

1. Report No. NASA TM X-3278		2. Government Accession No.		3. Recipient's Catalog No.	
4. Title and Subtitle NASTRAN: USERS' EXPERIENCES				5. Report Date September 1975	
				6. Performing Organization Code	
7. Author(s)				8. Performing Organization Report No. L-10436	
9. Performing Organization Name and Address NASA Langley Research Center Hampton, Va. 23665				10. Work Unit No. 506-17-21-02	
				11. Contract or Grant No.	
12. Sponsoring Agency Name and Address National Aeronautics and Space Administration Washington, D.C. 20546				13. Type of Report and Period Covered Technical Memorandum	
				14. Sponsoring Agency Code	
15. Supplementary Notes Compendium of papers prepared for Fourth NASTRAN Users' Colloquium, September 9-11, 1975, NASA Langley Research Center. **					
16. Abstract This technical memorandum is comprised of selected papers prepared for the Fourth NASTRAN Users' Colloquium held at the NASA Langley Research Center, September 9-11, 1975. The authors discuss the application of NASTRAN to a wide variety of static and dynamic structural problems. Specifically, the papers focus on the following topics: I. General Topics II. Statics III. Vibrations IV. Dynamics V. Computer Operations VI. Thermal Analysis VII. Special Topics					
17. Key Words (Suggested by Author(s)) NASTRAN, structures, finite element, NASTRAN Colloquium			18. Distribution Statement Unclassified - Unlimited Subject Category 39		
19. Security Classif. (of this report) Unclassified		20. Security Classif. (of this page) Unclassified		21. No. of Pages 639	22. Price* \$15.25

NASTRAN: USERS' EXPERIENCES

Compendium of papers prepared for the Fourth NASTRAN Users' Colloquium

September 9-11, 1975

NASA Langley Research Center

FOREWORD

NASTRAN (NASA STRUCTURAL ANALYSIS) is a large, comprehensive, nonproprietary, general-purpose finite-element computer code for structural analysis which was developed under NASA sponsorship and became available to the public in late 1970. It can be obtained through COSMIC (Computer Software Management and Information Center), Athens, Georgia, and is widely used by NASA, other government agencies, and industry.

NASA provides continuing maintenance and improvement of NASTRAN through a NASTRAN Systems Management Office (NSMO) located at Langley Research Center. Because of the widespread interest in NASTRAN, NSMO organized the Fourth NASTRAN Users' Colloquium at Langley Research Center, September 9-11, 1975. (Papers from previous colloquiums held in 1971, 1972, and 1973 are published in NASA Technical Memorandums X-2378, X-2637, and X-2893, respectively.) The Fourth Colloquium provided a comprehensive review of the current status of NASTRAN, future capabilities, unique applications, operational enhancements, and new approaches in its use.

Individuals actively engaged in the use of NASTRAN were invited to prepare papers for presentations at the colloquium. These papers are included in this volume. Only a limited editorial review was provided to achieve reasonably consistent format and content. The opinions and data presented are the responsibility of the authors and their respective organizations.

Deene J. Weidman, Manager
NASTRAN Systems Management Office
Langley Research Center
Hampton, Va. 23665
September 1975

CONTENTS

FOREWORD iii

I. GENERAL TOPICS

1. NASTRAN STATUS AND PLANS 1 ✓
Deene J. Weidman (NASA Langley Research Center)

2. SURVEY OF NASTRAN IMPROVEMENTS SINCE LEVEL 15.5 11 ✓
John R. McDonough (Computer Sciences Corporation)

3. NASTRAN MAINTENANCE AND ENHANCEMENT EXPERIENCES 23 ✓
Ronald P. Schmitz (Sperry Rand Corporation)

4. NASTRAN AS A RESOURCE IN CODE DEVELOPMENT 37 ✓
E. L. Stanton and L. M. Crain (Prototype Development Associates, Inc.) and T. F. Neu (Naval Air Development Center)

5. NASTRAN SOLUTIONS OF PROBLEMS DESCRIBED BY SIMULTANEOUS PARABOLIC DIFFERENTIAL EQUATIONS 65 ✓
J. B. Mason (NASA Goddard Space Flight Center) and W. H. Walston, Jr. (University of Maryland)

II. STATICS

6. NASTRAN APPLICATIONS TO AIRCRAFT PROPULSION SYSTEMS 91 ✓
John L. White (Boeing Commercial Airplane Co.) and David L. Beste (Boeing Computer Services, Inc.)

7. MODELING DAMAGED WINGS - ELEMENT SELECTION AND CONSTRAINT SPECIFICATION 105 ✓
W. J. Stronge (Naval Weapons Center)

8. APPLICATION OF NASTRAN TO A FLUID SOLIDS UNIT IN THE PETROLEUM INDUSTRY 121 ✓
Norman W. Nelson (Exxon Research and Engineering Co.)

9. SHUTTLE WING PANEL STABILITY ANALYSIS 137 ✓
T. Balderes, P. Mason, E. Ranalli, J. Zalesak, and A. Levy (Grumman Aerospace Corporation)

10. PRESSURE DEFORMATION OF TIRES USING DIFFERENTIAL STIFFNESS FOR TRIANGULAR SOLID-OF-REVOLUTION ELEMENTS 171 ✓
C. H. S. Chen (B. F. Goodrich Company)

11. A FAILSAFE ANALYSIS USING NASTRAN'S PIECEWISE LINEAR ANALYSIS WITH A NINE NODE LINEAR CRACK ELEMENT 181 ✓
R. F. Wilkinson and J. W. Kelley (Lockheed-Georgia Company)

12. APPLICATION OF NASTRAN FOR STRESS ANALYSIS OF LEFT VENTRICLE
OF THE HEART 201 ✓
Y. C. Pao (University of Nebraska), E. L. Ritman (Mayo Graduate
School of Medicine), and H. C. Wang (IBM Corporation)

III. VIBRATIONS

13. DYNAMIC SUBSTRUCTURE ANALYSIS OF THE INTERNATIONAL ULTRAVIOLET
EXPLORER (IUE) SPACECRAFT 221 ✓
William R. Case (NASA Goddard Space Flight Center)
14. ANALYTICAL AND EXPERIMENTAL STUDY OF TWO CONCENTRIC CYLINDERS
COUPLED BY A FLUID GAP 249 ✓
T. M. Mulcahy, P. Turula, H. Chung, and J. A. Jendrzejczyk
(Argonne National Laboratory)
15. NASTRAN NONLINEAR VIBRATION ANALYSES OF BEAM AND FRAME STRUCTURES . . . 259 ✓
Chuh Mei (LTV Aerospace Corporation) and James L. Rogers, Jr.
(NASA Langley Research Center)
16. ON EIGENVECTORS OF MULTIPLE EIGENVALUES OBTAINED IN NASTRAN 285
P. R. Pamidi and W. K. Brown (Computer Sciences Corporation)
17. THE EFFECTS OF LOCALIZED DAMPING ON STRUCTURAL RESPONSE 301 ✓
D. H. Merchant (Boeing Aerospace Company) and R. M. Gates,
M. W. Ice, and J. W. Van Derlinden (Boeing Computer Services, Inc.)
18. FINITE ELEMENT ANALYSIS USING NASTRAN APPLIED TO HELICOPTER
TRANSMISSION VIBRATION/NOISE REDUCTION 321 ✓
R. W. Howells and J. J. Sciarra (Boeing Vertol Company)
19. ANALYSIS OF NONLINEAR STRUCTURES VIA MODE SYNTHESIS 341
R. K. Gieseke (General Dynamics/Convair Aerospace)

IV. DYNAMICS

20. APPLICATION OF NASTRAN TO PROPELLER-INDUCED SHIP VIBRATION 361 ✓
Atis A. Liepins (Littleton Research and Engineering Corp.)
and John H. Conaway (Control Data Corporation)
21. TRANSIENT ANALYSIS OF BODIES WITH MOVING BOUNDARIES USING NASTRAN . . . 377 ✓
John W. Frye (Naval Underwater Systems Center)
22. APPLICATION OF NASTRAN IN NONLINEAR ANALYSIS OF A CARTRIDGE
CASE NECK SEPARATION MALFUNCTION 389 ✓
Jackson C. S. Yang (University of Maryland) and
Diana L. Frederick (U.S. Army, Frankford Arsenal)

- 23. NONLINEAR SEISMIC ANALYSIS OF A REACTOR STRUCTURE WITH IMPACT
BETWEEN CORE COMPONENTS 397 ✓
Ronald G. Hill (Hanford Engineering Development Laboratory)
- 24. THE DYNAMIC ANALYSIS OF SUBMERGED STRUCTURES 419 ✓
Gordon C. Everstine, Erwin A. Schroeder, and Melvyn S. Marcus
(Naval Ship Research and Development Center)

V. COMPUTER OPERATIONS

- 25. THE IMPACT OF "FOURTH GENERATION" COMPUTERS ON NASTRAN 431 ✓
James L. Rogers, Jr. (NASA Langley Research Center)
- 26. NASTRAN PRE- AND POSTPROCESSORS USING LOW-COST INTERACTIVE
GRAPHICS 449 ✓
E. D. Herness and H. Z. Kriloff (Boeing Computer Services, Inc.)
- 27. SCANNING NASTRAN OUTPUT DATA FOR MAXIMUM AND MINIMUM VALUES 461 ✓
Donald C. Walker (Control Data Corporation)
- 28. UNDERSTANDING THE NASTRAN STRUCTURE PLOTTER 475 ✓
Loren R. Kuusinen (Universal Analytics, Inc.)
- 29. THE NASTRAN ERROR CORRECTION INFORMATION SYSTEM (ECIS) 493 ✓
David C. Rosser, Jr., and James L. Rogers, Jr.
(NASA Langley Research Center)
- 30. RECENT IMPROVEMENTS TO BANDIT 511 ✓
Gordon C. Everstine (Naval Ship Research and Development Center)

VI. THERMAL ANALYSIS

- 31. NASTRAN THERMAL ANALYZER - STATUS, EXPERIENCE, AND NEW
DEVELOPMENTS 523 ✓
H. P. Lee (NASA Goddard Space Flight Center)
- 32. APPLICATION EXPERIENCES OF NASTRAN THERMAL ANALYSIS IN
ENGINEERING 529 ✓
James Chi-Dian Go (Computer Sciences Corporation)
- 33. COMPARISON OF NASTRAN AND MITAS NONLINEAR THERMAL ANALYSES
OF A CONVECTIVELY COOLED STRUCTURE 533 ✓
Earl A. Thornton (Old Dominion University) and
Allan R. Wieting (NASA Langley Research Center)

VII. SPECIAL TOPICS

34. RIGID FORMAT ALTER PACKETS FOR THE ANALYSIS OF ELECTROMAGNETIC
FIELD PROBLEMS 557 ✓
E. Spreeuw (Reactor Centrum Nederland) and R. J. B. Reefman
(Hazemeyer B.V.)

35. THE AUTOMATED MULTI-STAGE SUBSTRUCTURING SYSTEM FOR NASTRAN 571 ✓
E. I. Field, D. N. Herting, D. L. Herendeen, and R. L. Hoesly
(Universal Analytics, Inc.)

36. AUTOMATED MULTI-STAGE SUBSTRUCTURING ANALYSIS COMPARED WITH
SUPERELEMENT ANALYSIS 593 ✓
Lalit Shah (Rockwell International)

37. AN IMPROVED DMAP CAPABILITY 595 ✓
David L. Herendeen (Universal Analytics, Inc.)

38. DELTA WING FLUTTER BASED ON DOUBLET LATTICE METHOD IN NASTRAN 603 ✓
Howard Jew (Lockheed Electronics Company, Inc.)

39. NASTRAN MODELING AND ANALYSIS OF RIGID AND FLEXIBLE WALLED
ACOUSTIC CAVITIES 615 ✓
Joseph A. Wolf, Jr., and Donald J. Nefske (General Motors
Corporation)

NASTRAN STATUS AND PLANS

Deene J. Weidman
NASA Langley Research Center

N75 31486

SUMMARY

Current status and future NASA plans for the NASTRAN program are presented and discussed. Information is also presented to indicate the extent of NASTRAN use throughout the world.

INTRODUCTION

Use of the NASTRAN structural analysis computer program has become widespread since it was released to the public in 1970. The last status report on NASA's plans for NASTRAN was presented two years ago. (See ref. 1.) Since then, some fundamental changes have occurred both in technical aspects of the program and in NASA management policies. This paper summarizes the current status and NASA plans regarding the use, improvement, maintenance, and dissemination of NASTRAN.

CURRENT STATUS OF NASA ACTIVITIES

NASA's efforts are managed through the NASTRAN Systems Management Office (NSMO), which serves as a focal point for dissemination of NASTRAN information. The activities of this office are discussed subsequently in four different categories: use, improvements, maintenance, and dissemination.

Use

To get a better definition of NASTRAN use, 1200 Newsletter Address Up-dating forms were sent to users in May, 1974. Results from the 455 responses to that survey are shown in figure 1. The total number of known computer installations of the program is 269. Each respondent was asked to estimate the number of users at his installation, and an average number of users was determined from all of that company's respondents. Based on this process, the responding organizations have approximately 2300 users. Since not all users responded and not all users get the newsletter, these numbers are probably conservative. One significant fact is the large number of nonaerospace users that appear.

Survey results showing estimates of NASTRAN computer usage by the respondees in CPU hours/month are shown in figure 2. Also shown is the distribution of the number of users among various categories. A total of over 5000 CPU hours per month are being used on NASTRAN activities, with over 3/4 of this computer use being from nongovernment and non-aerospace users. The estimated number of users, however, indicate more persons in the government and aerospace categories.

Improvements

A broad overview of current improvements for NASTRAN is diagramed in figure 3. Since the last public release level, Level 15.5, a large number of improvements have been completed and are undergoing tests. These improvements were defined in some cases as long ago as the last NASTRAN colloquium, and will be included in Level 16. They include:

- (1) Static analysis using cyclic symmetry (Rigid Format 14)
- (2) Normal modes analysis using cyclic symmetry (Rigid Format 15)
- (3) Isoparametric solid hexahedra elements, C1HEX1
- (4) Subsonic modal flutter analysis (APP AERO, Rigid Format 10)
- (5) Static analysis with differential stiffness (Improved Rigid Format 4)
- (6) Normal mode analysis with differential stiffness (Rigid Format 13)
- (7) Axisymmetric solid of revolution elements, TRIAAX and TRAPAX
- (8) Identical element matrix generation (CNGRNT Feature)
- (9) Fully stressed design (OPTPR1 and OPTPR2 Modules)
- (10) Element strain energy and grid point force balance (GPFDR Module)
- (11) Complex modal displacement plots (CMODAL Plot Option)

The first four of these are mentioned in ref. 2 and are discussed elsewhere. The specific content of the last seven improvements is presented in detail in ref. 2, and is not discussed in the present paper.

Additional improvements identified as current improvements on figure 3 will also be incorporated in Level 16 before it is released. Estimated release date for Level 16 is now March 1976. The most important of these current improvements are discussed in two papers in the proceedings (refs. 3 and 4). Finally, there are also some planned improvements that are in progress or just beginning development and will not be available in time for Level 16 release. They will be incorporated in a post-Level 16 release and are identified in a later section of this paper.

Maintenance

As also shown on figure 3, error correction and dissemination by NASA is continuing and now embodies an Error Correction Information System (ECIS) that allows users to receive information more quickly on all reported errors. This system is described in still another proceeding's paper (ref. 5).

Dissemination

Since the last colloquium, NASA has implemented a new policy on dissemination of technology, including computer software, called FEDD (For Early Domestic Dissemination). This policy requires early dissemination to domestic users of any technology having significant commercial potential and which was developed at government expense. It also requires that such information be controlled for a period (typically two years) before foreign dissemination is permitted. NASTRAN levels above Level 15.5 are currently designated as "FEDD" information and therefore will be constrained from foreign distribution for a two-year period. The possibility of quid-pro-quo exchanges still exist, when it is to the advantage of the government.

Another important new NASA decision is to lease NASA funded software to domestic corporations at a yearly rate sufficient to support a portion of the maintenance costs of the software. Leases will be written to restrict the use of the software to a specific computer at a definite location and thus, facilitates the necessary control of dissemination of future levels, designated as FEDD. The entire leasing arrangement is handled for NASA by the Computer Software Management Information Center (COSMIC) at the University of Georgia. In the case of NASTRAN, levels that are not designated as FEDD information will be leased overseas at higher fees to recoup some of the large development costs of the present NASTRAN system.

CURRENT AND PLANNED IMPROVEMENTS

NSMO has three current improvements in progress. They are shown in figure 4, are nearing completion and, after testing, will be incorporated into Level 16 before it is released. The automated substructuring and DMAP language improvements are discussed in references 3 & 4. NASTRAN users also wanted more complete checks to be made on the condition of generated matrices before and during decomposition not after. These conditioning checks and accuracy estimates are being completed and also will be incorporated in Level 16 before it is released.

Also shown in figure 4 are a number of planned improvements that are scheduled for installation in the next level after Level 16. These capabilities include:

1. The FEER method of eigenvalue extraction (see ref. 6):

This fast tridiagonal modal reduction has been extended to complex eigenvalue problems and to allow specification of frequency ranges to be searched. This capability is being prepared for installation.

2. Supersonic flutter and gust response:

The aerodynamic theories include piston theory, strip theory, and Mach box theory. The calculation of gust loads and their power spectral density is included, and Fourier transform modules have been added. For a more detailed discussion of this capability, see references 7 and 8. The supersonic flutter and gust response package is nearly complete, and incorporation in a standard NASTRAN level will commence soon. Some improvements to the previously completed subsonic flutter capability have also been developed under contract.

3. A NASTRAN data generator:

A general program to generate NASTRAN input data from a minimum of geometric information will be contracted for and installed within NASTRAN, possibly in a link by itself. This effort is just starting.

4. Some new NASTRAN elements:

- A. A rigid element will be added to allow general connection of a number of grid points with a variety of degrees of freedom. This element would essentially allow constraint equations to be generated. The element is generated and currently being debugged.
- B. Two new ring elements will be added (triangular and trapezoidal). These axisymmetric elements would allow nonaxisymmetric loads and calculate the higher harmonics. These elements are also being debugged.
- C. A 6-node triangular membrane element will be added that will have linear varying strain and allow for linear thickness and temperature variations. This element is currently being checked out in a stand-alone version.
- D. A 6-node plate bending element is being developed that will allow a higher order bending displacement. (See ref. 9.)

This element would also allow a linear variation in thickness and temperature and is being checked out in a stand-alone version.

5. Automated modal synthesis:

Representing a portion of a structure by means of its natural modes is a common need of many users. This capability, sometimes termed automated modal synthesis, has only been defined and no development work has been started.

All five of these planned improvements will be received after Level 16 is frozen but will be available later. There are several other small improvements beyond the five listed, but these are not defined sufficiently for listing.

Also noted in figure 4 is the continual need for NASTRAN changes to keep abreast of computer hardware and operating system software developments. The required changes to NASTRAN caused by a new operating system on the IBM computers or a new compiler on the CDC computers are examples of recent changes of this type. This effort is hard to predict but is necessary for NASTRAN to remain state of the art.

FUTURE DEVELOPMENT PROCESS

NASA plans for future development of NASTRAN beyond Level 17 are not defined. If expanding user needs cannot be satisfied by NASA, cooperative procedures for new development might be needed. Such a process is illustrated in figure 5. Individual users would define, develop, and evaluate new capabilities they need. When a new development is complete and verified as correct by the developer, new decks and ALTERS to NASTRAN subroutines requiring modification would be submitted to the NSMO for possible incorporation into the next standard level of NASTRAN to be released. As a potential guide for possible future cooperative development activities, an Interface Requirements Document is being prepared by the maintenance contractor. This document will define general requirements (I/O, stress recovery, data card recognition, etc.) and coding standards to facilitate installation of new capability into the NASTRAN system.

CONCLUDING REMARKS

NASTRAN status and plans have been described and can be summed up with the following observations:

1. Use is widespread and growing.
2. Major improvements to the code (Level 16) and to the error communication process (ECIS) are at hand.
3. Plans for capability to be included in Level 17 are being completed. Future plans beyond Level 17 are not defined.
4. Future dissemination procedures will be different, with leasing, higher costs, and FEDD constraints being applied.
5. A possible cooperative pooling of user developed improvements is suggested as a means for continued enhancement of NASTRAN capabilities.

REFERENCES

1. Weidman, Deene J.: Future NSMO Plans for Maintenance of NASTRAN. NASTRAN: Users' Experiences, NASA TM X-2893, 1973, pp. 1-6.
2. McDonough, John R.: Survey of NASTRAN Improvements Since Level 15.5. NASTRAN: Users' Experiences, NASA TM X-3278, 1975, pp. 11-22.
3. Field, E. I.; Herting, D. N.; Herendeen, D. L.; and Hoesly, R. L.: The Automated Multi-Stage Substructuring System in NASTRAN. NASTRAN: Users' Experiences, NASA TM X-3278, 1975, pp. 571-591.
4. Herendeen, David L.: An Improved DMAP Capability. NASTRAN: Users' Experiences, NASA TM X-3278, 1975, pp. 595-602.
5. Rosser, David C., Jr.; and Rogers, James L., Jr.: The NASTRAN Error Correction Information System (ECIS). NASTRAN: Users' Experiences, NASA TM X-3278, 1975, pp. 493-509.
6. Anon.: NASTRAN: Users' Experiences. NASA TM X-2893, 1973, pp. 485-506.
7. Anon.: NASTRAN: Users' Experiences. NASA TM X-2378, 1971, pp. 779-795.
8. Harder, R. L.; MacNeal, R. H.; and Rodden, W. P.: A Design Study for the Incorporation of Aeroelastic Capability Into NASTRAN. NASA CR-111918, 1971.
9. Narayanaswami, R.: New Triangular and Quadrilateral Plate Bending Finite Elements. NASA TN D-7407, 1974.

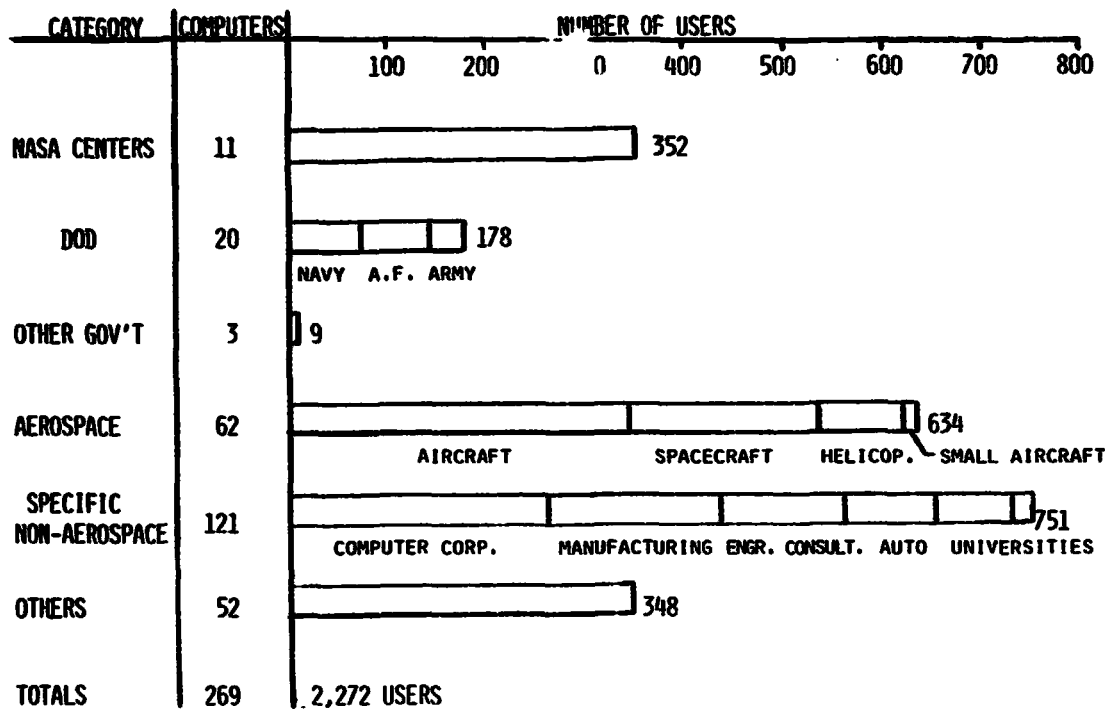


Figure 1.- NASTRAN User Community (For groups responding to Newsletter form - May 1974).

CATEGORY	INDIVIDUAL COMPUTER TIME USED (CPU HRS./MONTH)	% OF TOTAL COMPUTER USE	ESTIMATED NUMBER OF USERS	% OF TOTAL USERS
NASA CENTERS	156.9	3.0	352	15.5
DOD	81.4	1.6	178	7.8
OTHER GOV'T	.3	0.0	9	0.4
AEROSPACE	881.4	17.1	634	27.9
SPECIFIC NON-AEROSPACE	3887.5	75.4	751	33.1
OTHERS	146.8	2.9	348	15.3
TOTALS	5154.3	100.0	2272	100.0

Figure 2.- Computer time used by responding NASTRAN users.

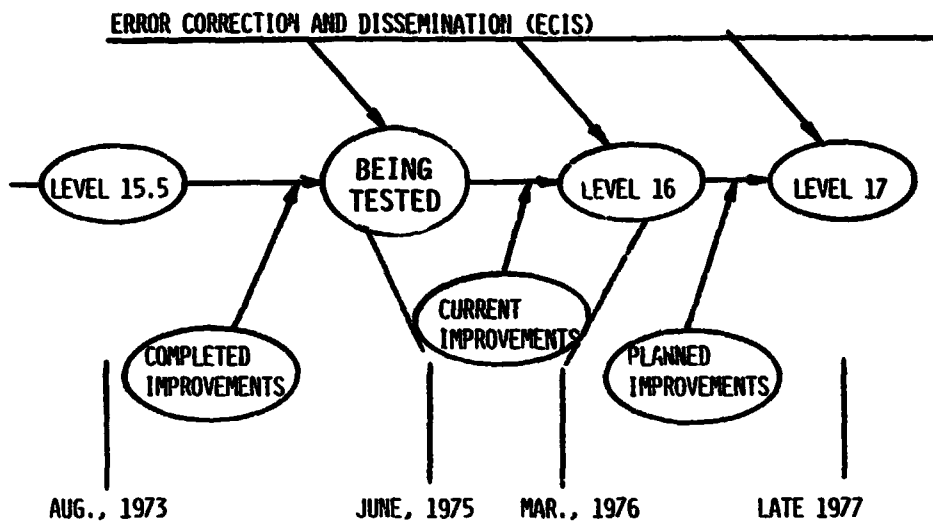


Figure 3.- Current status of NASTRAN improvements.

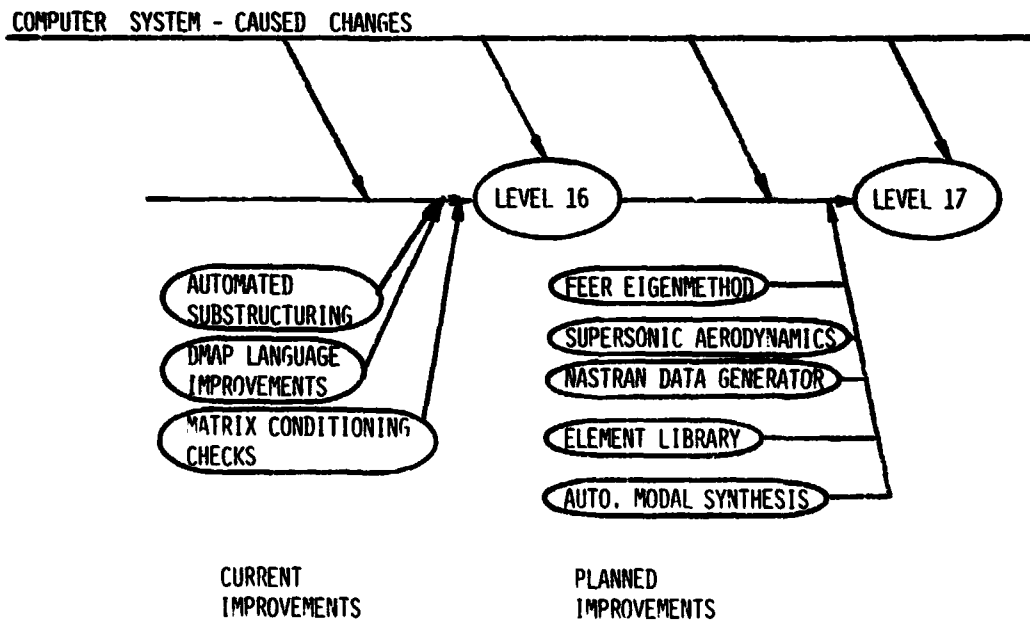


Figure 4.- NASTRAN improvements currently in progress.

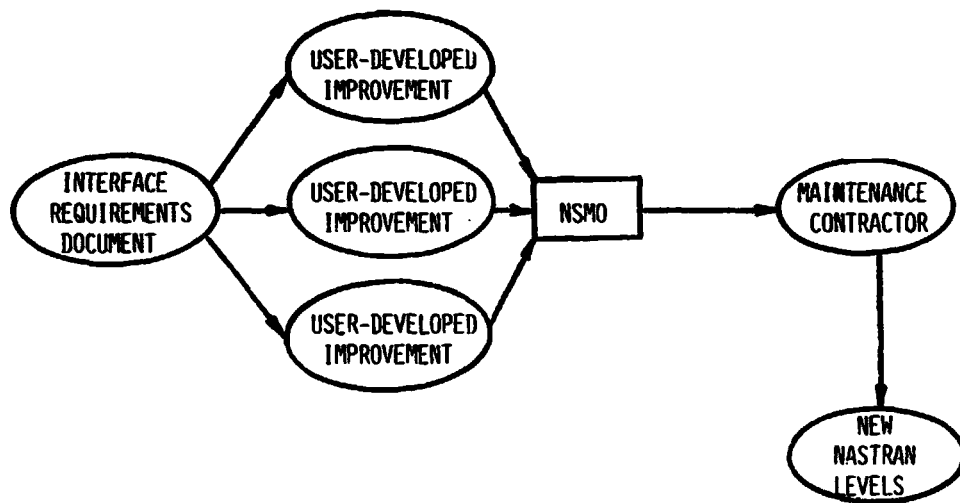


Figure 5.- A possible process for developing needed NASTRAN improvements.

A SURVEY OF NASTRAN IMPROVEMENTS SINCE LEVEL 15.5

John R. McDonough

N75 31487

Computer Sciences Corporation

SUMMARY

Since the last public release of NASTRAN (Level 15.5), several improvements and new capabilities have been developed and installed in intermediate levels and are being analyzed and evaluated. This paper presents a survey of current improvements to the program.

INTRODUCTION

Previous discussions of some of the improvements to NASTRAN have already been presented. These are: two axisymmetric solution techniques for identical structural segments called Static Analysis Using Cyclic Symmetry for APP DISP, Rigid Format 14 and Normal Modes Analysis Using Cyclic Symmetry for APP DISP, Rigid Format 15 (Reference 1), the inclusion of a library of linear-, quadratic-, and cubic-isoparametric solid hexahedra for DISP and HEAT APPROACHES called CIHEX1, CIHEX2, and CIHEX3, respectively (Reference 2), and a subsonic aeroelastic capability called Modal Flutter Analysis for APP AERØ, Rigid Format 10 (Reference 3).

Improvements in operational efficiency, such as matrix handling and processing (Reference 4), are not discussed here since this paper will highlight basic features which the user will implement to gain access to a specific capability.

Other improvements (Reference 5) which have not been previously discussed are: an improved differential stiffness technique (APP DISP, Rigid Format 4), a new normal modes with differential stiffness rigid format (APP DISP, Rigid Format 13), the inclusion of two axisymmetric solids of revolution elements to the NASTRAN library (TRIAAX and TRAPAX), an identical element matrix generator (CNGRNT), an experimental property optimization technique (Fully Stressed Design), two new static analysis output features to print element strain energy (ESE) and grid point force balance (GPFØRCE), and the ability to plot complex modal deformations (CMØDAL).

STATIC ANALYSIS WITH DIFFERENTIAL STIFFNESS RIGID FORMAT

The previous differential stiffness technique (Reference 6) uses the internal element forces obtained from the linear static solution to compute the individual element differential stiffness matrices. This technique is based on the assumption that the internal load is a linear multiple of the applied load and remains fixed in magnitude and direction. Thus the effects of nonlinearity on large displacement responses were approximated by a series of applied load factors.

Another approach (Reference 7) to solve the differential stiffness problem is to iterate the displacements to compute the differential stiffness matrix K^d by

$$[K + K^d(u_i)] \{u_{i+1}\} = \{P\} \quad (1)$$

where u_i and u_{i+1} are the set of displacements at two successive iterations, K is a stiffness matrix, and P is a load vector. To avoid a decomposition of

$$[K + K^d(u_i)]$$

at each iteration, $[K^d(u_i)]$ is removed from the left hand side and is replaced with the term $[K^d(u_e)]$ to give

$$[K + K^d(u_e)] \{u_{i+1}\} = \{P\} + [K^d(u_e) - K^d(u_i)] \{u_i\} \quad (2)$$

or

$$(K + K^d(u_e)) \{u_{i+1}\} = \{P\} + [K^d(u_e - u_i)] \{u_i\} \quad (3)$$

where u_e is an estimate initially equal to the linear elastic solution. With this technique the internal loads may change due to differential stiffness effects so that the solution is not linearly related to the applied load. Thus equation (3) treats the change in differential stiffness as a load correction.

Three PARAMETERS are provided to control the iterative process. The first, BETAD, limits the number of load corrections before adjusting the differential stiffness. The second, NT, limits the cumulative number of iterations. Thus load correction iterations can be performed up to the limit BETAD, at which time the differential stiffness is adjusted, and then more load correction iterations are performed and an adjustment is made to a new differential stiffness until NT is exhausted. Smaller values of BETAD allow more frequent adjustments to the differential stiffness. It is more economical to iterate via a larger value for BETAD so that fewer DMAP modules in the rigid format are re-executed. The third, EPSIØ, is a convergence criteria which terminates the process when successive iterations of the differential stiffness are sufficiently small. Convergence occurs when $\epsilon_i < \text{EPSIØ}$ where

$$\epsilon_i = \frac{| \{u_{i+1}\}^T \{P_{i+1} - P_i\} |}{| \{u_{i+1}\}^T \{P_i\} |} \quad (4)$$

A differential stiffness check functional module, DSCHK, performs convergence and timing tests and issues appropriate information each time it is executed. The differential stiffness coefficient functional module, DSMG2, is not used with this technique. The iterated differential stiffness solution does not match exact theoretical results, but shows a significant improvement over the one-step method, particularly where nonlinearity is pronounced.

NORMAL MODES WITH DIFFERENTIAL STIFFNESS RIGID FORMAT

It was possible to obtain the normal modes of a structure including differential stiffness effects by ALTERing the buckling analysis rigid format using NASTRAN Level 12.0 (Reference 8) or Level 15.1 (Reference 9). The obvious difference between the two was that the earlier version required two subcases and the later version required three. The three-subcase version is the one that is incorporated in a new, separate rigid format (SOL 13; APP DISP). Although the static analysis with differential stiffness rigid format solution technique has been substantially changed, as discussed above, the same technique has not been incorporated in this rigid format.

This rigid format requires three subcases to define the three steps of normal modes analysis with differential stiffness effects. The first subcase pertains to the linear solution step in which static loads are defined and output requests are specified. The second subcase is used to prescribe one differential stiffness loading scale factor and to prescribe output for second order effects. The third subcase contains the eigenvalue extraction method and output requests. Overall definitions can be placed above the subcase level and plot requests follow the third subcase in the usual convention. Since the previous differential stiffness technique allowed several loading factors to be prescribed (Reference 10), this approach can only be used with one load factor at a time. If the load factor technique is still preferred for differential stiffness analysis, this rigid format can be used with minor ALTERS to loop back for new loads and JUMP around the normal modes analysis.

This combination rigid format supports requests for static undeformed and deformed structural plots as well as mode shapes.

THE TRIAAX AND TRAPAX ELEMENTS

One of the types of elements included in the NASTRAN library has been the solid of revolution (Reference 11). Two specific cross sections available have been the triangle and the trapezoid which were defined by the CTRIARG and CTRAPRG data cards, respectively. These elements are, however, restricted to axisymmetric loading conditions. Two new axisymmetric ring elements have been developed for the asymmetric loading case. These are the TRIAAX and TRAPAX. Like the earlier elements they may not be used with other types of structural elements and they may be used alone or with each other. Because of the inherently different loading capabilities, the -RG type elements cannot be used with the -AX type elements.

In a manner similar to the development of the conical shell element, the radial, tangential and axial displacements of a point $p(r,z,\phi)$, expressed in terms of Fourier series, are

$$u(r,z,\phi) = u_0(r,z) + \sum_{n=1}^m u_n(r,z) \cos n\phi + \sum_{n=1}^m u_n^*(r,z) \sin n\phi \quad (5)$$

$$v(r,z,\phi) = v_0^*(r,z) + \sum_{n=1}^m v_n(r,z) \sin n\phi - \sum_{n=1}^m v_n^*(r,z) \cos n\phi \quad (6)$$

$$w(r,z,\phi) = w_0(r,z) + \sum_{n=1}^m w_n(r,z) \cos n\phi + \sum_{n=1}^m w_n^*(r,z) \sin n\phi \quad (7)$$

respectively.

The generalized displacement amplitudes are obtained for each n harmonic for the TRIAAX and TRAPAX elements at specified azimuth positions, ϕ . When $n = 0$, the degenerate displacement coefficients are obtained for the TRIARG and TRAPRG elements. Thus, with the use of new property cards, PTRIAAX and PTRAPAX, up to 14 azimuth coordinates can be specified for displacement and stress recovery. Displacements and forces are evaluated at the three (or four) corners. Stresses are evaluated for the triangular element on a circle generated by the centroid while stresses for the trapezoid are computed at the four corners as well as the centroid.

THE CNGRNT FEATURE

When a structural model is made up of elements which are truly identical, i.e., orientation, geometry, etc., an identical matrix generator feature is utilized with a CNGRNT bulk data card. One element is designated as the primary element, i.e., the one for which the stiffness, mass and damping matrices will be calculated and all other identical elements, declared as secondary, have identical matrix elements. This feature will then reduce the amount of time required to generate numerous matrices which are exactly identical. In a limited number of cases, the NASTRAN data generator module, INPUT, can be used in lieu of actual data cards to model bars, plates and scalar elements (Reference 12). The CNGRNT feature is automatically used by this module so it is therefore unnecessary to employ CNGRNT cards with it.

A structure can be modeled in one of three ways: (1) a complete data deck, (2) no connection cards but using the INPUT module or (3) a complete data deck with the CNGRNT feature. Using one of the NASTRAN demonstration problems (static analysis of a simply supported 5 x 50-inch plate subjected to a varying load across its transverse midplane), comparative computer CPU times were compiled to show the improvement using this technique. This problem contains 250 CQUAD1 plate elements, an initial stiffness matrix, $[K_{gg}]$, of order 1836 and a

constrained stiffness matrix, $[K_{\ell\ell}]$, of order 760 (Reference 13). With the complete data deck it took the CDC 6400 a total of 425 CPU seconds to build the individual stiffness matrices, whereas the same computer took about 2.5 CPU seconds to complete one stiffness matrix and duplicate the rest for the same problem set up the other two ways. Compared to Level 15.5, it took the CDC 6400 a total of 730 CPU seconds to build the individual stiffness matrices and about 400 CPU seconds with the original INPUT module. The differences achieved between Level 15.5 and the improved level cannot be attributed to the congruent feature but to an improved matrix generator (Reference 14). Thus these time studies are only valid when modeling techniques are compared within the same level. Table 1 shows the detailed results.

FULLY STRESSED DESIGN

The concept of a "fully stressed" design of a structure is to adjust some parameter so that each member is at a zero margin of safety since a pre-determined stress limit has been achieved. The parameters to be adjusted are cross-sectional area, thickness or moment of inertia. Properties may be scaled for common elements, such as the thickness for all plates, or they may be scaled for individual elements, each having its own design criteria.

The iteration process begins by performing a static analysis (APP DISP; SØL 1) for all loading conditions using the initial values for all element properties, p . A new property, p' , will be scaled from

$$p' = p \left[\frac{\alpha}{\alpha + (1-\alpha)\gamma} \right] \quad (8)$$

where p is the current property value, γ is an iteration factor set by the user and α is defined as

$$\alpha = \text{Max} \left| \frac{\sigma}{\sigma_{\ell}} \right| \quad (9)$$

where σ is a stress and σ_{ℓ} is the stress limit. The maximum value of α is taken for all loading conditions.

The value of the iteration factor, γ , is by default equal to unity. In this case Equation (8) is

$$p' = p\alpha \quad (10)$$

When $\gamma = 0$, Equation (8) is

$$p' = p \quad (11)$$

Thus the user can regulate the iteration process by choosing an intermediate value for γ .

The maximum change in any property is specified by the user to be

$$KMIN < \frac{P'}{P} < KMAX \quad (12)$$

The change ratio can be ignored by setting KMAX equal to zero, otherwise $KMAX > KMIN$.

The iteration process continues until a convergence criteria

$$\epsilon > \frac{|\sigma - \sigma_l|}{\sigma_l} \quad (13)$$

is achieved or until the number of iterations is reached, both of which are set by the user.

Optimization can be performed on bars, rods and tubes as well as shear panels and plate and membrane elements. The cross-sectional area or torsional constant of the bars, rods and tubes can be optimized. Additionally the moments of inertia of the bar can be optimized. The moments of inertia or thickness are optimized for the other elements, depending upon whichever is appropriate. The stress limit used is that in tension, compression, shear or torsion, as dictated by the type of element in question.

A PØPT bulk data card contains the number of iterations desired, the values for ϵ and γ , and PRINT and PUNCH options for new property bulk data cards. A PLIMIT bulk data card contains the values for KMIN and KMAX with reference to the element type involved.

Functional Module ØTPR1, in Link 2, processes the PØPT and PLIMIT bulk data cards and sets up appropriate tables. Functional Module ØTPR2, in Link 8, performs the new property calculations. These two modules re-execute until insufficient time or user criteria is met.

ELEMENT STRAIN ENERGY AND GRID POINT FORCE BALANCE

A Functional Module, GPFDR, in Link 13 of DISP Rigid Format 1, processes case control requests for grid point force balance and element strain energy output.

The card GPFØRCE $\left[\begin{array}{c} \text{PRINT} \\ \text{PUNCH} \end{array} \right] = \left\{ \begin{array}{c} \text{ALL} \\ n \\ \text{NONE} \end{array} \right\}$ requests a force balance output for

specified grid points. The output is arranged by grid or scalar point number

and lists the forces at the point due to applied loads $\{P_g\}$, forces of single point constraint $\{q_g\}$ and element forces $\{F_e\}$. These forces are summed and the total is ideally identical to zero for true balance; however, in some cases round-off errors cause extremely small force residuals when combining very large and very small quantities.

Element strain energy is output via the card ESE $\left[\begin{matrix} \text{PRINT} \\ \text{PUNCH} \end{matrix} \right] = \left\{ \begin{matrix} \text{ALL} \\ \text{NONE} \end{matrix} \right\}$

in the case control deck. From the equation for element forces,

$$\{F_E\} = - [K_E] \{u_E\} \quad (14)$$

where $[K_E]$ is an element stiffness matrix and $\{u_E\}$ is the displacement vector, the element strain energy is computed from

$$U = 1/2 | \{F_E\}^T \{u_E\} | \quad (15)$$

The total strain energy for all structural elements is printed followed by a listing of the strain energies of the individual elements, arranged by element type.

COMPLEX MODAL DISPLACEMENT PLOTS

The complex eigenvalue extraction rigid format (APP DISP, SØL 10) does not contain a deformed plot option, even for real mode shapes (Reference 15). The user would instead employ APP DISP, SØL 3 to compute real eigenvalues and plot only the real mode shapes. However, included with the subsonic aeroelastic flutter analysis (Reference 3) is the capability to plot complex mode shapes. To do this, the user defines a plot SET of interest in the case control deck, such as a wing surface (Reference 16), which may be modeled with structural or aerodynamic elements. Assuming the preliminary definitions and specifications following OUTPUT(PLØT) are complete, the plot command card PLØT MØDAL DEFØRMATIONetc.... will generate the real part of the mode shapes. The plot command card PLØT CMØDAL DEFØRMATIONetc.... will generate the imaginary part of the mode shapes. An eigenvalue frequency RANGE of interest may be included in both commands; otherwise all the frequencies at which solutions were obtained will be used for the plots. A MAGNITUDE or PHASE LAG may be specified on the complex plot command card; otherwise a default of zero degrees phase will be used.

DEMONSTRATION PROBLEMS

Levy has suggested a scheme to demonstrate the capabilities offered by NASTRAN with a comprehensive set of demonstration problems (Reference 17). Although total adoption of such a premise would necessitate revisions to many existing demonstration problems (and an extensive writing effort for the NASTRAN Demonstration Problem Manual), new demonstration problems have been devised and are still being devised to adequately exercise new capabilities. Also, a more compact table of options and features illustrated by each demonstration problem is in progress. Where one model is analyzed via more than one technique, such as user data cards versus INPUT data generation, the "duplicate" problem is simply referred to as another version of the first. Thus a proliferation of problem identification does not result and the user need not be familiar with a scattered set of examples in order to study aspects of the program in which he is interested.

The static analysis rigid format (APP DISP, SOL 1) contains the most demonstration problems and has had the most newly devised demonstration problems added to it. A thick walled cylinder, modeled with the TRAPAX and TRIAAX elements and subjected to a pressure load on a portion of its surface, is used to illustrate the use of these elements. A beam, modeled with general (GENEL) elements, described in terms of the flexibility matrix (Reference 18) is used to illustrate that feature introduced in Level 15.5. A reinforced arch, modeled with quadrilateral plates and reinforcing rods, is used to illustrate the property optimization technique in adjusting the plate thicknesses and rod cross sections. The isoparametric solid hexahedra are separately used to model the same section of a circular cylinder to demonstrate the utility of these elements. The biconvex wing demonstration problem (Reference 19) and the free rectangular plate with thermal loading (Reference 20) are used to separately demonstrate the comparable use of the CQDMEM1 and the CQDMEM2 elements (Reference 21) which were introduced in Level 15.5. The congruent feature is demonstrated as previously discussed. Steady state heat conduction through a washer (Reference 22) is converted to APP HEAT, SOL 1, with minor data changes to illustrate the updated methodology required by the completion of the heat transfer capability for Level 15.5. In addition, the convection and radiation heat transfer additions (Reference 23) lead to the inclusion of appropriate demonstration problems for APP HEAT, SOL 3 and APP HEAT, SOL 9. A beam-column, subjected to a compressive axial load, is used to illustrate the APP DISP, SOL 13 normal modes with differential stiffness effects rigid format. The example presented in Reference 1 is used to show the static cyclic symmetry technique for APP DISP, SOL 14 and a similar version of it demonstrates the normal modes analysis using cyclic symmetry for APP DISP, SOL 15. The example studied in Reference 3 is the basic problem used to model two aeroelastic demonstration problems for APP AERO, SOL 10 to show the computational and graphical capabilities.

CONCLUDING REMARKS

These are some of the user features, but certainly not all, which are currently in stages of development, testing and evaluation. The choice of an

--	--	--	--	--	--	--	--

appropriate demonstration problem illustrates the utility of a particular feature to verify theoretical cases. The real testing rests with the user.

REFERENCES

1. MacNeal, R. H., R. L. Harder and J. B. Mason, NASTRAN Cyclic Symmetry Capability, NASTRAN User's Experiences, NASA TM X-2893, September 1973, pp 395-421.
2. Johnson, Stephen E. and Eric I. Field, Three Isoparametric Solid Elements for NASTRAN, NASTRAN Users' Experiences, NASA TM X-2893, September 1973, pp 423-437.
3. Doggett, Robert V. and Robert L. Harder, Subsonic Flutter Analysis Addition to NASTRAN, NASTRAN Users' Experiences, NASA TM X-2893, September 1973, pp 507-529.
4. McCormick, Caleb W., Review of NASTRAN Development Relative to Efficiency of Execution, NASTRAN Users' Experiences, NASA TM X-2893, September 1973, pp 7-28.
5. NASTRAN NEWSLETTER, September 5, 1973, pp 3-5.
6. The NASTRAN Theoretical Manual, NASA SP-221(01), December 1972, Section 7.1.
7. Zienkiewicz, O. C. and G. C. Nayak, A General Approach to Problems of Plasticity and Large Deformation Using Isoparametric Elements, Proceedings Third Conference on Matrix Methods in Structural Mechanics, AFFDL-TR-71-160, U.S. Air Force, December 1973, pp 881-928.
8. NASTRAN NEWSLETTER, March 13, 1972, pp 7-9.
9. NASTRAN NEWSLETTER, November 7, 1972, pp 22-28.
10. The NASTRAN User's Manual, NASA SP-222(01), May 1973, Section 3.5.
11. The NASTRAN Theoretical Manual, NASA SP-221(01), December 1972, Section 5.11.
12. The NASTRAN User's Manual, NASA SP-222(01), May 1973, Section 2.6.
13. The NASTRAN Demonstration Problem Manual, NASA SP-224(01), June 1972, Section 1.4.
14. The NASTRAN Programmer's Manual, NASA SP-223(01), May 1973, Section 4.124.
15. The NASTRAN User's Manual, NASA SP-222(01), May 1973, Sections 3.11, 4.1 and 4.2.
16. McDonough, John R., NASTRAN Plotting Capabilities, NASTRAN Users' Experiences, NASA TM X-2378, September 1971, pp 709-735.

- | | | | | | | | |
|--|--|--|--|--|--|--|--|
| | | | | | | | |
|--|--|--|--|--|--|--|--|
17. Levy, Alvin, Design of NASTRAN Demonstration Problems, NASTRAN Users' Experiences, TM X-2637, September 1972, pp 497-516.
 18. The NASTRAN Theoretical Manual, NASA SP-221(01), December 1972, Section 5.7.
 19. The NASTRAN Demonstration Problem Manual, NASA SP-224(01), June 1972, Section 1.1.
 20. The NASTRAN Demonstration Problem Manual, NASA SP-224(01), June 1972, Section 1.3.
 21. The NASTRAN Theoretical Manual, NASA SP-221(01), December 1972, Section 5.8.
 22. The NASTRAN Demonstration Problem Manual, NASA SP-224(01), June 1972, Section 1.12.
 23. The NASTRAN Theoretical Manual, NASA SP-221(01), December 1972, Section 8.

TABLE 1 - SAMPLE PROBLEM CUMULATIVE TIMES ON THE CDC 6400

Step	Improved Level (CPU seconds)			Level 15.5 (CPU seconds)	
	Complete Data Deck	Partial Deck with INPUT	Complete Deck with CNGRNT	Complete Data Deck	Partial Deck with INPUT
ΔA	41.198	27.310	43.770	37.228	23.638
ΔB	425.852	2.496	2.788	398.850	398.600
ΔC	332.886	333.792	337.314	296.232	302.070
Total JOB Time	799.936	363.598	383.872	732.310	724.308

ΔA = Total time for initial processing up to beginning of stiffness matrix module

ΔB = Total time in stiffness matrix module

ΔC = Total time from end of stiffness matrix module to EXIT

' N75 31488

NASTRAN MAINTENANCE AND
ENHANCEMENT EXPERIENCES

Ronald P. Schmitz

Sperry Rand Corporation

ABSTRACT

This paper describes Sperry Support Services' recent experiences in maintaining and enhancing the NASTRAN Program. The Sperry Version of NASTRAN started with the adoption of Level 15.1.2 (NSRDC) in 1972 and has evolved through a series of program improvements and error corrections. The current capability, which has been added to Level 15.5, includes isoparametric elements, optimization of grid point sequencing and new eigenvalue routine. Overlay and coding errors were corrected for cyclic symmetry, transient response and differential stiffness rigid formats.

In addition to maintaining a Sperry version of NASTRAN, we are also publishing a newsletter quarterly, providing user training to world wide UNIVAC users and maintaining and developing a set of NASTRAN pre and post processors which include mesh generators and interactive graphics.

The enhancement of NASTRAN is a continuing effort with a primary motivation of providing state-of-the-art analytical capability to in-house analysts, and to offer Sperry UNIVAC and its customers a source for error corrections and program enhancements in a continuous and timely manner. Developments scheduled for the current year are described in the paper as well as a brief description of analyses being performed using the program.

INTRODUCTION

Although Sperry has been a user of finite element programs dating back to early versions of SAMIS (reference 1) and the initial release of NASTRAN, our interest in maintaining and enhancing a local version is of more recent origin. The Sperry version of NASTRAN started with the adoption of Level 15.1.2 (reference 2) in 1972 and has evolved since that time through a series of program improvements and error corrections. Our early work was performed on both UNIVAC and CDC versions. In recent years, a natural emphasis upon developments for the UNIVAC computer systems has occurred through our association and cooperation with other divisions of the Sperry Rand Corporation.

The enhancement of NASTRAN is a continuing effort with a primary motivation of providing state-of-the-art analytical capability to in-house analysts, and to offer Sperry UNIVAC and its customers a source of error corrections and program enhancements in a continuous and timely manner. In addition to maintaining a Sperry Version of NASTRAN, we are also publishing a Newsletter quarterly, (reference 3, 4, and 5), providing user training to world wide UNIVAC users and maintaining and developing NASTRAN pre and post processors which include mesh generators and interactive graphics.

The association and cooperation with Sperry UNIVAC has resulted in a two way exchange of new routines and error corrections; and Sperry Support Services has acted as a focal point for the Corporation, bringing together the experiences of many domestic divisions and foreign subsidiaries.

ERROR CORRECTION EXPERIENCES

Any in-house programming effort with NASTRAN invariably begins with error corrections. Error corrections account for 25 percent of all NASTRAN programming efforts at Sperry. These involve:

- Implementing corrections obtained from NSMO via the SPR LOG and Newsletters.
- Independently locating and correcting errors existing in Level 15.5.
- Locating and correcting errors in the Sperry enhanced Level 15.6.

In the period January to May 1975, Sperry has made 17 error corrections. Five of these errors were found in the original Level 15.5 and the remaining errors were found in new code implemented in the Sperry Version 15.6.

These errors are briefly described in Table I, and do not include corrections obtained from NSMO SPR LOG or Newsletters, since these sources of corrections were implemented prior to January 1975.

Our experience with Level 15.5 error corrections shows that overlay errors account for most of the remaining errors and since many of the overlay errors do not exist in CDC or IBM versions, it is our conclusion that past NSMO maintenance of NASTRAN has not done a thorough job in checking the UNIVAC version overlay structure. On the other hand, the inclusion of a reverse trace of subroutine calls has been a significant help in locating many of the overlay problems.

CURRENT CAPABILITIES

The current capabilities of Sperry Version NASTRAN, structured around the standard COSMIC release Level 15.5, are summarized as follows:

- **Isoparametric Elements** - Four isoparametric elements, two surface elements and an independent thermal analysis capability (Rigid Format 14) originally developed by NSRDC (reference 6), have been installed. These elements have been utilized extensively since 1972 for the analyses of high energy laser and large space telescope mirrors, shown in Figures 1 and 2. The thermal analysis capabilities were compared with the CINDA thermal analyzer (reference 7) and published at the 5th Navy NASTRAN Colloquium (reference 8). Figure 1 also illustrates a comparison of CINDA and Sperry NASTRAN Thermal Analyzers.

The implementation of this capability into Level 15.5 required the addition of 103 new subroutines, and 113 modified subroutines requiring over 4000 Fortran update cards. Since the basic capability already existed in Level 15.1, the major programming effort required updating data block tables and correcting any conflicts between the isoparametric elements and the improvements implemented by NSMO between 15.1 and 15.5.

- **LINKO** - Many users operate at computer installations where the cost algorithms include the number of input card images read. The conventional "CONTRL" file can introduce many hundreds of data cards during the execution of a rigid format. LINKO was developed to eliminate the large number of input cards and automatically generate the necessary @XQT instruction for each succeeding link. A typical NASTRAN run stream becomes:

```
@XQT *NASTRAN.LINK1
ID A,B
  :
  :
ENDDATA
@XQT *NASTRAN.LINKO
```

- **Improved LINK1** - The BANDIT and WAVEFRONT procedures (references 9 and 10) were added to LINK1 overlay to permit automatic grid point resequencing to minimize the stiffness matrix decomposition time. Resequencing is requested through the NASTRAN card. Either method may be selected separately or both may be used. The sequencing resulting in the minimum decomposition time is automatically inserted into the data deck. All of the normal options of BANDIT and WAVEFRONT have been retained through the use of control cards containing a \$ in column 1.
- **Plot Tape Parity Option** - Many UNIVAC users, especially those operating on 1110 systems, often find it necessary to generate plot tapes, PLT1 or PLT2, in odd or even parity. A program change was made in SGINO, and a new data card added to the case control deck to permit the selection of tape parity from within the NASTRAN plot data deck (case control) e.g.,

@AST,T PLT2,20N

:

PLOTID = NAME, LOCATION
OUTPUT (PLOT)
PLOTTER CALCOMP
PLT2 EVEN

This run stream will mount a 9 track tape for the CALCOMP plot tape. All plot commands will be written in odd parity.

- Rayleigh-Ritz with Stadola Iteration Eigenvalue Routine - A new eigenvalue routine was added to NASTRAN. The formulation was based on work performed by J. R. Admire, reference 11. The procedure had previously been implemented in the FORMA (reference 12) and SPAR (reference 13) programs and is, therefore, well established as a fast and accurate technique. Figure 3 illustrates the basic equations used in the formulation. Capability to solve symmetric and unsymmetric matrices has been included, and the Input Data Card EIGR was modified for use with the procedure and is illustrated in Figure 4.

The size of the analysis set (A-set) is limited only by the core required for matrix decomposition. Several test problems have shown the technique to be at least three times faster than the Inverse Power method.

Some statistics on the changes required for the Rayleigh-Ritz routines are:

- Seven new subroutines added
- Special logic for selecting FBS or INVFBFS routines
- A new incore inversion routine added
- Stadola and Jacobi incore eigenvalue routines were added
- Programming effort was approximately 3 months
- Subroutines were modified to accept the changes to the EIGR cards.

OTHER ACTIVITIES

Sperry has gone beyond normal program maintenance and improvements by publishing a NASTRAN newsletter, providing user training, and developing pre and post processors. The newsletters are similar to the NSMO newsletter. Publication started in September 1974 and we plan to continue publishing one every 3 or 4 months. The objective of the newsletter is to provide Sperry UNIVAC customers with timely information on the development of new capabilities, current developments, error corrections and user's experiences.

The user's contributions published in the newsletters are chosen to illustrate new capabilities incorporated in the Sperry version or to illustrate a solution to a UNIVAC users' problem which Sperry feels may be of general interest to the user community. Past papers have included examples in the use of the thermostructural rigid format 14, cyclic symmetry, and buckling analyses using conical shell elements.

NASTRAN short courses have been taught in the United States and in Europe for users of the Sperry version of NASTRAN. This writer has found the European NASTRAN user to be very competent. In general they are analyzing large structures (e.g., automobile bodies, off shore oil rigs and ship structures) utilizing substructuring, cyclic symmetry, DMAP alters and DMAP programs. Their major limitations are the high cost of computer time and the failure of management to recognize the value of finite element analyses or to allow sufficient budgeting for large scale problem solution.

The development of pre and post processors is also being undertaken at Sperry. The current trend in the development of these programs is to include the capability to work with more than one finite element program. The GEOMPLT program (reference 14) is an interactive graphics program which was initially developed to graphically display and edit NASTRAN Bulk Data. It has since been modified to work with SPAR and ICES/STRUDL (reference 15) data as well. The ICES/TOPOLOGY mesh generation subsystem (reference 16) is currently being modified to output NASTRAN data. This approach has been taken to give the Sperry analysts additional flexibility in problem solution.

FUTURE DEVELOPMENT

The list of current development priorities for the Sperry Version of NASTRAN are:

- Automated Substructuring
- Contour Plotting added to the PLOT module
- Improved I/O
- Improved matrix decomposition
- Improved matrix multiplication
- New modal shock response rigid format
- Non-linear shell analysis
- Post-buckling rigid format
- New elements including pipe bends, and rigid elements.

Due to the leasing policy and export restrictions placed on post 15.5 NSMO improvements, all of the future development improvements will be added to the 15.5 program structure. Further, it will be necessary to duplicate existing capabilities such as automated substructuring instead of investing our resources

in new enhancements of mutual benefit to NASA and Sperry. It is recommended that NASA consider alternatives to the current policies. In the past, the NASTRAN program has gained a reputation for being a low cost general purpose structures program with excellent documentation and on-going maintenance. For this reason a large number of companies large and small have adopted the program. The return on the tax payers investment should not be measured only by the monetary return or even the direct benefit derived by NASA projects, but by the greater productivity derived from its use by commercial companies, the excellent information exchange obtained from its common use, and finally the positive effect on the export sale of large scale computer systems.

REFERENCES

1. Melosh, R. J., et al, "Structural Analysis and Matrix Interpretive System (SAMIS) Program Report," NASA JPL Report TM 33-307, Rev. 1, December 1966.
2. McCormick, C. W., Editor, "The NASTRAN USER'S Manual (Level 15.0)," NASA SP-222(01), May 1973.
3. "Sperry NASTRAN Newsletter," Number 1 Sperry Support Services, Huntsville, Alabama, October 10, 1974.
4. "Sperry NASTRAN Newsletter," Vol. 2, No. 1, Sperry Support Services, Huntsville, Alabama, February 1, 1975.
5. "Sperry NASTRAN Newsletter," Vol. 2, No. 2, Sperry Support Services, Huntsville, Alabama, June 6, 1975.
6. Hurwitz, M. M., "Additions to the NASTRAN User's Manual and Theoretical Manual for a Thermostructural Capability for NASTRAN using Isoparametric Finite Elements," NSRDC Report 4134, Bethesda, Maryland, May 1973.
7. Gaski, J. D., Lewis, D. R. and Thompson, L. R., "Chrysler Improved Numerical Differencing Analyzer for Third Generation Computers," TN-AP-67-287, October 20, 1967.
8. Proceedings of the Fifth NAVY-NASTRAN Colloquium," NSRDC Report CMD-32-74, September 1974.
9. Everstine, G. C., "The Bandit Computer Program for the Reduction of Matrix Bandwidth for NASTRAN," NSRDC Report 3827, March 1972.
10. Levy, R., "Structural Stiffness Matrix Wavefront Resequencing Program (WAVEFRONT), JPL, Pasadena, California. (Cosmic Report NPO-13322).
11. Admire, J. R., "Modal Analysis of Substructures by an Iterative Rayleigh-Ritz Technique," NASA TMX-64528, MSFC, 1970.

12. Wohlen, R. L., "Synthesis of Dynamic Systems using FORMA - Fortran Matrix Analysis," Martin Marietta Corp. Report MCR-71-75, NASA Contract NAS8-25922, May 1971.
13. Whetstone, W. D., "SPAR Reference Manual," Lockheed Missiles and Space Co. Report LMSC D403168, NASA Contract NAS8-26352, June 1974.
14. Schmitz, R. P., "GEOMPLT, Interactive Graphics Program for Finite Element and Thermal Network Models," Sperry Support Services, Huntsville, Alabama, November 30, 1974.
15. Logcher, R. D., et al, "ICES STRUDL-II, The Structural Design Language Engineering User's Manual," MIT Report R70-77, 2nd Edition, Cambridge, Mass., December 1973.
16. Bjaaland, H. K., et al, "ICES TOPOLOGY, Engineering User's Manual," MIT Report R72-65, Cambridge Mass., October 1972.

Table I. Sperry NASTRAN Error Corrections.

LEVEL 15.6.2

<u>SPR NO.</u>	<u>DESCRIPTION</u>
S-110	An infinite loop in plot module.
S-111*	Problem stops during gravitation load evaluation in SSC1.
S-112	No element forces printed.
S-114	Format error when printing solid isoparametric element stresses.
S-115	Problem max times in GP3 when using PLOAD2, SURF4, SURF8, IS3D8 or IS3D20 Bulk Data cards.
S-116*	COSMIC source code error in KQDMM1.

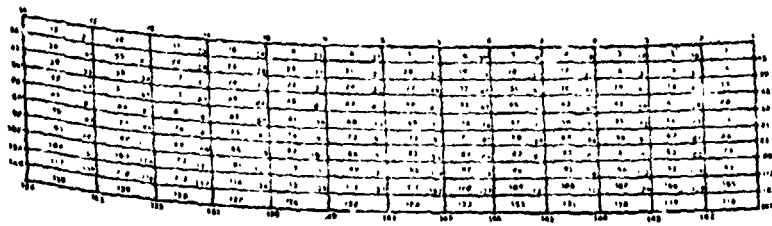
LEVEL 15.6.3

<u>SPR NO.</u>	<u>DESCRIPTION</u>
S-113	Restart error when restart with altered case control deck.
S-117	Plot error in IS3D8, IS3D20 and IS2D8 elements.
S-118	Mis-spelled word PQEMEM2.
S-119	NTRAN error, Unit 44/45 not available.
S-121*	Format error in Grid Point Singularity Table.
S-122	Force print error for CQDMEM2 element.

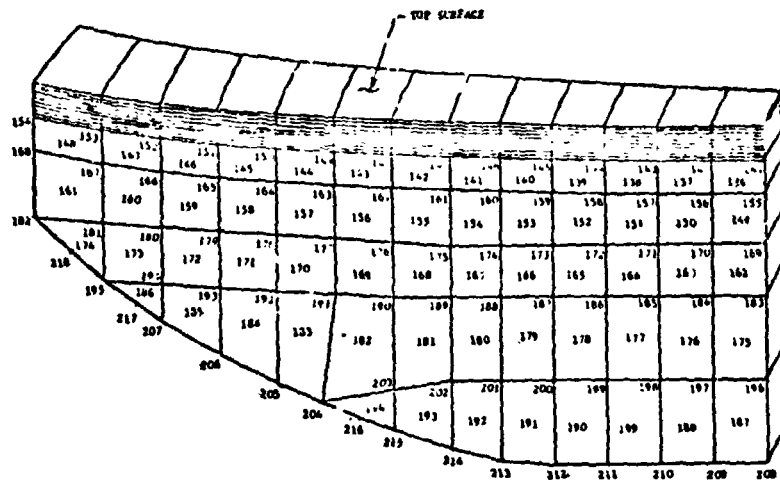
LEVEL 15.6.4

<u>SPR NO.</u>	<u>DESCRIPTION</u>
S-123, 128*	Error in NASTRAN General Plotter.
S-124*	Multiple time step error in Transient Analysis.
S-126	Incorrect time printed for RF 14 temperature output.
S-127	Permit plot tape parity change in Case Control Deck.
S-129	Add TAPEFLAG keyword to NASTRAN card of directing user tape files to DISK.

*Correction to original Level 15.5 code.



NEW PRIMARY MIRROR
FINITE ELEMENT MODEL
TOP 0.2 IN. THICKNESS



NEW PRIMARY MIRROR
FINITE ELEMENT MODEL

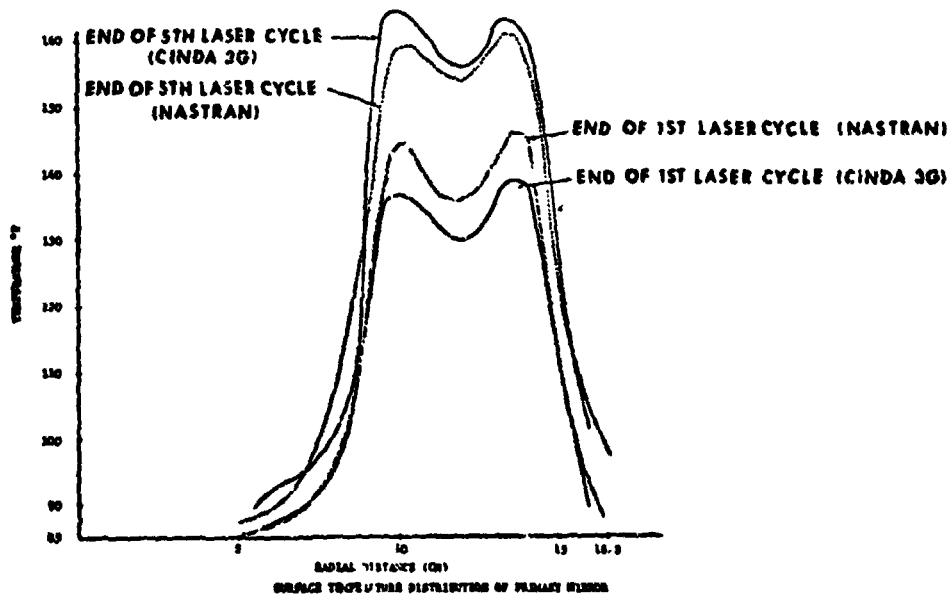
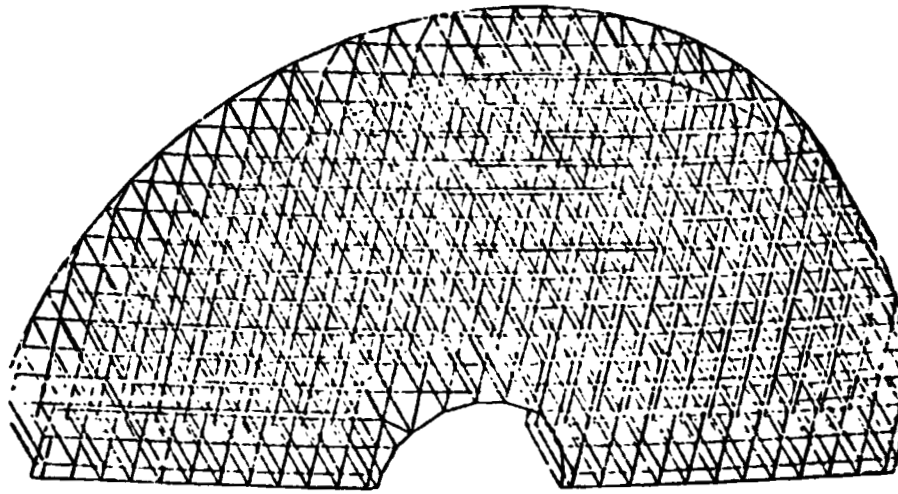
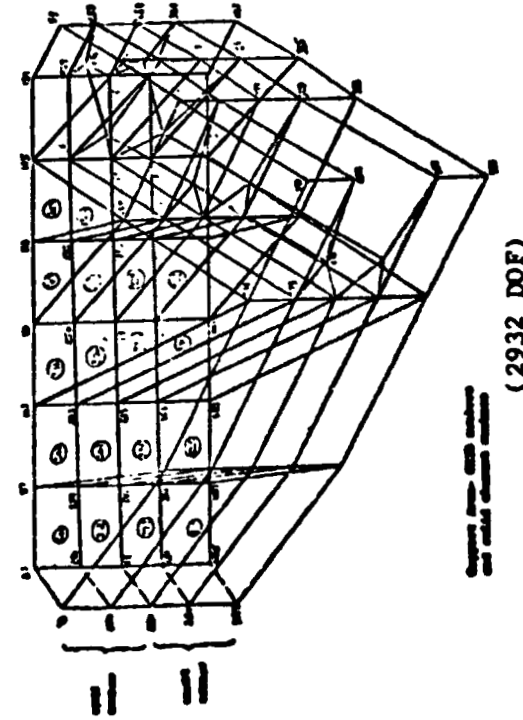
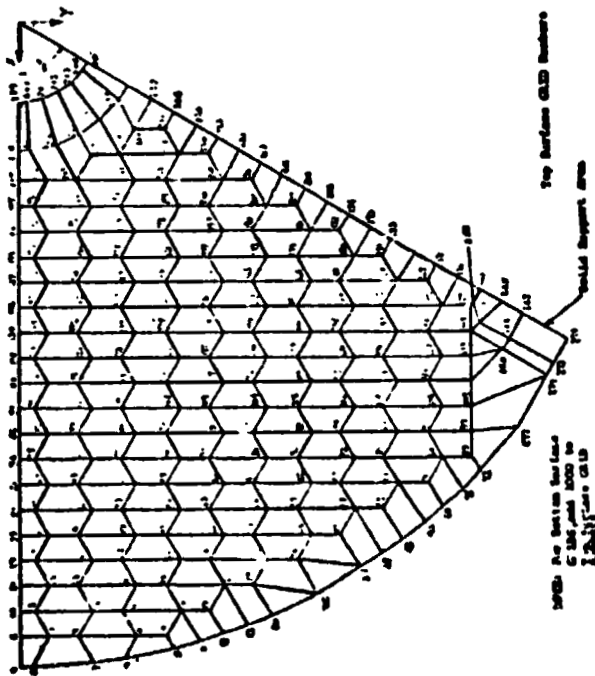


FIGURE 1. PRIMARY MIRROR, FINITE ELEMENT MODEL (648 DOF)



(5220 DOF)

(2932 DOF)

FIGURE 2. LST PRIMARY MIRROR, CERVI I AND ULE FINITE ELEMENT MODELS

- 1) Subtract $[K] - \lambda_g [M] = [\hat{K}]$;
- 2) Decompose $[\hat{K}] = [U]^T [D] [U]$;
- 3) Select initial modes $[Z]_0$;
- 4) Multiply $[M] [Z]_0 = [G]$;
- 5) Repress higher modes $[U]^T [\hat{K}] [Z] = [G]$;
- 6) Triple matrix product $[Z]^T [\hat{K}] [Z] = [\bar{K}]$, for 1st iteration only;
- 7) Multiply $[Z]^T [G] = [\bar{K}]$, skip this step for 1st iteration;
- 8) Multiply $[M] [Z] = [MZ]$;
- 9) Multiply $[Z]^T [MZ] = [\bar{M}]$;
- 10) Solve the eigenvalue/eigenvector problem

$$([\bar{K}] - \Omega^2 [\bar{M}]) \{q\} = \{0\}$$
 for eigenvalues $[\Omega^2]$ and eigenvector $[Y^*]$;
- 11) Calculate structural eigenvalues, $\omega_i^2 = \Omega_i^2 + \lambda_g$. Test ω_i^2 for convergence with previous iteration values. If converged, go to Step 13;
- 12) Multiply $[MZ] [Y^*] = [G]$, go to Step 5;
- 13) Multiply $[Z] [Y^*] = [Z]_{final}$;
- 14) End.

Figure 3. Rayleigh-Ritz Iterative Eigenvalue Formulation Used for Sperry Version NASTRAN.

BULK DATA CHECK

Input Data Card EIGR (continued) Real Eigenvalue Extraction Data

Description: Defines data needed to perform real eigenvalue analysis using the Rayleigh-Ritz with Stadola or Jacobi iteration method.

Format and Example:

EIGR	SID	METHOD	F1	F2	NE	ND	NZ	E	+abc
EIGR	13	RRTZ	0.0	50.0	20	10	-4	1.-3	+ER13
+abc	NORM	G	C						
+ER13	MASS								

Field

- SID** Set identification number (unique integer > 0)
- METHOD** Method of eigenvalue extraction, one of the BCD values "RRTZ" or "URRZ."
 RRTZ - Rayleigh-Ritz method, symmetric matrix operations.
 URRZ - Rayleigh-Ritz method, unsymmetric matrix operations.
- F1,F2** Frequency range of interest, F1 is the shift frequency, F2 is the upper limit of frequency of output eigenvectors. ($0.0 \leq F1 < F2$, Real)
- NE** Maximum number of iterations used (integer ≥ 3)
- ND** Number of roots desired, $2 \leq ND \leq 90$ (integer)
- NZ** Convergence criteria for accuracy of eigenvalues, $1F < 0$ $EPS1 = 10^{-NZ}$
 $1F \geq 0$ $EPS1 = .0001$
 (integer)
- E** Mass orthogonality test parameter (Default is 0.0 which means no test will be made (Real ≥ 0.0)).
- NORM** Method for normalizing eigenvectors, one of the BCD values "MASS", "MAX" or "POINT."
 MASS - Normalize to unit value of the generalized mass
 MAX - Normalize to unit value of the largest component in the analysis set.
 POINT - Normalize to unit value of the component defined in fields 3 and 4 - defaults to "MAX" if defined component is zero.
 G - Grid or Scalar point identification number (required if and only if "NORM" = "POINT") (integer ≥ 0)
 C - Component number (one of the integers 1-6) (required if and only if "NORM" = "POINT" and G is a geometric grid point.

Figure 4. EIGR Bulk Data Input Card.

NASTRAN DATA DECK

Remarks:

1. Real eigenvalue extraction data set must be selected in the Case Control Deck (METHOD = SID) to be used by NASTRAN.
2. The units of F1 and F2 are cycles per unit of time.
3. The continuation card is required.
4. If NE is omitted, NE is set equal to 1/3 the size of the A set or a maximum of 30, whichever is smaller.
5. The number of eigenvectors used for the iteration procedure is 1.3 times the number of roots desired (ND).
6. DIAG 16 may be used to obtain intermediate printout of the iteration procedure. Eigenvalues printed by this method have been shifted by F1. The final eigenvalue summary table has been corrected for the shift frequency.

Figure 4. EIGR Bulk Data Input Card. (Continued)

NASTRAN AS A RESOURCE IN CODE DEVELOPMENT*

E. L. Stanton and L. M. Crain
Prototype Development Associates, Inc.
Santa Ana, California

N75 31489

T. F. Neu
Naval Air Development Center
Warminster, Pennsylvania

SUMMARY

The heavy use of NASTRAN here and abroad has demonstrated its value as a resource for structural analysis. This paper presents another view of NASTRAN as a quite different resource. A case history is presented in which the NASTRAN system provided both guidelines and working software for use in the development of a major new discrete element program, PATCHES-III. At the 1973 Users' Colloquium, there were two papers presented on the addition of solid isoparametric elements to NASTRAN. At about the same time, development of PATCHES-III for general solids of composite material was begun. The grid point modeling system available in NASTRAN at that time was judged inadequate to efficiently support the modeling of general solids. However, there were many features of the program that would also be required in the new code. To avoid duplication and take advantage of the wide spread user familiarity with NASTRAN, the PATCHES-III system uses NASTRAN Bulk Data syntax, NASTRAN matrix utilities and the NASTRAN Linkage Editor. There were obvious problems that had to be overcome; GINO had to be transplanted to a new environment to mention only one. This paper reviews how these problems were solved and presents details on the architecture of the PATCHES-III parametric cubic modeling system. This system includes novel model construction procedures, new checkpoint/restart strategies and other features that may benefit future versions of NASTRAN.

* This development was sponsored by the Navy under contract number N62269-73-C-0736 and was performed at McDonnell Douglas Astronautics Company.

PRECEDING PAGE BLANK NOT FILMED

INTRODUCTION

At a recent NASTRAN Users' Colloquium, software eugenics was a topic of considerable interest, particularly as it related to the continued improvement of NASTRAN. Taking the symmetric view, NASTRAN can serve as a resource in the development of other finite element programs. A case history of one such development, PATCHES-III, is presented with emphasis on the mechanics of how this was accomplished. Among the reasons for taking this approach are the need for: (1) a standard finite element syntax familiar to all; (2) reliable, efficient, out-of-core matrix utilities; and (3) a standard file format for matrices. There are a great many finite element programs today (Ref. 1) and they seemingly all use a different syntax. Ideally the structural analyst would like to model his structure independently of the program selected for analysis just as one codes in FORTRAN independently (more or less) of the machine selected for processing. Although this goal remains unrealized, NASTRAN's Bulk Data syntax has proved durable in a dynamic growth period and is probably the most widely used data modeling system in structural mechanics today. Also the NASTRAN matrix utilities are evolving into a system that can serve as a standard both for operations and inter-program communication. For these reasons, as well as for economy, NASTRAN's Bulk Data syntax and matrix utilities were used in the development of PATCHES-III.

The first major integration step involved solving several interface problems between the Linkage Editor and the PATCHES-III program library. It was then necessary to create a NASTRAN environment in which the general input output system (GINO) could operate in support of the matrix utilities. This system functions in parallel with a random access utility system (RASTUS) in PATCHES-III. Installation of a NASTRAN module, such as XSCEI or RBMG2, then consists primarily of matrix file management. Matrix files including USET, the basic partitioning vector in NASTRAN, are constructed by various routines in the host program, PATCHES-III. The detailed link structure of a modified version of RBMG2 will be presented as an illustration of a major NASTRAN matrix module adapted for use in another finite element program.

There are important differences between PATCHES-III, a parametric cubic modeling system, and NASTRAN. The grid point modeling available in NASTRAN requires voluminous input for two-dimensional structures and truly staggering input for solid three-dimensional structures. To minimize this problem, PATCHES-III constructs finite line, surface and volume models using operations which can reference data to be created by other operations (construction-in-context); then a queuing algorithm orders the operations for serial processing. In the case of one interlaminar stress analysis, input data requirements were reduced from 2750 NASTRAN Bulk Data cards (Ref. 2) to only 46 PATCHES-III Bulk Data cards (Ref. 3). There are also differences in the approach to spill during decomposition and the checkpoint/restart strategy that will be discussed. The final difference to receive attention is the way in which the two programs interface with post-processor programs. This issue is particularly important for graphic output and data editing.

NASTRAN USAGE IN CODE DEVELOPMENT

Early in the design phase of PATCHES-III it became obvious that we could not afford the luxury of reinventing the wheel. Numerous programs had solved in numerous ways many of the basic matrix processing functions that would be needed in the timely construction of this major new software system. However, the NASTRAN modules under consideration were shown to rely heavily upon the NASTRAN environment, in particular GINO and the open core concept as well as an intrinsic dependence upon the linkage editor. In addition, NASTRAN on the CDC system utilized a non-standard RUN compiler and timing considerations had already indicated the necessity for certain of the inner loop routines to be compiled with full optimization under the FTN compiler. Thus in order to use the NASTRAN utilities, it was necessary to simulate an environment within PATCHES-III in which an FTN NASTRAN system could be adapted.

The first major step in the incorporation of NASTRAN modules into PATCHES-III was made through the acquisition of an FTN NASTRAN Linkage Editor (Ref. 4) as well as an FTN version of NASTRAN level 15.1 from the Naval Ship Research and Development Center (NSRDC). Certain difficulties arose in the use of the linkage editor. In the first attempt, the LINKLIB file, from which externals are satisfied, contained relocatables from NSRDC as well as from our own site. Such a hybrid system must be avoided as system and site idiosyncracies can conflict. As long as the LINKLIB file is self-consistent, the resultant system will operate identically at all facilities with no changes required. A second problem with the use of the linkage editor arose from a small set of PATCHES-III routines written in CDC machine language, COMPASS. The loader places a word of traceback information in the word prior to the primary entry point of the routine. However, certain of the COMPASS routines in the PATCHES-III library had their primary entry point at other than the first word of the routine which would result in execution of the traceback word in some circumstances yielding obviously unpredictable results. When this and other operational problems were circumvented (Ref. 5), a fundamental drawback of the linkage editor became evident; it was designed for a large and relatively stable system - NASTRAN, and not for a program in its development cycle, subject to almost daily modifications. For example, if a referenced routine is not explicitly positioned, it will "float" to the highest segment in the link rather than being positioned in the segment from which it was referenced. The impact of this problem was diminished by breaking the system into a structure consisting of a resident link 0 and 18 subordinate parallel links, Figure 1, thereby also minimizing the restriction that a routine can exist at only one location within a link. Another difficulty is that any references to such unpositioned routines are satisfied only from the LINKLIB file therefore requiring concatenation of all program libraries onto LINKLIB. The linkage editor also contains little diagnostic capability.

A job procedure library, essentially a set of control card subroutines, was created to minimize the potential for error in the development cycle. One of these procedures, for example, effects a modification to the source code and to the program structure and also handles all file management associated with the creation of the new system. This procedure, diagramed in Figure 2, requires three input card files: the UPDATE modifications to the PATCHES-III source, the UPDATE modifications to the linkage editor directives and an input Case Control/Bulk Data deck to test the system. Typically, the linkage structure of the system remains unchanged and only the code in a few links is modified. For example, assume that subroutines referenced in links 1 and 17 are to be modified. Having placed the linkage editor directives for each link in a separate *DECK, it is possible in this instance to generate the input to the linkage editor with only one card:

```
*COMPILE LINKM, LINK1, LINK17, END
```

where deck LINKM contains the directives to modify an existing executable file and deck END contains the ENDLINKS directive. In our example then the following steps would be performed:

- (1) UPDATE the PATCHES-III source and send the modified routines to the FTN compiler
- (2) Augment/modify the previous version of the PATCHES-III relocatables per the updates
- (3) Create the new LINKLIB file
- (4) UPDATE the linkage directives
- (5) Execute the linkage editor using directives created in step 4, and create the new executable file
- (6) Execute the PATCHES-III system as created

Armed with a functioning linkage editor, we could then begin the process of adding selected portions of NASTRAN to the new system. The devices used to solve these problems may not always have been the most efficient or general, but they satisfied our needs given the time constraints. First it was necessary to add the basic NASTRAN utilities and resident common blocks to link 0 through the use of linkage editor directives. Figure 3, from Ref. 4, diagrams the current configuration of the merged PATCHES-III/NASTRAN link 0. Block data routines TIME and GINO66 should also be loaded.

To follow the flow of a typical execution will serve to illustrate the necessary steps in a combined PATCHES-III/NASTRAN run. Table 1 gives a brief description of each of the links diagramed in Figure 1. Figures 4, 5, and 6 describe the basic flow of a PATCHES-III execution. In links BEGIN and INITNS, the program initializes the NASTRAN subsystem. Toward this end, a call is made to BTSTRP which determines the machine type and sets machine dependent constants. Then the time-to-go clock is initialized via a CALL KLOCK (TBEGIN) where TBEGIN is located in common block/SYSTEM/. A call to GNFIAT is made to determine the number of logical files available and to place an entry for each in the file entry table XFIA T. A call to GNFIST then sets up proper linkage between data blocks and the files upon which they reside. This call to GNFIST should be followed by an OPEN and CLOSE operation on file NPTP setting a necessary first pass flag. Room must be allocated for the NASTRAN system working storage beyond the open core region and this is accomplished by decrementing word 76_g of core by 4000_p in a small COMPASS routine CORE76, called from the initialization link. It is this word which is queried on each call to CORESZ, the open core utility, and this action then prevents any utility from referencing the NASTRAN system region. The PATCHES-III executive modifies the field length of the program as necessary prior to the execution of each link. Therefore, the CORE76 routine must be utilized to modify word 76_g on each change of field length. At the same time, the NASTRAN system region must be translated to its new location below open core. As NASTRAN modules utilizing the time-to-go feature are employed, a TIME Case Control card should be processed setting the first word of common block STIME to TBEGIN + 60 times the time estimate in minutes.

At this point, we are able to reference any of the NASTRAN utilities including GINO. The above steps have created entries in the FIA T and FIST tables such that references may be made to any GINO file numbered 201 through 216 and 301. References to other file numbers should not be made. For example, a reference to file number 301 + i results in an actual reference to file 200 + i. As this was an adequate number of GINO files for our application, we did not use pooling and unpooling of files. Whenever a file is no longer necessary, it is made available for use by a new module simply through a close with rewind request. Since the communication to most NASTRAN utilities references the CINO file number through either calling parameters or common blocks, in most cases only the driving routine needs consider the bookkeeping problem and the NASTRAN routines can usually remain unmodified.

Many of the NASTRAN modules require some additional information in the form of the USET table and trailer. The major constituents of this file are mask words - one per degree of freedom of the problem indicating the types of constraints associated with each degree of freedom. The USET trailer contains in location three the number of degrees of freedom and in location five the logical OR of all the mask words in the table. The entire file can be constructed in approximately a dozen lines of FORTRAN, primarily through calls to GINO utilities.

The above operations have succeeded in creating an environment suitable for many NASTRAN utilities. All that remains is to establish the proper interface to drive them. A number of the modules in the PATCHES-III system such as the input processor, model generation and data verification links consist almost exclusively of PATCHES-III routines, Figure 7 (Ref. 6). Certain other links consist primarily of NASTRAN routines, for example XSCE1 the single point constraint eliminator, and SSG the static solution generator. The other links are a marriage of both systems and as an example, consider the matrix decomposition link, RBMG2D, shown schematically in Figure 8. The driver routine determines if a checkpoint or restart is requested and calls the PATCHES-III controller CKPTL or RESTL as appropriate. These routines then write or read the necessary files on the restart tape through the use of the NASTRAN utilities OUTPT1 or INPTT1. Matrix decomposition is performed, when required, under the supervision of RBMG2D through a call to the NASTRAN driver FACTOR which in turn calls RSPSPC, a slightly modified version of NASTRAN's RSPSDC. There are certain steps which, in general, must be performed to create a NASTRAN environment for a module such as RBMG2:

- (1) The driver routine must allocate storage for the appropriate COMMON blocks used to communicate file numbers and header records within the module.
- (2) The input, output, and scratch GINO file numbers should be placed in the appropriate common blocks or subroutine parameter lists consistent with their usage in other links.
- (3) The linkage editor must be used to position any necessary open core arrays to a REGION following the segment from which it is referenced.
- (4) Any files which are opened should be closed and rewound prior to exit from the link.

Experience has indicated that a typical major module such as the decomposition module requires approximately three weeks of iteration to install and debug. Adaptation of a smaller utility, such as INPTT1 and OUTPT1 requires substantially less time.

DIFFERENCES IN PHILOSOPHY

There are a number of significant differences in philosophy between PATCHES-III and NASTRAN that may be useful to consider for future versions of NASTRAN and other systems. Prior to illustrating these differences, an overview of the capabilities of PATCHES-III is appropriate. More detailed discussions can be found in References 3, 7, and 8. PATCHES-III determines the linear elastic response of a general heterogeneous anisotropic solid under thermal loads, mechanical loads and imposed displacements. The analysis model is based on a sixty-four point isoparametric solid discrete element with variable material properties. This element efficiently models the strain discontinuities at heterogeneous material boundaries as well as the continuous strains at homogeneous boundaries. The program constructs models for both geometry and physical data using parametric cubic interpolation over lines, surfaces and volumes. This system automates the construction of discrete element models and can reduce input data requirements by more than an order of magnitude. In this system, construction operations are available that reference data to be created by other operations (construction-in-context). Conceptually and in practice, this system is analogous to an interactive model generation system. Instead of sequentially processing requests from a terminal, all requests are made at once (batch mode via Bulk Data) and a queuing algorithm orders the requests for serial processing. This approach is also used to create models for physical data and imposed displacement constraints. Thus the same interpolation functions and most of the construction tools used to model the geometry are also available to model any physical data input to PATCHES-III. Both zero and non-zero constraint options are available that constrain the entire face of an element with a single bulk data card using either the reference frame or the local surface frame.

Consider the construction of a hyperpatch for one segment of a thick-walled circular cylinder. Two quite different but nearly equal constructions illustrate the procedure for a simple shape. In the first, Figure 9, grid points 1 and 3 are input and a straight line connecting them is created with a LINEPC Bulk Data card. This line is rotated about the e_3 axis through 90° to form one quadrant of a cylindrical surface using a PATCHR card. In this process grid points 7 and 5 are automatically created. The surface 1-3-7-5 is expanded a unit amount in the direction of its normal to create a hyperpatch using the HPN card. The grid points 2, 4, 6 and 8 are automatically created in this process along with the parameters defining the element or hyperpatch. The final figure is a 90° segment of a circular cylinder of unit thickness. The construction of this 192 parameter hyperpatch required five (5) cards of very simple format. Now consider the same construction problem but this time input grid points 1, 2, 3 and 4, Figure 10. A quadrilateral surface is created with a PATCHQ card and this surface is rotated about the e_3 axis through 90° to form the hyperpatch using the HPR card. The construction this time required six (6) bulk data cards. These examples illustrate the method, not the complexity of the geometric shapes that can be created (c.f. Ref. 7, page 2-22). In fact the geometry for all of the general elements in NASTRAN, including isoparametric elements, can be constructed using the modeling system in PATCHES-III.

Consider next a PATCHES-III analysis of an interlaminar normal stress problem. One of the few three-dimensional composite laminate problems for which corroborative solutions exist is a four ply graphite-epoxy plate under uniaxial load. A finite difference solution of the elasticity equations (Ref. 9), a stress-function discrete element solution of the elasticity equations (Ref. 10), an analytic solution of certain higher order laminated plate theory equations (Ref. 11) and the PATCHES-III displacement-function discrete element solution of the elasticity equations all agree well for the interlaminar normal stress. Stresses are computed for the $0^{\circ}/90^{\circ}/90^{\circ}/0^{\circ}$ laminate shown in Figure 11 under a uniform imposed displacement in the axial direction. Taking full advantage of symmetry, a simple four element PATCHES-III model was created from the forty-six bulk data cards shown in Figure 12. This is a substantial reduction from the 2750 Bulk Data cards necessary for a comparable solution using NASTRAN (Ref. 2) and the savings in the user's model definition and debugging cycle is of comparable magnitude. Figure 13, from the PATCHES-III plotting post-processor, shows a six element model of the interlaminar stress problem; an additional pair of elements has been used in the vicinity of the free edge to improve transverse shear stress accuracy. Lines in addition to the element boundaries are also drawn to show surface effects. Figure 14 shows the deformed geometry view of the model with hidden surfaces removed. The magnitude of the displacements has been magnified substantially to make the deformations visible. Figure 15 is a data surface plot; the lower surface represents the undeformed geometry along the laminate mid-plane; the upper surface represents the normal strains such that each point in the upper surface lies in the normal direction to the undeformed surface and at a distance proportional to the magnitude of the normal strain at that point plus an initial offset.

Although similar in many ways, there are some basic philosophical differences in the operation of the programs. A fundamental policy in PATCHES-III which is sometimes absent from NASTRAN concerns the diagnostic package. In PATCHES-III, an attempt is made to detect every error in model or data generation including Case Control-Bulk Data cross references prior to execution of any of the time consuming modules. Any diagnostic messages are explicit and informative and reference the card which precipitated the error condition. In concert with this philosophy, a "DRY" Case Control directive exists which indicates that this is to be a dry run of the data for the purpose of diagnosing any input errors. Another difference is that the field length used by PATCHES-III varies automatically during a run. This can result in a significant reduction in computing charges for larger analyses in a multiprocessing environment.

Although conditions may change with the release of Level 16, the current release of NASTRAN consumes large amounts of I/O time for a matrix decomposition operation that "spills." In PATCHES-III when the spill condition is detected, the program switches to a combination decomposition-conjugate gradient solution scheme which allows the user to buy as much accuracy as he requires up to and including complete convergence at a substantially reduced cost.

Bulk Data processing and model generation consume relatively little time in PATCHES-III when compared to generation of the element stiffness matrices or decomposition. Accordingly, the checkpoint/restart strategies employed by PATCHES-III differ from those of NASTRAN in that a checkpoint dictionary is not required. Rather, the Bulk Data deck is resubmitted on a restart run and the necessary tables and files are recreated. For design applications, the ELEMENT checkpoint is of use when a few elements are being modified. The LOADS checkpoint is utilized in analysis applications in which only the loads are changed.

A special output called the User Information Messages file is printed subsequent to all output from PATCHES-III. This listing details CP times and field lengths of each of the major modules encountered during execution. It also summarizes additional information concerning the dimension of certain matrices, the usage of random access storage, and other salient features of the execution.

A major departure from NASTRAN involves PATCHES-III's generation of a post-processing data file, PPDATA. This file uses a straightforward format written with unformatted binary FORTRAN write statements, and serves as an easy-to-use data base for post-processor programs. By no means a replacement for the OUTPT2 capability in NASTRAN, the PPDATA file does offer significant advantages: (1) it makes possible a wide range of DMAP independent post-processors; (2) it is far easier for the average structural analyst to use and adopt to his own requirements; (3) use of the post-processing scheme permits support of the blossoming array of hardware devices, in particular plotters, to be offloaded from the primary system; and (4) the post-processing environment is a necessity for experimental or special case analyses such as failure models which would be inappropriate to include in NASTRAN. In PATCHES-III the PPDATA tape contains $n+1$ files: one file containing the invariant data such as geometry, and n subcase files containing the load conditions and the results of the analysis.

PATCHES-III itself assists in the creation of post-processor programs by supplying a library of utilities which the post-processor may reference within the framework of a procedure library designed to aid in the construction of such systems. The most obvious and highly used post-processing system for PATCHES-III is the plot system. This program accepts free form inputs similar to Case Control cards to direct the plotting of the deformed or undeformed three dimensional elements. Surfaces may be subdivided to any requested extent and labeled contours of data surfaces may be requested on the data or geometry surfaces. Many options similar to those in NASTRAN for view, perspective and hidden line control are available.

CONCLUDING REMARKS

NASTRAN has shown itself to be a valuable resource in code development, both as a reference and a source of software. Once the steps have been identified, it is not difficult to implement any of the NASTRAN utilities in an existing or developing code. Since a major expense in code development is usually associated with the debugging and optimization phases, it is a tremendous asset to have NASTRAN as a source of efficient and effectively error-free software.

The NASTRAN Case Control-Bulk Data syntax was used to make a new finite element program, PATCHES-III, easier to learn for many users. More needs to be done to make structural modeling less dependent on the syntax of individual applications programs.

A number of major differences in the operations of PATCHES-III and NASTRAN have been noted. In particular, the construction-in-context of geometry and data models and the post-processor data file should be given serious consideration for inclusion in future versions of NASTRAN.

REFERENCES

1. **W. Pilkey, K. Saczalski, and H. Schaeffer, Structural Mechanics Computer Programs, University Press of Virginia (1974).**
2. **T. F. Neu, "Finite-Element Analysis of Edge Effects in Angle-Ply Composite Laminates," Naval Air Development Center Report No. NADC-74051-30, March 1974.**
3. **E. L. Stanton and L. M. Crain, "PATCHES-III User's Manual," McDonnell Douglas Astronautics Company, Report No. MDC G5538, November 1974.**
4. **Roger J. Martin, "A General Purpose Overlay Loader for CDC-6000 Series Computers; Modification of the NASTRAN Linkage Editor," Report 4062, Naval Ship Research and Development Center.**
5. **E. L. Stanton and L. M. Crain, "Three-Dimensional Parametric Discrete Element Program for the Analysis of Composite Structures," Progress Report Number 6, Contract Number N62269-73-C-0736, pp. 12-15, June 1974.**
6. **L. M. Crain, "PATCHES-III Program Structure and Subroutine Descriptions," McDonnell Douglas Automation Company, Report No. MDC G5795, April 1975.**
7. **E. L. Stanton, "A Three Dimensional Parametric Cubic Discrete Element Program for the Analysis of Composite Structures," McDonnell Douglas Astronautics Company, Report No. MDC G5716, January 1975.**
8. **E. L. Stanton, L. M. Crain, and T. F. Neu, "A Parametric Cubic Modeling System for General Solids of Composite Material." McDonnell Douglas Astronautics Company, Paper No. WD2606, July 1975.**
9. **R. Byron Pipes, "Solution of Certain Problems in the Theory of Elasticity for Laminated Anisotropic Systems," Ph. D. Dissertation, University of Texas (1972).**
10. **E. F. Rybicki, "Approximate Three-Dimensional Solutions for Symmetric Laminates Under Inplane Loading," Journal of Composite Materials, Vol. 5, 1971, pp. 354-360.**
11. **N. J. Pagano, "On the Calculation of Interlaminar Normal Stress in Composite Laminate," Journal of Composite Materials, Vol. 8, 1974, pp. 65-81.**

Table 1
PATCHES-III LINK DESCRIPTIONS

<u>LINK</u>	<u>NAME</u>	<u>FUNCTION</u>
0	MAIN	Executive control and common storage
1	BEGIN	Initialize PATCHES-III system
2	INPCN	Input control. Construct geometry and data models
3	GET	Initialize integration tables
4	MATCN	Material properties module
18	LOADS	Generate element load vectors
6	INTNS	Initialize NASTRAN sub-system
7	BIGMSH	Generate element meshpoint connectivity
8	IMDISP	Imposed displacement module
9	MPC	Multipoint constraints (not active)
5	*EKIJ	Generate element stiffness matrices
10	TTEKTD	Transform element matrices to analysis coordinates
12	SMA	Structural matrix assembler
13	XSCE1	Single point constraint eliminator
14	MCE1	Multipoint constraint eliminator (not active)
15	*RBMG2D	Matrix decomposition
16	SSG	Static solution generator
17	SDR	Stress recovery
11	SUBCØM	Subcase combinations

*Links that use majority of the CP time.

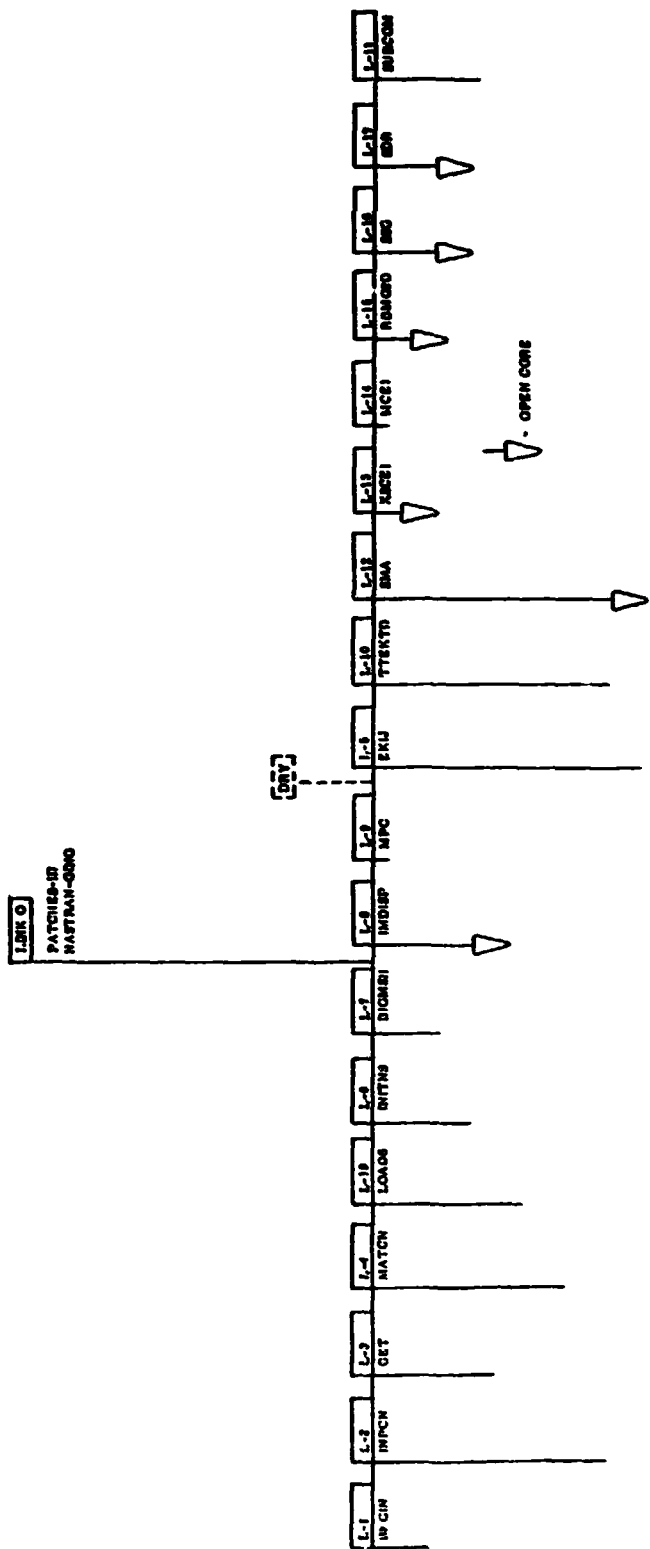


Figure 1: PATCHES-III/NASTRAN Schematic Load Map

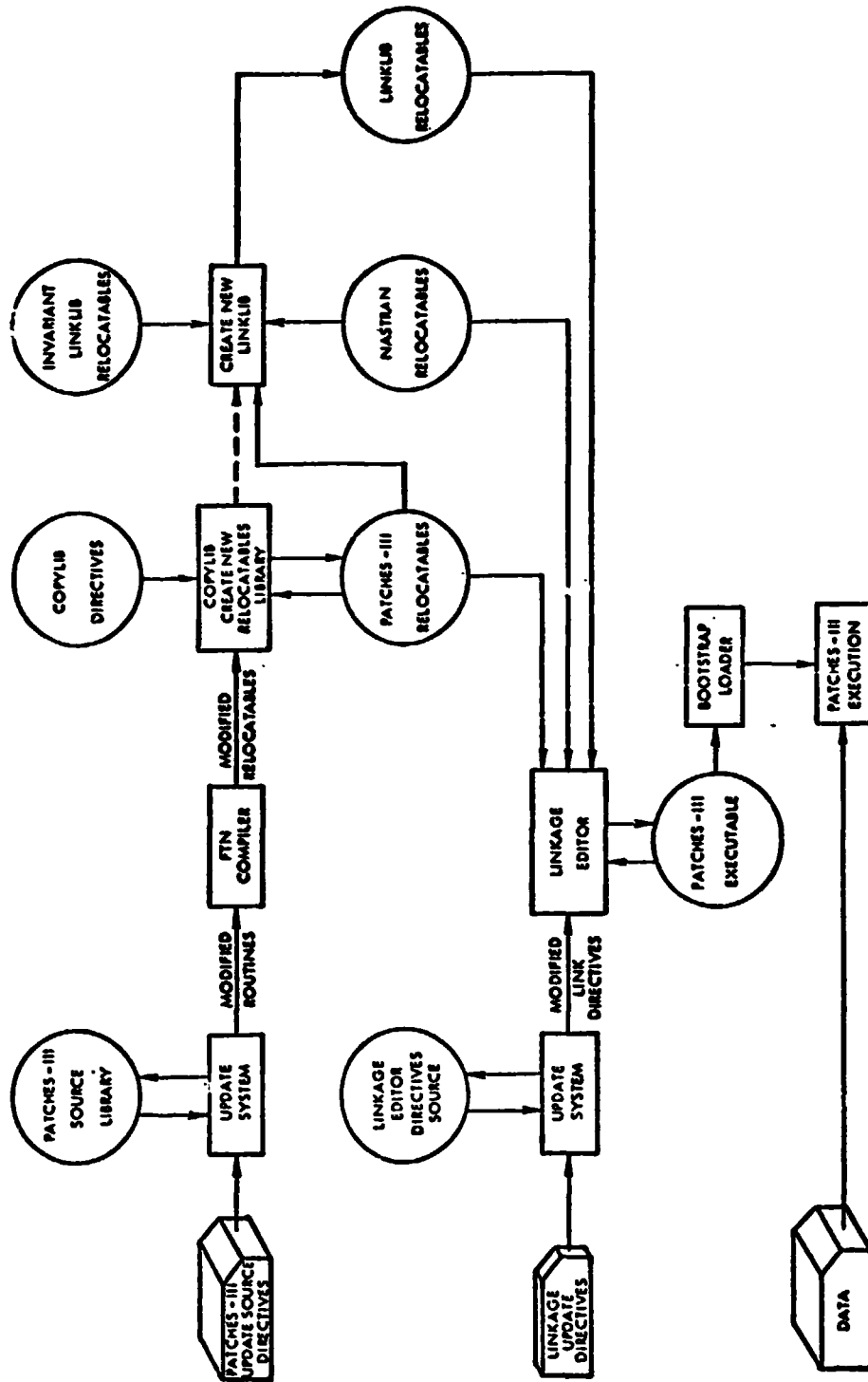


FIGURE 2. PROCEDURE TO MODIFY AND EXECUTE PATCHES-III

LINK 0 Structure

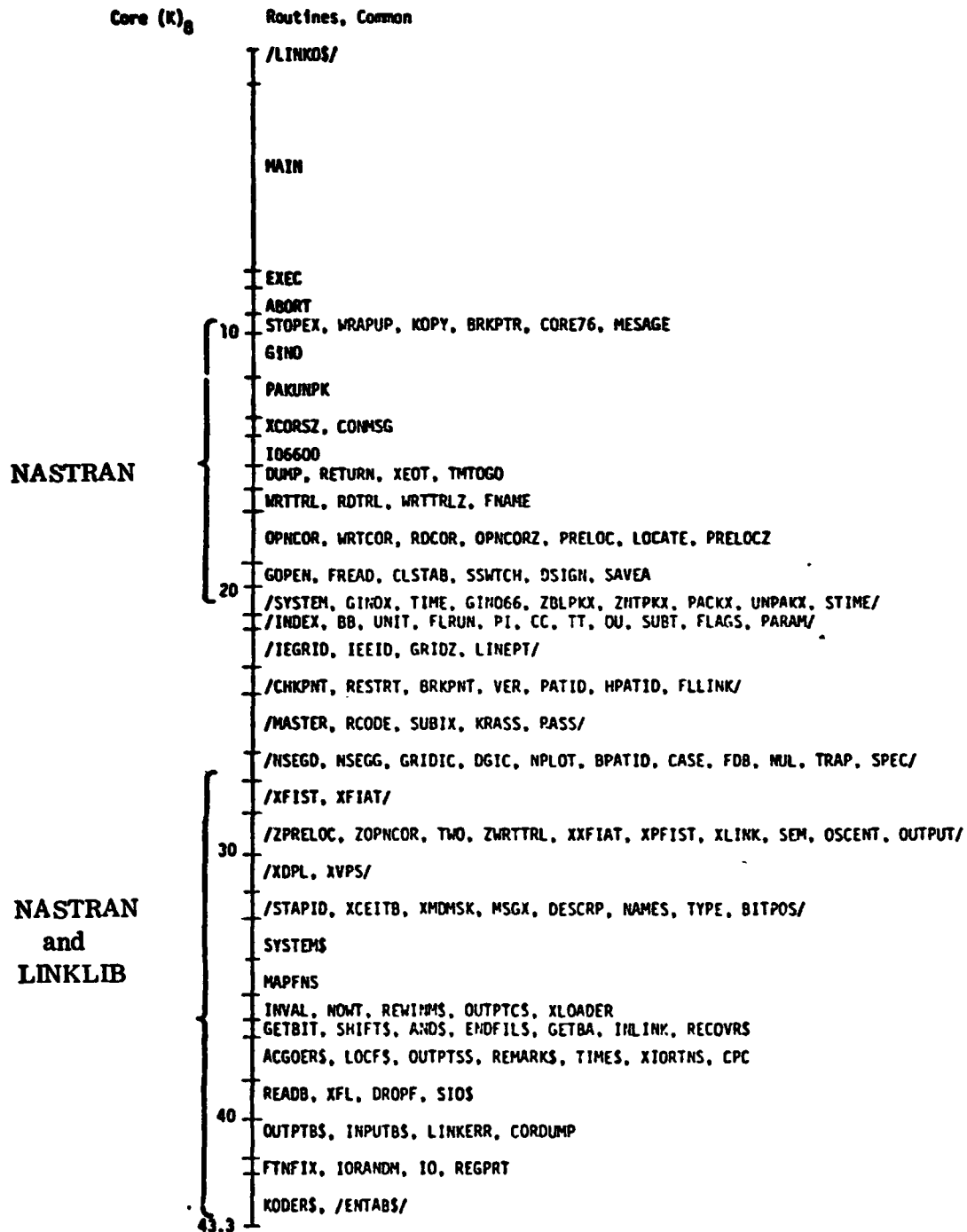


Figure 3: PATCHES-III Link 0 Structure

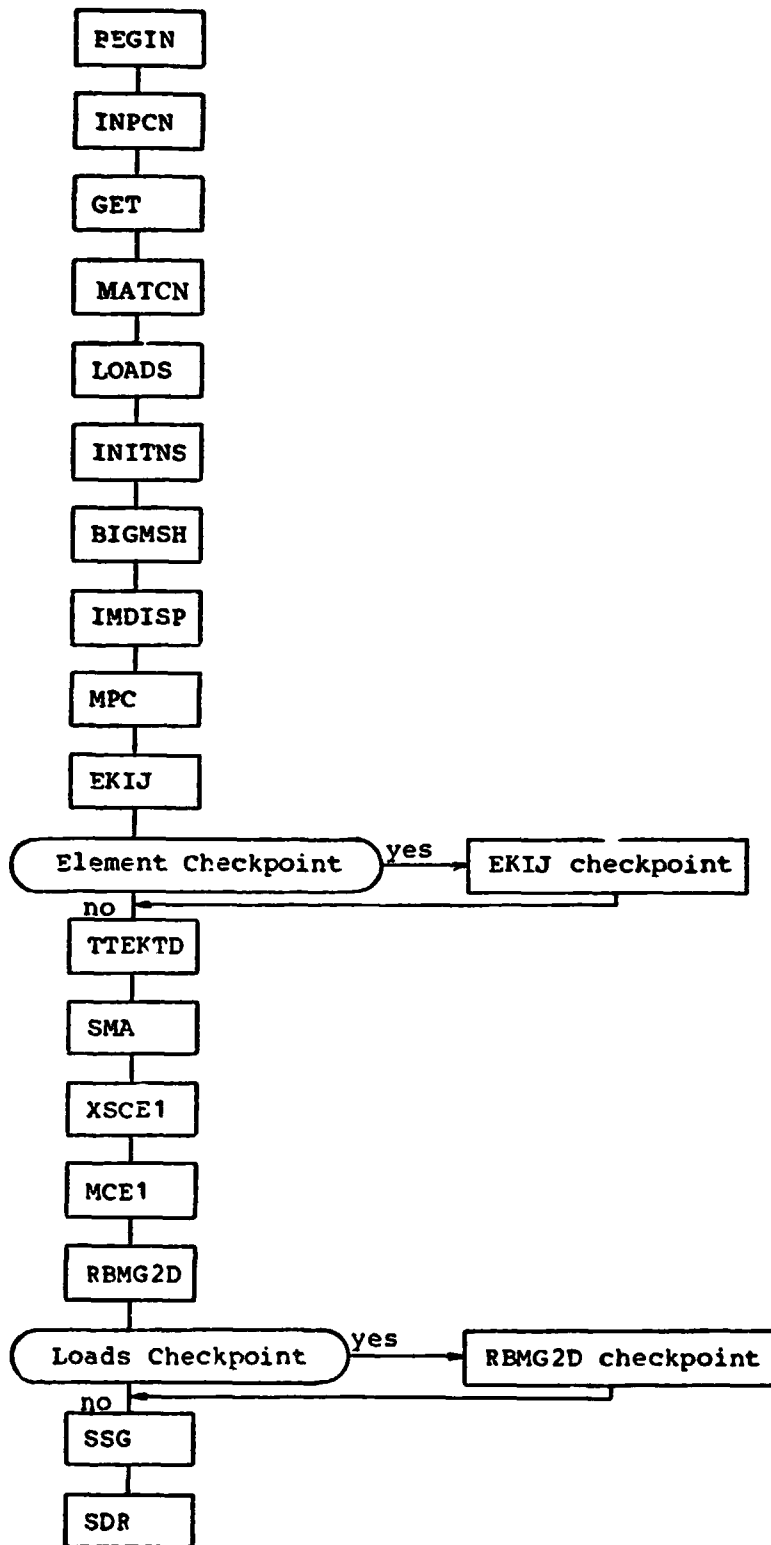


Figure 4: Basic PATCHES-III Flow

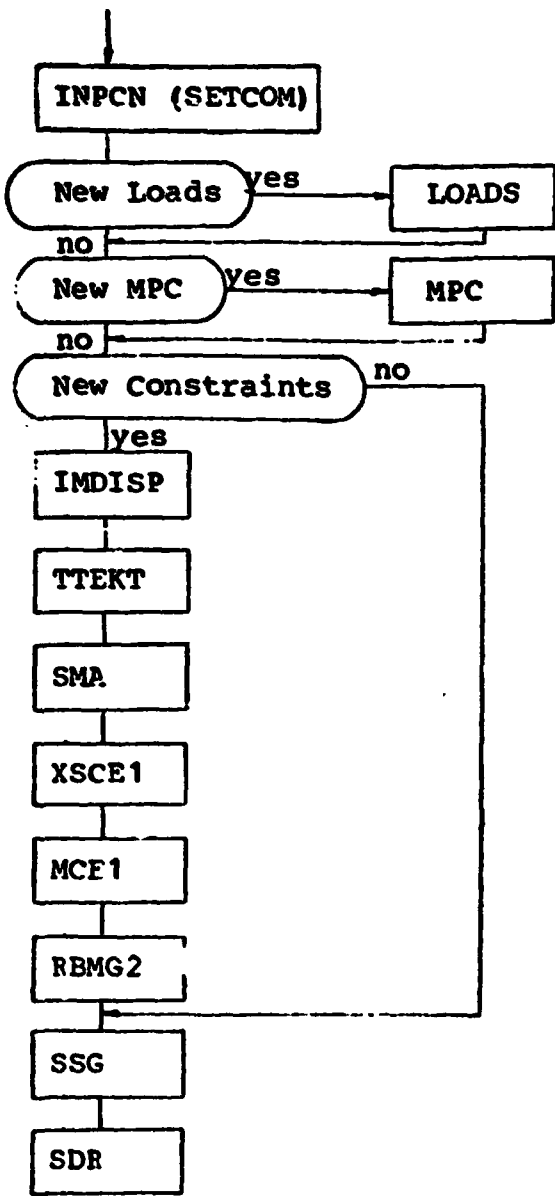


Figure 5: Additional Subcase Flow

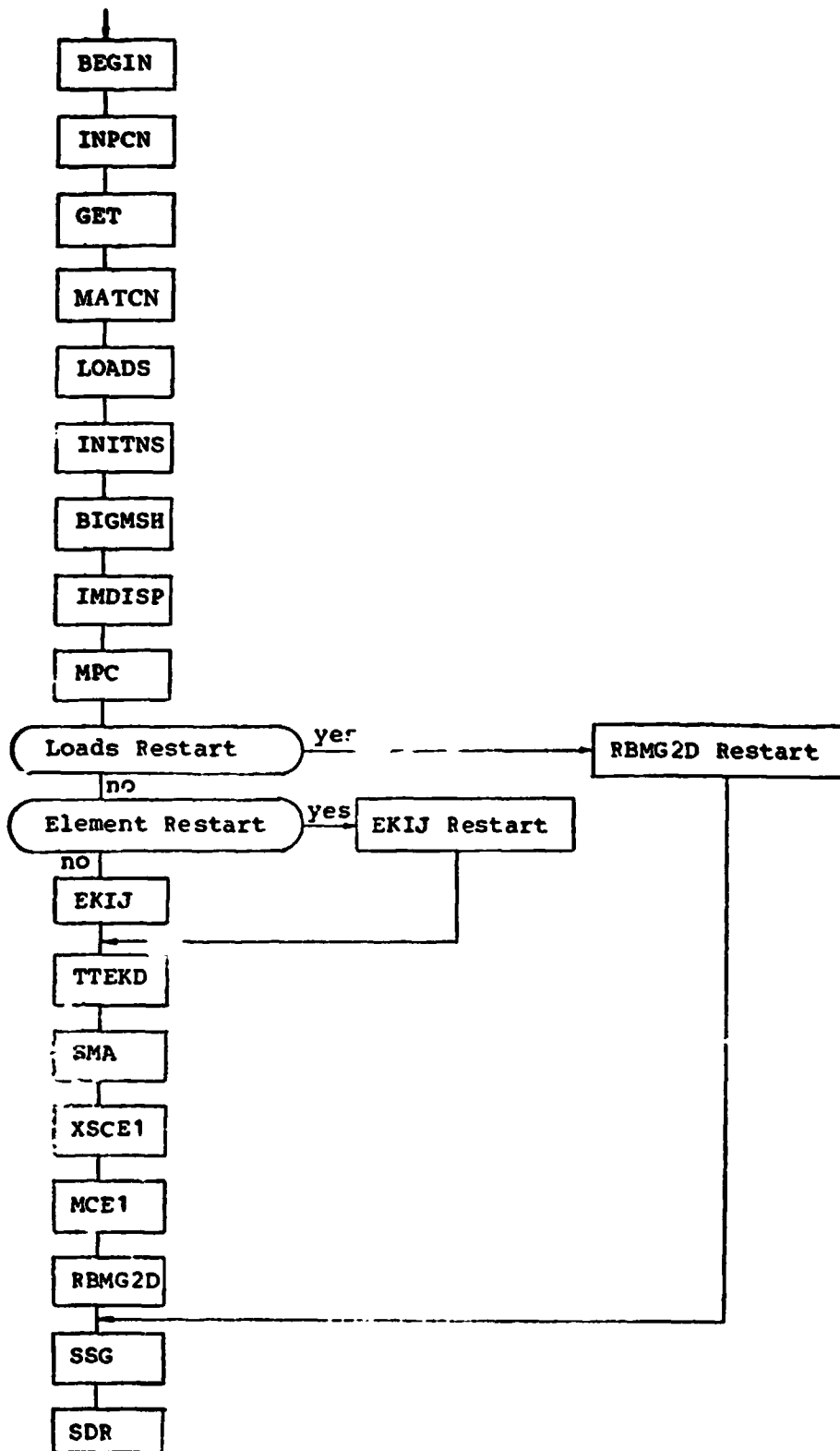


Figure 6: Restart Flow

LINK 2 Structure

43.3.R

INPCR

/CONA/

/FORCE/

60

INFO, TITLE0, ERFAG, UNPAK, DEBLK
 INPUTCS, ZEROUT, EDFILE, STOREE, SQRTS, PLACE, SINCSSE
 STOREP

SRCHO, MOVE, DETN, MCARD, POMP
 DROPF, WRITMSS, INITHSS, READMSS, ZHYP

ERAKERS

66K

CASEA
 ATTACH, PFNAME,
 ACTFDB, ZPACK
 RASTUS

BULK

CTYPE, BDCET, IRANGE
 RANGE, GRIDPT, FIFIT
 MULT, UNIQUE, SRCN, ALMOST

/BO/
 /LINEC/

/PAIRS/

CASEB

TITLE1

CASEC

CASEP

DATOUT

DETRU

HYBTP, LBTP, NISAIT
 HYPRNT, HYPRN1, PTPRNT, PTPPNI
 SCALER

SETCOM

76K

INIT	PGRID PNTX PPARAN	PHATC PPATL PPAT1	PCPDE3	PFORCE	LSORT PLARC PLINE PLINEB PLINEC LSPLN SEQENC LDIPC SEQDET LINE LARC1 NSU ARCPC1	PPATL PPATB PPATP PPATQ PSCALP PATSAV PATCXL	PHP2P PHPB PHP6P PHPL PHPHEX PHPR PHPR PSCLP HP2PAT NORMAL HYRFY CKHYP HYGRID BTNODE FOR4J ABCT GETGR NSR MIDNRH HP6PAT	PPPDE3	PCATAG	FILPC GAP STLINE PDLINP LPTB	PPATL PPATQ PPATP PPATX PPATA	PCMPL POPEQ	PDP2P	PPLOD3 PFORT	PSCC1	PCATLG DISCARD CATALOG DISFDB CATFDB
														PTDOP PFORL3 POMPS		

110K

THRU THROB SETLST FIELD	MENT MONTN PISHIT SCALP	ALLG EXCLUD SEARCH	PATCH1 SEPCE	PAKE1 CLRBIT SETBIT	SSGL SGRIDL SPLINE	PATCHR PATCPO SFFPEV TAPERP LINEPC	HP6P1 PATL4 FBFT JATEPG GGGT, HP2P1 PAIP, FLINE MYSORT, HYPTB	BLDFDB
----------------------------------	----------------------------------	--------------------------	-----------------	---------------------------	--------------------------	------------------------------------------------	---------------------------------------------------------------------------------	--------

Figure 7: PATCHES-III Link 2 Structure

LINK 15, STRUCTURE

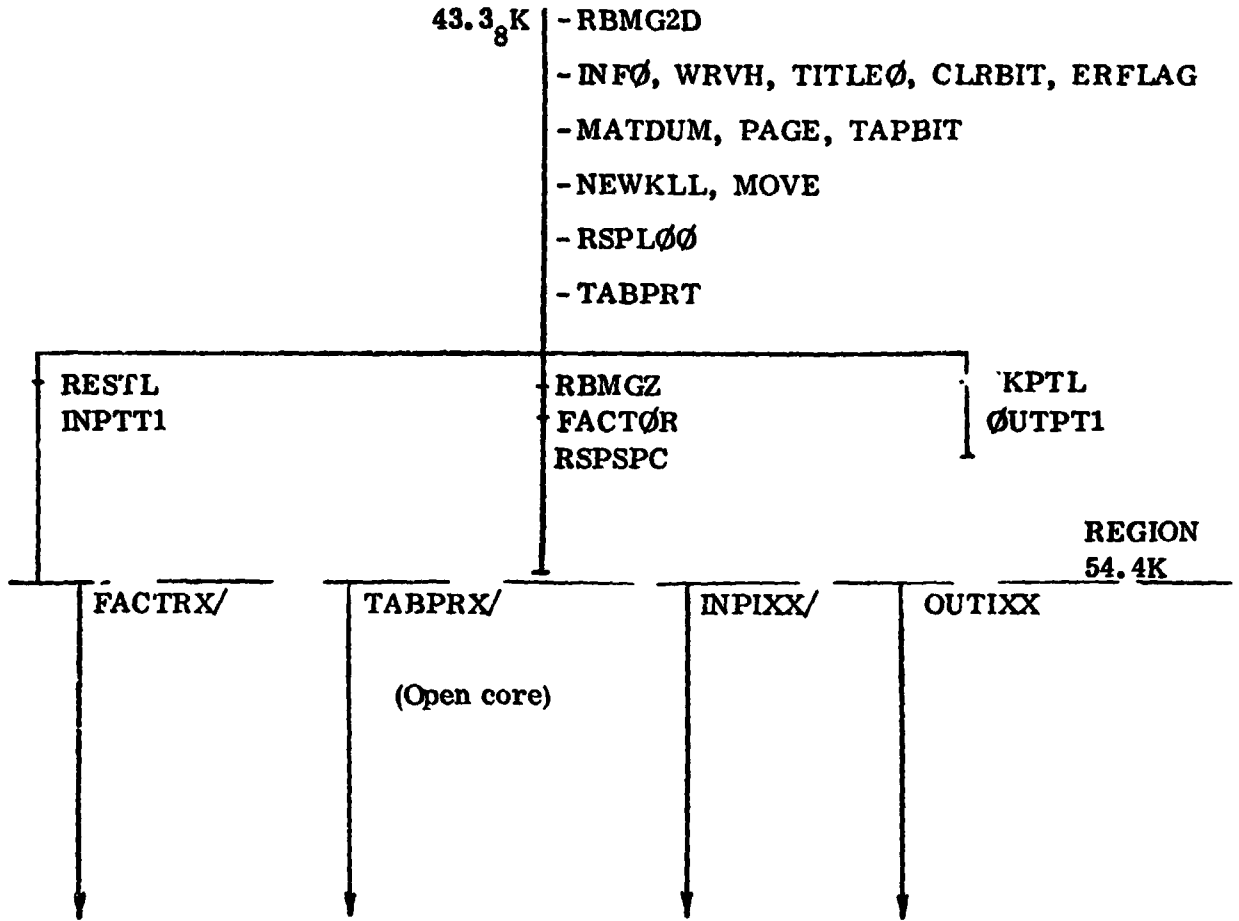
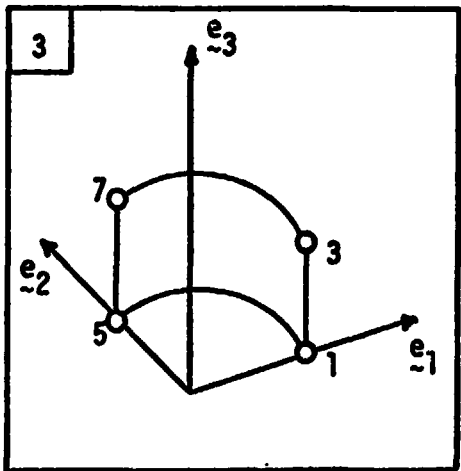
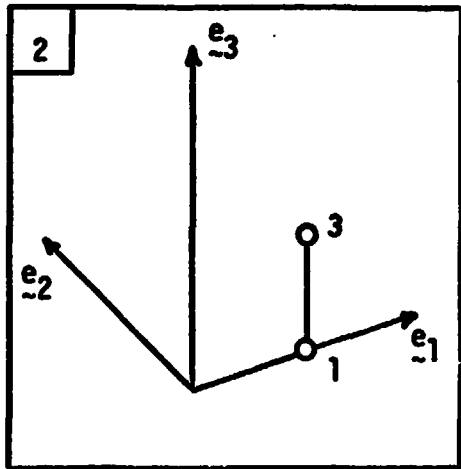
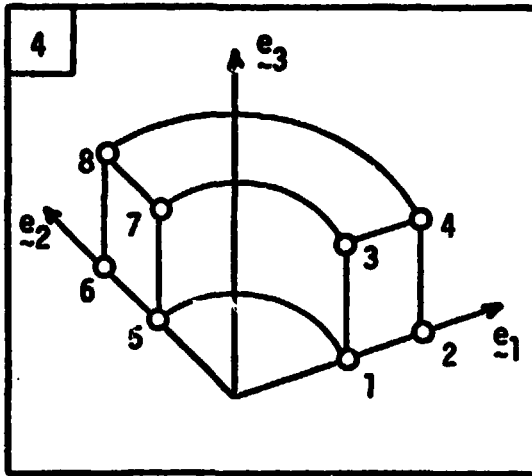
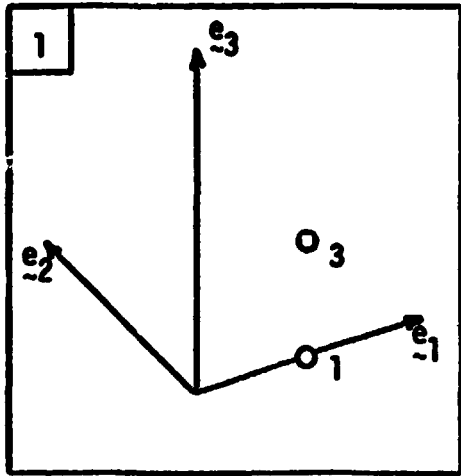
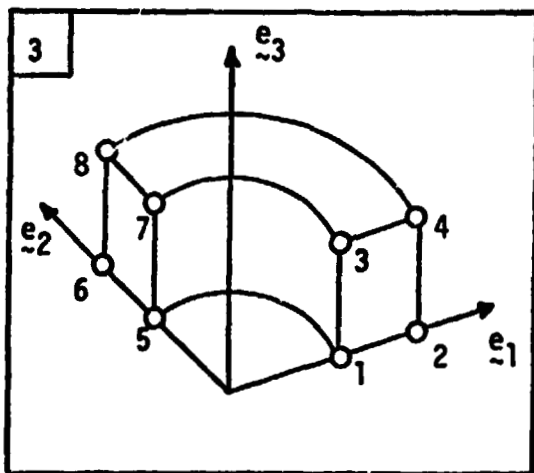
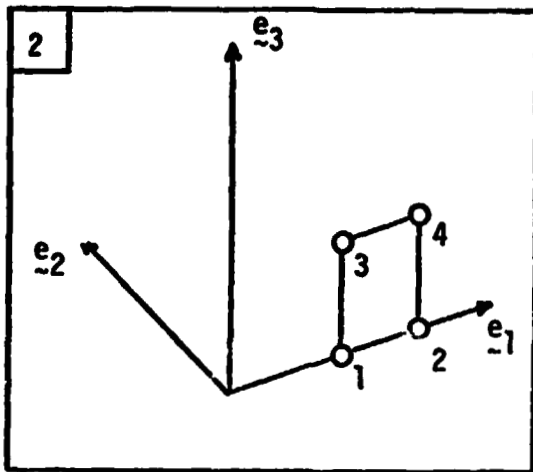
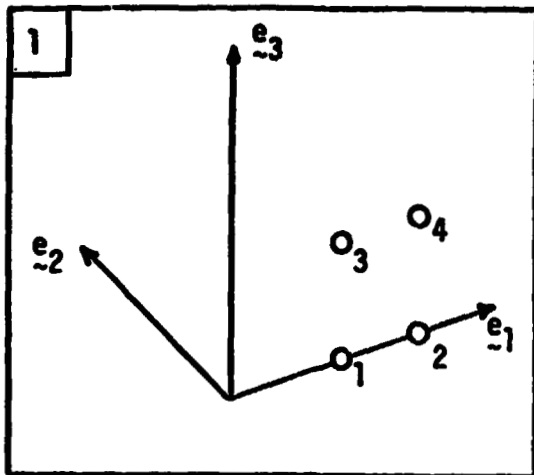


Figure 8: PATCHES-III Link 15 Structure



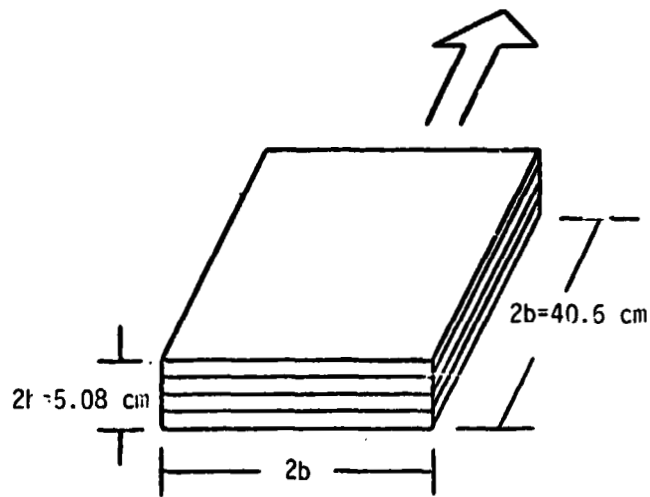
Step	Bulk Data Option	Cards
1	GRID	2
2	LINEPC	1
3	PATCHR	1
4	HPN	1

Figure 9: Hyperpatch Construction Example - Method One



Step	Bulk Data Option	Cards
1	GRID	4
2	PATCHQ	1
3	HPR	1

Figure 10: Hyperpatch Construction Example - Method Two



0°/90°/90°/0° Laminate

Elastic Stiffness of 0° Layers

$C_{11} = 139 \text{ GPa}$

$C_{22} = 15.7 \text{ GPa}$

$C_{12} = 3.9 \text{ GPa}$

$C_{23} = 3.3 \text{ GPa}$

$C_{44} = C_{55} = C_{66} = 5.9 \text{ GPa}$

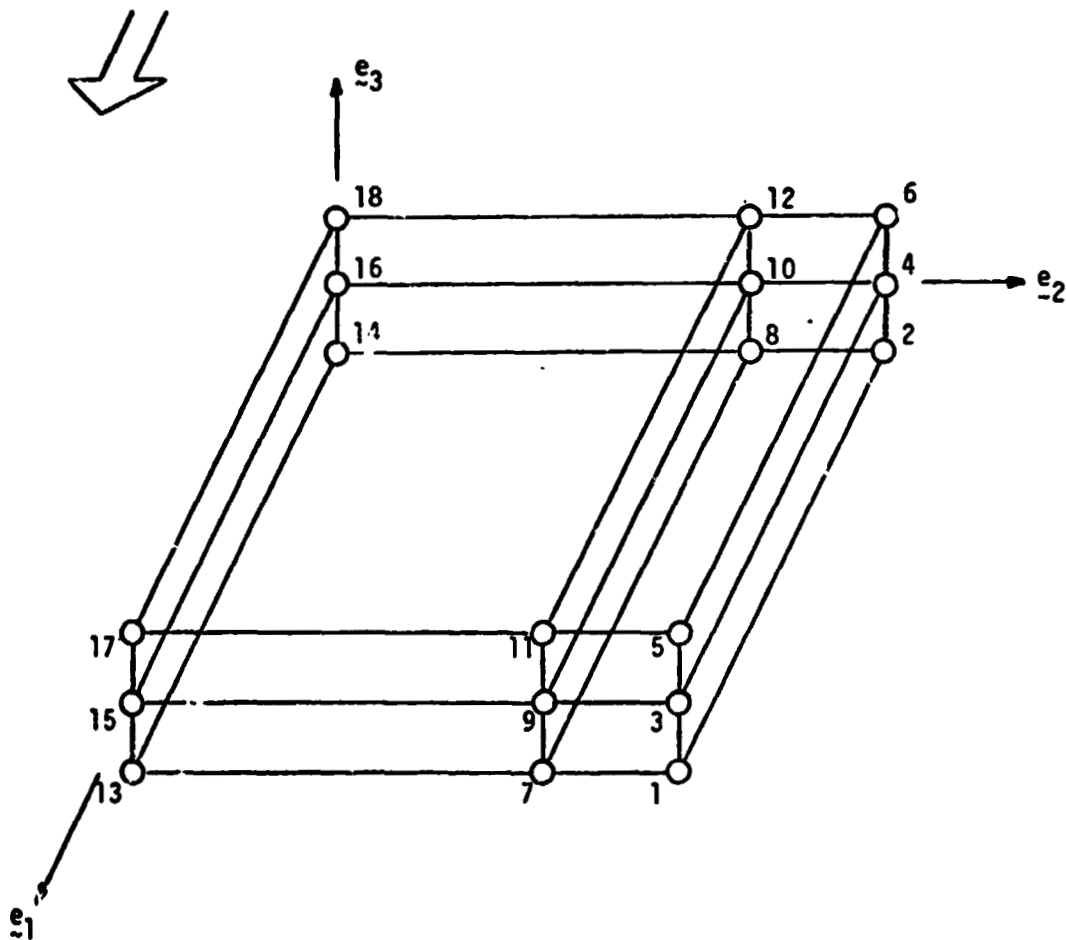


Figure 11: Four Element Model of a Graphite Epoxy Laminate

ORIGINAL PAGE IS
OF POOR QUALITY

BULK DATA CARDS

CARD FIELD-1, FIELD-2, FIELD-3, FIELD-4, FIELD-5, FIELD-6, FIELD-7, FIELD-8, FIELD-9, FIELD-10

CARD	FIELD-1	FIELD-2	FIELD-3	FIELD-4	FIELD-5	FIELD-6	FIELD-7	FIELD-8	FIELD-9	FIELD-10
1-	CPDE3	10	14	8	7	13				
2-	CP1	16	10	9	15					CP2
3-	CPDE3	20	A	2	1	7				CP2
4-	CP2	10	4	5	9					CP3
5-	CPDE3	30	16	14	9	15				CP4
6-	CP3	18	12	11	17					
7-	CPDE3	40	10	4	3	9				
8-	CP4	17	6	5	11					
9-	UATAG	1	1	0.01	3	0.01	5	0.01	5	0.01
10-	CP1	7	0.01	9	0.01	11	0.01	13	0.01	0.01
11-	CP2	15	0.01	17	0.01	19	0.01	21	0.01	0.01
12-	UPATO	10	1	13	15	9	7			
13-	UPATO	20	1	7	9	3	1			
14-	UPATO	30	1	15	17	11	9			
15-	UPATO	40	1	9	11	5	3			
16-	GRID	15	8	6	0	0				
17-	GRID	9	8	6	0	0				
18-	GRID	3	8	6	0	0				
19-	GRID	16	0	0	0	0				
20-	GRID	10	0	0	0	0				
21-	GRID	4	0	0	0	0				
22-	MPN	10	1	15						
23-	MPN	20	2	15						
24-	MPN	30	1	15						
25-	MPN	40	2	15						
26-	PPDE3	10	1		90					
27-	PPDE3	20	1		90					
28-	PPDE3	30	1							
29-	PPDE3	40	1							
30-	MATC	1	1	1	1	1				
31-	MTRX-1	20.2+6	0.56+6	0.50+6	2.21+6	0.48+6	2.21+6	0.89+6	0.0	0.0
32-	MP1	0.0	0.85+6	0.0	0.85+6					
33-	PATCHO	1	16	10	9	19				
34-	PATCHO	2	10	4	3	9				
35-	SDC10	10	10	1	14	16	10	0		
36-	SDC10	10	10	2	14	13	15	16		
37-	SDC10	10	10	3	14	8	7	15		
38-	SDC10	10	20	1	8	10	4	2		
39-	SDC10	10	20	3	8	2	1	2		
40-	SDC10	10	30	1	16	18	12	10		
41-	SDC10	10	30	2	16	15	17	18		
42-	SDC10	10	40	1	10	12	6	6		
43-	SNC1	10	10	10						
44-	SNC1	10	20	20						
45-	SNC1	10	30	30						
46-	SNC1	10	40	40						

Figure 12: Bulk Data for Laminate

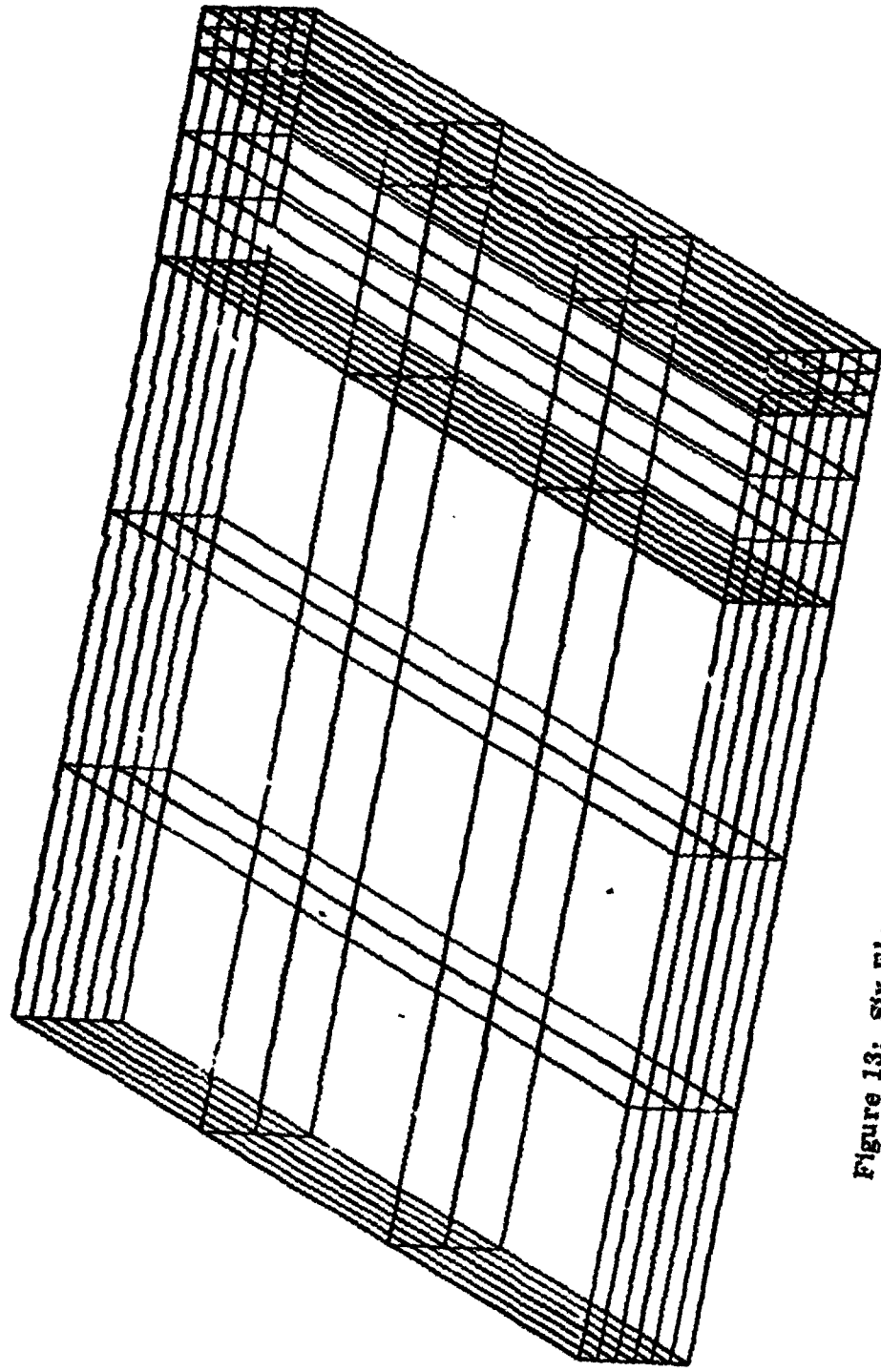


Figure 13: Six Element Model, Undeformed

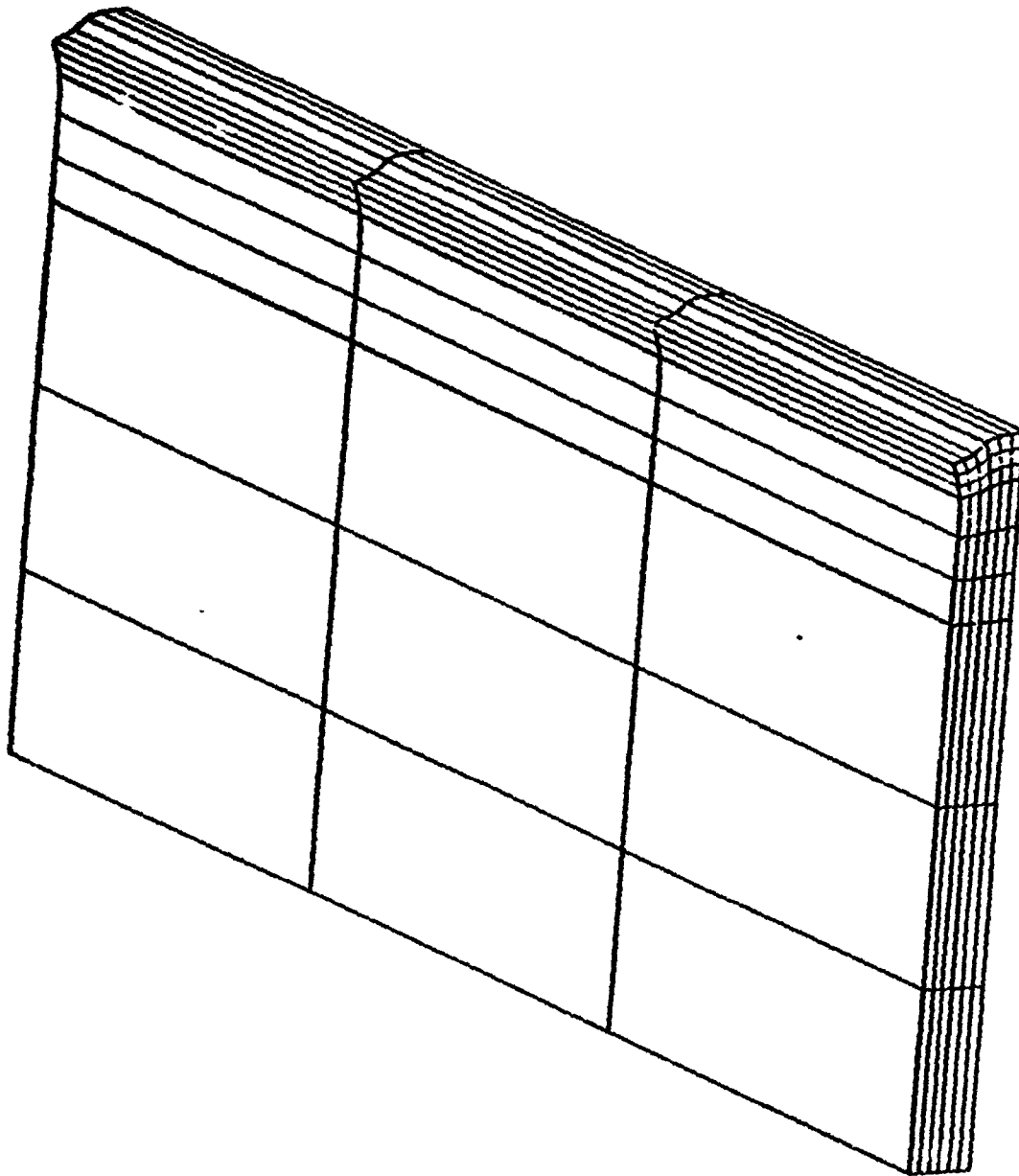


Figure 14: Six Element Model, Deformed

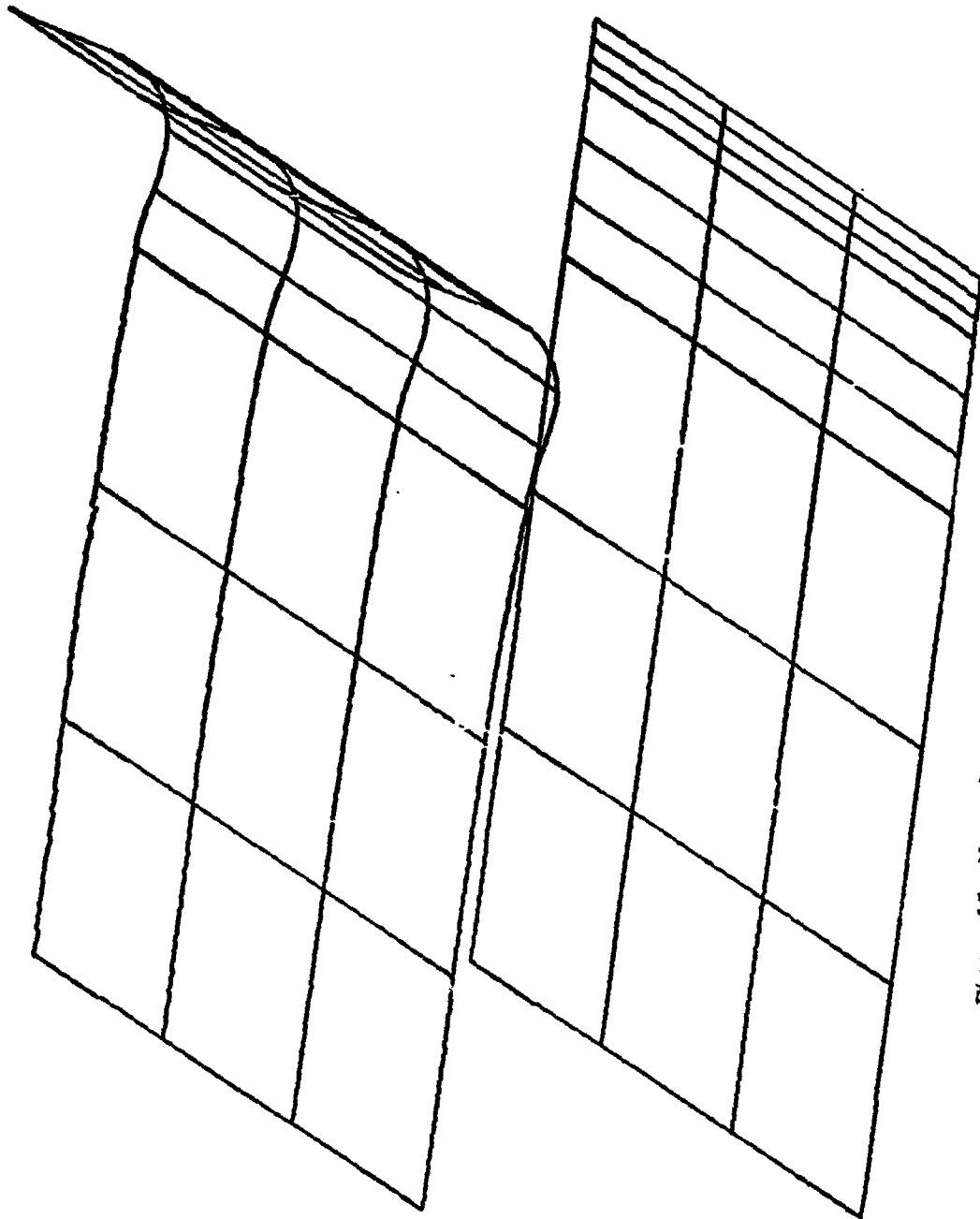


Figure 15: Normal Stress Data Surface

NASTRAN SOLUTIONS OF PROBLEMS

DESCRIBED BY

N75 31490

SIMULTANEOUS PARABOLIC DIFFERENTIAL EQUATIONS

J. B. Mason
NASA Goddard Space Flight Center

W. H. Walston, Jr.
University of Maryland

INTRODUCTION

NASTRAN solution techniques are shown for a numerical analysis of a class of coupled vector flow processes described by simultaneous parabolic differential equations. To define one physical problem type where equations of this form arise, the differential equations describing the coupled transfers of heat and mass in mechanical equilibrium with negligible mass average velocity are presented and discussed. Also shown are the equations describing seepage when both electrokinetic and hydrodynamic forces occur. Based on a variational statement of the general problem type, the concepts of scalar transfer elements and parallel element systems are introduced. It is shown that adoption of these concepts allows the direct use of NASTRAN's existing Laplace type elements for uncoupled flow (i.e., the heat transfer elements) for treating multi-component coupled transfer. Sample problems are included which demonstrate the application of these techniques for both steady-state and transient problems.

5

IRREVERSIBLE THERMODYNAMICS

Based on the linear phenomenological laws of irreversible thermodynamics and the general conservation laws, generalized flow equations describing the simultaneous transfer of vector processes may be developed. A brief development for coupled energy and mass flow is presented here and the reader is referred to the literature [references 1 to 8] for more details and applications.

Consider a motionless fluid, i.e., a fluid with zero or negligible mass average velocity, consisting of N chemical components K and contained in a mathematically well-defined geometric volume V which is separated from its surroundings by an equally well-defined boundary surface S . Within this system the coupled diffusion of matter and energy takes place. Assume that no chemical reactions are occurring and that the effects of external forces and viscous phenomena may be neglected. For this nondeforming system, therefore, the diffusion of momentum and its associated conservation law need not be directly considered. The conservation laws of mass and energy are applicable.

Adopting the repeated indices summation convention on i, j and designating rectangular Cartesian coordinates as x_i , the conservation of energy for the system under consideration can be written as

$$\rho C \frac{\partial T}{\partial t} = - \frac{\partial J_i^q}{\partial x_i} \quad (1)$$

and the conservation of mass as

$$\rho \frac{\partial C_K}{\partial t} = - \frac{\partial J_i^K}{\partial x_i} \quad (K = 1, 2, \dots, N) \quad (2)$$

where

- C = specific heat
- C_K = mass fraction of chemical component K ($C_K = \frac{\rho_K}{\rho}$)
- J_i^q = i^{th} spacial component of the heat flux vector with respect to the mass average velocity
- J_i^K = i^{th} spacial component of the diffusion flux vector of chemical component K with respect to the mass average velocity
- t = time
- T = absolute temperature
- ρ = total mass density
- ρ_K = mass density of chemical component K

The conservation equations (1) and (2) are of similar form and can be generalized to account for distributed external sources. Thus, a general conservation law for the M generalized fluxes γ can be written as

$$\rho C_\gamma \frac{\partial f_\gamma}{\partial t} = - \frac{\partial J_i^\gamma}{\partial x_i} + Q_\gamma \quad (\gamma = 1, 2, \dots, M) \quad (3)$$

where

- C_γ = specific mass capacity for flux γ
- J_i^γ = i^{th} spacial component of the γ^{th} generalized flux vector with respect to the mass average velocity
- f_γ = scalar thermodynamic potential corresponding to flux γ
- Q_γ = external source strength corresponding to flux γ

According to the linear laws of irreversible thermodynamics, the M generalized fluxes \vec{J}^Y result from the action of M generalized forces \vec{X}_ϵ ($\epsilon = 1, 2, \dots, M$) and are proportional to these forces. For general anisotropic coupled transfer, therefore, we may write

$$J_i^Y = - \sum_{\epsilon=1}^M L_{Yi}^{\epsilon j} \bar{X}_{\epsilon j} \quad (4)$$

where

$\bar{X}_{\epsilon j}$ = jth spacial component of the ϵ th generalized thermodynamic force

$L_{Yi}^{\epsilon j}$ = phenomenological coefficient expressing the effects of the jth component of the thermodynamic force \vec{X}_ϵ on the ith component of the flux \vec{J}^Y

In addition, it can be shown that the appropriate selection of fluxes and forces through examination of the local rate of entropy production leads to the important results:

$$L_{Yi}^{\epsilon j} = L_{\epsilon j}^{Yi} \quad (5)$$

$$\bar{X}_{\epsilon j} = \eta_\epsilon \frac{\partial f_\epsilon}{\partial x_j} \quad (6)$$

where

η_ϵ = proportionality factor depending on the choice of generalized thermodynamic fluxes and forces; η_ϵ is assumed constant for the range of operating conditions considered here.

That is, the phenomenological coefficient matrix is symmetric and the generalized thermodynamic forces are expressible as gradients of the scalar potentials. When written in the above form, the quantities are known as Onsager coefficients.

Combining equations (3), (4) and (6) results in a general set of simultaneous differential equations of the parabolic type describing the coupled irreversible transfer phenomena

$$\rho C_Y \frac{\partial f_Y}{\partial t} = \frac{\partial}{\partial x_i} \left[\sum_{\epsilon=1}^M L_{Yi}^{\epsilon j} n_{\epsilon} \frac{\partial f_{\epsilon}}{\partial x_j} \right] + Q_Y \quad (\gamma = 1, 2, \dots, M) \quad (7)$$

For the case of isotropic transfer equations (4) and (7) become, respectively

$$J_i^Y = - \sum_{\epsilon=1}^M L_Y^{\epsilon} \bar{X}_{\epsilon i} \quad (8)$$

$$\rho C_Y \frac{\partial f_Y}{\partial t} = \frac{\partial}{\partial x_i} \left[\sum_{\epsilon=1}^M L_Y^{\epsilon} n_{\epsilon} \frac{\partial f_{\epsilon}}{\partial x_i} \right] + Q_Y \quad (\gamma = 1, 2, \dots, M) \quad (9)$$

Equations (9) in their most simple form may be used to describe the steady-state diffusion of uncoupled heat or mass in an isotropic medium. In their most general form, equations (7) may be utilized to describe the transient diffusion of general anisotropic coupled flows such as multi-component mass and/or heat.

As examples of the above developments, consider first the one-dimensional ($i = j = 1$) coupled transfer of heat and mass. For this case,

$$\begin{aligned} J_1^1 &= -L_{11}^{11} \bar{X}_{11} - L_{11}^{21} \bar{X}_{21} \\ J_1^2 &= -L_{21}^{11} \bar{X}_{11} - L_{21}^{21} \bar{X}_{21} \end{aligned} \quad (10a)$$

where J_1^1 is the heat flux and J_1^2 the mass flux. The coupling term L_{11}^{21} expresses the effects of the concentration gradient on the heat flux while L_{21}^{11} establishes the effects of the temperature gradient on the mass flux. The Onsager coefficient L_{11}^{21} is proportional to the Soret coefficient and L_{21}^{11} to the Dufour coefficient. Recall that $L_{11}^{21} = L_{21}^{11}$.

The equations describing coupled electrokinetic and hydrodynamic flow in porous media offer a second example. In reference 9 a finite element approach is used to analyze the movement of fluid relative to a solid phase and the migration of ionized soil particles relative to a fluid phase, both occurring in an electric force field. For this case,

$$J_i^1 = - \sum_{\epsilon=1}^2 L_1^\epsilon \bar{X}_{\epsilon i} \quad (10b)$$

$$J_i^2 = - \sum_{\epsilon=1}^2 L_2^\epsilon \bar{X}_{\epsilon i}$$

where J_i^1 is the i^{th} component fluid discharge velocity and J_i^2 is the i^{th} component of the current density. The coefficient L_1^1 expresses the effects of hydrostatic potential gradients \bar{X}_{1i} on the discharge velocities while L_2^2 expresses the effects of voltage gradient \bar{X}_{2i} on the current. The L_1^2 and L_2^1 terms express the cross coupling between voltage gradient and fluid velocity and between potential gradient and electrical current, respectively.

VARIATIONAL FORMULATION

Equation (7) is a set of simultaneous parabolic differential equations describing the coupled transport processes in the continuum. While a Galerkin approach can be employed in a straightforward manner to evolve a finite element statement of the problem, the approach used here is based on a variational formulation similar to the principle of virtual work used in mechanics. Because of this similarity, it is designated as a principle of virtual generalized work and has the advantage that physical interpretation can be associated with its use.

Consider the motionless fluid within the well-defined boundary. For each flow quantity γ , the boundary of the volume V in which the M generalized fluxes are transferred may be considered as consisting of three regions S_1 , S_2 and S_3 as follows:

1. Over the boundary S_1 the flux \tilde{J}_1^γ is prescribed.
2. Over the boundary S_2 the generalized convective flux \tilde{J}_1^γ is proportional to the thermodynamic potential differences between the boundary values $(\eta_{\gamma}^f)_{S_2}$ and the known ambient values $(\eta_{\gamma}^f)_\infty$.

3. Over the boundary S_3 the thermodynamic potential $(\eta_Y f_Y)_{S_3}$ is prescribed.

Now allow a fictitious variational change $\eta_Y \delta f_Y$ which does not violate the constraints of the system; i.e., $\eta_Y \delta f_Y$ is zero over S_3 and arbitrary elsewhere. Also, the virtual changes are assumed to occur without the passage of time while the various fluxes remain constant.

For this volume consider the sum of the products of the generalized fluxes J_i^Y and the variations in their conjugate thermodynamic potentials $\eta_Y \delta f_Y$, that is, the virtual generalized work

$$\sum_{\gamma=1}^M J_i^Y (\eta_Y \delta f_Y) \quad (11)$$

Integration of equation (11) over the total boundary area S and application of Gauss' Theorem yields

$$\int_S \sum_{\gamma=1}^M (J_i^Y \eta_Y \delta f_Y) v_i dS = \int_V \sum_{\gamma=1}^M \frac{\partial J_i^Y}{\partial x_i} (\eta_Y \delta f_Y) dV + \int_V \sum_{\gamma=1}^M J_i^Y \frac{\partial (\eta_Y \delta f_Y)}{\partial x_i} dV \quad (12)$$

where $v_i = i^{\text{th}}$ component of the unit vector along the outer normal to S . Since the general conservation of the various transfer quantities must apply, equation (7) is substituted for the first integral on the right-hand side of equation (12), yielding

$$\begin{aligned} \int_V \sum_{\gamma=1}^M J_i^Y \eta_Y \frac{\partial (\delta f_Y)}{\partial x_i} dV + \int_V \sum_{\gamma=1}^M \left(Q_Y - \rho C_Y \frac{\partial f_Y}{\partial t} \right) \eta_Y \delta f_Y dV \\ + \int_{S_1} \sum_{\gamma=1}^M \bar{J}^Y (\eta_Y \delta f_Y) dS + \int_{S_2} \sum_{\gamma=1}^M \bar{\bar{J}}^Y (\eta_Y \delta f_Y) dS = 0 \quad (13) \end{aligned}$$

Note that the surface integral appearing in equation (13) extends only over that portion of the boundary for which δf_Y is not prescribed and that the scalar

boundary fluxes per unit surface area

$$\begin{aligned}\bar{J}^Y &= -\tilde{J}_1^Y v_1 \\ \bar{\bar{J}}^Y &= -\tilde{\tilde{J}}_1^Y v_1\end{aligned}\tag{14}$$

have been employed in writing this equation. In addition, it should be noted that the generalized convective flux can be expressed in terms of the thermodynamic potential differences in the form

$$\bar{\bar{J}}^Y = \sum_{\epsilon=1}^M h_{\epsilon}^Y [(\eta_{\epsilon}^f)_{\infty} - (\eta_{\epsilon}^f)_{S_2}]\tag{15}$$

where

h_{ϵ}^Y = proportionality factor expressing the contribution from the ϵ^{th} thermodynamic potential difference to the flux $\bar{\bar{J}}^Y$ at the boundary S_2

The characteristics of the variational statement (13) are such that its Euler equations and boundary conditions are those governing the case of coupled vector transfer considered here when the expressions (4) or (8) are employed. As such, it may be viewed as an alternate expression of the mathematical problem posed by equations (7) or (9) and the associated boundary conditions discussed above. These results indicate the similarities between the variational principle for the coupled irreversible processes and the principle of virtual work for mechanical systems. From this presentation the analogies between the variation in thermodynamic potentials (or state variables) and mechanical deformations, between surface flux and mechanical surface forces, and between thermodynamic sources/sinks and mechanical body forces are clearly indicated.

GENERAL FINITE ELEMENT FORMULATION

For irreversible coupled flows, the thermodynamic potentials at the grid points of the element are taken as the degrees of freedom. Element properties are determined using the principle of virtual generalized work together with functions expressing the state of the thermodynamic potentials within the element in terms of their grid point values. With this information the gradients of the potentials and alternately the various fluxes within the element may be uniquely defined in terms of the grid point values of the potentials. Assembly of the element equations to describe the complete system is accomplished with

the aid of the variational principle. This assembly is accomplished by requiring that the thermodynamic potentials be compatible between elements and that flow conservation apply at the grid points. In essence, only compatible states are considered and the true values of the potential are those for which flow conservation holds, a condition which is enforced by the principle of virtual generalized work.

Details of the general finite element formulation are presented in reference 8 and only the form of the resulting matrix equations of motion describing the coupled processes are presented here as follows:

$$[D]\left\{\frac{dP_{\alpha}}{dt}\right\} + ([K] + [K_C])\{P_{\alpha}\} = \{F_Q\} + \{F_B\} + \{F_C\} \quad (16)$$

where

- $\{P_{\alpha}\}$ = values of the thermodynamic potentials at the α grid points of the assembled model
- $[D]$ = generalized capacitance matrix for the assembled model
- $[K]$ = generalized conduction matrix for the assembled model
- $[K_C]$ = generalized boundary convection matrix for the assembled model
- $\{F_Q\}$ = generalized source vector for the assembled model
- $\{F_B\}$ = generalized boundary flux vector for the assembled model
- $\{F_C\}$ = generalized boundary convection vector for the assembled model

Note that $\{P_{\alpha}\}$ is a column vector of length equal to the number of grid points of the assembled model times the number of transport quantities (i.e., $\alpha \times M$).

NASTRAN SOLUTIONS

The previous developments are general in nature and can be applied for the finite element description of coupled anisotropic transfer in one, two and three dimensions. Once suitable interpolation functions have been chosen, the finite element matrices can be obtained and assembled to form the set of equations (16) describing the idealized system using well-known procedures (refs. 8 and 9). In what follows, the reader will be assumed familiar with these procedures and the discussion will center on special techniques which may be employed to permit the direct use of NASTRAN for the analysis of M coupled transfer processes.

One-Dimensional Element Formulation

A one-dimensional element suitable for use in the analysis of two coupled flows is presented below and shown to be equivalent to a combined system

of parallel one-dimensional Laplace elements, representing uncoupled transfer, connected by "molar transfer elements," representing coupling. With this information the extension to the case of M coupled flows is discussed.

Consider a one-dimensional finite element of constant cross-sectional area A connecting grid points ξ and θ on the r axis. Assume a linear variation in the two thermodynamic potential variables $p_1(x,t)$ and $p_2(x,t)$ along the axis of the element. Thus,

$$\begin{aligned} p_1 &= \eta_1 f_1 = \bar{a} + \bar{b}x \\ p_2 &= \eta_2 f_2 = \bar{c} + \bar{d}x \end{aligned} \quad (17)$$

where $\bar{a}(t)$, $\bar{b}(t)$, $\bar{c}(t)$ and $\bar{d}(t)$ are generalized coordinates which can be related to the four unknown grid point values of the thermodynamic potentials, i.e., p_1^ξ , p_1^θ , p_2^ξ , p_2^θ , using equation (17). Evaluating the generalized coordinates in terms of the grid point potential values results in the matrix equation

$$\begin{Bmatrix} p_1 \\ p_2 \end{Bmatrix} = \begin{bmatrix} 1 + \frac{x_\xi}{l} - \frac{x}{l} & \frac{x}{l} - \frac{x_\xi}{l} & 0 & 0 \\ 0 & 0 & 1 + \frac{x_\xi}{l} - \frac{x}{l} & \frac{x}{l} - \frac{x_\xi}{l} \end{bmatrix} \begin{Bmatrix} p_1^\xi \\ p_1^\theta \\ p_2^\xi \\ p_2^\theta \end{Bmatrix} \quad (18)$$

where

p_1^ξ = value of the thermodynamic potential p_1 at grid point ξ , etc.

l = length of element ($l = x_\theta - x_\xi$)

x_ξ, x_θ = coordinates of element end points

For two coupled flows, the Onsager coefficient matrix can be written as

$$\begin{bmatrix} L_{11} & L_{12} \\ L_{12} & L_{22} \end{bmatrix} \quad (19)$$

Using equations (18) and (19), a generalized conduction matrix for the element is found in reference 8 as

$$[K^e] = \frac{A}{l} \begin{bmatrix} L_{11} & -L_{11} & L_{12} & -L_{12} \\ -L_{11} & L_{11} & -L_{12} & L_{12} \\ L_{12} & -L_{12} & L_{22} & -L_{22} \\ -L_{12} & L_{12} & -L_{22} & L_{22} \end{bmatrix} \quad (20)$$

The one-dimensional element for the analysis of two coupled processes has two grid points and two degrees of freedom at each of these points. This representation results in the four by four element matrix (20) which may be partitioned into the form

$$[K^e] = \frac{A}{l} \left[\begin{array}{c|c} K_{11}^e & K_{12}^e \\ \hline K_{12}^e & K_{22}^e \end{array} \right] \quad (21)$$

with

$$[K_{11}^e] = \left[\begin{array}{c|c} L_{11} & -L_{11} \\ \hline -L_{11} & L_{11} \end{array} \right] \quad (22)$$

$$[K_{22}^e] = \left[\begin{array}{c|c} L_{22} & -L_{22} \\ \hline -L_{22} & L_{22} \end{array} \right] \quad (23)$$

$$[K_{12}^e] = \left[\begin{array}{c|c} L_{12} & -L_{12} \\ \hline -L_{12} & L_{12} \end{array} \right] \quad (24)$$

Examination of these indicates that $[K_{11}^e]$ represents the two by two element matrix describing the uncoupled transfer of J^1 through the thermodynamic potential gradient in $p_1 = \eta_1 f_1$. Similarly, $[K_{22}^e]$ is the two by two matrix describing the uncoupled transfer of J^2 through the gradient in $p_2 = \eta_2 f_2$ while $[K_{12}^e]$ is the two by two matrix representing coupling between the two processes. At this point, it is useful to introduce the concept of a "scalar transfer element" which may connect any two degrees of freedom and is defined by the two by two generalized conductivity matrix

$$[K_s] = \begin{matrix} \text{Scalar transfer element} \\ \text{conductivity matrix} \end{matrix} = k \begin{bmatrix} 1 & -1 \\ -1 & 1 \end{bmatrix} \quad (25)$$

where

k = conductivity of the scalar transfer element

With the above observations and use of the scalar transfer element concept, it can be shown that a "parallel element system" composed of two one-dimensional Laplace elements (i.e., NASTRAN ROD heat transfer elements) connected by four scalar transfer elements (i.e., SCALAR CONDUCTION elements), see Figure 1, can be utilized to represent the single coupled transfer element of equation (20).

This new model has four grid points with one degree of freedom at each point. Grid points ξ and θ are connected by ROD 1 of area A and length $l = x_\theta - x_\xi$. The degree of freedom at grid point ξ is p_1 and at grid point θ is p_2 . The element properties of ROD 1 are those of equation (22) and represent the uncoupled transfer of J^1 . ROD 2 is also of length l and area A (since the geometric location of ξ' is identical to ξ and θ' identical to θ) and represents the uncoupled transfer of J^2 between p_2 and p_1 at grid points ξ' and θ' as given by equation (23). The four scalar transfer elements represent the effects of coupling as described by equation (24). The conductivities of these are

$$\begin{aligned} k_1 &= \text{Generalized conductivity of SCALAR 1 transfer element} = \frac{A}{l} L_{12} \\ k_2 &= \text{Generalized conductivity of SCALAR 2 transfer element} = \frac{A}{l} L_{12} \end{aligned} \quad (26)$$

Several advantages are gained using this assembly. One advantage is that physical insight is gained into this complex transfer problem. Another is that existing Laplace finite elements, like those in NASTRAN for the analysis of uncoupled heat transfer processes, can be utilized for the parallel models of the primary flows and then interconnected by the scalar transfer elements. A

third advantage to be gained is that a simple and practical method to automate in the computer for treating an arbitrary number of M coupled processes is to model the primary uncoupled flows by M parallel systems using existing NASTRAN elements and to then automatically interconnect these with scalar transfer elements representing the coupling.

Two-Dimensional Element Formulation

The developments will now be extended to the case of coupled two-dimensional isotropic flow. The most general element for use in the investigation of two-dimensional flow is a triangle of thickness \bar{t} . Two coupled flows will be considered for a triangular element lying in the xy plane and defined by the three grid points (ξ, θ, ϕ) with six unknown degrees of freedom.

Proceeding as before, assume that the potentials $p_1(x, y, t)$ and $p_2(x, y, t)$ are distributed linearly within the element by the relations

$$\begin{aligned} p_1 &= \bar{a} + \bar{b}x + \bar{c}y \\ p_2 &= \bar{d} + \bar{e}x + \bar{f}y \end{aligned} \tag{28}$$

where $\bar{a}(t)$, $\bar{b}(t)$, . . . , $\bar{f}(t)$ are again generalized coordinates. Anticipating the results from the one-dimensional parallel element system, it is chosen here to express the Onsager coefficient matrix for two coupled isotropic flows as the sum of three matrices

$$[L^e] = [L_1^e] + [L_2^e] + [L_3^e] \tag{29}$$

where

$$[L_1^e] = \begin{bmatrix} L_{11} & 0 & 0 & 0 \\ 0 & L_{11} & 0 & 0 \\ 0 & 0 & 0 & 0 \\ 0 & 0 & 0 & 0 \end{bmatrix} \tag{30}$$

$$[L_2^e] = \begin{bmatrix} 0 & 0 & 0 & 0 \\ 0 & 0 & 0 & 0 \\ 0 & 0 & L_{22} & 0 \\ 0 & 0 & 0 & L_{22} \end{bmatrix} \quad (31)$$

$$[L_3^e] = \begin{bmatrix} 0 & 0 & L_{13} & 0 \\ 0 & 0 & 0 & L_{13} \\ L_{13} & 0 & 0 & 0 \\ 0 & L_{13} & 0 & 0 \end{bmatrix} \quad (32)$$

From the previous results and the form of equations (30) and (31), it is concluded that the uncoupled transfer of \vec{J}^1 and \vec{J}^2 may be included by two parallel Laplace triangular elements of a type available in NASTRAN. With this approach, only the $[L_3^e]$ contribution of equation (32) due to coupling need be presented here.

Using equations (28) and (32) and employing standard procedures lead to the element matrix $[K]_{\text{coupling}}$ representing between the parallel element system (see reference 8), thus

$$[K]_{\text{coupling}} = \frac{\bar{\epsilon}L_{13}}{4\Delta} \begin{bmatrix} 0 & 0 & 0 & K_{\xi\xi'} & K_{\xi\theta'} & K_{\xi\phi'} \\ 0 & 0 & 0 & K_{\xi\theta'} & K_{\theta\theta'} & K_{\theta\phi'} \\ 0 & 0 & 0 & K_{\xi\theta'} & K_{\theta\phi'} & K_{\phi\phi'} \\ K_{\xi\xi'} & K_{\xi\theta'} & K_{\xi\theta'} & 0 & 0 & 0 \\ K_{\xi\theta'} & K_{\theta\theta'} & K_{\theta\phi'} & 0 & 0 & 0 \\ K_{\xi\phi'} & K_{\theta\phi'} & K_{\phi\phi'} & 0 & 0 & 0 \end{bmatrix} \quad (33)$$

where

$$\begin{aligned} K_{\xi\xi'} &= b_\xi^2 + c_\xi^2, & K_{\theta\theta'} &= b_\theta^2 + c_\theta^2 \\ K_{\xi\theta'} &= b_\xi b_\theta + c_\xi c_\theta; & K_{\theta\phi'} &= b_\theta b_\phi + c_\theta c_\phi \\ K_{\xi\phi'} &= b_\xi b_\phi + c_\xi c_\phi; & K_{\phi\phi'} &= b_\phi^2 + c_\phi^2 \end{aligned}$$

and

$$a_{\xi} = x_{\phi}y_{\theta} - x_{\theta}y_{\phi}$$

$$b_{\xi} = y_{\phi} - y_{\theta}$$

$$c_{\xi} = x_{\theta} - x_{\phi}$$

(etc., in cyclic order
 ξ, θ, ϕ)

Δ = area of the triangular element
 x_{ξ}, y_{ξ} = coordinates of element corner points, etc.

With the above results a parallel element system composed of two NASTRAN heat transfer triangular elements and connected by scalar transfer elements can be constructed, see Figure 2. Grid points ξ, θ, ϕ are connected by TRIANGLE 1 of thickness \bar{t} and properties $[L_1^e]$ of equation (30). Grid points ξ', θ', ϕ' are connected by TRIANGLE 2 also of thickness \bar{t} but with properties $[L_2^e]$ of equation (31). The two triangular elements are connected by nine scalar transfer elements with properties $[K]_{\text{coupling}}^*$ obtained from equation (33). The extension to three-dimensional problems is not difficult since one need only utilize existing three-dimensional heat transfer elements in the program for the uncoupled parallel flows and utilize the variational principle and the scalar transfer elements to include the effects of thermodynamic coupling.

SAMPLE PROBLEMS

Two sample problems are presented to demonstrate aspects of the above developments. Parallel and scalar transfer elements are employed and solutions obtained using the NASTRAN program.

Problem 1 - One-Dimensional Steady-State Process, Three Coupled Flows

The one-dimensional transfer of $\vec{J}^1, \vec{J}^2,$ and \vec{J}^3 along the x axis of a continuum due to gradients in the potentials $p_1(x), p_2(x),$ and $p_3(x)$ is considered. Find the steady-state distributions in the potentials. The continuum is of length $L = 4.0$ and cross-sectional area $A = 1.0,$ and there is internal generation within the continuum given by

* $K_{\xi\xi'}$ is the generalized conductivity for the scalar transfer element connecting degree of freedom ξ with degree of freedom $\xi',$ etc.

$$\begin{aligned}
 Q_1(x) &= -(4.6 + 1.2x) \\
 Q_2(x) &= 24.4 - 1.8x \\
 Q_3(x) &= 1.0 - 12.0x
 \end{aligned}
 \tag{34}$$

The boundary conditions are specified as

$$\begin{aligned}
 p_1(0) &= 0.0 & p_1(4) &= 32.0 \\
 p_2(0) &= 0.0 & p_2(4) &= -48.0 \\
 p_3(0) &= 0.0 & p_3(4) &= 64.0
 \end{aligned}
 \tag{35}$$

and the Onsager relations have been determined as

$$\begin{pmatrix} J_x^1 \\ J_x^2 \\ J_x^3 \end{pmatrix} = - \begin{bmatrix} 1.0 & -0.1 & 0.2 \\ -0.1 & 4.0 & 0.3 \\ 0.2 & 0.3 & 2.0 \end{bmatrix} \begin{pmatrix} \partial p_1 / \partial x \\ \partial p_2 / \partial x \\ \partial p_3 / \partial x \end{pmatrix}
 \tag{36}$$

From equations (9), (34), and (36) the equations describing the process are found as

$$\begin{aligned}
 1.0 \frac{\partial^2 p_1}{\partial x^2} - 0.1 \frac{\partial^2 p_2}{\partial x^2} + 0.2 \frac{\partial^2 p_3}{\partial x^2} + [-4.6 - 1.2x] &= 0 \\
 -0.1 \frac{\partial^2 p_1}{\partial x^2} + 4.0 \frac{\partial^2 p_2}{\partial x^2} + 0.3 \frac{\partial^2 p_3}{\partial x^2} + [24.4 - 1.8x] &= 0 \\
 0.2 \frac{\partial^2 p_1}{\partial x^2} + 0.3 \frac{\partial^2 p_2}{\partial x^2} + 2.0 \frac{\partial^2 p_3}{\partial x^2} + [1.0 - 12.0x] &= 0
 \end{aligned}
 \tag{37}$$

The solution satisfying equations (37) and the boundary conditions is given by

$$p_1(x) = 2.0x^2 ; p_2(x) = -3.0x^2 ; p_3(x) = 1.0x^3
 \tag{38}$$

The finite element model is shown in Figure 3. Figure 3(a) shows the fifteen grid points connected by a total of twelve rod elements of length $l = 1.0$, i.e.,

three parallel systems each consisting of four unit-length rod elements and representing, respectively, the three primary flows \vec{J}^1 , \vec{J}^2 , and \vec{J}^3 . Figure 3(b) shows a typical parallel system connecting grid points 2, 2', and 2'' (i.e., location $x = 1.0$) and 3, 3', 3'' (i.e., location $x = 2.0$). The properties of the rod and scalar transfer elements for this system are found using our previous conclusions and are presented in Table 1.

The vector $\{F_Q\}$ representing the effects of distributed sources $Q_1(x)$, $Q_2(x)$, $Q_3(x)$ is obtained by simple lumping procedures and applied to the grid points as thermal loads. The boundary conditions (35) are satisfied by constraining the boundary point potentials to their appropriate values using single point constraints (SPC).

Table 2 presents a comparison between analytical results (AN.) from equation (38) and results from the finite element solution (F.E.).

Problem 2 - Two-Dimensional Transient Process, Two Coupled Flows

The two-dimensional coupled transport of the fluxes \vec{J}^1 and \vec{J}^2 in a square continuum of planform dimension 4.0 and thickness $\bar{t} = 2.0$ due to gradients in the potentials $p_1(x,y,t)$, $p_2(x,y,t)$ is considered. Find the transient distribution of the two potentials when there is internal generation within the continuum given by

$$\begin{aligned} Q_1(x,y,t) &= \left[\sin \frac{\pi x}{4} \sin \frac{\pi y}{4} \right] [t + t^2] \\ Q_2(x,y,t) &= - \left[\sin \frac{\pi x}{4} \sin \frac{\pi y}{4} \right] [t + 3t^2] \end{aligned} \quad (39)$$

The initial and boundary conditions are specified as

$$\begin{aligned} p_1(0,y,t) &= 0.0 & p_2(0,y,t) &= 0.0 \\ p_1(4,y,t) &= 0.0 & p_2(4,y,t) &= 0.0 \\ p_1(x,0,t) &= 0.0 & p_2(x,0,t) &= 0.0 \\ p_1(x,4,t) &= 0.0 & p_2(x,4,t) &= 0.0 \end{aligned} \quad (40)$$

The Onsager relations for the isotropic material have been determined as

$$\begin{Bmatrix} J_x^1 \\ J_y^1 \\ J_x^2 \\ J_y^2 \end{Bmatrix} = - \begin{bmatrix} 2.0 & 0.0 & 1.0 & 0.0 \\ 0.0 & 2.0 & 0.0 & 1.0 \\ 1.0 & 0.0 & 4.0 & 0.0 \\ 0.0 & 1.0 & 0.0 & 4.0 \end{bmatrix} \begin{Bmatrix} \partial p_1 / \partial x \\ \partial p_1 / \partial y \\ \partial p_2 / \partial x \\ \partial p_2 / \partial y \end{Bmatrix} \quad (41)$$

and the specific mass capacities as

$$\begin{aligned} \rho C_1 &= 0.61685 \\ \rho C_2 &= 0.61685 \end{aligned} \quad (42)$$

From equations (9), (39), (41), and (42), the equations describing the process are found as

$$\begin{aligned} 0.61685 \frac{\partial p_1}{\partial t} &= 2.0 \left[\frac{\partial^2 p_1}{\partial x^2} + \frac{\partial^2 p_1}{\partial y^2} \right] + 1.0 \left[\frac{\partial^2 p_2}{\partial x^2} + \frac{\partial^2 p_2}{\partial y^2} \right] + \left[\sin \frac{\pi x}{4} \sin \frac{\pi y}{4} \right] [t + t^2] \\ 0.61685 \frac{\partial p_2}{\partial t} &= 1.0 \left[\frac{\partial^2 p_1}{\partial x^2} + \frac{\partial^2 p_1}{\partial y^2} \right] + 4.0 \left[\frac{\partial^2 p_2}{\partial x^2} + \frac{\partial^2 p_2}{\partial y^2} \right] - \left[\sin \frac{\pi x}{4} \sin \frac{\pi y}{4} \right] [t + 3t^2] \end{aligned} \quad (43)$$

The solution satisfying (43) and the boundary and initial conditions is

$$\begin{aligned} p_1(x, y, t) &= \frac{8.0}{\pi} \left[\sin \frac{\pi x}{4} \sin \frac{\pi y}{4} \right] t^2 \\ p_2(x, y, t) &= - \frac{8.0}{\pi} \left[\sin \frac{\pi x}{4} \sin \frac{\pi y}{4} \right] t^2 \end{aligned} \quad (44)$$

The finite element model is shown in Figure 4. It consists of two parallel five by five grid point arrays connected by a total of sixty-four right triangular elements, i.e., thirty-two in each array. The two parallel systems represent, respectively, the two primary flows J^1 and J^2 . Figure 4(b) shows a typical parallel system connecting grid points 7, 8, and 13 with 7', 8', and 13'. The properties of the triangular elements and scalar transfer elements for this system

are found using our previous conclusions for triangular and scalar elements. For the 7,8,13 system we find, using equation (33) for the scalar elements, that

$$\begin{aligned}
 K_{7,7'} &= (b_7^2 + c_7^2) \frac{\bar{t}_{L13}}{4\Delta} = \frac{\bar{t}_{L13}}{4\Delta} & K_{7,8'} &= (b_7 b_8 + c_7 c_8) \frac{\bar{t}_{L13}}{4\Delta} = -\frac{\bar{t}_{L13}}{4\Delta} \\
 K_{7,13'} &= (b_7 b_{13} + c_7 c_{13}) \frac{\bar{t}_{L13}}{4\Delta} = 0 & K_{8,8'} &= (b_8^2 + c_8^2) \frac{\bar{t}_{L13}}{4\Delta} = \frac{\bar{t}_{L13}}{2\Delta} \\
 K_{8,13'} &= (b_8 b_{13} + c_8 c_{13}) \frac{\bar{t}_{L13}}{4\Delta} = -\frac{\bar{t}_{L13}}{4\Delta} & K_{13,13'} &= (b_{13}^2 + c_{13}^2) \frac{\bar{t}_{L13}}{4\Delta} = \frac{\bar{t}_{L13}}{4\Delta}
 \end{aligned} \tag{45}$$

This information is presented in Table 3.

The vector $\{F_Q\}$ representing the effects of the distributed sources $Q_1(x,y,t)$ and $Q_2(x,y,t)$ was obtained by simple lumping procedures. The boundary and initial conditions (40) were satisfied by constraining the boundary grid point potentials to their appropriate values.

Table 4 presents a representative comparison between analytical results (AN.) from (44) and results from the NASTRAN analysis (F.E.). Numerical integration was performed using 100 time steps with integration interval $t = 0.05$ and maximum error was less than five percent.

REFERENCES

1. DeGroot, S. R., and Mazur, P.: *Non-Equilibrium Thermodynamics*. North-Holland Pub. Co., Amsterdam, 1962.
2. Fitts, D. D.: *Nonequilibrium Thermodynamics*. McGraw-Hill Book Co., Inc., 1962.
3. Veinik, A. I.: *Thermodynamics*. Israel Program for Scientific Translations, Jerusalem, 1964.
4. Taylor, S. A., Gary, J. W.: *Linear Equations for the Simultaneous Flow of Matter and Energy in a Continuous Soil System*. Soil Sci. Soc. Proceedings, Jan. - Feb. 1964.
5. Lykov, A. V., and Mikhailov, Yu. A.: *Theory of Heat and Mass Transfer*. Israel Program for Scientific Translations, Jerusalem, 1965.
6. Schechter, R. S.: *The Variational Method in Engineering*. McGraw-Hill Book Co., New York, 1967.
7. Tsoi, P. V.: *Thermodynamics of Irreversible Processes and Derivation of a System of Differential Equations for Molecular Transfer*. J. Eng. Phys., Vol. 9, No. 3, 1967.
8. Mason, J. B.: *Finite Element Analysis of Coupled Irreversible Vector Processes*. Ph.D. Thesis, University of Maryland, College Park, Maryland, August 1971.
9. Lewis, R. W., and Garner, R. W.: *A Finite Element Solution of Coupled Electrokinetic and Hydrodynamic Flow in Porous Media*. Int. J. Numerical Methods Eng., Vol. 5, 1972.

Table 1
 Element Connection Table for Parallel
 System Between Grid Points 2,2',2'' and 3,3',3''

Element Type	Connecting Grid Points	A	ℓ	$L_{\gamma\epsilon}$	$k = I \frac{A}{\ell} L_{\gamma\epsilon}$
ROD 1	2 - 3	1.0	1.0	$L_{11} = 1.0$	
ROD 2	2' - 3'	1.0	1.0	$L_{22} = 4.0$	
ROD 3	2'' - 3''	1.0	1.0	$L_{33} = 2.0$	
Scalar 1	2 - 2'	1.0	1.0	$L_{12} = -0.1$	0.1
Scalar 1	2 - 2''	1.0	1.0	$L_{13} = 0.2$	-0.2
Scalar 1	2' - 2''	1.0	1.0	$L_{23} = 0.3$	-0.3
Scalar 1	3 - 3'	1.0	1.0	$L_{12} = -0.1$	0.1
Scalar 1	3 - 3''	1.0	1.0	$L_{13} = 0.2$	-0.2
Scalar 1	3' - 3''	1.0	1.0	$L_{23} = 0.3$	-0.3
Scalar 2	2 - 3'	1.0	1.0	$L_{12} = -0.1$	-0.1
Scalar 2	2' - 3	1.0	1.0	$L_{12} = -0.1$	-0.1
Scalar 2	2 - 3''	1.0	1.0	$L_{13} = 0.2$	0.2
Scalar 2	2'' - 3	1.0	1.0	$L_{13} = 0.2$	0.2
Scalar 2	2' - 3''	1.0	1.0	$L_{23} = 0.3$	0.3
Scalar 2	2'' - 3'	1.0	1.0	$L_{23} = 0.3$	0.3

Table 2
Problem 1 Results

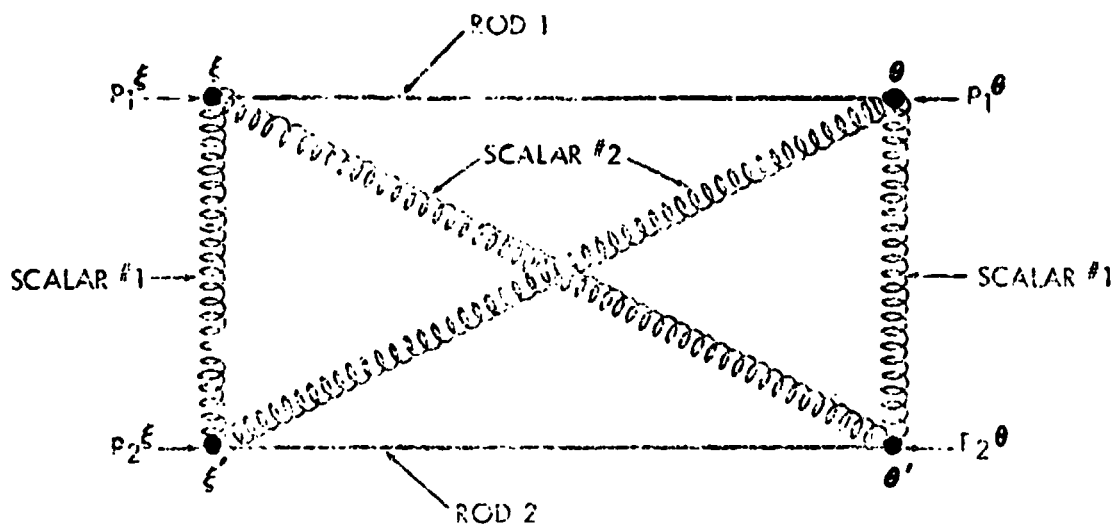
Location x =	P ₁ (x)		P ₂ (x)		P ₃ (x)	
	AN.	F.E.	AN.	F.E.	AN.	F.E.
0.0	0.0	0.0	0.0	0.0	0.0	0.0
1.0	2.0	2.0 ⁻	-3.0	-3.0	1.0	1.0 ⁺
2.0	8.0	8.0 ⁻	-12.0	-12.0	8.0	8.0 ⁺
3.0	18.0	18.0 ⁻	-27.0	-27.0	27.0	27.0 ⁺
4.0	32.0	32.0	-48.	-48.0	64.0	64.0

Table 3
Element Connection Table for Parallel System
Connecting Grid Points 7,8,13 and 7',8',13'

Element Type	Connecting Grid Points	\bar{c}	Δ	$L_{y\epsilon}$	$k = -K_{\text{coupling}}$
TRIANGLE 1	7 -8 -13	2.0	0.5	2.0	
TRIANGLE 2	7'-8'-13'	2.0	0.5	4.0	
Scalar	7 -7'	2.0	0.5	1.0	$-k_{7,7'} = -1.0$
Scalar	8 -8'	2.0	0.5	1.0	$-k_{8,8'} = -2.0$
Scalar	13 -13'	2.0	0.5	1.0	$-k_{13,13'} = -1.0$
Scalar	7 -8'	2.0	0.5	1.0	$-k_{7,8'} = 1.0$
Scalar	8 -7'	2.0	0.5	1.0	$-k_{8,7'} = 1.0$
Scalar	8 -13'	2.0	0.5	1.0	$-k_{8,13'} = 1.0$
Scalar	13 -8'	2.0	0.5	1.0	$-k_{13,8'} = 1.0$
Scalar	7 -13'	2.0	0.5	1.0	$-k_{7,13'} = 0.0$
Scalar	13 -7'	2.0	0.5	1.0	$-k_{13,7'} = 0.0$

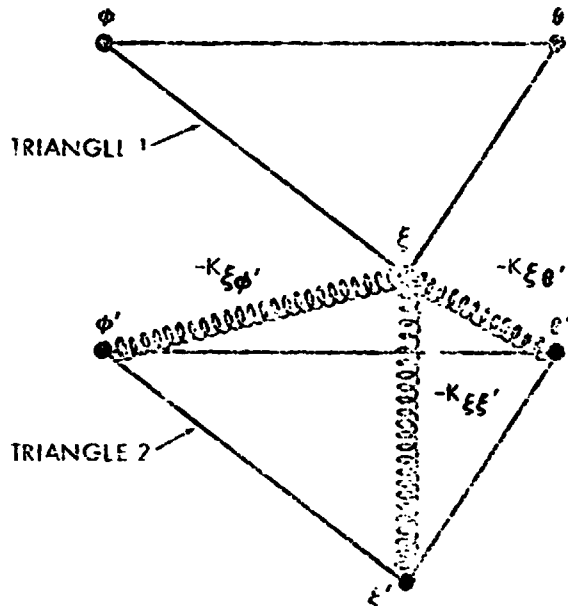
Table 4
Problem 2 Results

Time	$p_1(x,y,t)$				$p_2(x,y,t)$			
	$x = 2.0, y = 2.0$		$x = 3.0, y = 3.0$		$x = 2.0, y = 1.0$		$x = 1.0, y = 1.0$	
	AN.	F.E.	AN.	F.E.	AN.	F.E.	AN.	F.E.
t=1.0	0.811	0.832	0.573	0.588	-0.811	-0.839	-0.405	-0.420
t=2.0	3.242	3.361	2.293	2.376	-3.242	-3.381	-1.621	-1.690
t=3.0	7.295	7.596	5.516	5.371	-7.295	-7.629	-3.648	-3.814
t=4.0	12.969	13.538	9.171	9.573	-12.969	-13.584	-6.485	-6.792



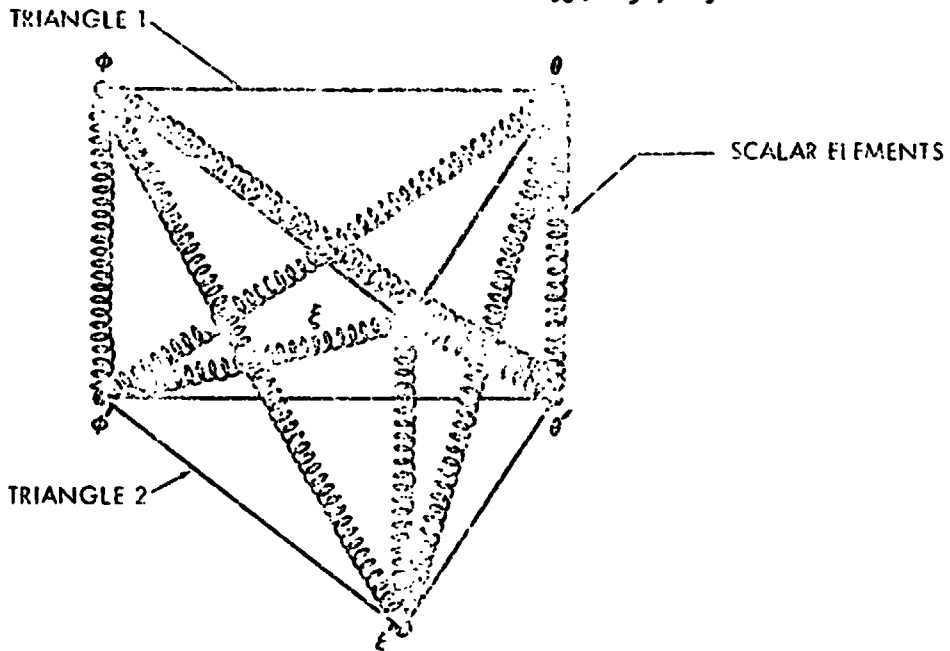
NOTE:
 Geometric Coordinates of Grid Points ξ, θ
 Correspond to those of ξ', θ' respectively

Figure 1. ONE DIMENSIONAL PARALLEL ROD ELEMENT SYSTEM FOR TWO COUPLED FLOWS.



Note: Geometric Coordinates of Grid Points ξ, θ, ϕ Correspond to Those of ξ', θ', ϕ' Respectively

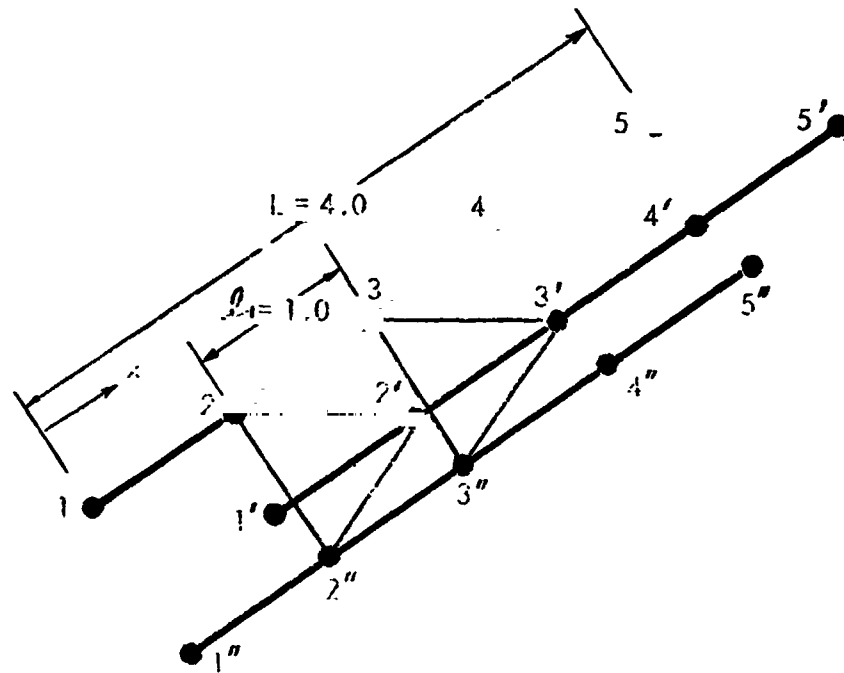
(a) Showing Typical Scalar Connections $K_{\xi\xi'}$, $K_{\xi\theta'}$, $K_{\xi\phi'}$.



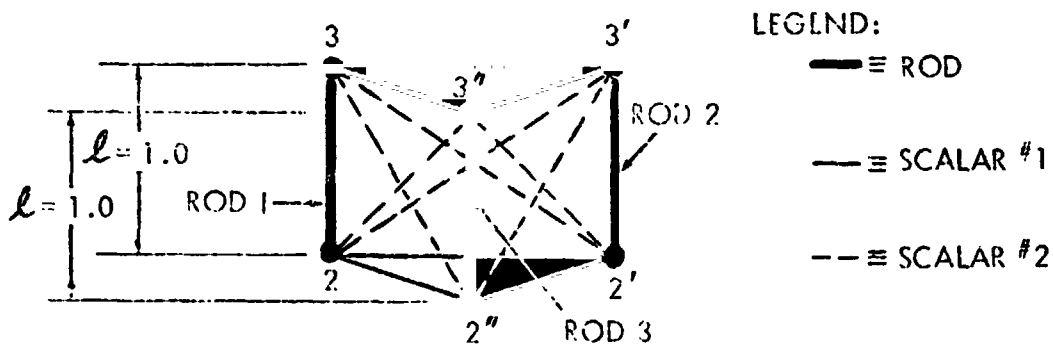
(b) Showing All Scalar Transfer Elements.

Figure 2. TWO DIMENSIONAL PARALLEL TRIANGULAR ELEMENT SYSTEM FOR TWO COUPLED FLOWS.

NOTE: Geometric Location of Grid Points 1 Through 5 Correspond to Those of 1' Through 5' and 1'' Through 5'', Respectively

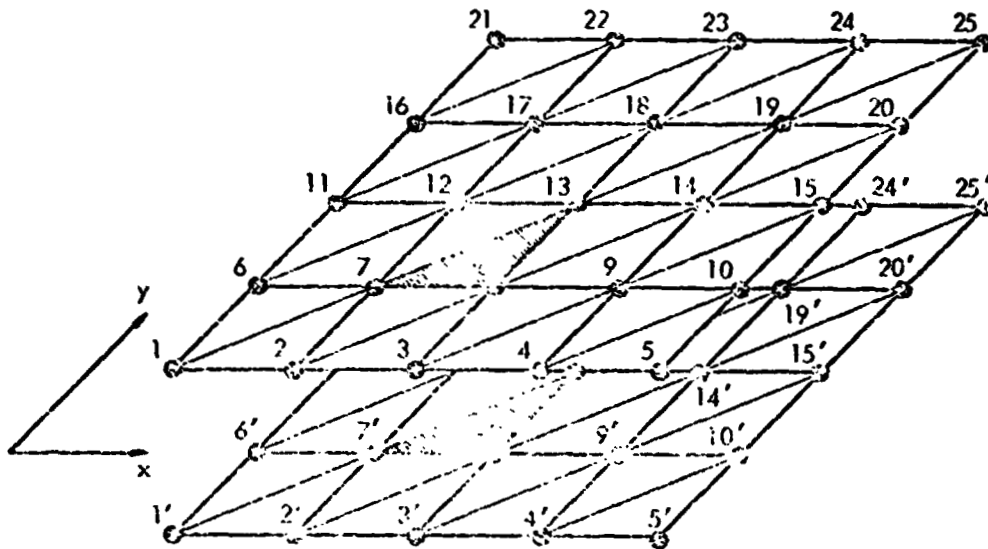


(a) Assembled Model Showing Grid Points and Parallel Rods.

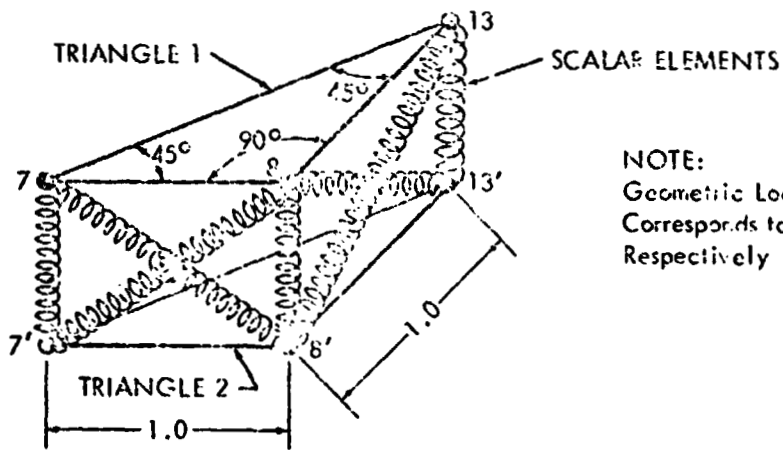


(b) Showing Typical Parallel Element System.

Figure 3. ONE DIMENSIONAL, THREE COUPLED FLOWS.



(a) Assembled Model Showing Grid Points and Parallel Triangles.
(Viscous Dampers Not Shown)



NOTE:
Geometric Location of Points 1 Through 25
Corresponds to Those of 1' Through 25',
Respectively

(b) Showing Typical Parallel Element System.

Figure 4. TWO DIMENSIONAL, TWO COUPLED FLOWS.

NASTRAN APPLICATIONS TO AIRCRAFT PROPULSION SYSTEMS

John L. White, Boeing Commercial Airplane Company

and

David L. Beste, Boeing Computer Services, Inc.

N75 31491

SUMMARY

The use of NASTRAN in propulsion system structural integration analysis is described. Computer support programs for modeling, substructuring and plotting analysis results are discussed. Requirements on interface information and data exchange by participants in a NASTRAN substructure analysis are given. Static and normal modes vibration analysis results are given with comparison to test and other analytical results.

INTRODUCTION

The versatility of NASTRAN makes it an ideal tool for the complex analysis problems associated with aircraft propulsion systems. These systems experience a great variety of loads and environments requiring sophisticated analysis tools for accurate analysis.

A particularly attractive advantage of NASTRAN is its low initial cost of acquisition and its common availability. Thus, it can serve as a unifying structural analysis language in joint engine and airframe company structural integration efforts. This has been the major use of NASTRAN in the Boeing Commercial Airplane Company, although some detailed analysis of engine components has been carried out for risk evaluation. This paper is therefore directed primarily at overall propulsion system structural analysis rather than detailed component analysis.

This paper describes NASTRAN history at Boeing, the various pre and post processors developed for enhanced utilization, propulsion system modeling, substructuring procedures, and various analysis cases with some correlation with test and other analyses.

NASTRAN BACKGROUND

NASTRAN has been operational on Boeing computers since release 8.0 was available in 1969. Currently release 15.5 is running on the IBM 370/168's under HASP and LASP, the IBM 360/65 under OS and the CDC 6600's under KRONOS 2.1. During this time NASTRAN has been used in the analysis of a large number of aerospace and other structures, e.g., MVM, LST, Minuteman, Lunar Rover, Roland, turbine blades, HLH combustor, YC-14 propulsion system, and a large cable-stayed bridge.

To aid in the various analyses and to improve "ease of use" of NASTRAN, various computer programs have been developed. SAIL, SPAN and XFETCH are three such computer programs. Also routines have been developed to provide an overall equilibrium check, to generate multipoint constraints, and to recover multipoint constraint forces.

SAIL II (Structural Analysis Input Language II) (Reference 1) is a language for describing NASTRAN bulk data. Basic finite-element input data such as gridpoints, element connections, and loads are defined in an easy, straightforward manner, using the SAIL II statements. The SAIL II features include looping, data block transformation, and external data generators plus all the capabilities of FORTRAN. The NASTRAN bulk data deck is generated from a relatively small number of SAIL II statements, making it very convenient to incorporate structural and geometry changes into a NASTRAN model.

SPAN (Substructure Partition Automation for NASTRAN) (Reference 2) is a NASTRAN support program that automatically generates the partition vectors required for assembling Phase I matrices during Phase II of a NASTRAN substructure analysis. The partition vectors generated can be based on identical grid or scalar point identifications, identical XYZ coordinates, or specified connection points. User labels can be retained during Phase II to allow loads, constraints, and elements to reference the original grid points. The displacement results are identified by the original gridpoint labels. Structural plots can be produced during Phase II.

SPAN uses the Phase I checkpoint tapes and a small amount of card input to determine the substructure definition. The SPAN output is the NASTRAN Phase II input deck that includes the required partition vectors. Extensive error checks are made to insure proper matrix ordering and consistency.

XFETCH is a subroutine that reads NASTRAN data files from a checkpoint/restart tape. The NASTRAN data can be returned to an incore storage array, or copied and reformatted to data sets easily read by FORTRAN. The copy and reformat feature is useful in applications where the data sets are too large for convenient incore processing. Both tables and matrices can be read.

PROPULSION SYSTEM STRUCTURES BACKGROUND

In the development of aircraft propulsion systems, major structural components are provided by both the engine manufacturer and the airframe manufacturer. Typically the strut and nacelle, including inlet, nozzles, reversers, tail-cone, cowlings and systems equipment - or about 20 percent of the propulsion system below the wing weight - are produced by the airframe manufacturer.

The engine manufacturer ordinarily develops and tests the bare engine on a rigid test stand, exclusive of flight hardware. The airframe manufacturer provides design envelope loads to the engine manufacturer who then determines if the engine will function properly under such loads.

Because the propulsion system is usually not tested on the wing as an integrated structure until flight testing begins, it is important that at an early stage of the engine/airframe development program an integrated structural analysis of the total propulsion system be carried out. A structural integration tool such as NASTRAN can provide this analysis by accurately simulating the real propulsion installation and providing detailed knowledge of internal loads, running clearances, and total system vibration response. The needs for propulsion system and airframe structural integration are discussed further in Reference 3.

PROPULSION SYSTEM MODELING

For enhanced utilization of NASTRAN, comprehensive modeling procedures have been developed. Because of the axisymmetry or cyclic symmetry of most of the propulsion structure, automation of the modeling is particularly easy.

Figure 1 illustrates how the engine structure is modeled utilizing the SAIL II general purpose input language described earlier. An engine fan frame is shown whereby half of one strut is idealized, then by SAIL II built-in transformation subroutines, it is reflected, rotated and joined with other structure to generate the entire fan frame substructure. Where practicable, geometry is digitized directly from engineering drawings including grid point coordinates, plate section properties, beam offsets, section properties and orientation grid points.

One of the most beneficial aids for model checkout has been large size CALCOMP plots identifying grid points and the different element types and their numbers. However, model checkout is never assumed complete until a successful loads case has been fully executed and results plotted.

Figure 2 is a NASTRAN plot of a high bypass ratio, fan jet propulsion system. The models shown are symmetric halves made up essentially of quadrilateral plate and beam elements and include a beam-lumped mass representation of the rotors. Multipoint constraints simulate the bearing housings as rigid rings which are coupled to the rotor by scalar spring and damper elements. Direct matrix input is used to input rotor spin stiffening and Coriolis terms when applicable.

The vibration and dynamic response models are obtained from the static models shown in Figure 2 by the standard methods of Guyan reduction or possibly, more economically by mass lumping. In either case considerable non-structural mass lumping is required due to the many propulsion system accessories. The NASTRAN generated gross mass matrix has been found useful for manually redistributing the mass for vibration analysis.

MULTICOMPANY INTEGRATION ANALYSIS

Since NASTRAN is in the public domain and is available to everyone, it is quite straightforward for many companies to join in performing a substructure analysis of the complete structure. Phase I for a particular component is done by the company responsible for the component at its computing facility; Phase II is done at a mutually acceptable computing facility; and Phase III is run at the company responsible for the component. Before a joint effort is undertaken, however, the participating companies should establish the following ground rules to aid the effort:

- 1) A basic XYZ coordinate system for the entire structure.
- 2) Unique grid point numbers for the entire structure so that Phase I grid points instead of scalar points can be used in Phase II.
- 3) Compatible displacement coordinate system at interface points.
- 4) Grid point numbers at an interface increasing in the same direction for all substructures.
- 5) Unique coordinate system numbers for each substructure.
- 6) Agree on a common buffer size.
- 7) Compatible user and checkpoint tapes.
- 8) Unique substructure plot element ID's for Phase II plots.

If SPAN is used, then the ASET degrees of freedom at an interface grid point are required to be the same for all substructures that connect to the interface point.

ANALYTICAL RESULTS - STATICS

NASTRAN models of the type illustrated in Figure 2 have been used to analyze a variety of static loads cases, including thrust, inlet lift, inertia, and gyroscopic moments. Typical loadings and the manner in which they are introduced onto the model are illustrated in Figure 3. A best guess distribution and force balance provided thrust loads which were distributed circumferentially at various axial locations. The distributed gravity load is calculated within NASTRAN using the GRAV card. Inlet lift was distributed over the fan case/inlet attach flange in this early study prior to the availability of an inlet model. Gyroscopic moments, a case requiring antisymmetric boundary conditions, were applied at the major inertia locations of the rotor and were based on overall rigid body pitch velocity of the aircraft.

The deflections of the engine structure under load are shown in Figure 4 which were plotted using the standard built in NASTRAN plot capability.

Engine performance depends heavily on maintaining tight running clearances between the rotors and case, particularly in the fan and high pressure compressor. Rubbing increases clearances and decreases engine efficiency causing increased specific fuel consumption. Therefore, detailed knowledge of clearance changes under load is desired. To exhibit change of clearance contours between the engine case and rotors, a NASTRAN postprocessor was written (Reference 4). This postprocessor utilizes XFETCH, previously described, to read NASTRAN restart tapes then plots contour maps for the entire engine under the various loads. Two such plots are shown in Figure 5. Absolute values are not given because of engine proprietary information agreements between the airframe and engine companies.

The accuracy to be expected from NASTRAN analyses for propulsion system type structure has not been determined. The few known correlations with test data indicate it should be within the realm of 5 to 10 percent on peak deflections. The prevalence of bolted flanges in the engine case, slop in the installation system, and non-linear seal interface stiffnesses probably make the analysis less accurate than the 5 percent accuracy usually associated with the finite element methods.

A comparison of test and analysis is shown in Figure 6 for an engine compressor case. The model was produced independently by the airframe company from engine drawings and the analysis run without any knowledge of the tests which were run independently by the engine company. Under such circumstances the correlation should not be considered too bad.

ANALYTICAL RESULTS - VIBRATION

The ability to predict dynamic behavior of the propulsion system is of utmost importance. This includes the response to external gust loads, turbulence, takeoff, maneuver and landing loads in addition to critical rotor speeds and various off design conditions for safety and reliability. The interface problem between the engine and airframe manufacturer is of particular importance here since much of the airframe produced structure is hung at the extremities of the engine, magnifying the dynamic effects.

NASTRAN's dynamics capability provides an excellent tool for propulsion system vibration and dynamic response analysis. The normal modes vibration analysis of a typical high bypass ratio turbine engine is shown in Figure 7. The model shown had 51 lineal masses, 7 rotary inertias and retained 151 freedoms from the static stiffness model. A total of 120 symmetric and 120 antisymmetric modes were extracted, three of which are shown in Figure 7. Mass lumping was used due to excessive computing cost of Guyan reduction which has been found to be typically four times higher than the mass lumping approach.

The versatile plotting capability in NASTRAN is a great help in understanding vibration behavior as illustrated in the mode plots of Figure 7. Correlation has been attempted between NASTRAN normal modes analysis and test data, and with other analyses, i.e., simpler beam-spring-mass simulations.

Certain NASTRAN analysis and test frequencies are very close as indicated in Table I but there is not enough available test data to be sure if the mode shapes correlate. Much the same situation exists in comparing NASTRAN results to the simpler beam-spring-mass simulations, also noted in Table I. A revision of the NASTRAN plot elements and plot viewing angles will be helpful in this regard.

CONCLUSIONS

The success of an engine/airframe structural integration effort depends greatly on the timely exchange of interface information between the engine and airframe manufacturers including not only elementary geometry and loads but also comprehensive finite element models. A good tool for doing this is NASTRAN since it has common availability.

Application of the general purpose finite element programs such as NASTRAN to propulsion system structure is more recent than to airframe structure. More analysis and test correlation is needed to establish better standards for propulsion system modeling and analysis. Experience to date indicates that NASTRAN accuracy for overall engine structures may not be as good as for other more intensively analyzed structures.

ACKNOWLEDGEMENTS

The support and encouragement of M. N. Aarnes and E. D. Herness and the assistance of V. L. Iverson, T. F. Yantis, and F. L. Yen in modeling and postprocessor development is gratefully acknowledged. Also the cooperation of General Electric and Pratt and Whitney in providing engine data is gratefully acknowledged.

REFERENCES

1. Ice, M. W., "SAIL II - Structural Analysis Input Language II", 10204-001 Functional Description, 10204-002 Users Manual, Boeing Computer Services, Inc., May 1974.
2. Beste, D. L., "SPAN - Substructure Partition Automation for NASTRAN", 10204-003, Boeing Computer Services, Inc., May 1974.
3. Aarnes, M. N. and White, J.L., "Propulsion System and Airframe Structural Integration Program", Journal of Aircraft, Vol. 12, No. 4, April 1975, p. 234.
4. Yantis, T. F., "IFPLOT - Interference Contour Plotter", BCS-G0697, Boeing Computer Services, Inc., July 1975.

TABLE 1 NASTRAN VIBRATION ANALYSIS COMPARED TO TEST AND OTHER ANALYSIS

NASTRAN MODE NO.	NASTRAN FREQUENCY, HZ	ENGINE TEST, HZ	BEAM-SPRING-MASS ANALYSIS, HZ	POSSIBLE CORRELATION
1	11.04		10.9	NO
8	25.2	25		YES
12	38.18	34		YES
13	49.25	51	48	YES
18	76.75	62	62	YES

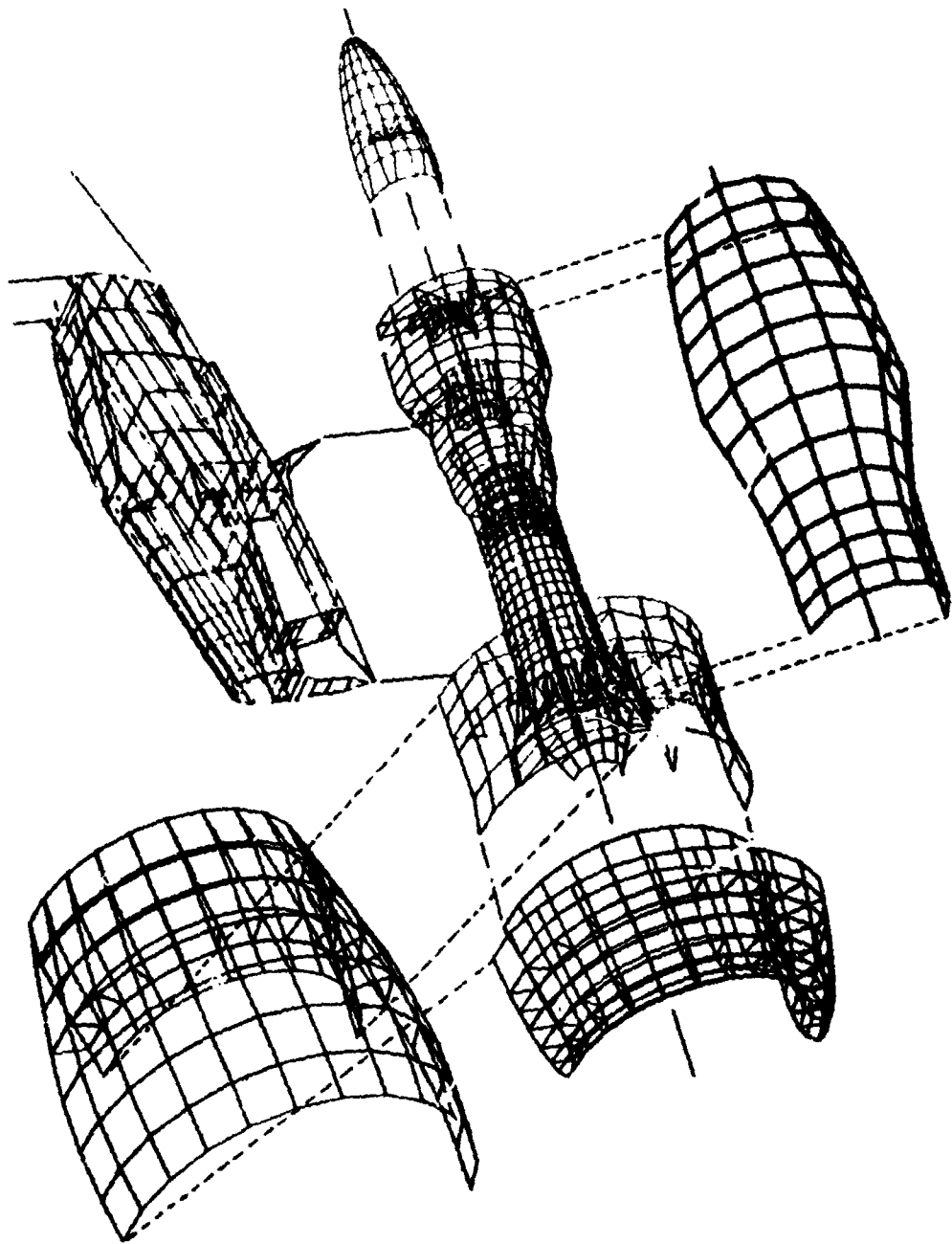


Figure 2.- Propulsion system substructures.

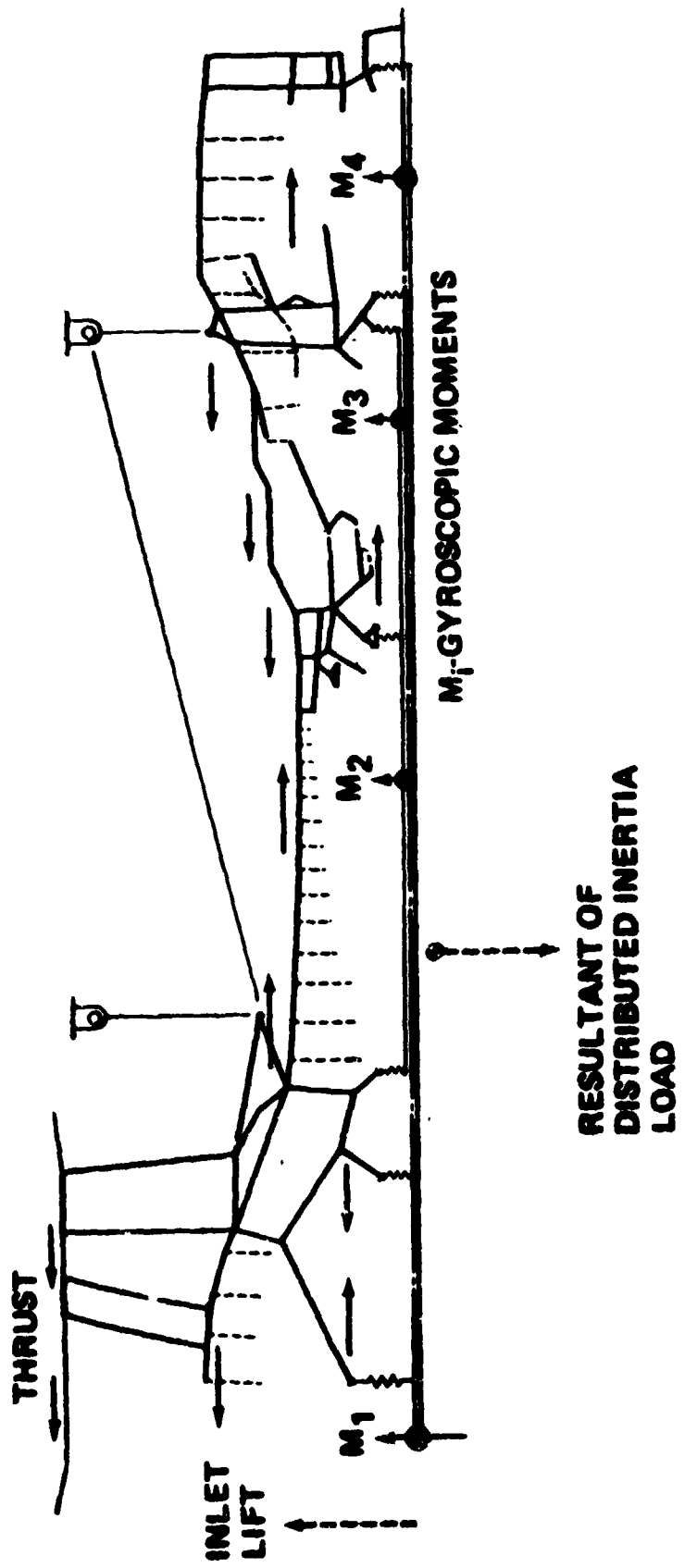


Figure 3.- Propulsion system static loads simulation.

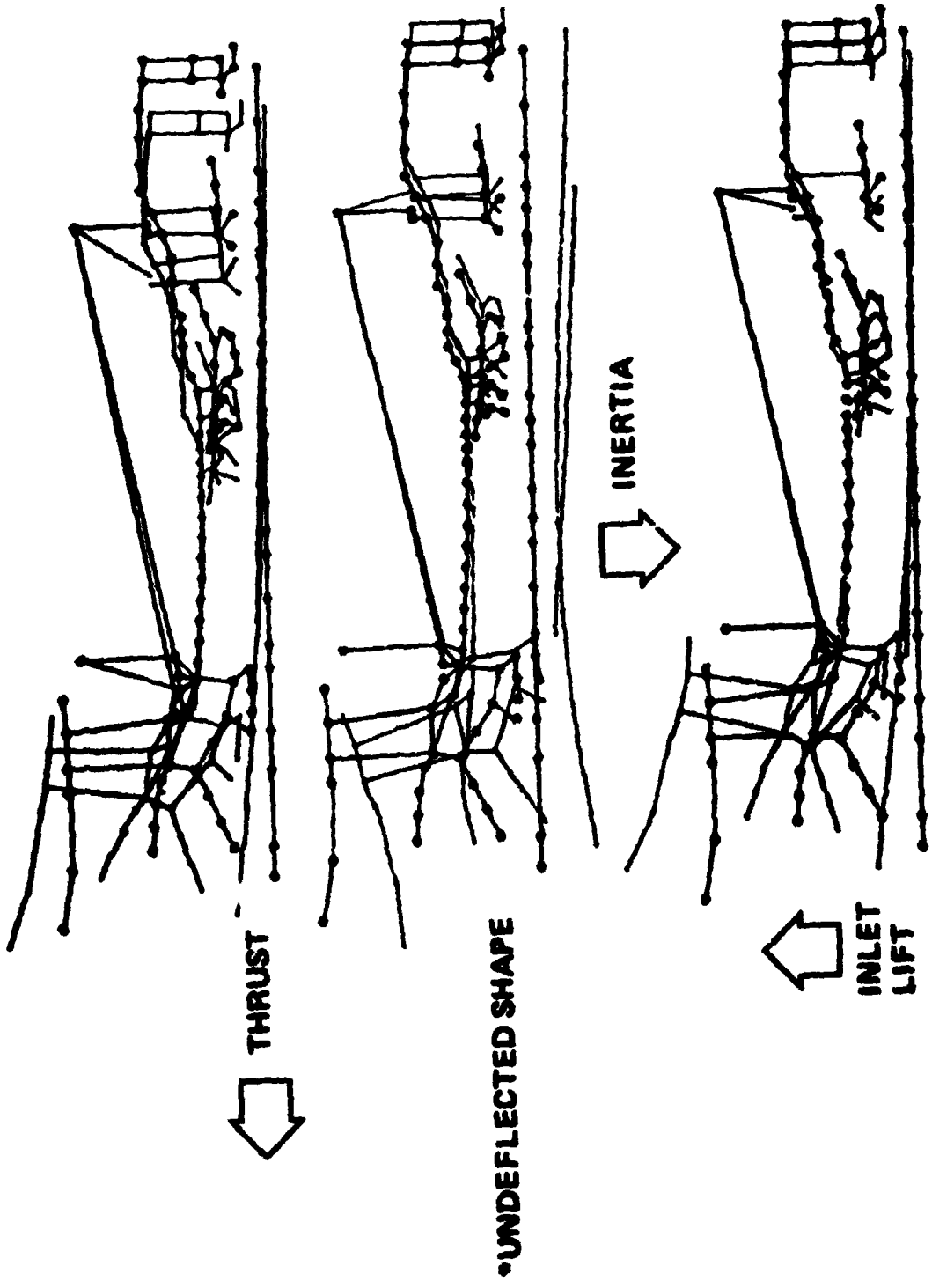
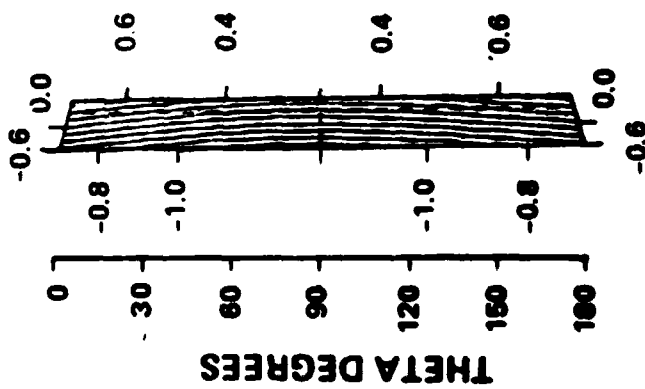


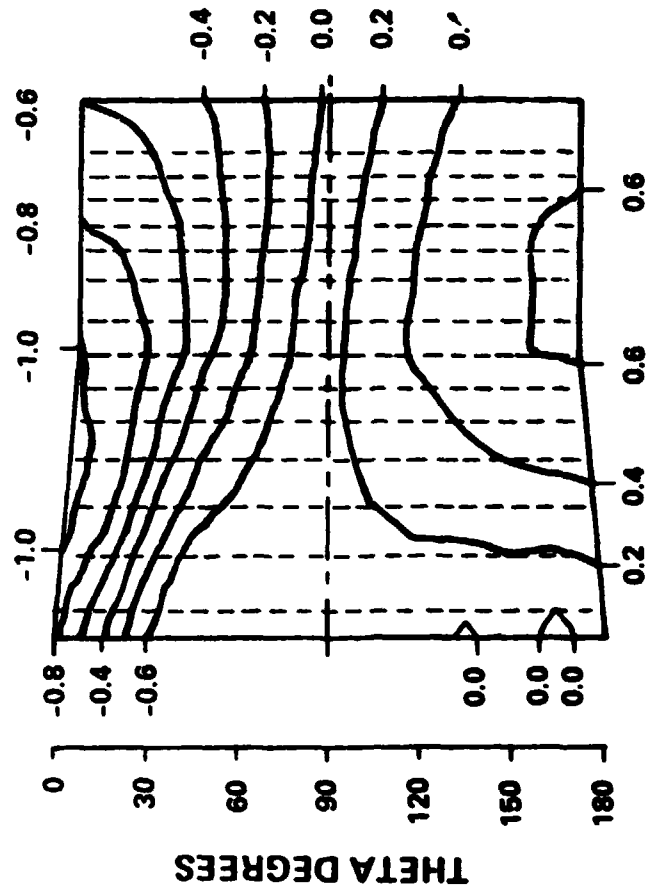
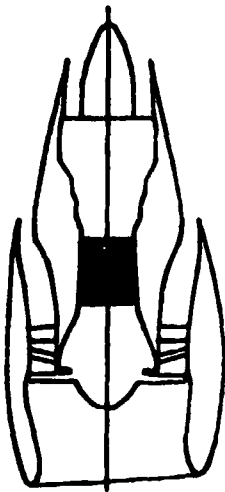
Figure 4.- Propulsion system static deflections.

**FAN
GYROSCOPIC LOADS,
1 RAD/SEC PITCH**



STAGE 1

**HIGH PRESSURE COMPRESSOR
51000 LBS THRUST**



STAGE 1 2 3 4 5 6 7 8 9 11 13

Figure 5.- Rotor/case change of clearance under load.

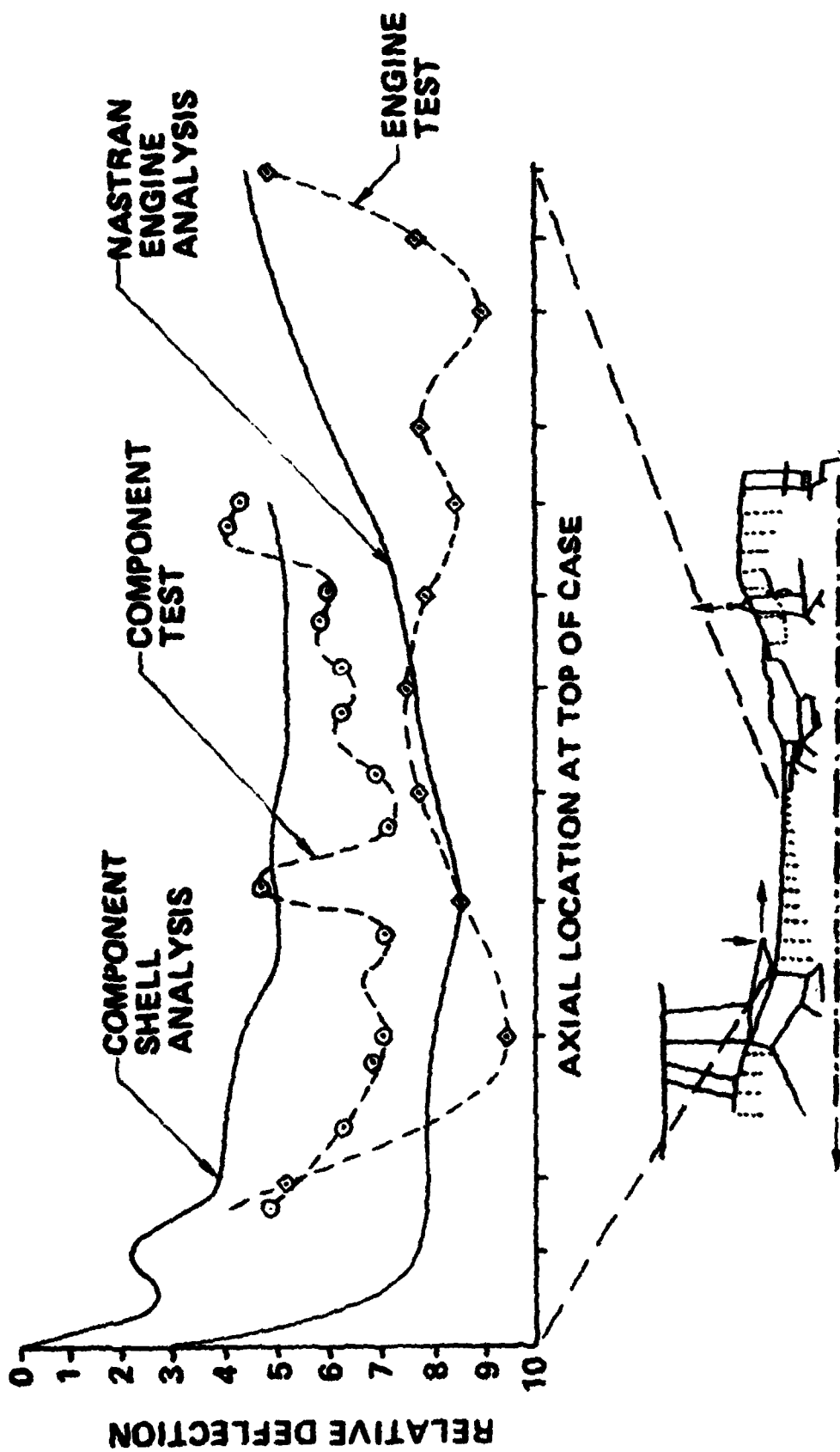


Figure 6.- Comparison of test and analysis results for engine case deflections under thrust load.

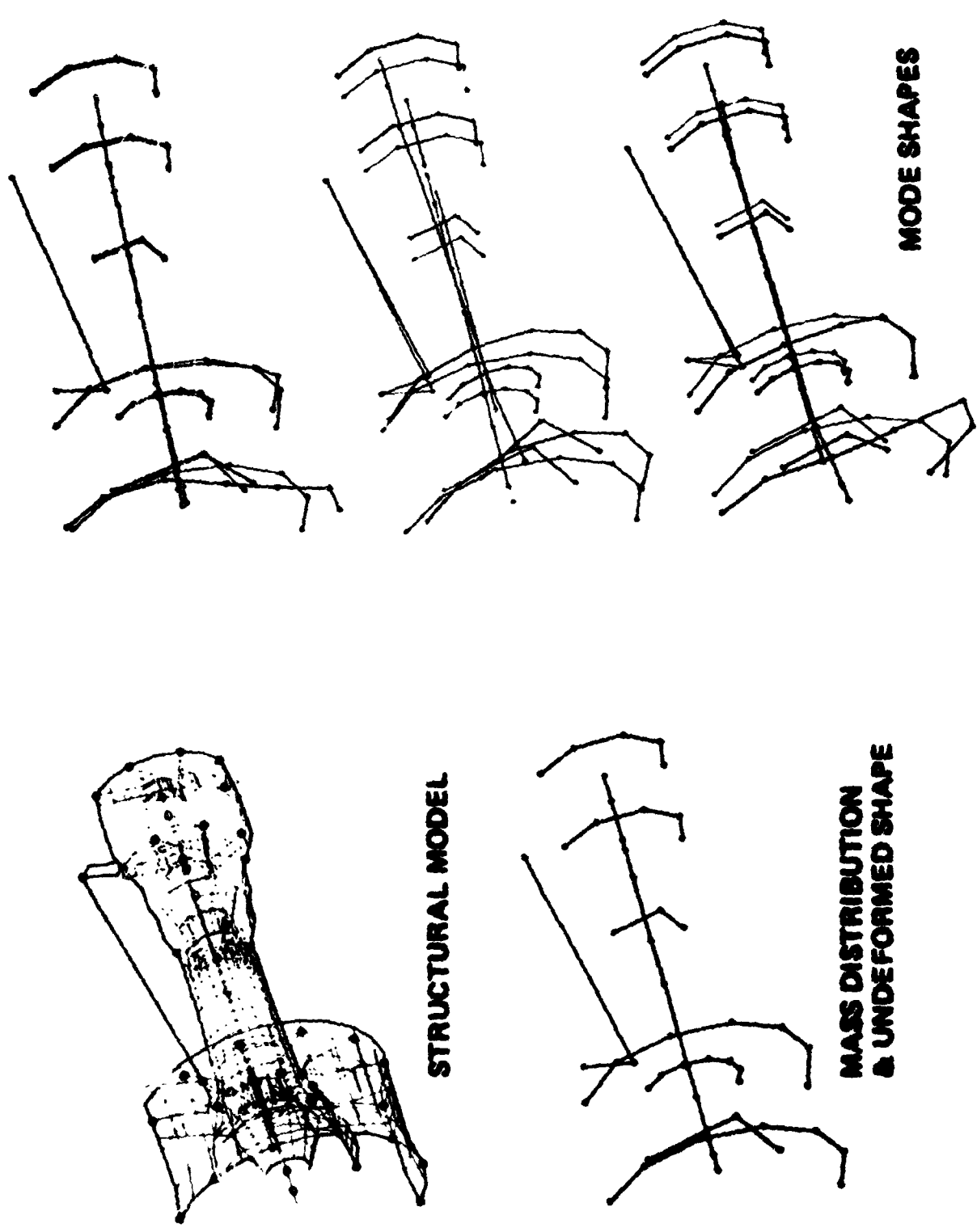


Figure 7.- Engine vibration analysis.

N75 31492

MODELING DAMAGED WINGS -

ELEMENT SELECTION AND CONSTRAINT SPECIFICATION

W. J. Stronge

Naval Weapons Center

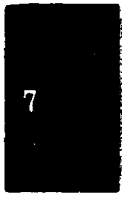
INTRODUCTION

The NASTRAN analytical program has been primarily used for structural design. Nevertheless, no problems were anticipated in applying this program to a damaged structure as long as the deformations were small and the strains remained within the elastic range. In this context, NASTRAN was used to test three-dimensional analytical models of a damaged aircraft wing under static loads. A comparison was made of calculated and experimentally measured strains on primary structural components of an RF-84F wing. This comparison brought out two sensitive areas in modeling semimonocoque structures. The calculated strains were strongly affected by the type of elements used adjacent to the damaged region and by the choice of MPC (multipoint constraints) sets on the damaged boundary.

DESCRIPTION OF STRUCTURE

Left wings from RF-84F aircraft were tested in this program. This fighter, designed for high subsonic speeds, had a wing span of 10 m. Its loaded weight was approximately 11 Mg. The wings were two-spar semimonocoque structures with the quarter-chord line swept back at 40 degrees. Both spars and four major ribs in each wing were aluminum forgings. Three outboard ribs were built up from extrusions. This basic framework (Figure 1) was covered by stringers and a skin of sheet aluminum. The entire structure was composed of 7075-T6 material with the exception of a few 2024-T3 skin panels.

An undamaged wing and five damaged wings were tested. The extent and location of damage for three of the wings are illustrated. (For example, see Figure 2.) These three cases had substantial damage to either the front or rear spar, a condition that previously caused large differences between predicted and measured strains (ref. 1). The damage cases investigated were all roughly 0.6-m diameter holes at 40 percent of the wing span. The damaged areas were cut out of the wings with a welding torch. Burned edges were ground back about 1 cm to reduce the heat-affected zone. In each of the three cases shown,



damage reduced the area moment-of-inertia of the wing about a chord line passing through the damaged region by 10 to 15 percent.

STATIC LOADING TESTS

The wings were cantilevered horizontally from a test fixture by their mounting lugs. Hydraulic jacks located at B and C in Figure 1 provided a static vertical force. Eighty-five percent of the force was applied to the front spar and fifteen percent to the rear spar to simulate a load distribution due to aerodynamic lift. With the undamaged wing, a 45-kN force applied in this way resulted in a uniform deflection of approximately 15 cm at the wing tip. With the damaged wings, deflections at the point of load application sometimes exceeded the 30-cm stroke of the jacks before failure. When this happened the wings were supported in the deformed configuration while the load was removed from the jack for shimming. Elimination of strain relaxation during shimming was a goal. In three tests where damage had been done to the main spar, the loads were slowly increased until failure occurred. In the other three tests, limitations of the test fixture prevented forces large enough to cause failure from being applied.

In these tests strains were measured at eight locations on major structural elements of the wings. The location of four pairs of SR4 strain gages is shown on Figure 1. These gages were mounted parallel to the spar axis on the top and bottom of the spar caps. In most cases, measured strains were linear up to failure since the gages were not near the critical section (ref. 1). Gages near where failure occurred (particularly 3 and 4) recorded nonlinear strains at loads as small as 50 percent of maximum. The measured strain data shown for a 45-kN load were determined by extrapolation of data from the 9 kN-to 27-kN range. At these lower load levels the data were linear, hence comparable with linear theoretical analysis.

ANALYTICAL MODEL DEVELOPMENT

Element Selection

A finite element model of the RF-84F wing structure was developed based on measurements made in the field. The first model (A in Figure 3) used simple elements in the interest of economy. ROD and SHEAR elements represented the spars. The skin in Model A is composed of quadrilateral SHEAR elements that are bordered by ROD's representing both stringers and in-plane skin stiffness. This model had about 250 degrees-of-freedom.

In this structure, the spars carry most of the bending loads. The ROD elements representing bending stiffness of the spars were located on the wing surface. Their cross-sectional area was chosen to provide the correct moment-of-inertia for each spar about its centroid. This representation resulted in a cross-sectional area for the model that was smaller than that of the structure. Since the cross-sectional area of the spar and its model were not the same, stresses caused by axial loads were not correct. Stresses on the wing surfaces caused by bending loads were correct when a principal axis of inertia for the wing cross-section passed through the spar centroid. Generally, the bending stiffness of a model created in this way would be somewhat smaller than the stiffness of the structure. In these wings, this influence of modeling technique was less than 5 percent.

The later Model C (Figure 4) varied from A in two respects: the number of elements was increased and in-plane stiffness was retained in the skin elements. After introducing additional grid points along the wing, elements in the three large bays were made one-half their original length. This increased the problem size to 340 degrees-of-freedom. Further, the SHEAR elements that represent skin in Model A were replaced by TRMEM elements. These smaller elements with wider load carrying capability were expected to improve load distribution around damaged regions.

Although the strains predicted by these models were reasonable for the undamaged structure, they compared very poorly with measured values when either spar was damaged. In these cases of damage, differences were as large as an order of magnitude. Consequently, the structural representation around the damaged region was reconsidered. The simple ROD and SHEAR elements representing beams were found to be inadequate for the complex load distribution in the vicinity of damage. In damage cases 2 and 5 where half of the beam was removed over a 76-cm length, the ROD representing the residual spar section was replaced by BEAM elements through the damaged region. MPC's were required at the ends of these elements to enforce compatibility with the slope of adjacent structure. In damage case 3 where the rear spar was cut completely, the bending forces carried by that spar were transferred to the short intermediate spar. The transfer occurred mainly through ribs at each end of the intermediate spar. Hence, torsional stiffness of the ribs became important and was added to the properties of the ROD elements representing these components. Twist in the ribs was determined by MPC's relating relative displacements of top and bottom grid points. These local modifications to the analytical model greatly improved the correlation of analytical and experimental results.

Constraints Around Holes

The simple structural elements used in the analytical model require special consideration on free boundaries. When elements are removed to represent damage, grid points bordering the hole can be left with

unrestrained degrees of freedom. A fatal error due to grid point singularity will result. This can be remedied by providing displacement constraints on these grid points by means of multipoint constraints. The choice of constraint conditions is not unique. It is easy to specify large displacements that are not compatible with the free edge of a hole. Forces required to achieve MPC constraints are not output directly so the degree of compatibility is not easily checked. Equilibrium considerations on free body sections passing through the hole can be used to determine these forces. Comparison with element forces at the cross-section has been used to test how well an MPC set satisfies the stress-free boundary condition of a hole. Generally, insignificant boundary forces have resulted from specifying a rigid body displacement relative to spanwise adjacent grid points.

COMPARISON OF MEASURED AND CALCULATED STRAINS

For comparison with the experimental results, a 45 kN static force was applied normal to the midplane of the model wing. Of the total, 85 percent was applied at point B of Figure 1 and 15 percent at point C. Stresses in the elements and nodal displacements were calculated using the NASTRAN static analysis rigid format.

Comparisons of calculated and measured strains on the undamaged wing encouraged confidence in the model that was first developed. With both Model A and Model C, calculated strains were within 17 percent of measured values for all gage locations on the undamaged wing. Hence, the large differences that occurred in damaged wings - in some cases as large as an order of magnitude - were a surprise. Since these large differences were only present when the spars were damaged, it first seemed that the skin structure in the vicinity of the damage must be carrying large strain gradients and significant in-plane loads. Models B and C were developed to deal with these possibilities. They had a smaller element size and membrane rather than shear elements. These models did not substantially improve the correlation of analytical and experimental results (compare ROD models in Figures 5 and 6). Subsequently, the simple elements adjacent to damage were replaced by higher order elements that could also carry bending or torsional loads. This markedly improved the correlation of calculated and measured strains.

Spar strains calculated by the analytical models are compared with the few measured values in Figures 5 and 6. Figure 7 illustrates damage to the rear spar while Figure 8 shows the measured and calculated strains with this damage. Similarly, Figures 9 and 10 illustrate damage to the underside of the front spar and corresponding strains. These axial strains are along the top and bottom of the front and rear spars on a wing subject to a 45-kN vertical force near the wing tip. In each case of damage to a spar and with both models A and C, the introduction of higher order

elements (H.O.E.) adjacent to damage greatly improved correlation with measured values. This improvement was a result of developing a numerically stable analytical model rather than refinements in the model.

Numerical stability problems are associated with ill-conditioning of the stiffness matrix. In NASTRAN, an index of this problem is the residual load vector,

$$\{\delta P_{\ell}\} = [I - KK^{-1}]\{P_{\ell}\}$$

where [I] is the identity matrix, [KK] is a stiffness matrix, and $\{P_{\ell}\}$ is the applied load vector. A nondimensional index can be defined as the error vector

$$\{\epsilon\} = \{\delta P_{\ell}\} / \|\{P_{\ell}\}\|$$

where $\|\{P_{\ell}\}\|$ is the norm of the applied load vector. For this wing, comparable results were obtained from the model when all components of $\{\epsilon\}$ were less than 10^{-14} . A component of the order of 10^{-12} or larger indicated poor modeling. The largest component of $\{\epsilon\}$ has been shown in Figures 5, 6, 8 and 10 for each model. Another indication of numerical problems caused by poor modeling was the large jump in nodal displacements across the damaged region. Displacements normal to the wing surface just outboard of damage were as large as 25 m. Replacement of elements around damage by higher order elements cured the conditioning problem.

CONCLUSIONS

Large differences between calculated and measured strains in damaged wings have been associated with numerical instability. This was caused by the simple elements initially used to represent structure adjacent to the damaged region. Load distribution around damage was significantly affected by the stiffness of adjacent structural components in planes that had only negligible loads in the undamaged structure. The simple elements provided no stiffness in these planes. More complex elements were required to handle the unusual loads around the damaged region.

Analyses of semimonocoque structures are sensitive to structural discontinuities. Holes and cutouts in particular can be troublesome. The considerations which greatly improved the accuracy of this damaged wing analysis are believed to be generally applicable.

REFERENCE

1. Stronge, W. J.: Failure Prediction for Damaged Aircraft Wings. Proceedings of the Fifth Navy-NASTRAN Colloquium, NSRDC, 1974.

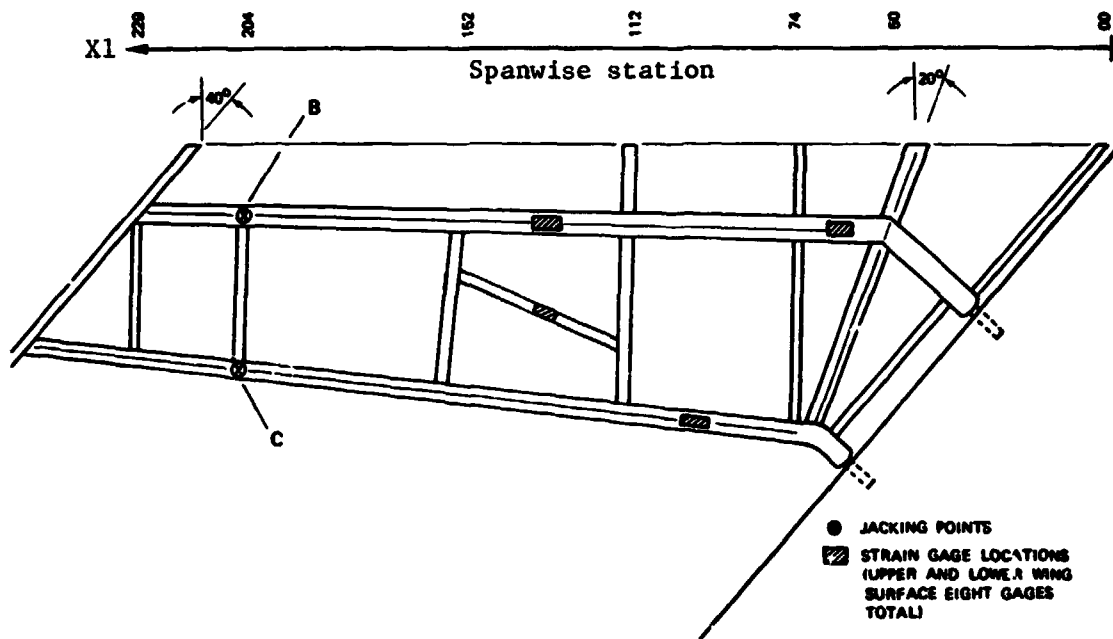
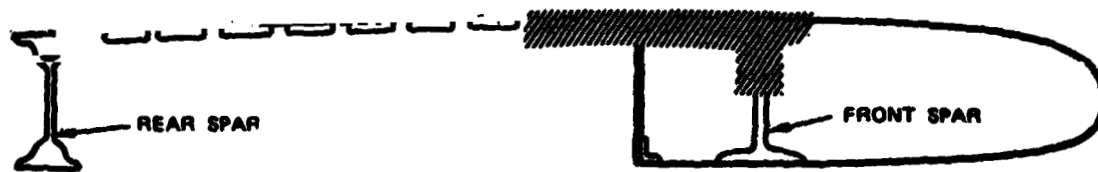


Figure 1.- F84 wing spars and ribs.



SECTION A-A

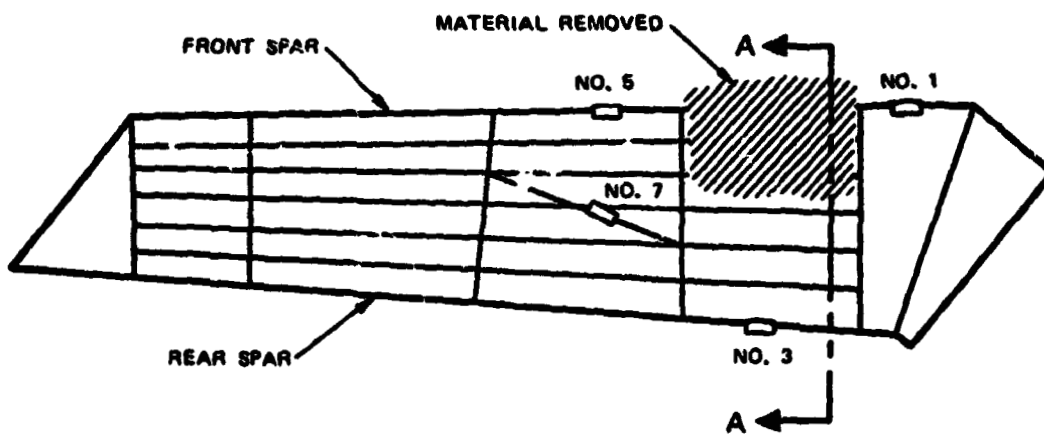


Figure 2.- Wing no. 2.

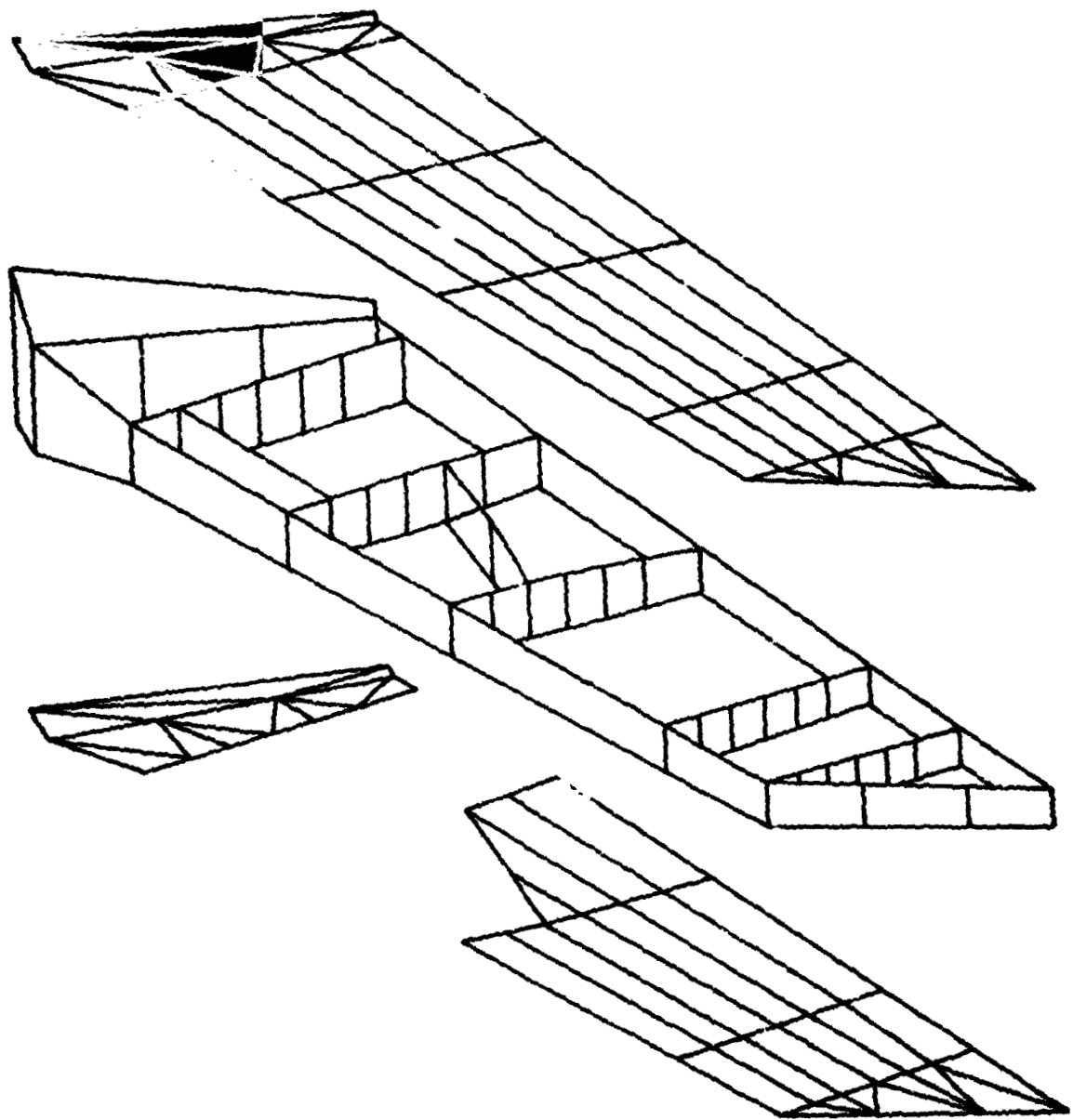


Figure 3.- Model A.

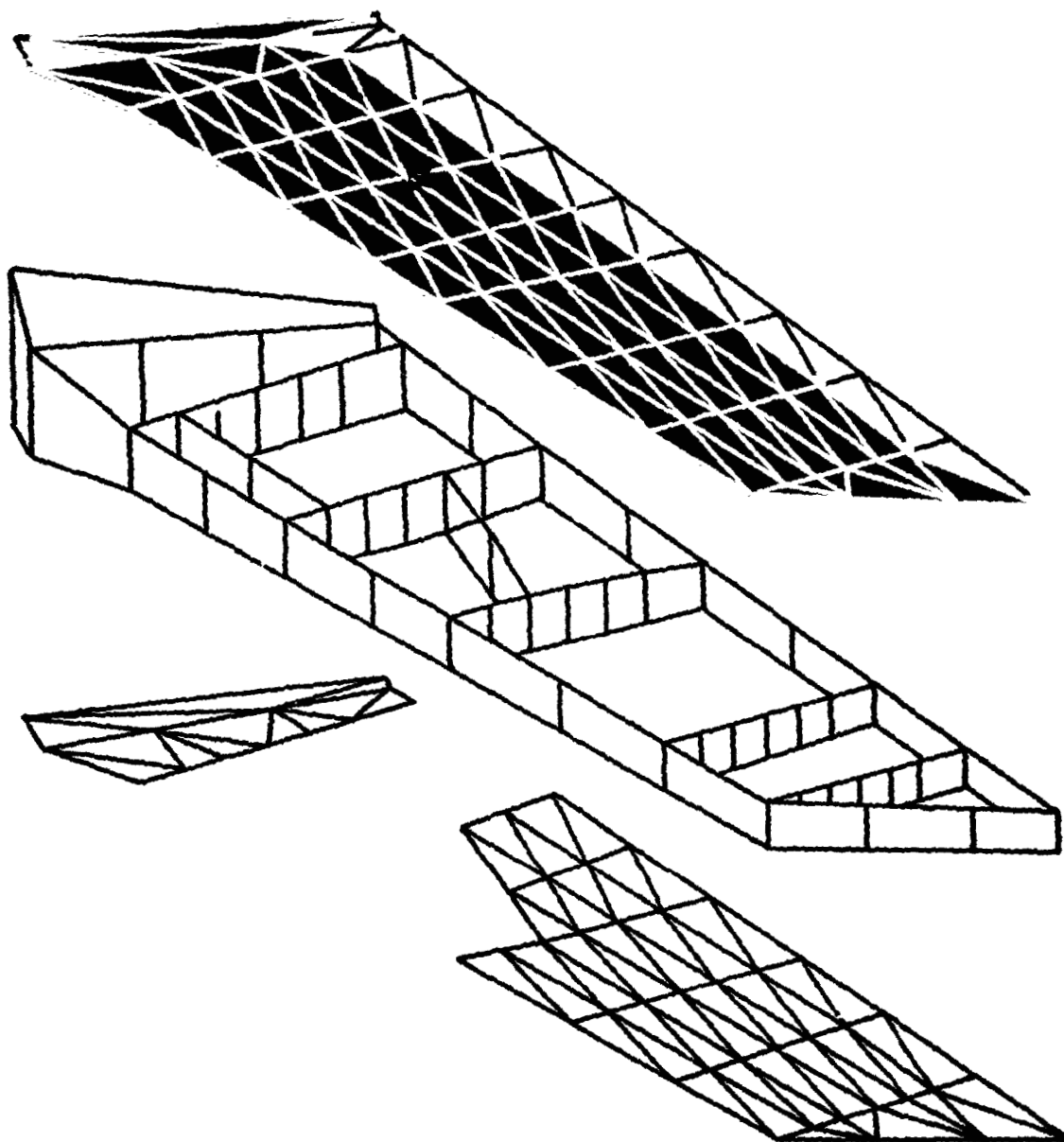


Figure 4.- Model C.

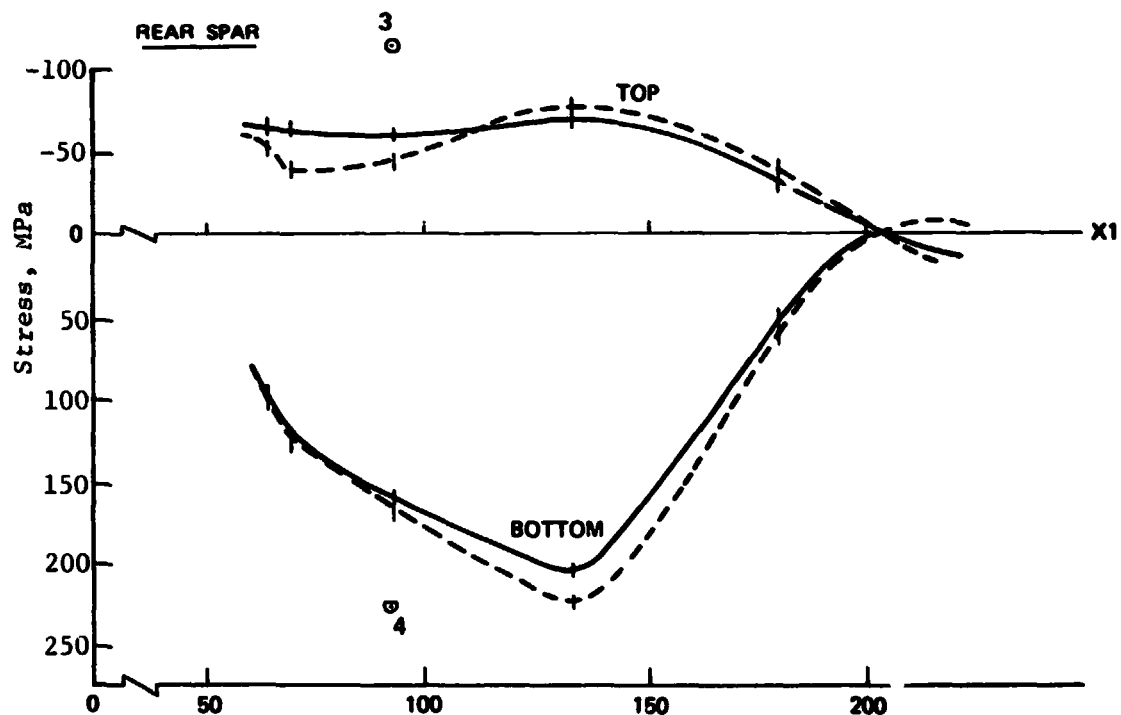
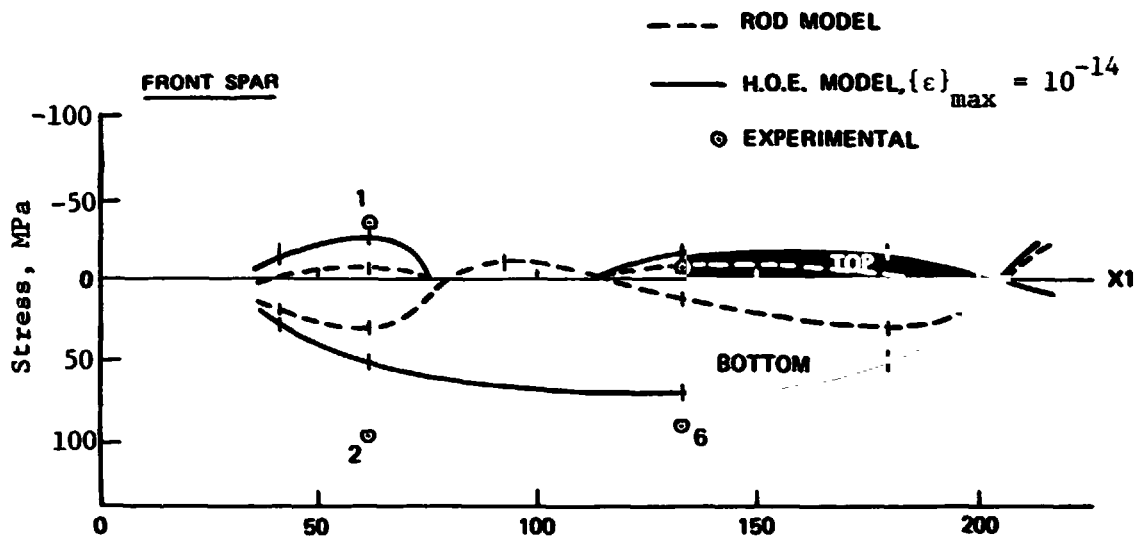


Figure 5.- Damage no. 2, model A.

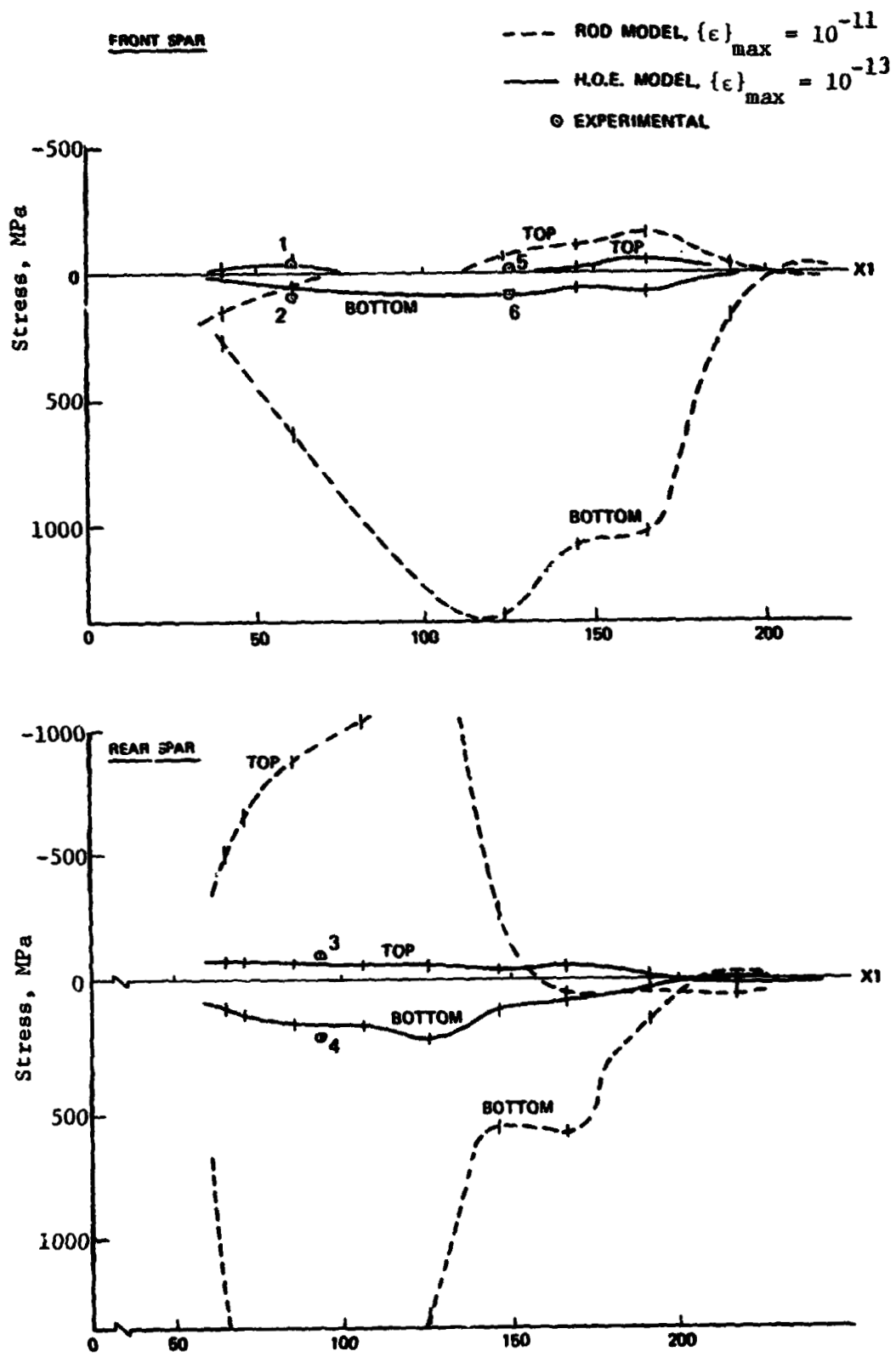
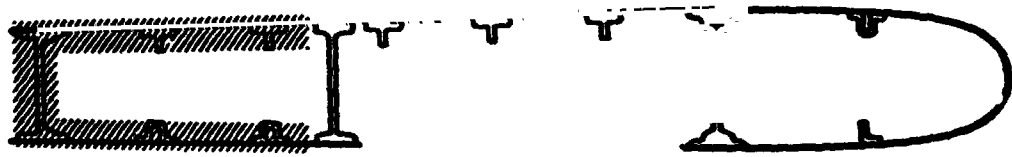


Figure 6.- Damage no. 2, model C.



SECTION A-A

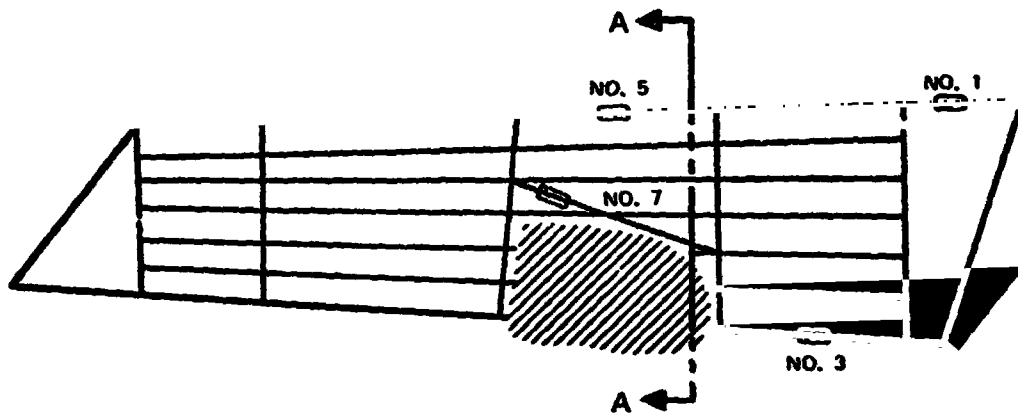
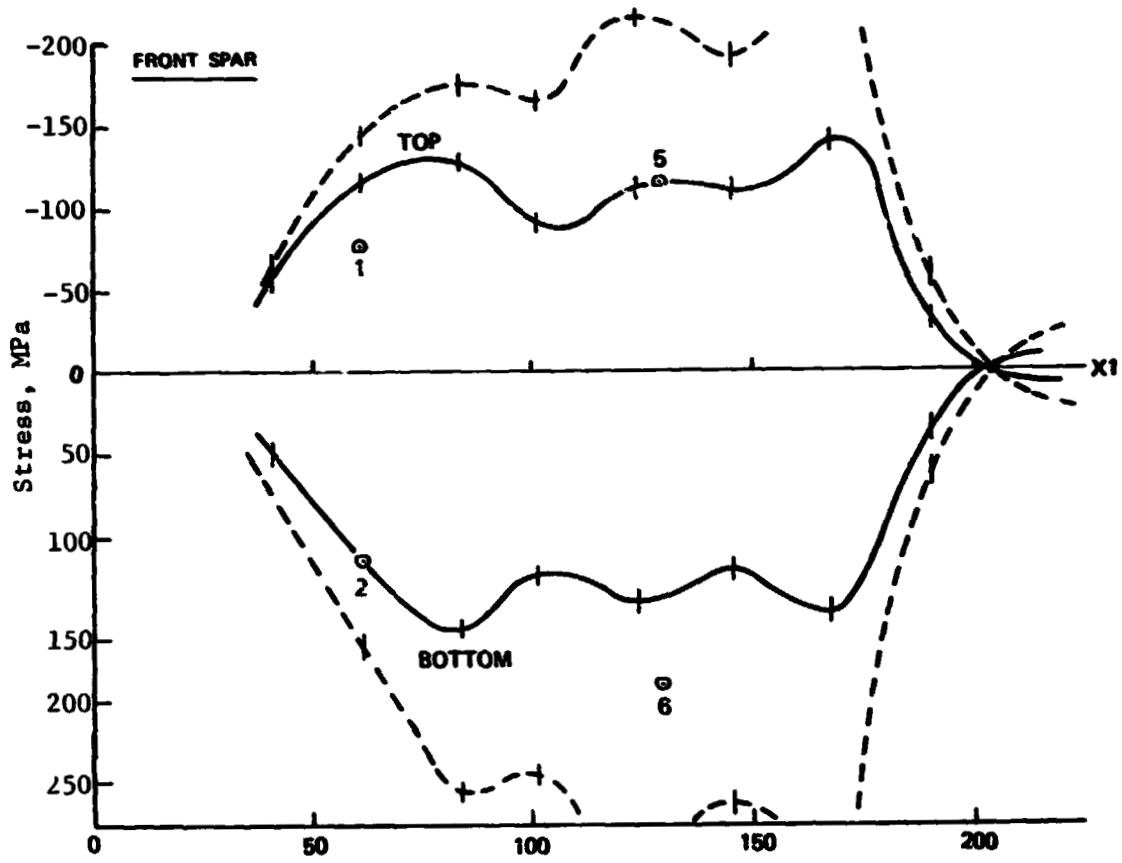


Figure 7.- Wing no. 3.



--- ROD MODEL, $\{\epsilon\}_{\max} = 10^{-13}$
 — H.O.E. MODEL, $\{\epsilon\}_{\max} = 10^{-14}$
 ⊙ EXPERIMENTAL

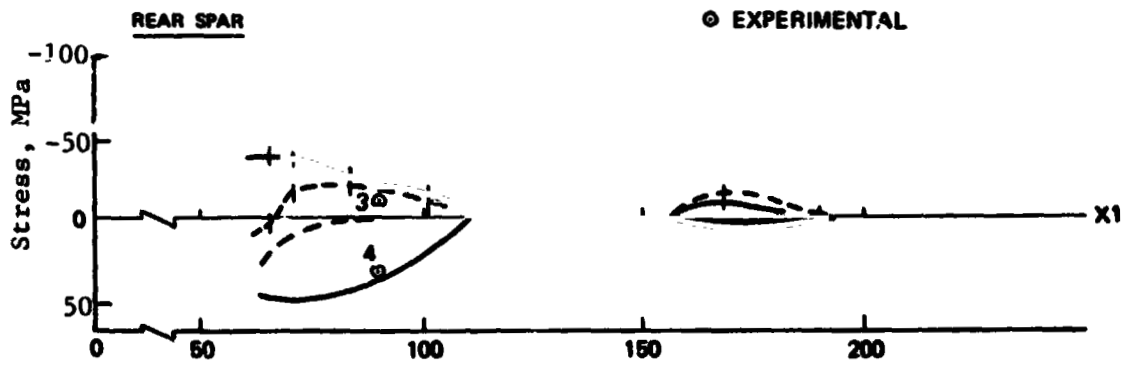


Figure 8.- Damage no. 3, model C.

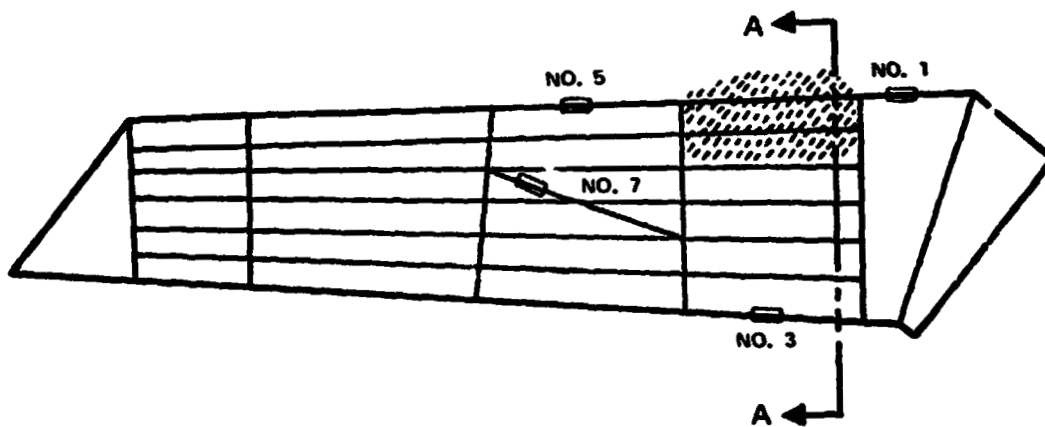
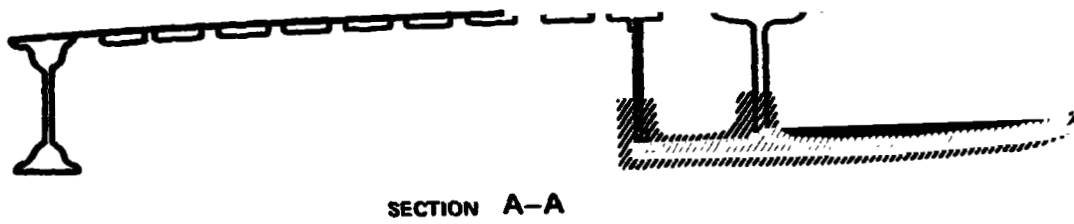


Figure 9.- Wing no. 5.

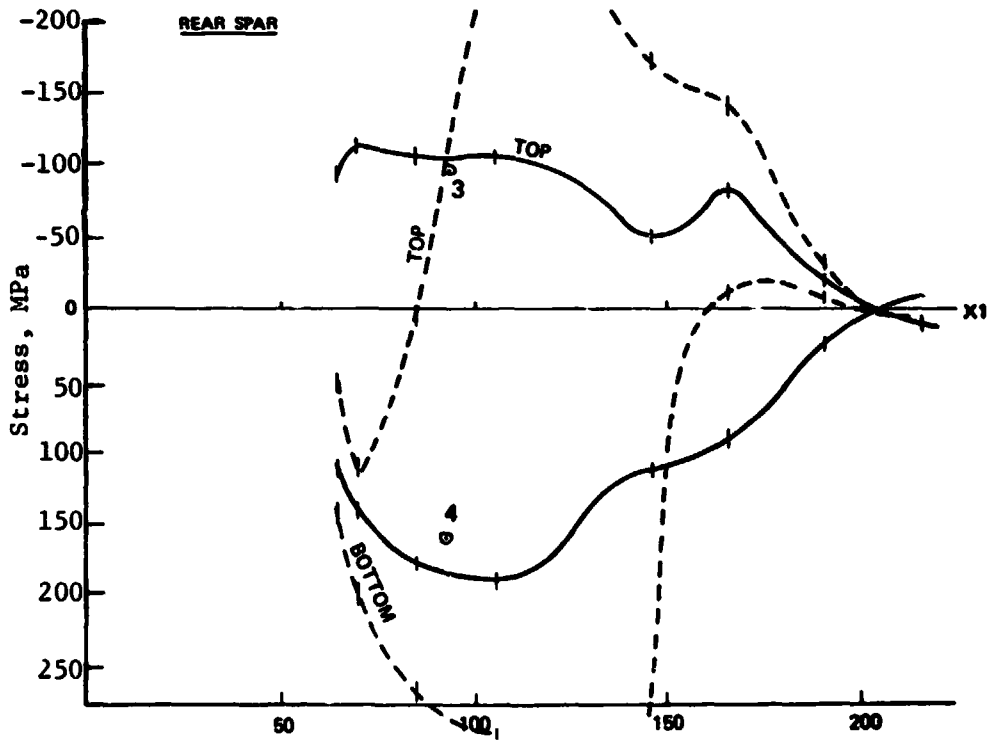
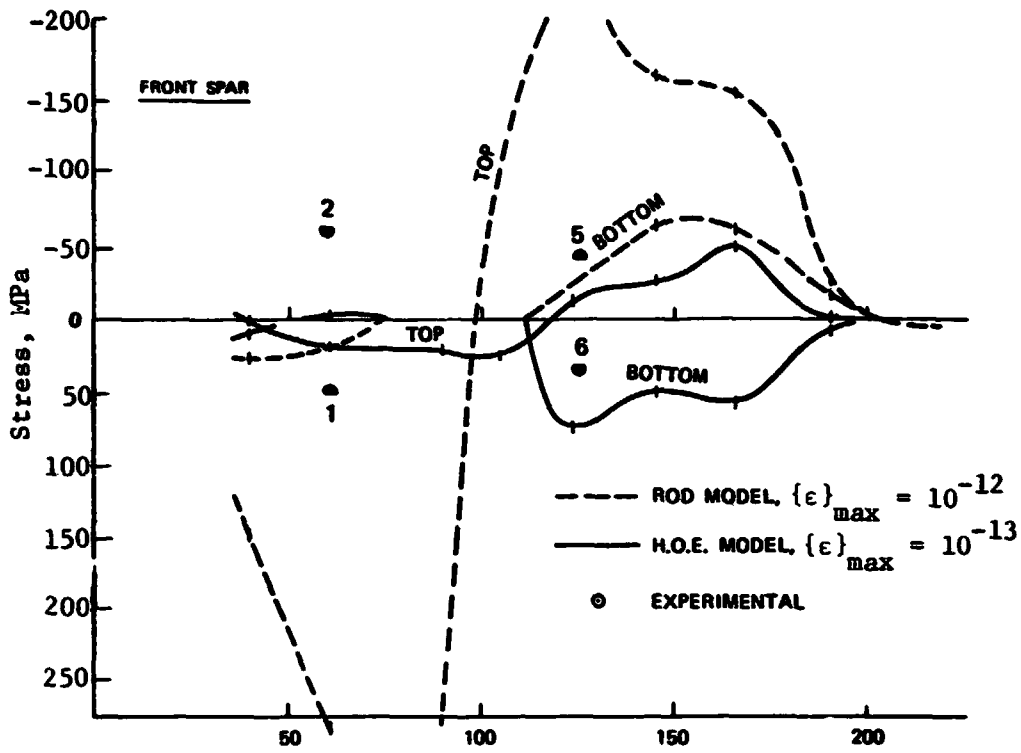


Figure 10.- Damage no. 5, model C.

! N75 31493

APPLICATION OF NASTRAN TO A FLUID SOLIDS UNIT

IN THE PETROLEUM INDUSTRY

Norman W. Nelson

**Exxon Research and Engineering Company
Florham Park, New Jersey**

SUMMARY

The application of NASTRAN to the design of a fluid solids unit plenum/cyclone/dipleg assembly is described. The major loads considered are thermal, pressure and gravity. Such applications are of interest in the petroleum industry since the equipment described is historically critical, and, to the best knowledge of the author, has not previously been fully analyzed.

INTRODUCTION

Traditionally, mechanical equipment engineers at Exxon design and specify certain pressure vessel internals which are deemed critical to good process unit performance. Of the many unit operations carried out in a refinery, the design of the internals for the fluid solids process presents perhaps one of the most difficult challenges to the designer. Until recently, such designs were based upon many years of cumulative company experience, and whatever strength of materials and pressure vessel code approximations were available. This paper deals with the relatively new application at Exxon of design by use of numerical analysis computer codes. This change in approach has occurred for a number of reasons, including continually increasing thermal and pressure loadings for greater processing efficiency, higher cost of labor and materials and the availability of numerical computer codes such as NASTRAN. This paper describes the first plenum chamber/cyclone/dipleg assembly numerically analyzed at Exxon.

STRUCTURAL LOADINGS IN THE FLUID SOLIDS REGENERATOR

A brief description of the fluid solids process is essential to understanding the nature of the loadings on fluid solids unit internals. Figure 1 is a schematic drawing of the process flow. In the reactor, oil is "cracked" at high temperature in the presence of a finely divided fluidized catalyst. This cracked gaseous hydrocarbon passes through several stages of cyclones to recover the catalyst, through the reactor plenum and out for further processing. The cracking process leaves a carbon deposit on the catalyst, which is continuously transferred to a regenerator where the carbon is burnt off. The combustion gases pass through several stages of cyclones, a plenum and from there out of the regenerator.

Both vessels are internally lined with an insulating refractory. However, since air is injected to cause combustion, the regenerator plenum runs at a higher temperature (usually 650 to 750°C) and is, therefore, structurally much more critical than the reactor plenum. Occasionally, combustion occurs for short periods in the dilute phase above the fluid bed, and, in the cyclones. This can raise local cyclone temperatures by several hundred °C during an upset.

In addition to the thermal loadings described above, another major loading occurs due to the pressure differential across the cyclone stages separating the plenum from the reactor. This differential is usually about 14 kPa but may double during unit upsets.

The final major loading is the gravity loading. In addition to the structural masses of the diplegs, cyclones and plenum, there exist substantial nonstructural mass gravity loadings due to erosion-resistant refractory linings in the cyclones and, in some applications, the mass of catalyst in a plugged cyclone.

PHYSICAL LAYOUT AND MODELLING ASSUMPTIONS

Figures 2 and 3 give the plenum planform and elevation for the particular regenerator plenum which was analyzed. In this application, the plenum is joined to the head by an inner and outer skirt. There are ten primary/secondary cyclone pairs which are arranged with the primaries alternately inside and outside the secondaries. The secondaries are supported directly from the plenum floor, whereas the outer and inner primaries are partly supported by rods. Determination of rod loads under the various loadings was one of the objectives of the analysis.

As shown in Figure 2, a 36° segment of the planform was modelled. Since only symmetrical loadings were applied, symmetry boundary conditions were enforced along these meridional planes. Study of Figure 2 will show that true symmetry is not quite satisfied along these boundaries. However, the approximation is close, and, furthermore, the usual compromise with cost must be made. Future NASTRAN levels which permit periodic symmetry will be of great value in such applications.

The model is delineated circumferentially as shown in Figure 3. Displacement boundary conditions for the skirt cylinders were calculated by hand.

In setting up the load cases for the NASTRAN analysis, three general load categories were recognized, i.e., gravity, pressure, and thermal. Since the thermal displacement boundary conditions along the circumferential cuts were at least one order greater than pressure displacement boundary conditions, thermal displacement boundary conditions were assumed for all loadings in the region, and a separate load case was run for the thermal displacement boundary conditions alone. This permitted all solutions to be developed with only one decomposition and the use of the NASTRAN LOAD and SUBCOM cards.

Figure 4 shows the coordinate systems utilized in mesh generation. The ability of NASTRAN to accept multiple coordinate systems worked to great advantage in applying in-house computer codes for mesh generation.

THE NASTRAN MODELS

The complete model is shown in Figure 5. Figure 6 shows the upper portion of the model in more detail. CQUAD2 and CTRIA2 bending/membrane elements were used to model the cylindrical skirts, the head, the floor and part of the secondary cyclone barrels. These cyclone barrels were terminated one cylinder decay length below the floor by a CBAR beam element "spider" at which point a transition was made to stepped CBAR beam elements to model the remainder of the cyclone, the dipleg, and the dipleg bracing. The primary cyclones, their diplegs, and the connecting ducts between primary and secondary cyclones were all modelled using CBAR beam elements. The hanger rods were modelled using CROD rod elements. COMMEM membrane elements were used for the floor beams.

As mentioned earlier, separate models were developed for the outer cylinder skirt to head intersection. In addition to a high meridional thermal gradient in this area, there is a change in material properties where the stainless steel skirt joins the cooler mild steel shell. By studying stress response to thermal fields arising from various insulation and structural arrangements of the skirt cylinder, it was possible to optimize this detail.

The model in Figure 7 is a symmetry wedge of this skirt to head intersection which utilizes a pad plate. The "tails" are sufficiently long such that temperature boundary conditions calculated from one-dimensional solutions could be applied at the ends. For the plate elements, film coefficients and environmental temperatures on either side were combined to form an equivalent one-sided film coefficient and environmental temperature. In the solid elements film coefficients and environmental temperatures were applied in the usual way, except for the gap behind the pad plate. Here, the environmental temperature was guessed, and an iterative approach adopted.

Symmetry conditions were enforced on the meridional planes for both thermal and stress solutions. In both cases, the number of unknowns was halved by using multipoint constraints, NASTRAN MPCs, to tie like meridional points. NASTRAN, CHEXA2, and CWEDGE solid elements were used in the junction zone and CQUAD2 plate-membrane elements were used in the "tails".

Figure 8 shows an alternative model studied wherein the junction between stainless and mild steel components is located 5 cm below the intersection point. Boundary conditions were developed as described previously for the solid model. This model consists entirely of CQUAD2 elements.

The large overall model contained 6787 degrees of freedom. It was solved on the IBM 360-168 computer, with high speed multiplier, at a region size of 2048K bytes. The semibandwidth was 279 and there were 258 active columns. The large semibandwidth was due to the lack of a bandwidth optimizer being operational at Exxon at that time. Decomposition time was 2458 CPU seconds.

DISCUSSION OF RESULTS

In assessing the results, much use was made of NASTRAN deformed plots. Because of the different nature of thermal and sustained loads, three general load case categories were established. These are mechanical loads (which consist of pressure and gravity loadings), thermal loads, and combined loads (which are the sum of the first two).

Figure 9 is a meridional cut near the center of the wedge showing underlaid deformations due to mechanical loads. The effects of pressure on the outer skirt and head, as well as the effect of the hanger rod on the head are clearly evident. The effect of the gravity load of the cyclone/dipleg assembly on the floor deformations is also clear.

Figure 10 shows the effect of combined loads along the same meridian. Since the thermal load induced displacement field is at least an order greater than the mechanical load induced displacement field, essentially only thermal displacements can be seen. High local bending at the outer skirt to shell junction can be clearly identified in this plot.

A study of the stress printout showed that the structure as designed, with a few minor modifications, was indeed good for all the intended loads. The design pressure differential across the plenum was found to be easily accommodated within allowable stresses. This was found to be true in spite of the fact that it was twice that which would have been allowed by previously developed empirical procedures. These procedures limit the pressure differential over the planform area to the equivalent gravity effect of the head, floor, cyclones and diplegs.

The one point of very high stress was the junction area between the outer cylindrical skirt and the head under thermal load. Figure 11 shows the underlaid deformed plot of the design utilizing a mild steel pad plate. Figure 12 shows deformation vectors for the design employing a 5 cm long mild steel skirt stub, at which point the junction to the stainless steel skirt is made. Of the two designs, the latter shows lower stresses, and is the one which was finally adopted.

CONCLUSIONS

This analysis has shown that modern applied mechanics computer codes such as NASTRAN can be effectively used in the petroleum industry to remove overly conservative empirical restrictions which have developed over the years. In this instance, not only was the empirical restriction on differential plenum pressure removed, but the analysis also focused attention upon the real area of high stress; namely, the skirt to head intersection. Using NASTRAN heat transfer and structural capabilities, a junction design was developed which brought stresses within allowable limits.

Various improvements planned for future NASTRAN levels would be most valuable now. Specifically, the ability to treat periodic symmetry, as well as the ability to handle constitutive nonlinearities under thermal loadings would be most welcome.

FLOW DIAGRAM OF TYPICAL FLUID SOLIDS UNIT

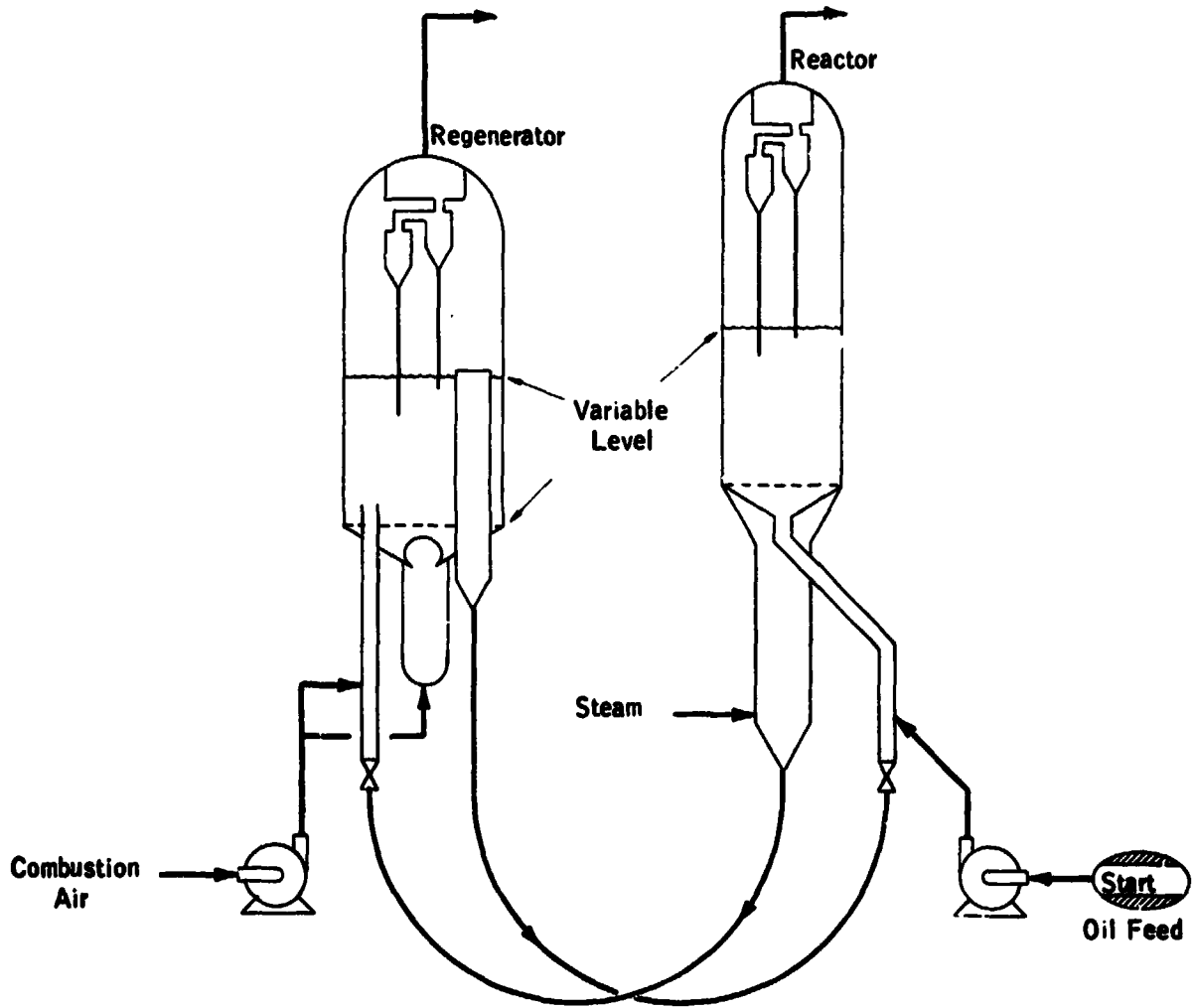


Figure 1

PLANFORM OF PLENUM CHAMBER AND CYCLONES

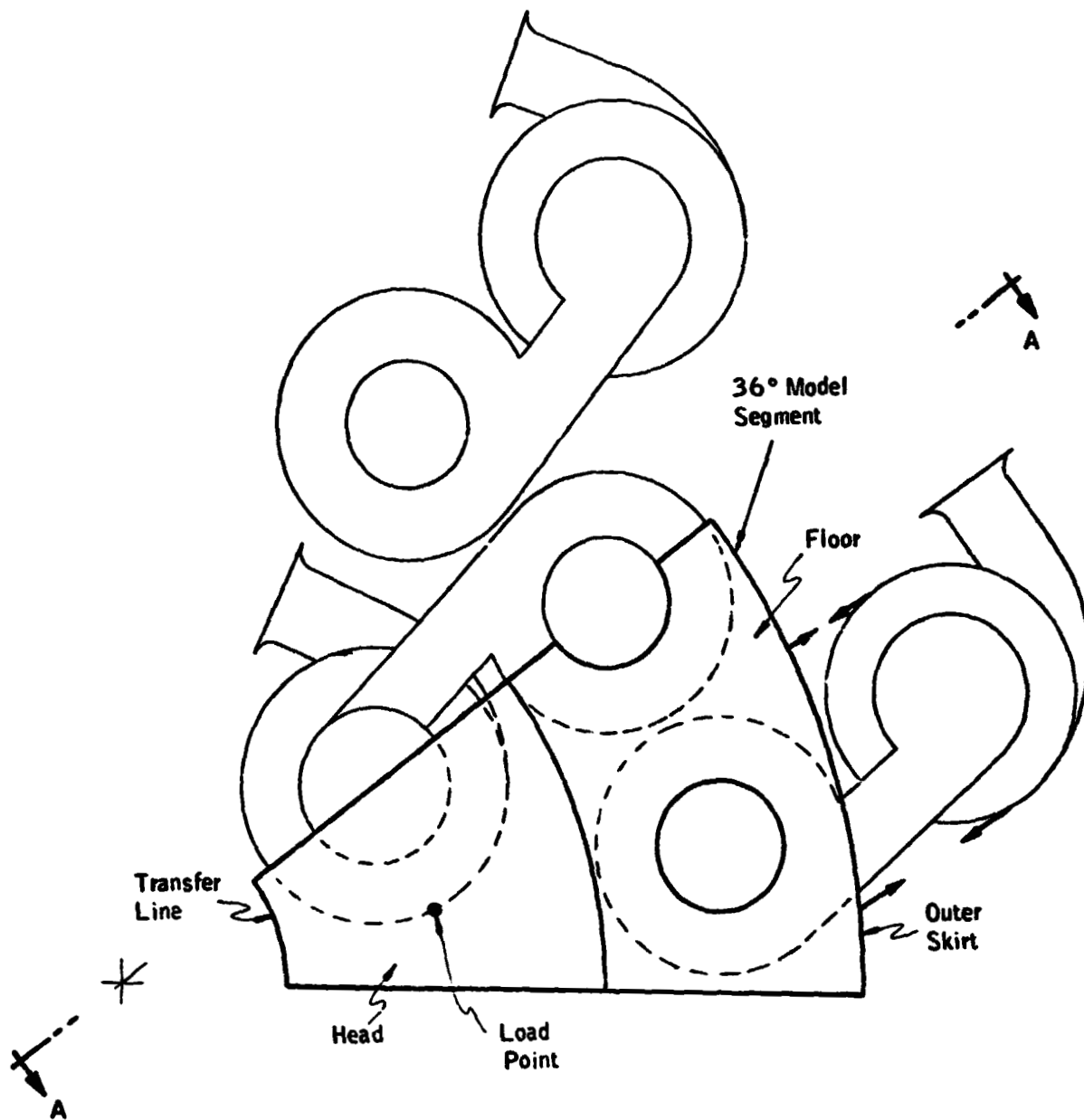


Figure 2

ELEVATION VIEW OF PLENUM CHAMBER AND CYCLONES

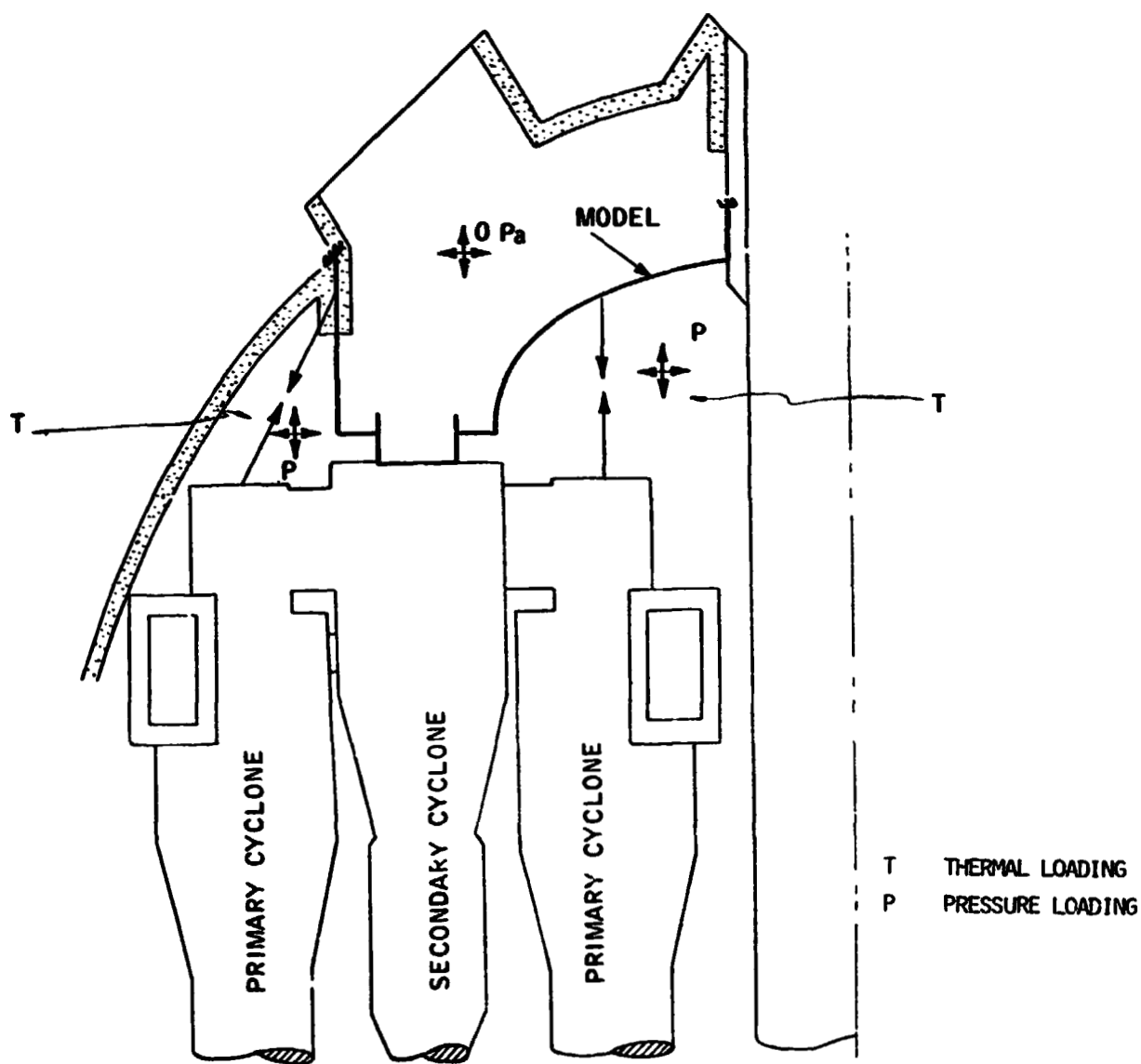
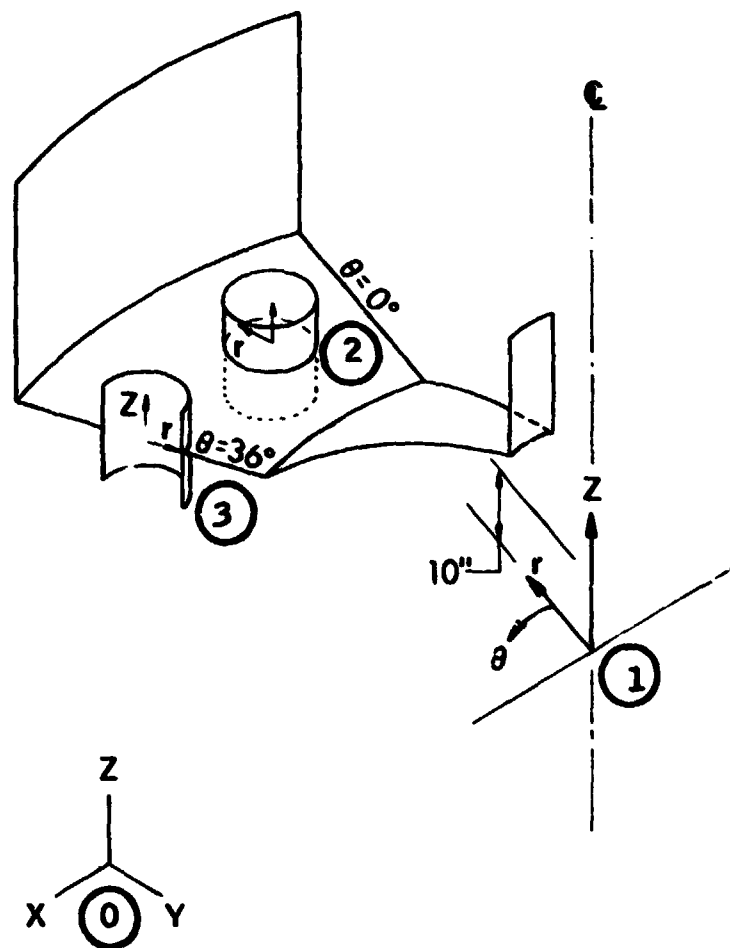


Figure 3

COORDINATE SYSTEM IDENTIFICATION



Notes:

- 0 = Implicit Cartesian System**
- 1 = Cylinder System For Skirts, Floor And Head**
- 2 = Cylinder System For Full Cyclone Barrel and Dipleg**
- 3 = Cylinder System For One-Half Cyclone Barrel and Dipleg**

Figure 4

**PLENUM CHAMBER
OVERALL VIEW**

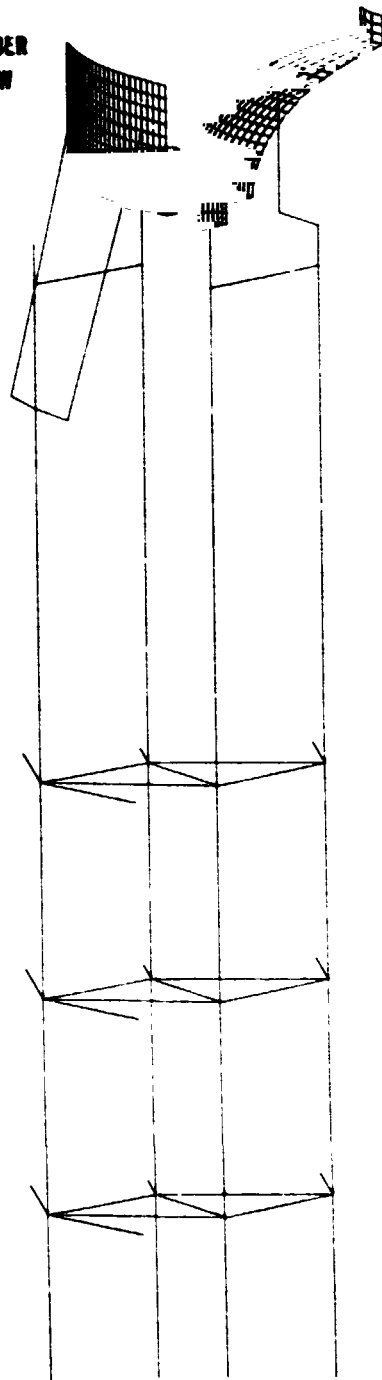
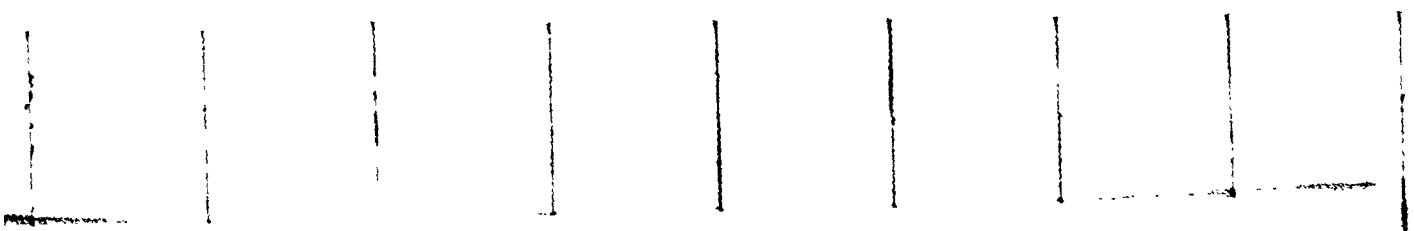


Figure 5



OVERALL VIEW

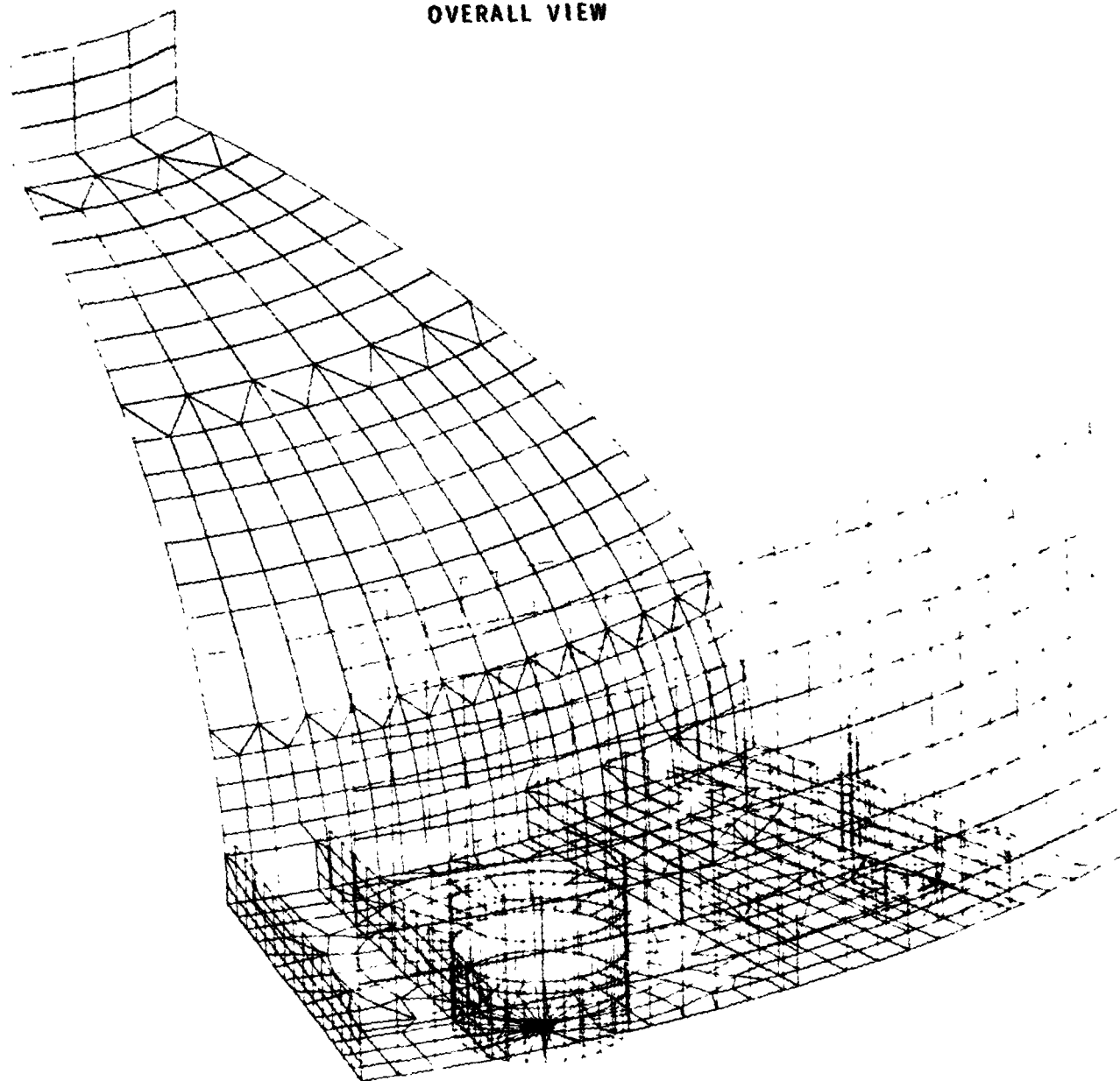


Figure 6

**CARBON STEEL PLATE MOUNTING OF SKIRT TO HEAD
(3-D MODEL)**

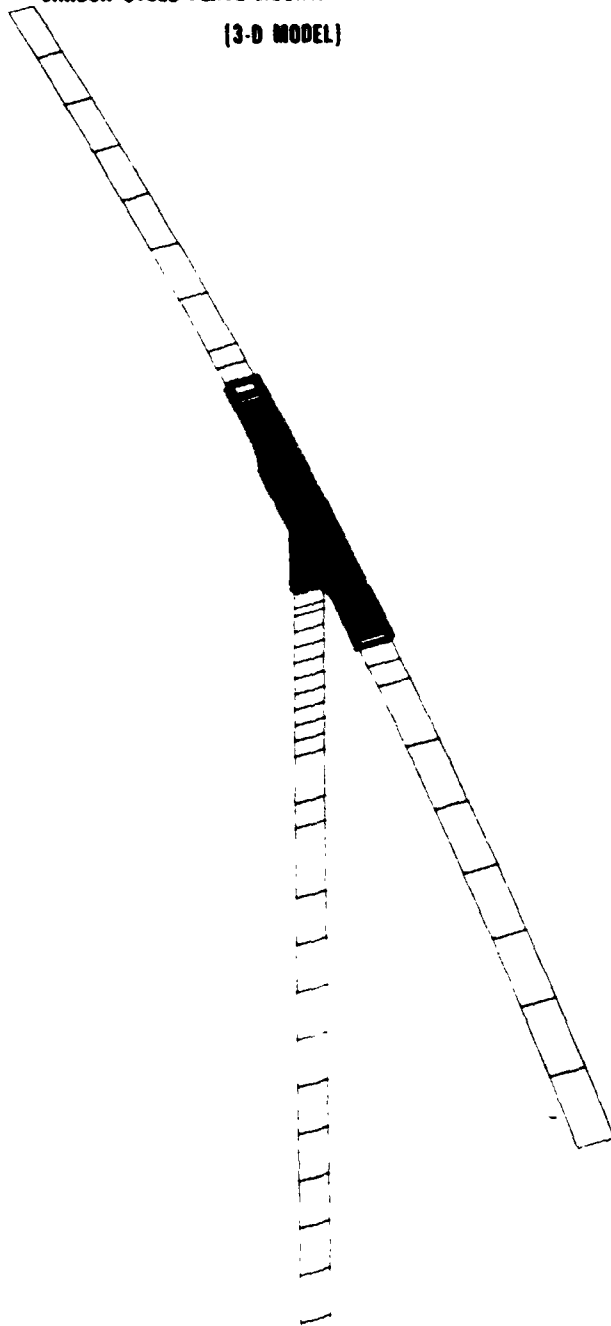


Figure 7

STC'B MOUNTING OF SKIRT TO HEAD
(3-D MODEL)

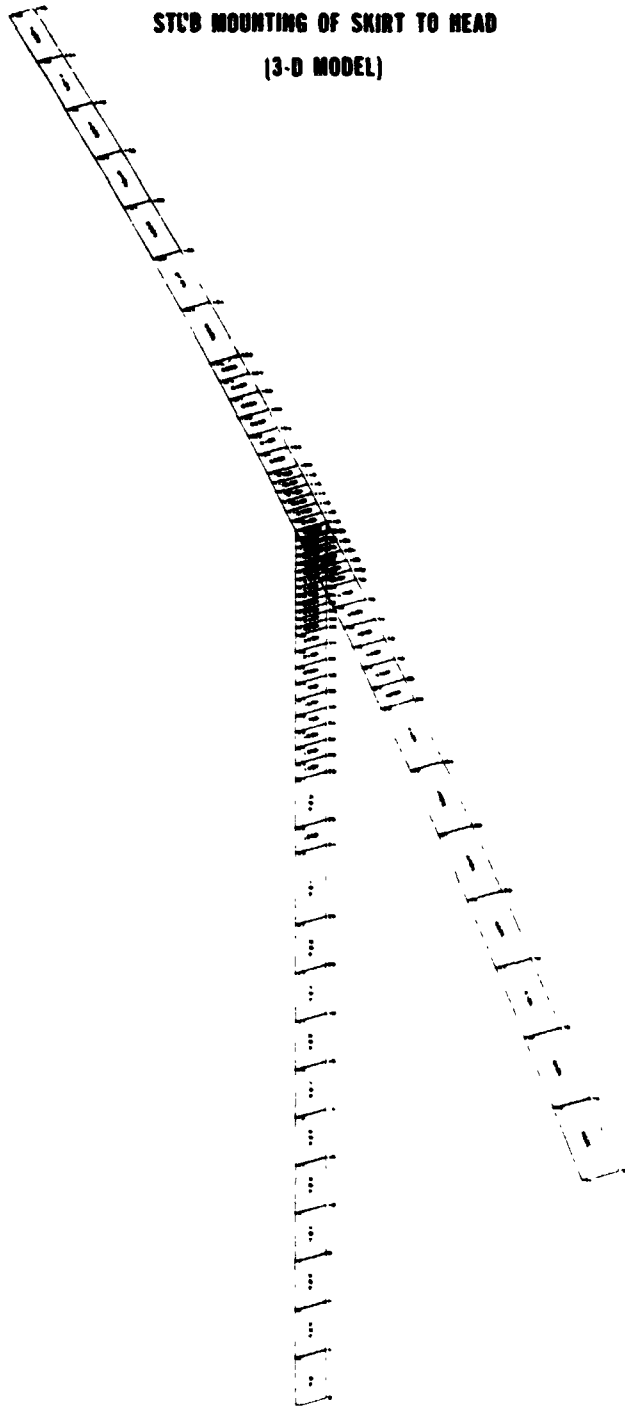


Figure 8

PROFILE VIEW
(UNDEFORMED AND DEFORMED)
MECHANICAL LOADS

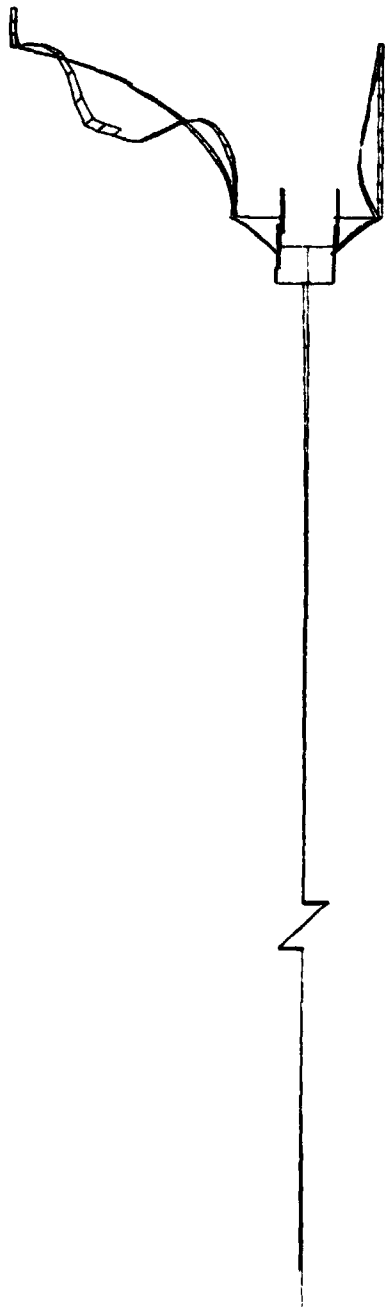


Figure 9

MODEL PROFILE
(UNDEFORMED AND DEFORMED)
COMBINED THERMAL AND MECHANICAL LOADS



Figure 10

**CARBON STEEL PLATE MOUNTING OF SKIRT TO HEAD
(THERMAL STRESS SOLUTION)**

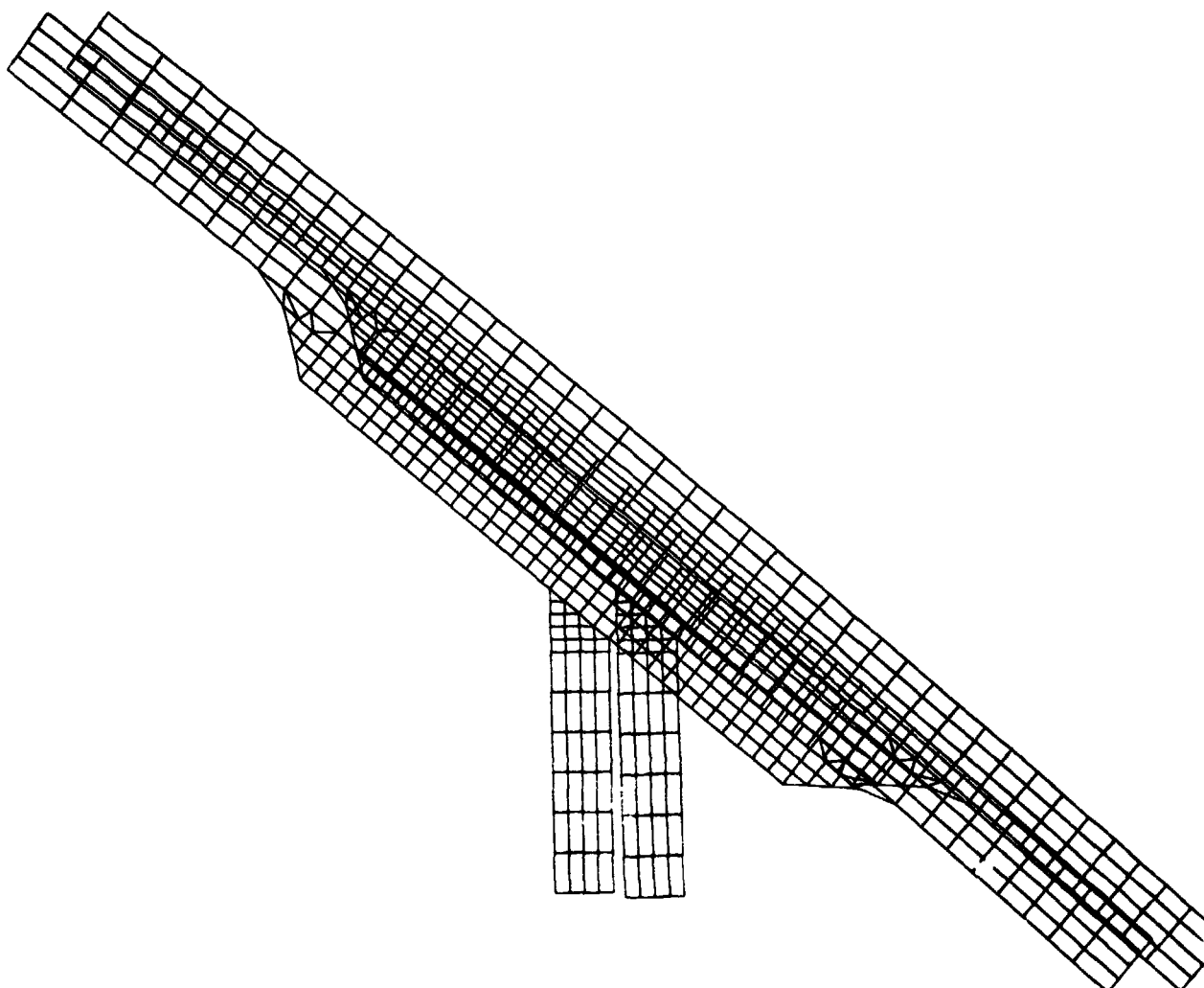


Figure 11

**CARBON STEEL STUB MOUNTING OF SKIRT TO HEAD
(THERMAL STRESS SOLUTION)**

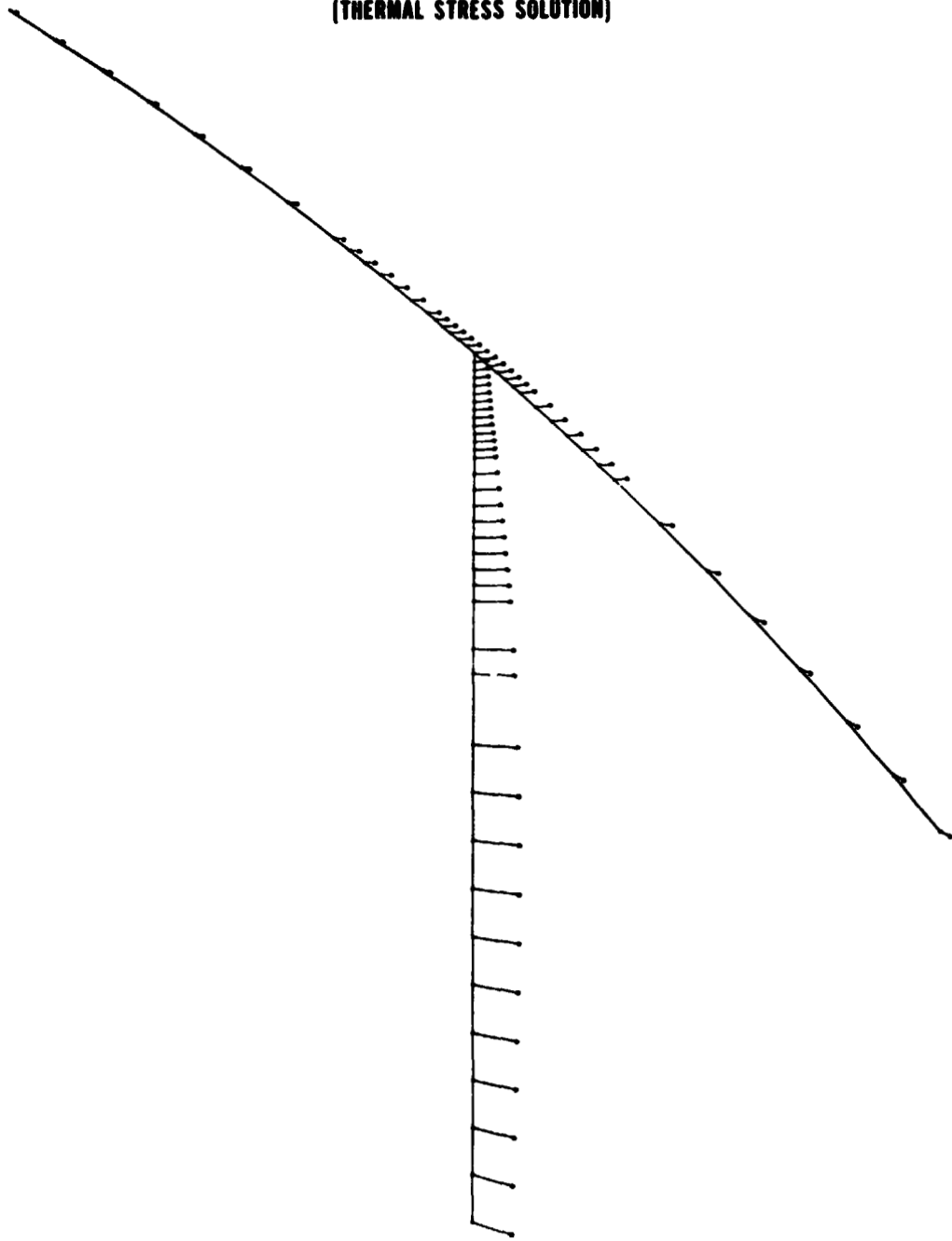


Figure 12

N75 81494

SHUTTLE WING PANEL STABILITY ANALYSIS

T. Balderes, P. Mason, E. Ranalli,
J. Zalesak, and A. Levy

Grumman Aerospace Corporation

SUMMARY

The use of the NASTRAN program in the Shuttle wing stability analysis is described. Details of the actual structure, the finite element idealization, and the NASTRAN results are given. A comparison of the NASTRAN results with those obtained with another computer program and with hand generated results indicates good agreement. An alternate approach for solving eigenvalue problems is illustrated and shows a considerable savings in computer time. Some emphasis is placed on the relationship of the NASTRAN analysis in the design process bringing out more clearly the contribution of the results and showing the importance of the mode plots. Finally, a deficiency in the NASTRAN plate elements when used to model structures made up of intersecting plates is discussed.

INTRODUCTION

The Space Shuttle wing structure (illustrated in Figure 1) is a low aspect ratio double delta with relatively light spanwise compressive load intensity (up to 875 kN/m (5000 lbs/in.) ultimate). The external skin surfaces are required to be buckle free during vehicle operation in order to insure the integrity of the Thermal Protection System (TPS) tiles. These tiles, which are composed of silica fibers, protect the vehicle's aluminum primary structure on reentry such that the maximum temperature is limited to 176°C (350°F). The design consists of closely spaced lightweight stringers which meet the dual requirements of a low cover weight and a buckle free surface. This is fairly typical of structures that have been built around the concept of the optimum compression panel, modified for shear and lateral loading. The stringer that was selected is a roll-formed stretched aluminum and is illustrated in Figure 2. The unique shape of the stringer (eight internal corners and only two hinged free elements) permitted the use of gages as low as 0.65 mm (.022 in.) while maintaining a test crippling strength of 379 MPa (55 ksi).

Large chordwise loads (normal to the stringer) were identified when the thermal loads, resulting from temperature gradients in the primary structure due to reentry heating were calculated from a comprehensive wing-fuselage finite element analysis. These loads which are approximately 175 kN/m (1000 lbs/in.) became critical for design. Modifications to the structure were thus required to overcome the general instability problem of the stiffened cover panels subjected to large chordwise loads. These modifications included the addition of a light riblet midway between the main ribs plus stiffening of the stringer cross section with bulkheads to prevent their distortion.

This paper illustrates how the NASTRAN program significantly contributed to the efforts of the structural analysts in identifying the mode shapes and the critical parameters controlling the buckling strength of the cover panels.

SYMBOLS

A	enclosed area of stringer
D	flexural stiffness of plate = $\frac{Et^3}{12(1 - \nu^2)}$
E	Young's modulus of elasticity
G	shear modulus
$(GI)_{xy}$	average torsional rigidity of plate
I	moment of inertia
J	torsional constant for stiffeners
L	length of plate, distance between main ribs
N	applied load intensity
T	work of external loads
T'	torque
V	strain energy
a	width of plate, distance between spars
b	distance between stiffeners
m	number of half waves in width of plate
t	thickness of plate
w	displacement normal to plate
λ	wavelength parameter
ν	Poisson's ratio
Subscripts:	
cr	critical
p	plate
SB	stringer bending
ST	stringer torsion

DISCUSSION

Structural Model

A typical cover panel, spanning two adjacent spars and two adjacent ribs, is shown in Figure 3. One quarter of the panel (ABCD) which included seven and one-half stiffeners was modeled. Conditions of simple support were imposed on the rib AB to simulate a half sine wave mode existing between ribs on the continuous cover. Simple support conditions were also imposed on spar AD. Symmetric or antisymmetric boundary conditions were assumed along the symmetry planes BC and CD. The finite element model consisted of approximately 570 nodes and 600 plate elements (QUAD2). The modified hat section was modeled as a Y section as shown in Figure 3 with BAR elements added at the base of the Y to obtain the appropriate properties. Although this model represented the basic stiffness of the section, it did not account for the local distortion which proved to be significant. Local distortion of the real stringer can drop the effective torsional stiffness GJ to 12% of the St. Venant value. Connecting the two legs of the stiffener to form a Y produces a closed cell that has a GJ of about 30% of the theoretical value of the modified hat. Note that a Y section when modeled as shown in Figure 3 is virtually distortionless due to the built in truss feature and hence the full torsional stiffness calculated by the St. Venant equations for closed cells is appropriate. This closed cell value, however, is close to an effective value of 40% that would be obtained if the waist of the modified hat is included with the upper cell. This is consistent with the insertion of "blocks" to form stiffening bulkheads in the real stringer.

Figure 4 shows a CALCOMP plot of the NASTRAN model where the cover skin has been separated from the stiffeners for clarity.

NASTRAN Analysis and Results for the Basic Structure

For the NASTRAN analysis Rigid Format 5 was used, employing the inverse power method to obtain the eigenvalues and eigenvectors.

The NASTRAN results, for the basic stiffened panel without modifications, are shown in Figures 5, 6, 7 and 8. Chordwise compressive loading (perpendicular to the stringers) was applied and two different sets of boundary conditions were considered. For the modes depicted in Figures 5 and 6, symmetric conditions were enforced along boundaries BC and CD, while for the modes shown in Figure 7 antisymmetric conditions were applied along BC and symmetric along CD. The first buckling mode (for symmetric conditions) is shown in Figure 5 where the displacements of the skin and the stringers are depicted. Also included is an end view at CD which clearly shows the number of half waves (m) and the location of node lines. Figure 6 shows the next four modes with symmetric conditions. It is noted that the first four modes are coupled; that is, they involve both bending and torsion of the stiffeners while the fifth mode is a pure bending mode since the stiffeners bend only. In a similar fashion the first five buckling modes for the antisymmetric conditions are illustrated in Figure 7. The NASTRAN results have been plotted in nondimensional form against m , the number of half waves in the full

length of the panel, in Figure 8. Note that while the results for the symmetric and antisymmetric boundary conditions are very close, they do not overlap. The reason for this is that the stresses in the prebuckled state are slightly different due to the difference in the boundary conditions.

Comparison of NASTRAN Results

The NASTRAN results can be compared with results obtained with another computer program, VIPASA, which is described in Reference 1. This program treatsismatic structures consisting of long plates connected along longitudinal lines. Thus the cover sheet and stringers were modeled with a series of 0.762-m- (30 in.) long, flat plates. The VIPASA model did not employ a Y-section representation of the stringer, as did the NASTRAN model, but followed closely the actual geometric outline accounting for chem milling patterns as shown in Figure 2. The first five VIPASA mode shapes, along with the critical loads, are shown in Figure 9, for the case of symmetric boundary conditions. The mode shapes obtained with the VIPASA program are identical to those obtained with NASTRAN; however, the order of the modes and the values of the critical loads differ.

A further comparison of the NASTRAN results involved the use of hand computations. Two different approaches were employed. In the first, the stiffened cover panel was treated as an orthotropic plate, and in the second, the energy method was used to obtain critical loads. Figure 10 illustrates the application of orthotropic plate theory to the stiffened panel. The governing equations (see Reference 2) together with the assumed mode shape, which takes on a half sine wave along the length of the stiffeners and varies in the other direction, are shown. Note that the orthotropic plate equations in Figure 10 neglect the torsional stiffness of the stiffeners and coupling between the membrane and bending stresses due to the shift in the neutral axis. The coupling effect can be taken into account by employing a more general orthotropic plate theory as in Reference 3. However, this leads to a complicated set of equations which must be solved using a computer. Furthermore, in the calculations employed herein, ν_x was taken to be zero and the stringer contribution to $(GI)_{xy}$ (the plate torsional rigidity) was neglected. Results are shown in Figure 8. Note that while the overall trend agrees with the NASTRAN results in general, lower buckling loads were obtained with the difference decreasing with m .

The use of the energy method is shown in Figure 11. Here a mode shape was assumed, and the strain energy due to plate bending, stringer bending and torsion and the potential of the applied loads was computed. Application of the principle of minimum potential energy then resulted in a value for the buckling load. Five different modes were assumed which are depicted in Figure 12 together with the respective buckling loads. Note that in this approach the interaction between the stringers and the plate is not fully accounted for. As shown in Reference 2 this interaction is a function of the mode shape. An approximate way of accounting for this effect is suggested by Timoshenko in Reference 4 and involves computing the moment of inertia of the stringers about the bottom of the plate. The torsional constant for the stiffeners was taken as 30% of the theoretical value of the modified hat section so that consistency with the finite element model is maintained. Results obtained with the energy method are also plotted in Figure 8 and show excellent agreement with the NASTRAN results.

Use of the ALARM Subprogram

The aforementioned NASTRAN analyses had between 2724 and 2853 degrees of freedom. Computer time is listed in Table 1. Also of considerable importance is the elapsed time or wall time which ranged from 5 to 10 hours for these runs. With such extensive computer residence periods, the computing system reliability becomes an important factor. In fact several computer system "crashes" were experienced during this effort which resulted in lost calendar time.

For these reasons, and in anticipation of analyses with an even greater number of degrees of freedom, an alternate approach was investigated for solving large eigenvalue problems. The concept was to use a very fast eigenvalue solution algorithm developed by Ojalvo and Newman (Reference 5) which was implemented into a working program for a NASA contract (Reference 6). This subprogram, called ALARM (Automatic Large Reduction of Matrices) employs an automatic tridiagonal reduction technique which is identical to the FEER routine described in Reference 7. The procedure was to generate the stiffness and incremental stiffness matrices in NASTRAN and then to use ALARM to obtain the desired number of eigenvalues and eigenvectors. The modes were then passed back to NASTRAN to be plotted. Table 2 shows a comparison of the eigenvalues obtained from NASTRAN and ALARM. The savings in computer time is evident from the comparison depicted in Table 3, which shows that the NASTRAN-ALARM-NASTRAN procedure reduced the computer cost by two-thirds. It should be noted that the ALARM values given in Table 2 are for the 17th iteration, and that after the first iteration the first five eigenvalues agree with those in Table 2 to four figures. Thus, the number of iterations could be cut to 2 or 3 which would result in a decrease of one-half in computer time for the ALARM step.

THE RELATIONSHIP OF THE NASTRAN ANALYSIS

TO SHUTTLE WING DESIGN CONSIDERATIONS

In the previous discussion comparisons have been made between the NASTRAN results and values obtained by using other approaches. It is advantageous to attempt to tie the various analytical and design activities together to obtain a more comprehensive view of the problem. Figure 13 illustrates the relationship of several activities that have taken place relative to the Shuttle Wing instability problem.

Initially all stability calculations were performed using hand methods (energy techniques using assumed mode shapes). Obviously these methods are limited, the results being only as good as the assumed mode shape. Attempting to guess at the lowest mode for overall instability can be difficult if not impossible (needless to say it is dangerous as well). Thus the NASTRAN analysis was undertaken to provide an overall check on the assumptions that were employed in the hand calculations. As such, the first NASTRAN analysis duplicated the design without the intermediate riblet, while the second analysis incorporated the riblet. The main purpose of the riblet is to prevent the mode that consists of alternate bending of the stringers. Having prevented this type of motion, it was discovered from the NASTRAN analysis that the stringer was still twisting as it passed over the intermediate riblet. (See Figure 14(a).) In order to prevent this, it was decided to control the clearance between the stud and the flange of the riblet (see Figure 15), such that when the stringer twisted it would come into contact with the flange of the riblet. The riblet flange was modeled as a tie bar and the results of this modification are shown in Table 4 and Figure 14(b).

Cross-sectional NASTRAN plots indicated that the stringer section was still distorting as it passed over the riblet. At this point we began to question the adequacy of the NASTRAN representation of the torsional stiffness of the stringer and in fact the effective GJ of the real stringer. To answer some of these questions a series of stiffener studies was initiated. An individual stringer and a .102 m (4 in.) width of skin was modeled as an assemblage of bars, beams, torque tubes and shear panels. This model more accurately preserved the geometric shape of the real stringer. The model was analyzed for a sine wave distribution of torque applied at the skin stringer attachment and for a concentrated torque applied at the end of the .381m (15 in.) length. Results of this latter analysis were correlated with test data. A cross-sectional plot of the model and the deformed shape at different stringer stations is shown in Figure 16. Note the severe bending distortion of the cross section at the loaded end and that the distortion decreases with the stringer station. If the stringer were long enough, the distortion would completely disappear, an indication that the total torque would then be taken by St. Venant torsion. The sine wave torque loading (comparable to the distribution of torsion that the stringer would have to resist to prevent buckling) was used to calculate an effective GJ value for the stringer. The calculated value was approximately 12% of the St. Venant torsional stiffness. At this point several design changes were considered. These included adding "blocks" at various spacings which tied the two sides of the stringer together at the waist (see Figure 17(a)). This scheme tends to mobilize the upper portion

of the stringer. A second concept was to insert a vertical "spike" through the stringer to tie the cover to the bottom and two sides of the stringer (see Figure 17(b)). This scheme is far more effective than the block scheme but also weighs more. A third possibility was also initiated, which was to investigate an alternate stringer concept that would not be subject to large distortion under torsional loading.

The Shuttle Wing design 101 used a combination of blocks and spikes. A spike was placed adjacent to each of the riblet attachment points. This configuration was investigated by modifying the previous NASTRAN model. The results of the analysis are shown in Table 4. The final NASTRAN analysis consisted of adding a beam element to the skin parallel to the intermediate riblet. This last modification which prevented bending of the skin along the riblet did little to increase the buckling allowable.

Some concern was developed at this time over the adequacy of elements in NASTRAN to predict the buckling behavior of structures composed of QUAD2 plate elements that intersect at an angle. In the QUAD2 elements, the inplane motion is assumed to be linear between node points while the out of plane motion is essentially a cubic. An incompatibility problem thus inherently exists such that elements connected at angles to each other do not continuously reinforce one another, but instead are "stitched" together at the nodes. In addition to this, the elements lack torsional stiffeners normal to their plane. Thus, as a separate study, the QUAD2 elements were used to obtain the buckling modes of an equal leg angle column. It was discovered that while the torsional buckling mode of the angle could be obtained using a refined grid, convergence was from the low side. Furthermore, some peculiar modes were observed and the Euler buckling mode could not be obtained. In order to clarify this problem, an investigation to determine the applicability of higher order plate elements (as described in Reference 8) has been initiated. These concerns caused us to turn to an alternate analytical approach, the VIPASA program. VIPASA can model continuous structure in detail. It cannot, however, account for discrete stiffening or items that do not fit into a Fourier series expansion. The correlation of the VIPASA results has been discussed previously.

As discussed above, work was initiated to develop an alternate stringer concept with the prime goal of minimizing the local distortion. This involved the analysis of a typical unit width of stringer with a torsion load applied at the skin line which is balanced with a $\left(\frac{T}{2A}\right)$ shear flow distribution. The stringer behaves as a frame, and hence has an internal force and moment distribution. Dividing the moment by the force gives the location of the load line. The geometric shape of the stringer was then modified to straddle the load line, keeping in mind other considerations such as local crippling requirements, fabrication restrictions and clearances dictated by the present design. The process of analysis and geometric modification was iterated until a stringer of the shape shown in Figure 17(c) was obtained. The effective GJ of this stringer is approximately 5 times the effective GJ of the unreinforced modified hat. Work is not yet complete on this concept but strong consideration is being given to it for inclusion in future Shuttle Wing designs.

A useful plot that illustrates the effects of the various design parameters is shown in Figure 18 where the critical stress is plotted as a function of the

unsupported stringer length. The plot was obtained using the energy equations given in Figure 11. The plot illustrates the improvement in allowable buckling stress in using the frame stiffened hat over the modified hat. Buckling stresses are indicated for a range of modified hat effective GJ values; the particular value within the range depends on the combination of block and spike spacing and stringer length. Note that the effective GJ for a stringer varies with length and is equal to the St. Venant value at $L = \infty$ and virtually zero for $L = 0$. It also should be noted that from a practical point of view one can question the real effectiveness of the blocks and spikes as these quantities are related to various manufacturing procedures. The four lowest NASTRAN values from Table 4 have been superimposed on the plot at spacings of 0.762m (30 in.) and 0.381m (15 in.). NASTRAN analysis I did not include the riblet; analysis II did but did not prevent twisting at the riblet support (hence it is lower than the value predicted by the hand calculations which tacitly assume zero rotation at the supports). NASTRAN analysis III prevented rotation at the support but not distortion. Analysis IV prevented rotation and distortion by inserting a spike at the riblet.

The plot also indicates the improvement in buckling stress due to inserting the riblet (spacing changes from 0.762m (30 in.) to 0.381m (15 in.)) which prevents the first bending mode.

It is important to note that simplified tests of the stiffened panel, under transverse compressive loading, correlated well with some but not all of the analytical results. In general, the large strength increases in the bending and coupled modes due to the addition of the riblet were attained. Also, the improvement in the effective torsional stiffness of the stringer with the block and spike modifications was corroborated. For the torsion modes, however, an effective length reduction from 0.762m (30 in.) to 0.381m (15 in.) proved difficult to attain. Subsequent analysis, using hand computations, showed that these lower than expected strength levels could be traced to the low torsional stiffness provided at mid bay. In effect the torsional restraint at the riblet was too flexible and allowed twisting as the plate buckled. This agreed with test observations. These results demonstrate the need to provide and model accurately the local stiffness which affect the behavior of the actual structure.

CONCLUDING REMARKS

The use of the NASTRAN program in the stability analysis of the Shuttle wing panels has been described. Moreover, the role of the NASTRAN analysis in the design process has been discussed to illustrate how it impacted the design. The NASTRAN results helped to identify the critical modes and show the importance of the torsional properties of the stiffeners. In this effort, the NASTRAN plots of the mode shapes were indispensable in that they indicated where the fixes should be made and clearly demonstrated their effectiveness. The results indicated that for future analyses (which will include spanwise loading in addition to the chordwise loading to determine the interaction effects) a better representation of the stringers is required.

It was demonstrated that a tridiagonal reduction scheme can greatly reduce the computer cost in solving large eigenvalue problems.

Finally, it was discovered that the plate bending elements in NASTRAN have incompatibilities which can lead to difficulties when the elements are used to model structures made up of intersecting plates. Further work in this area is clearly required to develop a plate bending element which would overcome the present deficiencies.

ACKNOWLEDGEMENTS

Acknowledgement is extended to the many contributors in the effort presented herein. Many of the design concepts were defined by I.G. Hedrick, L. Mead, T. Adey, D. Bone and J. Strakosch; specifically, the development of the frame stiffened hat concept is due to L. B. Wehle. The analysis using the VIPASA program was performed by M. Anderson of NASA Langley. A considerable part of the hand calculations was done by G. Kutz and L. Brown.

REFERENCES

1. Wittrick, W. H., and Williams, F. W., "Buckling and Vibration of Anisotropic or Isotropic Assemblies Under Combined Loadings," Int. J. Mech. Sci., Pergamon Press, 1974, Vol. 16, pp.209-239.
2. Seide, P., "The Effect of Longitudinal Stiffeners Located on One Side of a Plate or the Compressive Buckling Stress of the Plate Stiffening Combination," NACA TN 2873, Jan. 1953.
3. Ashton, J. E., Halpin, J. C., Petit, P. H., "Primer on Composite Materials: Analysis," Technomic Publishing Co., Stamford, CT, 1969.
4. Timoshenko, S. P., and Gere, J. M., "Theory of Elastic Stability," McGraw-Hill Book Co., 1961.
5. Ojalvo, I.U., and Newman, M., "Vibration of Large Structures by an Automatic Matrix Reduction Method," AIAA Journal, Vol. 8, No. 7, 1970, pp.1234-1239.
6. Ojalvo, I. U., Austin, F., and Levy, A., "Vibration and Stress Analysis of Soft-Bonded Shuttle Insulation Tiles," NASA CR-132553, Sept. 1974.
7. Newman, M., and Pipano, A., "Fast Modal Extraction in NASTRAN via the FEER Computer Program," Third NASTRAN User's Colloquium, NASA TM X-2893, Sept. 1973.
8. Pifko, A., Levine, H. S., and Armen, H., Jr., "PLANS--A Finite Element Program for Nonlinear Analysis of Structures - Vol. I - Theoretical Manual," Grumman Aerospace Research Dept., Report RE-501, August 1974.

TABLE 1 - NASTRAN BUCKLING ANALYSIS

MODE SET	NUMBER OF MODES	NO. OF D.O.F.	CFU MIN
1	11	2837	68.90
2	10	2853	81.16
3	10	2724	81.46
4	10	2724	73.51
5	10	2724	95.40
6	4	2724	38.00

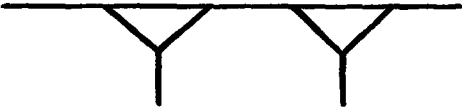
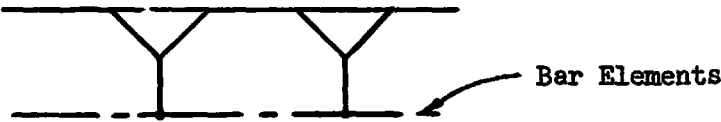
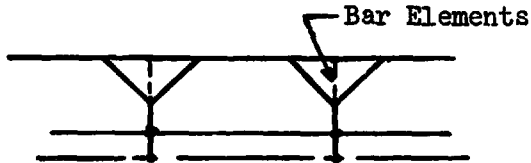
TABLE 2 - RESULTS FOR MODE SET 3

MODE	EIGENVALUE	
	NASTRAN	ALARM
1	.8352054	.8352112
2	.9625223	.9625288
3	1.147742	1.147748
4	1.363301	1.363310
5	1.592074	1.592082
6	1.828479	1.828488
7	2.053671	2.050866
8	2.057875	2.069090
9	2.058429	2.217536
10	2.060794	2.327002

TABLE 3 - NASTRAN-ALARM COMPARISON

	NASTRAN		ALARM	
	CPU	WALL TIME	CPU	WALL TIME
1) LINEAR ANALYSIS	9	72	9	72
2) EIGENVALUE	70	207	19	57
3) PLOTTING & RECOVERY	2	6	2	6
TOTAL	81	285	30	135
SYSTEM MIN.	621.55		224	

TABLE 4 - SUMMARY OF NASTRAN ANALYSES

CASE	N_{cr} , kN/m (lb/in.)		
	Mode 1	Mode 2	Mode 3
<p>I. Basic Structure</p> 	99.2 (566)	100.5 (574)	109.2 (623)
<p>II. Intermediate Rib Added with Vertical and Rotation Supports at Rib Tie</p> 	146.2 (835)	166.7 (952)	201.2 (1149)
<p>III. Tie Bar Added at Top of Intermediate Rib</p> 	215.2 (1229)	240.8 (1375)	271.3 (1549)
<p>IV. Spike Added</p> 	241.8 (1381)	264.3 (1509)	291.2 (1663)
<p>V. Beam Added to Skin Parallel to Intermediate Rib</p> 	242.7 (1386)	257.9 (1473)	280.2 (1600)

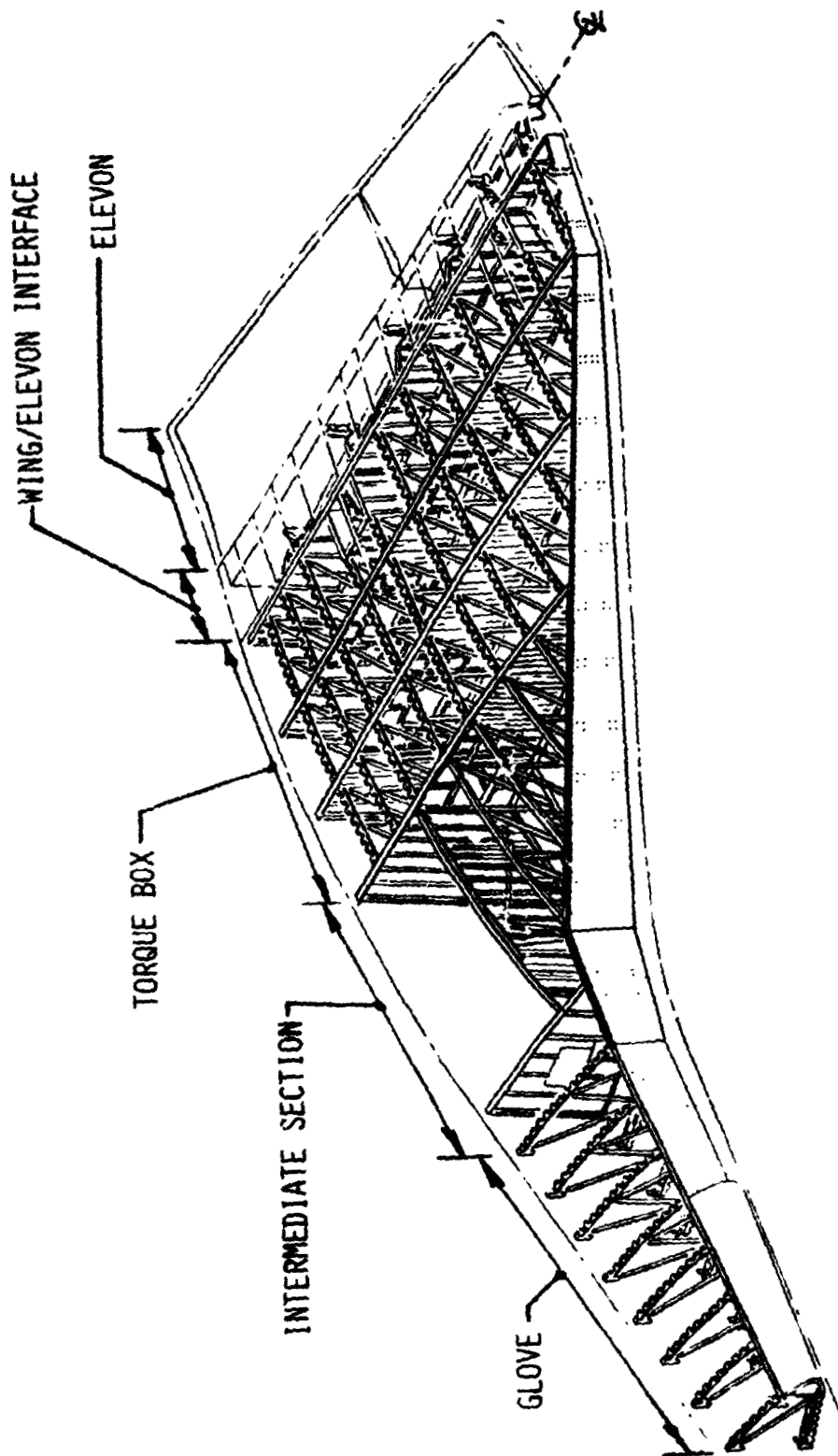


Figure 1.- Shuttle wing structure.

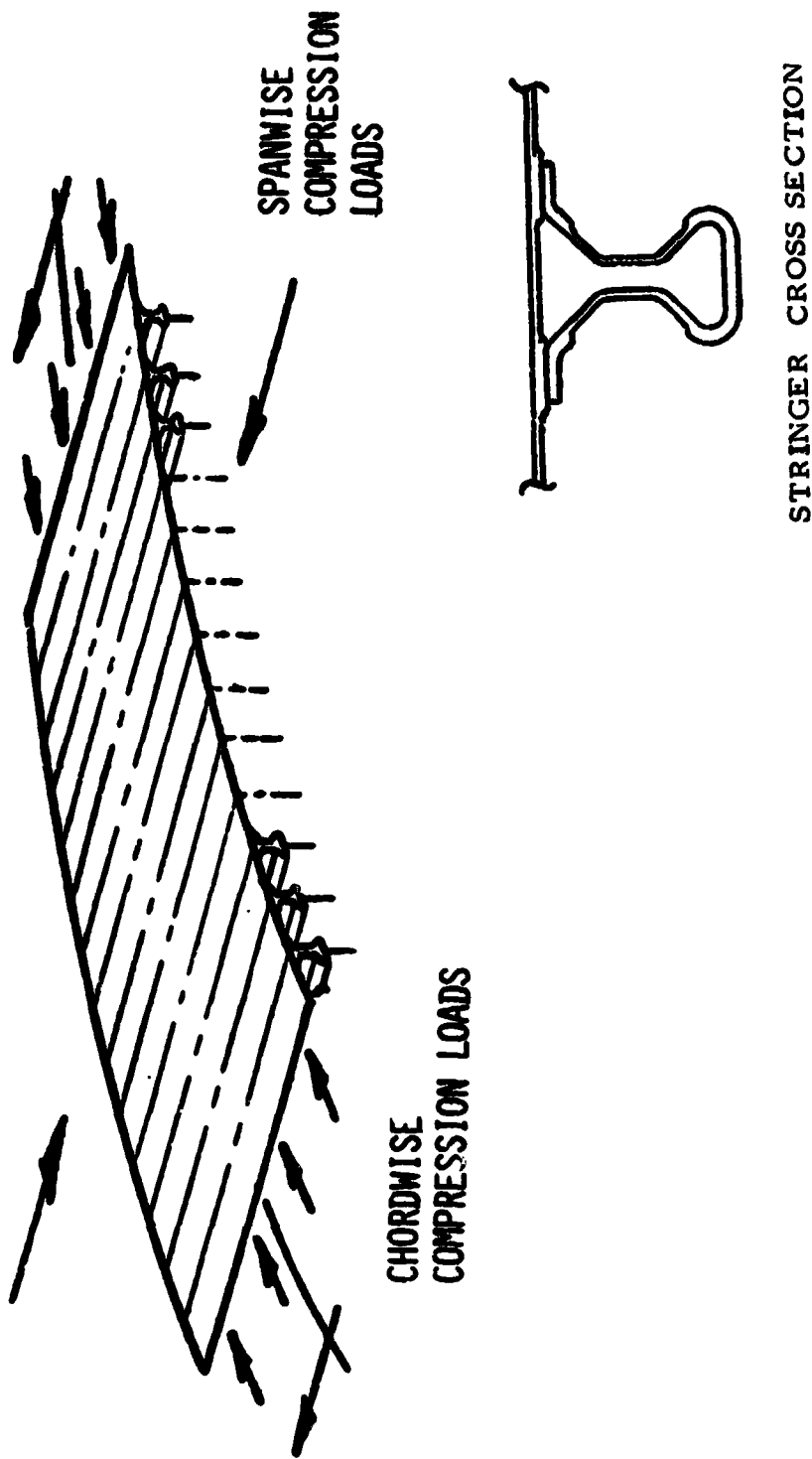


Figure 2.- Shuttle wing cover panel.

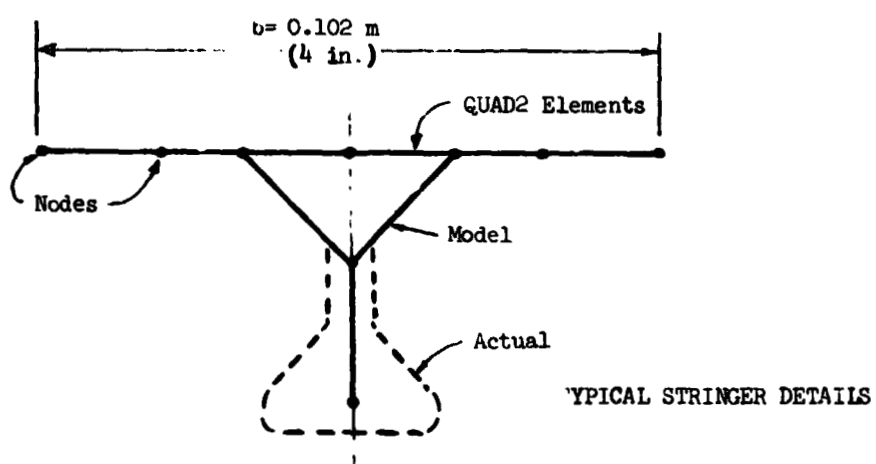
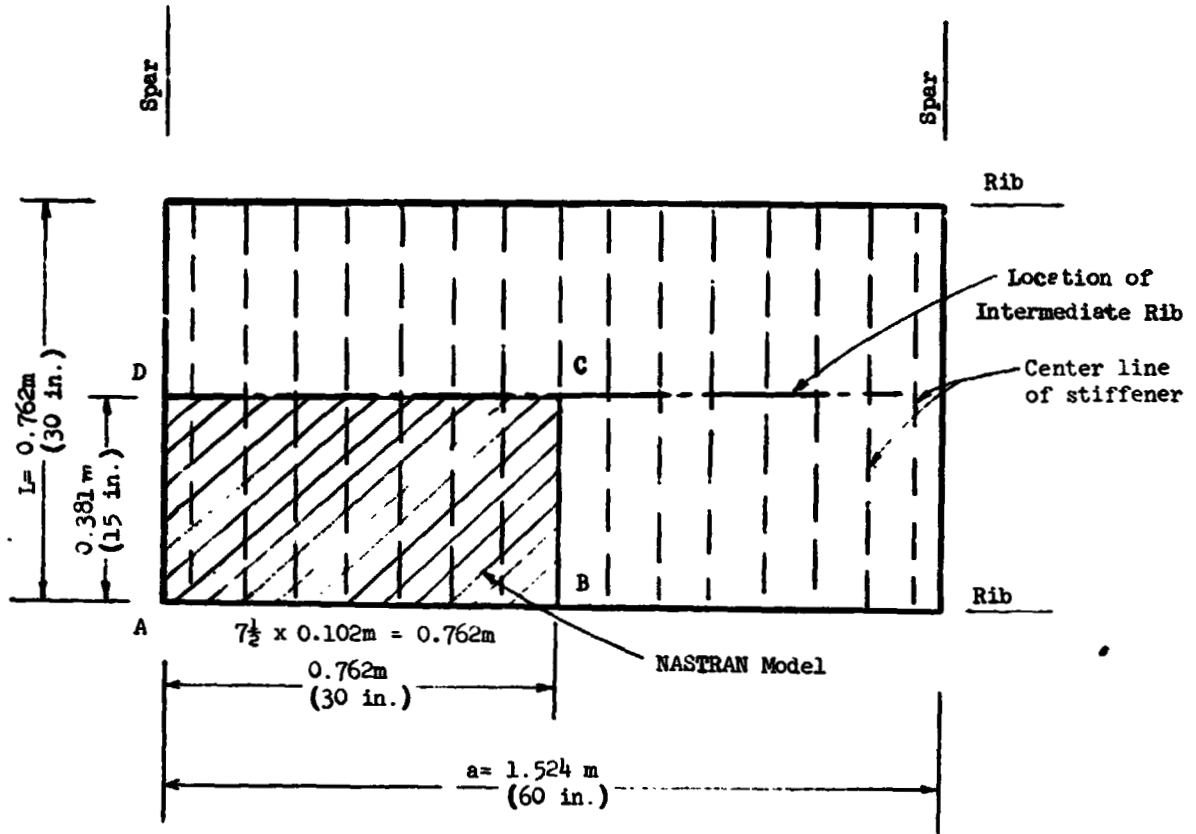
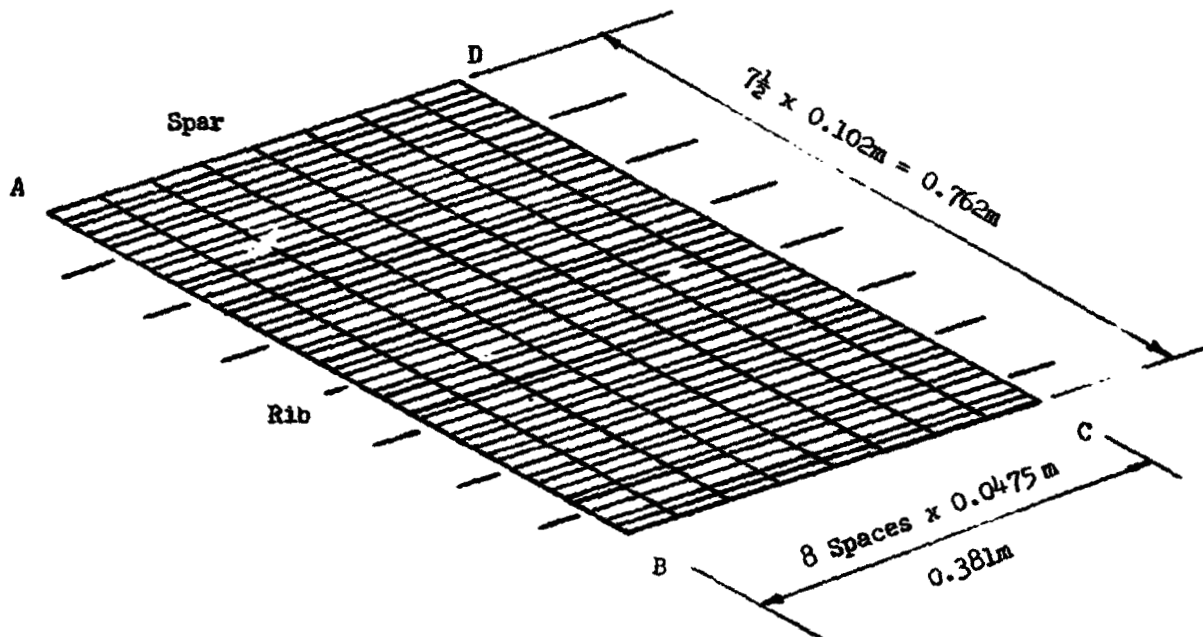
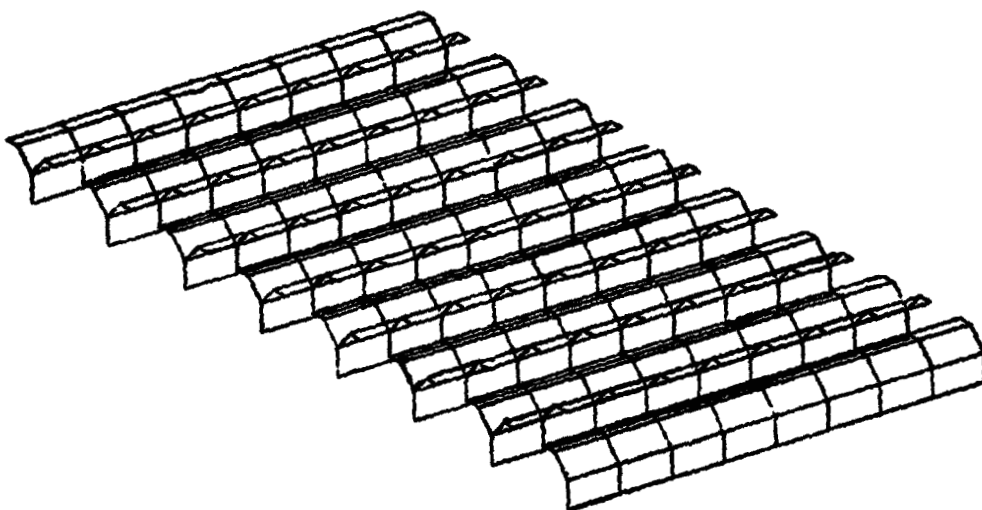


Figure 3.- Shuttle wing panel model.



Cover Sheet



Stiffeners

Figure 4.- Plot of NASTRAN model.



$\lambda = 1.36$, $N_{cr} = 99.17 \text{ kN/m (566 lb/in)}$ $m=11$

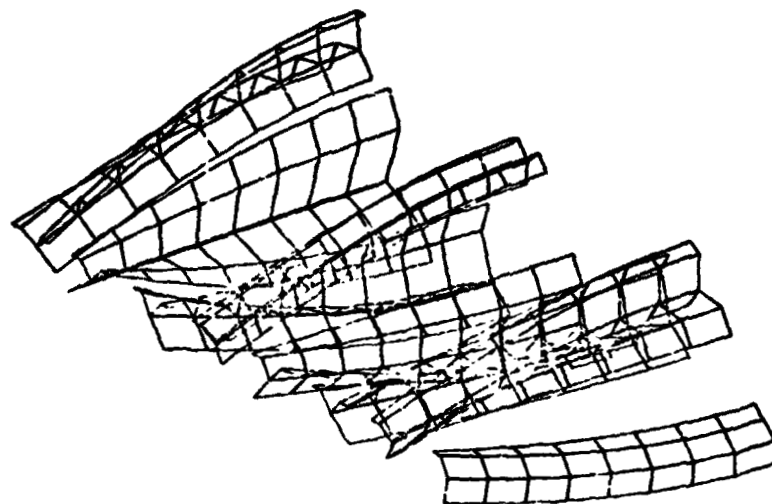
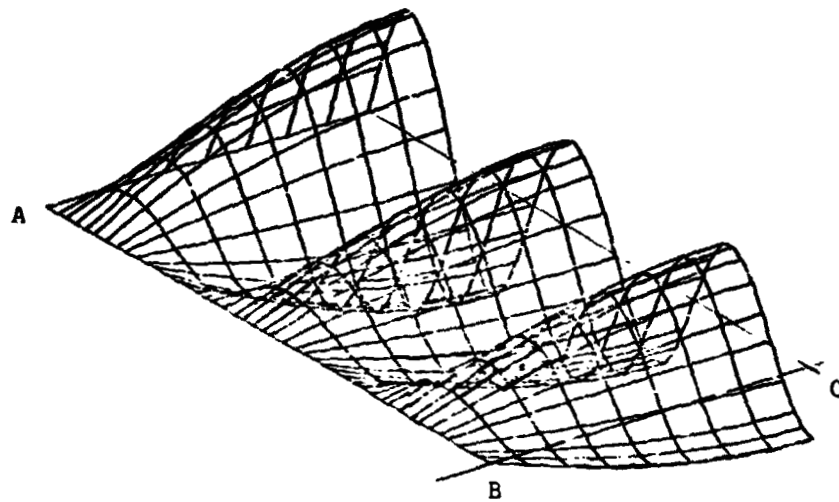


Figure 5.- NASTRAN results - mode 1 - symmetric conditions.



Mode 2 - $\lambda = 1.666$, $N_{cr} = 100.5 \text{ kN/m (574 lb/in)}$ $m=9$



Mode 3 - $\lambda = 1.154$, $N_{cr} = 109.2 \text{ kN/m (623 lb/in)}$ $m=13$



Mode 4 - $\lambda = 2.142$, $N_{cr} = 120.4 \text{ kN/m (688 lb/in)}$ $m=7$



Mode 5 - $\lambda = 1.0$, $N_{cr} = 129.0 \text{ kN/m (737 lb/in)}$ $m=15$

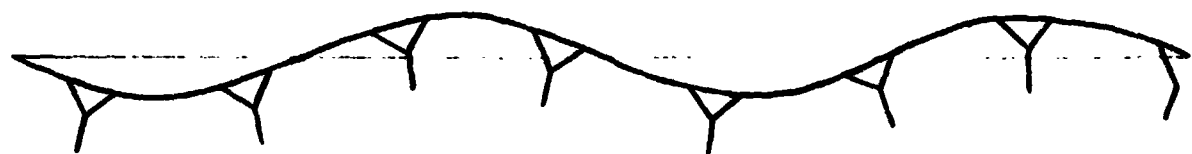
Figure 6.- NASTRAN results - modes 2-5 - symmetric conditions.



Mode 1 - $\lambda = 1.5$, $N_{cr} = 96.5 \text{ kN/m (551 lb/in)}$ $m=10$



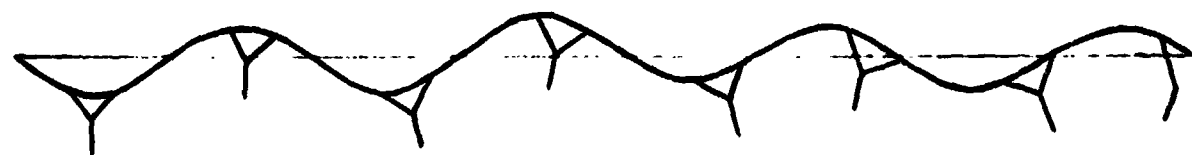
Mode 2 - $\lambda = 1.2666$, $N_{cr} = 101.6 \text{ kN/m (580 lb/in)}$ $m=12$



Mode 3 - $\lambda = 1.875$, $N_{cr} = 105.1 \text{ kN/m (600 lb/in)}$ $m=8$



Mode 4 - $\lambda = 1.071$, $N_{cr} = 114.5 \text{ kN/m (654 lb/in)}$ $m=14$



Mode 5 - $\lambda = 0.9375$, $N_{cr} = 134.9 \text{ kN/m (770 lb/in)}$ $m=16$

Figure 7.- NASTRAN results - modes 1-5 - antisymmetric conditions.

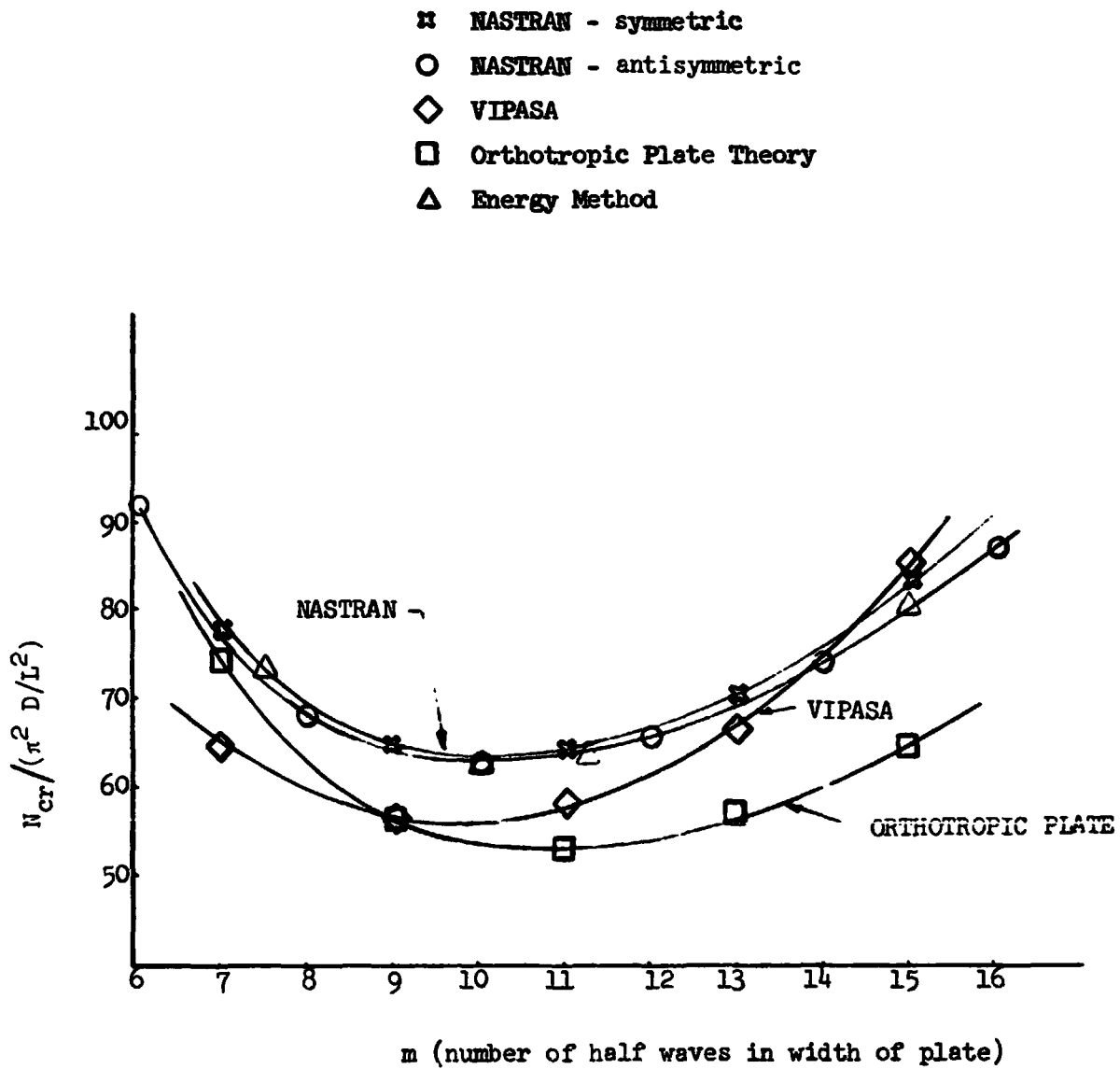
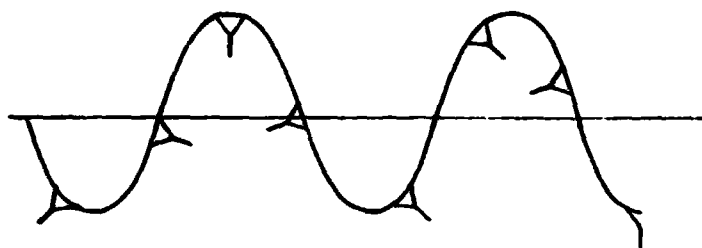
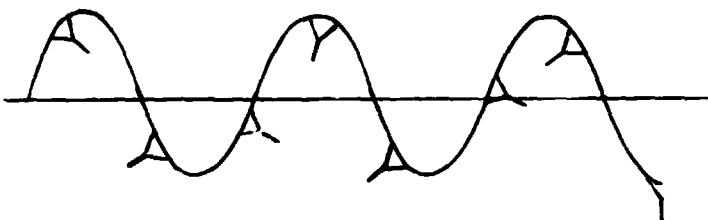


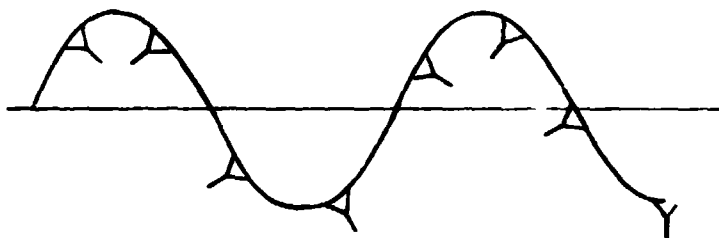
Figure 8.- Comparison of results.



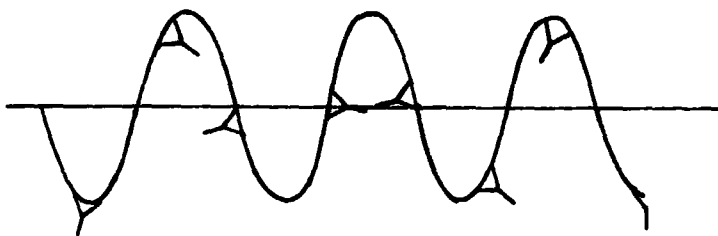
$N_{cr} = 86.8 \text{ kN/m (496 lb/in)}$
 $\lambda = 1.666$
 $m = 9$



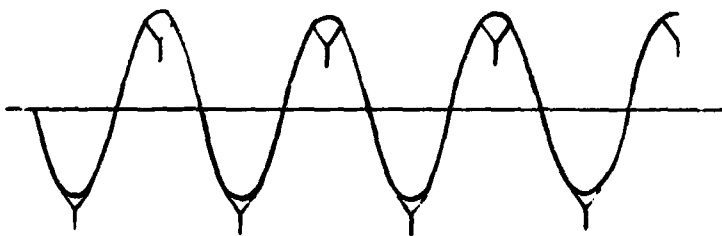
$N_{cr} = 90.2 \text{ kN/m (515 lb/in)}$
 $\lambda = 1.30$
 $m = 11$



$N_{cr} = 99.6 \text{ kN/m (569 lb/in)}$
 $\lambda = 2.142$
 $m = 7$

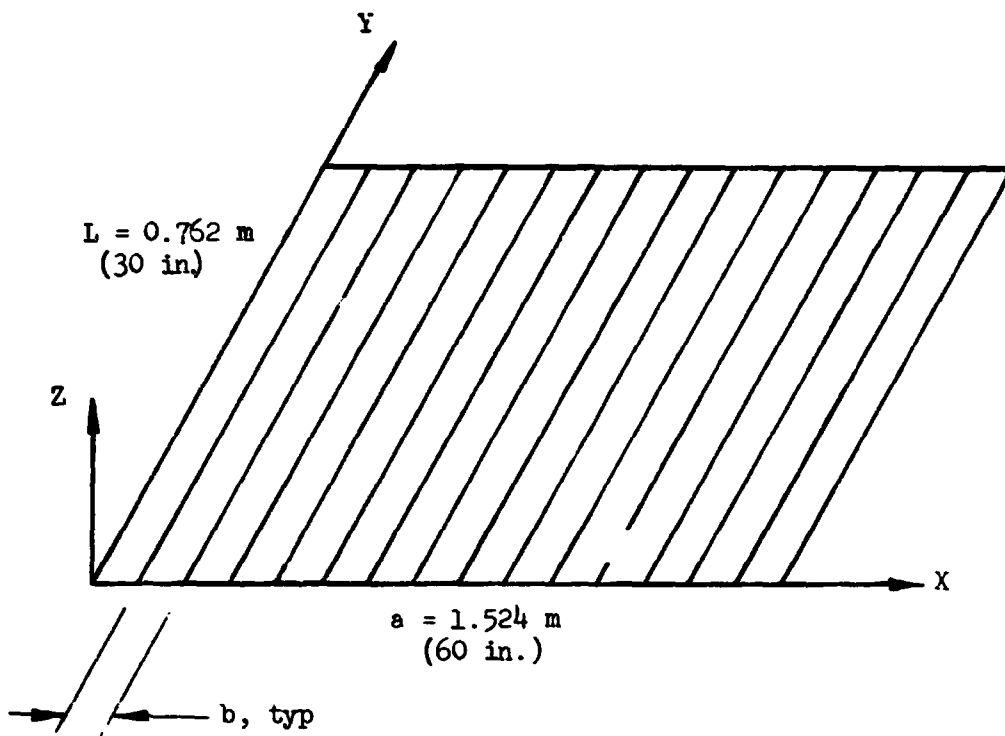


$N_{cr} = 101.9 \text{ kN/m (582 lb/in)}$
 $\lambda = 1.154$
 $m = 13$



$N_{cr} = 132.4 \text{ kN/m (756 lb/in)}$
 $\lambda = 1$
 $m = 15$

Figure 9.- Results obtained with VIPASA program.

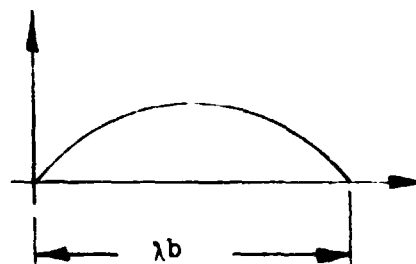


$$D_1 \frac{\partial^4 w}{\partial x^4} + 2D_3 \frac{\partial^4 w}{\partial x^2 \partial y^2} + D_2 \frac{\partial^4 w}{\partial y^4} + N_x \frac{\partial^2 w}{\partial x^2} = 0$$

where $D_1 = (EI)_x / (1 - \nu_x \nu_y)$
 $D_2 = (EI)_y / (1 - \nu_x \nu_y)$
 $D_3 = \frac{1}{2} (\nu_x D_2 + \nu_y D_1) + 2(GI)_{xy}$
 $N_x = \text{compressive load}$

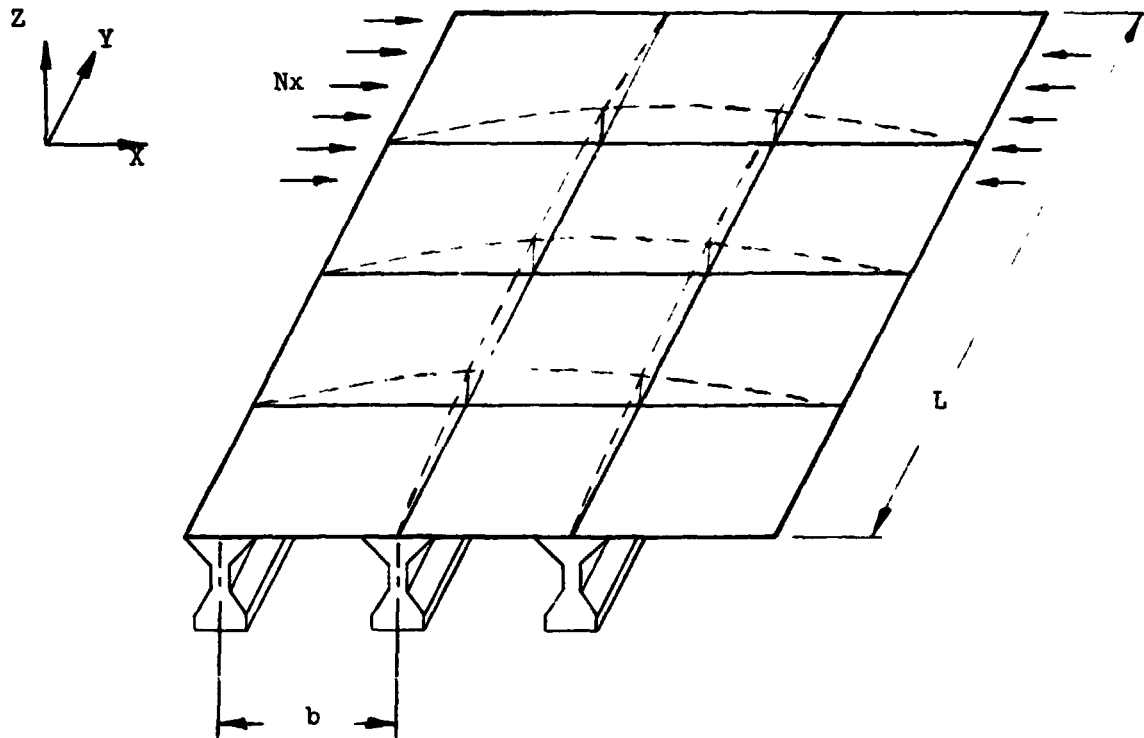
assumed mode shape

$$w = w_0 \sin \frac{\pi x}{\lambda b} \sin \frac{\pi y}{L}$$



$$N_x = D_1 \left(\frac{\pi}{\lambda b} \right)^2 + 2D_3 \left(\frac{\pi}{L} \right)^2 + D_2 \left(\frac{\pi}{L} \right)^2 \left(\frac{\lambda b}{L} \right)^2$$

Figure 10.- Orthotropic plate equations.



Assumed Mode Shape: $w = w_0 \sin \frac{\pi x}{\lambda b} \sin \frac{\pi y}{L}$

$$\Delta T = \Delta V_p + \Delta V_{SB} + \Delta V_{ST}$$

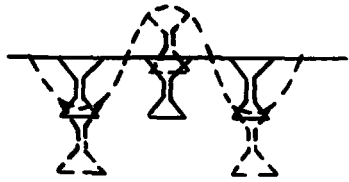
$$\Delta T = -\frac{1}{2} \iint \left[N_x \left(\frac{\partial w}{\partial x} \right)^2 + N_y \left(\frac{\partial w}{\partial y} \right)^2 + 2N_{xy} \frac{\partial w}{\partial x} \frac{\partial w}{\partial y} \right] dx dy$$

$$\Delta V_p = \frac{1}{2} D \iint \left[\left(\frac{\partial^2 w}{\partial x^2} \right)^2 + \left(\frac{\partial^2 w}{\partial y^2} \right)^2 + 2\nu \frac{\partial^2 w}{\partial x^2} \frac{\partial^2 w}{\partial y^2} + 2(1-\nu) \left(\frac{\partial^2 w}{\partial x \partial y} \right)^2 \right] dx dy$$

$$\Delta V_{SB} = \frac{EI}{2} \int \left(\frac{\partial^2 w}{\partial y^2} \right)^2 dy$$

$$\Delta V_{ST} = \frac{GJ}{2} \int \left(\frac{\partial \phi}{\partial y} \right)^2 dy \quad \phi = \frac{\partial w}{\partial x}$$

Figure 11.- Energy approach.



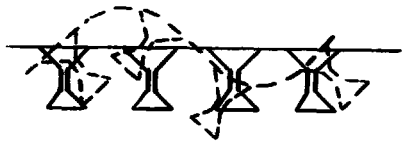
Stringer
Bending
 $\lambda = 1$
 $m = 15$

$N_{cr} = 129.9 \text{ kN/m}$
(742 lb/in)



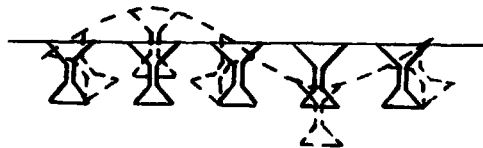
Stringer
Torsion
 $\lambda = 1$
 $m = 15$

$N_{cr} = 120.4 \text{ kN/m}$
(687 lb/in)



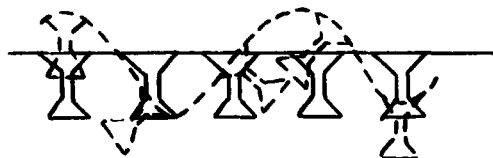
$\lambda = 1.5$
 $m = 10$

$N_{cr} = 100.9 \text{ kN/m}$
(576 lb/in)



$\lambda = 2$
 $m = 7.5$

$N_{cr} = 118.2 \text{ kN/m}$
(675 lb/in)



$\lambda = 1.333$
 $m = 11.25$

$N_{cr} = 101.9 \text{ kN/m}$
(582 lb/in)

Figure 12.- Results of energy approach.

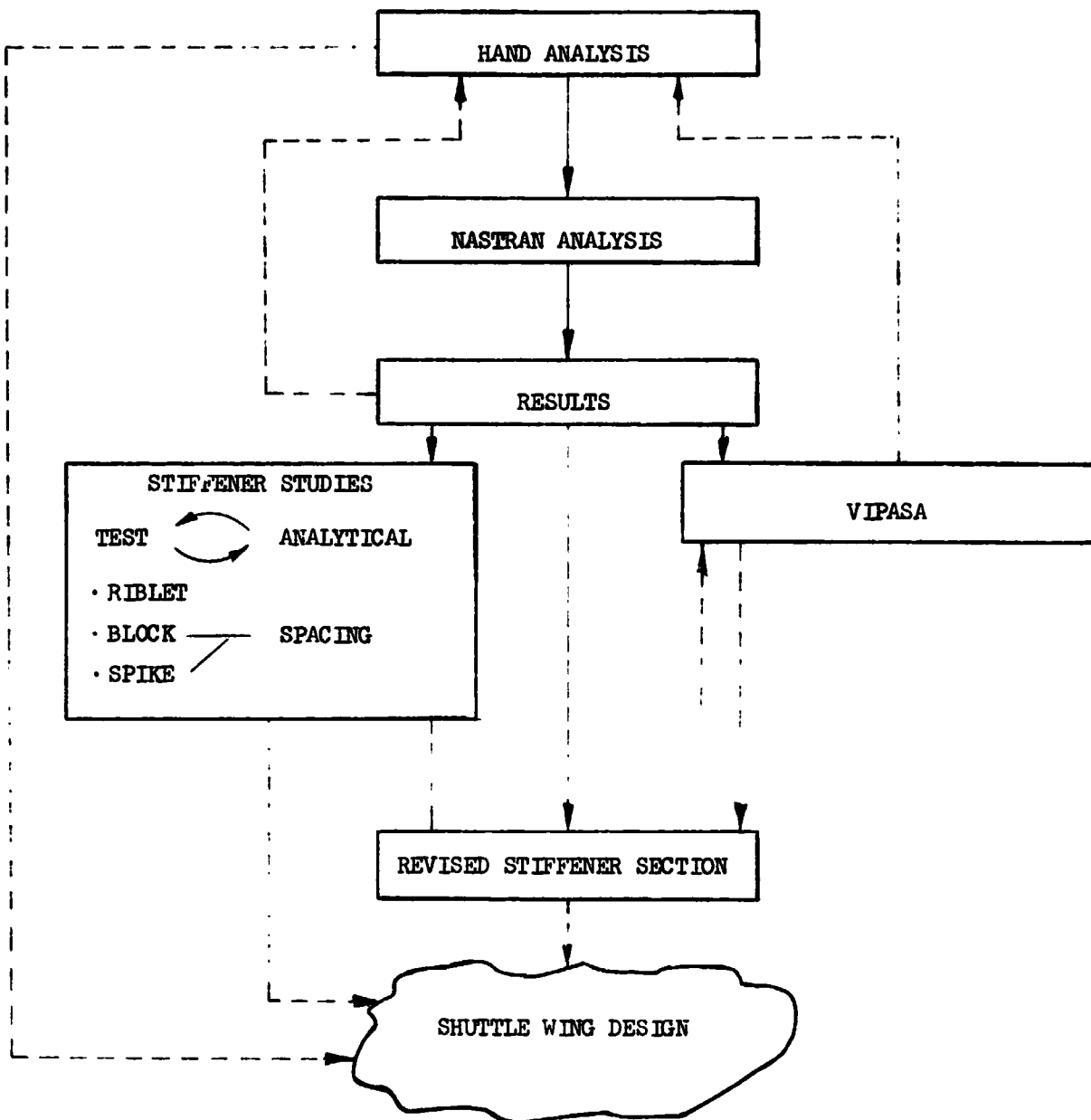
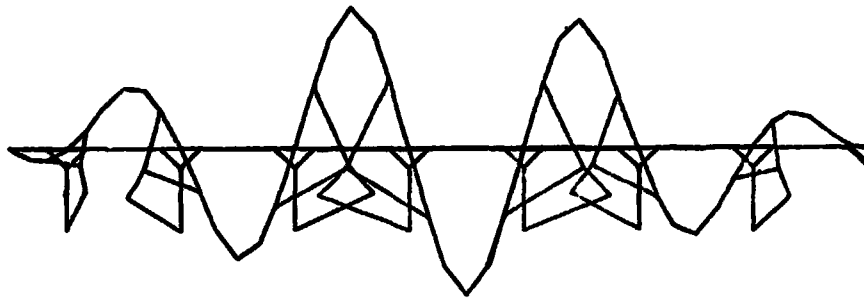


Figure 13.- Relationship of design analysis activities.



NASTRAN ANALYSIS - CASE II 1st MODE

$$N_{cr} = 146.2 \text{ kN/m (835 lb/in.)}$$

(A)



NASTRAN ANALYSIS - CASE III 1st MODE

$$N_{cr} = 215.2 \text{ kN/m (1229 lb/in.)}$$

(B)

Figure 14.- NASTRAN results for modified structure.

GENERAL INSTABILITY MODIFICATIONS - TYPICAL STIFFENER INSTALLATION

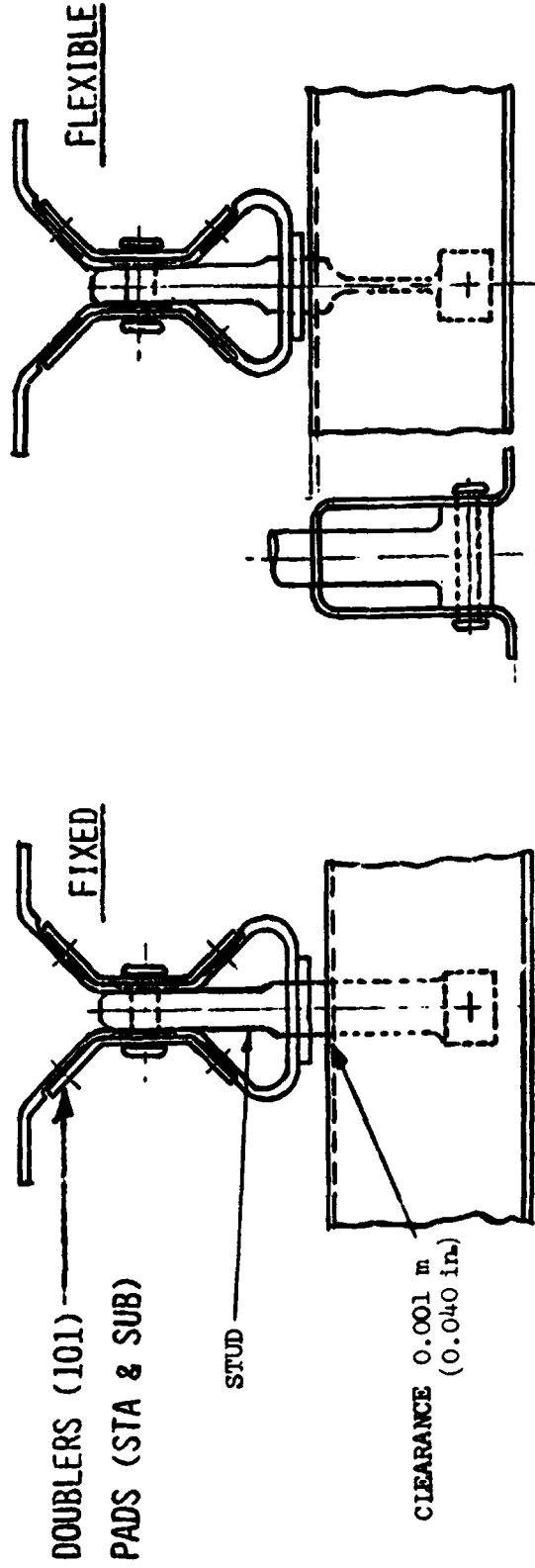
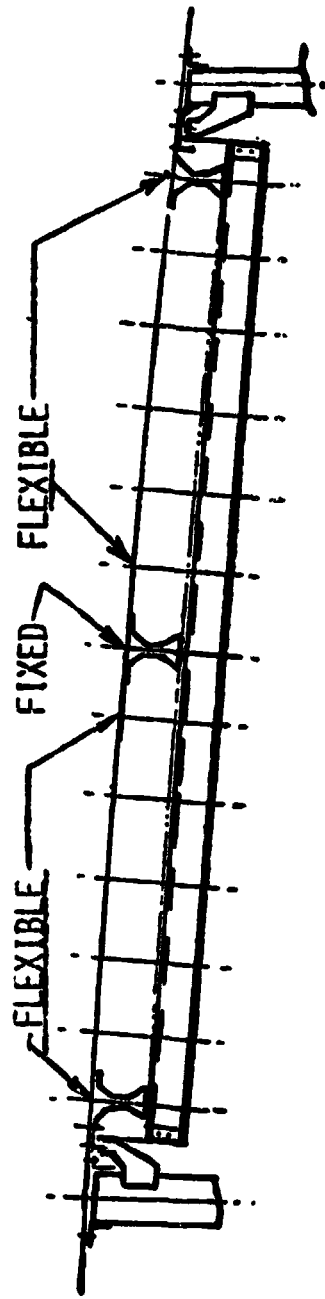


Figure 15.- Intermediate rib details.

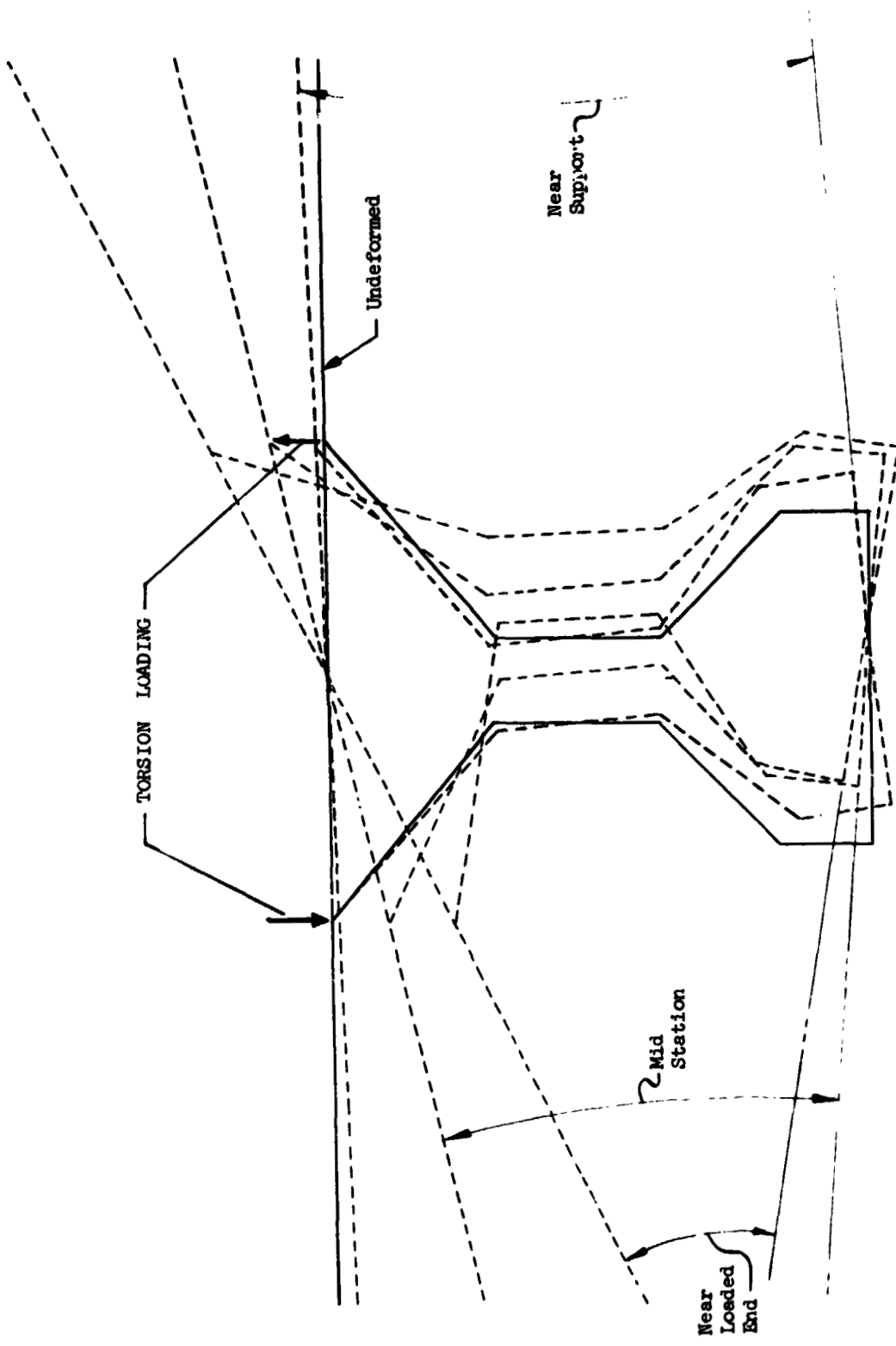
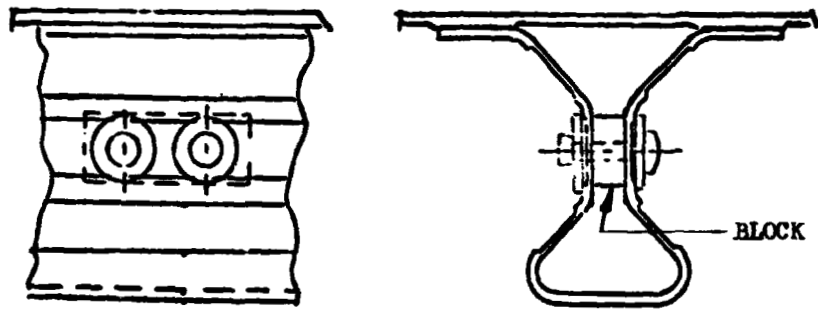
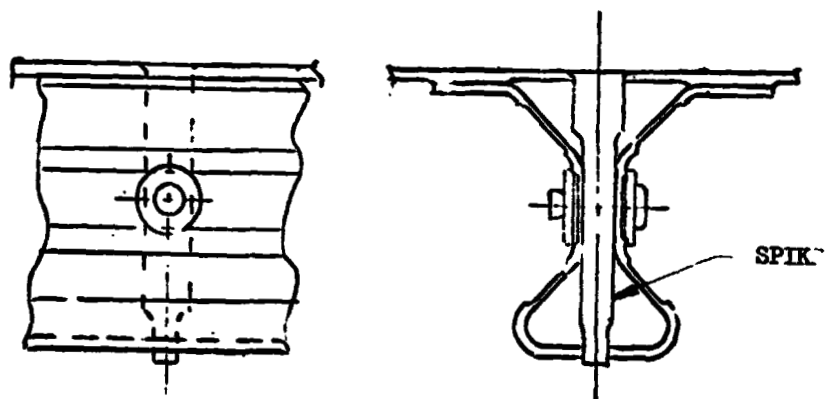


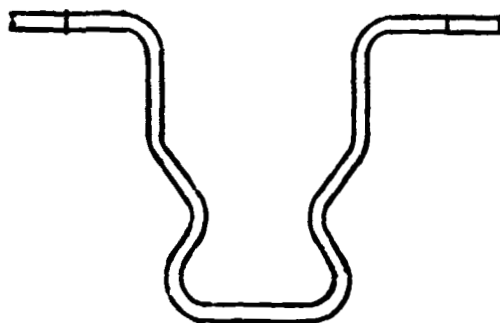
Figure 16.- Distortion of stringer.



(A) BLOCK STIFFENING



(B) SPIKE STIFFENING



(C) FRAME STIFFENED HAT
(chem milling patterns not shown)

Figure 17.- Stringer design concepts.

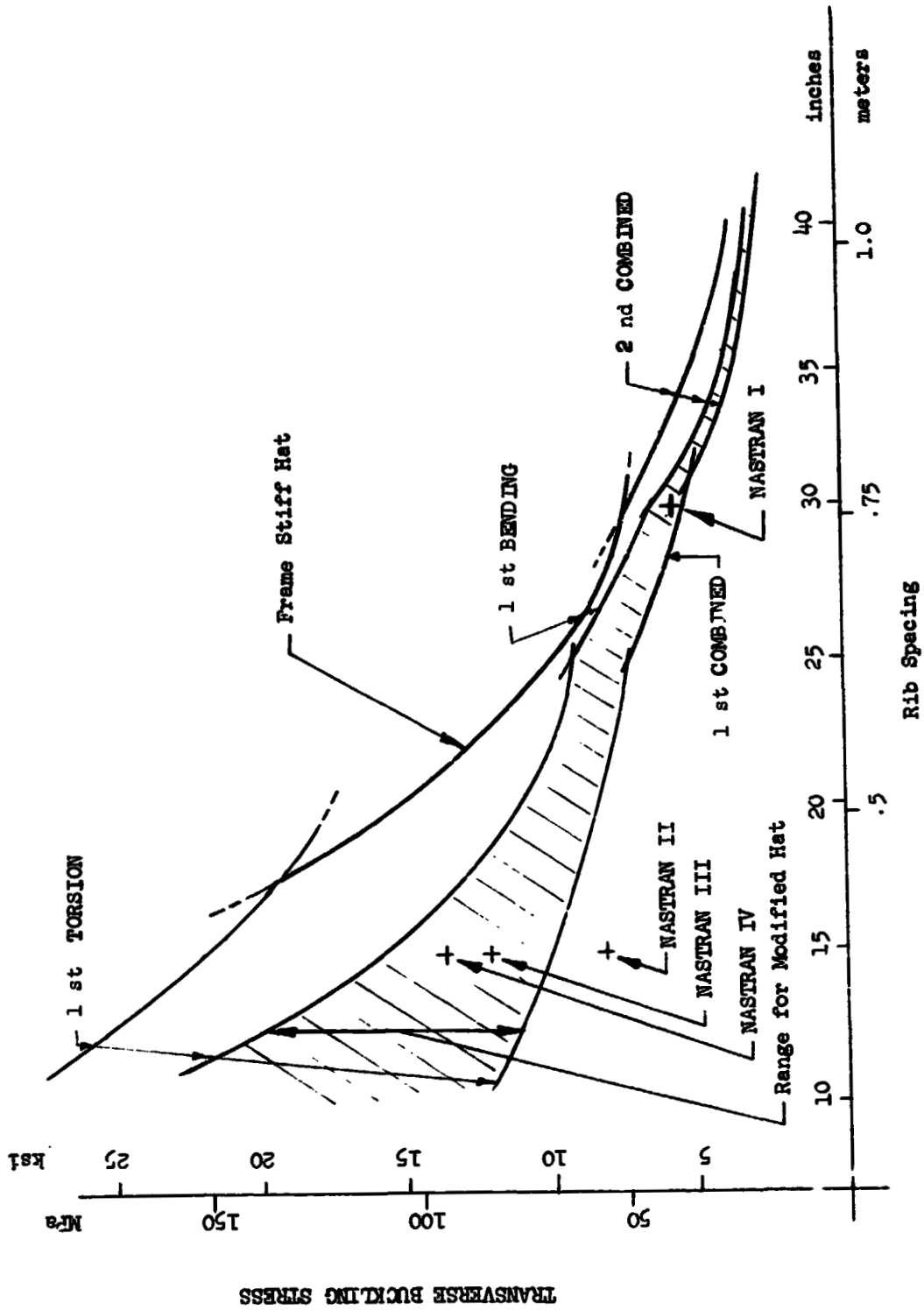


Figure 18.- Effect of design parameters.

N75 31495

**PRESSURE DEFORMATION OF TIRES USING DIFFERENTIAL STIFFNESS FOR
TRIANGULAR SOLID-OF-REVOLUTION ELEMENTS**

By C.H.S. Chen
B.F. Goodrich Co.
Akron, Ohio

SUMMARY

This paper presents the derivation of the differential stiffness for triangular solid of revolution elements. The derivation takes into account the element rigid body rotation only, the rotation being about the circumferential axis. Internal pressurization of a pneumatic tire is used to illustrate the application of this feature.

INTRODUCTION

In the NASTRAN computer code, the rigid format No.4 is the so-called static analysis with differential stiffness. This method of analysis is a first approximation to large deflection effects. The differential stiffness refers to the geometry stiffness which is generated using the stresses in the element which are computed from the initial linear stress analysis. The differential stiffness is available for rods, beams, shear panels, plates, and conical shell elements. However, sometimes one desires that the differential stiffness be available to solid elements. This is particularly true when one deals with a structure having thick wall yet flexible in nature. With this in mind, the differential stiffness for a triangular solid-of-revolution element is developed and incorporated into NASTRAN.

In the case of a ring element loaded axisymmetrically, there exists only one rotation of the element which is the rotation about the circumferential axis. We will assume that the stress and circumferential rotation are uniform through the element. Furthermore, in computing the work done by the forces in an element we will neglect the work done in conjunction with the normal and shear strains and the work done by the circumferential stress and strain. This is in accord with the derivation of the differential stiffness for a triangular membrane element presented in reference 1.

DERIVATION OF DIFFERENTIAL STIFFNESS MATRIX

The triangular ring element in NASTRAN assumes the following displacement field (Fig. 1)

$$u = \beta_1 + \beta_2 r + \beta_3 z \quad (1.a)$$

$$w = \beta_4 + \beta_5 r + \beta_6 z \quad (1.b)$$

where u, w are the displacements in the direction of the r, z coordinates respectively. Inverting the above yields

$$\{\beta\} = [r_{\beta q}] \{q\} \quad (2)$$

where $\{q\}^T = [u_1 \ w_1 \ u_2 \ w_2 \ u_3 \ w_3]$

$$\{\beta\}^T = [\beta_1 \ \beta_2 \ \beta_3 \ \beta_4 \ \beta_5 \ \beta_6]$$

Due to symmetry the only rotation of the element is the circumferential rotation ω_θ which according to reference 1 is given as

$$\omega_\theta = \frac{1}{2} \left(\frac{\partial w}{\partial r} - \frac{\partial u}{\partial z} \right) = \frac{1}{2} (\beta_5 - \beta_3) \quad (3)$$

Substituting β_5 and β_3 from equation (2) into equation (3) we obtain

$$\{\omega\} = [C] \{q\} \quad (4)$$

where $\{\omega\}^T = \{ \omega_r \ \omega_z \ \omega_\theta \}$

$$[C] = \frac{1}{2\Delta} \begin{bmatrix} 0 & 0 & 0 & 0 & 0 & 0 \\ 0 & 0 & 0 & 0 & 0 & 0 \\ r_{23} & z_{23} & r_{31} & z_{31} & r_{12} & z_{12} \end{bmatrix}$$

and

$$r_{ij} = r_i - r_j$$

$$z_{ij} = z_i - z_j$$

$$\Delta = r_{12} z_{13} - r_{13} z_{12}$$

Considering only the circumferential rigid body rotation and neglecting the effects of the normal and shear strains, then the work done by forces in an element of volume V reduces to

$$W = -\frac{V}{2} \omega_0^2 (\sigma_r + \sigma_z) \quad (5)$$

where σ_r and σ_z are the element normal stresses in the r and z directions, respectively. Hence the matrix of the differential stiffness coefficient for that element is simply

$$[K_{\omega\omega}^d] = V \begin{bmatrix} 0 & 0 & 0 \\ 0 & 0 & 0 \\ 0 & 0 & \sigma_r + \sigma_z \end{bmatrix} \quad (6)$$

We then have the differential stiffness matrix in terms of the generalized coordinate $\{\beta\}$

$$[K_{ee}^d] = [C]^T [K_{\omega\omega}^d] [C] \quad (7)$$

The above differential stiffness matrix is then transformed to grid point coordinates by means of equation (2) as

$$[K^d] = [\Gamma_{\beta q}]^T [K_{ee}^d] [\Gamma_{\beta q}] \quad (8)$$

This geometric stiffness matrix is then added to the elastic stiffness matrix to yield the total stiffness matrix of the structure.

APPLICATION TO PNEUMATIC TIRE INFLATION

We will apply the above formulation to the problem of inflating a pneumatic tire. This is an example which can be considered as an axisymmetric problem. Fig. 2 shows one-half of a typical meridian cross-section of a bias pneumatic tire. Its structural elements consist of (1) rubber which spreads from the tread area to shoulder area and to sidewall area and to the bead area, (2) casing or carcass which is the main load carrying member, and (3) bead, which seats the tire to the wheel rim. The carcass is a multi-layer composite which consists of a number of plies stacked together. The ply is a unidirectional composite made of many flexible high modulus cord of natural textile, synthetic polymer, glass fiber embedded in and bonded to a matrix of low-modulus polymeric material such as rubber. The plies are usually stacking together in a pair of symmetric bias cord angle with respect to the circumferential axis.

If we know the properties of the matrix and cord materials and their volume ratios, then the properties of the composite ply in its principal directions, directions 1 and 2 in Fig. 3, can be determined by the well-known Halpin-Tsai equation, reference 2. The ply is assumed to be transversely isotropic, i.e. Young's modulus $E_{33} = E_{22}$ and Poisson's ratios $\nu_{13} = \nu_{12}$, $\nu_{32} = \nu_{23}$. The well-known transformation matrix for elastic constants through a rotation is then applied to obtain the ply stiffness matrix in the laminate coordinate system x, y. For the present case, they are the meridional and circumferential directions. The

cord angle α which is also the angle of rotation of the transformation is calculated from the following equation known as "lift equation" in the tire industry.

$$\frac{r}{r_c} \frac{1}{1 + \epsilon} = \frac{\cos \beta}{\cos \alpha} \quad (9)$$

where α = cord angle in the body of tire which takes the molded shape
 β = cord angle in the initial cylinder before molding
 r = radius coordinate of the location in the body of tire
 r_c = radius of the initial cylinder before molding
 ϵ = estimated cord strain

The total effective carcass stiffness matrix is then obtained by the method in reference 3. In general, the laminate can be satisfactorily represented by two-ply laminate of $(+\alpha)$ and $(-\alpha)$ cord orientations.

The material properties used in our example are

$$\text{cord modulus } E_c = 0.52376 \times 10^5 \text{ kg/cm}^2 \text{ (} 7.45 \times 10^5 \text{ psi)}$$

$$\text{cord Poisson's ratio } \nu_c = 0.3$$

$$\text{rubber modulus } E_r = 52.7278 \text{ kg/cm}^2 \text{ (} 750 \text{ psi)}$$

$$\text{rubber Poisson's ratio } \nu_r = 0.48$$

Other data used are

$$\beta = 57 \text{ degrees}$$

$$r_c = 21.4846 \text{ cm (} 8.4585 \text{ in.)}$$

The cord strain ϵ is assumed to be constant and its value at the crown is used. The radius of the ply center line at the crown is 32.8308 cm (12.9255 in.) and the final cord angle at that point is assumed to be 32 degrees with reference to circumferential circle. The tire is subjected to internal pressure of

1.6873 kg/cm² (24 psi). For simplicity, the tire is assumed to be fixed at a section close to the bead. In all, 488 elements and 317 grid points are used for one-half of the tire cross-section. Figure 4 shows the shape of a deformed and undeformed tire section for the linear solution and for the differential stiffness solution. The radial displacement of the outer ply line using NASTRAN is 1.3785 cm (0.54277 in.) compared with 1.2217 cm (0.481 in.) from a shell theory. The shell theory neglects the rubber in the tread, shoulder, sidewall, and bead and only considers the carcass as a thin elastic shell of orthotropic material. The increase in the tire outer radius due to inflation is computed by NASTRAN to be 1.3419 cm (0.52829 in.) as compared with 1.0976 cm (0.448 in.) from measurement. The radial displacement of the same point from NASTRAN linear solution is 1.7499 cm (0.68895 in.). The inflated dimension of the outer carcass line in the z direction is 10.3045 cm (4.0569

in.) from NASTRAN and 9.9847 cm (3.931 in.) from shell theory. The section width of the tire (the maximum dimension of the tire outer profile in the z direction) after inflation is 21.116 cm (8.3134 in.) from NASTRAN as compared with 20.7772 cm (8.18 in.) from the measurement. As can be seen, the inclusion of the differential stiffness results in a great improvement over the linear solution. However, there are still discrepancies in the various results. The discrepancies can be attributed to factors such as material characterization, assumptions on the boundary conditions, initial shape, cord angles, cord strain, and the possibility of the residual stresses in the actual tire.

CONCLUDING REMARKS

We have presented here the derivation of the differential stiffness matrix for triangular solid-of-revolution elements. Its application is illustrated using the inflation of a bias tire as an example. The differential stiffness of a ring element is particularly useful when dealing with structure which has thick wall yet flexible enough to undergo large displacement and rotation. The example of the tire inflation demonstrates this point. The numerical results in the present example are quite satisfactory.

As mentioned earlier, the derivation of the differential stiffness presented in this paper is based on the information contained in the manual for Level 12, reference 1, since it was available to this author at that time. This author has learned since then that Level 15.5 (reference 4) has a refined derivation of the differential stiffness which includes the effects of the normal and shear strains in computing the energy. Hence, if a new derivation of the differential stiffness for a triangular ring element were made to include the effects of the normal and shear strains and also to include the effect of the circumferential strain, it would probably give a better solution than the present one.

REFERENCES

1. MacNeal, R.H., ed.: The NASTRAN Theoretical Manual (Level 12). NASA SP-221, 1970.
2. Ashton, J.E., et al.: Primer on Composite Materials: Analysis. Technomic, Stamford, Conn., 1969.
3. Chen, C.H.S., Tabaddor, F.: Effective Moduli of Layered Composites, J. Spacecraft and Rocket, vol. 11, no. 4, April 1974. pp. 262-264.
4. MacNeal, R.H., ed.: The NASTRAN Theoretical Manual (Level 15.5). NASA SP-221(01), 1972.

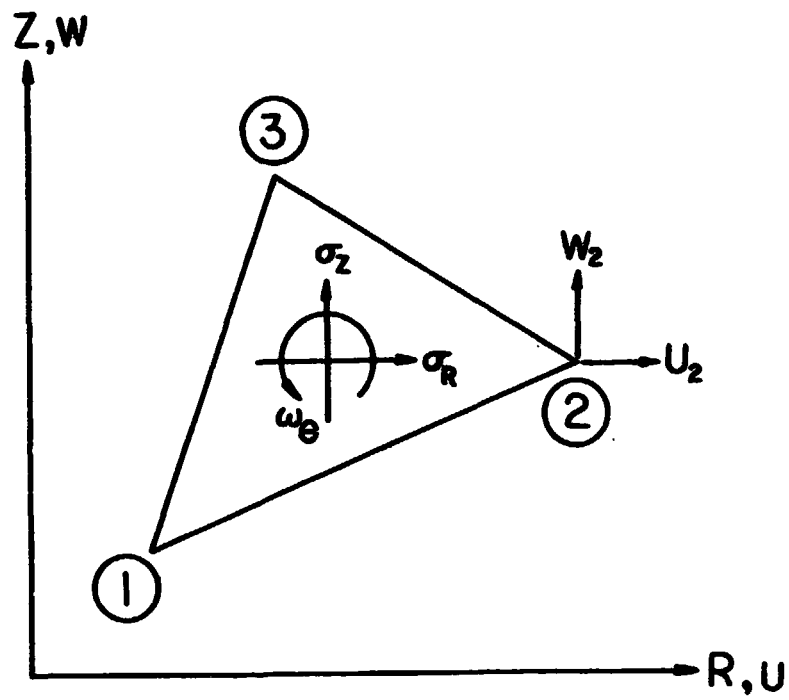


Figure 1.- Triangular solid of revolution element.

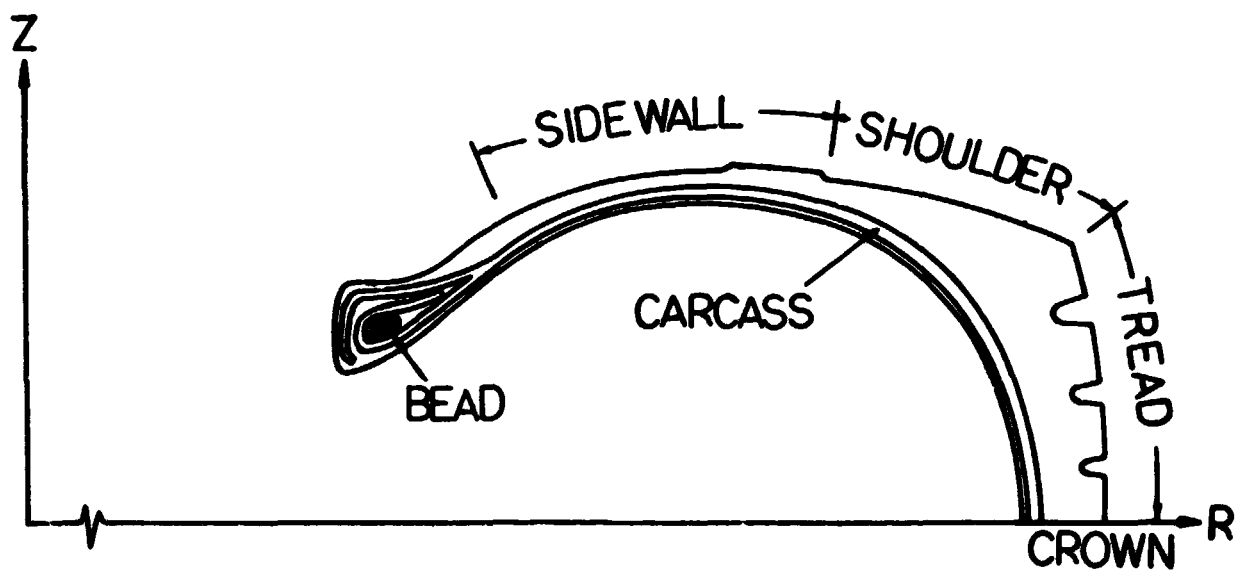


Figure 2.- Meridian cross section of a tire.

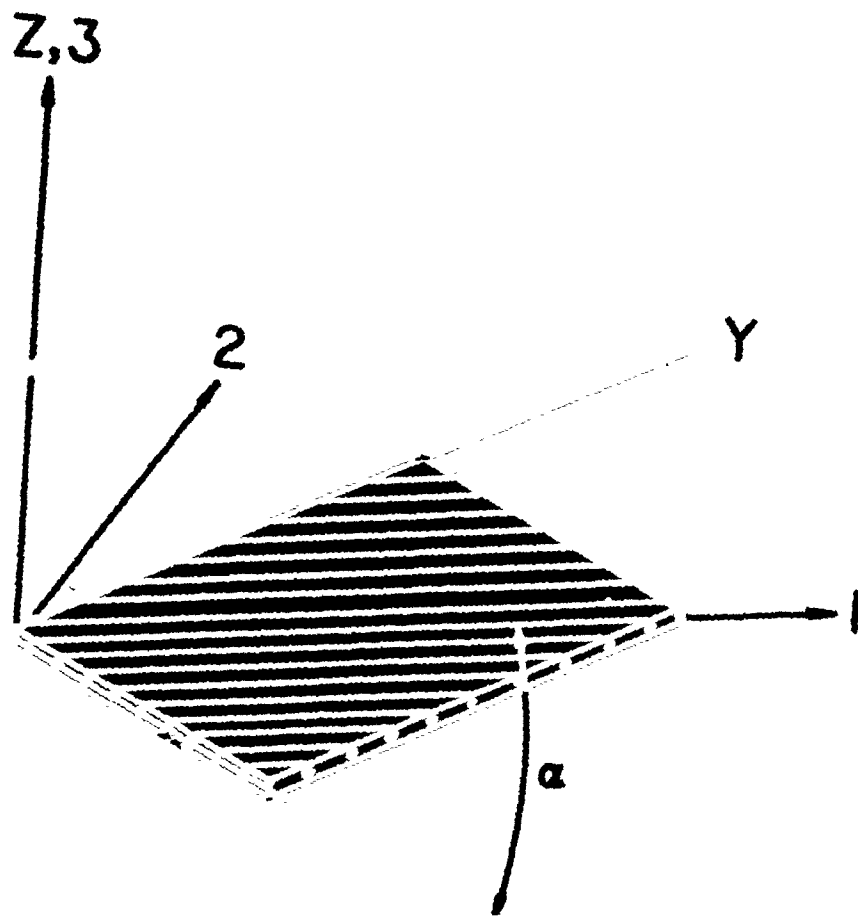
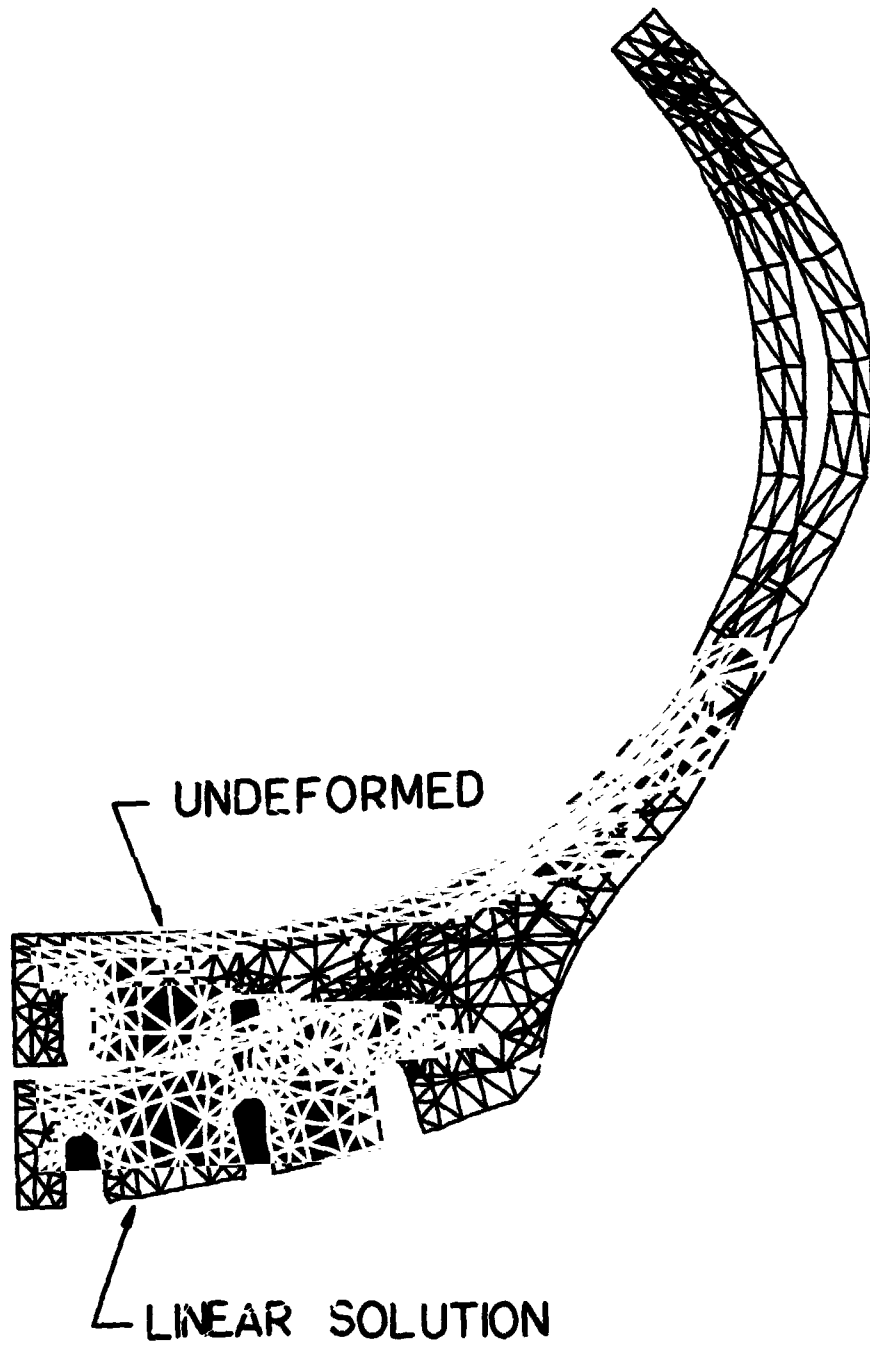
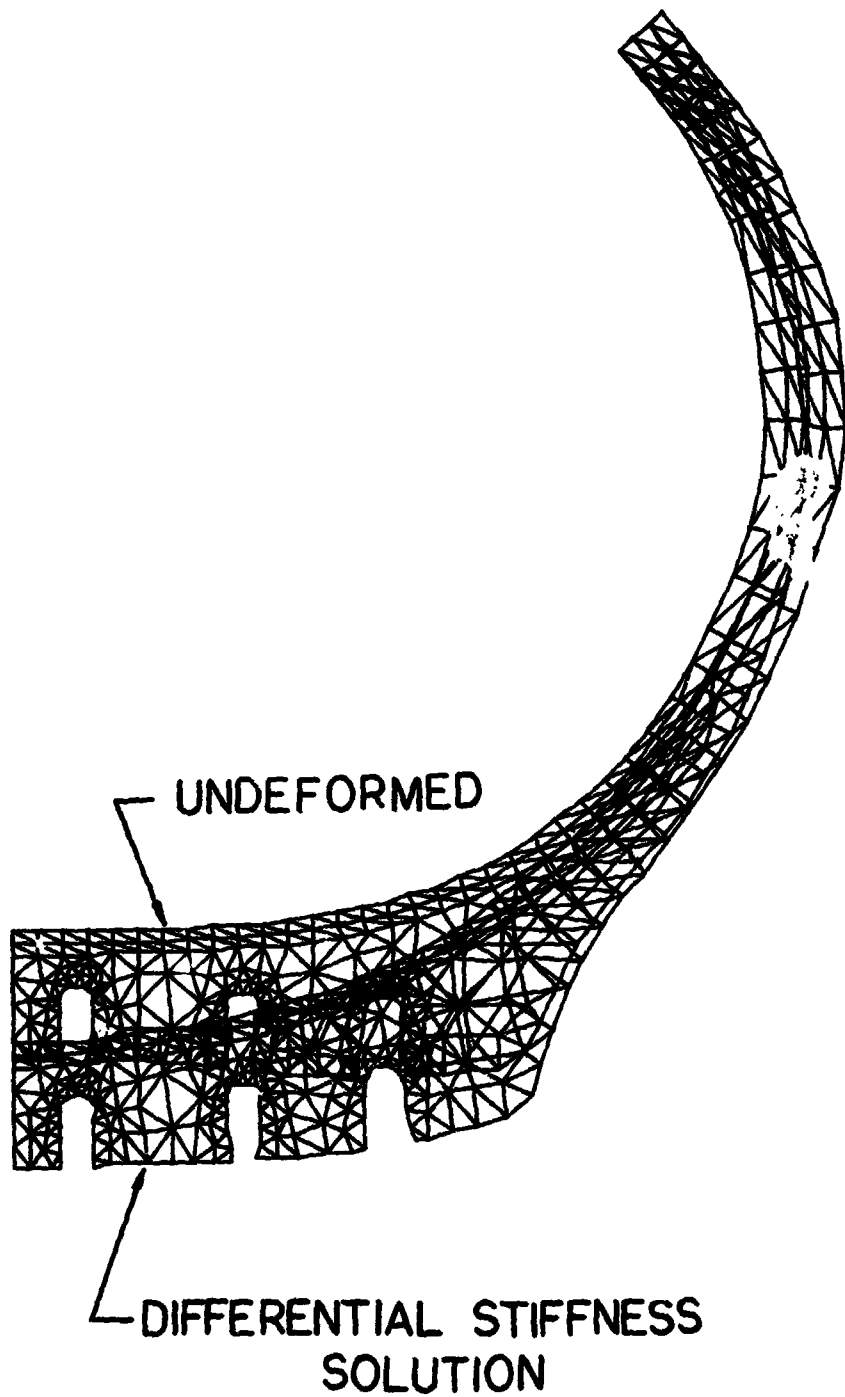


Figure 3.- Cord-reinforced composite ply.



(a) Linear solution.

Figure 4.- Deformed and undeformed tire cross section.



(b) Differential stiffness.

Figure 4.- Concluded.

N75 31496

**A FAILSAFE ANALYSIS USING NASTRAN'S PIECEWISE LINEAR
ANALYSIS AND A NINE NODE LINEAR CRACK ELEMENT**

R. F. Wilkinson and J. W. Kelley

Lockheed-Georgia Company

SUMMARY

This paper shows how a two-dimensional crack element was implemented into NASTRAN as a user dummy element and used to study failsafe characteristics of the C5A fuselage. The element is formulated from Reissner's functional requiring that it satisfy compatibility with the linear boundary displacement elements in NASTRAN. Its accuracy is demonstrated by analyzing for the stress intensity factors of two simple crack configurations for which there are classic solutions.

INTRODUCTION

A Lockheed requirement during the design of the C5A was for the pressurized fuselage structure to have the capability of sustaining a longitudinal crack in the skin. Circumferential straps are attached to the skin midway between the frames to provide this capability. Conventional methods for designing the straps and the system for attaching them to the skin are conservative and as a result dictate the use of high strength fasteners. It is now possible, due to the introduction of special crack tip singularity elements, to make a finite element analysis which eliminates much of this conservatism.

Part of the criterion for determining if a crack can be arrested is to find a configuration for which the stress intensity factor at the tip of the crack is lower than the critical stress intensity factor for the skin material. NASTRAN was considered the best analysis tool with which to analyze the various crack configurations. This was due to the ease with which a crack element can be incorporated into it as a user dummy element.

LIST OF SYMBOLS

σ	Stress
ϵ	Strain
u	Displacement
η	Vector normal to a surface
\bar{T}^*	Applied tractions
\bar{u}^*	Applied displacements
W_c	Complementary energy function
F	Body forces
V	Volume of an element
S_σ	Surface on which \bar{T}^* are specified
S_μ	Surface on which \bar{u}^* are specified
D	Interior boundary subdividing a region into finite elements
$[S]$	Compliance matrix
G	Shear modulus
ν	Poisson's ratio

SINGULARITY CRACK ELEMENT FORMULATION

In this section the stiffness matrix and the relationship between the nodal displacements and the stress intensity factors for a crack element are developed.

Reissner's functional, Reference 1, for a region subdivided by boundaries D into finite elements gives

$$(1) \quad J_R = \sum \left(\int_V \left[-W_C(\sigma_{LK}) - F_i \mu_i + \frac{1}{2} \sigma_{LK} (\mu_{L,K} + \mu_{K,L}) \right] dV \right. \\ \left. - \int_{S_\sigma} \eta_i^* \mu_i dS - \int_{S_\mu} \sigma_{LK} \eta (\mu_L - \mu_L^*) dS \right)$$

where the summation includes all the finite elements making up the region

If the displacements of the surfaces D are assumed compatible between finite elements, then the necessary conditions for J_R to be stationary due to a variation in the functions σ_{LK} , and μ_L are the following five Euler equations:

- (2) $\frac{\partial W_C}{\partial \sigma} = \frac{1}{2} (\mu_{L,K} + \mu_{K,L})$ in V (Hook's Law)
- (3) $\sigma_{LK,K} + F_L = 0$ in V (Equilibrium Equations)
- (4) $\sigma_{LK} \eta_K = \eta_i^*$ on S_σ (Traction boundary condition)
- (5) $\mu_L = \mu_L^*$ on S_μ (Displacement boundary condition)
- (6) $\langle \sigma_{LK} \eta_K \rangle = 0$ on D (Stress continuity between elements)

In which W_C has the property $\frac{\partial W_C}{\partial \sigma_{LK}} = \epsilon_{LK}$

A modified form of (1) is obtained by neglecting body forces and restricting the functions $\sigma_{i\kappa}$ and μ_i to the set which satisfy (3), (4), and (5)

$$(8) \quad J_1 = \sum \left[-\int_V w_c(\sigma_{i\kappa}) dV + \int_{S_n} \sigma_{i\kappa} \eta_\kappa \mu_i^* dS + \int_D \sigma_{i\kappa} \eta_\kappa \mu_i dS \right]$$

For this form of the functional the displacements μ_i only appear in the boundary integrals and hence do not have to be defined in the interior of the element.

In applying J_1 to the finite element shown in Figure 1 the stresses $\sigma_{i\kappa}$ are approximated by finite series and the displacements μ_i are required to vary linearly between nodal displacements $\{Q\}$. This ensures displacement compatibility with the linear boundary displacement elements already in the NASTRAN system. Expressing these approximate functions in matrix form

$$(9) \quad \{\sigma\} = [P] \{\beta\} \quad \text{stresses in } V$$

$$(10) \quad \{\mu_D\} = [L_D] \{Q\} \quad \text{displacements of the surface } D$$

$$(11) \quad \{\tau_D\} = [P_D] \{\beta\} \quad \sigma_{i\kappa} \eta_\kappa \quad \text{at the surface } D$$

where $[P]$ are the assumed series of stress functions and $\{\beta\}$ are the corresponding coefficients, $[L_D]$ are linear interpolations of the nodal displacements $\{Q\}$ along the boundary D , and $[P_D]$ are the values of $[P]$ that give the stresses $\{\sigma\}$ in Equation 9 normal to the boundary D . The stresses on the boundary S_n do not have to be defined as there are no enforced boundary displacements associated with this element.

Substituting (9), (10), and (11) into (8) gives the contribution of the crack element to J .

$$(12) \quad J_{1c} = -\frac{1}{2} [\beta] [KC] \{\beta\} + [\beta] [KA] \{Q\}$$

where

$$(13) \quad [KC] = \int_V [P]^T [S] [P] dV$$

$$(14) \quad [KA] = \int_D [P_0] [L_0] dS$$

Due to the fact that the coefficients, $\{\beta\}$, are independent between elements the necessary condition for J_{1c} to be stationary is $\frac{\partial J_{1c}}{\partial \beta} = 0$. This yields:

$$(15) \quad \beta = [KC]^{-1} [KA] \{Q\}$$

Substituting (15) into (12) and finding a stationary value of J_{1c} with respect to $\{Q\}$ give the contribution of the crack element to the total stiffness matrix

$$(16) \quad [KS] = [KA]^T [KC]^{-1} [KA]$$

Each term in the series used to approximate the stresses has to satisfy equilibrium and the stress boundary conditions. The series also has to include the known stress singularity near the tip of the crack. The form that has been assumed for this element is that which was developed from the Williams series of stress functions by Aberson and Anderson in Reference 2. The two dimensional stress distributions in polar coordinates are:

$$(17) \quad \sigma_r(R, \theta) = \sum_{n=1}^9 \beta S_n \left\{ \frac{n}{4} R^{n/2-1} \left[-(n+2) \cos(n/2+1)\theta + f(n)(n-6) \cos(n/2-1)\theta \right] \right\} \\ + \sum_{n=1,3}^9 \beta A_n \left\{ \frac{n}{4} R^{n/2-1} \left[g(n)(n+1) \sin(n/2+1)\theta - (n-6) \sin(n/2-1)\theta \right] \right\}$$

$$(18) \quad \sigma_\theta(R, \theta) = \sum_{n=1}^9 \beta S_n \left\{ \frac{n}{4} R^{n/2-1} \left[(n+2) \cos(n/2+1)\theta - f(n) \cos(n/2-1)\theta(n+2) \right] \right\} \\ + \sum_{n=1,3}^9 \beta A_n \left\{ \frac{n}{4} R^{n/2-1} \left[-g(n)(n+2) \sin(n/2+1)\theta + (n+2) \sin(n/2-1)\theta \right] \right\}$$

and

$$(19) \quad \tau_{R\theta}(R, \theta) = \sum_{n=1}^9 \beta S_n \left\{ \frac{n}{4} R^{n/2-1} \left[(n+2) \sin(n/2+1)\theta - f(n)(n-2) \sin(n/2-1)\theta \right] \right\} \\ + \sum_{n=1,3}^9 \beta A_n \left\{ \frac{n}{4} R^{n/2-1} \left[g(n)(n+2) \cos(n/2+1)\theta - (n-2) \cos(n/2-1)\theta \right] \right\}$$

in which

$$f(n) = \frac{n/2 + 1}{n/2 + (-1)^n}$$

and

$$g(n) = \frac{n/2 - (-1)^n}{n/2 + 1}$$

where βS_n and βA_n are the symmetric and antisymmetric parts of $\{\beta\}$.

The symmetric and antisymmetric coefficients βS_1 and βA_1 are associated with the singularity $R^{-1/2}$. They are related to the opening and sliding mode stress intensity factors K_I and K_{II} by the following formulas

$$(20) \quad K_I = 3 \sqrt{2\pi} \beta S_1$$

$$(21) \quad K_{II} = \sqrt{2\pi} \beta A_1$$

Hence once the displacements $\{Q\}$ have been determined the leading coefficients βA_1 and βS_1 can be recovered through (15) and subsequently the stress intensity factors through (20) and (21).

IMPLEMENTING THE CRACK ELEMENT INTO NASTRAN

The nine node crack element has been implemented into NASTRAN through the dummy element capability. This capability permits a user to enter his own element subroutines for the purpose of generating the stiffness and mass matrix contributions, the thermal load contributions and for the computation of various stresses and forces for output (see section 8.8.5 of the NASTRAN PROGRAMMERS MANUAL, Reference 3). This procedure is relatively simple compared to adding an entirely new element to the system.

The crack element has been implemented as a DUM2 element. The format for the ADUM2, CDUM2, and PDUM2 bulk data cards which are used to enter the geometry, property, and connectivity data is shown in Figure 2. The procedure used to implement the element is as follows.

- o Create an element stiffness subroutine KDUM2 which computes and outputs to functional module SMA1 one 6×6 matrix for each connecting grid point with respect to the connective pivot point.
- o Create two subroutines SDUM21 and SDUM22 to compute and output to functional module SDR2 the stress intensity factors.

- o Remap LINK3 to include the new routine KDUM2 and LINK13 to include the new routines SDUM21 and SDUM22.

All the element stiffness subroutines called by SMA1, including KDUM2, are overlaid. Therefore to avoid reducing the working core available to SMA1, KDUM2 was programmed in less core than the largest amount used by any of the existing element stiffness routines. To do this it was necessary to fix the shape of the element shown in figure 1. Chosen was a square with the nine grid points equally spaced around the boundary. This made it possible to compute the integrations involved in (13) and (14) externally to NASTRAN for a unit element size. Further (13) was integrated for a unit value of each of the two independent coefficients for an isotropic material in the compliance matrix $[S]$ i.e.

$$[S] = S_1 \begin{bmatrix} 1 & 0 & 0 \\ 0 & 1 & 0 \\ 0 & 0 & 2 \end{bmatrix} + S_2 \begin{bmatrix} 1 & 1 & 0 \\ 1 & 1 & 0 \\ 0 & 0 & 0 \end{bmatrix}$$

where

$$S_1 = 1/2 G$$

$$S_2 = \begin{cases} -\nu/2 G & \text{PLANE STRAIN} \\ -\nu/2 G(1+\nu) & \text{PLANE STRESS} \end{cases}$$

The resulting unit matrix for $[KA]$ and the two unit matrices for $[KC]$ are used as permanent data in the subroutines KDUM2 and SDUM21.

Subroutine KDUM2 forms the matrices $[KA]$ and $[KC]$ in double precision from the three unit matrices for a specific element size and material. It then uses these in (16) to compute the 2×2 stiffness matrices in the local element coordinate system for each grid point associated with the respective connective pivot point. Finally it transforms these 2×2 matrices into 6×6 matrices in the global coordinate system.

Similarly subroutine SDUM21 forms the matrices $[KA]$ and $[KC]$ in single precision for a specific element size and material. It then computes the two stress intensity factors K_1 and K_{II} for a unit value of each of the grid point displacements $\{Q\}$ in the global system using 15, 20, and 21. Subroutine SDUM22 computes the final stress intensity factors for specific grid point displacements.

ELEMENT EVALUATION

The capability of the element to predict accurate stress intensity factors has been demonstrated by numerous analyses. Two are presented here for which there are known classic solutions.

The opening mode stress intensity factor for an isotropic material can be expressed in the form, Reference 4.

$$(22) \quad K_1 = \sigma \sqrt{\pi a} f$$

Where $\sigma \sqrt{\pi a}$ is the stress intensity factor for a central crack of length $2a$ in an infinite plate loaded by a far field stress σ acting normal to the crack. f is either the correction factor associated with Bowie's analysis for the presence of a hole, Reference 5, or Isida's analysis for a finite width plate, Reference 6.

The finite element model shown in Figure 3 represents a crack in a finite width plate loaded by a far field stress acting normal to the crack. The plate is 81 cm wide 168 cm long and the crack length is varied between 10 and 51 cm. The model which idealizes one quarter of the plate represents the full structure thru the use of symmetric boundary constraints. The crack element which overlaps a symmetry boundary is forced to deflect symmetrically thru the use of multi-point constraint equations. It should be noted that when the multipoint constraint equations are used in this way the element that is being forced to act symmetrically should be specified with half its actual thickness. Besides the DUM2 crack element the model consists of 56 CQDMEM elements, and 36 CTRMEM elements. It has 124 grid points, 219 active freedoms, and a semiband width of 37. Figure 3 shows that for this type of idealization the crack element computes the stress intensity K_1 to within 3% of that given by equation (22).

The finite element model shown in Figure 4 represents symmetric cracks protruding from a hole in the center of an infinite plate. The plate is 102 cm wide and 102 cm long. The hole has a diameter of 5 cm and the crack lengths are varied between 0.8 and 8 cm. The model uses the same idealization techniques employed in the previous example to represent the plate. It consists of 154 CQDMEM elements, 5 CTRMEM elements and one DUM2 crack element. Figure 4 shows the results to be within 3% of equation 22.

C5A FAILSAFE ANALYSIS

The C5A fuselage has a failsafe criterion which requires that a 30 cm longitudinal crack in the cover skin will not result in a catastrophic failure when the structure is subjected to a normal operating internal pressure. To satisfy this requirement, circumferential failsafe straps are attached to the skin mid way between the frames for the purpose of arresting such a crack, see Figure 5. An analysis based on Lockheed data sheets is conservative and as a result dictates the use of expensive high strength fasteners to attach the strap to the skin. The following analysis using NASTRAN shows that less expensive aluminum rivets can be used instead.

As a longitudinal skin crack passes under the failsafe strap the stress intensity at the tip reduces. The crack will cease to propagate if the stress intensity becomes less than the critical stress intensity for the material, provided that the fasteners in the strap do not fail first. The finite element model shown in Figure 6 represents a typical region of the C5A aft fuselage. It considers the frame at fuselage station (F.S.) 1804 to be failed and is used to analyze various lengths of a skin crack which propagates towards the failsafe straps at F.S.'s 1794 and 1814. The model is two-dimensional, i.e. fuselage curvature and out of plane deflections are ignored. Advantage has been taken of two symmetry planes by idealizing only one quarter of the actual damaged region. The crack element which lies across a symmetry boundary is again forced to displace symmetrically through the use of multi-point constraint equations. The frame cap and the skin are represented as an integral structure through the use of CROD, CTRMEM, CQUAD, and the CDUM2 elements. The strap which is considered as a separate unit uses the CTRMEM and CQUAD elements. The twelve fasteners closest to the crack are each idealized by a system of CROD elements. The remaining fasteners are lumped into groups of approximately 4 and idealized by CELAS1 elements. The model is loaded by concentrated forces which represent the hoop loading on a 244 cm radius structure for a normal operating internal pressure with a dynamic factor of 1.15. The loading is applied to the model in proportion to the circumferential cross sectional area. This does not represent the true circumferential loading as it neglects the bulging effect of the skin between the frames. It is conservative however in that it overloads the frame at the center of the crack.

In order to show the fasteners capable of carrying the transfer load it is necessary to consider the nonlinear load deflection response for the twelve fasteners closest to the crack, see figure 7. Because the CELASI elements do not have the capability of representing nonlinearity it was necessary to idealize these fasteners by the system of CROD elements shown in Figure 8. The rods connect the coincidental grid points A and B on the skin and strap respectively through the grid point C. The elements have a combined length of 2.54 cm (1 in.) and a cross-sectional area of 6.45 cm² (1 in²). The use of English units allows the load deflection curves in Figure 7 to be input directly on Tables 1 cards as a stress strain curve for the rod elements. The only other region of the structure to experience plasticity is the tip of the crack and since this is ignored in linear fracture mechanics the most economical way of executing the analysis is to divide the model into two substructures: the skin, frame, and strap being included in substructure 1 and the fasteners in substructure 2. Substructure 1 is analyzed first for an increment of the external loads using rigid format 1. The freedoms for the grid points common to the fasteners are included in the 'A' set and the rigid format altered to terminate once the reduced A set stiffness and loads matrices are formed. Substructure 2 is then analyzed using rigid format 6, the piecewise linear analysis. Rigid format 6 is altered to read the A set stiffness and loads matrices for substructure 1 and add them to the appropriate terms in the G set stiffness and loads matrices for substructure 2. The results of the piecewise linear analysis give the desired fastener loads. To obtain the stress intensity factor it is necessary to restart the analysis for substructure 1 using the A set displacements resulting from the analysis of substructure 2.

Substructure 1 consists of one CDUM2, 56 CROD, 71 CTRMEM and 814 CQDMEM elements. It has 952 grid points, 1876 active freedoms and a semiband width of 84. There are 136 freedoms in the A set for which it took 31 CPU minutes, on a UNIVAC 1106 computer executed in a time sharing mode, to form the reduced stiffness and loads matrices. Substructure 2 consists of 56 CELASI elements and 24 CROD elements. It has 80 grid points, 148 active freedoms and a semiband width of 142. It took 10 iterations to obtain the elastic-plastic solution using 14 CPU minutes. The back feed into substructure 1 to obtain the stress intensity factor ran for 8 CPU minutes. All the above run times are for Level 15.1.

The analysis has been made for both the original 3.2 mm (1/8 in.) YBO TAPERLOKS and the proposed 4.0 mm (5/32 in.) aluminum rivets. Four crack lengths were considered for each system, the results being plotted in Figures 9 and 10 respectively. They show the ratio of the stress intensity to the critical stress intensity (K_1/K_C) and the ratio of the maximum fastener load to the allowable fastener load (P/P_a) plotted against the half crack length. Figure 9 shows that when the TAPERLOKS are used the stress intensity reduces to the critical value at a half crack length of 22 cm. At this length the fasteners are only working to 40% of their allowable load; hence they are shown to provide the necessary failsafe characteristics. This is only to be expected as the more conservative Lockheed data sheets also show the TAPERLOKS capable of arresting the crack. Figure 10 shows that when the rivets are used the stress intensity reduces to the critical value at a half crack length of 24 cm. At this length

the rivets are working to 67% of their allowable load therefore, unlike the conventional analysis, this analysis shows that they also are capable of providing the necessary failsafe characteristics. This analysis was validated by a test program which demonstrated that the rivets are capable of arresting the skin crack.

CONCLUSION

The NASTRAN capability of allowing a user to implement a dummy element was found to be relatively simple to use and exceedingly useful. Lockheed Georgia Company has plans to implement more elements into the system. In particular work is underway on a fastener element, similar to CELAS1, that has the capability of representing a nonlinear load deflection curve.

REFERENCES

1. Fung, Y.C.: Foundations of Solid Mechanics. Prentice-Hall Inc., 1965, pg 300.
2. Aberson, J.A., Anderson, J.M.: Cracked Finite Elements Proposed for NASTRAN. NASTRAN: User's Experiences. NASA TM X-2893, 1973
3. The NASTRAN Programmer's Manual. NAS SP-223 (01), Sept. 1972.
4. Bowie, O. L.: Analysis of an Infinite Plate Containing Radial Cracks Originating from the Boundary of an Internal Circular Hole. Journal of Mathematics on Physics, Vol. 35, 1956.
5. Isida, M.: On the Tension of a Strip with a Central Elliptical Hole. Transactions, Japanese Society of Mechanical Engineers, Vol. 22, 1956.
6. Wilhem, D.P.: Fracture Mechanics Guidelines for Aircraft Structural Application. AFFDL-TR-69-111, February 1970.

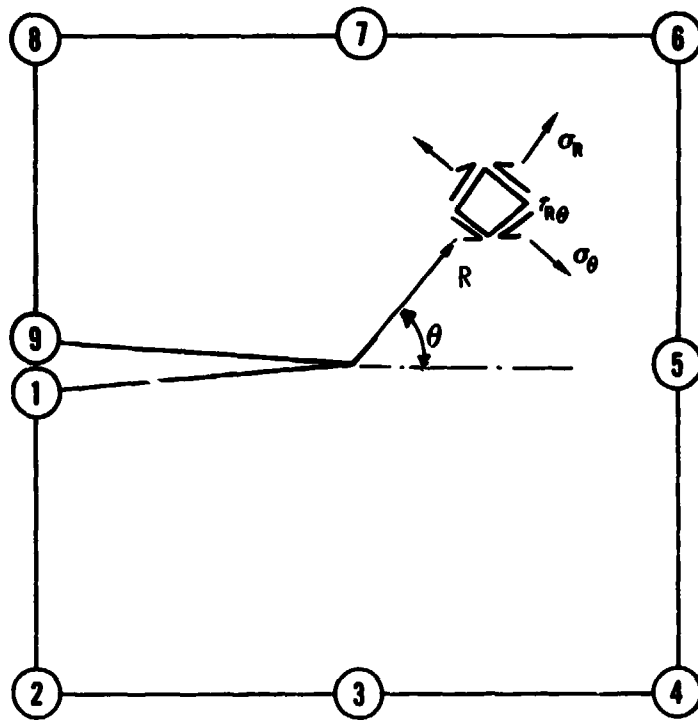


Figure 1. Nine Node Crack Element

ADUMi	NG	NC	NP	ND					
ADUM2	9	0	2	3					

CDUM2	EID	PID	G1	G2	G3	G4	G5	G6	abc
CDUM2	1	1	1	2	3	4	5	6	abc

+bc	G7	G8	G9						
+bc	7	8	9						

PDUM2	PID	MID	t	N					
PDUM2	1	1	.5	1					

WHERE

- NG NUMBER OF GRID POINTS CONNECTED BY DUM2 CRACK ELEMENT
- NC NUMBER OF ADDITIONAL ENTRIES ON CDUM2 CONNECTION CARD
- NP NUMBER OF ADDITIONAL ENTRIES ON PDUM2 PROPERTY CARD
- ND NUMBER OF DISPLACEMENT COMPONENTS AT EACH GRID POINT
- EID ELEMENT IDENTIFICATION NUMBER
- PID IDENTIFICATION NUMBER OF A PDUM2 PROPERTY CARD
- G_i GRID POINT IDENTIFICATION NUMBERS OF CONNECTION POINTS
- MID MATERIAL IDENTIFICATION NUMBER
- t ELEMENT THICKNESS
- N N=1 INDICATES PLANE STRESS
N=0 INDICATES PLANE STRAIN

Figure 2. Bulk Data Cards For a DUM2 Crack Element

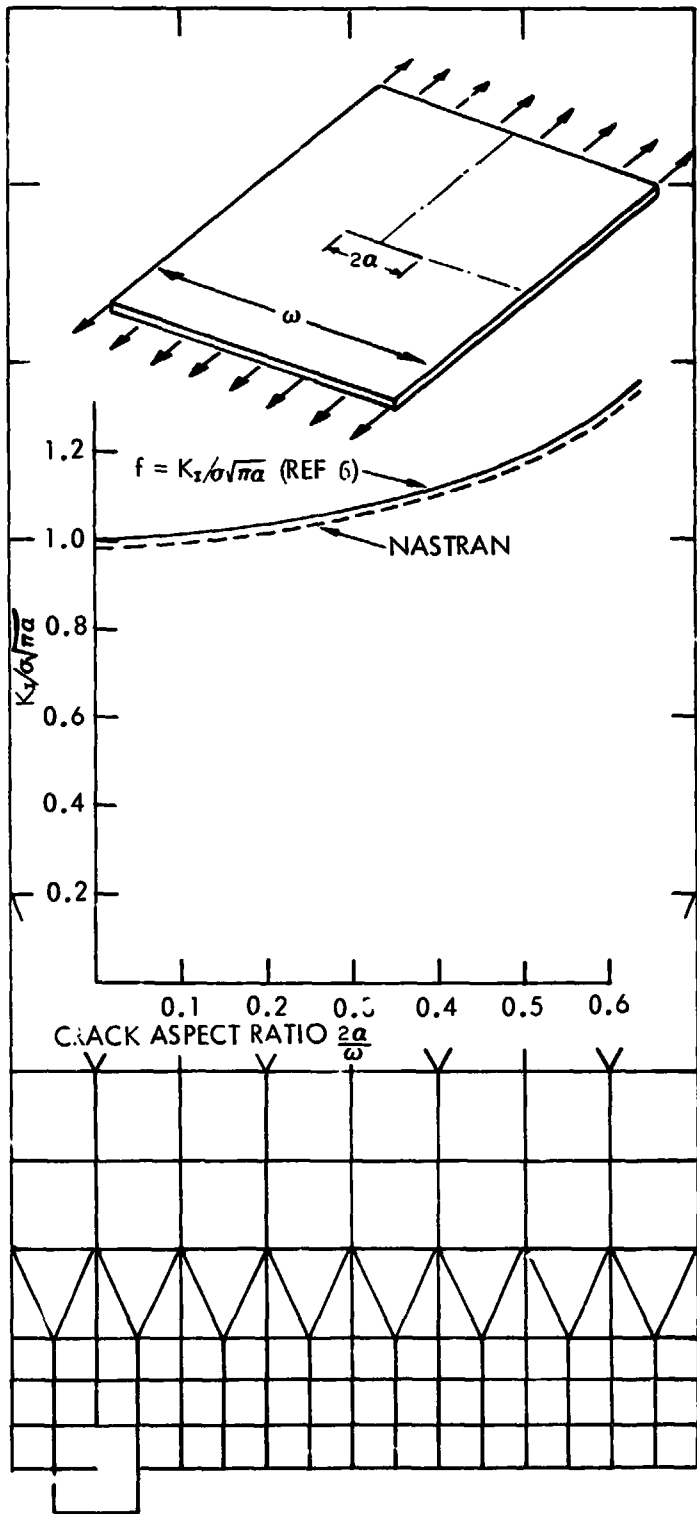


Figure 3. K_I Comparison For a Central Crack in a Finite Width Plate.

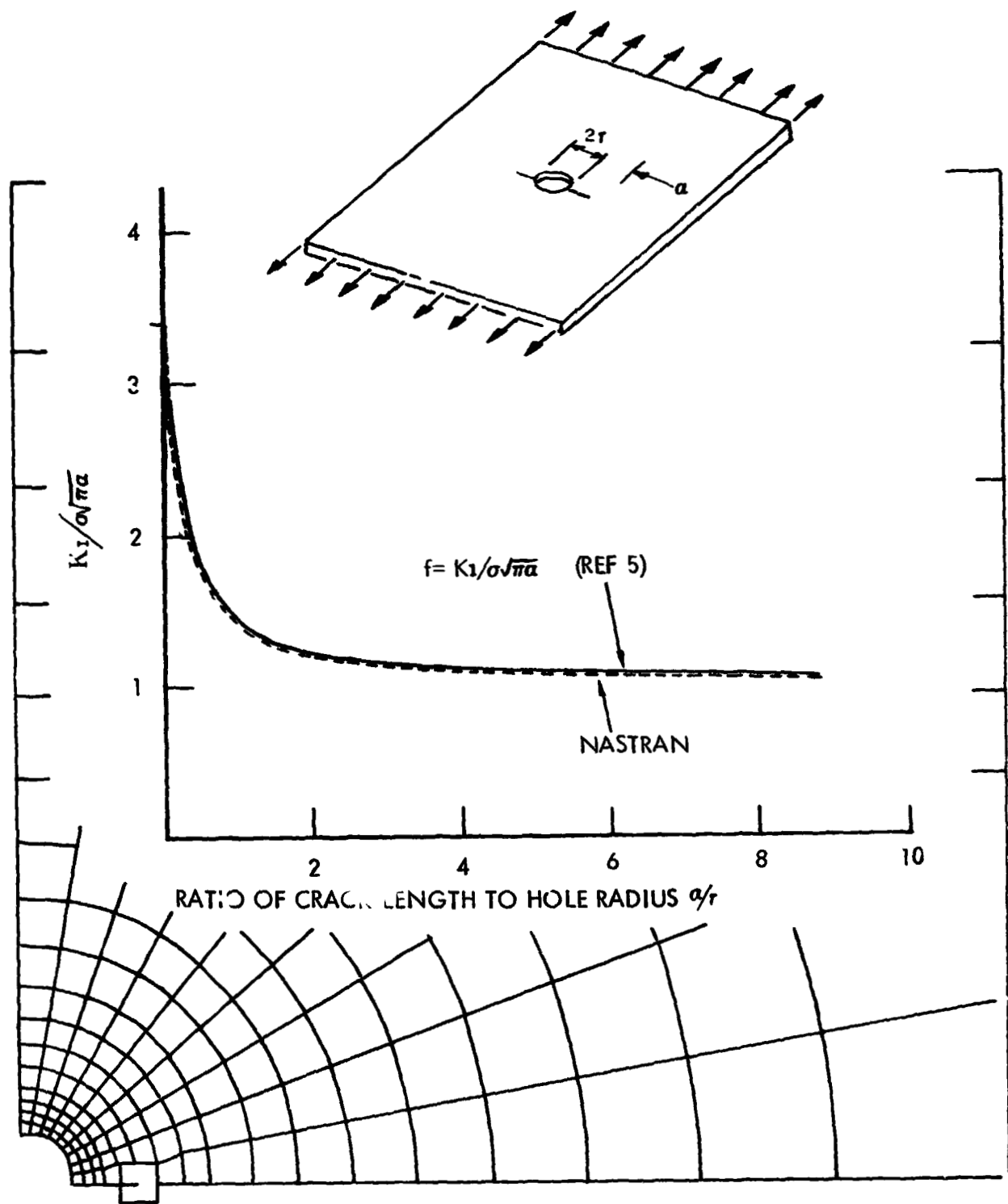


Figure 4. K_I Comparison For Symmetric Cracks at a Hole in an Infinite Plate

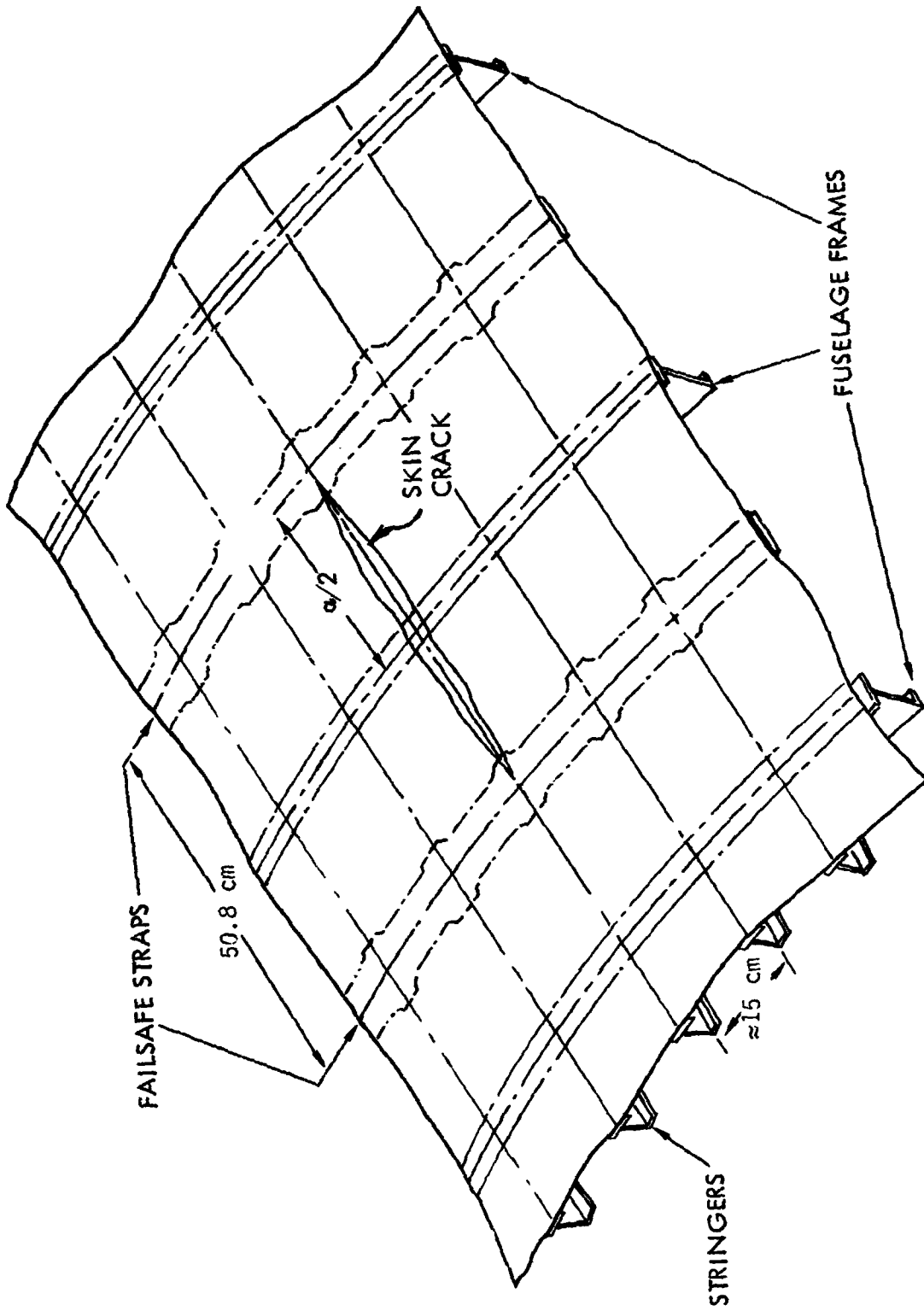


Figure 5. C5A Cracked Skin Configuration.

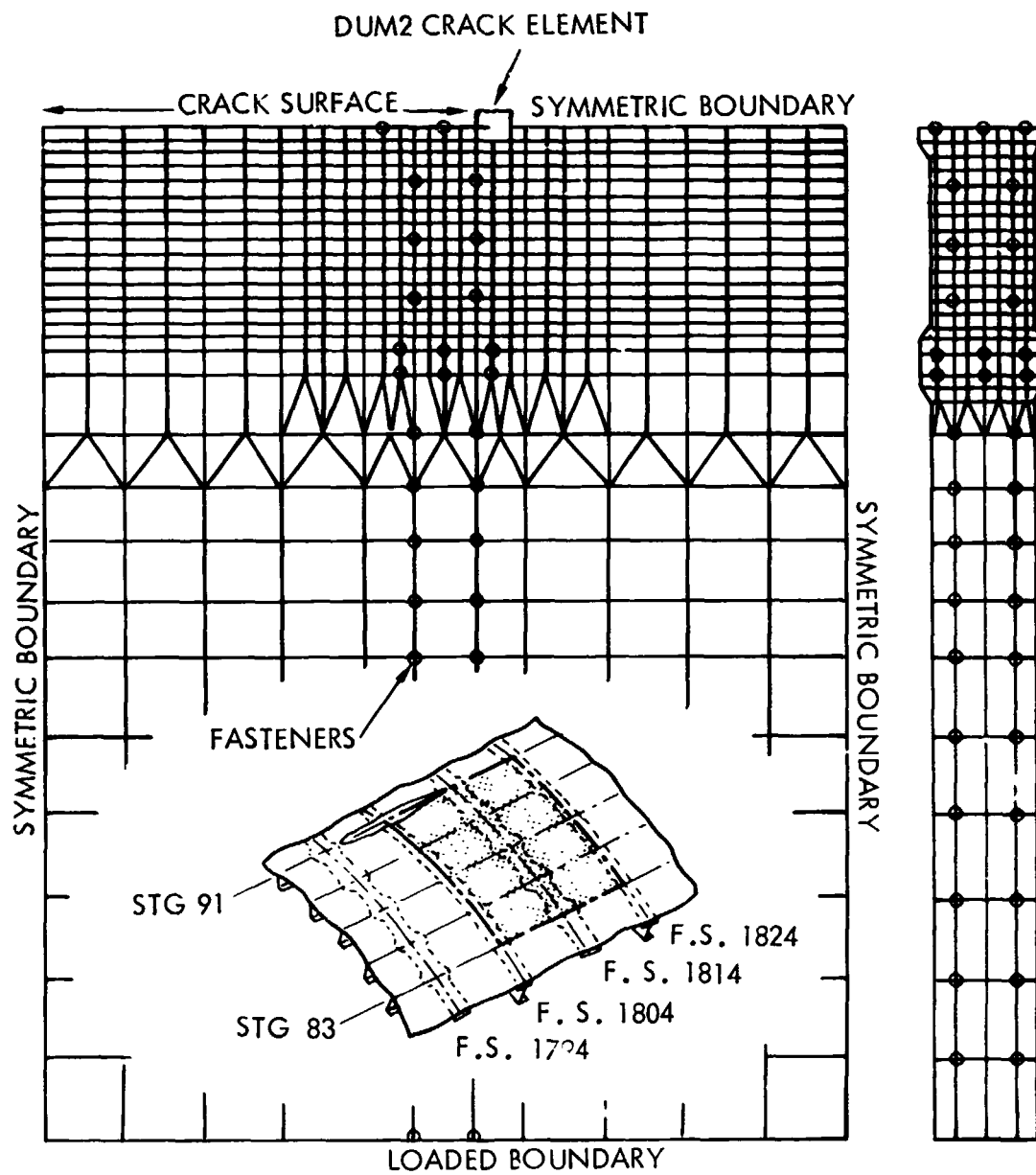


Figure 6. NASTRAN Model of a C5A Fuselage Skin Crack

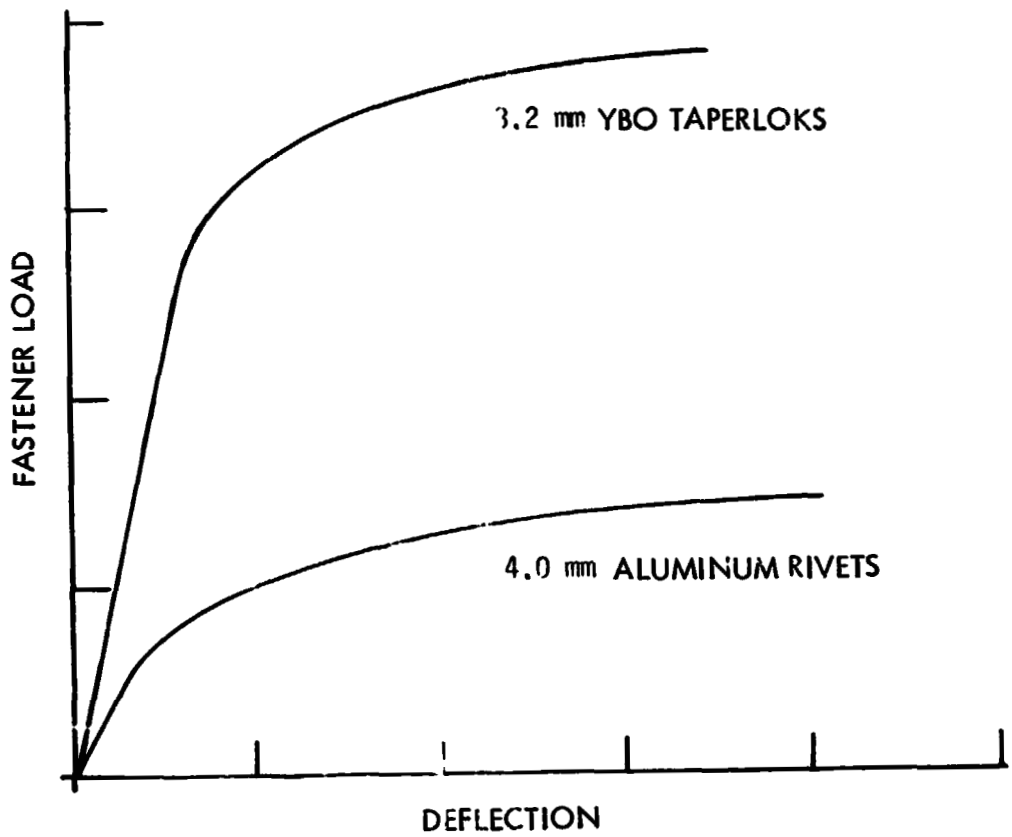


Figure 7. Nonlinear Fastener Load-Deflection Curves

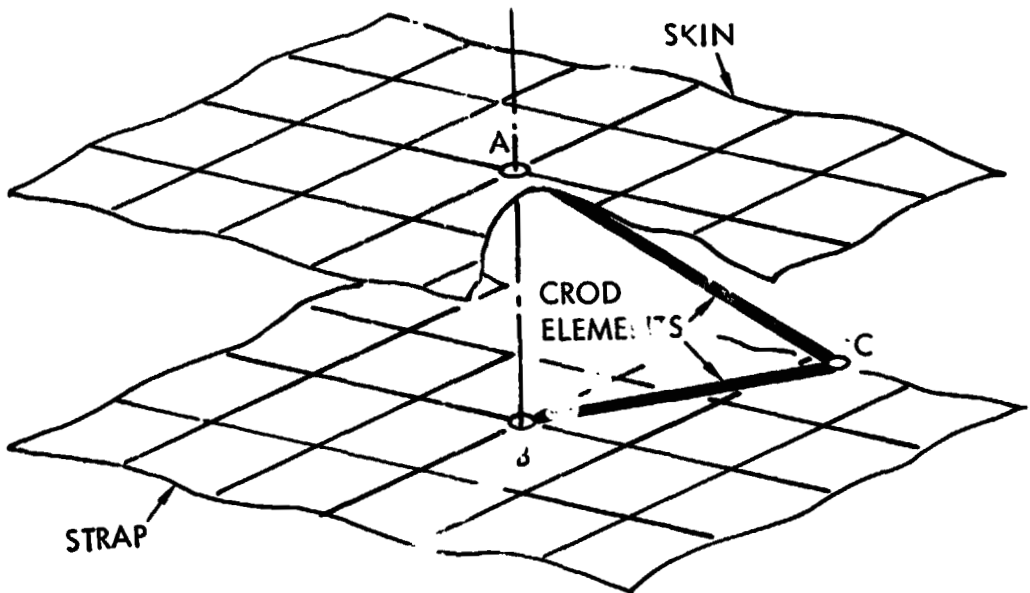


Figure 8. Fastener Idealization

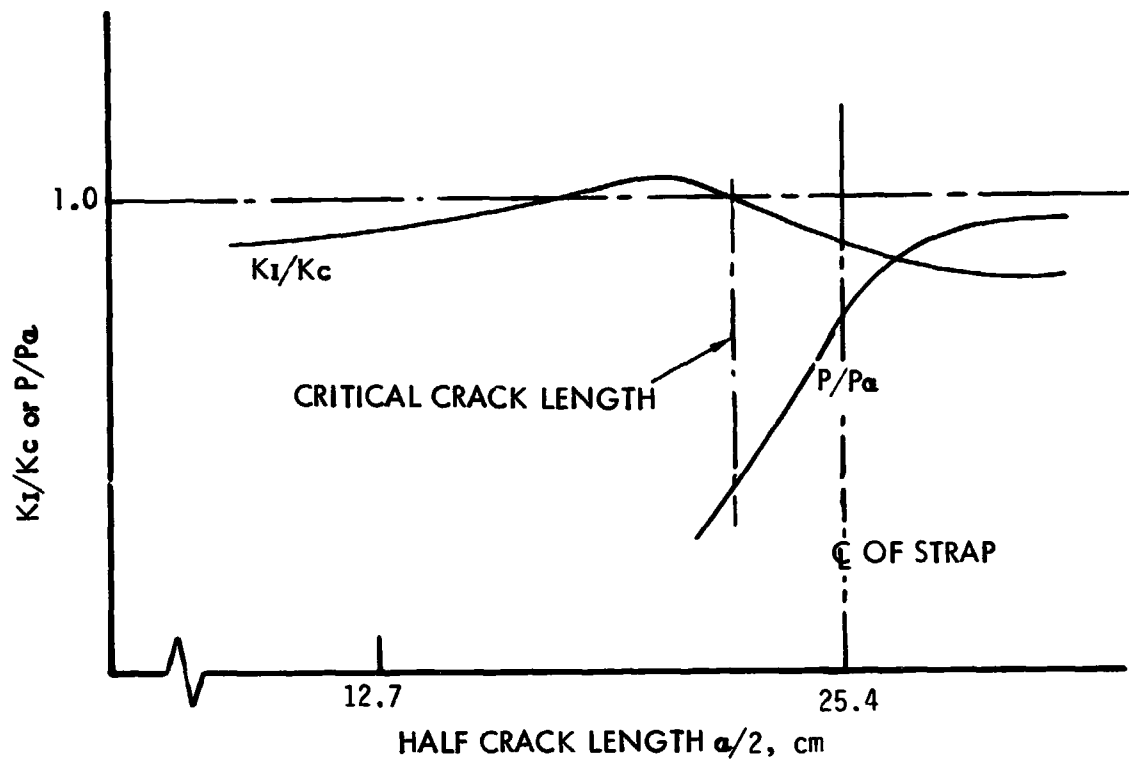


Figure 9. NASTRAN Results From the Finite Element Model Shown in Figure 6 for 3.2 mm TAPERLOKS.

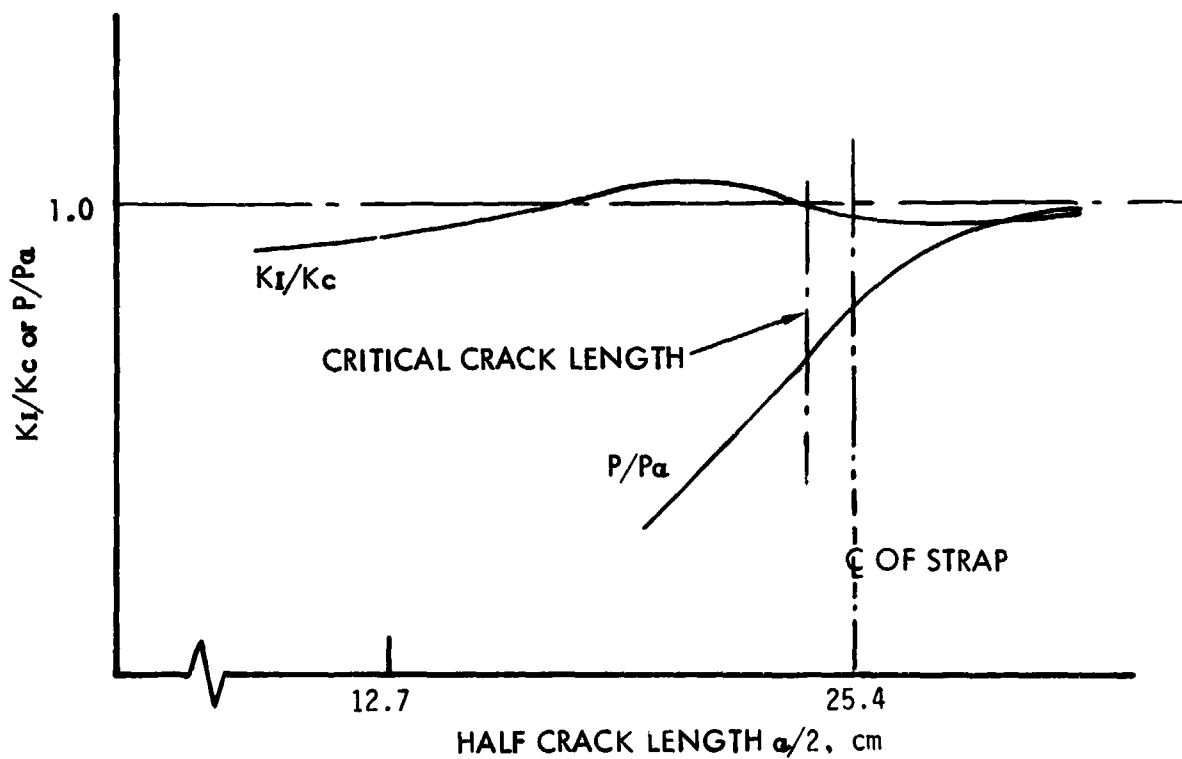


Figure 10. NASTRAN Results From the Finite Element Model Shown in Figure 6 for 4.0 mm Aluminum Rivets.

N75 31497

APPLICATION OF NASTRAN FOR STRESS ANALYSIS
OF LEFT VENTRICLE OF THE HEART*

12

Y. C. Pao
University of Nebraska-Lincoln
Lincoln, Nebraska

E. L. Ritman
Mayo Graduate School of Medicine
Rochester, Minnesota

H. C. Wang
IBM Corporation
Endicott, New York

SUMMARY

Knowing the stress and strain distributions in the left ventricular wall of the heart is a prerequisite for the determination of the muscle elasticity and contractility in the process of assessing the functional status of the heart. NASTRAN has been applied for the calculation of these stresses and strains and to help in verifying the results obtained by the computer program FEAMPS which was specifically designed for the plane-strain finite-element analysis of the left ventricular cross sections. Adopted for the analysis are the true shape and dimensions of the cross sections reconstructed from multi-planar x-ray views of a left ventricle which was surgically isolated from a dog's heart but metabolically supported to sustain its beating. A preprocessor has been prepared to accommodate both FEAMPS and NASTRAN, and it has also facilitated the application of both the triangular element and isoparametric quadrilateral element versions of NASTRAN. The stresses in several crucial regions of the left ventricular wall calculated by these two independently developed computer programs are found to be in very good agreement. Such confirmation of the results is essential in the development of a method which assesses the heart performance.

*This work was supported in part by research grants HL4664, HL3532, and RR7 from the National Institutes of Health, and by the Engineering Research Center, University of Nebraska-Lincoln.

INTRODUCTION

Structurally speaking, human and animal hearts are very complex not only in geometry but also in material characteristics. The finite element method therefore presents itself as an effective tool for analyzing the stresses and strains in the hearts. In order to assess whether or not a human or animal heart is functioning normally, it is necessary that the working characteristics of its left ventricular wall muscle (myocardium) be adequately ascertained, for it is the contraction of the left ventricular myocardium that pumps the oxygenated blood to circulate in the body. For the investigation of the left ventricle of the heart alone (not to be involved with the other chambers, right ventricle, and left and right atria), experiments of surgically isolated but metabolically supported, beating left ventricles of dogs are often prepared so that the dynamic changes of the shape and dimensions of the cross sections of the left ventricles during cardiac cycles can be recorded on videotape and by use of reconstruction techniques involving multiplanar x-ray projections or ultrasonic echoes of the cross sections (ref. 1).

The reconstruction technique using x-ray is schematically illustrated in Fig. 1. For a certain cross section of interest, a number of x-ray projections are taken by rotating the cross section with a chosen angle increment about its normal axis. The shape and dimensions of the cross section can then be reconstructed by use of algebraic algorithms (ref. 2). With a life supporting system (Fig. 2) for the isolated left ventricle of a dog experiment, any desired anatomic site selected at 0.7 mm intervals along the entire apical-to-basal axis of the ventricle can be reconstructed. Figure 3 shows a sample rectangular array of 35 apical-to-basal cross sections at a certain instant of a cardiac cycle. Further details and discussion of the reconstruction and data collection techniques are given in an internal publication (ref. 3), which is available upon request.

During relaxation (diastolic) phase of a cardiac cycle, the myocardium extends as the blood fills into the left ventricle. Based on the values of the left ventricular pressure and volume concomitantly recorded during the dog experiment, the history of the external work being done to the left ventricle can be calculated. Meanwhile, the finite element method can be applied for the analysis of the reconstructed instantaneous shapes of the left ventricular cross sections to determine the stresses and strains in the wall muscle and consequently the change of the strain energies. Upon relating the external work and the strain energies, the dependency of the elastic stiffness of the myocardium on the chamber pressure can then be estimated.

While the calculation of the external work is straightforward, it is for the calculation of the stresses and strains in the left ventricular cross sections that this paper reports the application of NASTRAN as a verifier for the plane-strain finite-element computer program FEAMPS which was specifically developed for the study of the left ventricles.

LEFT VENTRICLE MODEL AND FEAMPS

Since the thin-walled shell model was found to be adequate only for calculating the mean stresses across the wall thickness of the left ventricle, a number of thick-walled models have been proposed for obtaining the variation of the wall stresses (ref. 4). Most of the thick-walled models approximated the geometry of the left ventricle as a shell of revolution, either as a circular hollow cylinder, hollow sphere, or hollow prolate spheroid, all having uniform wall thickness. When biplane silhouettes of the left ventricle could be taken by application of the roentgen-, cine- and videodensitometry techniques (ref. 5), it became possible to incorporate some of the dimensions, such as the variations of wall thickness and chamber radii, of the left ventricle into the thick-walled models to determine the wall stresses by axisymmetric finite-element analysis. Now the advent of cross-sectional reconstruction from multiplanar x-ray views enables the thick-walled models of the left ventricle to be further improved by adopting the true shape and dimensions of the left ventricular cross sections.

However, the 35 apical-to-basal cross sections shown in Fig. 3 were obtained by a reconstruction system using only one x-ray source and one detector. The system requires the position and geometry of the left ventricle to be kept constant throughout successive cardiac cycles. This "stationarity" requirement is a serious disadvantage to be overcome by use of a spatial reconstruction system which will have multiple x-ray sources and multiple detectors. At present, the available data include (1) the dynamic changes of the cross-sectional shapes and dimensions at a few sites along the apical-to-basal axis of the left ventricle but are complete for several cardiac cycles, and (2) the shapes and dimensions for all apical-to-basal cross sections of the left ventricle but only at a few crucial instants of cardiac cycles. So these data suffice to investigate the cross-sectional behavior but not the ultimate three-dimensional analysis of the left ventricle.

FEAMPS is an abbreviation for Finite-Element Analysis of Myocardium by Plane-Strain Theory. The left ventricle is approximated as a hollow thick-walled cylinder with uniform cross section having the shape and dimensions reconstructed from multiplanar x-ray views. When the cylinder is subjected to uniform chamber pressure, it is assumed that all cross sections will deform identically. By looking at the silhouette shown in Fig. 4 constructed from stacking all cross sections in Fig. 3, it appears that plane-strain analysis should give a reasonably good prediction of the cross-sectional behavior in the vicinity of the base of the left ventricle.

It has been well established that the left ventricular myocardium is fibrous. Several investigations of the left ventricular wall with fibrous material properties had been reported (refs. 6,7). However, only scattered data are available regarding the changes of the fiber directions during cardiac cycles; the results of these investigations remain to be verified by more thorough experiments. FEAMPS follows the approach of assuming the left ventricle as a homogeneous, isotropic and elastic medium and proceeds to evaluate the effective elastic stiffness for such an equivalent model (refs. 8,9). Since the effective elastic stiffness is to be inversely determined on the basis of the

work-energy principle described in the Introduction, its value is assumed to be equal to 1 in the incremental-loading analysis of FEAMPS. Regarding the other material constant, Poisson's ratio, of the left ventricular myocardium, the issue whether it should be assumed equal to 0.415 (ref. 10) or nearly incompressible equal to 0.49 (ref. 11) is still not yet settled. So the results for both values will be discussed.

FORMATION AND ANALYSIS OF ELEMENTS

Figures 5(a) and 5(b) show a typical change of the shape and dimensions of a cross section near the base of the left ventricle reconstructed from multi-planar x-ray views during the early and ending stages of the diastole of a cardiac cycle, respectively. The diastolic phase is the resting period of the heart during which the relaxed left ventricular chamber is filling with blood and the wall muscles are passive and extended. The two-dimensional in-plane triangular elements of FEAMPS are generated by adopting 9 nodes across the wall thickness and 30 nodes around the perimeter of a reconstructed cross section. Additional elements may be necessary for the papillary muscle at certain levels within the ventricle. Figure 5(c) illustrates that the end-diastolic cross section shown in Fig. 5(b) is partitioned into 508 triangular elements using 290 nodes, of which 20 are for the formation of the 28 triangular elements for the peninsulalike papillary muscle.

The only input data required for FEAMPS are the coordinates of 30 pairs of points on the inner (endocardial) and outer (epicardial) boundaries of the cross section, plus additional pairs if necessary for the papillary muscle. A preprocessor which consists of several subroutines has been prepared to carry out the sequential numbering and calculation of the coordinates of all nodes, to compose the interconnected triangular elements by defining their respective constituent nodes, and to generate the nodal external loads. Plot subroutines are also made available for drawing of only the borders of the cross section or the partitioning pattern of the cross section either with or without the labelling of the node and element numbers.

The plane-strain finite-element analysis of FEAMPS follows closely the procedures delineated in Zienkiewicz's book (ref. 12). The displacements at any point within the triangular element are assumed as linear polynomials of its coordinates. This results in constant strains throughout the element. For saving computer storage spaces, the structural stiffness matrix is formulated in rectangular form by taking advantage of symmetry and discarding all of the zero elements that are on the outside of the diagonal band. In order to handle such a rectangular coefficient matrix, the Gauss-Jordan elimination method has been accordingly modified for the solution of the nodal displacements. This approach has reduced the computer storage core requirement for the structural stiffness matrix from 580x580 to 580x22 floating words in the analysis of the end-diastolic cross section partitioned as shown in Fig. 5(c). In case that further reduction of core storage in the computer is necessary, the zero elements inside the diagonal band of the structural stiffness matrix may also be discarded and all nonzero elements compacted into a vector, and the Gauss-Seidel iteration method can be applied for the solution of the nodal displacements (ref. 13).

Since the left ventricular cross sections are subjected to uniform internal pressure only on the inner (endocardial) boundary and there are no boundary constraints at all, the nodal displacements determined by machine computation may contain the superposition of a free body motion. To ascertain whether the sometimes very large free body motion will introduce significant errors in the subsequent calculation of the cross-sectional stresses, studies of the cross section with added fictitious boundary conditions have been conducted. More details on these studies are presented in the Discussion of Numerical Results.

FEAMPS also has the built-in provisions for the calculation of the nodal stresses by averaging the stresses of the adjoining elements, the extrapolation of the stresses for improved accuracy at the boundary nodes, the calculation of the strain energies, and for various plottings of the stress distributions of the cross section. Figure 6 displays a sample plot of the nodal circumferential stress distribution (normalized with respect to the uniform internal pressure) of the end-diastolic cross section with the exclusion of the almost uniformly compressed papillary muscle. Full details and computer program listing of FEAMPS are given in ref. 3. Nevertheless, the above synopsis should suffice for the discussion of the present paper.

APPLICATION OF NASTRAN

Attempts have been made to apply NASTRAN Rigid Format I to the two-dimensional plane-strain static analysis of the reconstructed left ventricular cross sections. With the availability of the FEAMPS preprocessor, preparatory works that can be expedited are the generation of the coordinates of the nodes, the division of the cross section into either triangular TRMEM or quadrilateral QDMEM1 elements, and the conversion of the uniform internal pressure on the inner (endocardial) boundary of the cross section into equivalent concentrated loads at the endocardial nodes.

As has been mentioned in the preceding section, there are no boundary constraints at all in the plane-strain analysis of the left ventricular cross sections. Test runs are necessary for the determination of acceptable fictitious points of support which can be adopted as the constraints data for the SPCI cards and will not introduce additional external loading. For instance, in the analysis of the cross section shown in Fig. 5(c), the decision to constrain node 6 in both the x and y directions and node 19 in the y direction was based on the verification by the printout, via SPCFORCE request, that the reactive forces at these two nodes were insignificantly small relative to the external loads at the endocardial nodes.

Since the left ventricle is assumed as a homogeneous, isotropic and elastic medium, the MAT2 cards specifying the material properties were prepared with the values of the Young's modulus, E , equal to 1 and the Poisson's ratio, ν , equal to 0.415 and 0.49, same as for the FEAMPS cases.

The extreme stresses are known to occur along the inner boundary of the left ventricular cross section; the four regions of primary concern have been

particularly pointed out in Fig. 7 to facilitate the comparison study of the FEAMPS and NASTRAN results. These regions are the inner borders of the posterior, septal, anterior and free walls in the vicinities of nodes 247, 253, 258 and 264, respectively. Figure 8 gives a close-up view of these four regions with the node and element numbers indicated.

DISCUSSION OF NUMERICAL RESULTS

Level 15.5 was used to generate all NASTRAN results reported herein. Table 1 shows that for $\nu=0.415$, the values of the principal stresses (normalized with respect to the chamber pressure) in the end-diastolic cross section determined by FEAMPS and NASTRAN are almost identical when both used triangular elements. The last two columns of Table 1 reveal that the principal stresses in a quadrilateral element are very close to the average values of those of the two adjacent triangular elements which have been combined to form the quadrilateral element. Since the number of the elements is reduced to half for the QDMEM1 analysis but the computer time is about doubled, the TRMEM analysis was selected for further studies.

For $\nu=0.415$ but for the early diastolic cross section shown in Fig. 5(a), Table 2 is presented to depict the effect of imposing fictitious boundary constraints to the cross section on the principal stresses. It is clearly indicated that restricting the x -displacement u of node 6 and the y -displacement v of nodes 6 and 19 causes no significant change to the values of the stresses. It also helps to demonstrate that the free body motion of the cross section which may result by FEAMPS analysis will not alter the values of the stresses.

The cases of treating the left ventricle as a nearly incompressible material with $\nu=0.49$ have also been investigated. Table 3 summarizes the normalized principal stresses for both the early and end diastolic cross sections shown in Figs. 5(a) and 5(b). The results exemplify the changes of the stresses during the diastolic phase of a cardiac cycle. As in Tables 1 and 2, these results obtained by FEAMPS and NASTRAN are in very good agreement.

Since FEAMPS has a feature for calculating the nodal stresses, the normalized principal stress distributions through the wall thickness at the four regions of concern during early and end diastole have been obtained and are presented in Fig. 9. It is noteworthy that some compressive circumferential stresses may develop at the innermost (0% of wall thickness in Fig. 9) myocardial layer in the septal and free walls where the curvature are small and sometimes even turn convex inward. Because other axisymmetric models of the left ventricle assumed cross sections to be of annular shape, in no portion of the cross section could the wall be curved inward. As a consequence, no compressive circumferential stress in the left ventricular wall had ever been determined by these models.

CONCLUDING REMARKS

The evaluation of the cross-sectional elastic stiffness (ref. 14) of the left ventricle during diastole depends in large measure on the accuracy of the values of the stresses and strains in the cross section. So it is indeed reassuring that these values can be confirmed by FEAMPS and NASTRAN.

This comparison study has also proved the applicability of NASTRAN for the plane-strain analysis of the left ventricular cross sections. Certainly, the other capabilities of NASTRAN can further help resolve some of the problems connected with the ongoing research of the three-dimensional analysis of the left ventricle, for which a special-purpose computer program is being developed. In the computer program, the true three-dimensional geometry of the left ventricle determined by the multiplanar x-ray views of its cross sections will be utilized and the analysis by treating the myocardium as a fibrous material using adjusted elastic stiffnesses and incremental loading will be incorporated.

It may also be anticipated that NASTRAN will contribute to the ultimate dynamic analysis of the left ventricle which will consider, among others, the effects of the myocardial contraction, the dynamics of the heart valves, and the interaction of the blood flow in the left ventricular chamber.

ACKNOWLEDGEMENT

We would like to thank Dr. Earl H. Wood for his encouragement and assistance throughout this project, Dr. Richard A. Robb for the reconstruction of the cross sections and Dr. David Donald for the surgical preparation of the isolated left ventricle. Their thanks are also extended to Mrs. Sharon Zahn, Mrs. Jean Frank and her coworkers at Mayo, and Mr. John L. Nikkila and Mrs. Louise Simmons at UNL for providing computer programming assistance and/or preparing the manuscript and illustrations.

REFERENCES

1. Robb, R. A., Greenleaf, J. F., Ritman, E. L., Johnson, S. A., Sjostrand, J. D., Herman, G. T., and Wood, E. H.: Three-Dimensional Visualization of the Intact Thorax and Contents, A Technique for Cross-Sectional Reconstruction from multiplanar X-Ray Views. Computers and Biomedical Research, Vol. 7, 1974, pp. 395-418.
2. Gordon, R., and Herman, G. T.: Reconstruction of Pictures from Their Projections. Communications of the Association for Computing Machinery, Vol. 14, 1971, pp. 759-768.
3. Pao, Y. C., Robb, R. A., and Ritman, E. L.: Plane-Strain Finite-Element Analysis of Reconstructed Left Ventricular Cross Sections. Technical

Report UHL/MAYO 7501, University of Nebraska-Lincoln, 1975. Presented at the Sixth Annual Meeting of the Biomedical Engineering Society, New Orleans, April 11-12, 1975.

4. Pao, Y. C., Ritman, E. L., and Wood, E. H.: Finite-Element Analysis of Left Ventricular Myocardial Stresses. Journal of Biomechanics, Vol. 7, 1974, pp. 469-477.
5. Ritman, E. L., Sturm, E., and Wood, E. H.: A Biplane Roentgen Videometry System for Dynamic (60/second) Studies of the Shape and Size of Circulatory Structures, Particularly the Left Ventricle. pp. 179-211 in Roentgen-, Cine- and Videodensitometry. Fundamentals and Applications for Blood Flow and Heart Volume Determination (Edited by Heintzen, P. H.), Georg Thieme Verlag, Stuttgart, 1971.
6. Janz, R. F., and Grimm, A. F.: Finite-Element Model for the Mechanical Behavior of the Left Ventricle. Circulation Research, Vol. 30, 1972, pp. 244-252.
7. Streeter, D. D., Jr., and Hanna, W. I.: Engineering Mechanics for Successive States in Canine Left Ventricular Myocardium, I. Cavity and Wall Geometry. II. Fiber Angle and Sarcomere Length. Circulation Research, Vol. 33, 1973, pp. 639-664.
8. Pao, Y. C., and Ritman, E. L.: An Energy Method for Evaluating the Global Young's Modulus of Left Ventricular Myocardium in the Passive State. Technical Report UHL/MAYO 7502, University of Nebraska-Lincoln, 1975.
9. Ghista, D. N., Sandler, H., and Vayo, W. H.: Elastic Modulus of the Human Intact Left Ventricle--Determination and Physiological Interpretation. Medical and Biological Engineering, Vol. 13, 1975, pp. 151-161.
10. Ross, A. L.: A Finite Element Computer Program for Nonlinear Structural Analysis of the Heart. General Electric Report 72SD213, King of Prussia, Pennsylvania, 1972.
11. Janz, R. F., Kubert, B. R., Moriarty, T. F., and Grimm, A. F.: Deformation of the Diastolic Left Ventricle--II. Nonlinear Geometric Effects. Journal of Biomechanics, Vol. 7, 1974, pp. 509-516.
12. Zienkiewicz, O. C.: The Finite Element Method in Engineering Science, McGraw-Hill, New York, 1971.
13. Pao, Y. C., and Ritman, E. L.: On Storage, Retrieval, and Gauss-Seidel Iteration Involving Nonzero Elements of a Sparse Stiffness Matrix Compacted as a Vector. Computers and Biomedical Research, Vol. 8, 1975, pp. 232-243.
14. Pao, Y. C., Ritman, E. L., Robb, R. A., and Wood, E. H.: A Finite-Element Method for Evaluating Cross-Sectional Young's Modulus of Diastolic Left Ventricle. Paper No. F3b.4, The 28th Annual Conference on Engineering in Medicine and Biology, New Orleans, September 20-24, 1975.

Table 1. Comparison of principal stresses for the end-diastolic cross section ($E=p_1=1$ and $\nu=0.415$).

REGION	Element Number	FEAMPS		NASTRAN			
		Triangular Elements		Triangular Elements		Isoparametric Quadrilateral Elements	
		σ_1	σ_2	σ_1	σ_2	σ_1	σ_2
POSTERIOR	425	2.14	-1.16	2.14	-1.16	1.95	-1.30
	426	0.34	-3.15	0.34	-3.15		
	427	9.64	3.53	9.62	3.53	7.50	1.55
	428	4.60	0.12	4.59	0.12		
	429	5.82	1.25	5.81	1.24	7.83	1.05
	430	8.54	0.59	8.53	0.58		
	431	6.41	-1.48	6.40	-1.48	5.80	0.16
	432	4.48	0.34	4.47	0.34		
SEPTAL	439	-0.61	-1.34	-0.61	-1.34	-0.42	-1.15
	440	0.07	-1.06	0.07	-1.06		
	441	-1.06	-1.55	-1.06	-1.55	-1.06	-1.62
	442	-0.76	-1.75	-0.76	-1.74		
	443	-0.88	-1.85	-0.87	-1.84	-1.09	-1.72
	444	-1.05	-1.70	-1.05	-1.69		
	445	-0.03	-1.08	-0.03	-1.07	-0.99	-1.64
	446	-1.16	-1.85	-1.16	-1.85		
ANTERIOR	453	4.96	0.37	4.95	0.37	6.43	0.08
	454	7.42	-0.99	7.40	-0.99		
	455	7.95	-0.23	7.93	-0.23	6.78	-0.48
	456	5.42	-0.35	5.40	-0.35		
	457	4.88	-0.65	4.87	-0.65	6.64	-0.17
	458	7.62	0.05	7.60	0.04		
	459	5.11	-1.36	5.10	-1.35	4.39	-0.48
	460	3.53	0.22	3.52	0.22		
FREE	463	-1.40	-2.11	-1.40	-2.11	-1.13	-1.59
	464	0.52	-0.43	0.52	-0.43		
	465	-1.55	-2.21	-1.54	-2.21	-1.11	-1.65
	466	-0.62	-1.58	-0.61	-1.58		
	467	-1.26	-2.10	-1.25	-2.09	-1.20	-1.81
	468	-1.12	-1.73	-1.12	-1.72		
	469	-0.15	-1.11	-0.15	-1.11	-1.04	-1.96
	470	-1.03	-1.97	-1.03	-1.96		

Table 2. Comparison of principal stresses for the early diastolic cross section ($E=p_1=1$ and $\nu=0.415$).

R E G I O N	Element Number	NASTRAN		FEAMPS			
		$u_6=v_6=v_{19}=0$		$u_6=v_6=v_{19}=0$		No Boundary Constraints	
		σ_1	σ_2	σ_1	σ_2	σ_1	σ_2
P O S T E R I O R	427	5.01	1.44	5.01	1.44	5.01	1.44
	428	2.76	0.48	2.76	0.48	2.76	0.48
	429	1.96	0.30	1.96	0.30	1.97	0.30
	430	7.14	2.73	7.14	2.73	7.14	2.73
	431	5.51	0.06	5.51	0.06	5.51	0.06
	432	0.15	-1.38	0.15	-1.38	0.15	-1.38
O R	433	1.66	-0.31	1.66	-0.31	1.66	-0.31
	434	2.63	0.11	2.63	0.11	2.63	0.11
S E P T A L	436	0.44	-0.83	0.44	-0.83	0.44	-0.83
	437	-0.10	-1.21	-0.10	-1.21	-0.10	-1.21
	438	-0.11	-0.82	-0.11	-0.82	-0.11	-0.82
	439	-0.81	-1.25	-0.81	-1.25	-0.81	-1.25
	440	0.004	-1.05	0.005	-1.05	0.004	-1.05
	441	-0.01	-1.02	-0.005	-1.02	-0.01	-1.02
	442	-0.54	-1.23	-0.54	-1.23	-0.54	-1.23
	443	0.26	-0.71	0.26	-0.71	0.26	-0.71
A N T E R I O R	446	0.11	-1.59	0.11	-1.59	0.11	-1.59
	447	2.07	-0.01	2.08	-0.10	2.08	-0.10
	448	1.51	-0.97	1.51	-0.97	1.51	-0.97
	449	2.63	-0.17	2.64	-0.17	2.64	-0.17
	450	3.13	-0.96	3.13	-0.96	3.13	-0.96
	451	3.60	-0.49	3.60	-0.49	3.60	-0.49
O R	452	2.45	-0.56	2.46	-0.56	2.46	-0.56
	453	2.54	-0.50	2.55	-0.50	2.55	-0.50
F R E E	454	4.08	0.02	4.09	0.02	4.09	0.02
	455	2.40	-1.32	2.40	-1.32	2.40	-1.32
	456	1.80	-0.56	1.80	-0.56	1.80	-0.56
	457	0.99	-1.19	0.99	-1.19	0.99	-1.19
	458	1.71	-0.22	1.71	-0.22	1.71	-0.22
	459	0.82	-1.22	0.82	-1.22	0.82	-1.22
	460	0.72	-0.88	0.72	-0.88	0.72	-0.88
	461	0.58	-1.07	0.58	-1.07	0.58	-1.07

Table 3. Comparison of principal stresses for the early and end diastolic cross sections considered as a nearly incompressible material $\nu=0.49$ ($E=p_i=1$).

R E G I O N	EARLY DIASTOLE				END DIASTOLE			
	FEAMPS		NASTRAN		FEAMPS		NASTRAN	
	σ_1	σ_2	σ_1	σ_2	σ_1	σ_2	σ_1	σ_2
P O S T E R I O R	5.69	2.81	5.68	2.81	2.84	0.26	2.67	0.19
	3.87	1.86	3.87	1.85	-0.67	-3.59	-0.64	-3.45
	1.83	-0.08	1.83	-0.09	1.63	-1.40	1.55	-1.37
	8.40	4.65	8.41	4.65	-3.25	-7.33	-3.14	-7.06
	6.96	0.29	6.98	0.29	15.23	10.21	14.56	9.74
	-1.54	-3.42	-1.53	-3.42	-0.15	-4.69	-0.15	-4.50
	2.72	0.68	2.72	0.67	10.31	5.51	9.83	5.22
	3.56	0.84	3.58	0.85	8.74	1.22	8.35	1.14
S E P T A L	0.30	-0.88	0.29	-0.88	5.75	-2.10	5.51	-2.03
	-0.24	-1.45	-0.25	-1.44	6.49	2.56	6.21	2.41
	0.88	-0.44	0.85	-0.45	1.15	-2.52	1.12	-2.43
	-1.57	-3.06	-1.56	-3.03	4.52	0.46	4.38	0.42
	2.73	1.24	2.67	1.20	2.17	-1.98	2.19	-1.91
	-0.44	-2.60	-0.45	-2.58	2.01	0.20	1.98	0.16
A N T E R I O R	3.47	1.10	3.40	1.07	-0.31	-2.04	-0.23	-1.98
	0.30	-2.33	0.26	-2.32	1.48	-0.12	1.52	-0.11
	3.76	0.96	3.69	0.94	3.86	1.40	3.80	1.37
	2.84	-1.00	2.78	-1.00	0.19	-3.04	0.28	-2.93
	3.31	-0.38	3.27	-0.38	5.15	1.22	4.99	1.13
	2.40	-0.43	2.34	-0.46	-0.38	-4.51	-0.29	-4.34
	2.12	-0.74	2.10	0.73	9.15	4.74	8.83	4.50
	4.09	0.34	4.05	0.22	6.56	-1.20	6.37	-1.19
	2.34	-1.50	2.33	-1.49	7.41	0.08	7.16	0.03
	2.29	0.13	2.27	0.12	4.97	-0.45	4.83	-0.43
F R E E	-0.10	-2.04	-0.10	-2.03	7.54	0.56	7.27	0.51
	1.72	0.10	1.71	0.10	4.31	-1.85	4.16	-1.81
	0.82	-1.35	0.83	-1.35	6.76	3.42	6.54	3.27
	0.91	-0.63	0.91	-0.63	-3.58	-6.32	-3.48	-6.13
	-0.07	-1.51	-0.06	-1.50	2.75	0.43	2.67	0.41
	-0.05	-1.10	0.06	-1.10	-1.25	-3.12	-1.19	-3.05
	0.45	-0.84	0.46	-0.83	2.59	2.07	2.47	2.00
	1.12	-0.30	1.11	-0.31	-3.14	-3.93	-3.03	-3.82

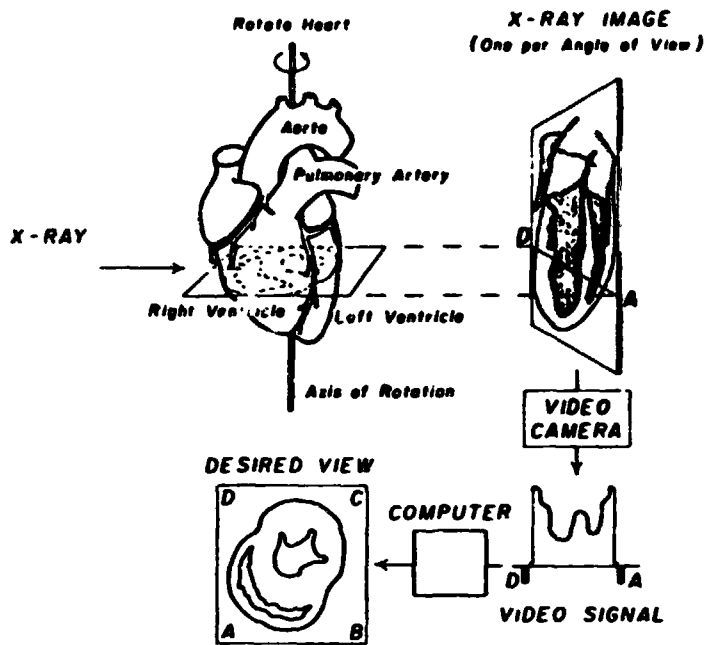


Figure 1. Reconstruction of cardiac cross section from multi-planar x-ray views and by use of algebraic algorithm.

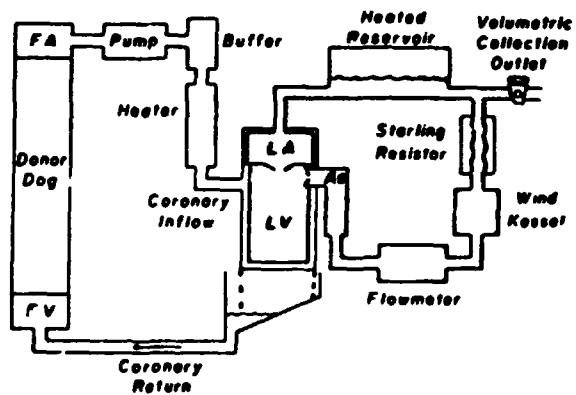


Figure 2. Schematic of the surgically isolated, metabolically supported canine left ventricle.

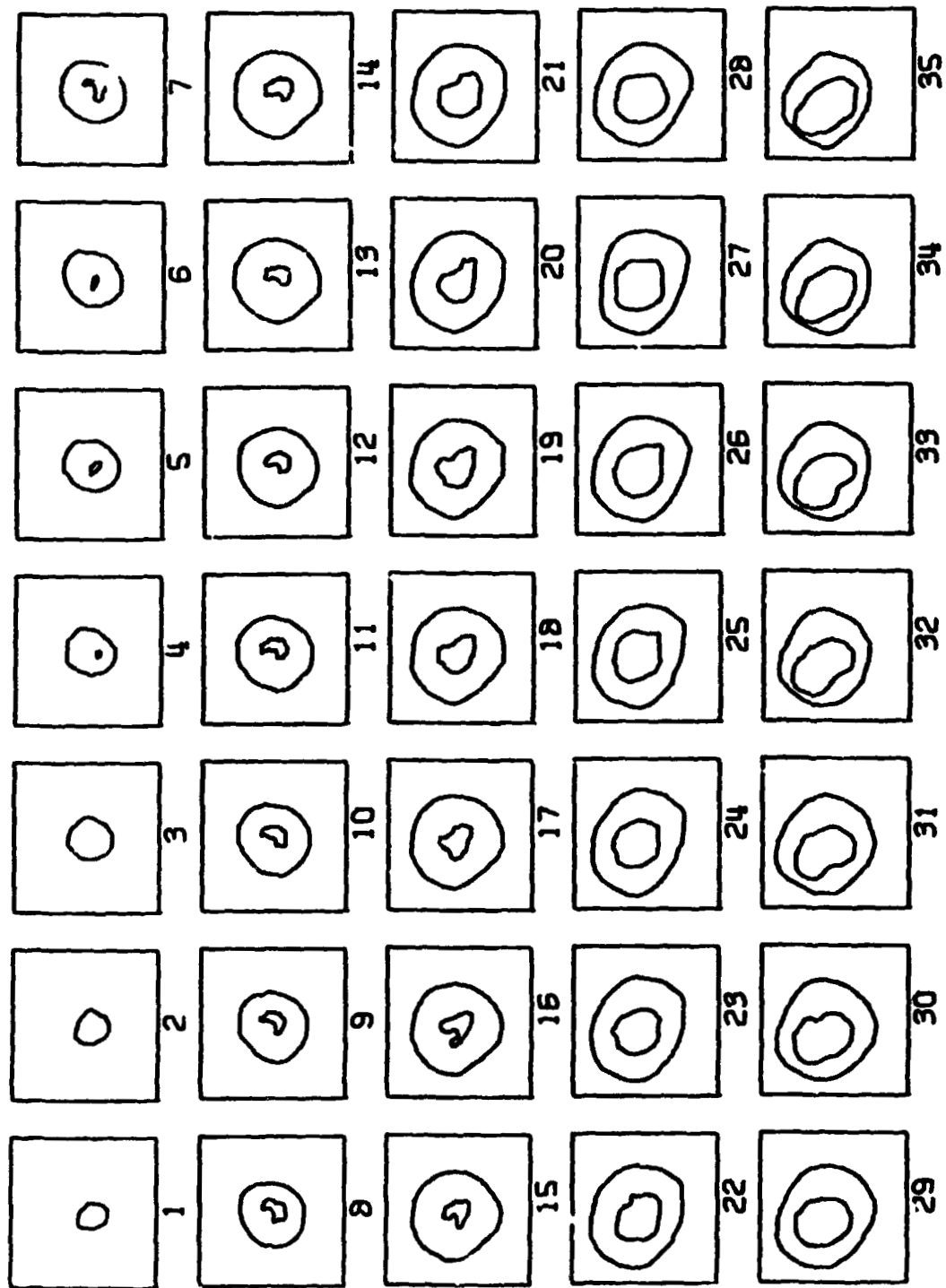


Figure 3. Sample plot of 35 reconstructed apical-to-basal cross sections of an isolated left ventricle during the end of diastole of a cardiac cycle.

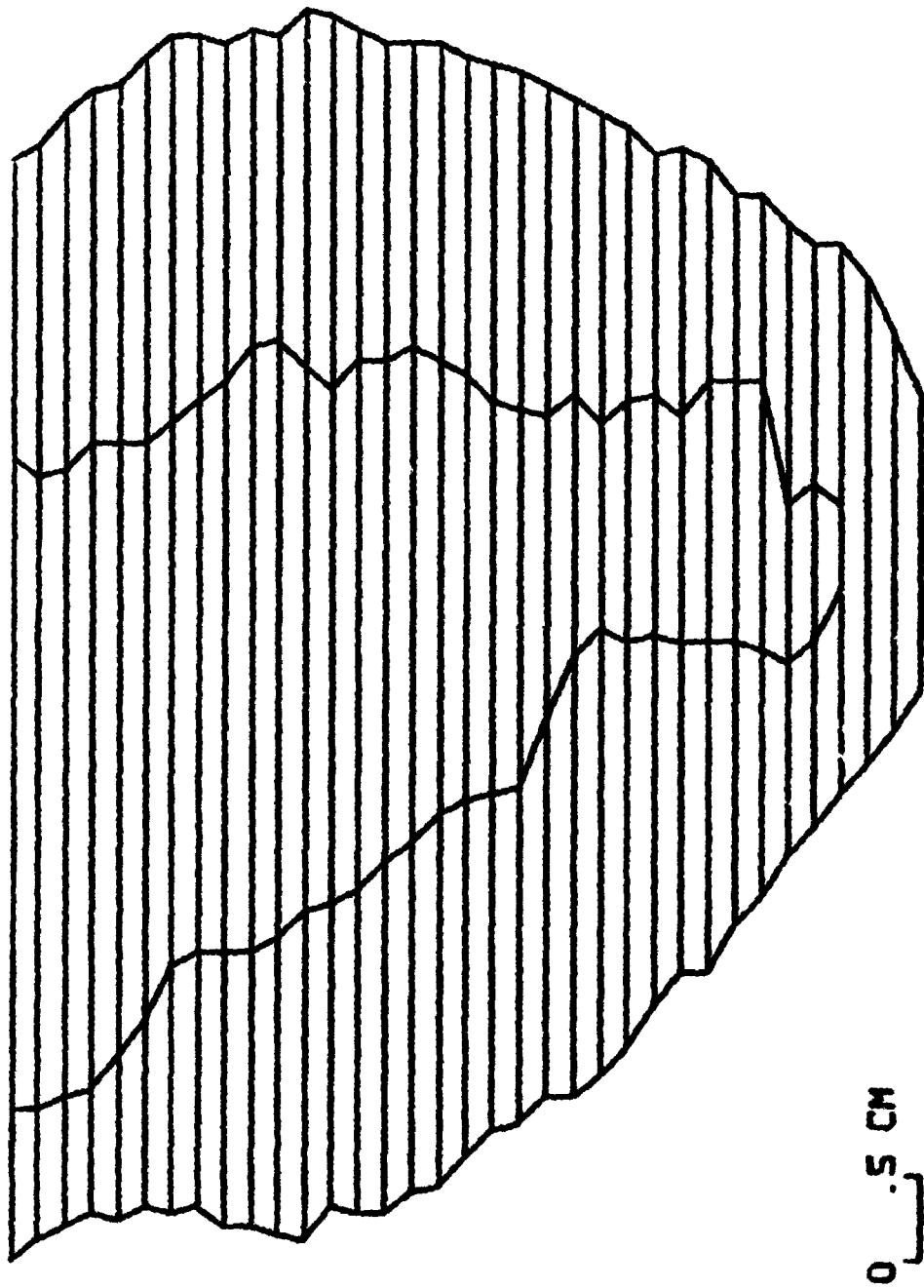
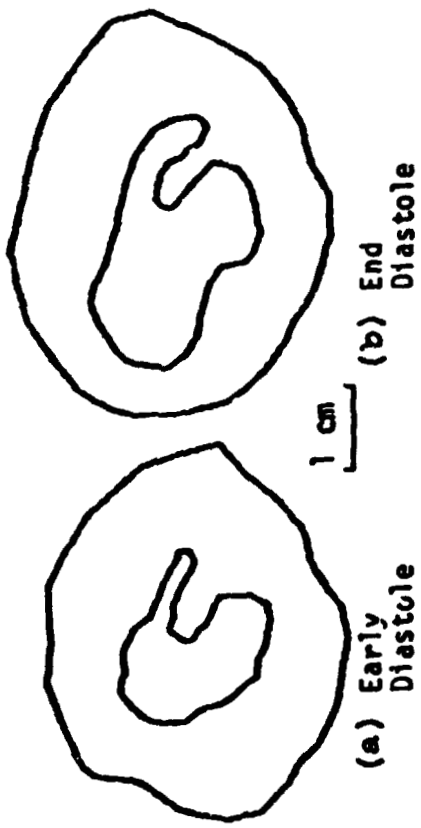


Figure 4. Formation of left ventricular silhouette from stacking the 35 cross sections shown in Fig. 3.



(c) Finite Element Partitioning Pattern

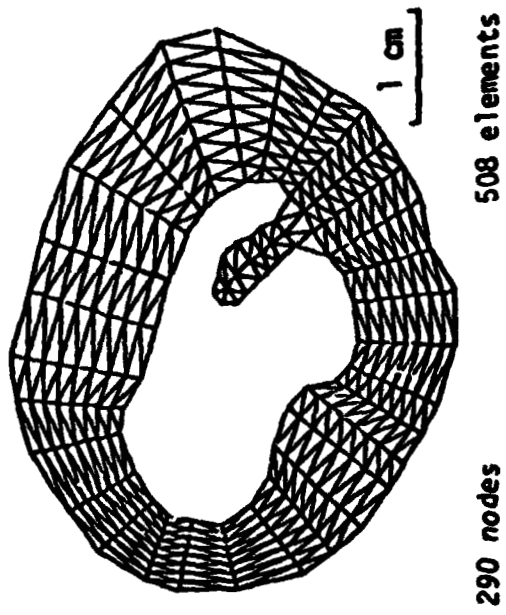


Figure 5. Typical shape and dimension changes of a cross section during diastole, and finite element partitioning pattern.

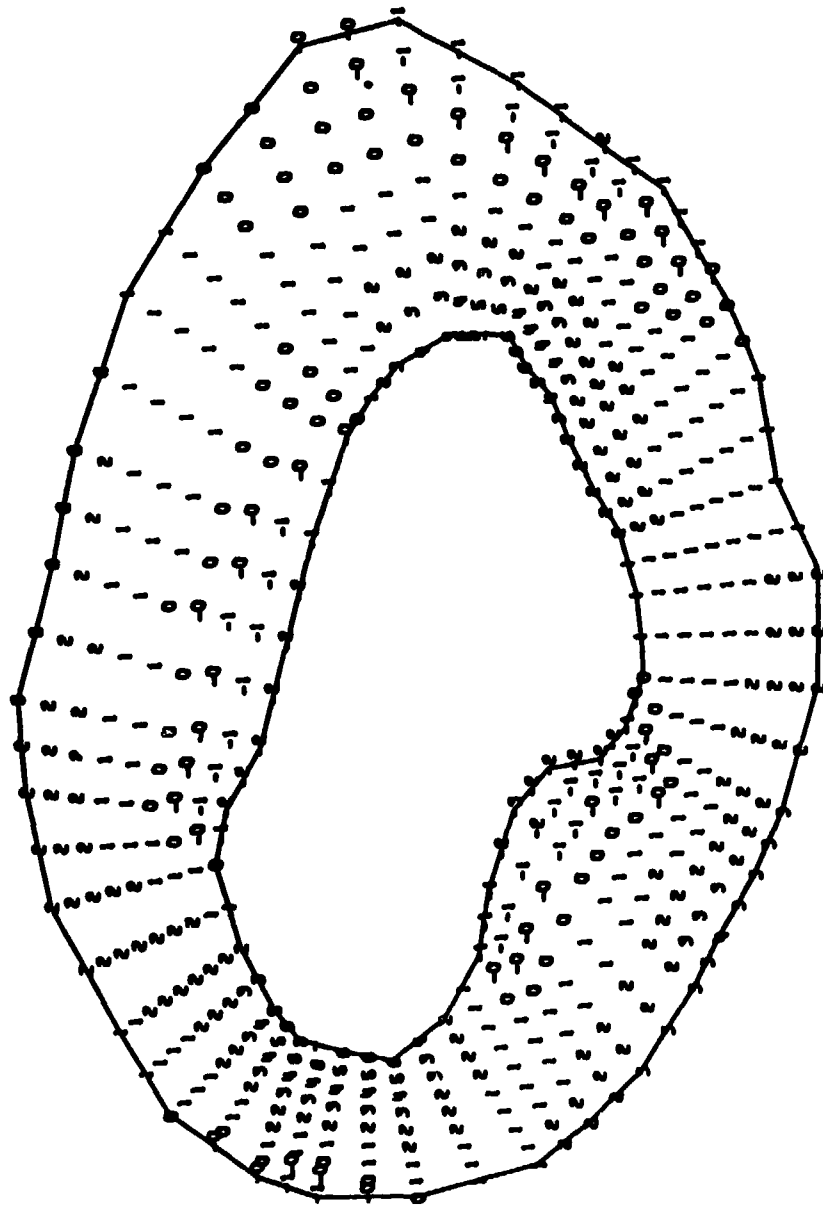


Figure 6. Sample plot of the normalized circumferential stress distribution in an isolated left ventricular cross section.

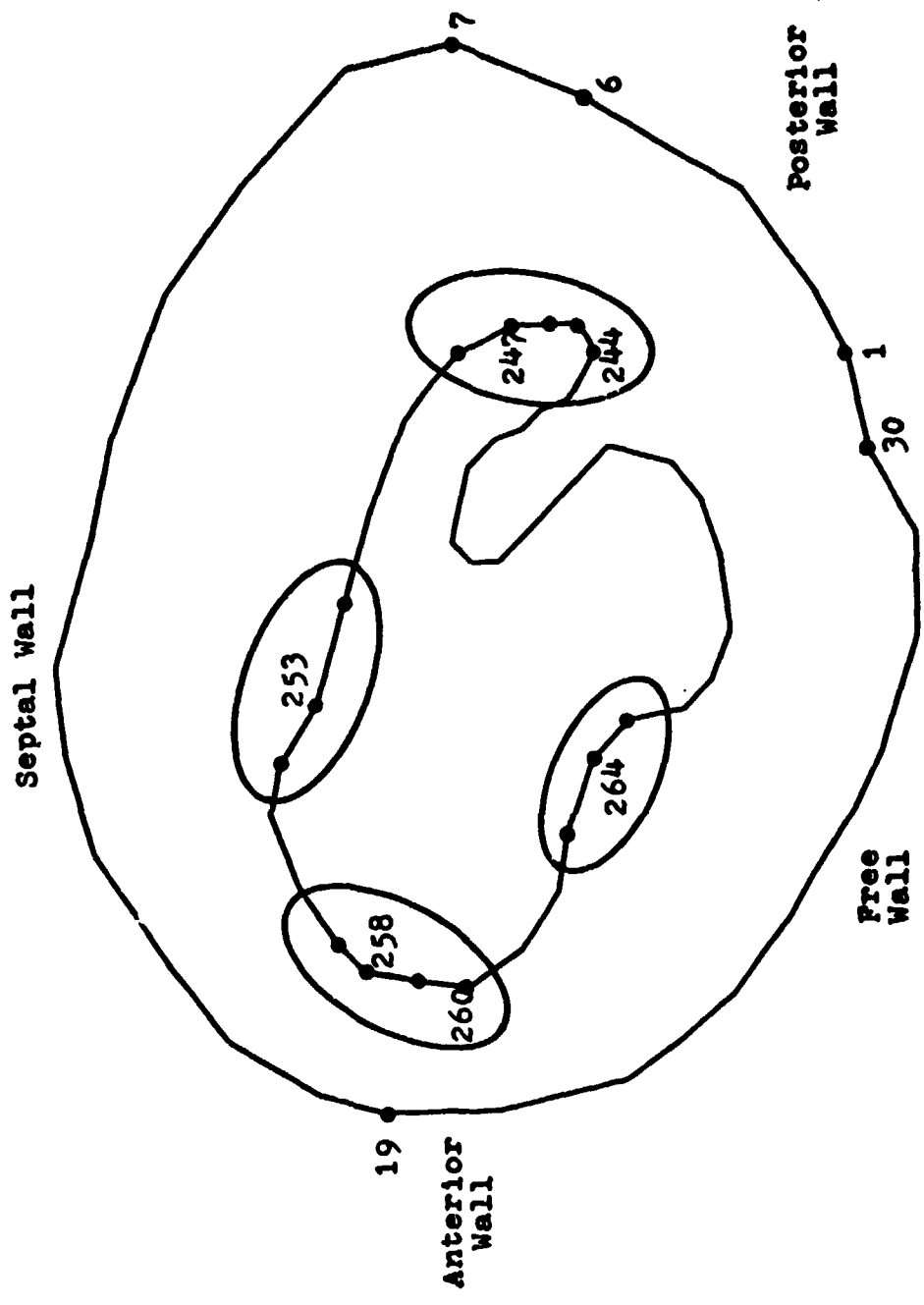


Figure 7. Some node numbers identifying the four regions of extreme stresses.

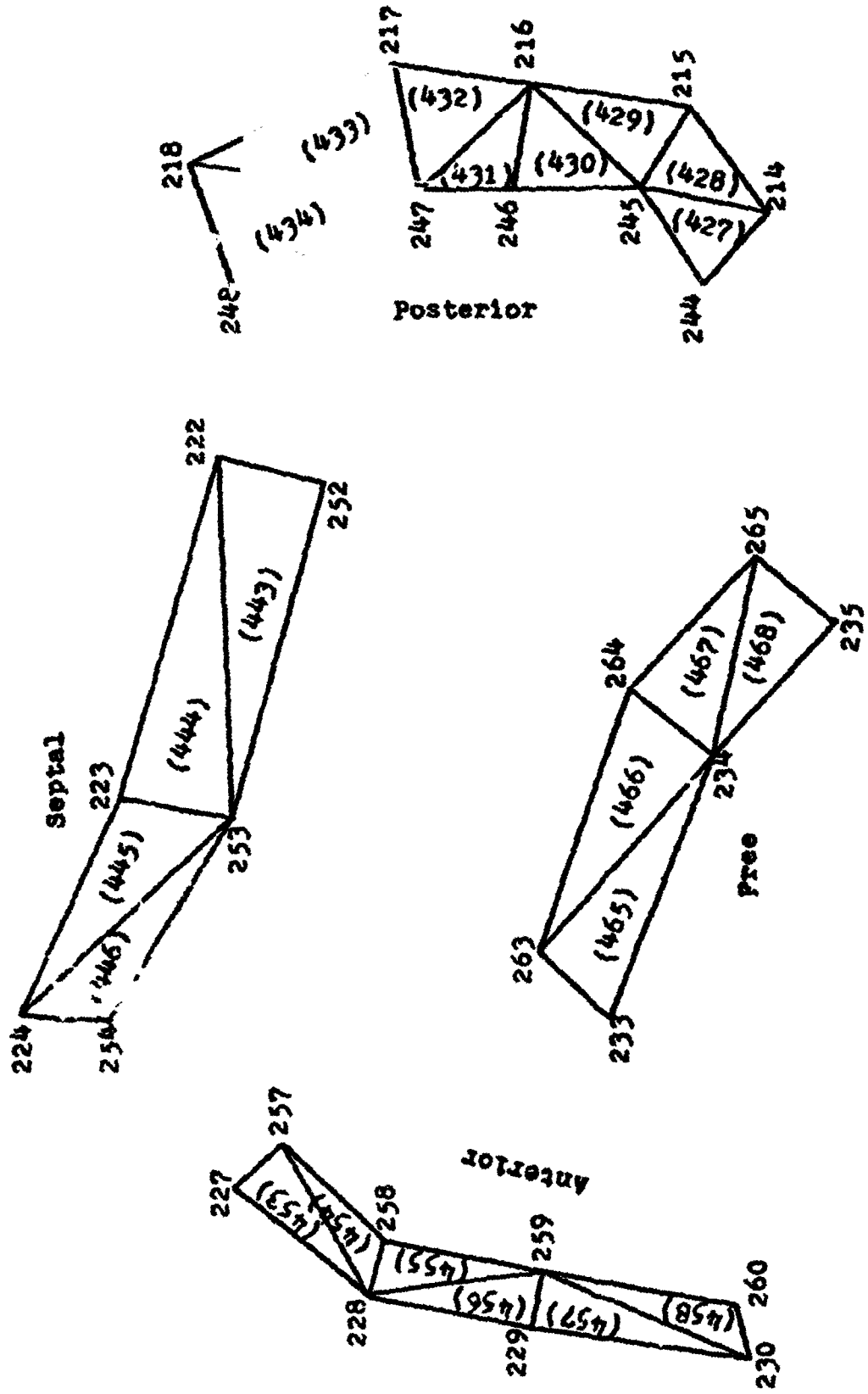


Figure 8. Close-up details of the four regions of extreme stresses with the node and element (parenthetical) numbers indicated.

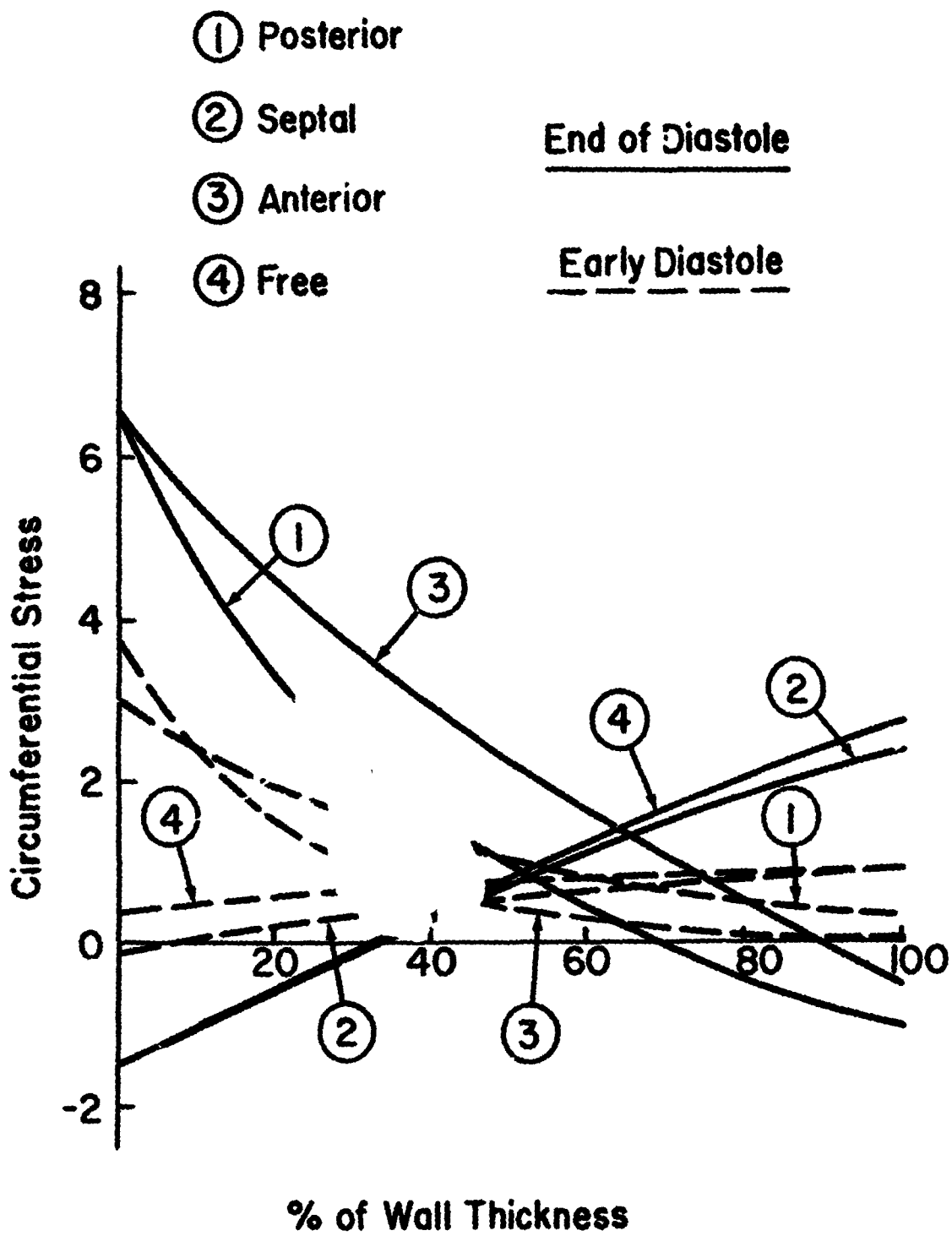


Figure 9. Normalized circumferential stress distributions across the wall thickness at the four regions of the left ventricular cross section.

N75 31498

DYNAMIC SUBSTRUCTURE ANALYSIS OF THE
INTERNATIONAL ULTRAVIOLET EXPLORER (IUE) SPACECRAFT

William R. Case
NASA Goddard Space Flight Center

SUMMARY

This paper presents the results of a steady state vibration analysis of the IUE spacecraft simulating its sinusoidal vibration test. The model of the spacecraft, including solar arrays and the scientific instrument consisted of three separate substructure models; one of which was used to represent the two identical solar arrays. Substructuring techniques were used since the large overall size of the problem precluded solving it utilizing a single model. The paper discusses the models used for each substructure, including reduction to an acceptable size for the combined dynamic analysis. Also discussed are the DMAP alters needed for performing the modal analysis and the subsequent modal frequency response and substructure data recovery. Comparison of the results with data obtained during vibration tests of the spacecraft are also included.

13

INTRODUCTION

The International Ultraviolet Explorer (IUE) is a 6670 N (1500 lb) Explorer class satellite designed to make astronomical observations in the ultraviolet spectrum. It is to be placed in synchronous orbit from which it will be in continuous contact with the control center at the Goddard Space Flight Center (GSFC). Guest observers, from this country as well as others, will come to GSFC to use the observatory, consisting of the ground control center and the orbiting satellite.

The IUE satellite, in its orbital configuration, is shown in figure 1. Figure 2 shows an exploded view of the satellite with only one of the two solar arrays indicated. The satellite consists of the basic spacecraft (S/C) structure, two solar arrays and the scientific instrument (SI) which is the heart of the IUE.

In the launch configuration the solar arrays are folded around the S/C upper body as indicated in figure 2. The arrays are latched to the top deck of the upper body structure at this time. The satellite is attached to the Delta launch vehicle through the use of a conical adapter which is clamped to the satellite at station 0.0 of figure 1. The adapter is not shown in the figure but is part of the structure that is vibrated during the design qualification vibration testing of the satellite. The analysis described herein was performed to estimate the vibration levels and dynamic loads that would be experienced by the IUE during the sinusoidal vibration tests.

IUE STRUCTURE DESCRIPTION

Spacecraft

The IUE S/C structure is shown in figure 2 (along with a solar array and the SI). It consists of the upper body structure, two equipment decks, an upper cone structure to which an apogee motor connects, a propulsion bay and a lower cone. The base of the lower cone, which is S/C station 0.0, is attached to a Delta launch vehicle conical adapter via a Marmon clamp. The S/C structure was designed and built at GSFC and is made mainly of aluminum.

The upper body structure is basically a truss with shear panels around the outer, octagonally shaped, periphery. The two equipment decks, which attach to the top and bottom of the truss, are aluminum skin honeycomb.

Solar Arrays

A schematic of one of the solar arrays is shown in figure 2; the other array attaches to the S/C 180° from the one shown. Each array is connected to the S/C during launch at five locations. At the upper S/C deck the arrays connect with ball joints that take all of the thrust axis loads from the arrays. The deployment mechanism is built to take shear in a plane perpendicular to the thrust axis. These are also swivel pins that partially restrain the motion at the lower corners of the arrays. The array structure is honeycomb panels stiffened by lightweight beams (not shown in figure 2). They are fabricated in Cannes, France by Societe Nationale Industrielle Aerospatiale (SNIAS) under subcontract to the European Space Research Organization (ESRO). Each solar array weighs approximately 89 N (20 lb).

Scientific Instrument

A cutaway view of the SI is shown in figure 3. It consists of a 45 cm Ritchey-Chretien telescope and an echelle spectrograph. The telescope structure consists mainly of an aluminum cylinder with stiffening rings at either end (strong ring and secondary mirror support spider). The SI is attached to the S/C upper body truss at three locations around the strong ring. The spectrometer structure is three main decks (camera, echelle and collimator decks) supported by three pairs of legs spaced 120° apart. The support legs are made of graphite fibre reinforced epoxy (GFRP) and the decks for the engineering test unit S/C were made of aluminum. Two smaller decks are mounted to the uppermost main deck (camera deck). Around the spectrograph is a non-structural dust cover. The spectrograph is designed and built at GSFC and weighs approximately 870 N (250 lb).

FINITE ELEMENT MODELS

Spacecraft

The original S/C structure finite element model was generated by Avco Corp. under a contract to the Mechanical Systems Division at GSFC. This model, following some modifications and updates was used in the combined dynamic analysis due to its availability and the fact that it appeared to be of sufficient detail to obtain the first few modes (in each axis) adequately. Figure 4 shows this model with the upper body truss shown separate for clarity. The main structural members are the two decks, the upper body truss, the shear panels (around the octagonal outside faces of the upper body truss), the upper and lower cones and the upper cone truss. The model contains 200 grid points with 1062 unconstrained degrees of freedom (DOF) and employs 426 elements (mainly CBAR, CQUAD, CTRIA). For the dynamic analysis, the 1062 DOF were reduced to 157 DOF using the Guyan reduction.

Solar Array

The solar array model used in the combined dynamic analysis was generated by the Mechanical Systems Division at GSFC from data supplied by ESTEC, the technical monitors for ESRO on the solar array contract. ESTEC supplied NASA with their finite element model and it was then converted to a NASTRAN model. Figure 5 shows the mesh used. The model consists mainly of CQUAD and CBAR elements. There are 165 grid points with 916 unconstrained DOF in the model for one array. For the dynamic analysis, the 916 DOF were reduced to 126 DOF.

In order to verify the solar array model with ESTEC results, an eigenvalue analysis of the cantilevered array was run. The array was constrained in all degrees of freedom to which it connects to the S/C. The modes of the NASTRAN model, compared to the ESTEC results (using the ASKA program) are shown below for the first few modes. Also shown are some preliminary test data identifying the first few modes of the array. In order to obtain better agreement with the test data so that a better representation of any S/C-array coupling problems could be assessed, the array model stiffness was lowered by 10% for the coupled dynamic analysis. The resulting frequency comparisons are also shown below.

Solar Array Mode	Frequencies (Hz)			
	ESTEC ASKA model	NASA NASTRAN model	Test Results	NASA NASTRAN model (10% reduced stiffness)
1st Sym.	59.8	55.5	53-55	52.9
2nd Sym.	77.5	73.5	65-68	70.2
1st Antisym.	50.5	50.8	46-48	48.4
2nd Antisym.	73.0	78.4	74-76	74.7

Some more recent test data indicate slightly lower frequencies but these have not as yet been documented by ESTEC.

Scientific Instrument

A detailed finite element model of the SI was formulated by the Test and Evaluation Division at GSFC for performing combined structural-thermal-optical analyses to assess the performance of the SI while in orbit. Figures 6 and 7 show the telescope and spectrometer portions of this model. For the dynamic analysis this model was reduced to only a few grid points for each of the three main decks plus several degrees of freedom for the telescope, which is quite stiff. In all, the original model contained 3006 unconstrained DOF with a reduction to 72 DOF by the Guyan reduction.

Verification of the spectrometer portion of the model was accomplished by comparison with test data on the SI with the telescope removed. This comparison is shown below for the modes of the spectrometer cantilevered at the strong ring with the NASTRAN results from reference 1.

Spectrometer Mode	Frequency (Hz)	
	NASTRAN model	Test
1st Y bending	16.2	} 15
1st Z bending	16.8	
1st torsion	23.8	25
2nd Y bending	37.3	} 37
2nd Z bending	37.3	

These theoretical modes are essentially the same with the telescope connected to the strong ring due to the high stiffness of the strong ring and the telescope tube.

DYNAMIC ANALYSIS

Formulation

From the preceding discussions it can be seen that the complete model, if run as a single finite element model without substructuring, would be very large. Due to this fact, as well as the fact that there are a relatively few DOF in which the solar arrays and the scientific instrument connect to the S/C, it was decided to use substructuring techniques to solve for the modes and steady state vibration response of the complete satellite. Another factor which makes this approach attractive is that the two solar arrays are identical and can be represented through the use of a single finite element model data deck if substructuring techniques are used. The table below shows the size of the models for each of the sub-

structures together with the computer time (CPU seconds on the IBM 360/95) required to generate the reduced stiffness and mass matrices for each substructure.

Substructure	Unconstrained DOF "F"	Reduced DOF "A"	Phase I CPU Time (seconds)
S/C	1200	157	478
Solar Array	990	126	245
SI	3006	72	1078
Totals (1)	6132	427	-

(1) Total DOF numbers reflect the fact that there are two solar arrays but do not include duplicated DOF at points where substructures attach to one another.

It can be seen that if the problem were solved as one structure it would contain 6132 DOF which is too large, even for the IBM 360/95. Taken as three separate substructures, the total time to generate all of the matrices needed to perform the eigenvalue analysis is 1801 CPU seconds indicated in the table. This includes the two solar arrays since only one set of matrices is needed due to the fact that they are identical. The grid point locations and the stiffness and mass matrices for the solar array DOF were generated in a local coordinate system. For the DOF on the S/C where the arrays attach, two coordinate systems were defined (one for each array) such that they would match the local system for that array. This coordinate system was then used for the global system for the DOF for the particular array and its S/C attach points.

In order to obtain the vibration modes and steady state response using substructure techniques, the problem is run in several phases as indicated below.

Phase	Description	No. of Runs
I	Formulate K_{AA} , M_{AA} for each distinct substructure model	3: S/C, solar array (once), SI
II-a	Combine substructures and do modal analysis	1
II-b	Restart II-a and do modal frequency response	1
III-a	Restart I with II-a tape of "A" set mode shapes to recover mode shapes for other DOF	4: S/C, solar array (twice), SI
III-b	Restart I with II-b tape of "A" set frequency responses to recover frequency response for other DOF	4: S/C, solar array (twice), SI

Notice that only one solar array Phase I run is needed although there are two solar arrays. When Phase II-a is run, the solar array stiffness and mass matrices are expanded and added to the S/C matrices twice (in the appropriate rows and columns) so that each array is represented in the combined model. When responses are calculated in Phase III (for the points reduced by Guyan reduction), the "A" set points from Phase II are used for the DOF corresponding to the appropriate array.

In order to implement the substructuring procedure described, Direct Matrix Abstraction Programming (DMAP) alters to NASTRAN Rigid Formats 3 and 11 were used. The basic DMAP alters for a similar substructuring problem were set up by Universal Analytics, Inc. under contract to GSFC and are described in reference 2. Those procedures were modified slightly to take advantage of the fact that the two solar arrays can be represented by one model, as already described. Appendix A lists the DMAP alters to NASTRAN level 15.5.1 that were used for the IUE analysis. The partitioning vectors (PV1, PV2, PV3, PV4) required in Phase II-a when the reduced substructures are combined are used to expand the matrices to the combined "A" set size and add rows and columns of substructure matrices at the DOF where substructures connect. The use and construction of these are discussed in reference 2 and in the NASTRAN User's Manual (ref. 3).

Modal Analysis

As indicated in the previous section, the three substructures were reduced to 157, 126 and 72 DOF for the S/C, one solar array and the SI respectively. When combined into the complete model (with two arrays and accounting for duplicate connection points) the model contained 427 DOF. From this model the modes of the structure cantilevered at the base of the Delta adapter, as in the sine vibration tests, were calculated. The particulars for this Phase II-a run are:

No. of DOF: "A"	Eigenvalue Method	No. Eigenvectors Computed	Computer Core Required (bytes)	Phase II-a CPU Time (seconds)
427	Givens	25	750K	665

The results of this Phase II-a run give the eigenvalues and the eigenvectors for the "A" set DOF. To recover the mode shapes for the other DOF for each substructure, the Phase III-a runs are executed. These use a restart tape from the Phase I set up run along with the OUTPUT1 tape (from Phase II-a) with the partitioned "A" set mode shapes for the particular substructure. As seen from Appendix I, the Phase II-a run partitions the "A" set mode shapes into four data blocks; one for each substructure. These go on one

physical tape and the appropriate data block is read from this tape during each Phase III-a run. In this manner, the mode shapes for all DOF in the problem are obtained and can be plotted, one substructure at a time. The Phase III-a mode shape recovery solution times are given below.

Substructure	Phase III-a CPU Time (seconds)
S/C	102
Solar Array No. 1	126
Solar Array No. 2	126
SI	342

Frequency Response

Once the eigenvalues and "A" set mode shapes are obtained, a modal frequency (or steady state) response analysis can be run. As mentioned previously, this is accomplished with a restart of Phase II-a and a switch from NASTRAN rigid format 3 to rigid format 11. The output from this phase, as with Phase II-a are solutions for the "A" set DOF. In this case, they are the frequency response solutions to whatever steady state loads were input. For the IUE vibration test simulation, the input "loads" are actually accelerations at the base of the Delta adapter. Since NASTRAN does not allow direct specification of base motions, this was accomplished by including, in the original model, a large mass at the base of the Delta adapter. During the Phase II-a modal analysis, the DOF to which the large mass was attached were not constrained but included in a SUPORT Bulk Data card. The resulting analysis gave rigid body "shaker" modes plus elastic modes that, due to the presence of the large mass, were essentially cantilevered from the large mass. The rigid body modes are then included in the frequency response analysis and the structure is excited with a load at the large mass whose value is the large mass multiplied by the desired acceleration at the large mass DOF (the shaker/structure interface). For this analysis, the desired acceleration at the base of the Delta adapter was 1.0g in order to obtain transmissibilities of the structure for base acceleration. The Phase II-b solution time is given below.

No. of Modes	No. of Frequencies	Phase II-b CPU Time
25	51	203

Once Phase II-b is run, the transmissibilities (in this case) for the "A" set DOF are available and the Phase III-b runs can be executed to obtain frequency responses for any desired output for any substructure. This is very similar to the restart to obtain mode shape data (Phase III-a) after completing Phase II-a. The

Phase III-b solution time to recover the frequency response output for each substructure is given below.

Substructure	Phase III-b CPU Time (seconds)
S/C	477
Solar Array No. 1	337
Solar Array No. 2	337
SI	858

Some of the results of the analysis for Z axis vibration are shown in figures 8 to 13. Figures 8 to 11 show transmissibilities representing the acceleration at each of four locations per unit acceleration at the base of the Delta adapter. Also included in these figures are test results. The test results were obtained from vibration tests at a low, 0.2g, input level as well as from the design qualification tests which were run at up to 2.0g. It can be seen that there is an appreciable difference in the high and low input test data due to nonlinearities in the structure. This is particularly evident on figure 9 where the 16 Hz spectrometer mode did not show up in the low level tests but did in the high level. Considering the spread in the high and low level test data, the theoretical results appear to give good agreement with the test data particularly below about 25 to 30 Hz. Above this frequency range the theoretical results follow the trend of the test data but is shifted higher in frequency. It therefore appears that the model is too stiff, as one would expect, as frequency increases.

From the frequency response plots the lowest mode is at 10.5 Hz which is the first S/C bending mode in the Z axis. The Y axis mode is also at 10.5 Hz. The next mode is at 15 Hz which is the first spectrometer mode. Modes in the range 30 to 40 Hz are due to S/C and SI second bending. Modal damping values of 10% critical were used for all lateral modes and was obtained from early tests on a structure using only a mass representation of the SI.

Figures 12 and 13 show data that are used to set limits on the test inputs. The design qualification bending moment is required not to exceed 26.2 kN-m (232 000 in-lb) during test. From figure 12 an input acceleration value of 0.23g must not be exceeded in order to prevent the bending moment from exceeding 26.2 kN-m (232 000 in-lb).

Figure 13 shows the relative deflection between the lowest spectrometer deck (at grid point 5007 in figure 7) and the S/C upper body truss leg which is nominally 2.2 cm (0.85 inches) away. If the input acceleration gets high enough the clearance will be exceeded resulting in banging of the deck on the S/C structure and possibly damaging of the sensitive alignment of the SI. At the 10 Hz fundamental mode the clearance will not be exceeded since the input has to be notched to 0.23g to avoid exceeding the bending moment at the separation plane. However, at 16 Hz it

can be seen that the relative deflection will be exceeded if the input is above about 2.0g. This is the level which is to be input during the design qualification tests. In fact, the tests did indicate that the IUE could just barely take 2.0g input and not have banging of the spectrometer on the S/C support legs.

CONCLUSIONS

Substructuring techniques have been used to solve a problem that would probably have been too large to solve as one computer submittal on the GSFC IBM 360/95. The total CPU time required for 3 Phase I, 1 Phase II-a and II-b, and 4 Phase III-a and III-b runs was 1 1/2 hr. The results of the analysis compare favorably with test data.

APPENDIX I

DMAP ALTERS FOR MODAL AND FREQUENCY
RESPONSE SUBSTRUCTURE ANALYSIS
(NASTRAN LEVEL 15.5.1)

PHASE I : Create KAA,MAA for each distinct substructure (three runs)
i=1 (S/C),i=2 (SI),i=3 (Solar Array)

SOL 3,0

ALTER 74

OUTPUT1 KAA,MAA,,,/C,N,-1/C,N,i/C,N,INPi

EXIT

ENDALTER

These are conventional rigid format 3 runs except that they terminate after the Guyan reduction. Any DOF that will connect to another substructure must be left in the "A" set in these runs, must be sequenced the same in all substructures and must have compatible coordinate systems.

PHASE II-a : Combine substructures and solve for eigenvalues and "A" set eigenvalues.

SOL 3,0

ALTER 47

PARAM //C,N,NOP/V,N,TRUE=-1

\$

\$Read S/C matrices in and incorporate into overall K,M

\$

INPUTT1 /K1,M1,,,/C,N,-1/C,N,1/C,N,INP1

MERGE, ,,,K1,PV1,/KG1

ADD KGG,KG1/KGG1

EQUIV KGG1,KGG/TRUE

MERGE, ,,,M1,PV1,/MG1

ADD MGG,MG1/MGG1

EQUIV MGG1,MGG/TRUE

\$
\$Read SI matrices in and incorporate into overall K,M

\$
INPUTT1 /K2,M2,,,/C,N,-1/C,N,2/C,N,INP2

MERGE, ,,,K2,PV2,/KG2

ADD KGG,KG2/KGG2

EQUIV KGG2,KGG/TRUE

MERGE, ,,,M2,PV2,/MG2

ADD MGG,MG2/MGG2

EQUIV MGG2,MGG/TRUE

\$
\$Read matrices for one Solar Array and incorporate
\$into overall K,M for both arrays using PV3,PV4

\$
INPUTT1 /K3,M3,,,/C,N,-1/C,N,3/C,N,INP3

MERGE, ,,,K3,PV3,/KG3

ADD KGG,KG3/KGG3

EQUIV KGG3,KGG/TRUE

MERGE, ,,,M3,PV3,/MG3

ADD MGG,MG3/MGG3

EQUIV MGG3,MGG/TRUE

MERGE, ,,,K3,PV4,/KG4

ADD KGG,KG4/KGG4

EQUIV KGG4,KGG/TRUE

MERGE, ,,,M3,PV4,/MG4

ADD MGG,MG4/MGG4

EQUIV MGG4,MGG/TRUE

CHKPNT KGG,MGG

ALTER 50,54

}
Solar Array No.1
(use K3,M3,PV3)

}
Solar Array No.2
(use K3,M3,PV4)

```

$
$Write partitioned modal data on tape for Phase III-a
$
OUTPUT1  LAMA,,,,//C,N,-1/C,N,4/C,N,INP4

PARTN    PHIG,,PV1/,PHIA1,,/C,N,1/C,N,1
PARTN    PHIG,,PV2/,PHIA2,,/C,N,1/C,N,1
PARTN    PHIG,,PV3/,PHIA3,,/C,N,1/C,N,1
PARTN    PHIG,,PV4/,PHIA4,,/C,N,1/C,N,1

OUTPUT1  PHIA1,PHIA2,PHIA3,PHIA4,,/C,N,0/C,N,4/C,N,INP4

ENDALTER

```

The Bulk Data deck should include a dummy scalar mass and stiffness just to get SMA1 and SMA2 to generate KGG and MGG data blocks to get started. It should also contain the direct matrix input (DMI) cards for the partitioning vectors for each substructure (including the second Solar Array) and an SPOINT card specifying as many scalar points as there are "A" set DOF.

PHASE II-b : Restart Phase II-a for modal frequency response

```

SOL 11,0

ALTER 146,146

ALTER 156

OUTPUT1  PPF,,,,//C,N,-1/C,N,4/C,N,INP4

PARTN    UPVC,,PV1/,UPVS1,,/C,N,1/C,N,3
PARTN    UPVC,,PV2/,UPVS2,,/C,N,1/C,N,3
PARTN    UPVC,,PV3/,UPVS3,,/C,N,1/C,N,3
PARTN    UPVC,,PV4/,UPVS4,,/C,N,1/C,N,3

OUTPUT1  UPVS1,UPVS2,UPVS3,UPVS4,,/C,N,0/C,N,4/C,N,INP4

CØND     LB14,NØP

ENDALTER

```

The data deck for this run is the same as any rigid format .1 restart of a rigid format 3 run. It should include all of the dynamic load data,damping and the excitation frequency list.

PHASE III-a : Recover mode shapes for each substructure (four runs)
i=1 (S/C),i=2 (SI),i=3 (Solar Array No.1),i=4 (Solar
Array No.2). These runs are restarts of the Phase I runs
with two restarts of the Solar Array model.

```
SOL 3,0  
ALTER 74  
PARAM //C,N,NOP/V,N,TRUE=-1  
JUMP LBPH3  
ALTER 94  
LABEL LBPH3  
INPUTT1 /LAMAS,,,,/C,N,-1/C,N,4/C,N,INP4  
EQUIV LAMAS,LAMA/TRUE  
INPUTT1 /UVSUB,,,,/C,N,i-1/C,N,4  
EQUIV UVSUB,PHIA/TRUE  
ENDALTER
```

The Case Control deck requests output desired and there is no
additional Bulk Data.

PHASE III-b : Recover frequency response data for each substructure
(four runs);i=1 (S/C),i=2 (SI),i=3 (Solar Array No.1),
i=4 (Solar Array No.2). These runs are also restarts of
Phase I runs

```
SOL 11,0  
ALTER 46  
PARAM //C,N,NOP/V,N,TRUE=-1  
ALTER 94,158  
INPUTT1 /PPF,,,,/C,N,-1/C,N,4/C,N,INP4  
INPUTT1 /UDV1f,,,,/C,N,i-1/C,N,4  
SDR1 USETD,,UDV1f,,,GO,GM,,KFS,,/UPVC,,QPC/C,N,1/  
C,N,DYNAMICS
```

```
CHKPNT  UPVC,QPC

SDR2    CASECC,CSTM,MPT,DIT,EQEDYN,SILD,,,,PPF,QPC,UPVC,
        EST,XYCDB/OPP_1,OQPC1,OUPVC1,OESC1,OEFC1,/C,N,
        FREQ/V,N,NOSORT2

ALTER 169,170

RANDOM   XYCDB,DIT,PSDL,OUPVC2,OPPC2,OQPC2,OESC2,OEFC2,
        CASECC/PSDF,AUTO/V,N,NORD

SAVE    NORD

ALTER 181,183

ENDALTER
```

The Case Control deck requests output desired. Dummy dynamic loads, damping, frequency response list should be included in the Bulk Data deck.

REFERENCES

1. Bruck, L. R.: Development of the IUE Spectrometer Finite Element Models, NASA-GSFC Memorandum Report No. 741-30.
2. Universal Analytics, Inc.: NASTRAN Substructuring Analysis Report, (to NASA-GSFC - no report number), July 9, 1974.
3. McCormick, Caleb W., ed.: The NASTRAN User's Manual (Level 15.0). NASA SP-222(01), 1973.

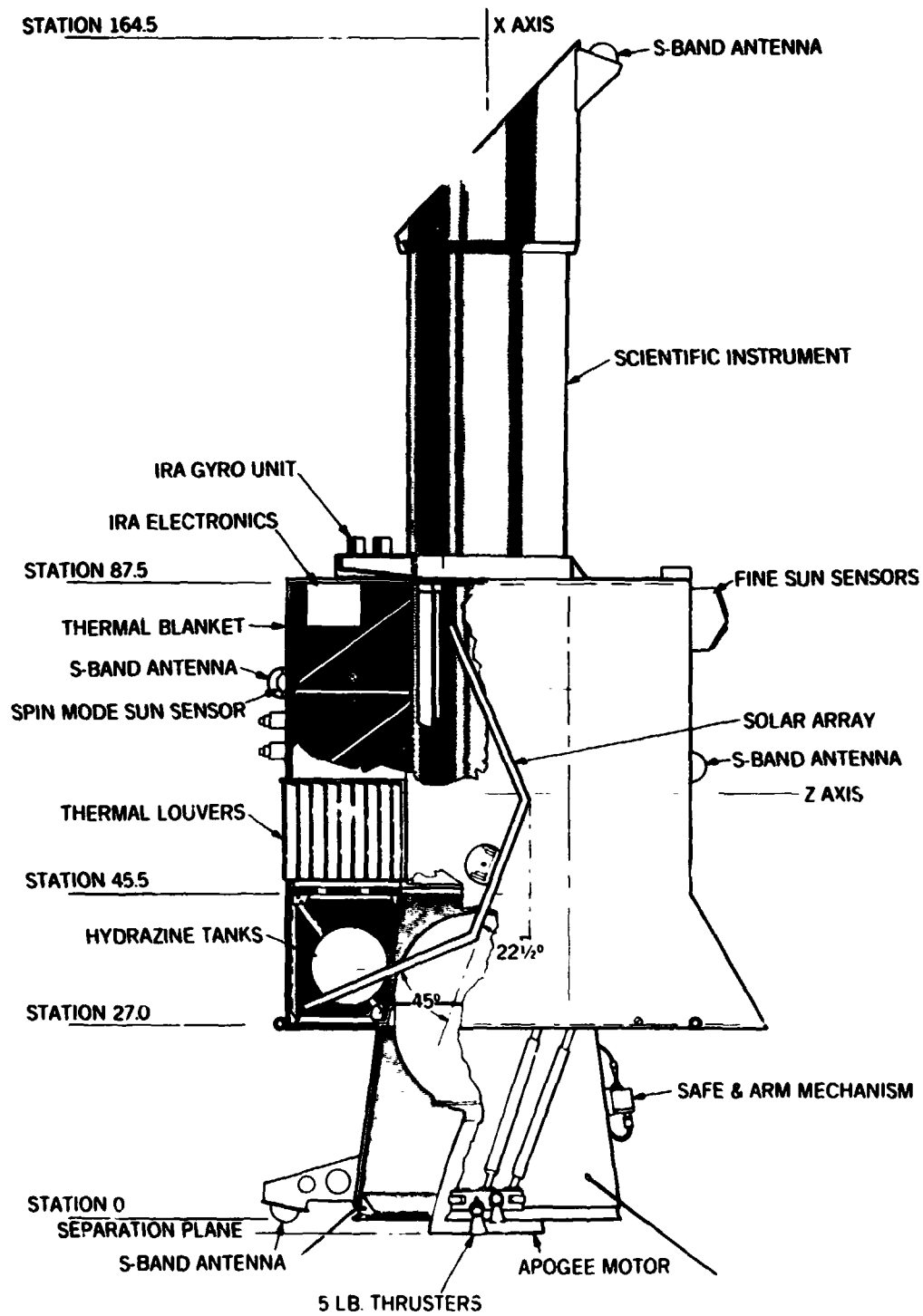


Figure 1.- IUE spacecraft with solar arrays deployed.
 1 lb = 4.448 N.

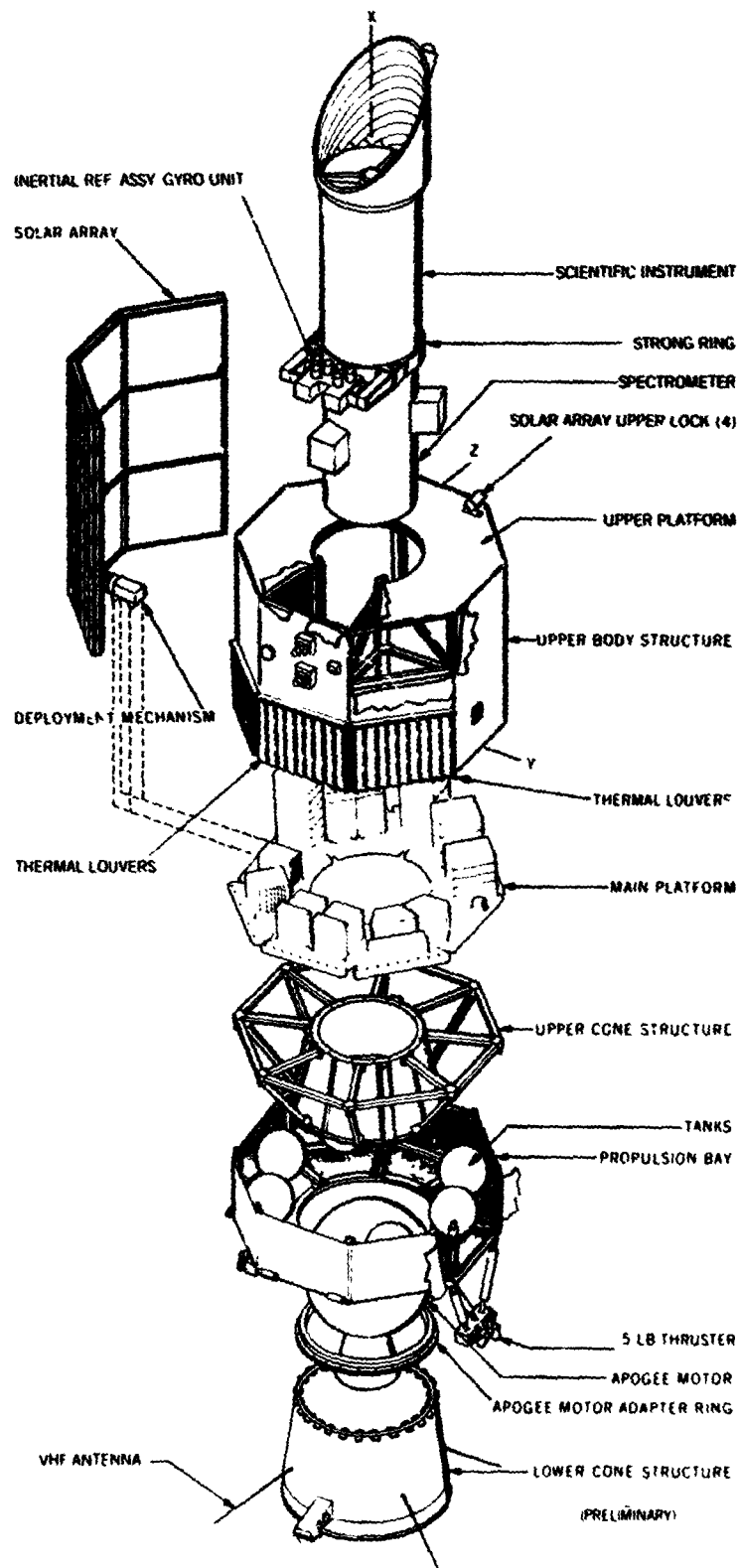


Figure 2.- Exploded view of IUF spacecraft. 1 lb = 4.448 N.

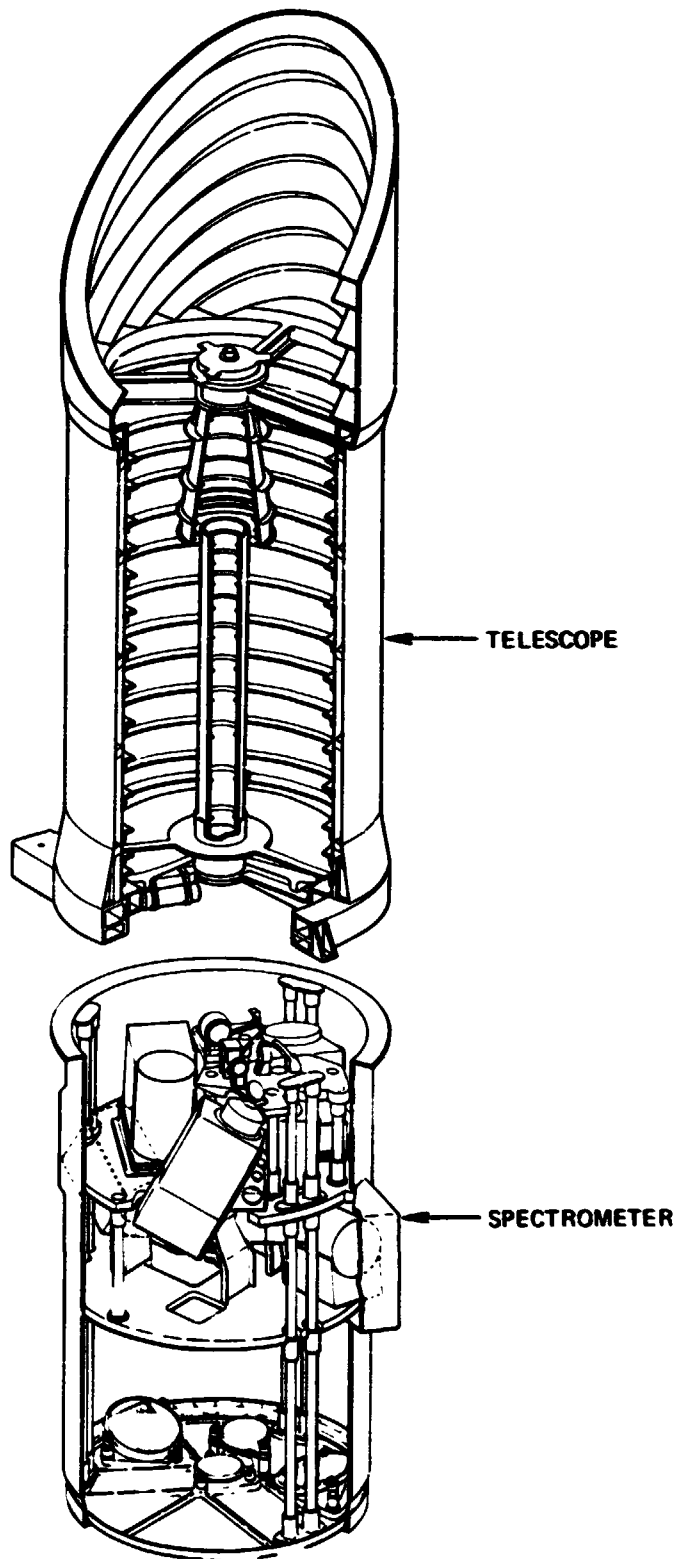


Figure 3.- IUE scientific instrument.

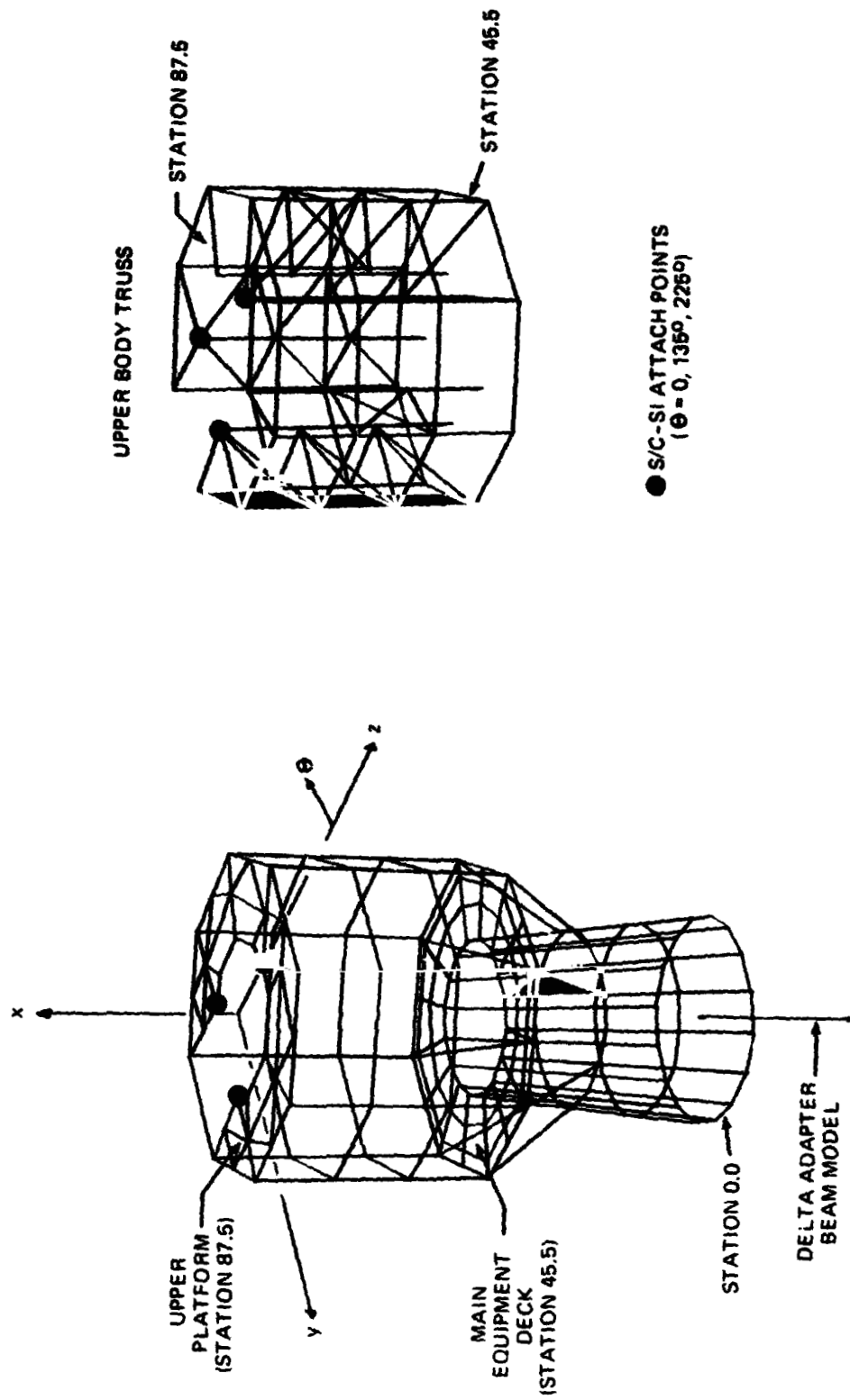


Figure 4.- Finite element model of S/C.

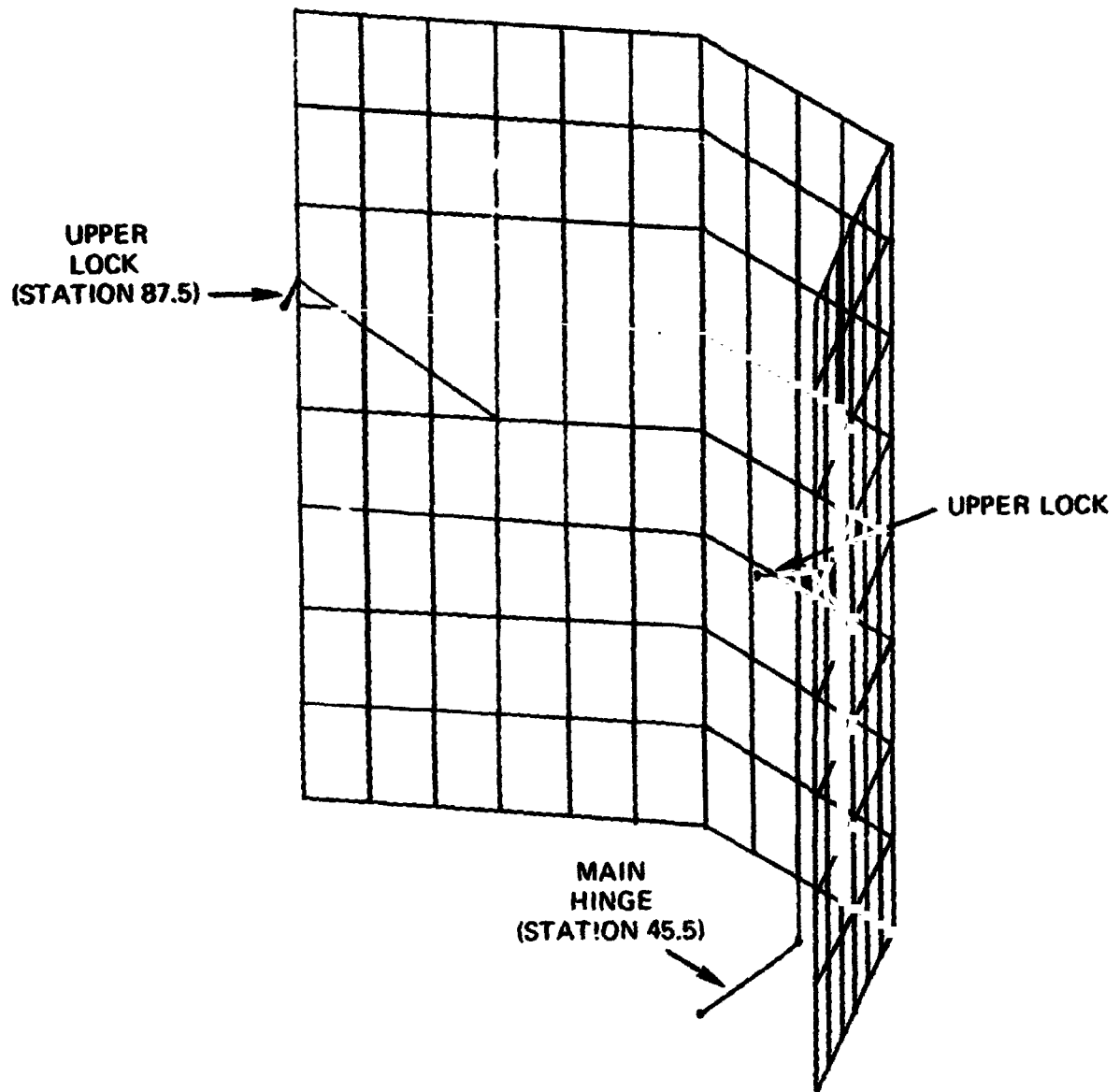


Figure 5.- Finite element model of one solar array.

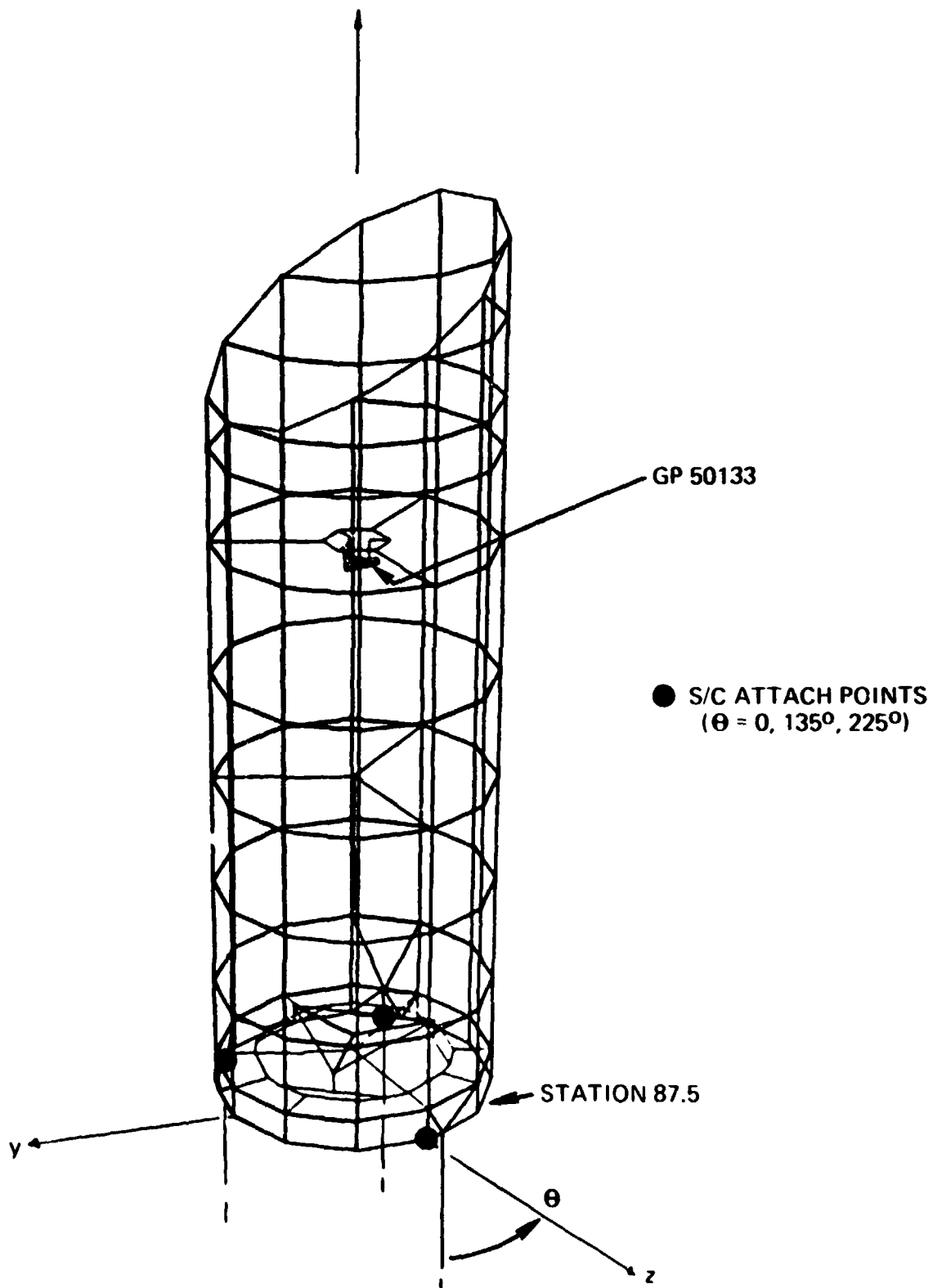


Figure 6.- Finite element model of telescope.

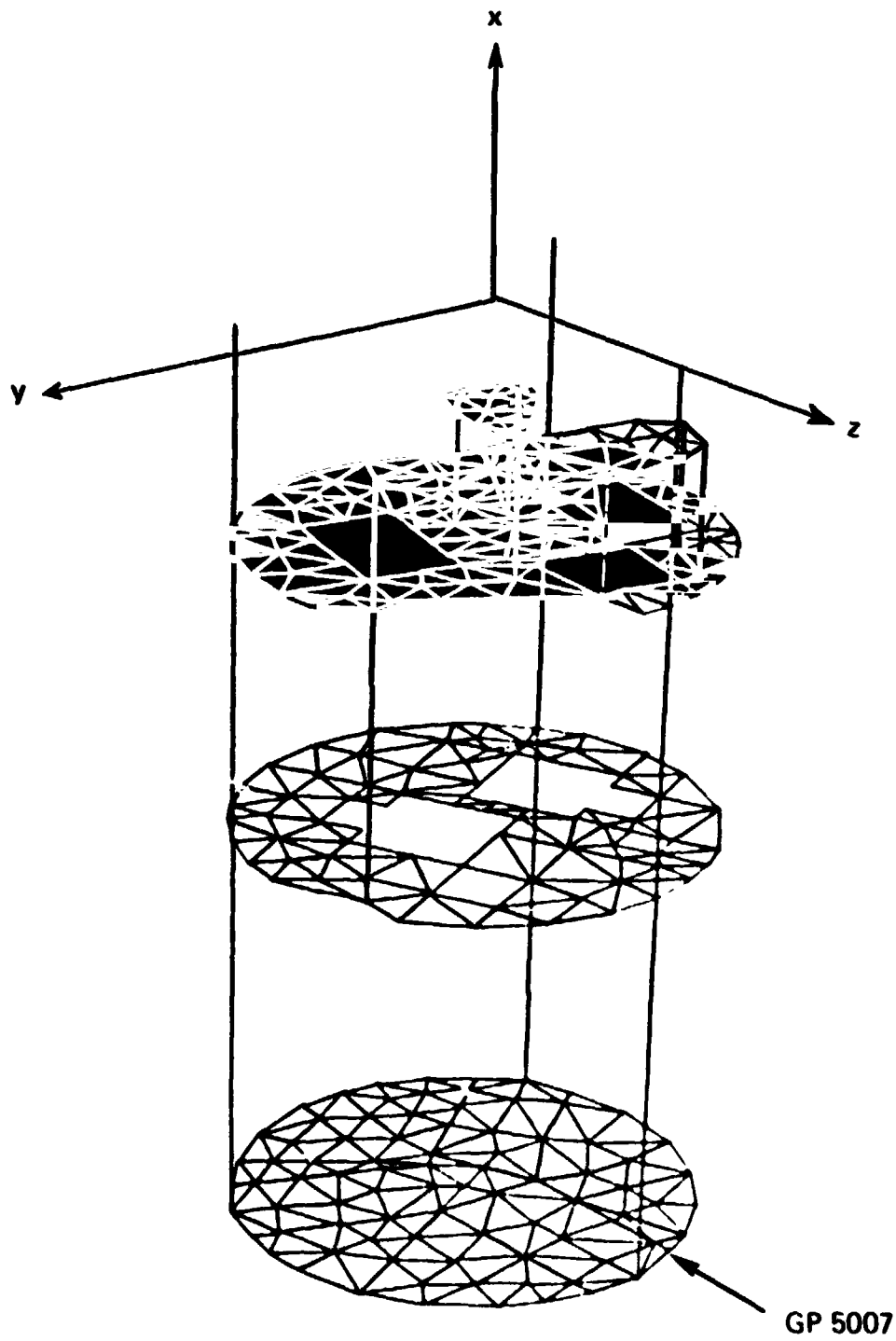


Figure 7.- Finite element model of spectrometer.

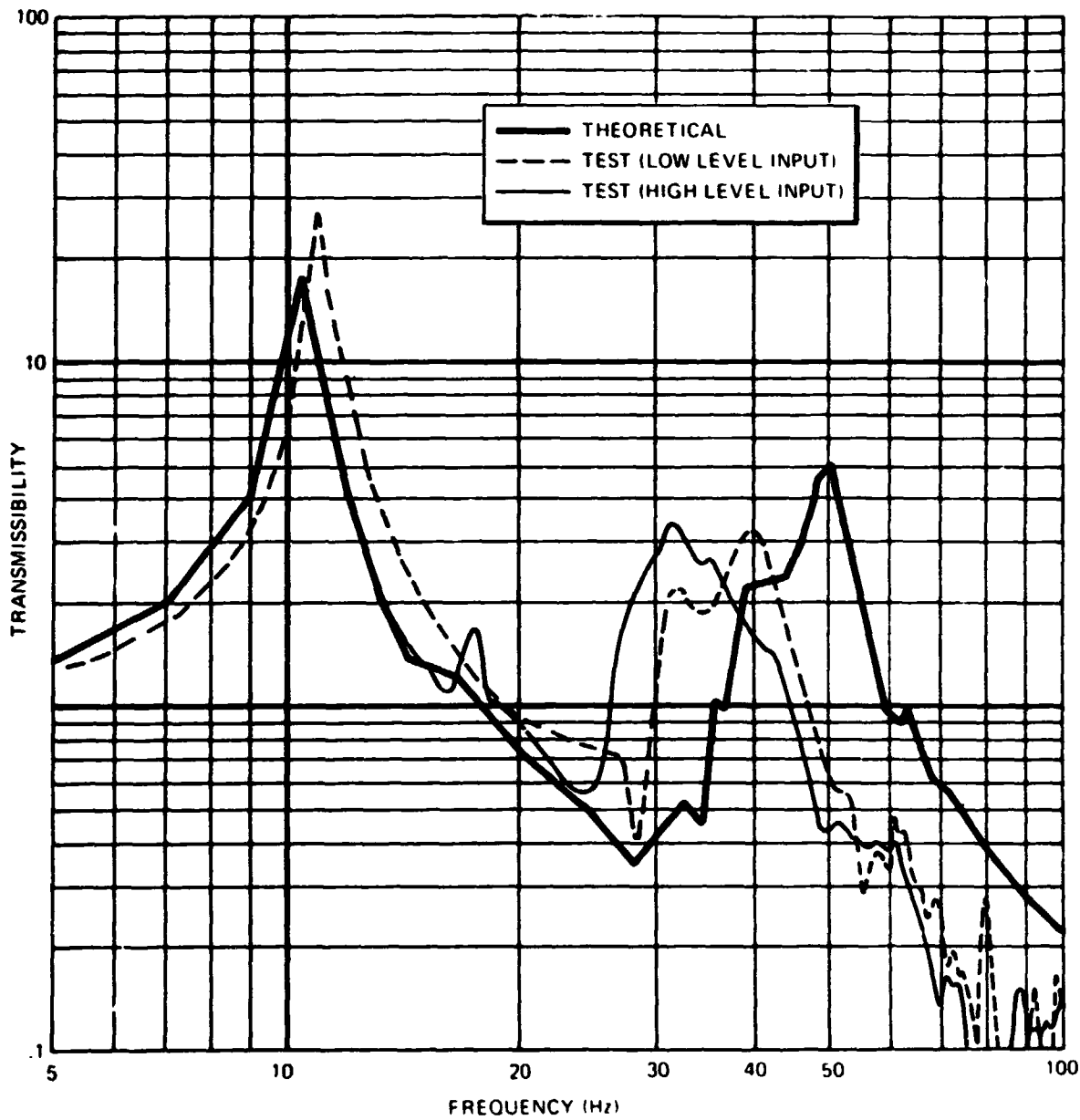


Figure 8.- Transmissibility at strong ring ($\theta = 135^\circ$) for Z axis vibration input to base of Delta adapter.

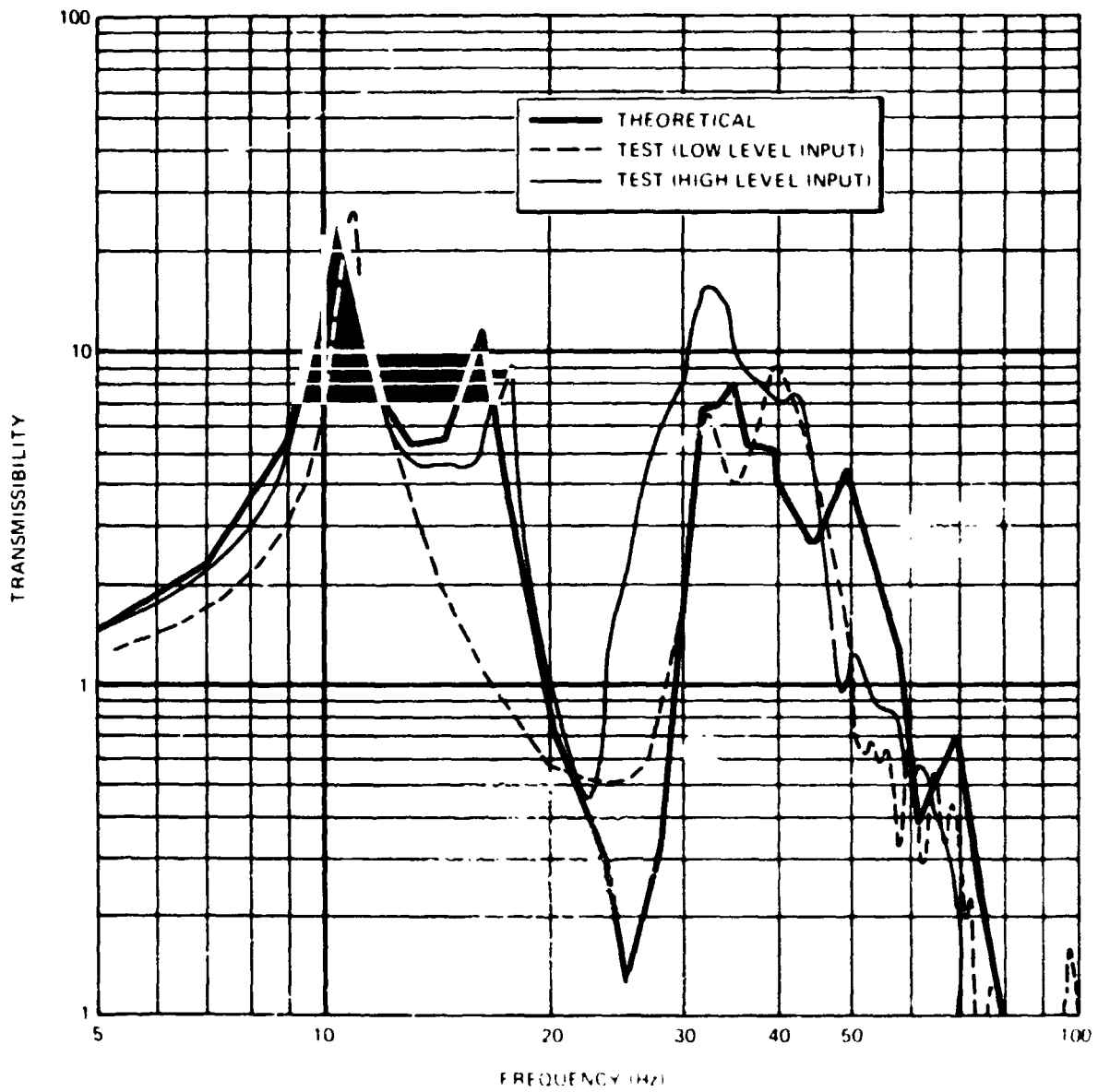


Figure 9.- Transmissibility at collimator deck (grid point 5007) for Z axis vibration input to base of Delta adapter.

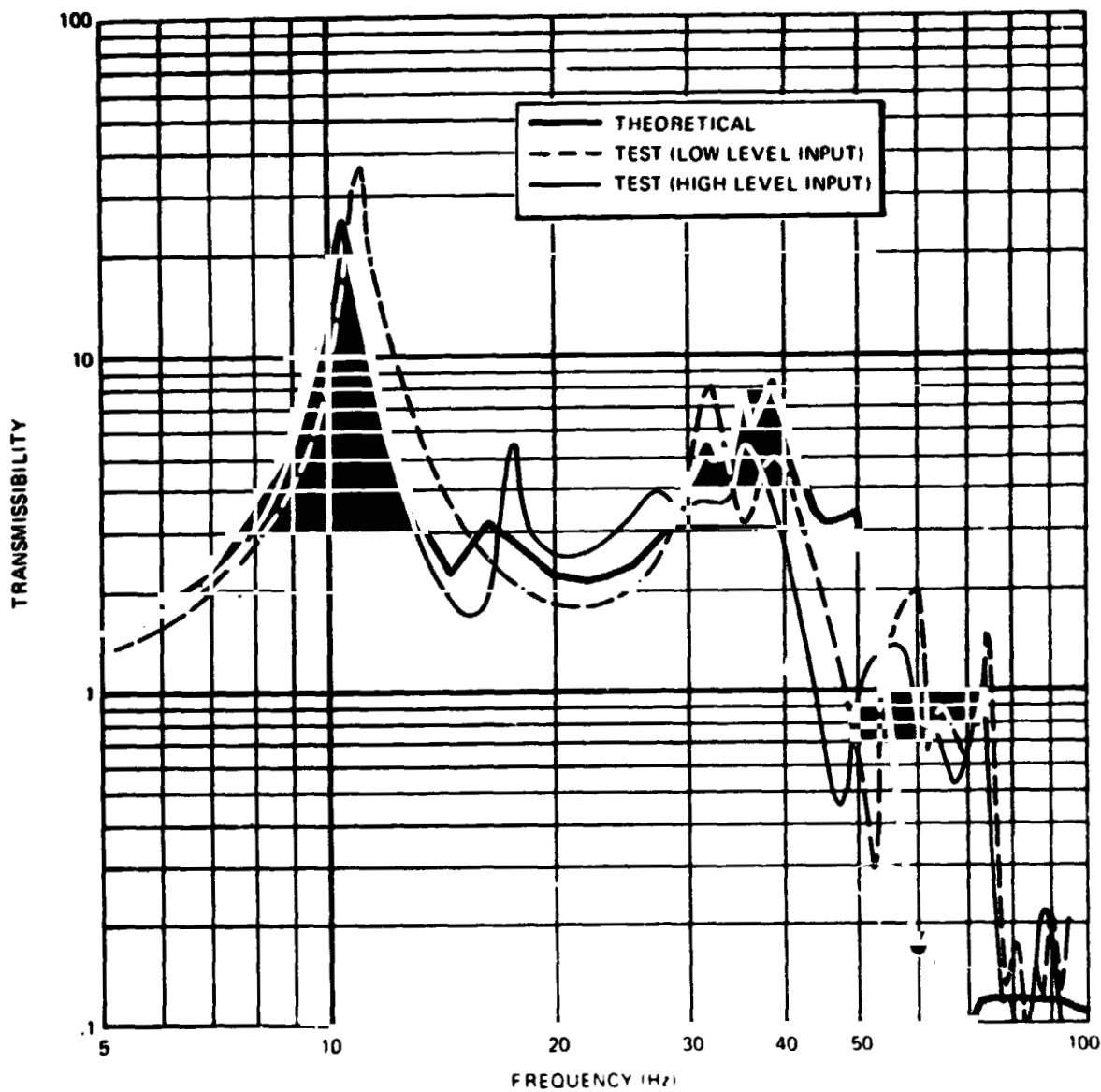


Figure 10.- Transmissibility at telescope secondary mirror (grid point 50133) for Z axis vibration input to base of Delta adapter.

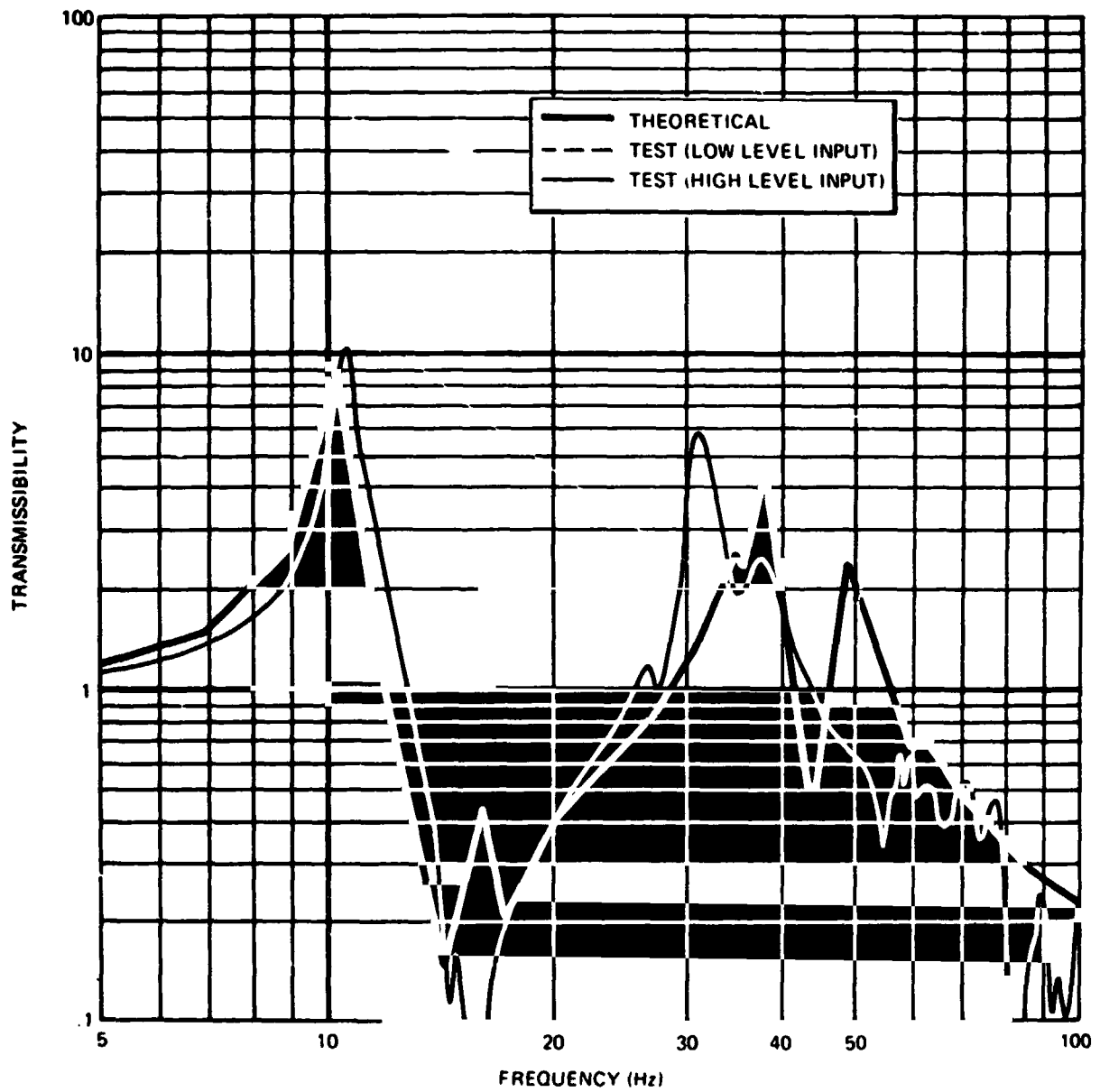


Figure 11.- Transmissibility at main deck (station 45.5) for Z axis vibration input to base of Delta adapter.

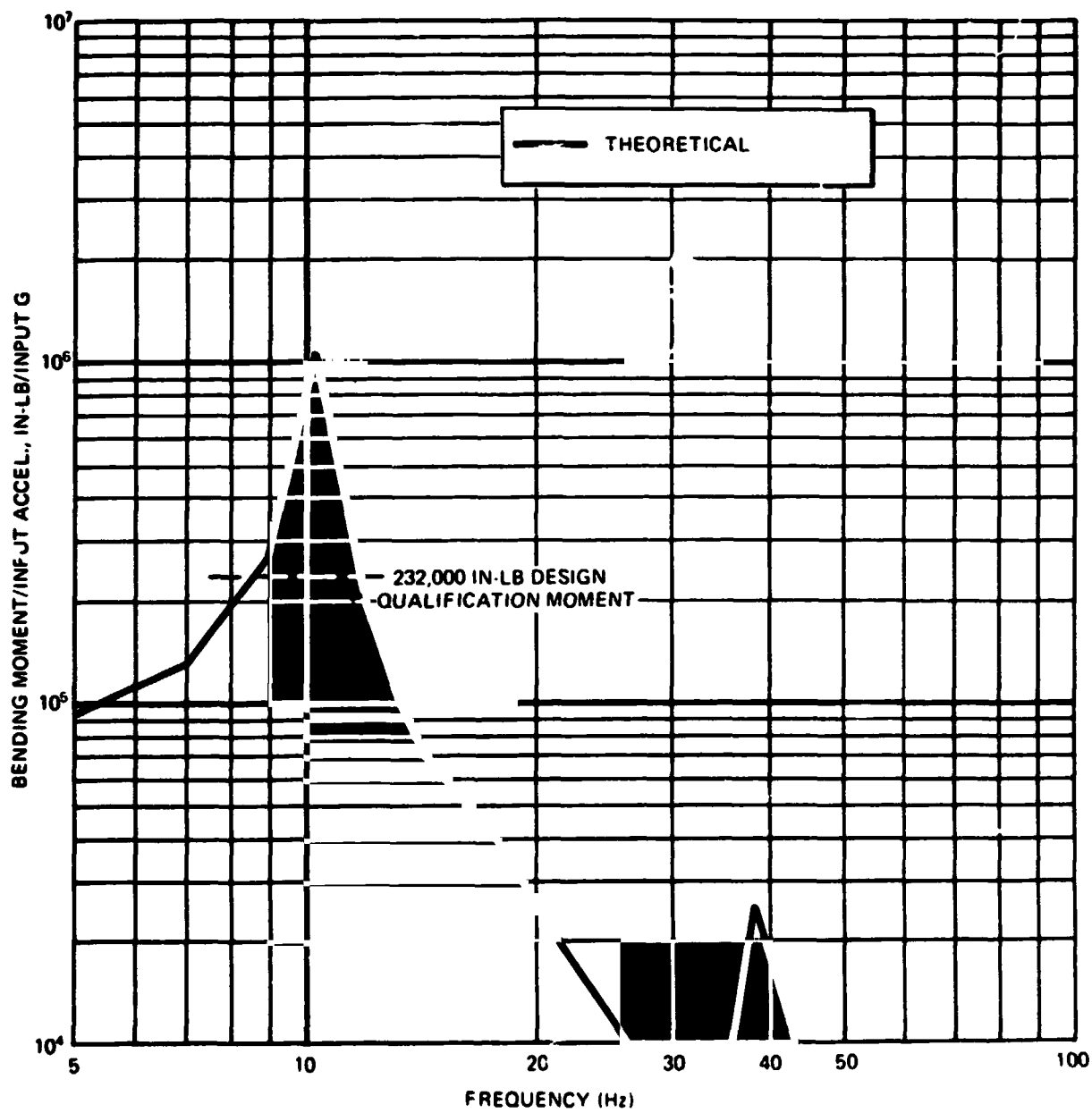


Figure 12.- Bending moment at separation plane (station 0.0)
 for Z axis vibration input to base of Delta adapter.
 1 in-lb = 0.11298 N-m.

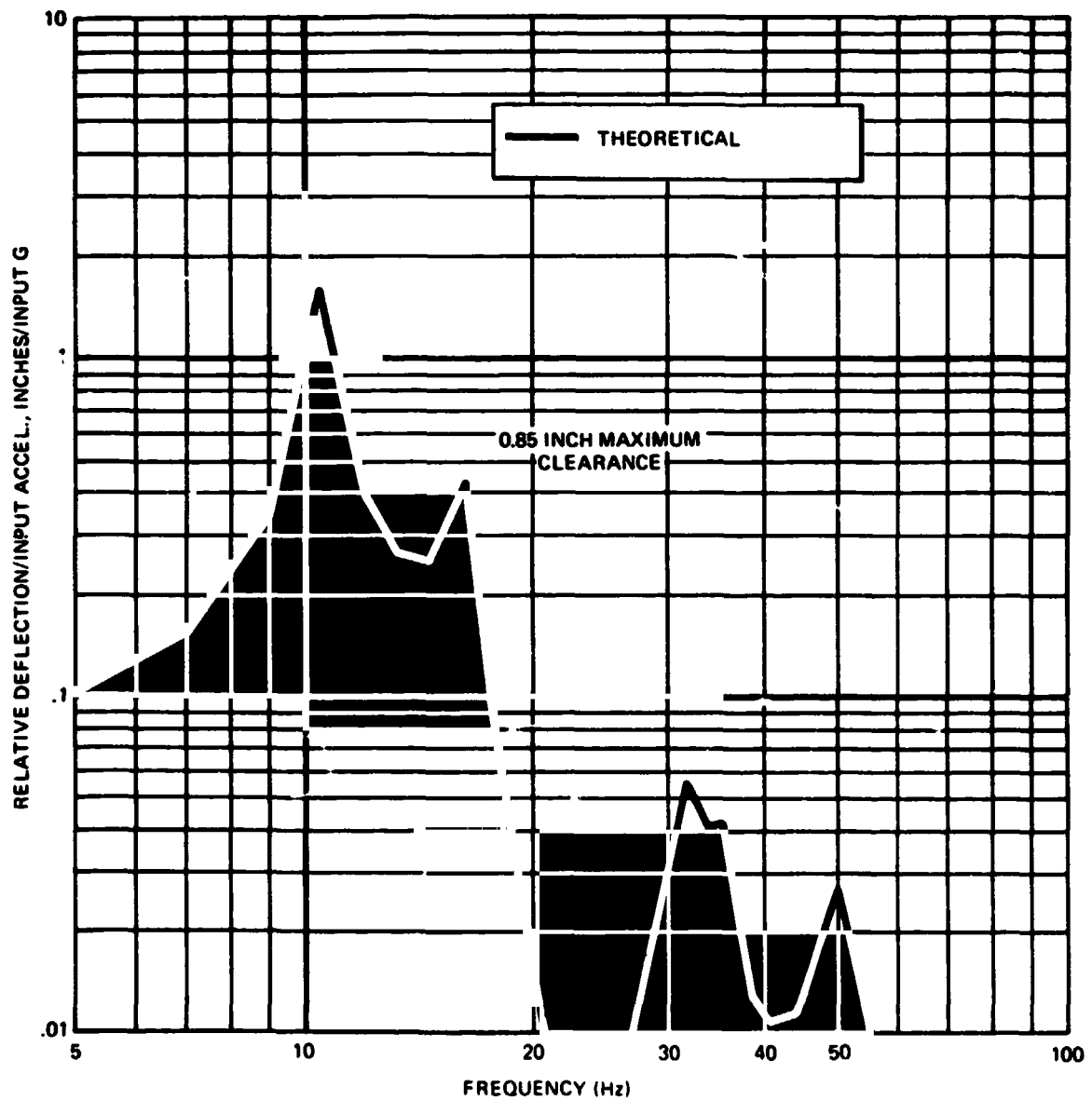


Figure 13.- Relative deflection between collimator deck and S/C support leg for Z axis vibration input to base of Delta adapter. 1 in. = 2.54 cm.

N75 31499

ANALYTICAL AND EXPERIMENTAL STUDY OF
TWO CONCENTRIC CYLINDERS COUPLED BY A FLUID GAP

By T. M. Mulcahy, P. Turula, H. Chung
and J. A. Jendrzeczyk

Argonne National Laboratory
Argonne, Illinois

INTRODUCTION

From a structural point of view a liquid coolant type nuclear reactor consists of a heavy steel vessel containing the core and related mechanical components and filled with a hot fluid. This vessel is protected from the severe environment of the core by a shielding structure, the thermal liner, which is usually a relatively thin steel cylinder concentric with the reactor vessel and separated from it by a gap filled with the coolant fluid. This arrangement leads to a potential vibration problem if the fundamental frequency, or one of the higher natural vibration frequencies, of this liner system is close to the frequency of some vibration source present in the reactor vessel. The natural vibration frequency of the liner shell vibrating in a vacuum is readily calculated by generally available techniques; e.g., references 1 and 2. However, it is felt that the influence of the fluid cannot be ignored since it may reduce the fundamental frequency by a factor of two to five, and thus may lower it into a range in which strong vibration sources may be present. Some natural frequency data for the case of a cylindrical shell filled with liquid has been presented in reference 3; however, the case of a cylindrical shell coupled to a concentric shell through a thin fluid gap was studied only for the case of simple support conditions at both top and bottom. (See references 4 and 5.) The study described here was undertaken to provide information for the shell rigidly clamped at its base and free at the top since this is a better description of the conditions encountered in typical reactor designs.

The dimensions of shell considered in this report were selected to model the liner used in the Fast Flux Test Facility reactor designed for the U. S. Atomic Energy Commission. The scale factor is approximately 1/14, giving nominal dimensions of 0.52 m (20.5 inches) height, 0.43 m (17 inches) diameter, and 1.6 mm (1/16 inch) thickness. All measurements were made in "customary" units. The behavior of prototype coolant liquid, sodium, is modeled by water which has density, compressibility, and viscosity properties that are adequately representative. In identifying mode shapes, this report will use the conventional designations: n to signify the number of complete waves in the circumferential direction ($n=0$ - axisymmetric, $n=1$ - translation, $n=2$ - "ovalling," etc.); and, m to signify the modal characteristic in the longitudinal direction ($m=1$ - simple cantilever beam type mode, $m=2$ - a mode with one nodal circle, etc.).

EXPERIMENTAL SETUP

The experimental model was fabricated by rolling a 1.5 mm (0.058 inch) thick, 0.51 m (20.125 inches) wide steel plate, seam welding, and soldering to a 13 mm (1/2 inch) brass plate which in turn was securely bolted to a 0.15 x 0.43 x 0.97 m (6 x 17 x 38 inch) steel block. Relatively rigid concrete outer cylinders were formed by casting around the cylindrical model utilizing a hard durometer neoprene spacer to obtain the nominal annular gap desired. The concrete was waterproofed and attached to the steel base as shown in Fig. 1.

The average outside diameter of the fabricated shell - .4338 m (17.08 inches) - was determined by taking the average of 36 measurements. The maximum diametral deviation was less than 0.5%. The shell wall thickness - 1.47 mm (0.058 inch) - was more uniform. The annular gap size - 3.8, 6.4, 13.7, 26.3 and 75 mm (0.151, 0.253, 0.538, 1.03 and 2.94 inches) - was determined by measuring the volume of water necessary to fill the annular region between the concrete shell and the steel shell to various levels. For any of the gap sizes used, the maximum deviation from the average value was about 0.10 (10%). The geometric accuracy of the model exceeds the uniformity expected in the prototype. Steel density - 7.5 Mg/m^3 (0.27 lb/cu. in.) - and elastic modulus - 193 GPa ($28 \times 10^6 \text{ psi}$) - were determined from test strips of the steel plate used in fabricating the shell by weighing and by a cantilevered beam frequency test.

A single exciter coil was situated close to the inside shell wall with an approximate 5 mm (3/16 inch) air space, and provided a magnetic force over approximately 0.016 m^2 (25 square inches) of the shell. Both a sinusoidal and a wide-band random current signal, controlled by signal generators were utilized during testing. The motion of the top of the test cylinder was monitored by miniature piezoelectric accelerometers cemented to the inside of the cylinder every 30° , with 0° defined to be opposite the center of the above coil. In addition, three accelerometers were cemented at equal spaces along the 0° longitudinal line on the cylinder and a movable accelerometer mounted on a magnet was used to search for node points.

TESTING PROCEDURE

Testing for each water-filled annular gap and the cylinder in air consisted of three phases. First, natural frequencies were determined by exciting the shell with a wide-band random force and inspecting power spectral density plots produced by a Fourier analyzer from the time history signals of several accelerometers. Second, the shell was excited with a sinusoidal current applied to the coil, using a range of frequencies in the vicinity of each of the natural vibration frequencies detected by random excitation. For each natural frequency, f_n , the accelerometer signal in a narrow band about this frequency was processed by the Fourier analyzer to provide a more accurate value of the peak frequency and to establish the RMS acceleration at each accelerometer position. This information was plotted to identify mode shapes corresponding to the natural frequencies. In the third phase of testing, the

transfer function between the RMS displacement and peak coil current was plotted at discrete points in a narrow frequency band about each natural frequency so that the equivalent viscous damping ratio could be calculated by the half power point bandwidth method as outlined in reference 6.

ANALYTICAL METHODS

Analytical solutions to the structural problems were obtained by using the NASTRAN finite element analysis program (see reference 7) with corroborating solutions obtained by using the SAP IV code (see reference 8) and through a Rayleigh-Ritz solution (see reference 9). The structural dimensions used for the analytical work were: height (i.e., length) - 0.5112 m (20.125 inches); radius to the mid-surface of the shell - .2160 m (8.505 inches); shell thickness - 1.473 mm (0.058 inch); elastic modulus - 182.7 GPa (26.5×10^6 psi); Poisson's ratio - 0.3; and, shell material mass density - 7497.55 kg/m^3 ($701 \times 10^{-6} \text{ lb-sec}^2/\text{in.}^4$). Analytical solutions for the coupled fluid-structure problem were obtained from the NASTRAN code only, using the following additional parameters: fluid mass density - 1000.11 kg/m^3 ($93.6 \times 10^{-6} \text{ lb-sec}^2/\text{in.}^4$); bulk modulus - 2.07 GPa (0.3×10^6 psi); and, gap sizes as noted above. The basic grid, as used in the reported structural finite-element formulations, consisted of 10 divisions vertically and 9 divisions over a quarter of the shell circumferentially (10° segments). Some comparison runs using a finer mesh were made to establish the adequacy of the mesh for the purposes of this study. For example, by using a mesh size with twice as many divisions in each direction, it was established that the basic grid gives results with the minimum frequencies (which were those with the most error) about 2% too high. Similarly, it was found that using a grid with divisions three times larger than the basic grid gives errors of 30 to 50 percent.

The basic grid used in the fluid-structural analyses had 5 divisions vertically, 6 divisions circumferentially (15° segments) and 5 divisions through the fluid in the radial direction. In solving the coupled problem, NASTRAN uses a finite-element representation of the fluid region. Compressible fluid with small motion is assumed to give a linear (acoustic type) formulation. The fluid is also assumed to be irrotational so that a scalar potential function (pressure) can be used as the solution variable in place of the three components of displacement.

VIBRATION IN AIR

Before considering the shell vibrating with a fluid, the shell in a vacuum was studied to establish the significance of variations in the boundary conditions and to establish the degree of correspondence to be expected between analytical and experimental results. Figure 2 presents a summary of these results. In all cases the top boundary of the shell was considered to be free. In comparing analytical results for the fixed base condition (rigidly

clamped) to the simply supported base condition (all edge displacements prevented but unrestrained rotation about the tangent), little difference was found. The degree of rotational restraint at the base does not affect the overall results significantly as it is primarily a local flexure condition. Hence it is not considered further. The base boundary condition was then further relaxed by allowing edge motion in the axial direction against an elastic spring restraint, K_z ; using $K_z = \text{infinite}$, 10^6 , 10^5 and 10 units, where each unit is 4.656 kN/m per m of circumference ($1 \text{ lb/in.} / 1.5 \text{ in.}$). The K_z infinite case corresponds to the simply supported condition, whereas $K_z = 10$ which is effectively $K_z = 0$ corresponds to a shear diaphragm boundary condition. The curves corresponding to each of these conditions are shown in the figure. Comparable results obtained by using the SAP IV program gave frequencies about 3% lower; frequencies obtained by the Rayleigh-Ritz method were up to 5% lower.

The results obtained experimentally for the shell vibrating in air (i.e., effectively in a vacuum) are shown as data points in Figure 2. Although the experimental setup was intended to simulate a fixed condition ($K_z = \text{infinite}$) at the base, it can be seen that effectively it is behaving as a shell supported by elastic springs in the axial direction with $K_z = 10^5$. Note that for both $m = 1$ and $m = 2$, the modes corresponding to the lower n values were not detected. Difficulties were encountered in this regard and explanations posed here and elsewhere are not totally satisfactory. Efforts to get response of these modes included the use of the local electromagnetic coil described previously as well as acoustic excitation at various amplitude levels applied by a loud speaker. Fourier analyzer processing of the acceleration response to a random excitation did show a frequency at 140 Hz which probably corresponds to the $m = 1$, $n = 3$ mode, but no corresponding response was generated when a single harmonic excitation at this frequency was applied. Frequency response analysis performed by the NASTRAN program indicated that the modes which failed to respond are of somewhat lesser intensity than modes at neighboring frequencies with high n values, but this difference was not large enough to justify the difficulties encountered in detecting these modes. One possible explanation is in the relation between flexural strain energy (associated with high n values) and membrane strain energy as discussed by Croll. (See reference 10.) The masking effect of the higher n value modes at frequencies close to that of the low n value mode may also be the difficulty. This is particularly suspect in the tests using the electromagnetic exciter since with a pure harmonic current applied to the device the resulting force function carries higher harmonic frequencies of an amplitude up to 20% of the fundamental harmonic. A factor which may be totally responsible for the difficulty of experimentally detecting these low n value modes is the geometrical imperfections of the shell as fabricated. NASTRAN is suited to the evaluation of this effect and a study to perform such an evaluation is contemplated. Finally, it should be noted that the frequencies of the low n value mode shapes are highly dependent on the stiffness K_z , as clearly shown in Fig. 2, so that the relatively undeterminable and possibly nonlinear nature of this restraint may greatly reduce the sharpness of the associated response. However, for the modes that gave a clear response, increasing the driving force by a factor of four lowered the peak response frequency by at most 1/2%; hence, support non-linearity appears to be negligible.

VIBRATION IN WATER

The vibration frequencies of the shell with a fluid gap were first approximated by applying the added mass factors, as described in reference 4 for infinitely long shells, to the frequencies obtained for the in air vibration case. A comparison between the experimental results and these extrapolations is shown in Fig. 3. This method appears to give frequency predictions that are somewhat low but generally within 10% of the experimental values.

Figure 4 shows the frequencies predicted by the NASTRAN program for the shell vibrating with four selected water gaps, and with the in-vacuum solutions shown for comparison. These frequencies are compared with the experimentally measured frequencies in Figure 3. The directly computed values are between 20 to 30 percent higher than the experimental results; however, by comparing results for problems run with several different models, it is expected that the mesh size used to generate the data in Figure 3 will give frequencies which are between 20% and 35% too high. The mesh size used for generating the data consisted of 5 divisions vertically, 5 divisions radially through the fluid, and 15° divisions circumferentially along the shell. However, for one particular fluid gap size, the mesh divisions were reduced in steps down to 10 by 5 by 6° , respectively. The number of divisions radially through the fluid was also varied, but this did not affect the results significantly; thus, the 5-division model can be considered fine enough for accurate results. This somewhat refined analysis gives results that are quite adequate for design purposes. However, the cost of running a series of fluid-solid interaction problems through NASTRAN, particularly with a much finer mesh than used here, would be prohibitive. The runs involving the (5, 5, 15°) mesh required about 1 minute of IBM S/370-195 CPU time; the (10, 5, 6°) case required 8 minutes. Both were run with NASTRAN level 15.1 using 180° of the shell modeled for analysis.

DAMPING

For purposes of determining the equivalent viscous damping ratios, the frequency-response curve was first determined in the 0.1 - 0.5 g acceleration range and then redetermined at the highest acceleration level compatible with the available equipment. The ratio of acceleration levels was at least two and usually five to ten. The damping ratio variation with amplitude level was in the 10 to 40 percent range. Figure 5 shows selected average values of damping for the shell vibrating with various water gaps and in air. Clearly, the smaller fluid gaps are associated with higher damping ratios than those measured in air, typically twice as large. Generally, larger damping is associated with smaller water gaps. For those few cases which do not follow this later trend, the frequency response curves probably were distorted (broadened) by superposition of the responses corresponding to an adjacent natural frequency which would make the half power bandwidth method inapplicable.

CONCLUDING REMARKS

Correspondence of experimental and analytical results is within acceptable limits for design purposes. Several vibration modes corresponding to solutions with low n values eluded experimental detection. The significance of these modes in design, as well as the reasons for the difficulty in detecting them experimentally, are not clear. The feasibility of using a coupled fluid-elastic finite-element analysis to solve vibration problems involving shells containing a fluid has been demonstrated; however, the computer time costs incurred with the present methods prohibit extensive application of this technique.

REFERENCES

1. Leissa, A. W.: Vibration of Shells. NASA SP-288, 1973.
2. Arnold, R. N., and Warburton, G. B.: "The Flexural Vibrations of Thin Cylinders." Proc. Inst. of Mech. Engrs., A167, 1953, pp. 62-80.
3. Arya, A. S., Thakkar, S. K., and Goyal, A. C.: "Vibration Analysis of Thin Cylindrical Containers." Journal of Engineering Mechanics Division, ASCE, Vol. 97, April 1971, pp. 317-331.
4. Chen, S. S., and Rosenberg, G. S.: "Dynamics of a Coupled Shell/Fluid System." Nuclear Engineering and Design, accepted for publication.
5. Krajcinovic, D.: "Vibrations of Two Coaxial Cylindrical Shells Containing Fluid." Nuclear Engineering and Design, accepted for publication.
6. Thomson, W. T.: Vibration Theory and Applications. Prentice Hall, 1965, p. 74.
7. McCormick, Caleb W., ed.: The NASTRAN User's Manual (Level 15). NASA SP-222(01), 1972.
8. Bathe, K-J., Wilson, E. L., and Peterson, F. E.: SapIV - A Structural Analysis Program for Static and Dynamic Response of Linear Systems. National Technical Information Service, EERC 73-11, June 1973.
9. Chung, H.: "A General Method of Solution for Vibrations of Cylindrical Shells." Ph.D. Thesis, Tufts University, March 1974.
10. Croll, J. G. A.: "Coupled Vibration Modes." J. of Sound and Vibration, 38(1), 1975, pp. 27-37.

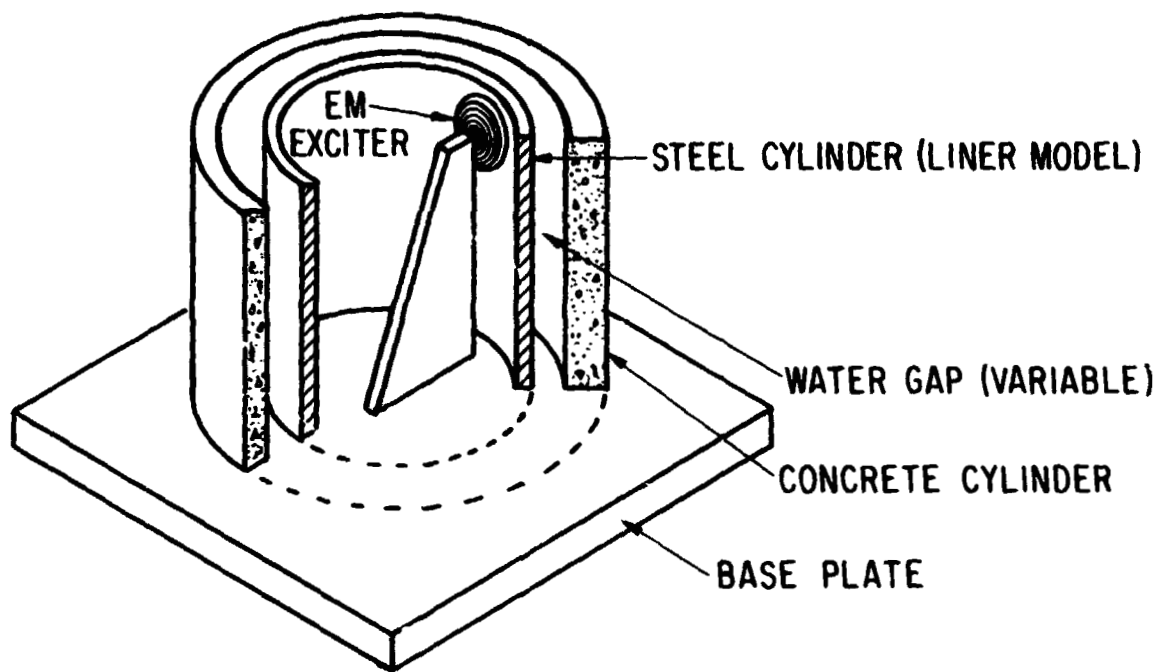


Figure 1. Experimental setup schematic.

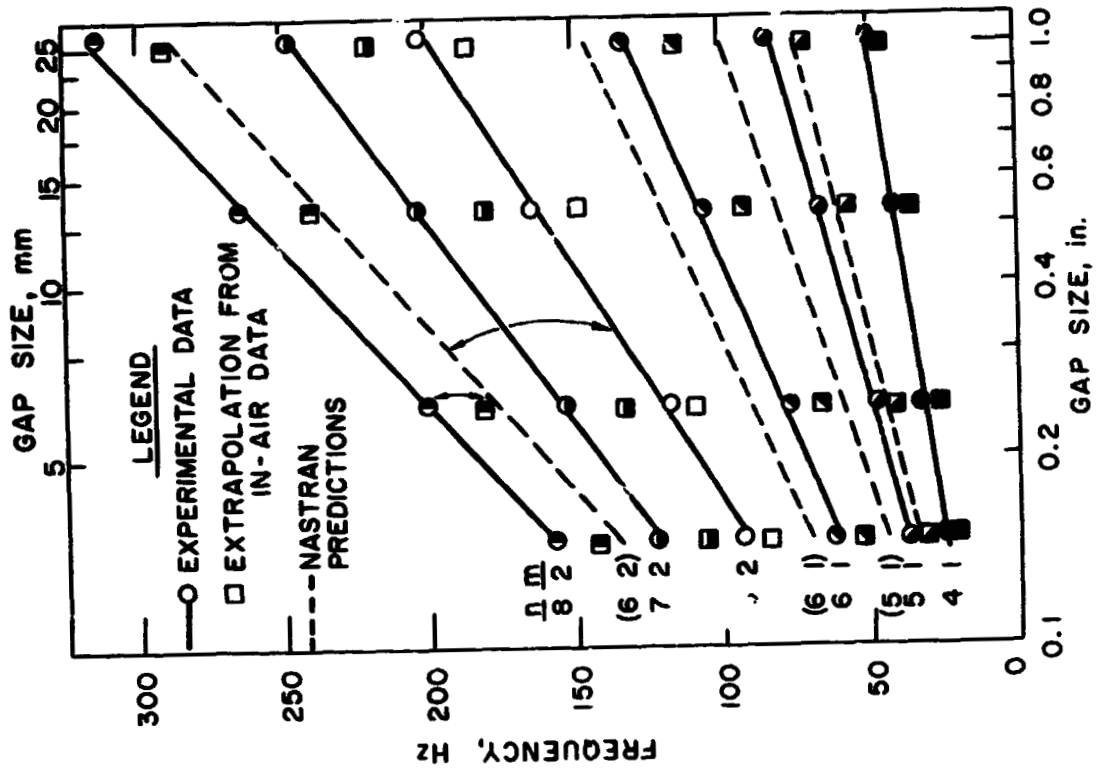


Figure 3. Comparison of experimental and predicted vibration frequencies for the shell with a fluid filled gap.

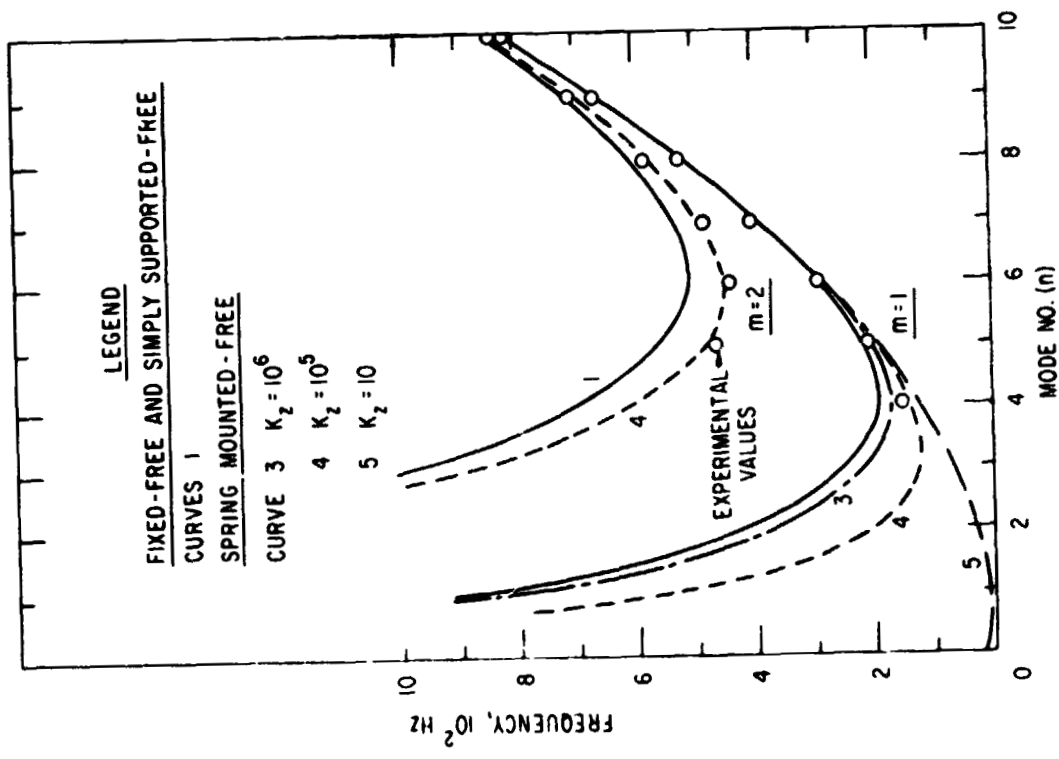


Figure 2. Comparison of experimental and predicted vibration frequencies for the shell without fluid.

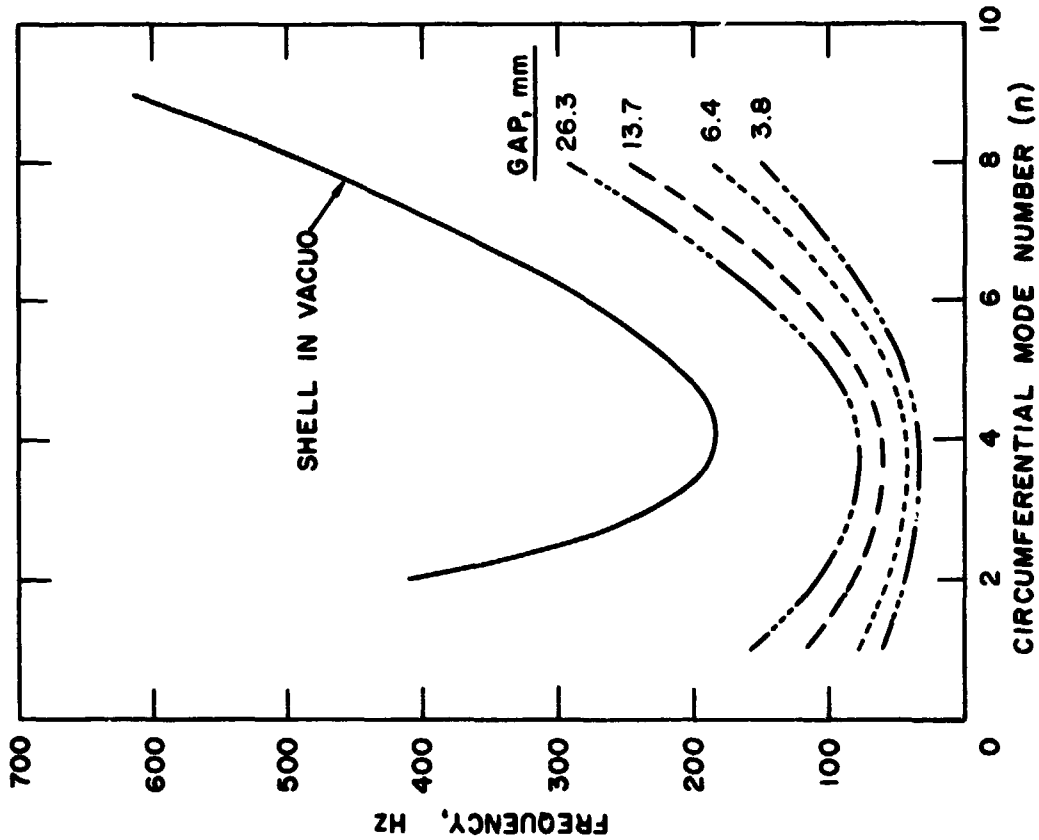


Figure 4. Computed $m = 1$ type vibration frequencies for the shell with and without fluid.

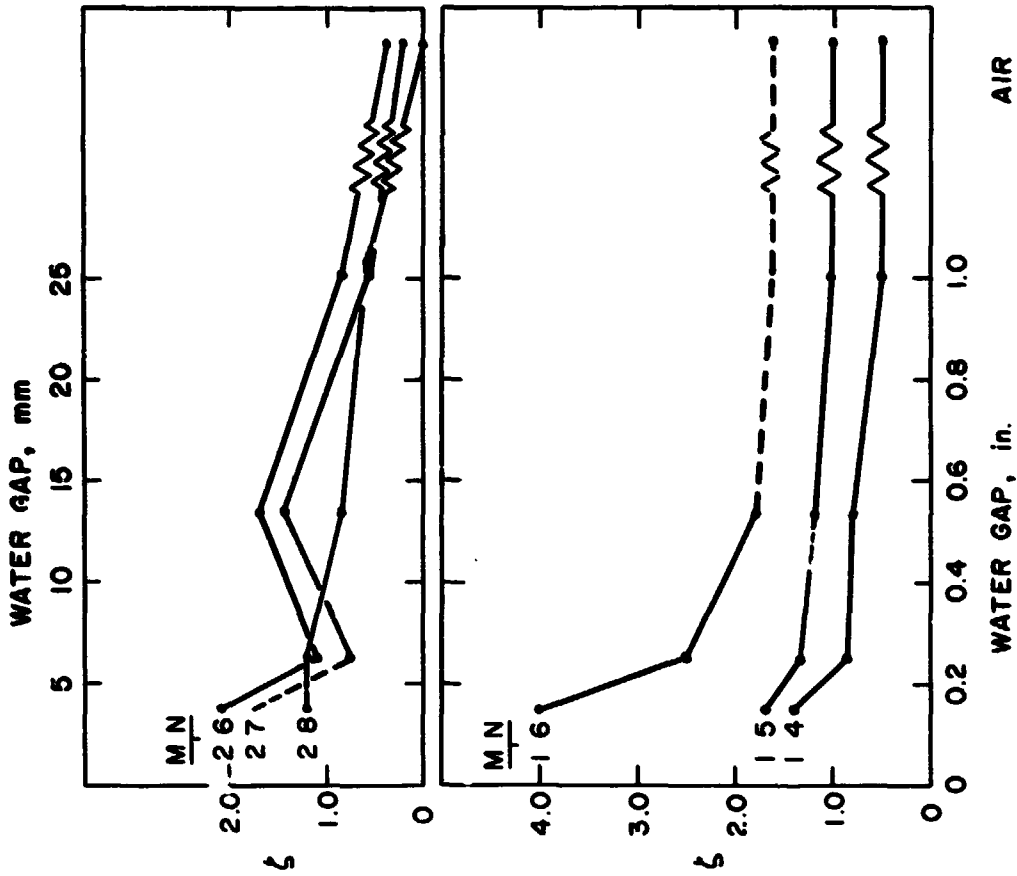


Figure 5. Experimentally determined damping coefficients.

N75 31500

**NASTRAN NONLINEAR VIBRATION ANALYSIS OF
BEAM AND FRAME STRUCTURES**

**Chuh Mei
LTV Aerospace Corporation, Hampton, Virginia**

and

**James L. Rogers, Jr.
NASA Langley Research Center, Hampton, Virginia**

SUMMARY

A capability for the nonlinear vibration analysis of beam and frame structures suitable for use with NASTRAN Level 15.5 is described. The nonlinearity considered is due to the presence of axial loads induced by longitudinal end restraints and lateral displacements that are large compared to the beam height. This paper includes a brief discussion of the mathematical analysis and the geometrical stiffness matrix for a prismatic beam (BAR) element. Also included are a brief discussion of the equivalent linearization iterative process used to determine the nonlinear frequency, the required modifications to subroutines DBAR and XMPLBD of the NASTRAN code, and the appropriate DMAP ALTERS to determine the frequency. To demonstrate this nonlinear vibration capability, four example problems are presented. Comparisons with existing experimental and analytical results show that excellent accuracy is achieved with NASTRAN in all cases.

15

INTRODUCTION

In practical beam vibration problems, transverse deflections may be greater than those assumed for linear theory. Considerable attention has been given, therefore, to the nonlinear flexural vibration of beams. Most studies have dealt with simple uniform beams with either hinged or fixed support conditions at both ends. An excellent literature survey is given by Easley (ref. 1) through 1964. More recent surveys are given by Ray and Bert (ref. 2), and Pandalai (ref. 3). Nonlinear vibrational behavior of non-uniform beam and frame structures found in many engineering applications, however, has not received much attention in the literature because of analytical difficulties. The use of the finite-element method overcomes these difficulties and removes the uniform beam and limited support condition restrictions.

The purpose of this paper is to describe a nonlinear vibrational analysis capability for determining fundamental frequency of beam and frame structures suitable for use with NASTRAN Level 15.5 and to present results demonstrating this capability. The paper includes a discussion of the mathematical analysis and the derivation of the geometrical stiffness matrix that represents the induced axial force in the governing equation, the appropriate modifications to the NASTRAN code, and solutions of example problems. Procedures for nonlinear vibration analysis with and without applied axial forces are available for NASTRAN Level 15.5 by means of DMAP ALTERS and modifications of the NASTRAN code given in the Appendices.

SYMBOLS

A	area
c	amplitude of vibration
d	amplitude ratio, $c/\sqrt{I/A}$
E	modulus of elasticity
{f}	element forces
h	height of beam
I	area moment of inertia of cross section
[k]	stiffness matrix
[k ^d]	differential stiffness matrix
[k ^g]	geometrical stiffness matrix
l	length
[m]	mass matrix
P _{xo}	applied axial force on undeformed beam
P _x	axial force due to deflection
P _E	Euler load
[p]	inplane force matrix
{u}	nodal displacements
t	time

x, y, z	element coordinate system
w	lateral deflection
ρ	mass density
$\{\phi\}$	normal mode
ω_0	fundamental linear frequency
ω	fundamental nonlinear frequency

Subscripts:

a, aa	system
e, ee	element
eq	equivalent

MATHEMATICAL ANALYSIS

Formulation of Matrix Equation of Motion

The strain energy in a deformed bar element of uniform cross section is given by:

$$U = \frac{EI}{2} \int_0^l \left(\frac{\partial^2 w}{\partial x^2} \right)^2 dx + P_{x0} \int_0^l \frac{1}{2} \left(\frac{\partial w}{\partial x} \right)^2 dx + \frac{P_x}{2} \int_0^l \frac{1}{2} \left(\frac{\partial w}{\partial x} \right)^2 dx \quad (1)$$

$$\text{where } P_x = \frac{EA}{l} \int_0^l \frac{1}{2} \left(\frac{\partial w}{\partial x} \right)^2 dx \quad (2)$$

The first two terms of the strain energy expression are due to bending and applied axial force, respectively. The last term is the nonlinear contribution of the axial force P_x induced by large deflections. If the axial force P_x is neglected from Eq. (1), the strain energy is reduced to that of the linear theory.

The kinetic energy is given by:

$$T = \frac{\rho A}{2} \int_0^l \left(\frac{\partial w}{\partial t} \right)^2 dx \quad (3)$$

where the rotatory inertia term has been neglected.

In the finite-element approach, transverse deflection of an element is expressed in terms of generalized displacements $\{u_e\}$ and interpolation functions. The function chosen to represent the e transverse deflection is given by:

$$w = \begin{bmatrix} (1 - 3 \bar{x}^2 + 2 \bar{x}^3) & -(1 - 2 \bar{x} + \bar{x}^2)x & (3 \bar{x}^2 - 2 \bar{x}^3) \\ (\bar{x} - \bar{x}^2) & x \end{bmatrix} \{u_e\} \quad (4)$$

$$\text{where } \bar{x} = \frac{x}{l} \quad (5)$$

This displacement function is the same as used for the NASTRAN bar element. The displacement vector describing bending of a bar element in the xz plane (see figure 1) is defined by:

$$\{u_e\} = \{u_{za} \quad \theta_{ya} \quad u_{zb} \quad \theta_{yb}\}^T \quad (6)$$

Substituting Eq. (4) into Eqs. (1) and (3), gives:

$$U = \frac{1}{2} \{u_e\}^T ([k_{ee}] + [k_{ee}^d] + [k_{ee}^g]) \{u_e\} \quad (7)$$

and

$$\dot{U} = \frac{1}{2} \{\dot{u}_e\}^T [m_{ee}] \{\dot{u}_e\} \quad (8)$$

where $[k_{ee}]$, $[k_{ee}^d]$, $[k_{ee}^g]$, and $[m_{ee}]$ represent the element stiffness, differential stiffness, geometrical stiffness, and mass matrices, respectively and $[k_{ee}^g]$ is a function of $\{u_e\}$. Substituting Eq. (4) into Eq. (2) yields

$$P_x = \{u_e\}^T [p_{ee}] \{u_e\} \quad (9)$$

where $[p_{ee}]$ is the inplane force matrix.

Substituting Eqs. (7) and (8) into Lagrange's equations, that is,

$$\frac{d}{dt} \left(\frac{\partial T}{\partial \dot{q}_i} \right) + \left(\frac{\partial U}{\partial q_i} \right) = 0 \quad i = 1, 2, \dots, n \quad (10)$$

where n is the number of elemental degrees of freedom, leads to the matrix equation of motion for the large amplitude free oscillations of a bar element which is given by

$$[m_{ee}] \{\dot{u}_e\} + ([k_{ee}] + [k_{ee}^d] + [k_{ee}^g]) \{u_e\} = \{f_e\} \quad (11)$$

The mass, stiffness, and differential stiffness matrices of the bar element are 12×12 matrices relating the forces and moments acting at the ends of the bar (see ref. 4). The portion of the differential stiffness matrix, for example, that describes bending in the xz plane of figure 1, is given by

$$[k_{ee}^d] = \begin{bmatrix} \frac{6 P_{x0}}{5l} & -\frac{P_{x0}}{10} & -\frac{6 P_{x0}}{5l} & -\frac{P_{x0}}{10} \\ & \frac{2l P_{x0}}{15} & \frac{P_{x0}}{10} & -\frac{l P_{x0}}{30} \\ & & \frac{6 P_{x0}}{5l} & \frac{P_{x0}}{10} \\ & & & \frac{2l P_{x0}}{15} \end{bmatrix} \quad (12)$$

The relations between $[k_{ee}^d]$, $[k_{ee}^g]$, and $[p_{ee}]$ can be found from Eqs. (1) and (2) and they are

$$[k_{ee}^g] = \frac{1}{2} \frac{P_{x0}}{P_{x0}} [k_{ee}^d] \quad (13)$$

where

$$p_x = \{u_e\}^T [p_{ee}] \{u_e\} \quad (14)$$

and

$$[p_{ee}] = \frac{\left(\frac{EA}{2L}\right)}{P_{x0}} [k_{ee}^d] \quad (15)$$

Solution Technique

The geometrical stiffness matrix $[k_{ee}^g]$ in Eq. (11) is displacement dependent (see Eqs. (13) and (14)). Therefore, the frequency for nonlinear vibration also depends on the amplitude of vibration. This phenomenon is different from the linear case, in which the frequency is independent of amplitude. In the following the frequency associated with the linear vibration problem is referred to as the linear frequency, and the frequency associated with the nonlinear vibration problem is referred to as the nonlinear frequency. To determine the nonlinear frequency, an iterative procedure with an equivalent linearization technique is used and is illustrated by the simplified flow chart shown in figure 2. The system matrices indicated in figure 2 are assembled from the element matrices by a standard finite-element procedure. The basic idea is to replace the displacement dependent geometrical stiffness matrix $[k_{ee}^g]$ by an equivalent matrix $[k_{ee}^g]_{eq}$ using the mode shape of the linear vibration problem as the first approximation to the displacement. This reduces the nonlinear system equation of motion to a linearized equation which can be solved as a standard eigenvalue problem. The mode obtained by solving this eigenvalue problem may be used to recompute $[k_{ee}^g]_{eq}$ for the next iteration in the nonlinear vibration iterative solution procedure. The solution procedure is illustrated as follows. The first step is to solve the linear vibration problem:

$$\omega_o^2 [m_{aa}] \{\phi\}_o = [k_{aa}] \{\phi\}_o \quad (16)$$

where ω_o is the fundamental frequency of the linear problem, $\{\phi\}_o$ represents the corresponding mode shape normalized by its maximum component, and the subscript aa represents the system matrices. Solving Eq. (16) provides the first approximate displacement in the form

$$\{u_a\}_1 = c \{\phi\}_o \quad (17)$$

where c is the amplitude of vibration. The equivalent geometrical stiffness matrix now can be obtained using $\{u_a\}_1$ which leads to a linearized eigenvalue equation of the form

$$\omega^2 [m_{aa}] \{\phi\}_1 = ([k_{aa}] + [k_{aa}^d] + [k_{aa}^g]_{eq}) \{\phi\}_1 \quad (18)$$

where ω is the fundamental nonlinear frequency associated with amplitude c , and $\{\phi\}_1$ is the corresponding mode shape. The iterative process can be repeated by using

$$\{u_a\}_2 = c \{\phi\}_1 \quad (19)$$

as the second approximation, and similarly the i -th iteration approximate displacement is of the form

$$\{u_a\}_i = c \{\phi\}_{i-1} \quad (20)$$

The iterative process can be continued until the nonlinear frequency converges to the desired accuracy or the mode shape $\{\phi\}_i$ satisfies some convergence criterion (e.g., the modified Euclidean norm of ref. 5).

MODIFICATIONS TO THE NASTRAN CODE

To compute the geometrical stiffness matrix $[k_{ee}^g]$, subroutine DBAR was modified to take advantage of the fact that the differential stiffness matrix and the geometrical stiffness matrix are related as shown in Eq. (13). Appendix A shows these changes in CDC UPDATE format. The core storage requirement for DBAR was increased by 6478 locations.

To avoid going through the modified section of code each time DBAR was called, a new parameter, NLVIB, was added to the DMAP calling sequence for module DSMG1. The contents of NLVIB are passed through blank common from DSMG1 to DBAR. The default value for NLVIB, set in block data subroutine XMPLEBD, is zero (0). When NLVIB = 0, the new code in DBAR will not be executed. To set NLVIB = 1 and execute the new DBAR code, the following calling sequence for the DSMG1 module is used:

```
DSMG1 CASECC,,SIL,,PHIG,CSTM,MPT,ECPT,GPC
      DIT/KGGG/V,N,DSCASET/C,N,1 $
```

The underlined parameter sets NLVIB to 1.

Once the changes shown in Appendix A were made to DBAR and XMP LBD, they were compiled and replaced the old DBAR and XMP LBD in the NASTRAN object library. Link 1 and Link 13 were relinked and a new executable NASTRAN was created. Although this procedure was done on a CDC computer, similar procedures will produce similar results on both the IBM and UNIVAC computers. In order to use this nonlinear vibration capability in NASTRAN, extensive alters have to be applied to either Rigid Format 5 and Rigid Format 13, depending on how the capability is needed. A summary of the applicable analyses, their governing equations and their appropriate Rigid Formats is given as follows:

<u>ANALYSIS</u>	<u>EQUATION</u>	<u>RIGID FORMAT</u>
Normal Modes	$\omega_o^2 [m] = [k]$	3
Buckling	$[k] + \lambda [k^d] = 0$	5
Normal Modes with Differential Stiffness	$\omega_o^2 [m] = [k + k^d]$	13
Nonlinear Vibration Analysis	$\omega^2 [m] = [k + k^g]$	5 with ALTERS
Nonlinear Vibration Analysis with Differential Stiffness	$\omega^2 [m] = [k + k^d + k^g]$	13 with ALTERS

where λ is an eigenvalue.

The appropriate DMAP alter sequences for both Rigid Formats 5 and 13 are shown in Appendix B. The alters between the statements

```
LABEL      CONV $
REPT       CONV, 1 $
```

will go through two iterations. If the user desires more iterations, the integer in the REPT statement must be increased. The only other input required to use this capability is the addition of a PARAM card in the Bulk Data deck. The parameter AMP is used to specify the amplitude of vibration of the structure.

EXAMPLES AND RESULTS

The nonlinear vibration capability developed for use with NASTRAN has been demonstrated by solving two examples of a nonlinear vibration analysis and two examples of a nonlinear vibration analysis with differential stiffness. NASTRAN solutions are compared with previously published results.

Nonlinear Vibration Analysis

The first example is the vibration of a uniform beam with various end support conditions. Evensen (ref. 6) obtained approximate amplitude-frequency relations for uniform beams with fixed-fixed, hinged-hinged, and fixed-hinged boundary conditions using a perturbation method. Good agreement is obtained between the NASTRAN and perturbation solutions as shown in Figure 3. For the hinged support case, the two amplitude-frequency curves coincide.

The second example demonstrates the effect of the amplitude of vibration on a rectangular frame structure. The frame is 304.8 cm (10.0 ft.) wide, 609.6 cm (20.0 ft.) long, and is made of 1.27 cm (0.5 in.) diameter steel rod. There are 10 equally spaced cells lengthwise and 4 equally spaced cells along the width. All four edges of the frame are fixed. A plot of the undeformed frame is shown in figure 4. Only one-fourth of the frame is used in the analysis due to symmetry. The linear frequency and nonlinear frequencies for values of the amplitude c (see Eq. 17) up to 7.62 cm (3 in.) are as follows.

<u>Amplitude, c</u>		<u>Frequency, Hertz</u>
<u>cm</u>	<u>(in.)</u>	
0	0	4.638 linear
1.27	0.5	5.319
2.54	1.0	6.830
3.81	1.5	8.565
5.08	2.0	10.295
6.35	2.5	11.940
7.62	3.0	13.478

The results indicate that the amplitude has an important influence on the frequency. In this example, a 5.08 cm (2 in.) amplitude at the center of the frame increases the fundamental nonlinear frequency to more than twice the linear one.

Nonlinear Vibration Analysis with Differential Stiffness

The third example is a hinged rectangular beam subjected to an applied axial tensile force of 105.4 N (23.7 lbf). The same problem was solved in ref. 2 using three different approximate analytical procedures, and results from these procedures, as well as experiment results, are given. One procedure is based on an assumption for the spatial dependence of the displacement function, one is based on an assumption for the temporal dependence of the displacement function, and the third procedure is the Galerkin procedure. The beam has the following properties:

Length	50.8	cm	(20.0	in.)
Width	1.27	cm	(0.50	in.)
Height	0.081	cm	(0.032	in.)
Material	Titanium Alloy			
Elastic Modulus	100.6	GPa	(14.6 x 10 ⁶	psi)
Specific Mass	5.15	Mg/m ³	(0.186	lb./in. ³)

One-half of the beam modeled by six BAR elements was used for the analysis. Three analytical fundamental frequencies and an experimentally measured one from ref. 2 and the NASTRAN solution are shown in figure 5. Comparing the results demonstrates that the NASTRAN results provide the closest comparison with the experiment.

The fourth example is a beam-column subjected to an applied compressive force with various support conditions. Based on linear theory, Lurie (ref. 7) has shown that the relation between the square of the frequency and the axial load is linear for a beam that has identically shaped vibration and buckling modes. He also showed that the condition of zero fundamental frequency corresponds to buckling. The linear vibration-stability problem studied by Lurie is actually the limiting case of a more general phenomenon of large amplitude vibrations under the influence of axial loads. Burgreen (ref. 8) obtained an exact solution in terms of elliptic functions for a uniform beam hinged at both ends and also verified his results experimentally. Srinivasan (ref. 9) used Galerkin's method to study beam-columns with both ends hinged. Table 1 shows good agreement between the NASTRAN solutions and the results given by Burgreen and Srinivasan, and NASTRAN gives better predictions than the one-term Galerkin method. The load-frequency curves for different amplitude ratios of vibration, d , for beams with various support conditions are given in figure 6, where d is the ratio of amplitude to the radius of gyration of the beam. No comparison is made for the cases of fixed-hinged and fixed-fixed because there appears to be no solution available in the literature. It has been found from this example that (1) the effect of amplitude is more pronounced for a less stiff structure, and (2) nonlinear theory shows that the frequency of a column at the Euler buckling load is not zero for finite amplitudes of vibration.

CONCLUDING REMARKS

Nonlinear vibration capability for beam and frame structures has been developed for use with NASTRAN Level 15.5 by means of DMAP ALTERS and modifications to the NASTRAN code. A geometrical stiffness matrix for a bar element has been developed for NASTRAN by modifying subroutine DBAR. An equivalent linearization technique and iterative process used to determine nonlinear frequencies are implemented into NASTRAN by the DMAP ALTERS. The versatility of the finite-element method enables the analyst to determine nonlinear frequencies of vibration for non-uniform beam and frame structures. Comparison with previously published results show that excellent accuracy is achieved with NASTRAN.

APPENDIX A
MODIFICATION OF CODE

```

*INSERT,DBAR,111
      DOUBLE PRECISION PXT,COEFF,HOLD(6),TEMP(36),PXP,STOR(36)
*INSERT,DBAR,185
C
C   INSERT NEW NLVIB PARAMETER INTO BLANK COMMON
C
      COMMON      ICOM,NLVIB
*INSERT,DBAR,638
      IF(NLVIB.NE.0.AND.FX.EQ.0.000) FX=1.000
*INSERT,DBAR,646
*INSERT,DBAR,766
      IF(NLVIB.EQ.0) GO TO 621
C
C   DIVIDE FX OUT OF KDGG MATRIX
C
      DO 900 KK=1,144
      KD(KK)=KD(KK)/FX
900 CONTINUE
C
C   COMPUTE
C
      T      F*A
      PXP = U * --- * (KDGG) * U
              2*L
C
C   WHERE U IS A 6X1 VECTOR
C
C      KDGG IS A 12X12 MATRIX DIVIDE INTO FOUR 6X6 MATRICES
C
      IF(IPVT.NE.1) GO TO 621
      COEFF=DA*E/(2.000*L)
      PXT = 0.000
      DO 920 IPI = 1,4
      JPX = 1
      JCNT=0
      IF(IPI.GE.3) GO TO 930
      ILO=)
      IHI=72
      GO TO 940
930  ILO=73
      IHI=144
940  DO 960 I = ILO,IHI,12
      JLO=I
      JHI=JLO+5
      DO 950 K = JLO,JHI

```

APPENDIX ..

```

JCNT = JCNT+1
IF (IP1.EQ.1.OR.IP1.EQ.3) TEMP(JCNT)=KD(K)
IF (IP1.EQ.2.OR.IP1.EQ.4) TEMP(JCNT)=KD(K+6)
950 CONTINUE
960 CONTINUE
IWLEFT=37
IF (IP1.GE.3) IWLEFT=73
IWRGHT=37
IF (IP1.EQ.2.OR.IP1.EQ.4) IWRGHT=73
CALL GMMATD(KE(IWLEFT),6.6.1,TEMP(1),6.6.0,STOR(1))
CALL GMMATD(STOR(1),6.6.0,KE(IWRGHT),6.6.0,TEMP(1))
912 DO 915 IP2 = 1,36
TEMP(IP2) = TEMP(IP2)*COEFF
915 CONTINUE
IF (IP1.EQ.2.OR.IP1.EQ.4) JPX = 2
IF (IP1.LE.2) CALL GMMATD(UA(1),6.1.1,TEMP(1),6.6.0,HOLD(1))
IF (IP1.GE.3) CALL GMMATD(UB(1),6.1.1,TEMP(1),6.6.0,HOLD(1))
IF (JPX .EQ.1) CALL GMMATD(HOLD(1),1.6.0,UA(1),6.1.0,PXP)
IF (JPX .EQ.2) CALL GMMATD(HOLD(1),1.6.0,UB(1),6.1.0,PXP)
C
C STORE SUM INTO PXT
C
PXT = PXT+PXP
920 CONTINUE
C
C PXT=.5 * PXP * KDGG
C
PXT = PXT*.5D0
621 CONTINUE
*INSERT,DBAR,790
IF (NLVID.EQ.0) GO TO 653
C
C CALCULATE KDGG AND STORE
C
DO 652 IPX=1,36
JPX=IPX+108
KEP(JPX)=PXT*KEP(JPX)
652 CONTINUE
653 CONTINUE
*COMPILE,DBAR
*DELETE,XMPLD,78
1, 10, 4HDSMG,4H1 , 1,10, 1, 1, -1, 1, 0
*DELETE,WT133-L14,39
DIMENSION MPL01(48), MPL02(178), MPL03(191), MPL04(179)

```

APPENDIX A

```
*DELETE.WT155-L16.8
COMMON/XGPI2/LMPL.MPLPNT.MPL(1621)
*DELETE.WT133-L14.42.WT133-L14.45
3      .(MPL( 227).MPL03(1)) .(MPL( 418).MPL04(1))
5      .(MPL( 597).MPL05(1)) .(MPL( 723).MPL06(1))
7      .(MPL( 858).MPL07(1)) .(MPL(1067).MPL08(1))
9      .(MPL(1172).MPL09(1)) .(MPL(1351).MPL10(1))
*DELETE.WT155-L16.9
1      .(MPL(1538).MPL11(1))
*COMPILE.XMPLBD
```

APPENDIX B

DMAP ALTERS

For Nonlinear Analysis

```

ID      NLVBF, BEAM FRAME
APP     DISP
SOL     5.0
TIME    5
$       NONLINEAR FREQ VIBRATIONS OF BEAM AND FRAME STRUCTURES
ALTER   19.23
GP3     GEOM3, EQEXIN, GEOM2/, GPTT/C, N, 123/V, N, NOGRAV/C, N, 123 $
CHKPNT  GPTT $
ALTER   31.31
ALTER   54
EQUIV   MGG, MNN/MPCF1 $
CHKPNT  MNN $
ALTER   66.76
MCE2    USET, GM, KGG, MGG, /KNN, MNN, $
CHKPNT  KNN, MNN $
LABEL   LBL2 $
EQUIV   KNN, KFF/SINGLE /MNN, MFF/SINGLE $
CHKPNT  KFF, MFF $
COND    LBL3, SINGLE $
SCE1    USET, KNN, MNN, /KFF, KFS, KSS, MFF, $
CHKPNT  KFS, KSS, KFF, MFF $
LABEL   LBL3 $
EQUIV   KFF, KAA/OMIT /MFF, MAA/OMIT $
CHKPNT  KAA, MAA $
ALTER   79
SMP2    USET, GO, MFF/MAA $
CHKPNT  MAA $
ALTER   81.129
ALTER   134.141
SETVAL  //V, N, BREAK/C, N, 1/V, N, LINK/C, N, -1 $
SAVE    BREAK, LINK $
LABEL   CONV $
EQUIV   KAA, KDAA/BREAK $
EQUIV   MAA, MDAA/BREAK $
READ    KAA, MAA, , EED, USET, CASECC/LAMA, PHIA, MI, OEIGS/C, N, MODES/V,
        N, NEIG/C, N, 2 $
SAVE    NEIG $
CHKPNT  LAMA, PHIA, MI, OEIGS $
OFF     LAMA, OEIGS, , //V, N, CARDNO $
SAVE    CARDNO $
COND    FINIS, NEIG $
SDR1    USET, , PHIA, , GO, GM, , KFS, , /PHIG, , BQG/C, N, 1/C, N, REIG $
CHKPNT  PHIG, BQG $
EQUIV   PHIG, PHIAMP/BREAK $
ADD     PHIG, /PHIAMP/ , Y, AMP $

```

APPENDIX B

```

CHKPNT PHIAMP $
EQUIV PHIAMP,PHIG/LINK $
DSMGL CASECC,,SIL,,PHIG,CSTM,MPT,ECPT,GPCT,DIT/KGGG/V,N,
DSCASET/C,N,1 $

CHKPNT KGGG $
ADD KGGG,KGG/KDGGG $
CHKPNT KDGGG $
EQUIV KDGGG,KDNN/MPCF2 /MGG,MDNN/MPCF2 $
CHKPNT KDNN,MDNN $
COND LBL2D,MPCF2 $
MCE2 USET,GM,KDGGG,MGG,,/KDNN,MDNN,, $
CHKPNT KDNN,MDNN $
LABEL LBL2D $
EQUIV KDNN,KDFF/SINGLE /MDNN,MDF/SINGLE $
CHKPNT KDFF,MDF $
COND LBL3D,SINGLE $
SCE1 USET,KDNN,MDNN,,/KDFF,KDFS,,MDF,, $
CHKPNT KDFF,KDFS,MDF $
LABEL LBL3D $
EQUIV KDFF,KDAA/OMIT /MDF,MDAA/OMIT $
CHKPNT KDAA,MDAA $
COND LBL5D,OMIT $
SMP1 USET,KDFF,,/GDO,KDAA,KDUO,LDOO,UDOO,,,, $
CHKPNT GDO,KDAA $
SMP2 USET,GDO,MDF/MDAA $
CHKPNT MDAA $
LABEL LBL5D $
EQUIV KDAA,KAA/LINK $
EQUIV MDAA,MAA/LINK $
REPT CONV,1 $
ADD MDAA,KDAA/KMAA $
ADD PHIAMP,/PHIM $
ALTER 157.158
ENDALTER
CEND

```

APPENDIX B

Nonlinear Vibration Analysis With Differential Stiffness

```

ID      NLVDS, BEAM FRAME
APP     DISP
SOL     13.0
TIME    5
$       NONLINEAR VIBRATION MODE WITH DIFFERENTIAL STIFFNESS FOR BEAM
$       AND FRAME STRUCTURES
ALTER   50
EQUIV   MGG, MNN/MPCF1 $
CHKPNT  MNN $
ALTER   62, 72
MCE2    USET, GM, KGG, MGG, /KNN, MNN, $
CHKPNT  KNN, MNN $
LABEL   LBL2 $
EQUIV   KNN, KFF/SINGLE /MNN, MFF/SINGLE $
CHKPNT  KFF, MFF $
COND    LHL3, SINGLE $
SCE1    USET, KNN, MNN, /KFF, KFS, KSS, MFF, $
CHKPNT  KFS, KSS, KFF, MFF $
LABEL   LBL3 $
EQUIV   KFF, KAA/OMIT /MFF, MAA/OMIT $
CHKPNT  KAA, MAA $
ALTER   75
SMP2    USET, GO, MFF/MAA $
CHKPNT  MAA $
ALTER   106, 125
ALTER   130, 130
SETVAL  /V, N, BREAK/C, N, 1/V, N, LINK/C, N, -1 $
SAVE    BREAK, LINK $
LABEL   CONV $
EQUIV   KAA, KSAA/BREAK $
EQUIV   MAA, MSAA/BREAK $
READ    KAA, MAA, EED, USET, CASECC/LAMA, PHIA, MI, CEIGS/C, N, MODES/V,
        N, N, C, N, 2 $
ALTER   136, 137
SDR1    USET, PHIA, GO, GM, KFS, /PHIG, BQG/C, N, 1/C, N, BKL1 $
CHKPNT  PHIG, BQG $
EQUIV   PHIG, PHIAMP/BREAK $
ADD     PHIG, /PHIAMP/V, Y, AMP $
CHKPNT  PHIAMP $
EQUIV   PHIAMP, PHIG/LINK $
DSMGI   CASECC, SIL, PHIG, CSTM, MPT, ECPT, GPCT, DIT/KGGG/V, N,
        DSCASET/C, N, 1 $
CHKPNT  KGGG $
ADD     K, KGGG, KGGG, /KSGG $
CHKPNT  KGGG $

```

APPENDIX B

```

EQUIV      KSGG,KSNN/MPCF2 / MGG,MSNN/MPCF2 $
CHKPNT     KSNN,MSNN $
COND       LBL2S,MPCF2 $
MCE2       USET,GM,KSGG,MGG,,/KSNN,MSNN,, $
CHKPNT     KSNN,MSNN $
LABEL      LBL2S $
EQUIV      KSNN,MSFF/SINGLE / MSNN,MSFF/SINGLE $
CHKPNT     KSFF,MSFF $
COND       LBL3S,SINGLE $
SCE1       USET,KSNN,MSNN,,/KSFF,KSFS,,MSFF,, $
CHKPNT     KSFF,KSFS,MSFF $
LABEL      LBL3S $
EQUIV      KSFF,KSAA/OMIT / MSFF,MSAA/OMIT $
CHKPNT     KSAA,MSAA $
COND       LBL5S,OMIT $
SMP1       USET,KSFF,,,/GSO,KSAA,KS00,LS00,US00,,,, $
CHKPNT     GSO,KSAA $
SMP2       USET,GSO,MSFF/MSAA $
CHKPNT     MSAA $
LABEL      LBL5S $
EQUIV      KSAA,KAA/LINK $
EQUIV      MSAA,MAA/LINK $
REPT       CONV,1 $
ADD        MSAA,KSAA/KMAA $
ADD        PHIAMP,/PHIM $
ENDALTER
CEND

```

REFERENCES

1. Eisley, J. G.: Nonlinear Deformation of Elastic Beams, Rings and Strings. Applied Mechanics Survey, Edited by H. Norman Abramson, Spartan Books, Washington, DC, 1966, pp. 285-290.
2. Ray, S. D., and Bert, C. W.: Nonlinear Vibrations of a Beam with Pinned Ends. Transactions of the ASME, J. of Engineering for Industry, Vol. 91, November 1969, pp. 997-1004.
3. Pandalai, K. A. V.: A General Conclusion Regarding the Large Amplitude Flexural Vibration of Beams and Plates. Israel J. of Technology, Vol. 11, 1973, pp. 321-324.
4. Anon.: The NASTRAN Programmer's Manual. NASA SP-223(01), May 1973.
5. Bergan, P. G. and Clough, Ray W.: Convergence Criteria for Iterative Processes. AIAA J., Vol. 10, 1972, pp. 1107-1108.
6. Evensen, D. A.: Nonlinear Vibrations of Beams with Various Boundary Conditions. AIAA J., Vol. 6, 1968, pp. 370-372.
7. Lurie, H.: Lateral Vibrations as Related to Structural Stability. J. Applied Mechanics, Vol. 19, 1952, pp. 195-204.
8. Bergreen, David: Free Vibrations of a Pin-Ended Column with Constant Distance Between Pin Ends. J. Applied Mechanics, Vol. 18, 1951, pp. 135-139.
9. Srinivasan, A. V.: Dynamic Stability of Beam Columns. AIAA J., Vol. 5, 1967, pp. 1685-1686.

TABLE 1. FREQUENCY RATIO OF A HINGED BEAM

Axial Load, $\frac{P_{xo}}{P_E}$	Method	Amplitude Ratio, $d = \frac{c}{\sqrt{I/A}}$			
		0.0	1.0	2.0	3.0
0.0	NASTRAN	1.0000	1.0889	1.3183	1.6260
	Ref. 8	1.0000	1.0892	1.3178	1.6257
	Ref. 9	1.0000	1.0897	1.3229	1.6394
0.2	NASTRAN	.8944	.9928	1.2401	1.5631
	Ref. 8	.8944	.9930	1.2389	1.5618
	Ref. 9	.8944	.9937	1.2450	1.5772
0.4	NASTRAN	.7746	.8864	1.1566	1.4976
	Ref. 8	.7746	.8864	1.1543	1.4949
	Ref. 9	.7746	.8874	1.1619	1.5125
0.6	NASTRAN	.6325	.7653	1.0666	1.4291
	Ref. 8	.6325	.7649	1.0627	1.4246
	Ref. 9	.6325	.7665	1.0724	1.4448
0.8	NASTRAN	.4472	.6210	.9682	1.3570
	Ref. 8	.4472	.6194	.9617	1.3502
	Ref. 9	.4472	.6225	.9747	1.3739
1.0	NASTRAN	.0026	.4309	.8586	1.2810
	Ref. 8	.0000	.4236	.8472	1.2708
	Ref. 9	.0000	.4330	.8660	1.2990
1.2	NASTRAN			.7329	1.2000
	Ref. 8			.7105	1.1851
	Ref. 9			.7416	1.2196

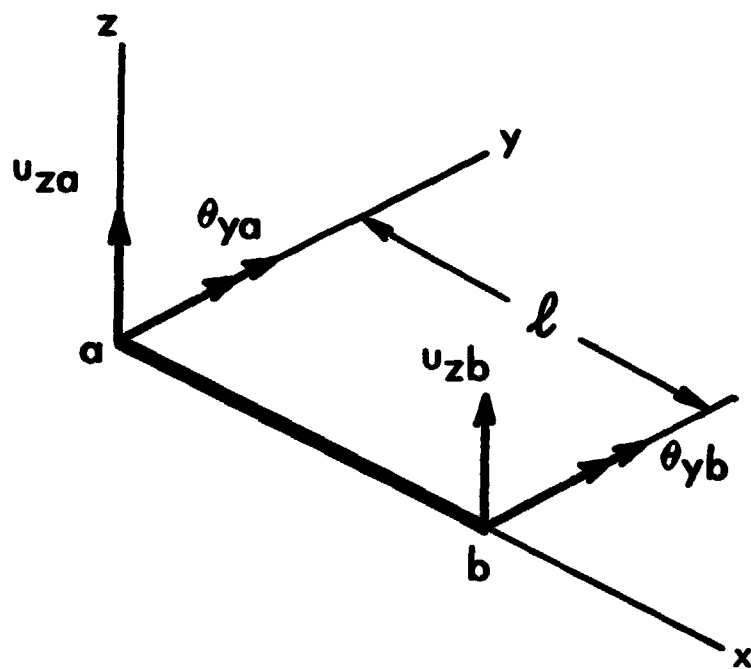


Figure 1. Bar coordinate system, showing displacements due to bending in the xz plane.

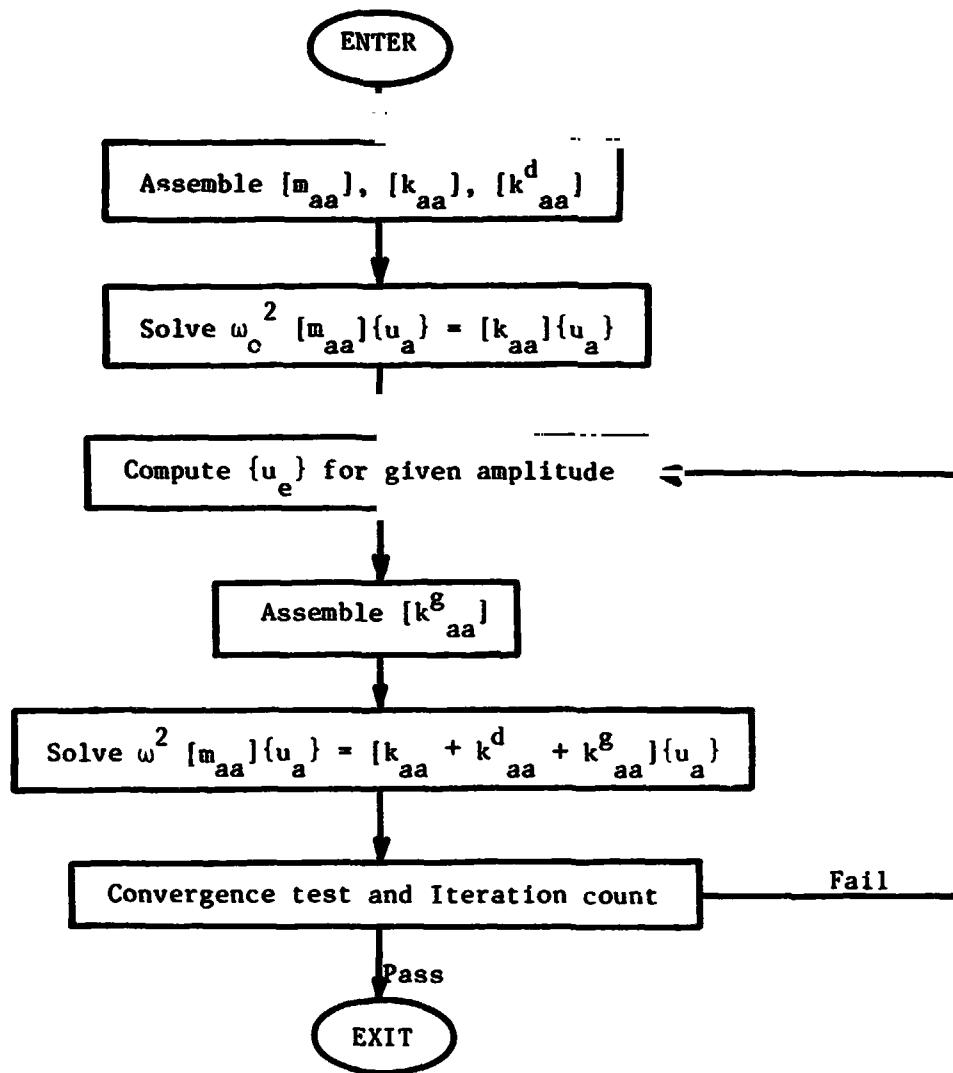


Figure 2. Simplified flow diagram for nonlinear vibration analysis.

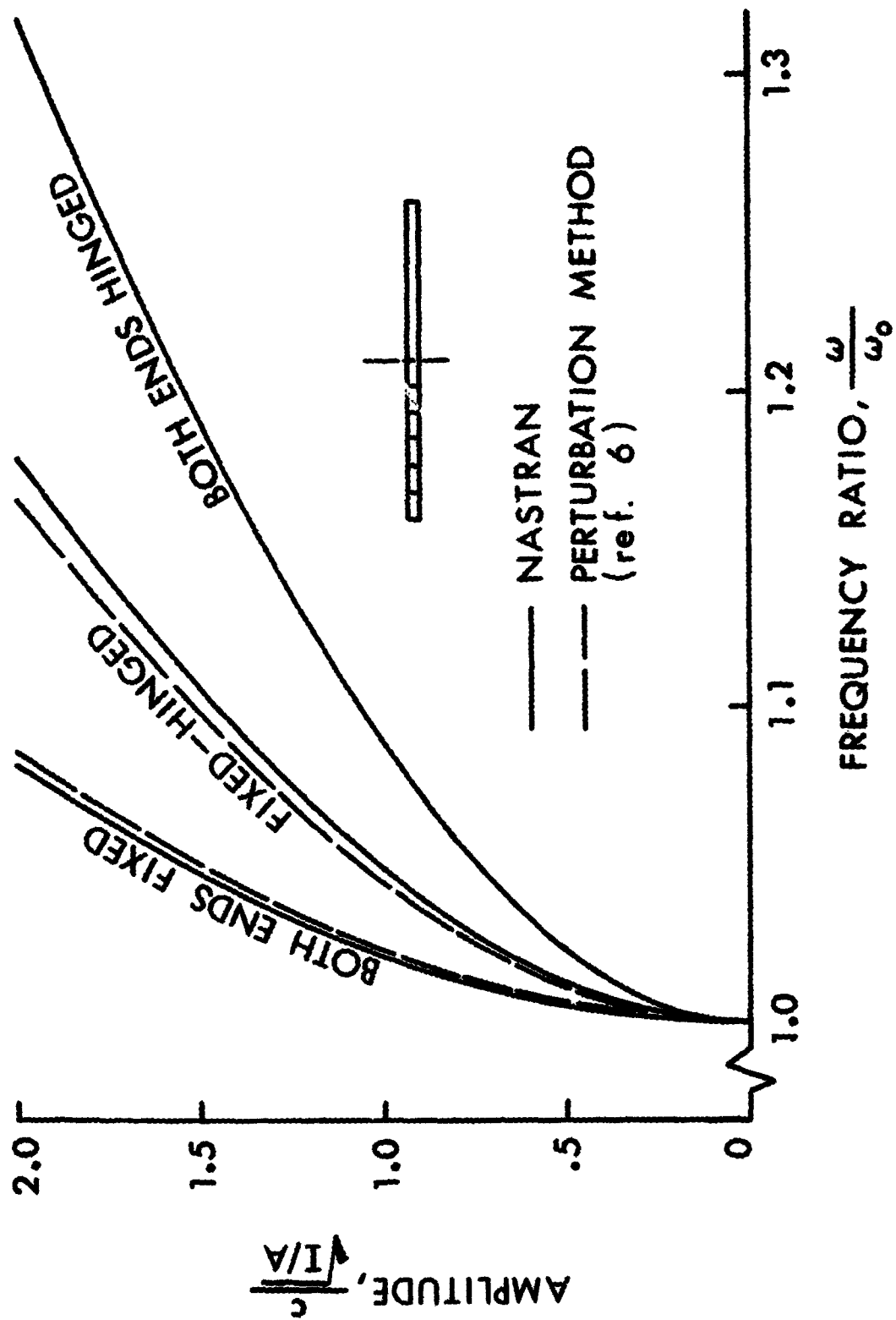


Figure 3. Amplitude-frequency curves for various support conditions.

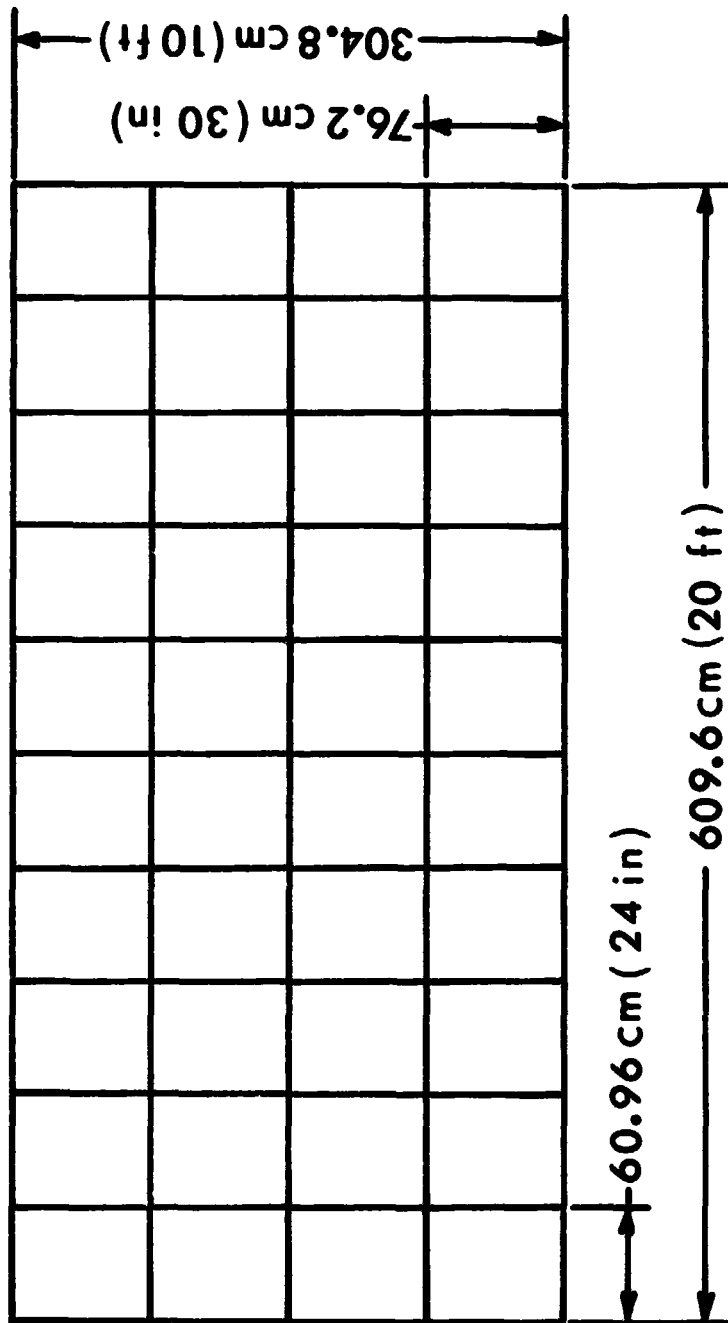


Figure 4. A rectangular frame constructed from bars with each edge fixed.

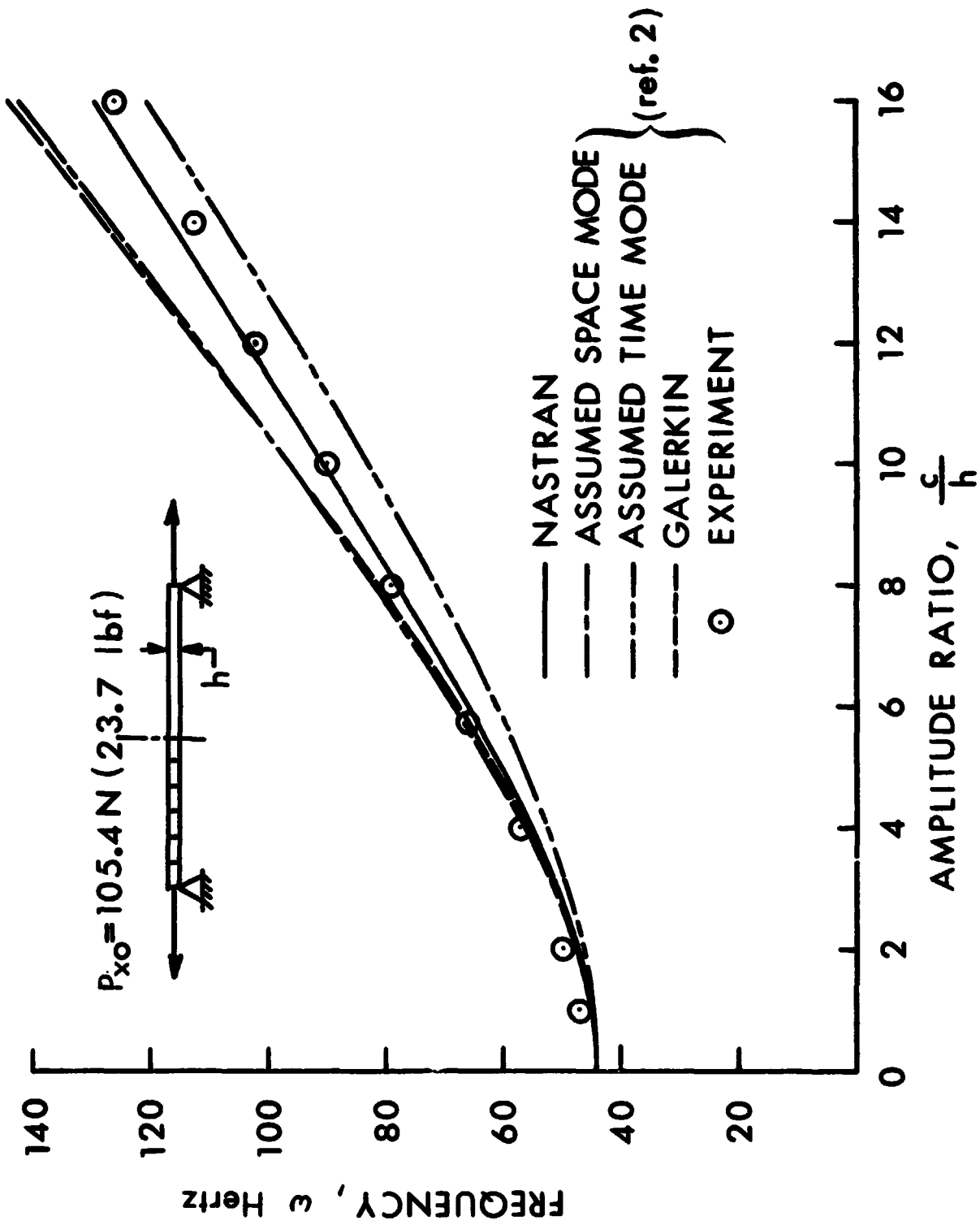


Figure 5. Comparison of experimental and analytical frequencies.

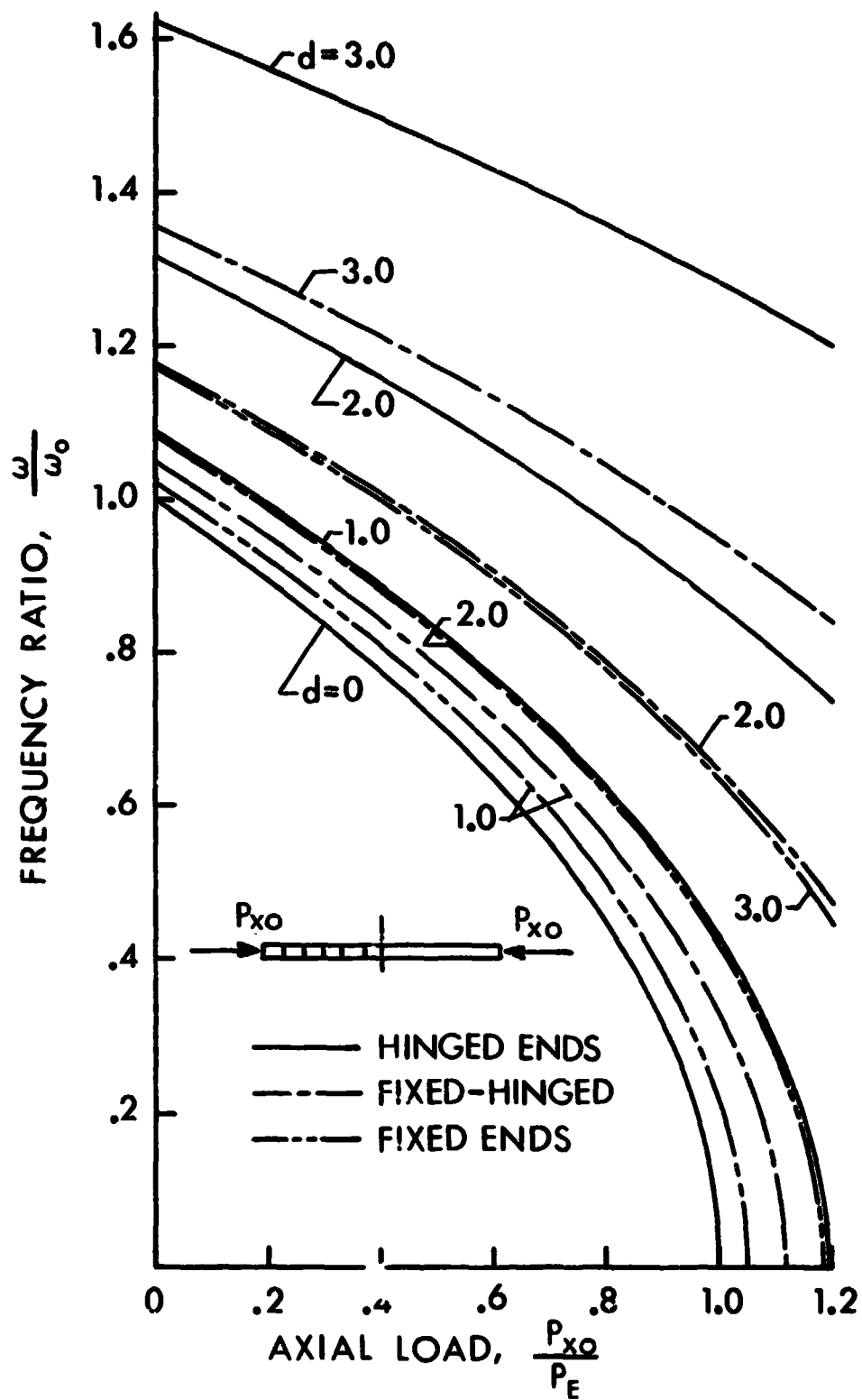


Figure 6. Variation of frequency with axial load for various support conditions.

N75 21501

ON EIGENVECTORS OF MULTIPLE EIGENVALUES OBTAINED IN NASTRAN

P. R. Pamidi

and

W. K. Brown

**Computer Sciences Corporation
System Sciences Division
Hampton, Virginia**

SUMMARY

In the case of non-multiple eigenvalues, each of the three real eigenvalue extraction methods available in NASTRAN will, for a given type of normalization, give essentially the same eigenvectors. However, this is not so in the case of multiple eigenvalues. This apparent discrepancy is explained and illustrated by considering the example of a NASTRAN demonstration problem that has both multiple and non-multiple eigenvalues.

INTRODUCTION

The NASTRAN program provides three basic methods for real eigenvalue extraction. In each of these methods, the eigenvectors obtained can be normalized in three different ways (see Appendix).

In the case of non-multiple eigenvalues, each of the three extraction methods will, for a given type of normalization, give essentially the same eigenvectors. However, in the case of multiple eigenvalues, the three extraction methods will, in general, give different eigenvectors even though they may employ the same type of normalization. Furthermore, in this case (of multiple eigenvalues), even a given method using a given type of normalization may yield different eigenvectors under different conditions (e.g., different frequency limits on the EIGR bulk data card) [1]¹. This discrepancy may seem disturbing, but it is explained in this paper where it is shown that the different eigenvectors corresponding to multiple eigenvalues obtained by different methods and under different conditions have certain definite relationships among them and

¹ Numbers in brackets indicate References given at the end of the paper.

that these relationships depend on the number of arbitrary constants that are inherently assumed in the computation of eigenvectors. This is illustrated by considering the example of a NASTRAN demonstration problem that has both multiple and non-multiple eigenvalues.

THEORETICAL BACKGROUND

The basic eigenvalue problem solved in NASTRAN can be formulated as

$$[K_{aa} - \lambda M_{aa}] \{x\} = 0 \quad (1)$$

where K_{aa} and M_{aa} are respectively the stiffness and mass matrices (both of which are real and symmetric) referred to the analysis set [2], λ is a scalar quantity, and $\{x\}$ is a column vector that comprises all the degrees of freedom in the analysis set. Non-trivial solutions for $\{x\}$ in the above equation are possible if and only if the resultant matrix within the brackets is singular [3,4]. The values of λ that satisfy this condition represent the required eigenvalues.

Let λ_ℓ be one of the eigenvalues of Equation (1). The eigenvector corresponding to this eigenvalue can be obtained from the equation by substituting $\lambda = \lambda_\ell$ and solving for $\{x\}$. We thus have

$$[K_{aa} - \lambda_\ell M_{aa}] \{x\}_\ell = 0 \quad (2)$$

where $\{x\}_\ell$ is the required eigenvector.

Let n be the order of the problem and let $x_1, x_2, x_3, \dots, x_n$ be the components of $\{x\}$. Equation (2) can then be rewritten as

$$\sum_{j=1}^n C_{ij} x_j = 0, \quad i = 1, 2, 3, \dots, n \quad (3)$$

where C_{ij} are constants that depend on K_{aa} , M_{aa} , and λ_ℓ .

Equation (3) represents a system of n linear equations in n unknowns. However, not all of these n equations are independent. The exact number of independent equations depends on the multiplicity of the eigenvalue λ_ℓ . If s ($1 \leq s \leq n$) is the multiplicity of λ_ℓ , then it can be shown that the rank of the resultant matrix in Equation (2) is $(n-s)$ [3,4]. The number of independent equations in (3) is also, therefore, $(n-s)$. Their solution thus involves s arbitrary constants. The total number of eigenvectors available is therefore equal to ∞^s . However, it can be shown that the number of linearly independent eigenvectors is only s [4].

--	--	--	--	--	--	--	--

Depending on the multiplicity s , it is useful to distinguish between the following two cases:

Case (a) Non-multiple Eigenvalues ($s = 1$)

In this case, $(n - 1)$ of the n equations in (3) are independent and their solution involves a single arbitrary constant. An infinite number of eigenvectors are thus available. However, the important thing to note here is that the relative values of the eigenvector components remain invariant.

Case (b) Multiple Eigenvalues ($1 < s < n$)

In this case, the number of independent equations in (3) is equal to $(n - s)$ and their solution involves s arbitrary constants. In contrast to the case of non-multiple eigenvalues, the most important thing to note in this case is that the relative values of the eigenvector components are not invariant, but depend on the relative values of the involved constants themselves. Also, it is clear that the solution space in this case is much larger than in the case of non-multiple eigenvalues.

EIGENVECTOR COMPUTATION IN NASTRAN

The exact procedure for eigenvector computation in NASTRAN depends on the method used for eigenvalue extraction and is described in detail in the Theoretical Manual [2]. Thus, in the Inverse power method, trial eigenvectors are assumed and iterated until convergence occurs. In the Determinant method, eigenvectors are computed by the method of backward substitution after each of the corresponding eigenvalues has been calculated. In the Givens method, all the eigenvalues are first obtained and then the required number of eigenvectors is computed by repeated use of backward substitution.

The orthogonality of eigenvectors of closely spaced eigenvalues is guaranteed by the procedure employed in the Inverse power method. NASTRAN employs the Gram-Schmidt orthogonalization procedure [4] for the purpose in the case of the Determinant and Givens methods.

Whatever the method employed, the eigenvectors obtained all exhibit the characteristics described in the previous section and also involve the inherent use of one or more arbitrary constants. In general, for a given mode, the involved constants for the computation of the corresponding eigenvector will not be the same in all the three methods. It should also be noted that the user has no control whatever on the selection or the choice of these constants.

EXAMPLE

To illustrate the points made in the paper, we consider the problem of the vibration of a square plate with hinged supports at all the four edges. (This is the same as NASTRAN Demonstration Problem 3-1. See Reference 5 for details.)

The finite element model employed is shown in Figure 1. Only half the plate has been modelled and symmetric boundary conditions used on the center-line in order to reduce the order of the problem as well as the bandwidth.

The parameters of the model are as follows:

Length = $l = 508.0$ mm (20.0 in.)

Width = $w = 508.0$ mm (20.0 in.)

Thickness = $t = 25.4$ mm (1.0 in.)

Young's modulus = $E = 2.06843 \times 10^{11}$ N/m² (3.0×10^7 psi)

Poisson's ratio = $\nu = 0.3$

Mass density = $\rho = 2.20197 \times 10^9$ Kg/m³ (206.04393 lb.-sec²/in.⁴)

The eigenvalues and eigenvectors for the first six modes of the model were obtained by the Inverse power and Determinant methods.² For each method, four separate runs were made with different eigenvalue extraction data. The detailed data for all the eight runs are given in Table 1. Since the number of degrees of freedom in the analysis set (or a-set) in this problem is as large as 590 and only the first few modes were required for the purpose of the present paper, the Givens method was considered unsuitable.

The eigenvalues and natural frequencies obtained in the eight runs (as well as the corresponding theoretical values [6]) are presented in Table 2. It can be seen from this that the third and fourth modes together represent an eigenvalue of multiplicity two, that is, a double root. The other modes yield non-multiple eigenvalues.³

Tables 3 through 7 present, for the first six modes, the eigenvector components corresponding to the vertical displacements at points 111 through 121 (along the line AB in Figure 1). The results for the third and fourth modes, which represent a multiple eigenvalue, are included together in Table 5.

² The runs were made on the CDC computer using an improved version of the 15.5 level of NASTRAN.

³ It is true that no conclusions can be drawn from Table 2 regarding the multiplicity of the eigenvalue for the sixth mode because in general, at least $(m + 1)$ eigenvalues must be obtained before one can examine the multiplicity of the m^{th} eigenvalue. However, in the present problem, the non-multiplicity of the sixth eigenvalue was confirmed from additional runs with more than six eigenvalues.

An examination of Table 3 (corresponding to the non-multiple eigenvalue of the first mode) reveals that the eigenvector components for all the runs are essentially the same. (Actually, the results for all the runs except Run 3 are identical. The extremely small differences between the results of Run 3 and those of others are so inconsequential as to be practically meaningless.) The results thus show that they are essentially unaffected by differences in the eigenvalue extraction data.

Tables 4, 6 and 7 (corresponding to the non-multiple eigenvalues of the second, fifth and sixth modes respectively) need some explanation. Note that all the eigenvector components given in these three tables are extremely small in magnitude. Actually, the corresponding theoretical values are all zero [6]. For all practical purposes, the differences among the various runs in these tables can, therefore, be considered as quite insignificant.

Table 5 (corresponding to the multiple eigenvalue of the third and fourth modes) is interesting. It can be seen that the results given by the runs employing the Determinant method are essentially the same and that they are essentially unaffected by differences in the eigenvalue extraction data. The same thing is not wholly true for the runs employing the Inverse power method because slight variations are noticeable among some of them. (In this connection, it should be emphasized that the association of a particular eigenvector with a particular mode number in this table is irrelevant because the numbering of the modes for this multiple eigenvalue is completely arbitrary.) The most important point to note in this table, however, is that the eigenvectors given by the Inverse power method are completely different from those given by the Determinant method. At first sight, this discrepancy in the results may seem disturbing. However, it can be explained from a theoretical viewpoint and the discrepancy may be shown to be apparent and not real.

Now, since the third and fourth modes involve a multiple eigenvalue of order two, it follows from the theory presented earlier that their eigenvectors involve two arbitrary constants in them and that the relative values of the eigenvector components depend upon the relative values of these two constants. The differences among the various eigenvectors shown in Table 5 are therefore clearly due to the fact that they represent different relative values of the two involved constants.

The theory also shows that, in the case of a multiple eigenvalue of order two, the total number of eigenvectors possible is doubly infinite. The solution space is thus much larger than in the case of non-multiple eigenvalues. The theory further shows that the number of independent eigenvectors in this case is only two. This means that every eigenvector in the solution field can be obtained by the linear combination of any two eigenvectors that are themselves linearly independent. This can be shown to be true in the case of the eigenvectors given in Table 5.

Let $\{x\}_{ij}$ represent any eigenvector in Table 5 where i denotes the mode number and j denotes the run number. It can be seen from the table that there are several eigenvectors that are identical and, therefore, linearly dependent. One such set, for instance, is given by the eigenvectors $\{x\}_{31}$ and $\{x\}_{42}$. Another such set is given by $\{x\}_{32}$ and $\{x\}_{43}$. Yet another such example is the set comprising $\{x\}_{35}$, $\{x\}_{36}$, $\{x\}_{37}$ and $\{x\}_{38}$. A fourth such set is given by $\{x\}_{46}$, $\{x\}_{47}$ and $\{x\}_{48}$.

As an example, consider the eigenvectors $\{x\}_{36}$ and $\{x\}_{46}$ in Table 5 which are clearly linearly independent. It can be shown that every eigenvector in Table 5 can be obtained as a suitable linear combination of these two eigenvectors. Simple algebra shows that, for instance, the eigenvector $\{x\}_{32}$ in Table 5 can be obtained from these two independent eigenvectors by the following (approximate) relationship:

$$\{x\}_{32} = 0.9850782\{x\}_{36} - 0.1917116\{x\}_{46} \quad (4)$$

Similarly, it can be shown that the following (approximate) relationship can be used to obtain the eigenvector $\{x\}_{34}$ from $\{x\}_{36}$ and $\{x\}_{46}$:

$$\{x\}_{34} = 0.9850979\{x\}_{36} - 0.1914862\{x\}_{46} \quad (5)$$

In a like manner, similar linear relationships can be shown to exist between any eigenvector and any two linearly independent eigenvectors in Table 5.

The above discussion and relationships clearly show that the discrepancy in the results presented in Table 5 is thus only apparent and not real.

It is interesting to note that the plate problem considered in this example yields multiple roots at many higher modes also. Thus, for instance, modes 9 and 10 represent a double root. So do modes 12 and 13. Results similar to the above can be expected to occur in these cases also.

CONCLUSIONS

NASTRAN provides three basic methods for real eigenvalue extraction. In the case of non-multiple eigenvalues, each of these three methods will, for a given type of normalization, give essentially the same eigenvectors. However, this is not so in the case of multiple eigenvalues. This apparent discrepancy has been explained and illustrated by considering the example of a NASTRAN demonstration problem that has both multiple and non-multiple eigenvalues.

APPENDIX

The NASTRAN program provides three basic methods for real eigenvalue extraction. These are:

- 1) The Inverse power method,
- 2) The Determinant method, and,
- 3) The Givens (or Tridiagonal) method.

The Inverse power and Determinant methods are "tracking" methods and as such are efficient in those cases where only a few of many eigenvalues are desired. On the other hand, the Givens method is a transformation method that is efficient only in those cases where all eigenvalues or a high proportion of all eigenvalues are required [2].

In each of the three methods, the eigenvectors obtained can be normalized in any one of three different ways. The three types of normalization (NORMS) available are [1]:

- a) normalizing to unit value of the generalized mass (MASS),
- b) normalizing to unit value of the largest component in the analysis set (MAX), and,
- c) normalizing to unit value of a specified component in the analysis set (POINT).

REFERENCES

1. The NASTRAN User's Manual (Level 15.0), NASA SP-222(01), May 1973.
2. The NASTRAN Theoretical Manual (Level 15.0), NASA SP-221(01), December 1972.
3. Hohn, F. E., Elementary Matrix Algebra, Second Edition, The Macmillan Company, New York, 1967.
4. Hildebrand, F. B., Methods of Applied Mathematics, Second Edition, Prentice-Hall, Inc., Englewood Cliffs, N. J., 1965.
5. NASTRAN Demonstration Problem Manual (Level 15), NASA SP-224(01).
6. Harris, C. M., and Crede, C. E., Ed., Shock and Vibration Handbook, Volume 1, McGraw-Hill Book Company, Inc., New York, 1961.

Table 1. Eigenvalue Extraction Data* for the NASTRAN Runs

Run no.	Eigenvalue extraction method	Normalization method	Frequency limits (Hz)		Number of desired roots
			f ₁	f ₂	
1	Inverse power	MAX	0.89	5.00	3
2			0.89	5.00	4
3			0.89	6.50	5
4			0.89	8.00	6
5	Determinant	MAX	0.89	5.00	3
6			0.89	5.00	4
7			0.89	6.50	5
8			0.89	8.50	6

* See Reference 1 for details.

Table 2. Eigenvalues and Natural Frequencies

Mode no.	NASTRAN results (Runs 1 through 8 --- See Table 1)		Theoretical values (Reference 6)	
	Eigenvalues (rad/sec) ²	Natural frequencies (Hz)	Eigenvalues (rad/sec) ²	Natural frequencies (Hz)
1 ^a	3.237408E+01	9.055634E-01	3.246970E+01	9.068997E-01
2 ^a	2.022407E+02	2.263364E+00	2.029356E+02	2.267249E+00
3 ^a	8.111597E+02	4.532870E+00	8.117425E+02	4.534499E+00
4 ^b	8.111597E+02	4.532870E+00	8.117425E+02	4.534499E+00
5 ^c	1.352052E+03	5.852169E+00	1.371845E+03	5.894848E+00
5 ^d	2.355330E+03	7.724066E+00	2.345936E+03	7.706648E+00

^a Obtained by all runs.

^b Obtained by all runs except Runs 1 and 5.

^c Obtained by Runs 3, 4, 7 and 8.

^d Obtained only by Runs 4 and 8.

Table 3. Eigenvector Components* Corresponding to Vertical Displacements for Mode 1

Eigenvalue = $3.237408E+01$ (rad/sec)² Natural frequency = $9.055634E-01$ Hz

Grid point (see Figure 1)	Run 1	Run 2	Run 3	Run 4	Run 5	Run 6	Run 7	Run 8	
111	1.000000E+00	1.000000E+00	1.000000E+00	1.000000E+00	1.000000E+00	1.000000E+00	1.000000E+00	1.000000E+00	
112	9.876883E-01	9.876883E-01	9.876883E-01	9.876883E-01	9.876883E-01	9.876883E-01	9.876883E-01	9.876883E-01	
113	9.510565E-01	9.510565E-01	9.510565E-01	9.510565E-01	9.510565E-01	9.510565E-01	9.510565E-01	9.510565E-01	
114	8.910065E-01	8.910065E-01	8.910064E-01	8.910065E-01	8.910065E-01	8.910065E-01	8.910065E-01	8.910065E-01	
115	8.090170E-01	8.090170E-01	8.090168E-01	8.090170E-01	8.090170E-01	8.090170E-01	8.090170E-01	8.090170E-01	
116	7.071068E-01	7.071068E-01	7.071065E-01	7.071068E-01	7.071068E-01	7.071068E-01	7.071068E-01	7.071068E-01	
117	5.877853E-01	5.877853E-01	5.877850E-01	5.877853E-01	5.877853E-01	5.877853E-01	5.877853E-01	5.877853E-01	
118	4.539905E-01	4.539905E-01	4.539902E-01	4.539905E-01	4.539905E-01	4.539905E-01	4.539905E-01	4.539905E-01	
119	3.090170E-01	3.090170E-01	3.090168E-01	3.090170E-01	3.090170E-01	3.090170E-01	3.090170E-01	3.090170E-01	
120	1.564345E-01	1.564345E-01	1.564344E-01	1.564345E-01	1.564345E-01	1.564345E-01	1.564345E-01	1.564345E-01	
121	0.0	0.0	0.0	0.0	0.0	0.0	0.0	0.0	
	Inverse power method						Determinant method		

* The eigenvalue analyses were done by using the British system of units. However, the eigenvector components obtained represent relative values and thus are independent of the system of units employed.

Table 4. Eigenvector Components* Corresponding to Vertical Displacements for Mode 2
 Eigenvalue = 2.022407E+02 (rad/sec)² Natural frequency = 2.263364E+00 Hz

Grid point (see Figure 1)	Run 1	Run 2	Run 3	Run 4	Run 5	Run 6	Run 7	Run 8
111	8.582833E-06	8.582833E-06	-8.804327E-07	2.867177E-11	7.498964E-14	7.498964E-14	7.498964E-14	7.498964E-14
112	8.476104E-06	8.476104E-06	-8.336322E-07	2.821834E-11	6.467638E-14	6.467638E-14	6.467638E-14	6.467638E-14
113	8.158775E-06	8.158775E-06	-7.022221E-07	2.688187E-11	3.426100E-14	3.426100E-14	3.426100E-14	3.426100E-14
114	7.639303E-06	7.639303E-06	-5.112464E-07	2.474057E-11	-1.083766E-14	-1.083766E-14	-1.083766E-14	-1.083766E-14
115	6.931394E-06	6.931394E-06	-2.964310E-07	2.192269E-11	-6.537558E-14	-6.537558E-14	-6.537558E-14	-6.537558E-14
116	6.053466E-06	6.053466E-06	-9.654166E-08	1.860159E-11	-1.164175E-13	-1.164175E-13	-1.164175E-13	-1.164175E-13
117	5.027983E-06	5.027983E-06	5.486849E-06	1.497935E-11	-1.438612E-13	-1.438612E-13	-1.438612E-13	-1.438612E-13
118	3.880710E-06	3.880710E-06	1.365259E-07	1.122344E-11	-1.422880E-13	-1.422880E-13	-1.422880E-13	-1.422880E-13
119	2.639977E-06	2.639977E-06	1.437853E-07	7.447627E-12	-1.153687E-13	-1.153687E-13	-1.153687E-13	-1.153687E-13
120	1.335955E-06	1.335955E-06	8.931819E-08	3.706543E-12	.467638E-14	.467638E-14	.467638E-14	.467638E-14
121	0.0	0.0	0.0	0.0	0.0	0.0	0.0	0.0
	Inverse power method				Determinant method			

* See note given under Table 3.

Table 5. Eigenvector Components Corresponding to Vertical Displacements for Modes 3 and 4

Natural frequency = 4.532870E+00 Hz

Mode no.	Grid point (see Figure 1)	Run 1	Run 2	Run 3	Run 4	Run 5	Run 6	Run 7	Run 8
3	111	1.000000E+00	-3.591128E-01	1.000000E+00	-3.588908E-01	-1.699369E-01	-1.699370E-01	-1.699370E-01	-1.699370E-01
	112	9.536365E-01	-2.786022E-01	9.536365E-01	-2.783910E-01	-9.874144E-02	-9.874148E-02	-9.874151E-02	-9.874146E-02
	113	8.231105E-01	-5.563910E-02	8.231104E-01	-5.545871E-02	9.802834E-02	9.802830E-02	9.802828E-02	9.802832E-02
	114	6.322864E-01	2.581424E-01	6.322863E-01	2.582780E-01	3.736201E-01	3.736201E-01	3.736201E-01	3.736201E-01
	115	4.152396E-01	5.893736E-01	4.152395E-01	5.894585E-01	6.616324E-01	6.616324E-01	6.616324E-01	6.616324E-01
	116	2.090134E-01	8.590667E-01	2.090132E-01	8.591037E-01	8.906449E-01	8.906449E-01	8.906449E-01	8.906449E-01
	117	4.579713E-02	1.000000E+00	4.579698E-02	1.000000E+00	1.000000E+00	1.000000E+00	1.000000E+00	1.000000E+00
	118	-5.377633E-02	9.715794E-01	-5.377648E-02	9.715579E-01	9.532895E-01	9.532895E-01	9.532895E-01	9.532895E-01
	119	-8.476043E-02	7.689300E-01	-8.476054E-02	7.689038E-01	7.466009E-01	7.466009E-01	7.466009E-01	7.466009E-01
	120	-5.856040E-02	4.242319E-01	-5.856046E-02	4.242148E-01	4.097170E-01	4.097170E-01	4.097170E-01	4.097170E-01
	121	0.0	0.0	0.0	0.0	0.0	0.0	0.0	0.0
	4	111	1.000000E+00	1.000000E+00	-3.591128E-01	1.000000E+00	1.000000E+00	1.000000E+00	1.000000E+00
112		9.536365E-01	9.536365E-01	-2.786022E-01	9.536270E-01	9.458695E-01	9.458695E-01	9.458695E-01	9.458695E-01
113		8.231105E-01	8.231105E-01	-5.563910E-02	8.230750E-01	7.939267E-01	7.939267E-01	7.939267E-01	7.939267E-01
114		6.322864E-01	6.322864E-01	2.581424E-01	6.322146E-01	5.732738E-01	5.732738E-01	5.732738E-01	5.732738E-01
115		4.152396E-01	4.152396E-01	5.893736E-01	4.151303E-01	3.254212E-01	3.254212E-01	3.254212E-01	3.254212E-01
116		2.090134E-01	2.090134E-01	8.590667E-01	2.088751E-01	9.540108E-02	9.540107E-02	9.540107E-02	9.540107E-02
117		4.579713E-02	4.579713E-02	1.000000E+00	4.564668E-02	-7.782729E-02	-7.782727E-02	-7.782727E-02	-7.782730E-02
118		-5.377633E-02	-5.377633E-02	9.715794E-01	-5.391728E-02	-1.695951E-01	-1.695951E-01	-1.695951E-01	-1.695951E-01
119		-8.476043E-02	-8.476043E-02	7.689300E-01	-8.486974E-02	-1.745788E-01	-1.745788E-01	-1.745788E-01	-1.745788E-01
120		-5.856040E-02	-5.856040E-02	4.242319E-01	-5.862008E-02	-1.075995E-01	-1.075995E-01	-1.075995E-01	-1.075995E-01
121		0.0	0.0	0.0	0.0	0.0	0.0	0.0	0.0

Determinant method

Inverse power method

* See note given under Table 3.

ORIGINAL PAGE IS
OF POOR QUALITY

Table 6. Eigenvector Components* Corresponding to Vertical Displacements for Mode

Eigenvalue = $1.352052E+03$ (rad/sec)²

Natural frequency = $5.852169E+00$ Hz

Grid point (see Figure 1)	Run 3	Run 4	Run 7	Run 8
111	-5.699912E-07	-1.843495E-06	-2.183520E-12	-7.436551E-12
112	-6.080192E-07	-1.758002E-06	-2.089282E-12	-6.985661E-12
113	-7.113474E-07	-1.517318E-06	-1.771927E-12	-5.644270E-12
114	-8.501140E-07	-1.165451E-06	-1.135621E-12	-3.503232E-12
115	-9.820411E-07	-7.652404E-07	-2.059582E-13	-8.178176E-13
116	-1.061947E-06	-3.849968E-07	7.125514E-13	1.746165E-12
117	-1.052001E-06	-8.408051E-08	1.267204E-12	3.572532E-12
118	-9.304697E-07	9.946076E-08	1.520344E-12	4.248741E-12
119	-6.970452E-07	1.565069E-07	1.396781E-12	3.669778E-12
120	-3.735721E-07	1.080931E-07	8.658139E-13	2.111212E-12
121	0.0	0.0	0.0	0.0
	Inverse power method		Determinant method	

* See note given under Table 3.

Table 7. Eigenvector Components* Corresponding to Vertical Displacements for Mode 6

Eigenvalue = 2.355330 (rad/sec)²

Natural frequency = 7.724066E+00 Hz

Grid point (see Figure 1)	Run 4	Run 8
111	-4.899823E-10	-6.518056E-12
112	-4.359024E-10	-5.832685E-12
113	-2.854791E-10	-3.934395E-12
114	-7.157563E-11	-1.252190E-12
115	1.590946E-10	1.593764E-12
116	3.561466E-10	3.982927E-12
117	4.764730E-10	5.414795E-12
118	4.937036E-10	5.612997E-12
119	4.039232E-10	4.588831E-12
120	2.265359E-10	2.571805E-12
121	0.0	0.0
	Inverse power method	Determinant method

* See note given under Table 3.

N75 81502

THE EFFECTS OF LOCALIZED DAMPING ON STRUCTURAL RESPONSE

D. H. Merchant, R. L. Gates,
Boeing Aerospace Company

M. W. Ice, and J. W. VanDerlinden
Boeing Computer Services, Inc.

SUMMARY

The effect of localized structural damping on the excitability of higher order normal modes of the Large Space Telescope is investigated. A preprocessor computer program was developed to incorporate Voigt structural joint damping models in a NASTRAN finite-element dynamic model. A postprocessor computer program was developed to select critical modes for (1) low-frequency attitude-control problems and for (2) higher frequency fine-stabilization problems. The mode selection is accomplished by ranking the flexible modes based on (1) coefficients for rate gyro, position gyro, and optical sensors and on (2) image-plane motions due to sinusoidal or random power spectral density force and torque inputs.

INTRODUCTION

The presence of distributed damping in spacecraft structures may significantly affect the predicted dynamic response of higher order normal modes. The purpose of this study was to develop and implement a general methodology framework for evaluating the effects of distributed structural damping on spacecraft structures. Identification of potential limitations in the conventional use of uncoupled normal modes for structural dynamic response analyses has resulted from the application of this methodology to the Large Space Telescope (LST) control system design (reference 1).

The methodology is concerned with two general aspects: (1) including distributed damping in a finite-element structural model and (2) selecting critical modes for subsequent dynamic analyses and assessing the effects of modal velocity coupling. Methodology for modeling distributed damping in a NASTRAN structural model was developed and implemented in a preprocessor computer program used to generate the required NASTRAN BULK DATA. This computer program was developed for convenience in preparing NASTRAN input, and its use is strictly optional. Methodology for selecting critical modes and assessing modal coupling was developed and implemented in a postprocessor computer program. Application of this methodology to the LST control and fine-stabilization problems was accomplished using a detailed LST NASTRAN structural model. Qualitative results and conclusions of the present study are discussed.

STRUCTURAL JOINT MODELING

Structural damping is comprised of both material (hysteretic) damping and energy dissipation in structural joints. Material damping may be represented in linear dynamic response analyses by uncoupled modal viscous damping ratios (ζ). Energy dissipation in structural joints is a nonlinear function of many parameters (references 2, 3, 4, 5, and 6). However, this phenomenon must also be represented by linear models so that linear analysis techniques may be used. Two linear joint models have been used to describe the frequency-dependent effects of distributed joint damping: the Maxwell model and the Voigt model. The three-parameter anelastic model, referred to as the Maxwell model, has been identified in the literature (references 2, 4, 5, 6, and 7) as a feasible model for representing hysteretic damping in materials. For a massless structural element and joint supporting a single mass, the Maxwell and Voigt models are essentially equivalent. Since the two-parameter Voigt model is simpler than the three-parameter Maxwell model, the Voigt model is used in the application to the LST control and vibration studies.

The two-parameter Voigt unit, shown schematically in Figure 1, consists of a spring in parallel with a viscous damper. It is the simplest complex-notation model and possesses hysteretic properties characteristic of damping in materials and structural joints. For sinusoidal excitation, the equivalent damping and stiffness coefficients (C_T and K_T) for the Voigt model, in series with a spring, are functions both of the structural parameters (K, K_V, C) and of the forcing frequency (β):

$$C_T = \frac{C K^2}{(K+K_V)^2 + C^2 \beta^2} \quad (1)$$

$$K_T = \frac{K K_V (K+K_V) + C^2 \beta^2 K}{(K+K_V)^2 + C^2 \beta^2} \quad (2)$$

These coefficients are determined for the single degree-of-freedom system shown in Figure 1 using Laplace transforms.

For very low frequencies,

$$C_T(\beta=0) = C \left(\frac{K}{K+K_V} \right)^2 \quad (3)$$

$$K_T(\beta=0) = K_V \left(\frac{K}{K+K_V} \right) \quad (4)$$

Equation (4) indicates that, at very low frequencies, the total Voigt joint/member stiffness coefficient is the static stiffness of the series spring arrangement.

For very high frequencies,

$$C_T(\beta=\infty) = 0 \quad (5)$$

$$K_T(\beta=\infty) = K \quad (6)$$

Equations (5) and (6) indicate that at very high frequencies the damper effectively becomes rigid; thus, the total Voigt joint/member damping coefficient is zero and the total stiffness coefficient is the member stiffness.

A preprocessor computer program was written to implement this methodology by adding structural joint models to a NASTRAN finite-element structural model. The preprocessor modifies the input data for a conventional finite-element structural model and generates additional inputs necessary to incorporate the Voigt joint damping model at the ends of specified BAR or ROD elements. The damping characteristics of the joints are modeled with the NASTRAN linear viscous damping element (VISC). The preprocessor is presently limited to incorporating joint damping at the ends of BAR and ROD elements defined in a rectangular coordinate system.

Schematics of NASTRAN BAR and ROD elements with joint damping models included at one end are shown in Figure 2. The original element lies between gridpoints a and b. When the user requests a joint damping model to be included at gridpoint a, the preprocessor establishes the model as follows:

- a. Gridpoint c is introduced on the BAR (ROD) axis at a specified distance from gridpoint a.
- b. Properties of the BAR (ROD) between gridpoints a and c are altered as specified, either by direct input or by default values, to provide desired stiffness characteristics.
- c. For a BAR element, gridpoints e and f are established such that gridpoints a, b, e and f form an orthogonal axis system at gridpoint a. Gridpoint e is in plane 1 of the BAR element, and gridpoint f is in plane 2. The distances from gridpoint a to gridpoints c, e and f are identical.
- d. Viscous damping (VISC) elements (m, n and p) with desired properties are inserted between gridpoints a and c, a and e, and a and f for a BAR element and between a and c only for a ROD element. The VISC elements used with BAR and ROD elements may have translational damping components, in addition to the rotational components, only when the VISC element axis is aligned with an axis of the displacement coordinate system.
- e. For a BAR element, gridpoints e and f are multipoint-constrained to gridpoint c.

The VISC element provides damping along its axis and in torsion about its axis. Therefore, for a BAR element, three VISC elements are required at each gridpoint to provide damping of all six degrees of freedom. The locations of gridpoints e and f in Figure 2(a) are calculated, in the rectangular coordinate system, by vector analysis.

Default values are automatically specified by the preprocessor for the NASTRAN data describing the structural joints. The default value specifying joint length results in a joint member whose length is ten percent of the original element length. The default values specifying joint member area, moments of inertia, and torsional constant are calculated to give a ten percent reduction in axial, bending, and torsional stiffnesses for a cantilever beam. This stiffness reduction results in a five percent reduction in the first resonant frequency for a massless cantilever beam with a concentrated mass at the tip. The five percent frequency reduction is consistent with the lower values measured from actual hardware compared with values predicted from standard finite-element analysis techniques.

The VISC elements and parameters chosen to define the joint damping characteristics must result in a physical damping matrix which satisfies kinematic compatibility. The compatibility relations for the damping matrix are represented by

$$[BGG]\{\phi_R\} = \{0\} \quad (7)$$

where $[BGG]$ is the NASTRAN viscous damping matrix in physical coordinates, and $\{\phi_R\}$ is an arbitrary vector of rigid-body translations and rotations. Equation (7) ensures that no damping forces are generated by rigid-body motions. With regard to kinematic compatibility, the NASTRAN VISC damping element is limited to two applications:

- a. With translational damping, the compatibility relations are satisfied only when the axis of the VISC element is aligned with an axis of the displacement coordinate system.
- b. Without translational damping, the compatibility relations involving only rotational damping are satisfied for any orientation of the VISC element.

For the general case of an arbitrarily oriented element having both translational and rotational damping components, the present NASTRAN VISC element does not provide the translation/rotation damping coupling terms required by Equation (7).

MODE SELECTION

Critical mode selection is accomplished by the postprocessor computer program using structural dynamic characteristics, including the coupled modal damping matrix, obtained from the NASTRAN restart tape. The NASTRAN calculation of the modal damping matrix is accomplished with DAMP ALTER statements in the NASTRAN EXECUTIVE CONTROL deck. The postprocessor has two major options. It will select critical modes for (1) low-frequency control problems involving sinusoidal analysis and (2) higher frequency fine-stabilization problems involving either sinusoidal or random vibration analysis. The methodology determines the critical normal modes in the low-frequency control range by comparing control-system coefficients associated with optical sensors as well as with rate and position gyro sensors. In the higher frequency fine-stabilization range, the methodology determines the critical normal modes by estimating the image-plane motion due to specified sinusoidal or random power spectral density (PSD) force and torque inputs. These calculations for ranking the modes use only the diagonal terms of the coupled modal damping matrix. The significance of the neglected damping coupling terms is therefore evaluated numerically in a separate series of calculations. The capability to convert between different systems of units is also available; the postprocessor input may be provided in the inch- $\frac{\text{pound}\cdot\text{second}^2}{\text{inch}}$ -second system or FSS (foot-slug-second) system and the output can be converted to the FSS or MKS (meter-kilogram-second) system. The general logic flow of the postprocessor is shown in Figure 3.

Low-Frequency Control Option

For the control option, the postprocessor reads the following structural dynamic characteristics from the NASTRAN checkpoint/restart tape:

- [ϕ] the matrix of mode shapes for selected modes and freedoms
- {M} the matrix of generalized masses for selected modes
- [D] the matrix of generalized coupled modal damping terms for selected modes
- { ω } the matrix of modal frequencies for selected modes

The optical amplification matrix, [B_0], and grid I.D.'s of image train components are input to the postprocessor by punched cards. The optical amplification matrix describes the three translations of the image plane in terms of physical translations and rotations of the image train components.

The coupled model damping matrix is calculated by applying the modal transformation to the viscous damping matrix [BGG] generated by NASTRAN in physical coordinates

$$[D] = [\phi]^T [BGG] [\phi] = [BHE] \quad (8)$$

The DMAP ALTER statements used to calculate and output the coupled damping matrix are included in the EXECUTIVE CONTROL deck as shown in Table 1.

Equivalent modal viscous damping (ζ_i) is calculated from the coupled modal damping matrix as follows:

$$\zeta_i = \frac{D_{ii}}{2 \omega_i M_i} \quad (9)$$

Rate or position coefficients for each requested mode are calculated for the selected freedoms and image plane motions as follows:

$$R(3014, 3024)_j = \frac{\phi_{3014,j} \phi_{3024,j}}{(2\zeta_j) \omega_j M_j} \quad (10)$$

$$P(3014, 3022)_j = \frac{\phi_{3014,j} \phi_{3022,j}}{(2\zeta_j) \omega_j^2 M_j} \quad (11)$$

$$P(3014, \quad)_j = [B_\sigma] \{ \phi_j^B \} \frac{\phi_{3014,j}}{(2\zeta_j) \omega_j^2 M_j} \quad (12)$$

where R and P denote rate and position coefficients, respectively. Grid-point freedoms for the input point and response point are specified in parentheses. The last digit of each I.D. is the input or output freedom specified at the gridpoint indicated by the preceding digits. For example, P(3014, 3022)_j requests a position coefficient to be calculated for the *j*th mode at gridpoint 302 in the freedom 2(y) direction due to a unit sinusoidal torque at gridpoint 301 in the freedom 4 (θ_x) direction. The three-component vector of displacement response at the image plane due to a unit sinusoidal torque at gridpoint 301 in the freedom 4 (θ_x) direction is calculated as shown in Equation (12). Position and rate coefficients for all selected modes are ranked and listed along with their mode numbers and frequencies.

High-Frequency Fine-Stabilization Option

For the fine-stabilization option, as with the low-frequency control option, the structural dynamic characteristics $[\phi]$, $[M]$, $[D]$ and $\{\omega\}$ for selected modes and freedoms are read from the NASTRAN checkpoint/restart tape, and the optical amplification matrix $[B_o]$ and grid I.D.'s of the image train components are input by cards. Equivalent modal viscous damping coefficients are calculated using Equation (9).

The inputs unique to this option are tables of sinusoidal peak or PSD force and torque levels versus frequency which are used in the sinusoidal or random analyses, respectively. Since the phase relationships among the sinusoidal force and torque inputs are not well defined, the generalized force for the j^{th} mode F_j is represented by

$$F_j = \max(|\phi_{ji}^F| * F_i) \quad (13)$$

where ϕ_{ji}^F is the j^{th} mode shape at the i^{th} forced freedom, and

F_i is the peak force (or torque) of the i^{th} forced freedom at the j^{th} mode frequency

The modal displacement at resonance q for the j^{th} mode is

$$q_j = \frac{F_j}{2\zeta_j \cdot \omega_j^2 \cdot M_j} \quad (14)$$

Physical displacements corresponding to the optical train components for the j^{th} mode are

$$\{x_B\}_j = \{\phi_j^B\} q_j \quad (15)$$

where $\{\phi_j^B\}$ is the j^{th} mode shape vector at the response freedoms corresponding to the optic train components.

Physical displacements of the image at the focal plane for the j^{th} mode are

$$\{x_1\}_j = [B_o] \{x_B\}_j \quad (16)$$

As previously noted, the optical amplification matrix, $[B_o]$, describes three translations of the image plane in terms of physical translations and rotations of the image train components.

For random force (or torque) inputs, the RMS modal displacements for the j^{th} mode are

$$(q_j)_{\text{RMS}} = \frac{1}{2\zeta_j \cdot \omega_j^2 \cdot M_j} \left(\pi f_j S_j \zeta_j \right)^{\frac{1}{2}} \quad (17)$$

where $S_j = \{\phi_j^F\}^T [S_F(f_j)] \{\phi_j^F\} = \sum_i (\phi_{ij}^F)^2 \cdot S_{Fi}(f_j)$

and $S_{Fi}(f_j)$ is the input force (torque) power spectrum at the i^{th} input freedom for frequency f_j

The individual input force PSD's, defined with frequency (f) in Hz, are assumed approximately constant within $\pm 20\zeta_j f_j$ of the j^{th} modal frequency. This frequency band accounts for approximately 98 percent of the RMS modal displacement for a constant PSD. No cross-spectra are assumed so that $[S_F(f_j)]$ is a diagonal matrix constructed, for each frequency, from one value of force PSD and one value of torque PSD.

Equations (15) and (16) are then used to calculate RMS values of physical displacements (x_B) and displacements of the image at the focal plane (x_1) for each mode. These calculated RMS displacements are ranked and listed along with their mode numbers and frequencies.

The degree of modal velocity coupling is calculated as the ratio of coupled to uncoupled response for all modes having potentially significant coupling. These modes are identified by numerically considering both the relative magnitudes of each pair of off-diagonal and diagonal damping terms and the proximity of the modal frequencies corresponding to these pairs of damping terms. To assess the degree of modal velocity coupling, the ratio of coupled response to uncoupled response is calculated and output for all modes selected as having potentially significant coupling. The coupled response is calculated for each mode using the admittance matrix at the resonant frequency and unit forces applied at selected gridpoints.

LST STRUCTURAL MODEL

The basic LST structural dynamics model (Model 1) includes detailed modeling of the Support Systems Module (SSM), the Orbital Telescope Assembly/Science Instruments (OTA/SI) and four deployed appendages. Table 2 shows the detailed breakdown into numbers of gridpoints, structural elements, and dynamic degrees of freedom for the various substructures comprising the complete structural dynamic model. The grid geometry and some of the element connections and gridpoint identifications for the SSM and OTA/SI structural dynamic models are shown in Figures 4 and 5, respectively.

The SSM model, shown in Figure 4, consists of the aft shell, the equipment section including reaction wheels and interface points, the forward shell, and appendages. The aft shell is modeled with coarse-grid plate elements as suggested by Figure 4. Four ring stiffeners, three on the cylinder and one around the access porthole on the aft end, are modeled with BAR elements. The forward end of the aft shell is connected to the smaller diameter inner shell of the equipment section through multipoint constraint equations.

The equipment section inner shell is modeled with 60 plate elements as shown in Figure 4. The equipment bays are formed by three large external ring frames and 15 longerons. These rings and longerons, not shown in the figure, are modeled with 105 BAR elements offset radially approximately one-half the bay depth. The forward gridpoints of the SSM equipment section are connected to the central gridpoint through multipoint constraint equations. Four reaction wheels are each supported by four BAR elements attached to the corners of the forward and aft compartments of the bays as shown in Figure 4. The gridpoints representing the reaction wheels have six dynamic degrees of freedom each. The three SSM interface gridpoints are each supported by two stiff BAR elements which distribute the interface loads to the aft and center ring frames at the intersection with the nearest longeron. These BAR elements are not shown in Figure 4. The forward shell is modeled as a beam consisting of 11 BAR elements cantilevered from the central gridpoint of the forward end of the equipment section.

The deployed high gain antennas (HGA) and solar arrays are modeled as beams consisting of 5 and 9 BAR elements each, respectively. The bases of the appendages are connected to the forward end of the SSM equipment section with 3 rotational and 3 translational scalar spring elements each.

The OTA/SI model, shown in Figure 5, consists of the metering truss including the secondary mirror, the primary support structure including the primary mirror and interface flexures, and the focal plane structure including the science instruments. The graphite/epoxy metering truss is modeled with BAR elements as shown in Figure 5. The secondary mirror is supported by four radial graphite/epoxy beams, each modeled with three BAR elements. The secondary mirror gridpoint, having six degrees of freedom, is connected to the four support points by multipoint constraint equations.

The primary support structure consists of six radial beams connecting inner and outer rings as shown in Figure 5. These beams and rings are modeled with 42 BAR elements. The metering truss is connected to the stiff outer ring with BAR's at 8 points which represent the eight fittings. The three primary mirror support gridpoints are connected to three of the radial beams by three axial bar elements. These three gridpoints are connected to the central primary mirror gridpoint through multipoint constraint equations. The three interface flexures are each modeled by two scalar spring elements, one providing axial stiffness and the other providing tangential stiffness. These scalar elements connect the SSM interface gridpoints to three stiff BAR elements extending radially outward from the OTA/SI primary support ring as shown in Figure 5.

The focal plane structure consists of two hexagonal rings connected by six axial and six diagonal truss members. This assembly is supported from three points on the primary support ring by nine truss members. The three fine guidance sensors are each supported from the focal plane structure by four BAR elements. The star tracker and two gyro sensors are supported by single stiff BAR elements from the primary support ring. The six gridpoints on the aft hexagonal ring of the focal plane structure are connected to a central gridpoint by multipoint constraint equations. This central gridpoint has six dynamic degrees of freedom. A single gridpoint located aft of the focal plane is used to represent the science instruments. A rigid link (multipoint constraint) connects the aft ring gridpoint to the SI gridpoint.

LST Model 1 was modified to include structural joint damping at 26 locations throughout the structure. This modified finite-element model was designated LST Model 2. Some joints were incorporated using the preprocessor and others were added manually. The manual data input was for joints in the basic structural model which were modeled using elements other than BARS or RODS. Voigt models were added at the appendage deployment hinges, the star tracker support, the metering truss supports, the OTA/SSM interface flexures, the SI focal plane structure supports, and the SSM forward shell support. The effects of material damping were included by adding modal viscous damping for all flexible modes to the modal damping matrix corresponding to the Voigt joint models.

The deployment hinges for the four appendages (two high-gain antennas and two solar arrays) in the basic LST model were idealized using scalar spring (ELAS) elements. The Voigt models were generated for the modified LST model by adding DAMP1 elements in parallel with these ELAS elements to provide joint damping in three rotational degrees of freedom. Joint damping characteristics for the star tracker, which is cantilevered from the primary support ring, were also input manually. Scalar damping elements (DAMP1) were used to provide damping in the three rotational directions. Damping in the eight metering truss/primary mirror support ring fittings was modeled using scalar damping (DAMP1) elements in the axial direction only. Damping in the OTA/SSM interface flexures was modeled using axial scalar damping elements in parallel with the axial scalar spring components.

The preprocessor was used to incorporate Voigt structural joint models in the nine BAR elements supporting the SI focal plane structure. The nine VISC elements, with only rotational damping components, were defined at the three gridpoints where the SI connects to the primary support ring. The preprocessor was also used to incorporate a structural joint at the base of the SSM forward shell.

Free-free mode shapes, frequencies, generalized masses, and the coupled modal damping matrix for 100 flexible modes were determined using NASTRAN rigid format 3. Modal frequencies range from less than 1 Hz for appendage modes to more than 130 Hz. The coupled modal damping matrix for the Voigt joint damping of LST Model 2 indicated off-diagonal terms frequently exceeding the corresponding diagonal terms, sometimes by as much as an order of magnitude.

RESULTS

The preprocessor and postprocessor methodology was applied to two different LST control system studies: 1) a time-domain control simulation and 2) a frequency-domain vibration analysis. LST fine-stabilization errors induced by the attitude control system cover a wide frequency spectrum from DC up to 300 Hz. In order to analyze the problem efficiently, it was divided into two efforts on the basis of frequency. Although there is some overlap in frequency, the low-frequency control analysis covers DC up to about 20 Hz, and the vibration frequency analysis covers from 10 Hz to above 100 Hz. A detailed discussion of this overall approach may be found in Reference 8.

Control frequency errors are studied using a closed-loop time-domain simulation of the control system. A nonlinear, digital, three-axis control simulation computer program (DTACS) is used to obtain the image position at the $f/24$ focus as a function of time. The higher frequency vibration errors are studied using an open-loop frequency-domain simulation of the actuator output vibrations exciting the LST structure. The vibration analysis program (VAP) is a linear, digital, three-axis simulation used to obtain image motions versus excitation frequency.

The postprocessor methodology was applied in selecting critical modes of LST Model 1 for DTACS and VAP and comparing these mode orderings with those obtained by conventional techniques. With the low-frequency control option, the postprocessor mode ordering for LST Model 1 was based on image-plane coefficients calculated using the optical amplification matrix (Equation 12). The conventional ordering was based on the product of mode shapes at applied torque and image sensor locations divided by the generalized mass. For the LST structural model, the conventional ordering technique omitted three of the eight critical modes identified by the postprocessor. However, since the modes identified by both techniques are the major contributors to the LST image motion, the postprocessor methodology and the conventional technique are equivalent for this particular simulation.

With the higher-frequency fine-stabilization option, the postprocessor mode ordering for LST Model 1 was accomplished using Equations (13) through (16), where the applied forces and torques were proportional to reaction wheel excitation frequency raised to the 1.7 power. The conventional ordering was again based on the product of input and output mode shapes normalized by the generalized mass. For the LST structural model, the conventional ordering technique omitted 17 of the 20 critical modes identified by the postprocessor. The LST image motions calculated from these two different sets of modes were, of course, significantly different. Those image motions calculated from the conventional ordering were in error by an order of magnitude compared with those from the postprocessor ordering.

The preprocessor methodology was applied in generating LST Model 2 with discrete damping components. The critical modes of this model were selected for DTACS and VAP by the postprocessor, and the simulation results using these modes were compared with the previous results from LST Model 1. For the DTACS low-frequency control simulation, the postprocessor mode ordering

and the calculated image motions were essentially identical for the two LST models, despite the fact that the damping of the critical low-frequency modes increased an order of magnitude for LST Model 2. The increased modal damping did not significantly affect the results since the control loop used in both cases was designed to be stable for the lower damping. For the VAP sinusoidal vibration simulation, on the other hand, the modal damping effects are very significant. Although the postprocessor mode orderings were quite similar for the two LST models, comparisons of calculated image motions indicate substantial reductions in response amplitudes due to the increase in modal damping from LST Model 1 to LST Model 2.

The data of LST Model 2 was used to assess the significance of damping (velocity) coupling among the normal modes. The measure used to assess the degree of coupling is the ratio of coupled response to uncoupled response. For the 20 most critical modes of LST Model 2, the maximum assessment ratio is 1.024. For all 100 modes, the minimum assessment ratio is 0.459 for the 68th mode. These data indicate that modal velocity coupling is a potentially significant effect for high-accuracy structural dynamic analysis.

CONCLUDING REMARKS

Methodology developed to improve structural joint modeling for distributed damping and to select critical structural modes for subsequent analytical studies has been successfully demonstrated. The NASTRAN viscous damping capability is adequate to represent the general characteristics of localized structural damping, although special care is required in using the VISC damping element. The preprocessor computer program automatically generates NASTRAN BULK DATA cards required for a specific class of Voigt joint damping models. The postprocessor methodology is sufficiently general to select critical modes for a broad class of subsequent analytical studies. LST studies indicate that modal velocity coupling resulting from damping in discrete structural joints has a potentially significant effect on dynamic responses.

ACKNOWLEDGEMENTS

The work described in this report was sponsored primarily by the George C. Marshall Space Flight Center under NASA Contract NAS8-30655. The work was performed under the technical direction of George L. von Pragenau and Larry A. Kiefling of the MSFC Systems Dynamics Laboratory. The basic LST NASTRAN structural model was developed as part of the Boeing-sponsored Orbiting Telescope Systems program under the direction of C. T. Golden. The control-system and sinusoidal vibration studies were performed by William W. Emsley and Patrick J. Hawkins of the Boeing Aerospace Company.

REFERENCES

1. Merchant, D. H., and Gates, R.M., "Effect of Damping on Excitability of High-Order Normal Modes", Boeing document D180-18835-1, May 30, 1975
2. Ungar, E. E., "The Status of Engineering Knowledge Concerning the Damping of Built-up Structures", Journal of Sound and Vibration, Vol. 26, No. 1, January 8, 1973, pp. 141-154
3. Ungar, E. E., "Energy Dissipation at Structural Joints: Mechanisms and Magnitudes", AFFDL-TDR-64-98, August, 1964
4. Rodgers, E. J., and Warrington, J. D., "A Survey of Material and Structural Damping", Saturn V/Apollo and Beyond, American Astronautical Society National Symposium, Huntsville, Ala., June 11-14, 1967, Transactions, Volume 3
5. De Veubeke, B. M. F., "Influence of Internal Damping on Aircraft Resonance", Manual on Aeroelasticity, Part 1, AGARD, October 1968, Chapter 3
6. Lazan, B. J., Damping of Materials and Members in Structural Mechanics, Pergamon Press, 1968
7. Goodman, L. E., and Klumpp, J. H., "Analysis of Slip Damping with Reference to Turbine-Blade Vibration", ASME Journal of Applied Mechanics, Vol. 23, September 1956, pp. 421-429
8. Jacot, A. D., and Emsley, W. W., "Assessment of Fine Stabilization Problems for the LST", AIAA Paper No. 73-881, presented at AIAA Guidance and Control Conference, Key Biscayne, Florida, August 20-22, 1973

Table 1.- DMAP ALTER Statements for
Damping Matrix Formulation

```

-----
N A S T R A N   E X E C U T I V E   C O N T R O L   D E C K
-----
FD LST, MODES 1
APP DISPLACEMENT
SOL 3.0
CHKPNT YES
TIME 30
ALTER 28,29
SMA2 ESTM,MPT,EEPT,GPET,DIT/HGG,BGG/V,Y,HTMASS#1,R/V,N,NOMGG/V,N,NDBGG/
V,Y,COUPMASS/V,Y,CPBAR/V,Y,CPRDD/V,Y,CPQUAD1/V,Y,CPQUAD2/V,
Y,CPTRIA1/V,Y,CPTRIA2/V,Y,CPTUBE/V,Y,CPODPLT/V,Y,CPTRPLT/V,
Y,CPTRBSC 1
SAVE NOMGG,NDBGG $
ALTER 74
MATGPR GPL,USET,SIL,MAA//E,N,AS
MATGPR GPL,USET,SIL,BGG//C,N,GS
ALTER 96
MPYAD PHIG,BGG,/XX/C,N,1/E,N,1/C,N,0 $
MPYAD XX,PHIG,/BHH/C,N,0/C,N,1/C,N,0 $
CHKPNT BHH $
MATPPN BHH,XXX// $
ENDALTER
CEND
-----

```

**ORIGINAL PAGE IS
OF POOR QUALITY**

Table 2.- Basic Structural Dynamic Model Description

Substructure	No. of Gridpoints*	No. of Structural Elements			No. of Dynamic D.O.F.
		Plate	Bar	Scalar Spring	
SSM Aft Shell	49	45	32		24
SSM Equip. Sect.					54
Inner Shell	75	60			
Ring Frames			45		
Longerons			60		
Reaction Wheels	4		16		24
Shuttle Attach.	4		8		
Fwd SSM Shell	12		11		33
HGA	12		10	12	24
Solar Arrays	20		18	12	48
OTA/SI-SSM Interface & Backup	6		9	6	
Metering Truss	32		80		48
Secondary Mirror & Support	13		12		6
Primary Mirror & Support	40		53		42
Focal Plane Struct.	19		48		24
SI	1		1		
	<u>287</u>	<u>105</u>	<u>403</u>	<u>30</u>	<u>327</u>

*Permanent SPC Gridpoints Excluded

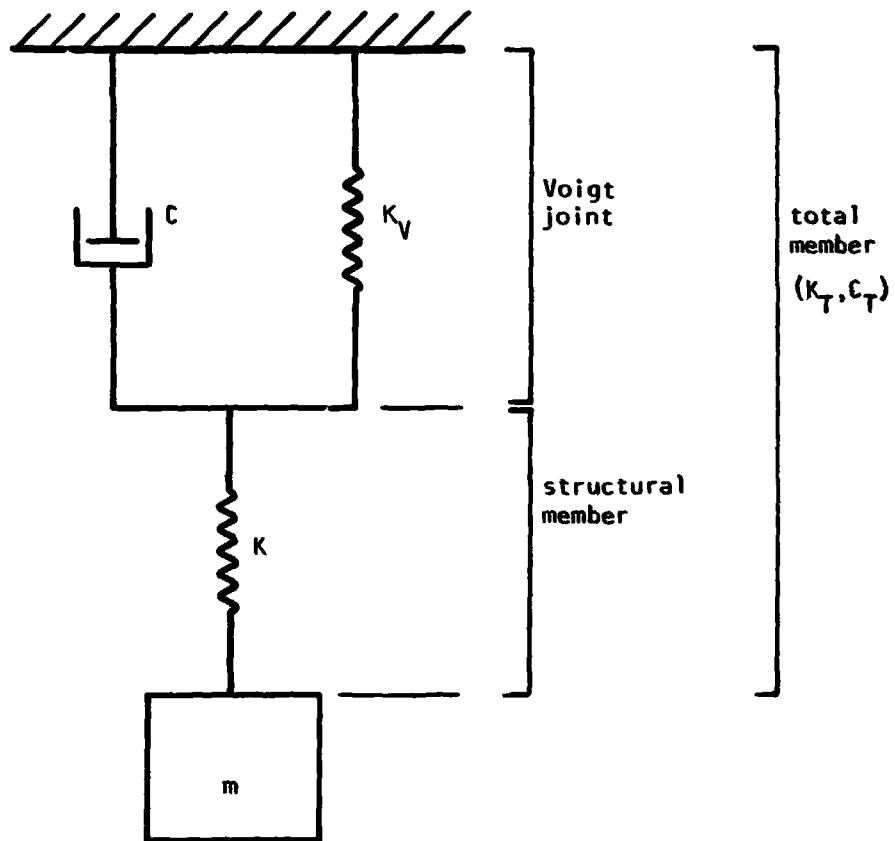
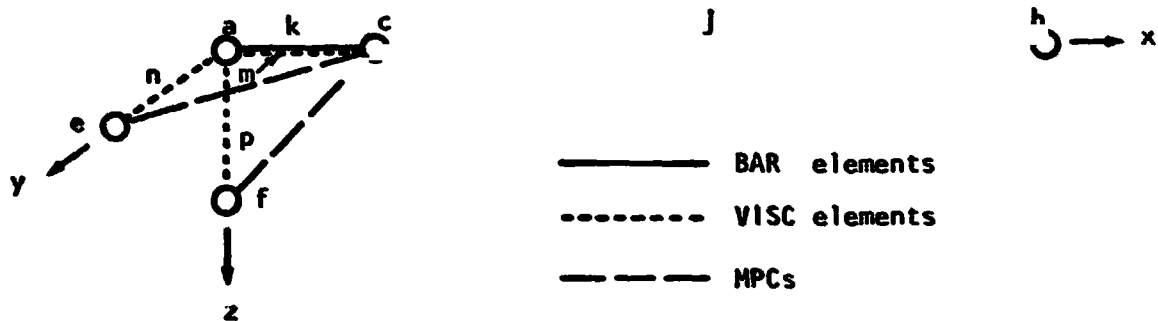
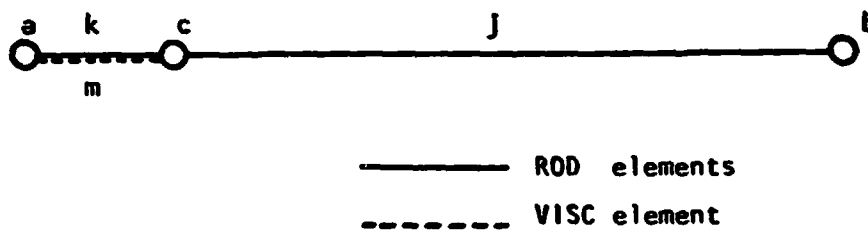


Figure 1.- Schematic of Single Degree-of-Freedom Voigt Joint Model



a) BAR Joint Schematic



b) ROD Joint Schematic

Figure 2.- NASTRAN Joint Damping Model Schematics

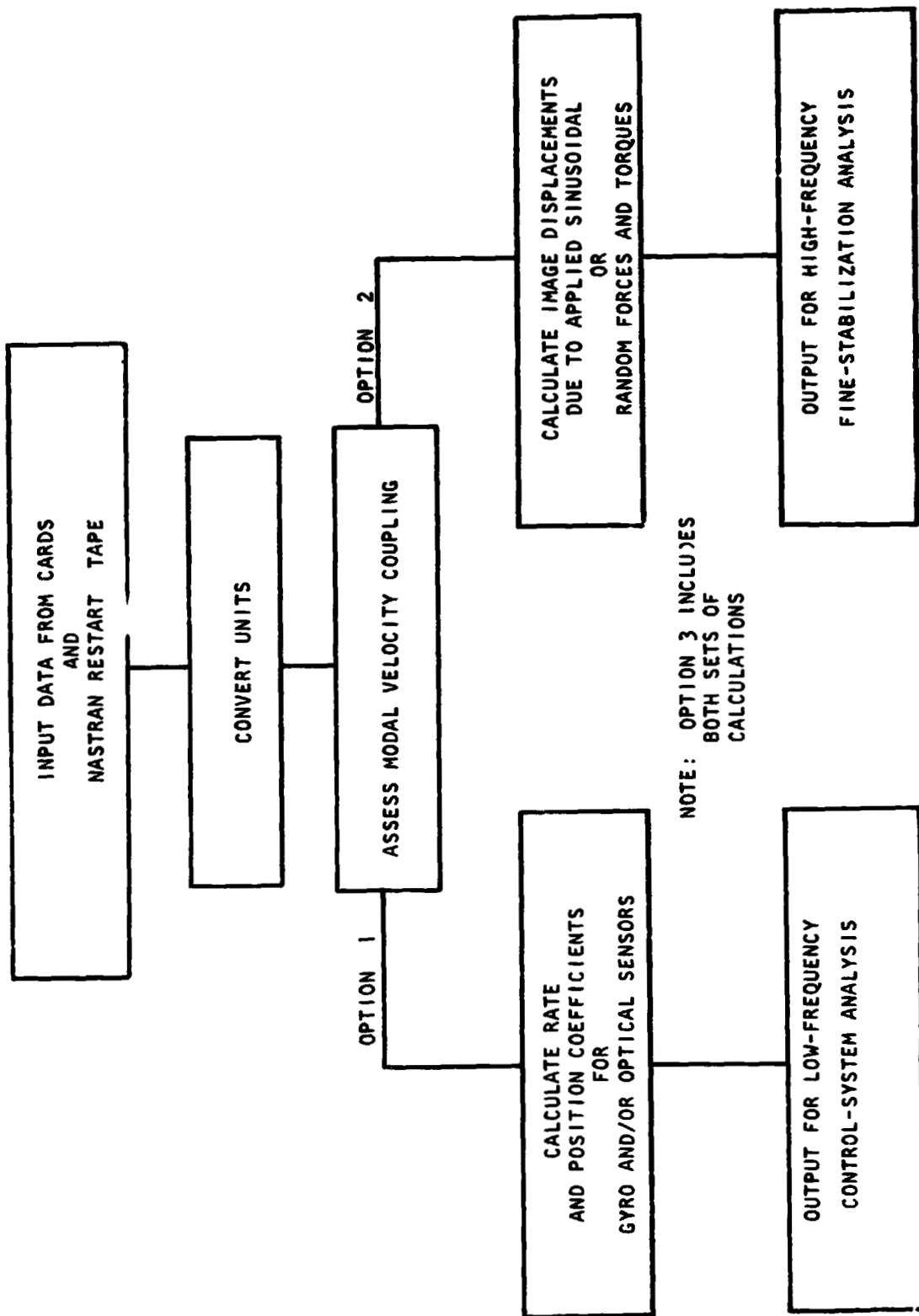


Figure 3.- Postprocessor Program Flow

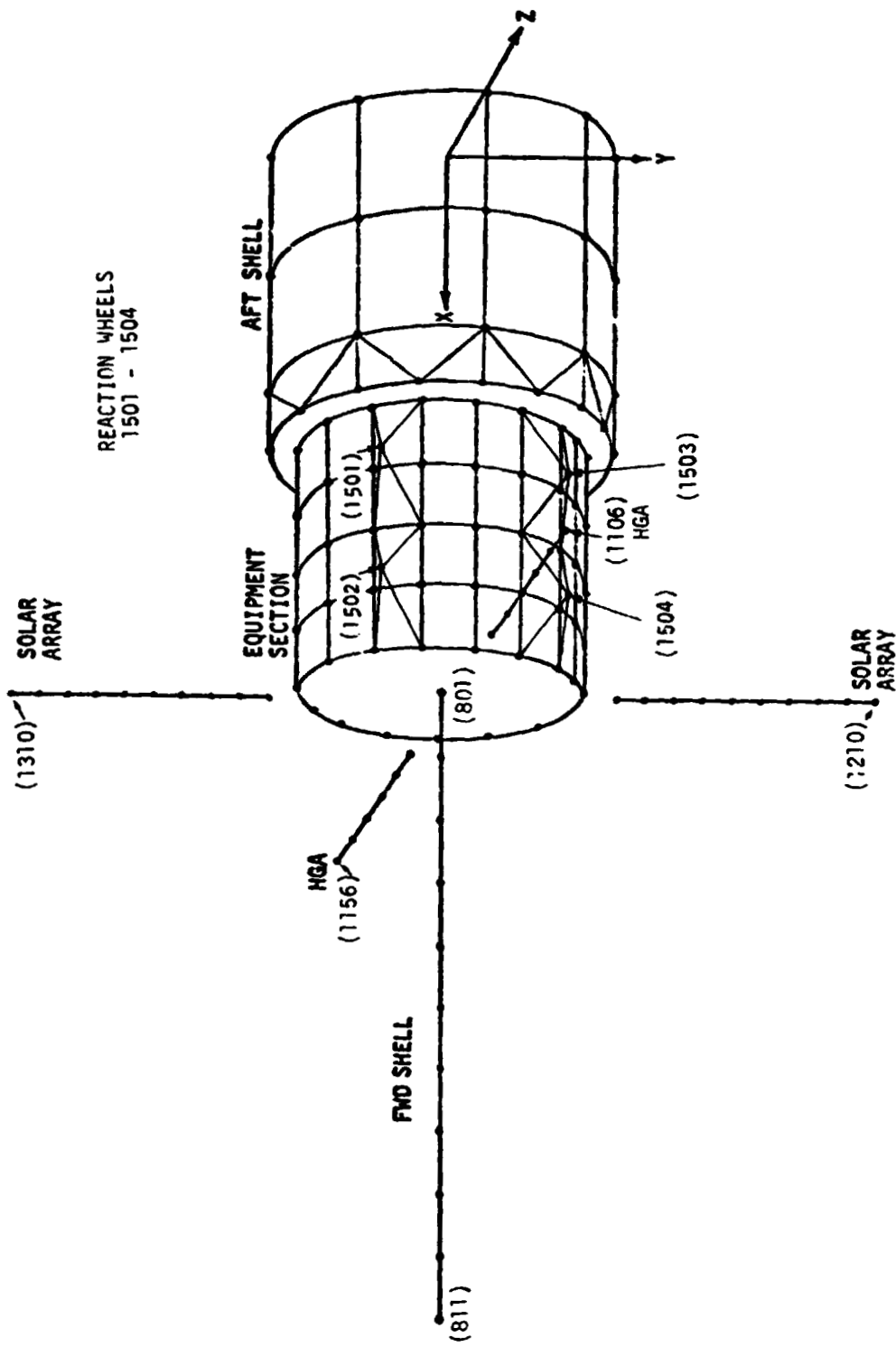


Figure 4.- SSM Finite-Element Model.

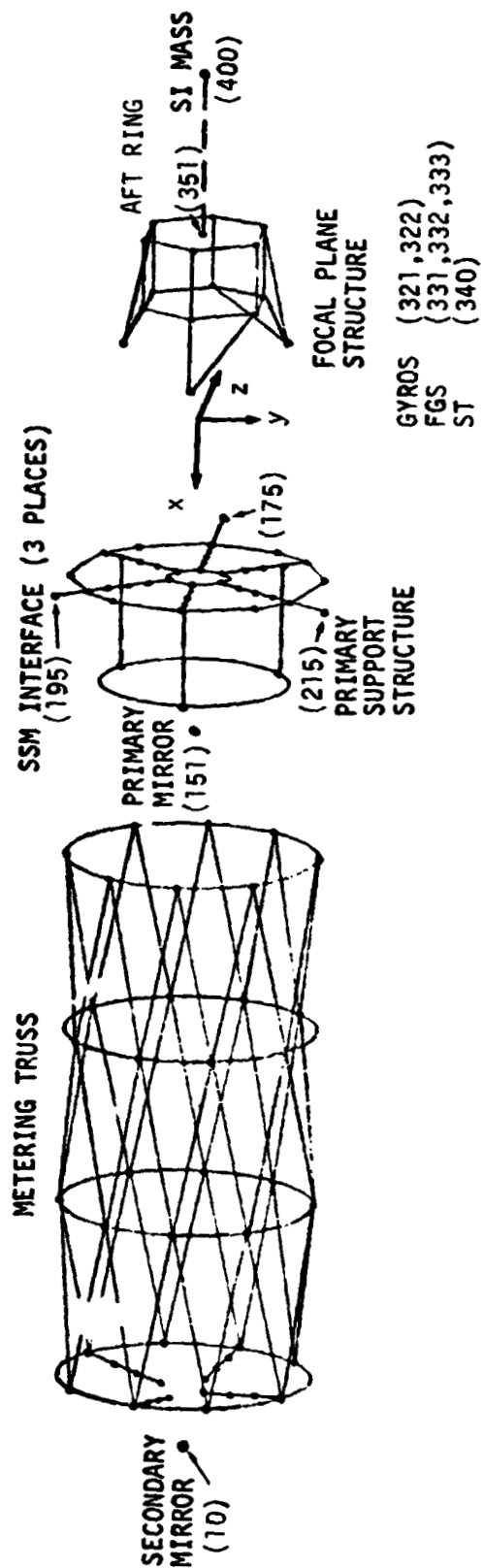


Figure 5.- OTA/SI Math Model.

FINITE ELEMENT ANALYSIS USING NASTRAN APPLIED TO
HELICOPTER TRANSMISSION VIBRATION/NOISE REDUCTION*

R. W. Howells and J. J. Sciarra
Boeing Vertol Company

N75 31503

SUMMARY

A finite element NASTRAN model of the complete forward rotor transmission housing for the Boeing Vertol CH-47 helicopter has been developed and applied to reduce transmission vibration/noise at its source. In addition to a description of the model, a technique for vibration/noise prediction and reduction is outlined. Also included are the dynamic response as predicted by NASTRAN, test data, the use of strain energy methods to optimize the housing for minimum vibration/noise, and determination of design modifications which will be manufactured and tested. The techniques presented are not restricted to helicopters but are applicable to any power transmission system. The transmission housing model developed can be used further to evaluate static and dynamic stresses, thermal distortions, deflections and load paths, fail-safety/vulnerability, and composite materials.

INTRODUCTION

Considerable attention has been focused in recent years on the reduction of noise levels for both military and civil helicopters. Helicopter noise emanates from three major sources - the rotor blades, engines, and transmissions. Exterior noise is dominated by the rotors and engines, although the transmissions also contribute to this noise. Minimization of the exterior noise is important to reduce the annoyance to communities near civil helicopter operations and to reduce the detectable noise signature of military helicopters. The interior cabin noise is predominantly due to the transmissions (Figure 1), with the engines and rotors being secondary sources. Interior noise not only degrades crew performance by causing annoyance and fatigue, but interferes with reliable communication and may cause hearing damage. Comfortable interior noise levels are essential for passenger acceptance of civil helicopters.

By any of the numerous standards in existence for scaling annoyance and reactions to noise (Reference 1), transmission noise is particularly objectionable. Noise in excess of 120 db has been

* This work has been performed under U. S. Army contract DAAJ02-74-C-0040, U. S. Army Air Mobility Research and Development Laboratory, Eustis Directorate, Fort Eustis, Virginia.

measured for the transmission of a medium transport helicopter (References 2 and 3) which, for comparison, approaches the noise level of an air raid siren. Not only is this noise level high, but its frequency typically falls within the sensitive 1000-5000 Hz range which is particularly annoying to the human ear (Figure 2). Furthermore, the pure tonal content, which results in a high-pitched whine, is subjectively much more annoying than broad-band noise (Figure 3).

Transmission noise and the inherent structural vibrations which generate this noise have been of concern to helicopter designers for many years. Until recently, analytical methods have not been available to predict and reduce transmission vibration/noise problems in advance. The conventional means of controlling transmission noise has generally been to add acoustical enclosures after the hardware is built and a noise problem has become evident. Since practical enclosures are limited in noise attenuation by unavoidable sound leaks in seams and access doors, adequate attenuation is not provided for advanced helicopter drive systems of increased power (References 2 and 3). Not only do these enclosures impose considerable weight and maintainability penalties, but they do not reduce the deleterious effect of the accompanying vibrations which contribute to material fatigue and fretting at joints.

A significant program in the area of transmission vibration/noise reduction is in progress at Boeing Vertol. The objective of this work is to generate analytical tools that will provide the capability to perform trade studies during the design stage of a program. This capability will yield optimized drive train components that are dynamically quiet with inherently longer life and reduced vibration and attendant noise levels.

MECHANISM OF TRANSMISSION NOISE GENERATION

The transfer of torque between mating gears is not uniform due to tooth profile errors and the elastic deformation of the gear teeth under load (References 2 and 3). This non-uniform transfer of torque produces a dynamic force at the gear mesh frequency (number of teeth x rpm) and its multiples which excites the coupled torsional/lateral vibratory modes of the gear shaft. This lateral vibration (or bending) produces displacements at the bearing locations which excite the housing and cause it to vibrate, thus radiating noise (Figure 4). Furthermore, the dynamic characteristics of the housing may magnify its displacements and the resulting noise.

NOISE REDUCTION

A three-pronged analysis for the reduction of vibration/noise at its source has been developed which includes the reduction of dynamic excitation, the reduction of dynamic response, and the use of auxiliary devices for vibration absorption. Controlling the dynamic response of the transmission is a desirable approach to noise reduction since avoidance of resonance reduces shaft deflections at the bearings which inherently increases the life of dynamic components and transmission reliability. The finite element modeling of the transmission housing using NASTRAN is an integral part of this analytical technique.

Detuning of Internal Components

Reduction of the dynamic excitation of the housing is accomplished by minimizing the dynamic forces at the shaft support bearings. This is a two-fold task. First, the excitation due to the dynamic tooth forces is calculated from the gear geometry and operating conditions. Second, the damped force response of the shafts responding to the tooth mesh excitation loads is calculated from a finite element model and the shaft is detuned using strain energy methods to minimize the displacement at the bearings. The development of this method, accomplishment of extensive dynamic testing, and correlation of data are described fully in References 2 and 3. Finally, the dynamic forces associated with the optimum configuration of the internal components are then applied to excite the model of the housing. To study the response of the transmission housing to these forces and to minimize the noise produced, a finite element model of the housing was developed and analyzed using NASTRAN.

Application of NASTRAN to Finite Element Model of Housing

The Boeing Vertol CH-47 forward rotor transmission housing is composed of three major sections: upper cover, ring gear, and case (Figure 5). The upper cover provides lugs for mounting the transmission to the airframe and transmits the rotor system loads. The case contains and supports the main bevel gears. The ring gear, which connects the upper cover and case, contains the planetary gear system. This natural division of the housing was adhered to for ease of modeling (Figure 5).

The geometric grid points for the model were defined from design drawings and by cross-checking on an actual housing. CQUAD2 (Quadrilateral) and CTRIA2 (Triangular) homogeneous

plate (membrane and bending) elements were used to connect the grid points and build the NASTRAN structural model. A Boeing Vertol preprocessor program (SAIL II - Structural Analyses Input Language) for the automatic generation of grid point coordinates and structural element connections was used. This preprocessor allows the user to take advantage of any pattern which occurs in the data by providing straight-forward techniques for describing algorithms to generate blocks of data. The extensive computer generated plotting capability of NASTRAN was used to de-bug the structural model.

For ease of identification the housing was subdivided into several regions and the grid points in each region were labeled with a specific, but arbitrary, series of numbers. Although these grid point numbers act only as labels, they affect the bandwidth of the stiffness and mass matrices. In order to minimize the matrix bandwidth for most efficient running of NASTRAN, the BANDIT computer program (Reference 4) was used to automatically renumber and assign internal sequence numbers to the grid points. The output from BANDIT is a set of SEQGP cards which are then included in the NASTRAN bulk data deck and which relate the original external grid numbers to the internal numbers.

The model includes grid points representative of the structure where the shafts are supported by their bearings as well as grid points representative of the planet-ring gear tooth meshes. These grid points are used to apply the dynamic excitations at the mesh frequencies to analytically excite the housing. Although each geometric grid point has six possible degrees of freedom (3 translational and 3 rotational), the displacements normal to the outer surface of the housing are of most interest for noise evaluation since it is this out-of-plane motion which generates sound waves (Figure 6). To conveniently evaluate the motion normal to the housing surface, numerous local coordinate systems were defined and oriented such that the displacements and accelerations calculated at each grid point could be referred to a coordinate system having an axis normal to the housing surface. One degree of freedom, rotation about the normal to the surface, was constrained since the stiffness for this component is undefined for NASTRAN plate elements. The other two rotational degrees of freedom were omitted. All translational degrees of freedom were retained to accurately represent the motion of the actual housing. Because of the large model size, the Guyan reduction technique was used to reduce the size of the analysis set. The Givens method of eigenvalue extraction was used and the model parameters are summarized in Figure 7.

Detuning of Housing Response (Strain Energy)

Each natural mode of a structure contributes to vibration in proportion to its amplification factor, which is the ratio of exciting frequency to natural frequency. Consequently, since each mode whose frequency is in the vicinity of a forcing frequency will be a major contributor to the overall dynamic response, it is desirable to alter the housing natural frequencies so that none fall close to an exciting frequency.

Strain energy techniques for structural optimization have evolved in recent years. For applications such as helicopters where weight is critical, it is more appropriate to evaluate the strain density (strain energy/volume) distribution within a structure which provides guidance for vibration reduction by identifying the structural elements participating in the modes (Reference 5). To optimize a housing for minimum vibration/noise, the NASTRAN normal modes analysis is used to obtain a dynamic solution; by employing the ALTER feature of NASTRAN, a checkpoint tape containing the stresses for each element is generated. The natural frequencies calculated are compared with the gear mesh exciting frequencies to identify each mode shape whose natural frequency is close to an exciting frequency and which it is desirable to shift. A post-processor program has been developed which uses the data stored on the checkpoint tape to calculate the strain density of NASTRAN plate elements and tabulate the elements in order of descending strain density. The structural elements with the highest strain density are the best candidates for effective modification of the natural frequency since a minimal weight change will yield a maximum shift in natural frequency (Reference 6). By locally altering the housing wall to change the mass and stiffness in these areas of high strain density, the natural frequency may be shifted away from an exciting frequency (Figure 8). Thus, the possibility of resonance is eliminated and the vibration and radiated noise are reduced. This strain density distribution concept can also be utilized statically to identify structural load paths and evaluate the efficiency of the housing structural design (stiffness/weight).

RESULTS

A complex gearbox such as a helicopter rotor transmission typically has more than one gear mesh, hence more than one exciting frequency. For instance, the Boeing Vertol CH-47C helicopter forward rotor transmission employs a spiral bevel gear mesh plus a two-stage planetary gear system. Additional

sources of exciting frequencies in the form of sidebands are introduced by planetary gear configurations (Reference 7) and manufacturing variations (Reference 8). This occurrence of multiple exciting frequencies, coupled with the fact that the housing possesses many natural frequencies, makes it a complex task to detune the housing so that none of the exciting frequencies coincides with a natural frequency. The primary frequencies for the CH-47 forward rotor transmission have been identified experimentally as the bevel gear mesh frequency and the lower planetary gear mesh frequency (LP1) and its second (LP2) and third (LP3) harmonics.

The experimental program described in References 2 and 3 included the dynamic testing of a CH-47C forward transmission with internal instrumentation to measure strains, displacements, and accelerations of the rotating components and external instrumentation to measure housing acceleration and noise. Correlation of this data with the analysis has indicated that by modifying the gear/shaft/bearing system geometry the internal components may be detuned to minimize excitation of the housing. Application of strain density techniques to these dynamic components has identified modifications which have analytically reduced the loads exciting the housing at the bevel mesh, LP2 and LP3 frequencies. Loads at the LP1 frequency increased. Since the effect of multiple noise sources are added logarithmically, the reduction of three out of four noise sources may not appreciably reduce the overall noise level.

Noise measurements have tended to confirm that housing responses exist and generate noise. This is evidenced, for example, by the LP2 and LP3 frequencies. Although the exciting source for these frequencies is within the ring gear, the maximum noise at these frequencies emanates from the mid-case region (Figure 9).

Some of the calculated natural frequencies of the housing and the main exciting frequencies are plotted on the spectrum shown in Figure 10. A NASTRAN plot of the housing 46th mode, which has a natural frequency closest to the LP2 exciting frequency, is shown in Figure 11. It is important to note that since the exciting frequencies will vary with changes in operating speed, the housing must be detuned at a specific operating speed. The use of strain density has led to preliminary identification of the areas (see shaded elements Figure 12) of the housing structure which will be modified to detune the housing for reduced vibration/noise. The strain density distribution was determined using the NASTRAN post-processor for the modes with frequencies nearest to the four main exciting frequencies and the elements with high strain density were identified. For each mode considered the elements with high strain density are generally different; however, some elements are common to two or more of the modes. Strictly speaking, the

elements with highest strain density for each mode should be modified to achieve the maximum frequency shift for each corresponding mode. This approach would be used during the design of a new housing. To modify an existing housing, however, it would be cumbersome to incorporate the numerous and varied modifications indicated by such a rigorous application of the analysis. Therefore, for practical application to the experimental housing herein, those elements with a relatively high strain density which are common to two or more modes have been identified (Figure 12) and will be used to shift the housing frequencies. In this manner a specified structural change will alter two or more frequencies, although perhaps no single frequency will be shifted maximally. It is more feasible to modify these elements since the actual changes to the existing housing design for testing will be limited to a few easily accessible areas on the exterior walls of the housing. This approach should provide sufficient detuning to demonstrate the validity of the analysis. Prior to finalizing the detuned design, the dynamic response of the model, with the structural modification incorporated, will be re-calculated using NASTRAN. Comparison with the baseline housing response will determine whether to proceed with the manufacture of the test hardware or to further evaluate the detuning procedure.

A test program described in Reference 9 was conducted to evaluate the effect of dynamic absorbers on transmission noise. The results indicated that internal dynamic absorbers provided some noise reduction, but the reduction was not sufficient to warrant practical application. External dynamic absorbers applied to the housing have been evaluated using NASTRAN rigid format 11. By applying absorbers on the housing at the points of load application (i.e. bearing supports) the excitation of the housing has been reduced. However, the absorbers are effective only for a very narrow range of frequencies. For a transmission housing with several excitation frequencies, absorbers may be useful to reduce a particularly troublesome frequency. As a general transmission noise reduction method, the use of absorbers must be further evaluated.

CONCLUDING REMARKS

The basic analytical approach as a design tool for transmission vibration/noise reduction has been partially validated. The method unites the internal components and the housing, and hence will optimize the transmission as a complete operating system. Since the housing provides structural support to the internal components, its physical characteristics grossly affect performance and life in terms of internal bearing

capacity, gear capacity, fretting, misalignments, etc. Therefore, housing optimization is essential if the full benefit of the advancements in gear and bearing technology are to be realized.

With the existing housing model, further investigations utilizing NASTRAN are planned to evaluate static and dynamic stress, thermal distortions, deflections and load paths due to any type loading, fail-safety, vulnerability, and composite materials (Figures 13 and 14).

REFERENCES

1. Munch, C., A STUDY OF NOISE GUIDELINES FOR COMMUNITY ACCEPTANCE OF CIVIL HELICOPTER OPERATIONS, Journal of the American Helicopter Society, January 1975, Pages 11-19.
2. Hartman, R., A DYNAMICS APPROACH TO HELICOPTER TRANSMISSION NOISE REDUCTION AND IMPROVED RELIABILITY, Paper Presented at the 29th Annual National Forum of the American Helicopter Society, Washington, D. C., May 1973, Preprint No. 772.
3. Hartman, R., and Badgley, R., MODEL 301 HLH/ATC TRANSMISSION NOISE REDUCTION PROGRAM, USAAMRDL TR 74-58, May 1974.
4. Everstine, G., BANDIT - A COMPUTER PROGRAM TO RENUMBER NASTRAN GRID POINTS FOR REDUCED BANDWIDTH, Naval Ship Research and Development Center Technical Note AML-6-70, February 1970.
5. Sciarra, J. J., VIBRATION REDUCTION BY USING BOTH THE FINITE ELEMENT STRAIN ENERGY DISTRIBUTION AND MOBILITY TECHNIQUES, 45th Shock and Vibration Symposium, Dayton, Ohio, August 1974.

6. Sciarra, J., USE OF THE FINITE ELEMENT DAMPED FORCED RESPONSE STRAIN ENERGY DISTRIBUTION FOR VIBRATION REDUCTION, U. S. Army Research Office - Durham, Final Report Contract DAH-C04-71-C-0048, July 1974.
7. Gu, A., Badgley, R., and Chiang, T., PLANET-PASS-INDUCED VIBRATION IN PLANETARY REDUCTION GEARS, ASME Paper 74-DET-93, Presented at the Design Engineering Technical Conference, New York, New York, October 5-9, 1974.
8. Gu, A., and Badgely, R., PREDICTION OF VIBRATION SIDEBANDS IN GEAR MESHES, ASME Paper 74-DET-95, Presented at the Design Engineering Technical Conference, New York, New York, October 5-9, 1974.
9. Sternfeld, H., Schairer, J., and Spencer, R., AN INVESTIGATION OF HELICOPTER TRANSMISSION NOISE REDUCTION BY VIBRATION ABSORBERS AND DAMPING, USAAMRDL TR 72-34, August 1972.

TWIN ENGINE RATING - 4474 kW AT 245 RPM
(6000 HP)
SINGLE ENGINE RATING - 2796 kW
(3750 HP)
GROSS WEIGHT - 20866 kg
(46,000 LB)

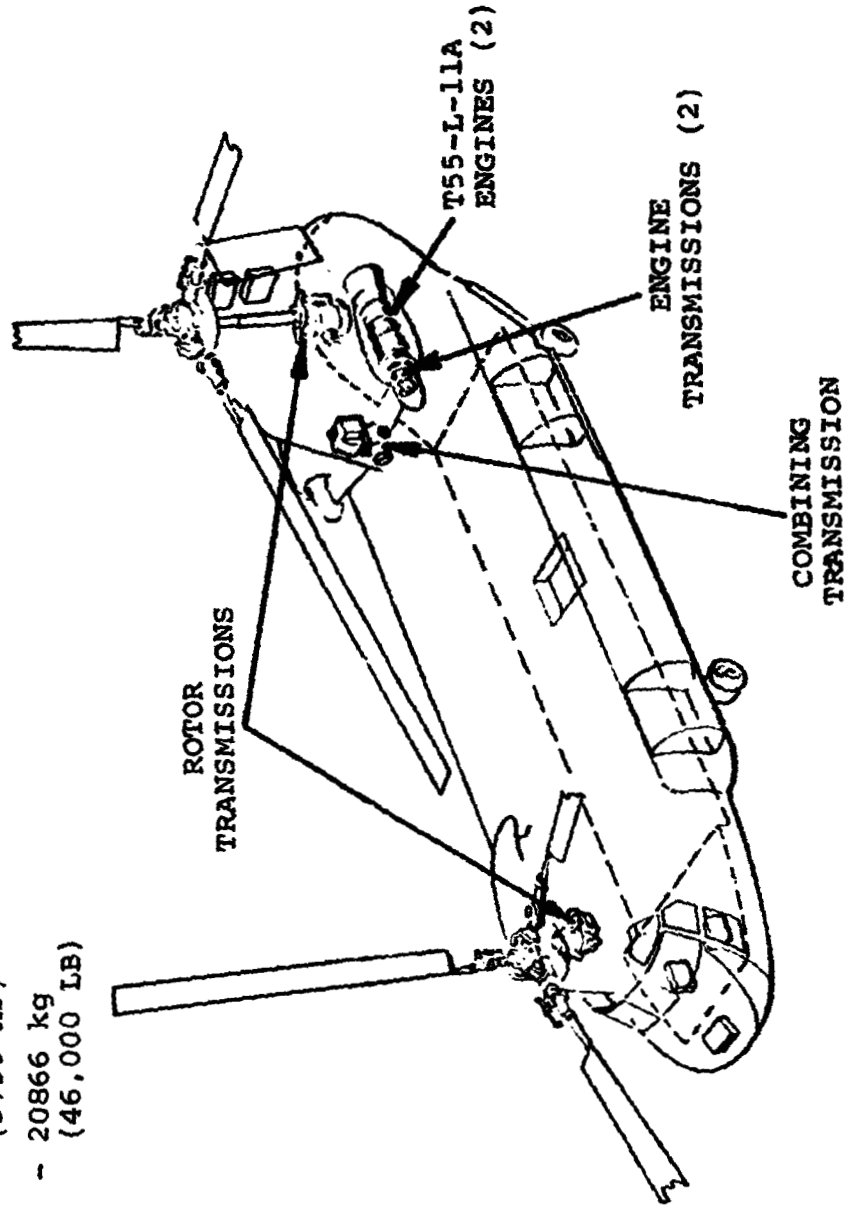


Figure 1. Boeing Vertol CH-47 Helicopter.

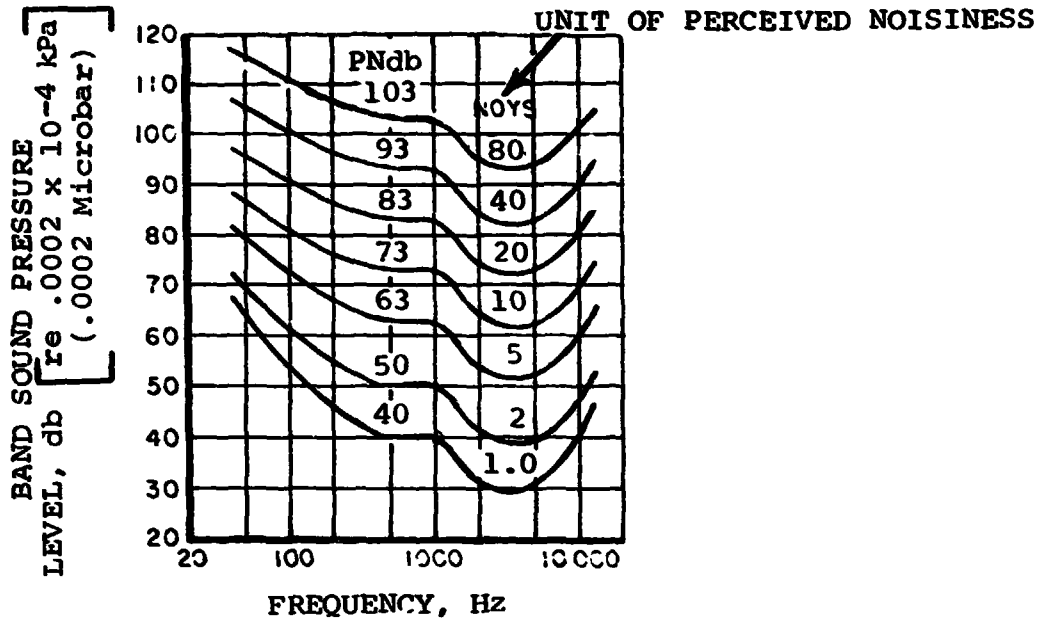


Figure 2. Perceived Noisiness of Bands of Sound.

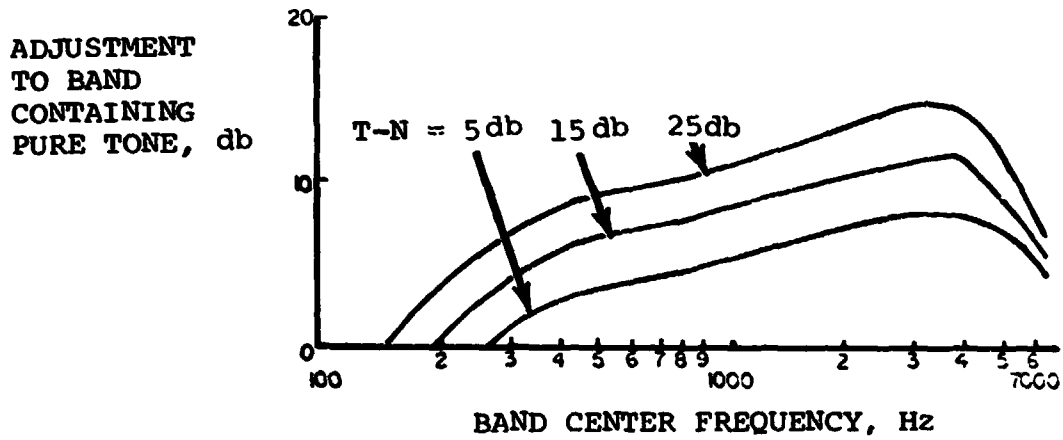


Figure 3. Tone Corrections - Adjustment to be Added to Broad Band Noise Level (N) When Pure Tone (T) is Present.

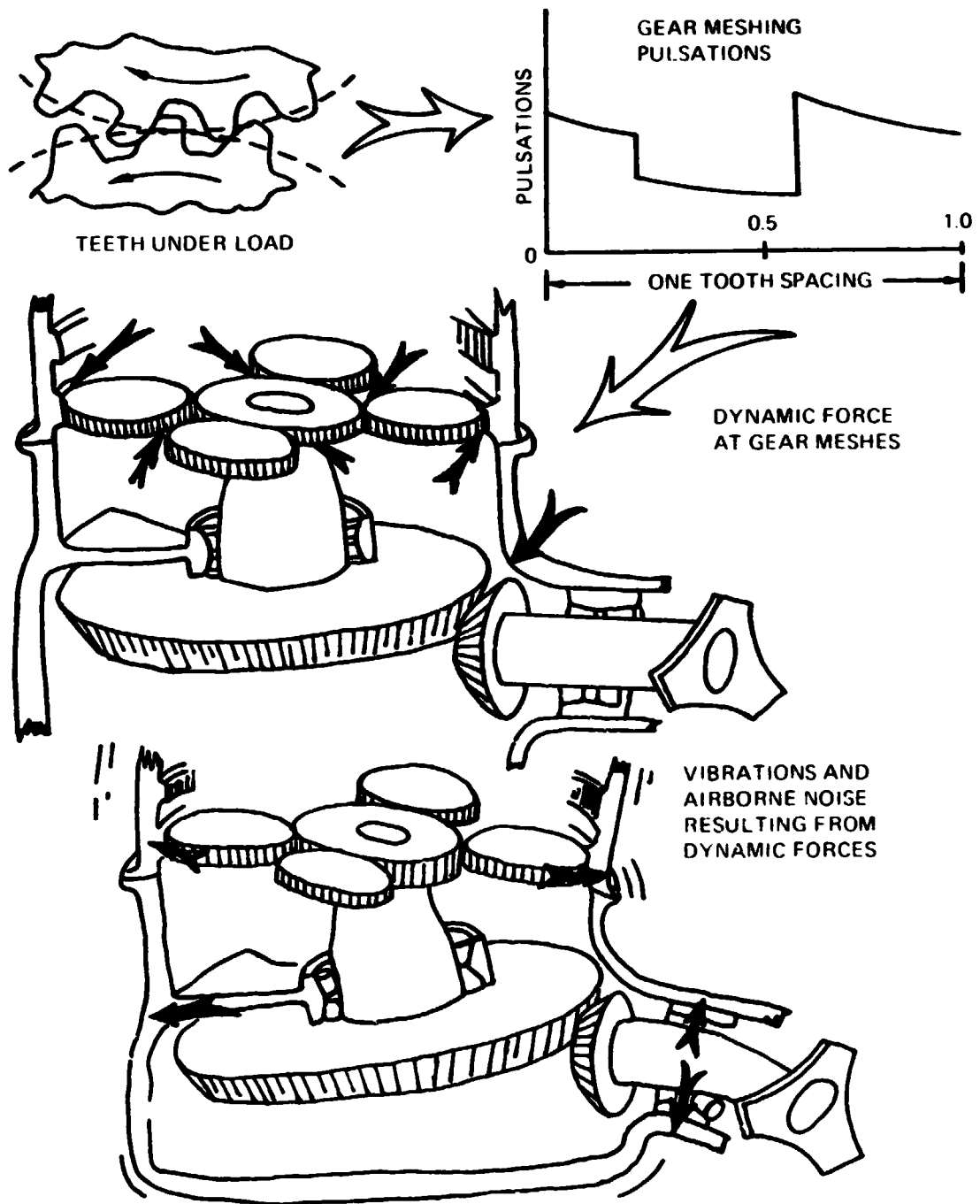
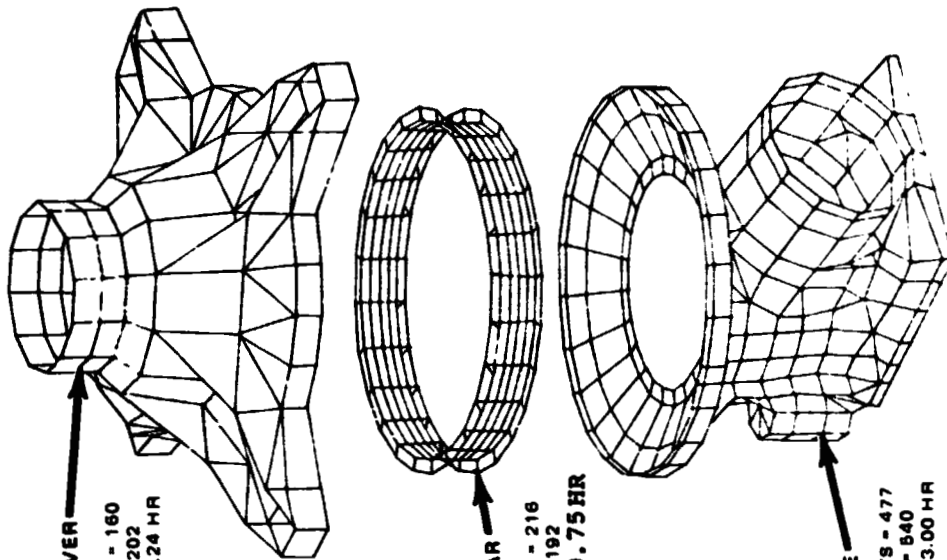


Figure 4. Sources of Transmission Noise.

**TRANSMISSION
HOUSING MODEL**



UPPER COVER
GRID POINTS - 160
ELEMENTS - 202
CPU TIME - 0.24 HR

RING GEAR
GRID POINTS - 216
ELEMENTS - 192
CPU TIME - 0.75 HR

CASE
GRID POINTS - 477
ELEMENTS - 540
CPU TIME - 3.00 HR

**CH-47
FORWARD TRANSMISSION**



Figure 5. Boeing Vertol CH-47 Helicopter Forward Rotor Transmission Housing and NASTRAN Model.

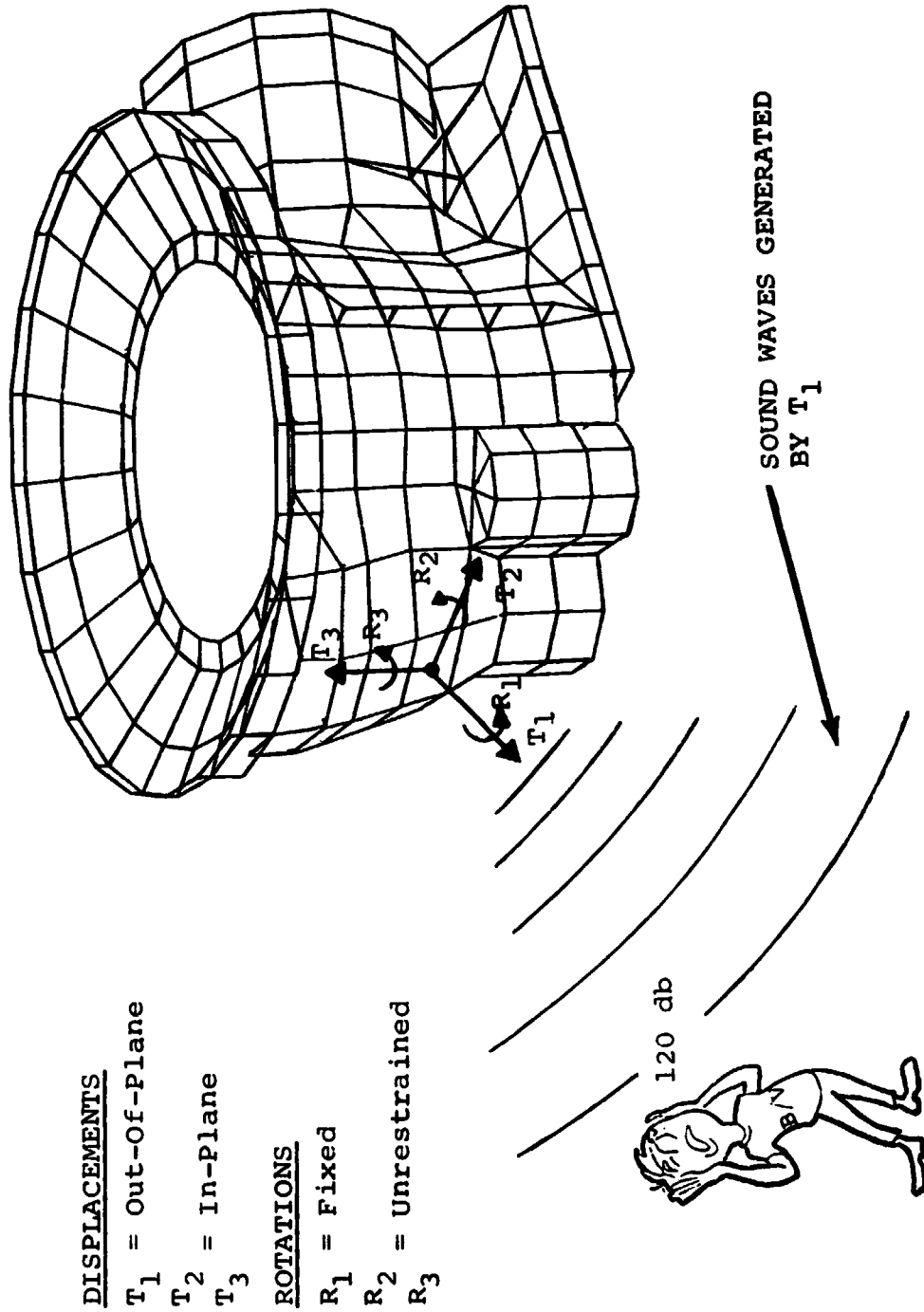


Figure 6. Transmission Noise Generated by Out-Of-Plane Displacements of Housing.

MODEL PARAMETERS

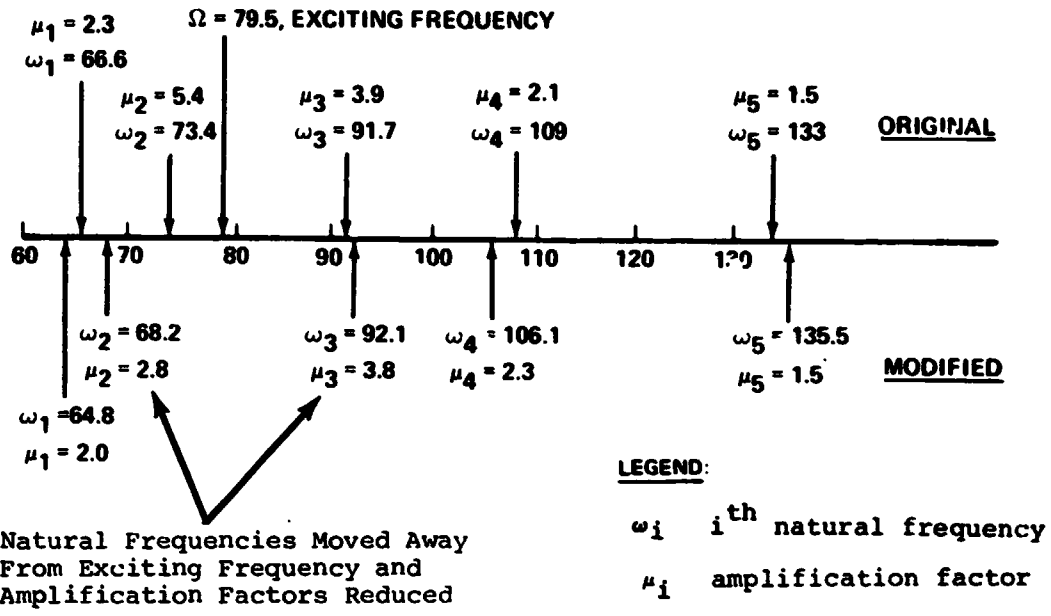
GRID POINTS ELEMENTS	NUMBER	NUMBER DEGREES OF FREEDOM	BANDWIDTH		CPU TIME (HOURS)*
			FULL REDUCED COLUMNS	ACTIVE	
Upper Cover	160	202	960 184 614 162	34 162	0 0.24
Ring Gear	216	192	1296 216 828 252	- 252	0 0.75
Case	477	540	2862 529 2024 309	61 309	0 3.00
TOTAL	853	934			

*RIGID FORMAT 3

COMPARISON OF CALCULATED AND ACTUAL WEIGHTS

	MODEL	HARDWARE	DIFFERENCE
Case	25.1 kg (55.4 lb)	24.6 kg (54.2 lb)	+ 2.2%
Ring Gear	28.6 kg (63.0 lb)	34.9 kg (77.0 lb)	-18.1% (No Teeth)
Upper Cover	62.8 kg (138.5 lb)	61.1 kg (141.4 lb)	- 2.0%

Figure 7. Summary of CH-47 Forward Transmission Housing NASTRAN Model.



Natural Frequencies Moved Away From Exciting Frequency and Amplification Factors Reduced

Figure 8. Example of Optimization of Natural Frequency Spectrum, CH-47 Helicopter Fuselage Forward Pylon Structure.

MICROPHONE INSTALLATION

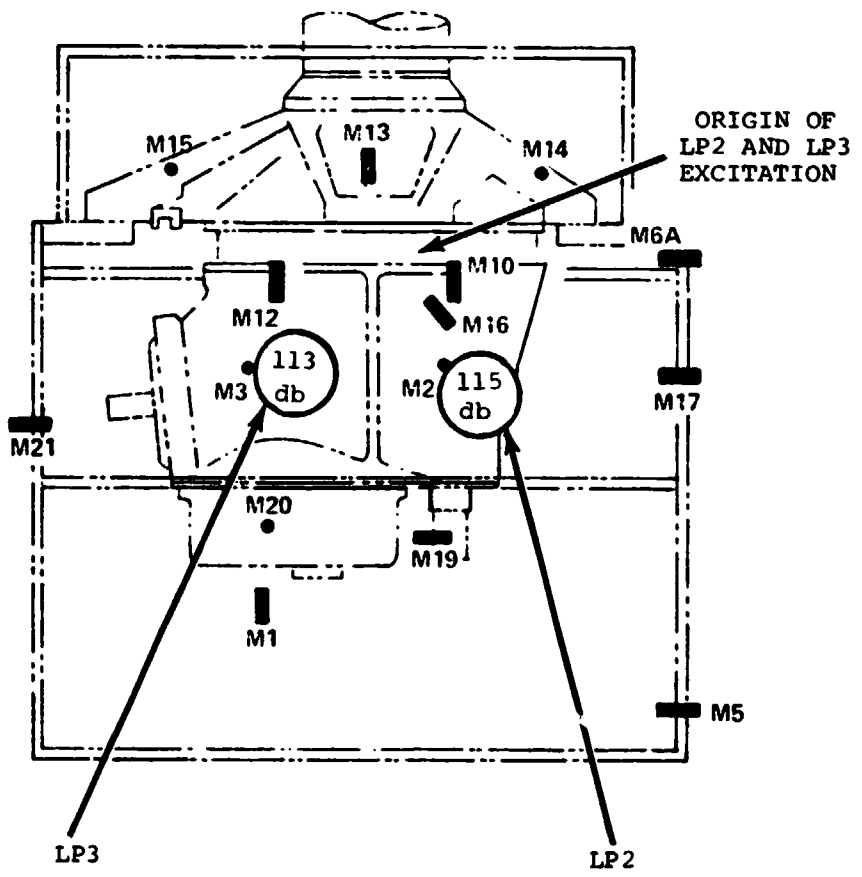


Figure 9. Maximum Measured Noise Levels (7460 RPM at 80% Torque).

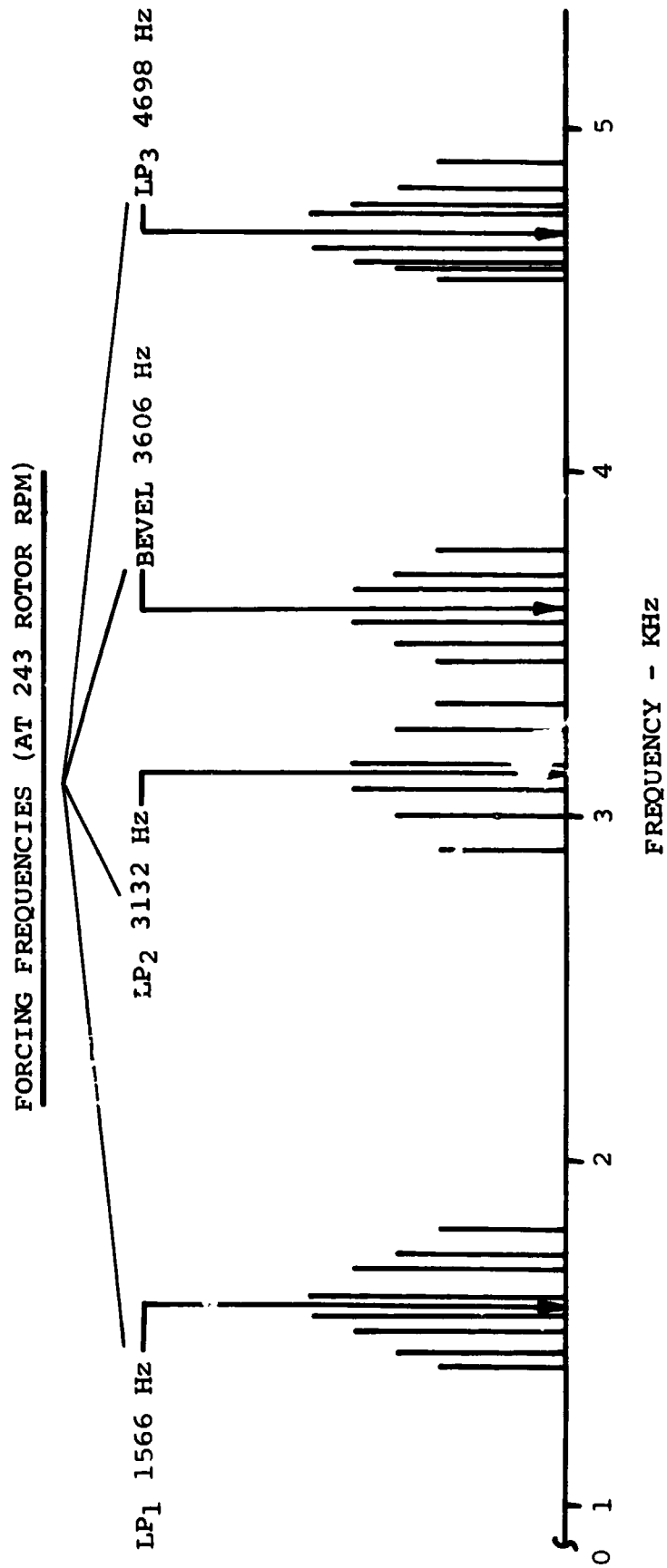


Figure 10. Spectrum of Forcing Frequencies Versus NASTRAN Predicted Natural Frequencies for CH-47C Forward Transmission Case.

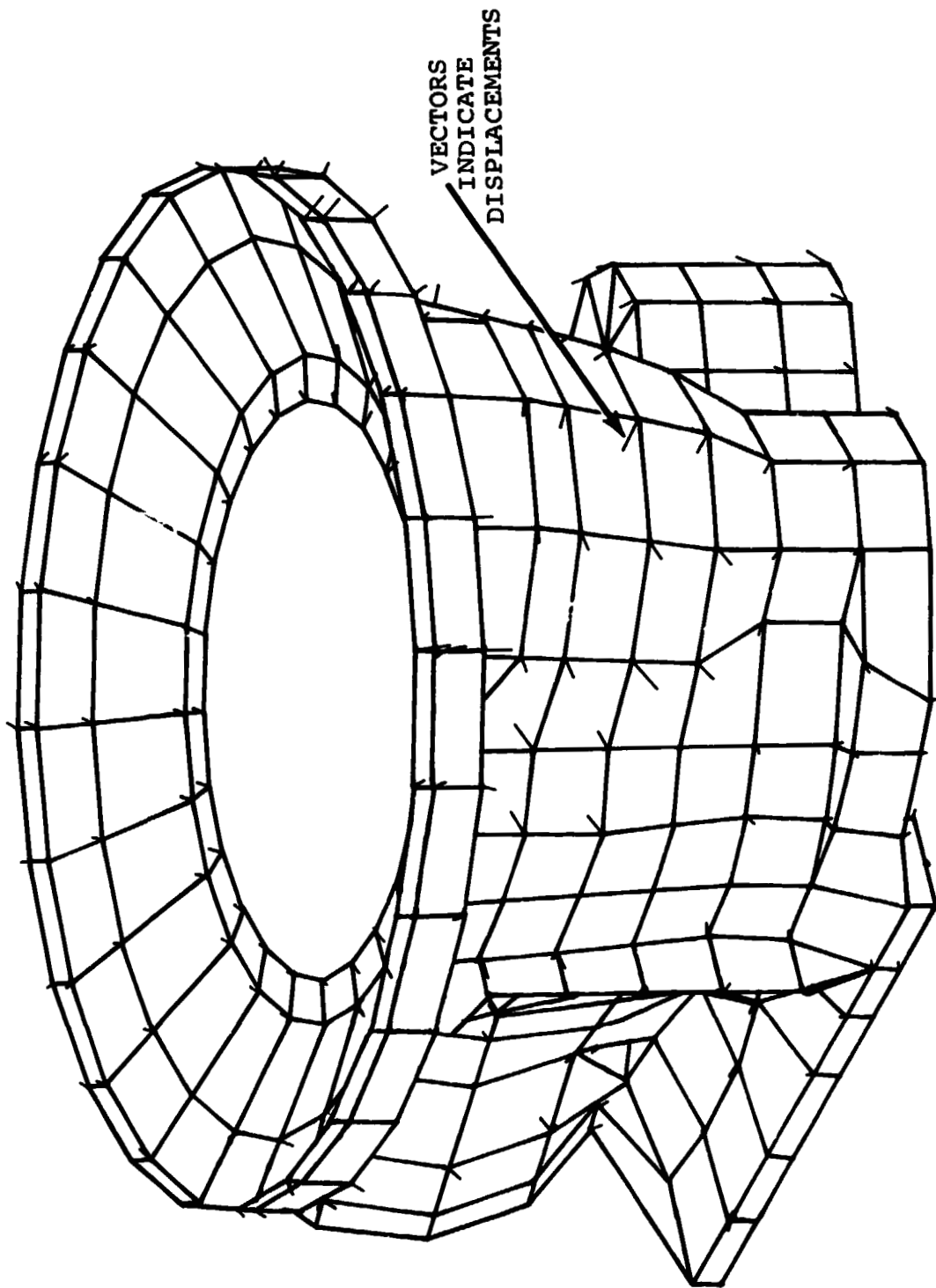
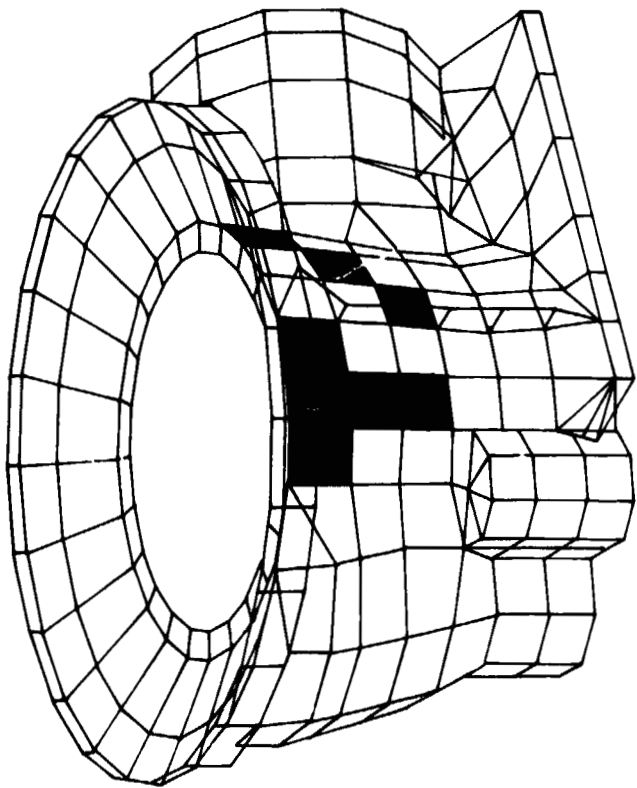
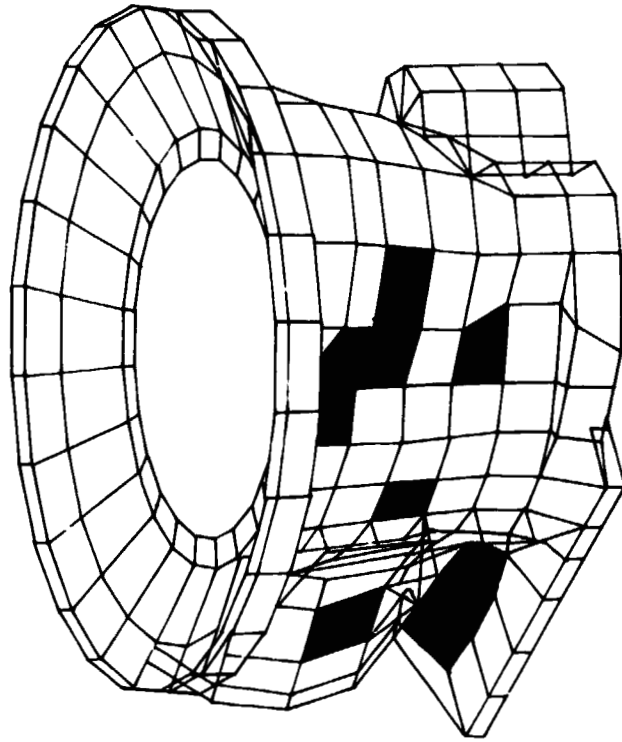


Figure 11. NASTRAN Plot of Deformed Housing,
Mode #46, Frequency 3141 Hz.



LEFT SIDE VIEW



FRONT VIEW

Figure 12. CH-47 Forward Transmission NASTRAN Model Areas of High Strain Density.

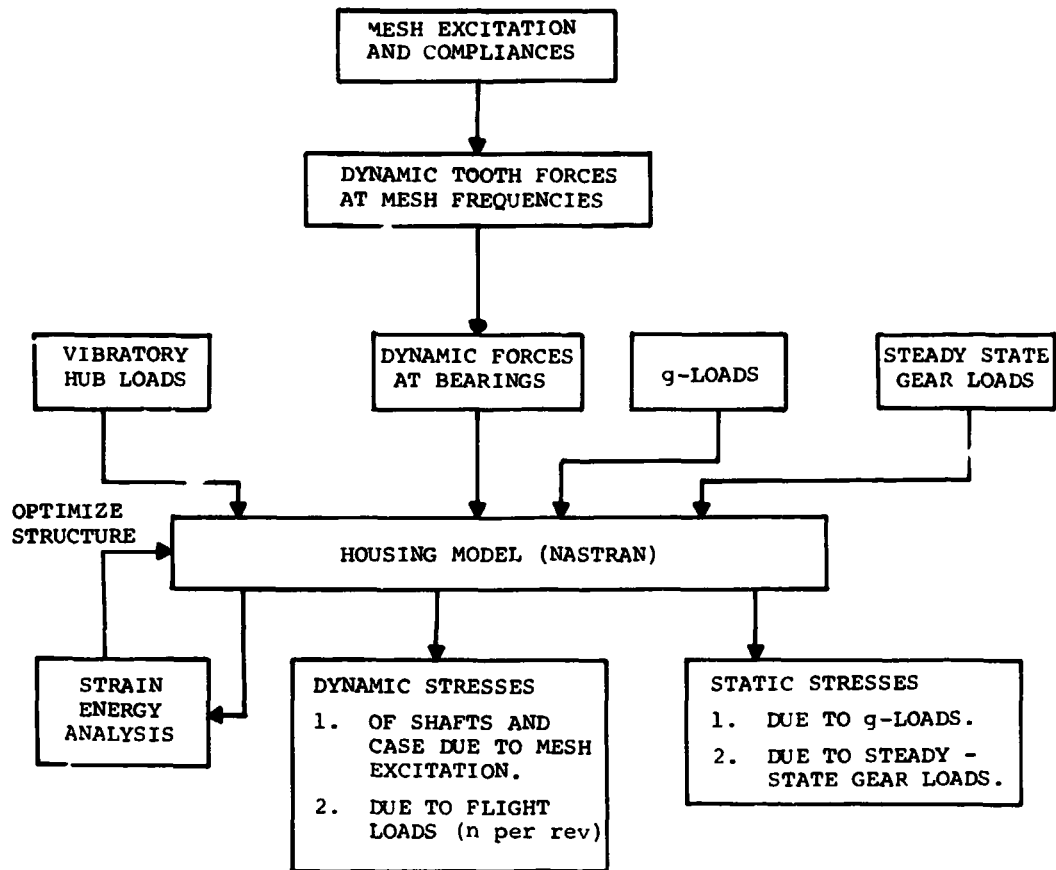


Figure 13. Flow Diagram of NASTRAN Stress Analysis.

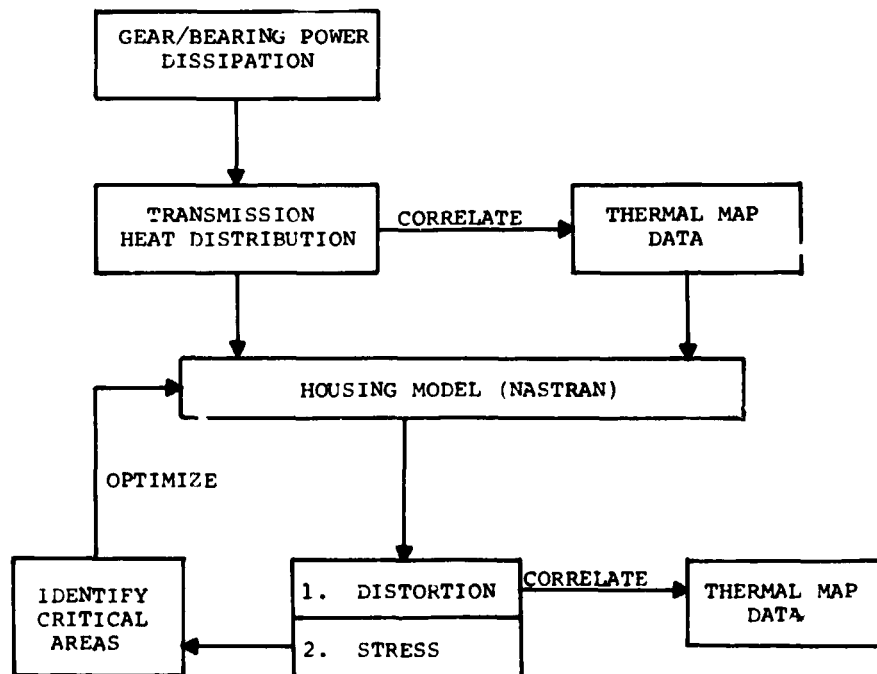


Figure 14. Flow Diagram of NASTRAN Thermal Analysis.

PN75 31504

ANALYSIS OF NONLINEAR STRUCTURES VIA MODE SYNTHESIS

R.K. Gieseke
General Dynamics Convair Division
San Diego, California

SUMMARY

An effective procedure for NASTRAN has been developed that permits any number of substructures of any size to be synthesized for the purpose of developing normal modes of vibration of the complete structural system. The technique is extended to permit modal transient analysis of the subdivided system. This latter procedure permits the use of NASTRAN's ability to include nonlinear forces in the problem. The five-phase process is accomplished using standard NASTRAN rigid formats with problem-independent alter packages and DMAP sequences.

INTRODUCTION

The advent of finite-element techniques has led to development of computer programs that perform efficient analyses of large-order structural systems of arbitrary geometry. Yet, for very large problems, it becomes impractical to attempt to develop and analyze a mathematical model of the entire structure. Questions of adequate data management and the cost of the analyses make such efforts difficult. Consequently, techniques have been developed to permit the structural system to be divided into smaller units, or substructures, which may then be modeled separately.

Substructure models, represented by some truncated set of degrees of freedom, are eventually brought together by the application of compatibility requirements at the interfaces. The resultant system representation is analyzed and the behavior of each substructure is determined by a back-substitution process.

The mode synthesis technique has been developed to permit dynamic analysis of such subdivided structures. A truncated set of vibration modes of a component is used as generalized coordinates to approximate dynamic characteristics. The several substructures are coupled by (1) compatibility relationships at the interfaces, and (2) modal transformations relating physical degrees of freedom with the generalized component modal coordinates. Solution of the resultant equations yields system eigenvalues and eigenvectors.

The use of vibration modes alone, however, usually fails to describe adequately the behavior of the system, particularly in the regions of the interior boundaries (interfaces). Consequently, the substructure vibration modes are augmented by other displacement functions. Numerous alternatives will be found in the literature. Hurty (Reference 1) and Craig and Bampton (Reference 2) employ "constraint" modes, defined by unit *displacements* of interface degrees of freedom on a fixed interface boundary. Bamford, *et al* (Reference 3) and Rubin (Reference 4) use "attachment" modes, defined by unit *forces* at each interface degree of freedom. Rubin has shown that this concept may be used for free interface boundaries, as well as fixed, to produce inertia relief deformations in unrestrained substructures. It is this latter arrangement that is employed in the development of mode synthesis via NASTRAN that follows. The technique can be easily modified to use constraint modes and fixed interface boundaries.

Synthesizing substructures for dynamic analysis via NASTRAN has been discussed previously. The NASTRAN Theoretical Manual (Reference 5) discusses the use of scalar elements and MPC sets to represent substructures. These procedures were reviewed and amplified by Courtney (Reference 6). The current approach exceeds this earlier work by explicitly including attachment modes and by providing automated communication of data between component and system levels. The ability to develop the structure characteristics and acquire results in spatial coordinates enhances the procedure, particularly when considered from a production environment viewpoint.

The synthesis may be performed using any number of independently formulated substructures of any size. No restrictions are placed on the identification schemes used in component model development, since they are not carried over into the synthesis. The technique uses standardized alter packages and DMAP sequences that are virtually independent of the problem characteristics; thus, the often present necessity for user specification of many data handling directives is avoided. Controls for matrix partitioning and merging are in the form of user-supplied partition vectors.

An extension of the mode synthesis procedure includes the modal transient response analysis for the synthesized system, wherein the required modal data is recovered on a substructure-by-substructure basis. Since the complete system may be quite large, the modal matrix is truncated to include only those degrees of freedom subjected to external loads or required to define the presence of nonlinear forces. Such nonlinear forces are included only after the mode synthesis has been completed. The responses of the system, including internal forces and stresses, if desired, are recovered by back-substitution into each substructure.

The complete analysis process is divided into five sequential phases, with communication between phases accomplished via User Tapes; e.g., INPT, and Problem Tapes (NPTP, OPTP).

SUBSTRUCTURE MODAL ANALYSIS

Phase I of the mode synthesis/transient response analysis using NASTRAN is the development of substructure, or component, modal data. This information is assembled in Phase II for system modal analysis. There are few restrictions and very little additional demands required for this phase over that associated with a standard NASTRAN analysis. It is necessary to give special consideration to those degrees of freedom in the component model that are involved in connection with other portions of the structural system. Additional information is required to direct the preparation of the component modal data for later synthesis.

The full range of NASTRAN's resources may be employed to define a substructure model. Since substructures are independently defined, no special restrictions are placed on identification or numbering schemes.

Components may have any form of boundary condition at their external boundaries; i.e., those boundary grid points not connected to other components. Connection grid points must be unrestrained in those coordinates that are used to join the components.

Since the interface degrees of freedom are by definition unrestrained, the collectivity of normal vibration modes cannot correctly define internal loads at the interface of the component. To correct this deficiency, the dynamic modes are augmented by a selected set of static deformations, which, when properly weighted and summed, will provide the internal loads at the interface degrees of freedom. The static modes are generated by applying a unit force at each interface degree of freedom in turn and letting the component deform. If rigid body motion is prevented by external constraints, a straightforward static analysis results. If, however, a rigid body component of motion does result from

the unit load at the interface, an inertia relief analysis is required to produce internal loads. For this reason, Phase I of the mode synthesis procedure is performed using Rigid Format No. 2, Static Analysis with Inertia Relief, as modified by the alter package of Figure 1.

```

$ PHASE ONE ALTER PACKAGE
ALTER 50, 50
PURGE KRR,KLR,QR,DM/REACT $
CHKPNT KKK,KLR,QR,DM $
ALTER 76
EQUIV KAA,KLL/REACT $
CHKPNT KLL $
COND LBL6,REACT $
ALTER 78
LABEL LBL6 $
ALTER 80
COND LBL7,REACT $
ALTER 84
LABEL LBL7 $
ALTER 88
EQUIV PL,PLI/REACT/PO,POI/REACT $
COND LBL10,REACT $
ALTER 89
LABEL LBL10 $
ALTER 110, 114
$ VIBRATION MODES
DPD DYNAMICS,GPL,SIL,USET/GPLD,SILD,USED,,,,,,,,EED,EQEYN/
V,N,LUSET/V,N,LUSETD/V,N,21/V,N,22/V,N,23/V,N,24/
V,N,25/V,N,26/V,N,27/C,N,0/V,N,29 $
SAVE 29 $
PARAM //C,N,ADD/V,N,VIBCASE/V,Y,NCON=0/C,N,1 $ MODES SUBCASE COUNT
READ KAA,MAA,MR,DM,EED,USET,CASECC/LAMA,PHIA,MI,OEIGS/
C,N,MODES/V,N,NEIGS/V,N,VIBCASE $
SAVE NEIGS $
CHKPNT LAMA,PHIA,MI,OEIGS $
OFF LAMA,OEIGS,,,,//V,N,CARDNO $
SAVE CARDNO $
COND FINIS,NEIGS $
$ RECOVER FULL MODE VECTOR
SUR1 USET,,PHIA,,,GO,GM,,KFS,,/PHIG,,UGX/C,N,1/C,N,REIG $
CHKPNT PHIG,UGX $
SUR2 CASECC,CSTM,MPT,DIT,EQEXIN,SIL,,,BGPDT,LAMA,UGX,PHIG,EST,/
,UGG2,OPHIG,OES2,DEF2,PPHIG/C,N,REIG $
CHKPNT PPHIG $
OFF UPHIG,UGG2,DEF2,OES2,,//V,N,CARDNO $
SAVE CARDNO $
$ DYNAMICS PORTION OF GENERALIZED MATRICES
GKAM, ,PHIA,MI,LAMA,,,,,CASECC/MHH,BHH,KHH,PHH/V,N,Z9/
C,N,100/C,N,0./C,N,0./C,N,-1/C,N,-1/C,N,-1/V,N,NOC/V,N,FMODE $
$ ATTACHMENT MODE PARTITION OF GENERALIZED MASS AND STIFFNESS MATRICES
MPYAD UGV,MGG,/AM/C,N,1 $
MPYAD AM,UGV,/MGEN/C,N,0 $ GENERALIZED MASS (ATTACHMENT)
MPYAD UGV,KGG,/AK/C,N,1 $
MPYAD AK,UGV,/KGEN/C,N,0 $ GENERALIZED STIFFNESS (ATTACHMENT)

```

Figure 1. Phase I alter package.

```

CHKPNT  MGEN,KGEN $
$ OFF-DIAGONAL PARTITIONS
MPYAD   AM,PHIG,/ML/C,N,0 $ L.L. PARTITION (MASS)
MPYAD   AK,PHIG,/KL/C,N,0 $ L.L. PARTITION (STIFFNESS)
TRNSP   ML/MU $ U.R. PARTITION (MASS)
TRNSP   KL/KU $ U.R. PARTITION (STIFFNESS)
$ GENERALIZED MATRICES AND CONNECTION PARTITION OF MODES
MERGE   MHH,ML,MU,MGEN,STATIC,/MASS/C,N,-1/C,N,2/C,N,6 $
MERGE   KHH,KL,KU,KGEN,STATIC,/STIFF/C,N,-1/C,N,2/C,N,6 $
MERGE   PHIG,,UGV,,STATIC,/MODES/C,N,1/C,N,2/C,N,2 $
PARTN   MODES,,CDOF,,INTER,,/C,N,1/C,N,2/C,N,0/C,N,2 $
MERGE   UGA,,QG,,STATIC,/QQG/C,N,1/C,N,2/C,N,2 $
CHKPNT  MODES,QQG $
PARAM   //C,N,NOP/V,Y,PRINT=-1 $
COND    LIST,PRINT $
MATPRN  MASS,STIFF,INTER,,// $
LABEL   LIST $
$ WRITE MATRICES ONTO USER TAPE -INPT-
PARAM   //C,N,SUB/V,N,KOUNT/V,Y,COMP=0/C,N,1 $
PARAM   //C,N,MPY/V,N,COUNT/V,N,KOUNT/C,N,3 $
COND    FINIS,COUNT $ EXIT IF SEQUENCE NUMBER IS LESS THAN U
PARAM   //C,N,SUB/V,N,IOTEST/V,N,COUNT/C,N,1 $
COND    I01,IOTEST $ JUMP IF FIRST COMPONENT
INPUTT1 /,,,/C,N,-1 $ REWIND -INPT-
JUMP    A02 $
LABEL   I01 $
OUTPUT1 ,,,,/C,N,-1 $
LABEL   I02 $
OUTPUT1 MASS,STIFF,INTER,,//V,N,COUNT $
ENDALTER

```

Figure 1. Phase I alter package (concluded).

The DMAP alterations supplied for Phase I add the eigenvalue extraction module and other modules that merge the results of the static and dynamic processes to form the final component mode matrix.

Data required by Phase II is output to a User Tape. These data include the generalized mass and generalized stiffness matrices associated with the merged mode vector matrix and the merged mode vector matrix truncated to include only the interface degrees of freedom. The truncation is directed by a partitioning vector supplied by the user. The Phase I analysis should be checkpointed for later use in recovery activity in Phases III and V.

Additional data required beyond the model description include special control parameters, entered via bulk data card PARAM, and partition vectors, entered via bulk data card DMI. The special parameters required for Phase I include:

1. COMP - The sequence number of the component. Used to position the User Tape before writing component data.
2. NCON - The number of interface degrees of freedom for the component. The number of static load subcases/static modes must agree with NCON.
3. PRINT - A positive value causes printing of the matrices written on the User Tape.

The partition vectors needed are:

1. **STATIC** - Used to merge static and dynamic modes into one mode vector matrix. M = sum of all modes computed (static and dynamic, including rigid body). An element value of 1 locates a static mode in the merged matrix. There must be exactly the same number of positive elements in the vector as there are static modes.
2. **CDOF** - Used to identify the interface degrees of freedom. $M = g$ size. Vector contains 1 for elements corresponding to the internal sequence number of all interface degrees of freedom

The Case Control deck must include $(n + 1)$ subcases, where n is the number of interface degrees of freedom for the component (and, consequently, the number of static load cases). The first n subcases are static cases, with a **LOAD** reference in each. The last subcase is the modal extraction subcase, with a **METHOD** card. Figure 2 illustrates a typical Case Control Deck.

```
REQUEST(NPTP,HD,5) RING IN
REQUEST(INPT,HD,5) RING IN
ATTACH(N15,NASTRAN15, ID=TONE90970)
REWIND(NPTP,INPT)
MAP(OFF)
N15.ATTACH
RETURN(NPTP,INPT)
EXIT.
DMP(140000)
RETURN(NPTP,INPT)
(7-8-9)
ID      PHASE,   ONE
APP     DISP
SUL     2,1
CHKPNT  YES
TIME    2
$ (PHASE ONE ALTER PACKAGE GOES HERE)
CEND
TITLE=DEMONSTRATION OF PHASE ONE DECK SET-UP
      SPC = 173
      MPC = 4177
OUTPUT
      SET 37 = 201 THRU 287
      VECTOR = ALL
      SPCFORCES = 37
$ THIS EXAMPLE ASSUMES FOUR CONNECTION
$ DEGREES OF FREEDOM.
SUBCASE 100
      LOAD = 57
SUBCASE 200
      LOAD = 371
SUBCASE 300
      LOAD = 66
SUBCASE 400
      LOAD = 331
SUBCASE 500
      METHOD = 850
BEGIN BULK
$ (BULK DATA DECK GOES HERE)
ENDDATA
(6-7-8-9)
```

Figure 2. Typical deck setup for Phase 1.

MODE SYNTHESIS

Phase II of the mode synthesis analysis involves generation of system dynamic characteristics through synthesis of component information. This is performed using Rigid Format 3, Normal Mode Analysis, modified by the alter package of Figure 3. Direction is required from the user regarding compatibility relations among the various components, and selection of component generalized coordinates. User attention to certain aspects of internal data storage arrangements is required; in most cases, however, this is a trivial consideration. Since the activity involves operations on generalized, rather than physical, coordinates, the intuition and understanding of the user become much more necessary than in a normal study. Further, component coupling is accomplished by imposing transforms (developed from physical coordinate relationships) on the generalized coordinates. This requires the use of some mathematical sleight-of-hand that can lead to confusion unless the user is alert.

```

$ PHASE TWO ALTER PACKAGE
ALTER 6,74
$ STORE COMPONENT PARTITIONING VECTORS ON TEMPORARY DISK FILE
OUTPUT2 POS1,LOC1,TRUNK1,,//C,N,-1/V,Y,HOLD=11 $
OUTPUT2 POS2,LOC2,TRUNK2,,//C,N,0/V,Y,HOLD $
$ INSERT ADDITIONAL -OUTPUT2- STATEMENTS
$ UNTIL ALL COMPONENTS ARE TREATED
INPUTT2 /,,,/C,N,-1/V,Y,HOLD $
PARAM //C,N,NOP/V,N,TRUE=-1 $
$ PARAMETER K IS COMPONENT LOOP COUNTER
PARAM //C,N,SUB/V,N,K/V,Y,NCOMP=1/C,N,1 $
PURGE SUMK,SUMM,SUMC/TRUE $
INPUTT1 /,,,/C,N,-1 $
JUMP TOP1 $
INPUTT2 /SUMK,SUMM,SUMC,,//C,N,0/V,Y,XTRA=13 $
$ LOOP OVER ALL SUBSTRUCTURES, TRUNCATING COMPONENT DATA AND
$ MERGING TO FORM UNCOUPLED SYSTEM MATRICES
LABEL TOP1 $
INPUTT2 /CP,RP,TRUNK,,//C,N,0/V,Y,HOLD $ PARTITION VECTORS
INPUTT1 /MASS,STIFF,INTER,,//C,N,0 $ COMPONENT DATA
PARTN MASS,TRUNK,/MM,,//C,N,-1/C,N,2/C,N,6 $
PARTN STIFF,TRUNK,/KK,,//C,N,-1/C,N,2/C,N,6 $
PARTN INTER,TRUNK,/CC,,//C,N,1/C,N,2/C,N,2 $
MERGE, ,,,CC,CP,RP/CCX/C,N,1/C,N,2/C,N,2 $
ADD SUMC,CCX/CCXX $
EQUIV CCXX,SUMC/TRUE $
MERGE, ,,,MM,CP,/MMX/C,N,-1/C,N,2/C,N,6 $
ADD SUMM,MMX/MMXX $
EQUIV MMXX,SUMM/TRUE $
MERGE, ,,,KK,CP,/KKX/C,N,-1/C,N,2/C,N,6 $
ADD SUMK,KKX/KKXX $
EQUIV KKXX,SUMK/TRUE $
PARAM //C,N,SUB/V,N,K/V,N,K/C,N,1 $DECREMENT COUNTER
COND END1,K $
REF TOP1,20 $
LABELL END1 $
CHKPNT SUMC,SUMM,SUMK $
PARAM //C,N,NOP/V,Y,PRINT=-1 $

```

Figure 3 Phase II alter package

```

COND      PRNT1,PRINT $
MATPRN    SUMC,SUMM,SUMK,,,// $ PRINT SYSTEM UNCOUPLED MATRICES
LABEL     PRNT1 $
PARAM     //C,N,NOP/V,N,NSKIP=0 $
GP4       CASECC,GEOM4,EGEXIN,SIL,GPD/ROG,,,USET,/
          V,N,USET/V,N,MPCF1/V,N,MPCF2/V,N,SINGLE/V,N,OMIT/
          V,N,REACT/V,N,NSKIP/V,N,REPEAT/V,N,NOSET/V,N,NOA/V,N,NOL $
SAVE      MPCF1,MPCF2,SINGLE,OMIT,REACT,NSKIP,REPEAT,NOSET,NOA,NOL $
CHKPNT    RGG,USET $
$ COMPATIBILITY RELATIONS YIELD REDUCTION TRANSFORM
VEC       USET/VF/C,N,G/C,N,COMP/C,N,F $
PARTN     RGG,VF/RG,,,/C,N,1/C,N,2/C,N,2 $
MPYAD     RG,SUMC,/A/C,N,0 $ COMPATIBILITY IN GENERALIZED COORDS.
VEC       USET/VO/C,N,F/C,N,COMP/C,N,0 $
PARTN     A,VO,/AI,,AD,/C,N,1/C,N,2/C,N,2/C,N,0/C,N,1 $
SOLVE     AD,AI/B/C,N,0/C,N,-1 $
COND      PRNT2,PRINT $
MATPRN    A,B,,,// $
LABEL     PRNT2 $
SMP2      USET,B,SUMM/MAA $ REDUCED SYSTEM MASS MATRIX
SMP2      USET,B,SUMK/KAA $ REDUCED SYSTEM STIFFNESS MATRIX
COND      PRNT3,PRINT $
MATPRN    MAA,KAA,,,// $
LABEL     PRNT3 $
$ CONTINUE WITH STANDARD ANALYSIS METHODS USING -MAA- AND -KAA-
ALTER     80,80
FBS       LLL,ULL,KLR/DM/C,N,1/C,N,-1/C,N,2/C,N,2 $
ALTER     95, 112
MPYAD     B,PHIA,/DEPEND/C,N,0 $ RECOVER DEPENDENT COORDS
MERGE     PHIA,DEPEND,,,VO/FULL/C,N,1/C,N,2/C,N,2 $
OUTPUT2   LAMA,MI,FULL,,,/C,N,0/V,Y,HOLD $
$ PRINT ON DEMAND
PARAM     //C,N,NOP/V,Y,VECTOR=-1 $
COND      PRNT4,VECTOR $
MATPRN    FULL,,,// $
LABEL     PRNT4 $
ENDALTER

```

Figure 3. Phase II alter package (concluded).

All component data required for mode synthesis is, at the beginning of Phase II, contained on a User Tape in a sequential manner. In most cases, the number of component generalized coordinates (modes) to be used in the synthesis task will be less than the number provided through the individual component analyses of Phase I. The user identifies the modes to be used by supplying partitioning vectors for each component.

The key to the mode synthesis task is the compatibility relationship among the interface coordinates, expressed in the following equation:

$$S_1 X_c^{(1)} + S_2 X_c^{(2)} + \dots + S_j X_c^{(j)} = 0 \quad (1)$$

where $X_c^{(i)}$ are the interface coordinates for component i and S_i is a transformation employed to

express the interface motions of all components in a common coordinate system. In matrix form, this becomes

$$[S_1 \ \dots \ S_2 \ \dots \ \dots \ S_j] \begin{Bmatrix} X_c^{(1)} \\ \dots \\ X_c^{(2)} \\ \dots \\ X_c^{(j)} \end{Bmatrix} = 0 \quad (2)$$

To represent this relation in terms of component generalized coordinates, a modal transformation is imposed, which yields

$$[S_1 \ S_2 \ \dots \ S_j] \begin{bmatrix} \phi_c^{(1)} & & & \\ & \phi_c^{(2)} & & \\ & & \dots & \\ & & & \phi_c^{(j)} \end{bmatrix} \begin{Bmatrix} q^{(1)} \\ \dots \\ q^{(2)} \\ \dots \\ q^{(j)} \end{Bmatrix} = 0 \quad (3)$$

For simplicity, the compatibility equation (Eq. 3) is rewritten as

$$[A] \{q\} = 0 \quad (4)$$

Motion at the interfaces is redundantly defined in the above equation. A set of dependent coordinates must be identified such that they are equal in number to the excess interface coordinates, which, in turn, are equal in number to the compatibility equations. The choice is essentially arbitrary, except that for a singular system an appropriate set of rigid-body modes must be retained as independent coordinates for reasons explained below. This set must be adequate to supply rigid-body motion in all directions that are singular in the complete structural system. The compatibility equation is partitioned into dependent and independent coordinates:

$$[A_I \ \dots \ A_D] \begin{Bmatrix} q_I \\ \dots \\ q_D \end{Bmatrix} = 0 \quad (5)$$

The relationship between dependent and independent coordinates is thus

$$\{q_D\} = -[A_D]^{-1} [A_I] \{q_I\} \quad (6)$$

It is apparent from Eq. 6 that the dependent coordinates must be chosen so that $[A_D]$ is nonsingular, and hence invertible. The full set of generalized coordinates can now be defined in terms of the independent coordinates.

$$\begin{Bmatrix} q_I \\ \dots \\ q_D \end{Bmatrix} = \begin{bmatrix} I \\ \dots \\ -[A_D]^{-1} [A_I] \end{bmatrix} \{q_I\} \quad (7)$$

This equation supplies the necessary coupling of component generalized coordinates required to define the behavior of the full structural system. Letting

$$[\beta] = \begin{bmatrix} I \\ \dots \\ -[A_D]^{-1} [A_I] \end{bmatrix} \quad (8)$$

the uncoupled component generalized mass and stiffness matrices are transformed into coupled system matrices. If the assembled uncoupled matrices are $[m]$ and $[k]$ where

$$[m] = \begin{bmatrix} m^{(1)} & & & \\ \dots & & & \\ & m^{(2)} & & \\ \dots & & & \\ & & \dots & \\ & & & m^{(j)} \\ \dots & & & \\ & & & \dots \end{bmatrix}$$

$$[k] = \begin{bmatrix} k^{(1)} & & & \\ \dots & & & \\ & k^{(2)} & & \\ \dots & & & \\ & & \dots & \\ & & & k^{(j)} \\ \dots & & & \\ & & & \dots \end{bmatrix}$$

then application of the transformation results in

$$[M] = [\beta]^T [m] [\beta]$$

$$[K] = [\beta]^T [k] [\beta]$$

where $[M]$ and $[K]$ are coupled system mass and stiffness matrices in terms of the independent set of generalized coordinates. These are used in the eigenvalue extraction to acquire system model data. The mode vectors obtained are the system vibration modes, expressed in terms of the independent component generalized coordinates.

The system mode vectors are expanded to include the dependent generalized coordinates and stored, along with the eigenvalue table and system generalized mass matrix, on another User Tape. These data are accessed in Phase III for purposes of recovering mode data in component physical coordinates.

Each component generalized coordinate is represented in the NASTRAN analysis by a scalar point. In addition, the interface degrees of freedom are mapped on a one-to-one basis on another set of scalar points. It is advantageous to employ a numbering sequence that can be used to distinguish easily between those scalar points representing component generalized coordinates and those representing interface degrees of freedom. The numbering scheme for the scalar points is arbitrary; however, partitioning vectors described below must be compatible with the internal sequence of points; thus, it is desirable that some logical numbering scheme be employed to facilitate bookkeeping. Both component mode and component interface degree of freedom internal sequences cannot be altered from the Phase I condition. Regardless of what scalar point numbering scheme is employed, compatibility with these sequences must be maintained. Note that, if necessary, SEQGP cards can be used to resequence scalar points.

The definition of interface compatibility relationships (Eq. 2) is introduced by means of multi-point constraint equations. It is the responsibility of the user to verify the coordinate relationships defined by the MPC equations, including any necessary coordinate transformations. The MPC cards supply these relationships in terms of the scalar point equivalents of the interface degrees of freedom. The relationships defined must be sufficient to eliminate all redundancy in describing interface motion. To illustrate, if there are n components interfacing at a grid point, then there must be $(n - 1)$ MPC equations supplied for every direction in which motion can occur at that grid point. Within that requirement, the choice of dependent degrees of freedom is arbitrary, since the actual synthesis activity does not consider the distinction. The scalar points used as *independent* coordinates in the MPC equations are placed in the S-set by SPC cards. This is done solely for the purpose of internal bookkeeping and does not impose any real constraint on the actual structure. The transform to generalized coordinates (Eq. 3) is performed automatically.

The division of component generalized coordinates into independent and dependent sets, as required by Eq. 5, is done by specifying the dependent set on OMIT cards. The number of coordinates omitted must be identical to the number of interface dependency equations defined by MPCs. The specification is in terms of the scalar points representing the generalized coordinates. Based on this set selection, NASTRAN automatically generates the coupled system matrices required by the eigenvalue module.

If the full structure being analyzed exhibits singularities, temporary supports should be specified via a SUPORT card. The scalar points that should be supported in this manner are those that represent

a set of component rigid-body modes sufficient to define rigid-body motion of the full structure. Note that the number of supports used must be equal to the number of rigid-body modes of the full system. The normal choice of temporary support location will be the rigid-body modes of a single component.

It is recommended that normalization of eigenvectors be done to a unit generalized mass to maintain a recognizable standard through the transformation back to physical coordinates.

Special parameters required for this phase are:

1. **NCOMP** – The number of components in the synthesis (and for which data have been placed on a User Tape).
2. **PRINT** – A positive value will cause the printing of intermediate matrices.
3. **VECTOR** – A positive value will cause the printing of a matrix containing mode vectors in component generalized coordinates.

The partition vectors required are:

1. **TRUNKi** – Identifies modes of component *i* present on the User Tape that are to be deleted (i.e., not used for the synthesis). *M* = number of component *i* modes computed and stored on the User Tape. An element corresponding to a mode to be deleted has value of 1.
2. **POSi** – Locates component modes in uncoupled system matrix. *M* = sum of all component modes to be used in the synthesis. Element has a value of 1 when corresponding to a mode of component *i*. (The sum of all POSi vectors is a unity vector.)
3. **LOCi** – Locates interface degrees of freedom for component *i* in truncated uncoupled mode vector matrix. *M* = sum of all interface degrees of freedom. Element has a value of 1 when corresponding to a degree of freedom of component *i*. (The sum of all LOCi vectors is a unity vector).

References for MPC, SPC, and eigenvalue METHOD must be present in the Case Control Deck, along with the titles, etc. None of the usual output options is available in this phase. A sample case control deck is given in Figure 4.

RECOVERY OF SYSTEM MODE SHAPES

The system modal information in physical coordinates can be recovered on a component-by-component basis using the DMAP sequence of Figure 5, the problem tapes generated in Phase I, and the User Tape created in Phase II. The User Tape contains not only the modal data but also the partitioning vectors supplied in Phase II to define the positioning of the component generalized coordinates. These are applied to the system mode vector matrix to truncate it to the generalized coordinates for a selected component, $\{q_s^{(j)}\}$. The portion of the system mode shape for the *j*th component $\{\phi_s^{(j)}\}$ is expressed in the component global coordinate system by means of back-substitution, using the component mode matrix $\{\phi_c^{(j)}\}$, as a transformation:

$$\{\phi_s^{(i)}\} = \{\phi_c^{(j)}\} \{q_s^{(j)}\} \quad (9)$$

If transient analysis is to be performed, these data are stored on a User Tape for use in Phase IV. Once the modal amplitudes of the physical coordinates have been determined, full use of NASTRAN's output option is available; this option permits printing and/or punching of displacements, constraint forces, internal forces, and internal stresses.

```

REQUEST(UT1,*PF)
REQUEST(INPT,HD,S,VSN=XXXXX)
REWIND(UT1,INPT)
ATTACH(N15,NASTRAN15,ID=TONE90970)
MAP(OFF)
N15.ATTACH
CATALOG(UT1,YOURPERMFILE,ID=YOURZZZZZ)
RETURN(INPT)
EXIT.
DMP(140000)
RETURN(INPT)
CATALOG(UT1,YOURPERMFILE,ID=YOURZZZZZ)
(7-8-9)
ID          PHASE,    TWO
APP         DISP
SOL         3,0
TIME        2
$(PHASE TWO ALTER PACKAGE GOES HERE)
CEND
TITLE=DEMONSTRATION OF PHASE TWO DECK SET-UP
      MPC = 381
      SPC = 16
      METHOD = 517
BEGIN BULK
$(BULK DATA DECK GOES HERE)
ENDDATA
(6-7-8-9)

```

Figure 4. Typical deck setup for Phase II.

```

$ PHASE THREE DMAP SEQUENCE
BEGIN $
INPUTT2 /,,,,/C,N,-1/V,Y,HOLD=11 $
PARAM //C,N,SUB/V,N,M/V,Y,COMP/C,N,1 $
PARAM //C,N,MPY/V,N,OVER/V,N,M/C,N,3 $
INPUTT2 /CP,RP,TRUNK,,,/V,N,OVER/V,Y,HOLD $
INPUTT2 /LAMA,MI,FULL,,,/C,N,-5/V,Y,HOLD $
PARTN FULL,,CP/,COMPMODE,,,/C,N,1/C,N,2/C,N,0/C,N,2 $
PARTN MODES,TRUNK,/MODEA,,,/C,N,1/C,N,2/C,N,2 $
PARTN QGG,TRUNK,/QA,,,/C,N,1/C,N,2/C,N,2 $
MPYAD MODEA,COMPMODE,/PHIGG/C,N,0 $
MPYAD QA,COMPMODE,/QGGG/C,N,0 $
SUR2 CASECC,CSTM,MPT,DIT,EGEXIN,SIL,,,BGPDT,LAMA,QGGG,
      PHIGG,EST,/,OQ,OPHI,OS,OF,PPHIG/C,N,REIG $
OFP OPHI,OQ,OF,OS,,,/V,N,CARDNO $
SAVE CARDNO $
PARAM //C,N,SUB/V,N,MM/V,N,M/C,N,1 $
COND OUT1,MM $ JUMP IF FIRST SUBSTRUCTURE
INPUTT1 /,,,,/C,N,-1/V,Y,INP1=1 $
JUMP OUT2 $
LABEL OUT1 $
OUTPUT1, ,,,,/C,N,-1/V,Y,INP1 $
LABEL OUT2 $
OUTPUT1 PHIGG,,,,,/V,N,M/V,Y,INP1 $
END $

```

Figure 5. Phase III DMAP sequence.

Since this phase uses a DMAP approach, only output requests have meaning in the Case Control Deck and no bulk data are needed. The restart dictionary generated in Phase I is used, to which is added a last card reading:

n, RE-ENTER AT DMAP SEQUENCE NUMBER 1

where n is the appropriate sequence number (see Section 2.2.1 of the NASTRAN User's Manual). A typical deck setup is given in Figure 6.

```

REQUEST(OTPT,HD,S, VSN=YYYYY)
REQUEST(INP1,HD,S) RING IN
ATTACH(UT1,YOURPERMFILE, ID=YOURZZZZZ)
REWIND(OTPT,INP1,UT1)
ATTACH(N15,NASTRAN15, ID=TONE90970)
MAP(OFF)
N15.ATTACH
RETURN(OTPT,INP1)
EXIT.
DMP(140000)
RETURN(OTPT,INP1)
(7-8-9)
ID PHASE, THREE
APP DMAP
TIME <
$(PHASE THREE DMAP SEQUENCE GOES HERE)
$(PHASE ONE RESTART DICTIONARY GOES HERE)
CEND
TITLE=DEMONSTRATION OF PHASE THREE DECK SET-UP
$ SPC AND MPC REFERENCES ARE THE SAME AS FOR PHASE ONE
SPC = 173
MPC = 4177
OUTPUT
SET 16 = 1,3,4 THRU 16, 30,35
SET 31 = 106 THRU 135, 187 THRU 194
VECTOR = ALL
SPCFORCES = 16
ELSTRESS = 31
BEGIN BULK
ENDDATA
(6-7-8-9)

```

Figure 6. Typical deck setup for Phase III.

MODAL TRANSIENT RESPONSE ANALYSIS

The transient response analysis via NASTRAN mode synthesis requires user direction to merge the required modal data from the component partitions and then perform the response analysis. Since the system being analyzed may be quite large, only those degrees of freedom involved in defining external loadings or associated with extra points are used. Rigid Format 12, Modal Transient Analysis, modified by the alter package of Figure 7, is used.

The system mode vector matrices for each substructure, written on a User Tape in Phase III, are partitioned to extract the portions associated with externally loaded degrees of freedom. If extra points are to be added at this stage (e.g., for nonlinear force definitions), the degrees of freedom

needed to define the relationship of the extra points to the physical structure must also be included. These truncated mode vector sets are merged to form a single truncated system mode matrix. The system modes to be used in the response analysis are selected by the user via frequency limits or mode count.

```

$ PHASE FOUR ALTER PACKAGE
ALTER 23,42
ALTER 48, 91
$ STORE SUBSTRUCTURE LOAD AND ASSIGN PARTITION VECTORS
INPUTT1 /,,,/C,N,-1/V,Y,INP1=1 $
OUTPUT1 LOAD1,ASSIGN1,,,//V,Y,NCOMP=1/V,Y,INP1 $
OUTPUT2 LOAD1,ASSIGN1,,,/C,N,-1/V,Y,TEMP=12 $
$ INSERT ADDITIONAL -OUTPUT2- STATEMENTS
$ UNTIL ALL COMPONENTS ARE TREATED
$ TEMPORARY DISK FILE (TEMP = 12) TO REDUCE TAPE MANIPULATIONS
OUTPUT1 LOAD2,ASSIGN2,,,/C,N,0/V,Y,INP1 $
OUTPUT2 LOAD2,ASSIGN2,,,/C,N,0/V,Y,TEMP $
$ CONTINUE UNTIL ALL SUBSTRUCTURES HAVE BEEN TREATED
INPUTT1 /,,,/C,N,-1/V,Y,INP1 $
INPUTT2 /,,,/C,N,-1/V,Y,TEMP $
PARAM //C,N,NOP/V,N,TRUE=-1 $
PARAM //C,N,SUB/V,N,K/V,Y,NCOMP/C,N,1 $
PURGE PHIA,MAA/TRUE $
JUMP TOPLoop $
INPUTT1 /PHIA,MAA,GO,GM,KFS/C,N,0/V,Y,INP1 $ DUMMY READ
LABEL TOPLoop $
INPUTT1 /SUBMODE,,,/C,N,0/V,Y,INP1 $
INPUTT2 /LOAD,ASSIGN,,,/C,N,0/V,Y,TEMP $
$ TRUNCATE MODE VECTOR TO LOADED AND E.P. REFERENCED DOF ONLY.
PARTN SUBMODE,,LOAD/,LOADMODE,,/C,N,1/C,N,2/C,N,0/C,N,2 $
$ ASSEMBLE SYSTEM MATRIX
MERGE, ,LOADMODE,,,ASSIGN/LDMD/C,N,1/C,N,2/C,N,2 $
ADD PHIA,LLMD/NEwMODE $
EQUIV NEwMODE,PHIA/TRUE $
PARAM //C,N,SUB/V,N,K/V,N,K/C,N,1 $
COND ENDLLoop,K $
REPT TOPLLoop,20 $
LABEL ENDLLoop $
CHKPNT PHIA $
INPUTT2 /LAMA,MI,,,/C,N,-5/V,Y,HOLD=11 $
CHKPNT LAMA,MI $
$ MODE MATRIX CONTAINING ONLY NEEDED DOF HAS NOW BEEN FORMED.
$ CONTINUE STANDARD ANALYSIS
ALTER 94,94
ALTER 98,103
ALTER 125
EQUIV UHVT,UHVTX/NOUE/PPT,PPG/NOUE $
COND EOFF,NOUE $
PARTN UHVT,,EP/UHVTX,,,/C,N,1/C,N,2/C,N,2 $
LABEL EOFF $
$ OUTPUT SOLUTION SET RESPONSE HISTORY AND LOAD HISTORY
PARAM //C,N,MPY/V,N,SKIP/V,Y,NCOMP/C,N,2 $
OUTPUT1 UHVTX,PPT,,,/V,N,SKIP/V,Y,INP1 $
ENDALTER

```

Figure 7. Phase IV alter package.

Phase IV is similar to Phase II in that only scalar points are used. The scalar points represent all loaded coordinates and all interface coordinates for extra points, if any. The numbering scheme for the scalar points is arbitrary; however, the partitioning vector described below must be compatible with the internal sequence of each component, which cannot be altered. Some logical number scheme to facilitate bookkeeping is obviously desirable. SEQGP cards may be used to resequence scalar points.

Note that no boundary conditions are specified. They are implicit in the modal information that will be used in the analysis. All system data are entered in terms of the physical degrees of freedom or, more exactly, their scalar point equivalents. NASTRAN automatically performs the required transformation to modal coordinates.

Standard NASTRAN methods for defining external loads sets are used. The loads are applied to the scalar points representing the appropriate physical degrees of freedom. It is the user's responsibility to ensure that this assignment is correctly specified as no internal check can be made.

The interactions between any extra points and the structure are defined by supplementary matrices added to structural mass, damping, and stiffness matrices, expanded to accommodate the additional degrees of freedom. These matrices are input directly via DMIG bulk data cards or formed from transfer functions entered via TF bulk data cards.

There is but one special parameter required for this phase: NCOMP - the number of substructures in the system. Partition vectors required include:

1. **LOADi** - Identifies the degrees of freedom in substructure *i* to be used in the transient response analysis. $M = g$ size of the substructure. The element corresponding to the coordinate to be used is given a value of 1. Degrees of freedom to be loaded by external forces or that are to be referenced by extra points are included.
2. **ASSIGNi** - Identifies the portion of retained degrees of freedom of substructure *i* in the assembled system representation. $M =$ the sum of all coordinates in the structure to be employed in the transient analysis. The element corresponding to a coordinate from substructure *i* has a value of 1.
3. **EP** - Identifies position of extra points in augmented modal matrices. $M =$ number of modes used in transient analysis plus number of extra points. This vector is required only if extra points are used. Further, extra points are always sequenced last in such matrices. A value of 1 indicates position of extra point degree of freedom.

The Case Control deck includes all references required to perform a transient response analysis. In addition, output requests for solution set responses as well as applied and nonlinear force histories are made. A typical deck setup is illustrated in Figure 8.

RECOVERY OF PHYSICAL RESPONSES

The response of the entire structural system can be recovered on a substructure-by-substructure basis by using the DMAP sequence of Figure 9, the Phase I Problem Tapes, and the Phase IV User Tape. The solution set response matrix generated in Phase IV is pre-multiplied by the appropriate partition of the system mode shape matrix to form the substructure response matrix. Then by using standard NASTRAN recovery methods, the full complement of output options may be exercised.

This phase is executed in a restart mode; consequently, the mathematical model data are available from the OPTP. (The restart dictionary must be augmented as for Phase III.) The additional

```

REQUEST(INP1,HD,S, VSN=PPPP) RING IN
ATTACH(UT1, YOURPERMFILE, ID=YOURZZZZ)
REWIND(INP1,U)1)
ATTACH(N15, NASTRAN15, ID=TONE90970)
MAP(OFF)
N15.ATTACH
RETURN(INP1)
EXIT.
DMP(140000)
RETURN(INP1)
(7-8-9)
ID PHASE, FOUR
APP DISP
SOL 12.3
TIME 2
$(PHASE FOUR ALTER PACKAGE GOES HERE)
CEND
TITLE=DEMONSTRATION OF PHASE FOUR DECK SET-UP
$ K2PP AND NONLINEAR REFERENCES NOT REQUIRED
$ FOR LINEAR PROBLEMS.
K2PP = TRA
NONLI = 5
DLOAD = 75
TSTEP = 70
OUTPUT
SET 784 = 1 THRU 12,501 THRU 508
SET 208 = 1 THRU 6
SET 611 = 1 THRU 12
SET 1800 = 117,159,170,182,197
SET 960 = 960 THRU 969
NLLOAD = 960
SDISPLACEMENT = 784
SVELOCITY = 208
SACCELERATION = 611
OLOAD = 1800
BEGIN BULK
$(BULK DATA DECK GOES HERE)
ENDDATA
(6-7-8-9)

```

Figure 8. Typical deck setup for Phase IV.

information required consists solely of a partition vector, DISCARD, required to identify the system modes not employed in the transient analysis. M = number of system modes originally found in Phase II. Excluded modes are identified by a corresponding element value of 1.

Because this phase employs a DMAP approach, no references to boundary conditions, etc., are needed. Tiling and output requests are chosen as the user wishes for each substructure. Output selections are for physical degrees of freedom and associated functions. A sample deck setup is shown in Figure 10.

NASTRAN MODE SYNTHESIS SAMPLE PROBLEM

The mathematical model of Figure 11 has been developed as an aid to demonstrating the procedures associated with NASTRAN mode synthesis. While the system is small, it does provide the opportunity

```

$ PHASE FIVE DMAP SEQUENCE
BEGIN $
PARAM //C,N,SUB/V,N,MARK/V,Y,COMP=1/C,N,1 $
INPUTT1 /,,,/C,N,-1/V,Y,INP1=1 $
INPUTT1 /SUBMODE,,,/V,N,MARK/V,Y,INP1 $
PARTN SUBMODE, DISCARD, /MODEMAT,,,/C,N,1/C,N,2/C,N,2 $
INPUTT1 /UHVTX,PPT,,,/C,N,-5/V,Y,INP1 $
MPYAD MOUEMAT,UHVTX,/UDV1T/C,N,0/C,N,1/C,N,1/C,N,1 $
CASE CASECC,/CASEXX/C,N,TRAN/V,N,REPEAT=-1/V,N,NOLOOP $
DPD DYNAMICS,GPL,SIL,USET/6PLD,SILD,USED,,,,,EGDYN/
V,N,LUSET/V,N,LUSETD/V,N,NOTFL/V,N,NODLT/V,N,NOPSDL/
V,N,OFRL/V,N,NONLFT/V,N,NOTRL/V,N,IOEED/
C,N,0/V,N,NOUE $
VEC USETD/VD/C,N,P/C,N,D/C,N,COMP $
PARTN UUV1T,,VD/UDSET,,,/C,N,1/C,N,2/C,N,2 $
SDR1 USETD,,UDSET,,,GO,EM,,KFS,,/U,,OP/C,N,1/C,N,DYNAMICS $
SDR2 CASEXX,CSTM,MPT,DIT,,EQDYN,SILD,,,6GPD,PPT,OP,UUV1T,EST,XYCDB/
OP,00,0U,0S,0F,PUGV/C,N,TRANRESP $
CHKPNT PUGV $
SDR3 OP,00,0U,0S,0F,/OP2,0Q2,0U2,0S2,0F2,$
OFF 0U2,OP2,0Q2,0F2,0S2, //V,N,CARDNO $
END $

```

Figure 9. Phase V DMAP sequence.

```

REQUEST(OPTP,HD,S,VS=YYYYY)
REQUEST(INP1,HD,S,VS=PPPPP)
REWIND(OPTP,INP1)
ATTACH(N15,NASTRAN15, ID=TONE90970)
MAP(OFF)
N15.ATTACH
RETURN(OPTP,INP1)
EXIT.
DMP(14000)
RETURN(OPTP,INP1)
(7-8-9)
ID PHASE, FIVE
APP DMAP
TIME 2
$(PHASE FIVE DMAP SEQUENCE GOES HERE)
$(PHASE ONE RESTART DICTIONARY GOES HERE)
CEND
TITLE=DEMONSTRATION OF PHASE FIVE DECK SET-UP
OUTPUT
SET 23 = 1,3,26,18,12 THRU 16
SET 38 = 38,24,36
SET 90 = 12,18,24,36,60,66
SET 91 = 12,18,24,36,60
SET 92 = 12,18,24,36
SET 187 = 122,132
DISPLACEMENT = 90
VELOCITY = 91
ACCELERATION = 92
SPCFORCES = 187
ELSTRESS = 23
ELFORCE = 38
BEGIN BULK
$(BULK DATA DECK ADDITIONS GO HERE)
ENDDATA
(6-7-8-9)

```

Figure 10. Typical deck setup for Phase V

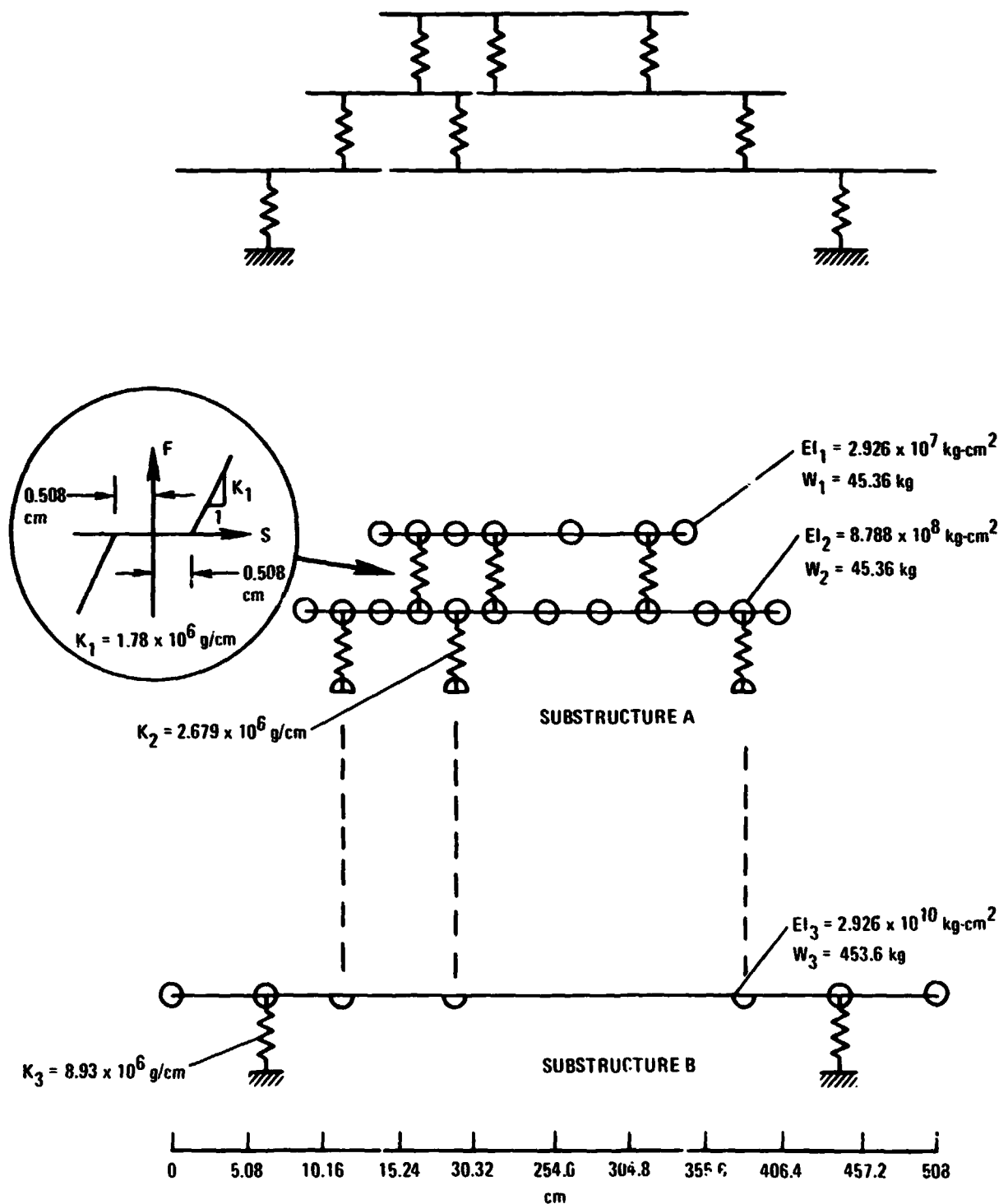


Figure 11. Sample problem mathematical model.

to demonstrate the major flexibilities of the technique. The problem exhibit a redundant interface, both free-free and constrained component modes, and nonlinear elements.

The system to be analyzed consists of three uniform elastic beams in parallel, connected by spring elements. The springs connecting the upper beam to the middle one are nonlinear and exhibit a

dead zone about the null deflection point. Excitation is provided by a sinusoidal force acting vertically at the end of the lowest beam.

For demonstration purposes, the structure is modeled as two components (see Figure 11). The first, identified as substructure A, consists of the upper and middle beams and the springs between middle beam and the lower beam. The second component, substructure B, is composed of the lower beam and its support springs. The component modes for substructure A are developed for the linear portions of the structure only – the nonlinear portions are added when the transient studies are performed.

The first user judgment comes immediately when he must decide which component modes to use in the synthesis. For the transient response study to follow, the 30 Hz sinusoidal applied force suggests the desirability of good system definition up to about 100 Hz. Based on this objective, a nominal cutoff of 300 Hz for component modes was chosen. For substructure A this presents no problem – the 14 lowest frequency modes plus the three static modes are selected. For substructure B, however, this criterion conflicts with the distribution of modal frequencies. Five vibration modes exist for substructure B that have frequencies under 300 Hz. Adding the three static modes gives a total of eight. However, the substructure only has seven independent degrees of freedom. The solution of the conflict was chosen to be a violation of the 300 Hz component mode criterion. For demonstration purposes, still another mode was deleted; thus the three static modes and three dynamic modes with a highest frequency of 33.7 remain. The resulting system modal frequencies did not show significant error until the 11th elastic mode (70 Hz), where just under 1% error in frequency is observed. However, some degradation of response accuracy results from this compromise modeling technique.

The nonlinear elements between upper and middle beams are integrated with the elastic structure definition by addition of extra points and use of a direct input matrix.

Comparison of the results obtained via mode synthesis with those acquired from the standard modal transient study indicates excellent correlation for component A (see Table 1), with errors limited to under 1% for displacements and accelerations and under 3% for internal loads. The effect of the severe truncation of the substructure B mode set is apparent when comparing results with the standard study (Table 1). Displacement and acceleration values are quite good, with errors of less than 1%, even though the error terms are substantially larger than those for substructure A. Bending moments and shears for the selected beam element are in error by 10.7%, because the limited number of elastic modes used in the study was inadequate to give good representation. For the more general case, with a great many more degrees of freedom in the substructure, it will be possible to employ an adequate number of substructure modes to provide sufficient description of elastic behavior.

REFERENCES

1. Hurty, W.C., "Dynamic Analysis of Structural Systems Using Component Modes," AIAA Journal, Vol. 3, No. 4, April 1965, pp 678-685.
2. Craig, R.R. and Bampton, M.C.C., "Coupling of Substructures for Dynamic Analysis," AIAA Journal, Vol. 6, No. 7, July 1968, pp 1313-1319.
3. Bamford, R., Wada, B.K., Garba, J.A., Chisholm, J., "Dynamic Analysis of Large Structural Systems," ASME Synthesis of Vibrating Systems, November 1971, p 63.
4. Rubin, S., "An Improved Component-Mode Representation," AIAA/SAME/SAE 15th Structures, Structural Dynamics, and Materials Conference, AIAA Paper 74-386, Las Vegas, Nevada, April 1974.
5. MacNeal, R.H., ed., "The NASTRAN Theoretical Manual," NASA SP-221(01), April 1972.
6. Courtney, R.L., "NASTRAN Modeling Studies in the Normal-Mode Method and Normal-Mode Synthesis," NASA TM-X-2378, "NASTRAN: Users' Experiences," September 1971.

Table 1. Summary of peak responses.

Response Quantity				
Grid or Element ID	Quantity	Standard Analysis	Synthesized Analysis	Error %
101	DISP	-4.29	-4.29	<0.01
201	DISP	-3.10	-3.10	<0.01
301	DISP	1.11	1.11	0.22
101	ACC	5.84×10^4	5.84×10^4	0.02
201	ACC	7.12×10^4	7.13×10^4	0.06
301	ACC	1.65×10^4	1.66×10^4	0.59
51	FORCE	1.43×10^4	1.44×10^4	0.28
53	FORCE	4.58×10^4	4.58×10^4	0.02
3	(BM) _A	1.49×10^5	1.48×10^5	0.29
3	(BM) _B	-6.60×10^4	-6.60×10^4	0.06
3	SHEAR	1.16×10^4	1.15×10^4	0.80
10	(BM) _A	4.10×10^5	3.97×10^5	2.95
10	(BM) _B	4.58×10^5	4.72×10^5	2.95
10	SHEAR	6.65×10^3	6.78×10^3	1.91
31	(BM) _A	0	0	-
31	(BM) _B	1.31×10^6	1.17×10^6	10.7
31	SHEAR	-5.25×10^4	-4.69×10^4	10.7

N75 31505

APPLICATION OF NASTRAN TO
PROPELLER-INDUCED SHIP VIBRATION

By Atis A. Liepins
Littleton Research and Engineering Corp.

John H. Conaway
Control Data Corporation

SUMMARY

An application of the NASTRAN program to the analysis of propeller-induced ship vibration is presented. Described are the essentials of the model, the computational procedure, and experience. Desirable program enhancements are suggested.

INTRODUCTION

The propeller, operating in the uneven wake of a ship, generates harmonic forces which are transmitted to the hull partly through the shaft and partly through the water as hull surface pressures. The frequency of the propeller forces is determined by the number of blades on the propeller and the revolving speed of the shaft. For modern commercial ships this frequency is, at full power, in the range of 5 to 15 Hz. The fundamental frequency of these ships is of the order of 1 Hz or lower. Thus, the propeller excitation is of high frequency relative to the fundamental of the ship. The response of the ship to this excitation can be expected to be found primarily in complicated modes that are far above the fundamental.

The concern about propeller-induced vibration is seldom for its effect on the ship's structural integrity or fatigue, but rather for its effect on the habitability of crew quarters and the excessive wear of propulsion machinery.

The prediction of vibration levels is thus of considerable importance in ship design, but it has been and continues to be a difficult problem. Vibration levels have been predicted from models which idealize the ship as a system of beams (Ref. 1 and 2). Although these models can handle the beam-type vibrations of the hull and the propulsion shaft, the finite-element method is better suited to the vibration of more localized structures such as the shaft bearing supports, and superstructures are also to be

predicted (Ref. 3). Because of interest in relatively high frequency response, the finite element models tend to be large. NASTRAN was selected for this problem because of its ability to handle large models. The MacNeal-Schwendler NASTRAN available at Control Data Corporation Data Centers was used. At the time that the computations were performed, Version 13 was current.

MODEL

The model is expected to represent the major types of ship vibration modes. These include the hull vertical bending, lateral bending coupled with torsion, and longitudinal extension (accordion type); the shaft longitudinal, vertical and lateral modes; the vertical motion of the double bottom and its interaction with the shaft longitudinal modes; and the motions of the superstructure. The torsional modes of the propulsion shafting and machinery are of little importance to hull vibration and are not included in the model. The local motions of the decks and shell panels are also excluded. In the operating frequency range there are typically a dozen vertical, four or five lateral-torsional, one or two longitudinal hull modes and several shafting modes.

The structure and weight distribution of the ship are nearly symmetrical about the longitudinal center plane. The minor asymmetries that exist were ignored and only one-half of the ship (the port side) was modeled.

Approximately, the forward third of the ship was modeled as a beam (fig. 1). This gross simplification of the structure is justified because it is far removed from the excitation and generally experiences low levels of vibration. The remaining structure was represented in three dimensions (figs. 2 and 3). In the three dimensional part the vertical spacing of the grid points was determined largely by the decks and the double bottom. The lateral spacing was determined by the location of longitudinal girders and bulkheads, and the attempt to limit the aspect ratio of triangular and quadrilateral elements to 2.0. The longitudinal spacing varies. Below the second deck and aft of FR 106, the longitudinal grid spacing is the finest. At shaft support structures each frame was represented. Away from these structures two or three frames were lumped. In the engine room the longitudinal spacing was also determined in part by the depth of the double bottom. Above the second deck and forward of the engine room, the grid spacing was determined by the location of major transverse bulkheads and the expected wave length of vertical vibration at a frequency corresponding to 150% of full power RPM. This resulted in the lumping of four to six frames.

The center shaft is raked and the wing shafts are raked and splayed. For these reasons the grid points of each shaft were referred to a special coordinate system. Grid points were also assigned to the centers of gravity of major machinery items such as boilers, condensers, turbines, and reduction gears.

The shell plate, double bottom, decks, bulkheads, transverse diaphragms (floor) and major machinery foundations were modeled with triangular and quadrilateral membrane elements CTRMEM and CQDMEM1. The CQDMEM1 element was selected because of its linear strain gradient (Ref. 4). Membrane elements rather than plate bending elements were used since, in vibration, the principal action of these structures is in their plane with negligible bending.

Shafts, longitudinal girders, frames, and columns were modeled with CBAR elements. Stiffeners and flanges of machinery foundations were represented by CONRODs. Shaft bearings were represented with rigid elements RBEL and spring elements CELAS2.

The mass of the ship for vibration purposes consists of the structure, machinery, outfit, liquids in tanks, stores, cargo, and the added mass of water associated with vibration in the vertical and horizontal directions. In the forward part of the ship, represented by beam elements, mass moments of inertia, as well as masses were assigned to grid points. This was accomplished with CONM1 elements. CONM2 elements were used for machinery items, outfit, liquids in tanks, and stores. CMASS2 elements were used for the added mass of water. The structure weight generator together with an adjusted material density was used to compute the structural weight.

Multipoint constraints were used to connect the beam part of the ship hull model to the three-dimensional part, to connect the centers of gravity of major machinery items to the ship's structure, and to transfer moment from a beam element into the plane of a membrane element. MPCs were also used to interpolate displacements at grid points which, if connected by membrane elements, would result in too large aspect ratios or, if not connected, would result in gaps between membrane elements.

Single point constraints were used to eliminate singular displacement coordinates and to specify symmetry and antisymmetry conditions on the center plane.

The model consisted of 1657 grid points connected by 5667 elements, approximately evenly divided among CBAR, CONROD, CTRMEM and CQDMEM1 elements. The coordinates and constraints of the symmetric and

antisymmetric models are summarized below:

	<u>Symmetric</u>	<u>Antisymmetric</u>
Multipoint constraints	332	328
Single point constraints	4,104	4,254
Unconstrained degrees of freedom	5,506	5,360
Dynamic degrees of freedom	258	228

COMPUTATIONAL PROCEDURE

For debugging purposes the model was divided into three sections: forebody, superstructure, and engine room. The forebody extends forward of FR 106, the superstructure aft of FR 106 and above the second deck, and the engine room aft of FR 106 and below the second deck (See fig. 1). Since there is interest in the modes of the engine room section when it is supported at its periphery, this division is logical.

The debugging of each section proceeded as follows using Rigid Format 3:

- 1) Data errors were corrected and a half a dozen undeformed geometry plots were made. The plots were examined and, if necessary, the geometry and connectivity corrected.
- 2) The BANDIT (ref. 5) program was used to resequence grid points.
- 3) The stiffness and mass matrices were assembled. The total mass in each of three directions was computed and the GPSP table, corresponding to the case of no single point constraints, was printed. This run was checkpointed and execution stopped after the GPSP table.
- 4) The structural weight as computed by the structural weight generator was brought into agreement with the section weight information by adjusting the density of the material. The singularities in the GPSP table were examined and for each singularity a single point constraint coded. The problem was restarted and mode shapes were computed. For the first few modes the forces of single point constraint were also computed.

- 5) Modes were examined for "soft spots", that is, coordinates with low stiffness and/or large mass concentration. The frequencies of some modes were checked against hand calculations, preliminary computer calculations, and general experience. If necessary, stiffness and/or mass connectivity was changed to improve the model. The single point constraint forces were inspected for their reasonableness.

Next the three sections were merged and the debugging steps 1-4, used for each section, were repeated. The BANDIT run for the merged model resulted in a bandwidth too large for NASTRAN. Apparently, this was caused by the large number of multipoint constraints. Since the multipoint constraints generally involved coordinates at three grid points, a dummy triangular membrane element CTRMEM was coded for each multipoint constraint. BANDIT then produced a resequence, which resulted in 294 active columns and a bandwidth of 19. The dummy CTRMEMs were not used in NASTRAN runs.

To insure that the more than 4000 single point constraints would suppress all singular coordinates but not destroy rigid body modes, the model was subjected to static enforced displacements. This was done through the SPCD cards. The same coordinates which later in modal extraction were specified on the SUPORT card were forced to displace so as to produce rigid body motions of the model. This calculation was first performed on the symmetric model by using Rigid Format 1.

After the symmetric model had passed the enforced rigid-body displacement check, the problem was restarted in Rigid Format 3 and 68 mode shapes were computed in the frequency range 0 to 20 Hz. For each mode shape five plots were produced:

- 1) An elevation view at the center plane of the engine room and superstructure,
- 2) An elevation view of the center plane of the forebody,
- 3) An elevation view of the center shaft,
- 4) Elevation and plan form views of the wing shaft.

Representative mode shape plots are shown in figures 4, 5, 6 and 7.

Largely as a result of the thorough checking of the three sections and the enforced rigid-body displacement check of the merged model, the modal

extraction run was immediately successful.

The problem was then restarted into Rigid Format 1 and the anti-symmetric enforced rigid body displacements were calculated. This was necessary since the symmetric and antisymmetric multipoint constraint sets were different, and resulted in different grid point singularity tables, and therefore different single point constraints. Subsequent to this check, the anti-symmetric model was restarted into Rigid Format 3 and 64 mode shapes in the frequency range 0 - 20 Hz were computed. Since antisymmetric modes are difficult to plot, only one plot, a fore and aft view at FR 106, was produced for each mode shape.

The running times, in ARUs (Application Resource Units, a billing unit for the CDC 6600 computer) for the symmetric and antisymmetric mode extraction runs were as follows:

	<u>Input/ Output ARUs</u>	<u>Central Processor ARUs</u>	<u>Total ARUs</u>
Symmetric model	11,690	18,518	26,674
Antisymmetric model	8,366	14,187	19,959

The ARUs for the major modules in the case of the symmetric model were as follows:

	<u>Input/ Output ARUs</u>	<u>Central Processor ARUs</u>
SMA 1	418	975
MCE2	147	888
SMP1	4,925	9,328
SMP2	1,959	3,975
READ	197	832
SDR1	824	1,428

The above table indicates that the most time-consuming operation is the condensation of stiffness and mass matrices.

Response to harmonic propeller excitation was calculated at 65 frequencies in the frequency range of 0 -20 Hz. This was done by restarting the checkpointed mode shape runs of Rigid Format 3 into Rigid Format 11.

Rigid Format 11 was altered with RF11/15 (Ref. 6) to suppress the calculation of single point constraint forces. All computed modes were used in the superposition and the same damping value was used for all modes. Responses for the following loadings were calculated:

- 1) The response of the symmetric model to the symmetric load components of the center propeller.
- 2) The response of the symmetric model to all load components of the wing propeller.
- 3) The response of the antisymmetric model to the antisymmetric load component of the center propeller.
- 4) The response of the antisymmetric model to all load components of the wing propeller.

In each of the above four cases, displacements were calculated and plotted at the propellers and several locations on the shafts, major machinery items, the bridge deck, and in the crew quarters. This resulted in 45 symmetric and 23 antisymmetric response curves. A typical response plot of displacement and phase is shown in figure 3.

The response calculation times for each of the four loading cases were 5536, 5458, 5006 and 4796 ARUs. Approximately 55 percent of the above ARUs were spent in recovering the dependent components of displacements.

CONCLUSIONS AND DESIRED ENHANCEMENTS

NASTRAN was successfully applied to the problem of propeller-induced ship vibration. All goals set at the beginning of the analysis were accomplished except those associated with damping. It was intended that the model dissipate energy through structural damping and viscous dashpots. These, however, could not be handled in an economic way, within the computational procedure described above, with Rigid Format 11 and the published RF ALTERS (Ref. 6).

NASTRAN's ability to handle the model without substructuring was especially advantageous. The aversion to substructuring resulted from experience with a previous ship vibration analysis, in which the logistics of the substructuring process were found to be time consuming. However, use of

the new MacNeal-Schwendler NASTRAN superelement capability, which simplifies the substructuring process considerably, should receive consideration in future ship vibration analyses.

As a result of this computational experience, the following program enhancements are suggested:

- 1) Coding a large number of single point constraints to eliminate singular displacement coordinates for a three-dimensional model with complex geometry and connectivity is a time-consuming and error-prone process. An option to instruct NASTRAN to remove all singular coordinates would be desirable. This need not result in blind trust in the program if all singularities removed by the program are printed.
- 2) The singularities in the GPSP table can be unreliable when displacement coordinates and grid point geometry are referred to a special coordinate system. This deficiency should be corrected.
- 3) An automatic grid resequencing option within NASTRAN would be desirable. This option would streamline the computational process.
- 4) Rigid Format 11 automatically recovers the dependent coordinate displacement responses. In the present analysis there was no interest in the responses of the dependent coordinates, but more computer time was spent in their recovery than in computing the response of the independent coordinates. It is suggested that an option be included in Rigid Format 11 to avoid this computation.
- 5) Upon restarting, changes in mass connectivity and material density on the MAT1 card result in the recomputation of the unconstrained stiffness matrix KGGX. In this analysis a considerable amount of computer time could have been saved if mass changes did not cause the recomputation of the stiffness matrix.
- 6) It would be desirable to have structural damping (i. e., proportional to displacement and independent of frequency) in Rigid Format 11. Although the User's Manual (Ref. 7) describes the TABDMP1 card as

"Structural Damping", it is used as viscous modal damping as indicated by the equations in Section 3.12.2 of the User's Manual. The published ALTER RF 11/4 (Ref. 6) inserts structural damping into Rigid Format 11. This ALTER worked successfully when tested in a cold start sample problem, but failed in the computational procedure described in the preceding section.

Many restart failures were experienced during this analysis. Some failures were due to acknowledged program errors. Others resulted from the use of multiple restarts in conjunction with published Rigid Format ALTERS. These restart failures demonstrated that in order for the structural dynamicist to compute effectively with NASTRAN, access to an analyst, knowledgeable in NASTRAN restart logic, is essential.

REFERENCES

1. McGoldrick, R. T., "Ship Vibration", David Taylor Model Basin Report 1451, December 1960.
2. Reed, F. E., "The Design of Ships to Avoid Propeller-Excited Vibration" SNAME, Vol. 79, 1971, pp. 244-296.
3. Restad, K., et al, "Investigation of Free and Forced Vibrations of an LNG Tanker with Overlapping Propeller Arrangement" SNAME, Vol. 81, 1973, pp. 307-347.
4. Adelman, H. M., et al, "An Isoparametric Quadrilateral Membrane Element for NASTRAN", in NASTRAN: Users' Experiences, NASA TM X-2639, Sept. 1972, pp. 315-336.
5. Everstine, G. C., "The BANDIT Computer Program for the Reduction of Matrix Bandwidth for NASTRAN", Naval Ship Research and Development Center, Report 3827, March 1972.
6. Joseph, G. A., MSC/NASTRAN Applications Manual, The MacNeal-Schwendler Corporation, November 1972.
7. McCormick, C. W., The NASTRAN Users' Manual, NASA SP-222(01), June 1972.

C-5

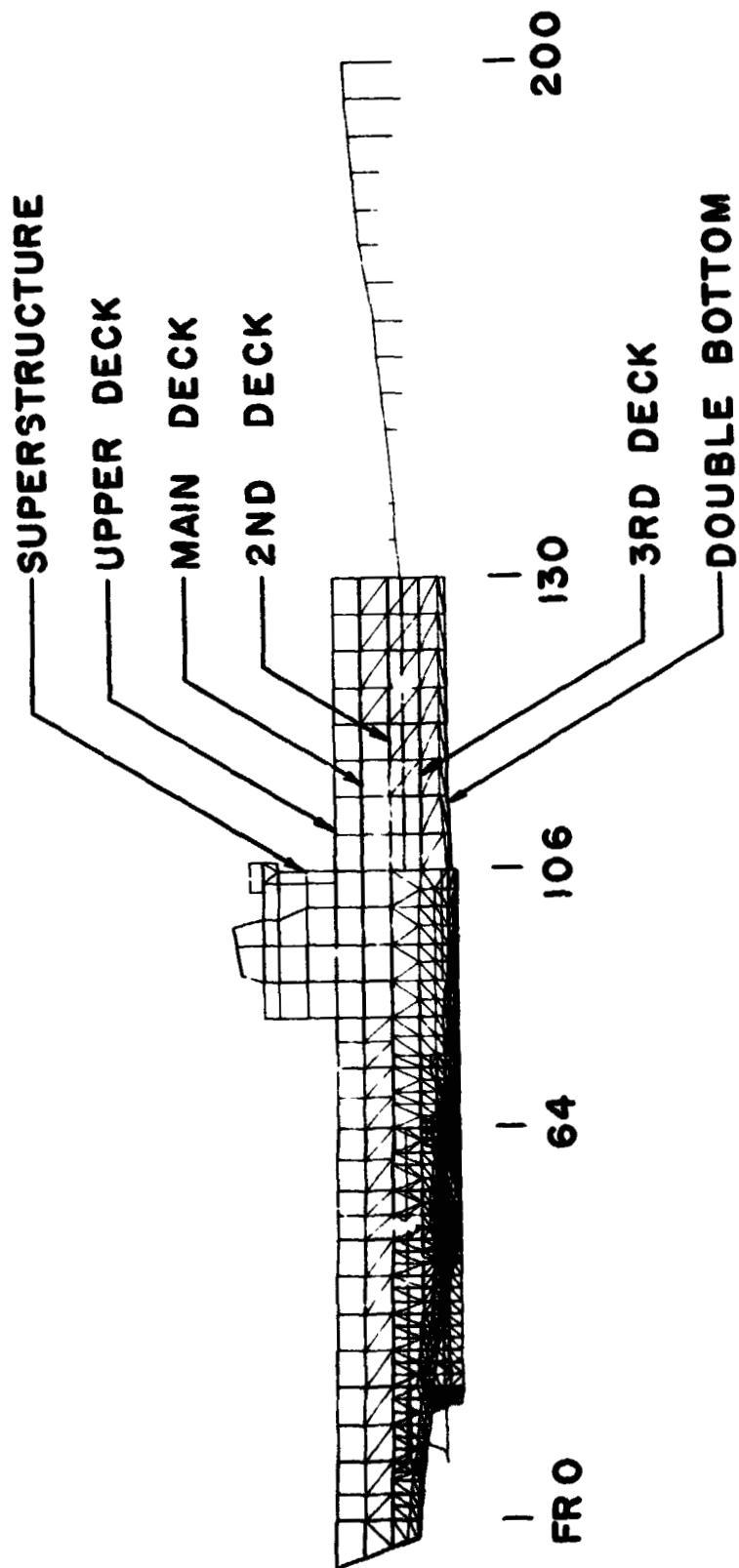


FIGURE 1. ELEVATION VIEW OF MODEL

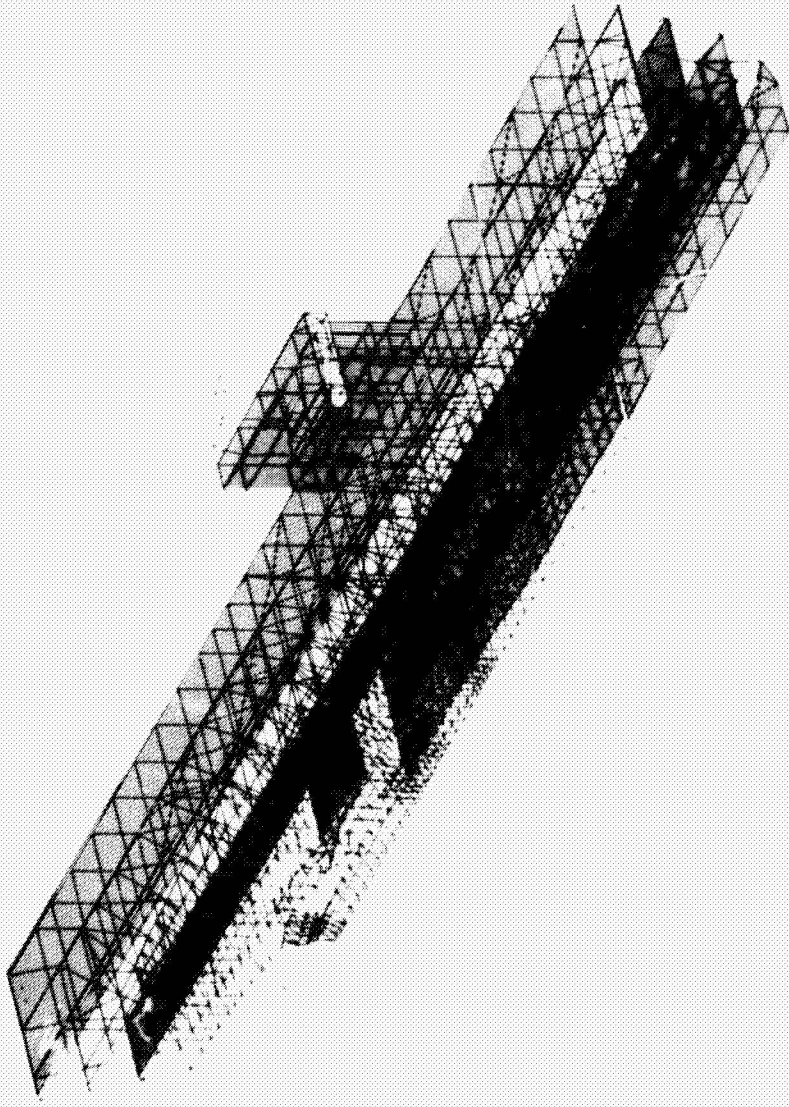


FIGURE 2. ROTATED VIEW OF MODEL – DECKS AND SUPERSTRUCTURE

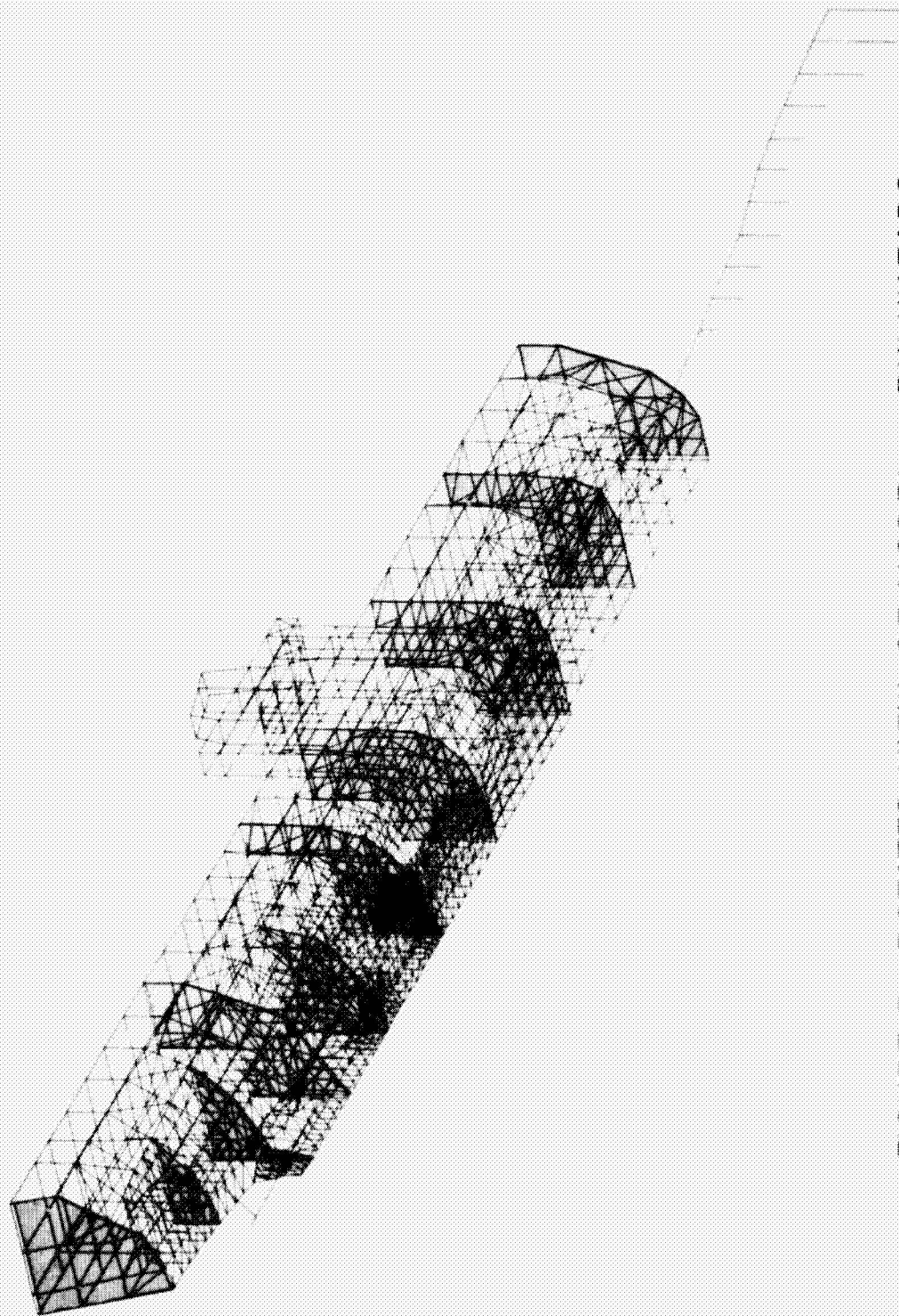
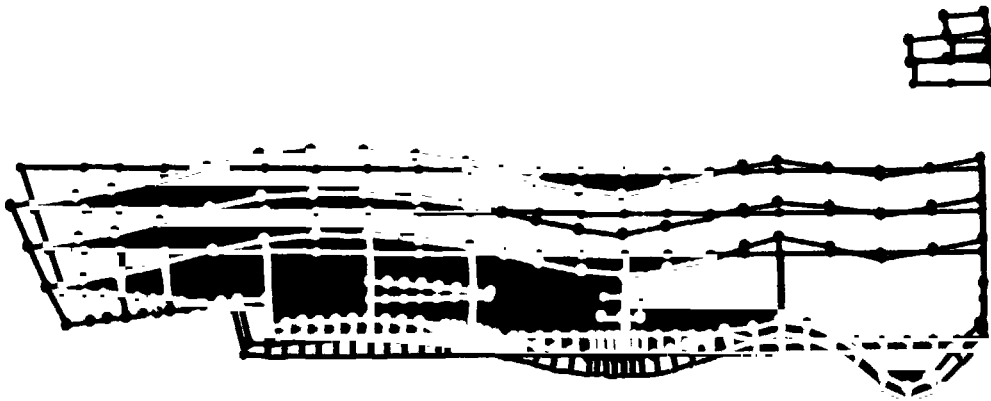


FIGURE 3. ROTATED VIEW OF MODEL -- BULKHEADS

00 8/ 8/74 NAE-SEP. - 2.00200700
CENTER PLANE AFT OF FR100

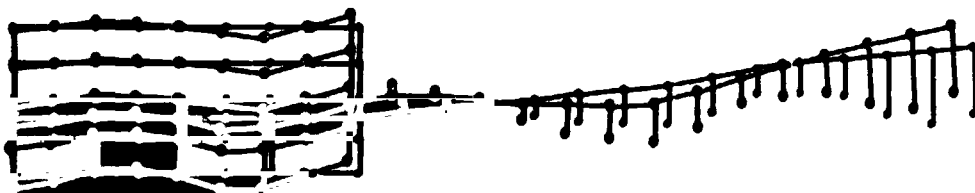


COMPLETE SHIP, SYMMETRIC CASE
NODAL DEFORM. SUBCASE 0 MODE 12 FREQ. 5.700480

FIGURE 4. AFTERBODY ELEVATION ON CENTER LINE,
SYMMETRIC MODE 12, 5.76 HZ.

100 8/ 8/74 NAE-SEP. - 11.0000100
CENTER PLANE FWD OF FR100

100

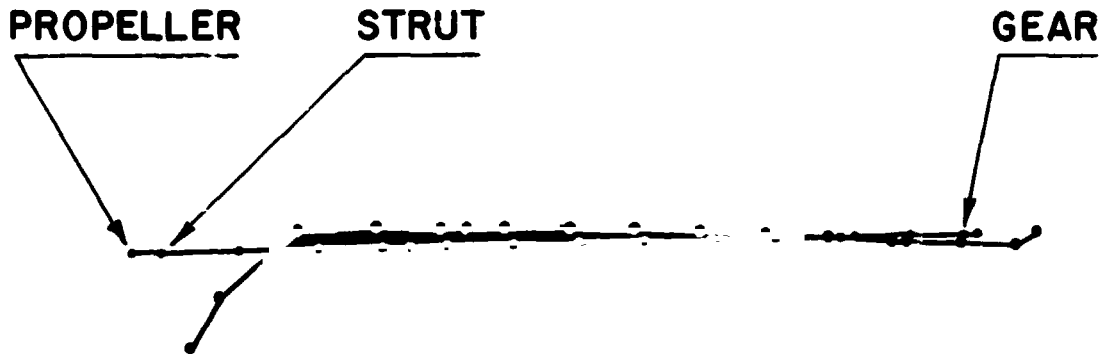


COMPLETE SHIP, SYMMETRIC CASE
NODAL DEFORM. SUBCASE 0 MODE 16 FREQ. 6.900175

FIGURE 5. FOREBODY ELEVATION ON CENTER LINE,
SYMMETRIC MODE 16, 6.90 HZ.

10 9/ 8/76 NAS-REP. - 11.000100
CENTER SHAFT ELEVATION

10

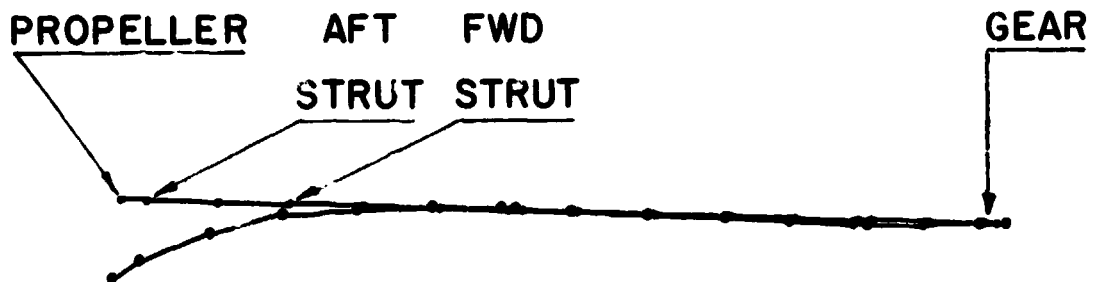


COMPLETE SHIP, SYMMETRIC CASE
RIGID DEFORM. SURFACE 0 MODE 10 FREQ. 6.900175

FIGURE 6. CENTER SHAFT ELEVATION,
SYMMETRIC MODE 16, 6.90 HZ.

9/ 8/76 NAS-REP. - 2.72000010
WING SHAFT PLAN VIEW

70



COMPLETE SHIP, SYMMETRIC CASE
RIGID DEFORM. SURFACE 0 MODE 30 FREQ. 10.96201

FIGURE 7. WING SHAFT PLAN VIEW, SYMMETRIC
MODE 30, 10.96 HZ.

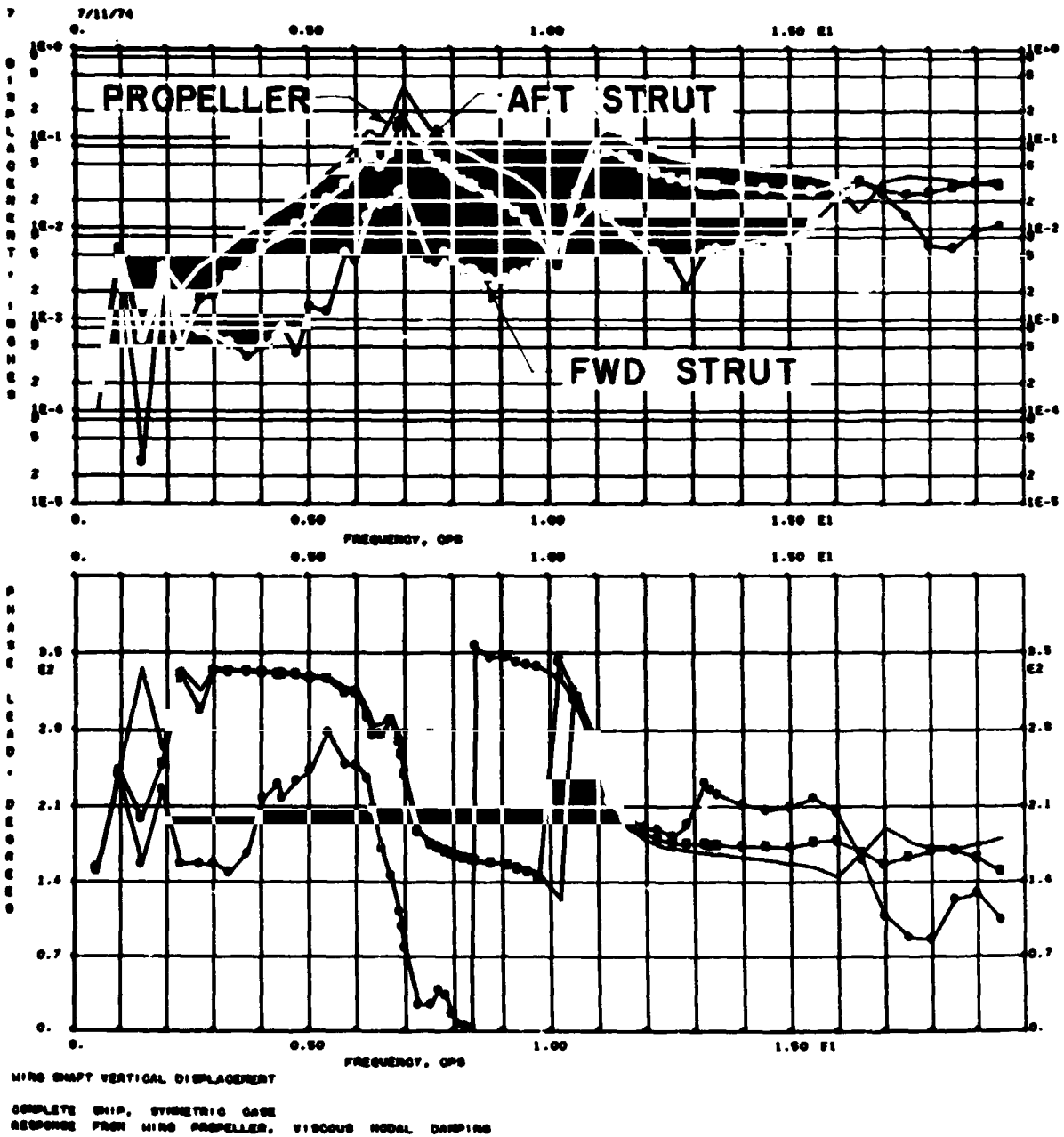


FIGURE 8. SYMMETRIC RESPONSE OF WING SHAFT TO WING PROPELLER EXCITATION

N75 31506

TRANSIENT ANALYSIS OF BODIES WITH
MOVING BOUNDARIES USING NASTRAN

John W. Frye

Naval Underwater Systems Center

21

SUMMARY

A scheme is presented which allows the modeling of a moving boundary with NASTRAN NOLIN cards. Various aspects and limitations of the approach are explained. Recommendations are given as to the procedure to be used in implementing the method.

INTRODUCTION

Situations occasionally arise when the boundary conditions of a theoretical model change as a result of the response of the model. The case under consideration is that where the boundaries of the model move as a function of rigid body displacement. The problem which motivated the development of the technique which we are presenting is that of a shaft under both axial and transverse loading moving between two stationary bearings. Figure 1 is a diagram of such a shaft.

The reactions at the bearings are dependent on the applied loadings and the inertial forces generated by transverse motions of the shaft. The applied loadings are known beforehand. The inertial loadings of the shaft are unknown since the transverse motion of the shaft is an unknown. Therefore, the reactions of the bearings cannot be predetermined before the start of the analysis.

Constraints cannot be directly applied to the model to account for the bearings since such constraints would be useful for only a short time of the analysis covering a small axial displacement of the shaft. It is possible to solve the problem by dividing the total time of the analysis up into many small time increments each with a different constraint condition. The idea here would be to start the analysis with the bearings in one position; run the problem for a short time; stop the analysis; change the constraints; and restart the problem with initial conditions equal to the state of the model at the end of the first time segment. This process is repeated until the shaft has moved as far as desired. This technique, while being possible, is awkward from the standpoint of data handling, the number of runs required, and the total number of days needed to obtain an answer.

SYMBOLS

a distance between grid points
 F_1, F_2 nonlinear loads at grid point accounting for moving boundary

377

PRECEDING PAGE BLANK NOT FILMED

$F_x(t), F_y(t)$	applied time dependent axial and transverse loads
i	index number of grid point
K	maximum slope of nonlinear loading curve
K_B	stiffness of bearing
s	scale factor
u_x, u_y	grid point axial and transverse displacements
x, y	axial and transverse coordinates of model
ξ	integration variable in axial direction

DISCUSSION

The approach which accounts for the moving bearings treated the bearings as stiff springs which moved along the model of the shaft as the shaft moved with respect to the bearings. These springs were fabricated artificially by the use of the nonlinear load option in NASTRAN. Each grid point along the shaft model over which the bearings could pass had two nonlinear loadings applied to it for each bearing. Figure 2 shows a diagram of these loadings for a typical grid point on the shaft model. For simplicity we consider the case of only one bearing.

The force F_2 is shown as a positive ramp function with a slope equal to the bearing stiffness and is a function of the displacement u_x of the shaft. The second force F_1 is shown as a negative ramp function with a slope equal to the bearing stiffness and is a function of the shaft displacement u_x added to the transverse deflection of the grid point u_y . Note here that since u_y is several orders of magnitude smaller than u_x , the magnitude of $u_x + u_y$ is mainly determined by u_x alone. Both F_1 and F_2 are zero until u_x is greater than x_{i-1} , the distance from the bearing at the start of motion to grid point $i-1$. F_1 and F_2 are equal and opposite and, hence, negate each other when u_x is greater than x_{i+1} , the distance from the bearing at the start of the motion grid point $i+1$. Therefore, the loadings F_1 and F_2 add to zero at all times except those times when the bearing is between grid points $i-1$ and $i+1$.

Now consider a case when the bearing is between grid points $i-1$ and $i+1$. Figure 3 illustrates such a condition.

$$\text{NET LOAD} = F_1 + F_2 = -K(u_x + u_y - x_{i-1}) + K(u_x - x_{i-1})$$

$$\text{NET LOAD} = -Ku_y$$

As can be seen, the net load on the grid point i is equal to $-Ku_y$ which is a restoring force proportional to the bearing spring constant and the lateral deflection of the shaft at i . Thus, the combination of two nonlinear loadings at i results in simulating a bearing spring which turns itself on when the bearing is in the vicinity of grid point i and turns itself off when the bearing is outside the vicinity of grid point i .

It is possible to allow the spring constant of the bearing to vary as a function of its distance from a grid point. There is some advantage to this since when a bearing is between two grid points, its stiffness ought to be shared in some way by the two grid points. See figure 4.

We have used the proportional sharing scheme where the stiffness of the bearing is distributed in proportion to that of a load shared between two ends of a pinned ended beam. To establish the loading curve for this kind of stiffness sharing scheme, notice that

$$(1) \quad dF = Kd\xi = \left(K_B\right) \frac{\xi}{a} d\xi \quad 0 < \xi < a$$

$$(2) \quad dF = Kd\xi = \frac{K_B(2a - \xi)}{a} d\xi \quad a < \xi < 2a$$

From (1) noting $F = 0$ at $\xi = 0$

$$(3) \quad F = \int_0^x \left(K_B\right) \frac{\xi}{a} d\xi = \frac{K_B \xi^2}{2a} \Big|_0^x = \frac{K_B x^2}{2a} \quad 0 < x < a$$

$$\frac{\partial F}{\partial x} = \frac{K_B x}{a} \quad \frac{\partial F}{\partial x} = 0 \quad \text{at } x = 0$$

$$\frac{\partial F}{\partial x} = K_B \quad \text{at } x = a$$

$$F = \frac{K_B a}{2} \quad \text{at } x = a$$

From (2) noting $F = \frac{K_B a}{2}$ at $x = a$

$$F = \int_a^x \frac{K_B(2a - \xi)}{a} d\xi + \frac{K_B a}{2}$$

$$F = \frac{-K_B(2a - \xi)^2}{2a} \Big|_a^x + \frac{K_B a}{2} = K_B a - \frac{K_B(2a - x)^2}{2a}$$

$$(4) \quad F = K_B \left[a - \frac{(2a - x)^2}{2a} \right] \quad a < x < 2a$$

$$\frac{\partial F}{\partial x} = \frac{K_B(2a - x)}{a} \quad \frac{\partial F}{\partial x} = K_B \quad \text{at } x = a$$

$$\frac{\partial F}{\partial x} = 0 \quad \text{at } x = 2a$$

$$F = \frac{K_B a}{2} \quad \text{at } x = a$$

Equations (3) and (4) establish the shape of the loading functions for the proportional stiffness loading scheme. Other stiffness sharing schemes could be devised and their loading curves easily arrived at in a similar manner to that shown here. Figure 4 shows a plot of the nonlinear load function for the proportional stiffness sharing scheme we use[†].

The scheme depends completely on accurately determining the difference between the quantities $K(u_x + u_y)$ and Ku_x . Theoretically, this presents no difficulty. If the value of u_x is six or seven orders of magnitude larger than u_y , a numerical difficulty arises since a computer may only work to eight significant figures using single precision arithmetic. Even if double precision arithmetic is used, there will come a point where large values of u_x start to degrade the numerical accuracy of the differencing operation $K(u_x + u_y) - Ku_x$.

There is a way around this numerical difficulty. The objective of the differencing operation is to obtain the quantity Ku_y . If the u_x quantity is multiplied by a scalar constant the differencing operation remains unchanged.

$$K(su_x + u_y) - Ksu_x = Ku_y$$

Here u_x was multiplied by the scalar s . To remove the numerical difficulty, the scalar constant is assigned such that u_x is no more than three or four orders of magnitude greater than values of u_y which can possibly be of interest. su_x cannot be too small or else the larger values of u_y will start to affect the first few significant figures of the quantity $su_x + u_y$. This would result in inaccuracies in the determination of the spring constant since the spring constant should be a function of u_x only and not $su_x + u_y$. Thus, some judgment must be used in the determination of s ; that is to say it cannot be made some very small number without considering the values which u_y are expected to be in the neighborhood of a bearing.

When using the scalar multiplier the nonlinear loading diagram changes such that the nonlinear loads start to act at sx_{i-1} rather than at s_{i-1} , since the lock up function or independent variable is su_x rather than u_x . Figure 5 shows the forcing function set up using the scalar multiplier.

The equation for the nonlinear load as a function of su_x or $su_x + u_y$ now becomes

$$\frac{dF}{ds\xi} = K = K_B \frac{s\xi}{sa} \quad 0 < \xi < a$$

$$dF = sK \frac{\xi}{a} d\xi$$

$$F = \frac{sK_B x^2}{2a} \quad 0 < x < a$$

$$F = sK_B \left[a - \frac{(2a - x)^2}{2a} \right] \quad a < x < 2a$$

Differentiating with respect to sx yields

$$\frac{dF}{dsx} = \frac{d}{dsx} \left(\frac{K_B (s^2 x^2)}{2sa} \right) = \frac{2K_B sx}{2sa} = \frac{K_B x}{a} \quad 0 < x < a$$

$$\begin{aligned} \frac{dF}{dsx} &= \frac{dK_B}{dsx} \left[sa - \frac{(2as - sx)^2}{2sa} \right] \\ &= K_B \left[2 \frac{(2as - sx)}{2sa} \right] = K_B \frac{(2a - x)}{a} \quad a < x < 2a \end{aligned}$$

The slope of the nonlinear force curve with respect to the scaled coordinate remains the same as the slope of the force curve using an unscaled coordinate.

Figure 6 shows a typical result for the transverse displacement of a grid point in the analysis of a shaft moving between two bearings. The results show the expected suppression of transverse displacement while the bearings are in the vicinity of the grid point.

The application of nonlinear loads raises questions as to the numerical stability of the solution. The numerical stability will depend on the time step used and the maximum slope of the nonlinear force curves. If the moving boundary is a rigid one, some compromise must be made on the stiffness of the moving boundary. An infinite stiffness will always result in an unstable condition. In our case, we ran several short problems with our model using what we considered as a reasonable time step. We reduced the slope of the nonlinear load curves

until we obtained a stable solution and then reduced the time step until the solution appeared reasonably converged. This trial and error approach may not always work out, but it did in our case. We were able to arrive at an acceptable time step and loading slope within a few days. It is best when setting up the tables for the loading curves to set the maximum slope in the table to unity and to use the NOLIN cards to scale the slope. Thus, the maximum slope values will appear directly on the NOLIN cards. The tables are tedious to construct as there is a table for each grid point on the model over which the moving boundary must pass, whereas it is relatively easy to change the slope values on the NOLIN cards.

If the time steps are large, the slope of the nonlinear load curve must be very small in order to give good convergence and numerical stability. In such a case, the moving boundary cannot be accurately modeled using this method. This is unfortunate but as far as we can see, there is no alternative for solving the problems of convergence and stability other than to reduce the time step or the loading slope.

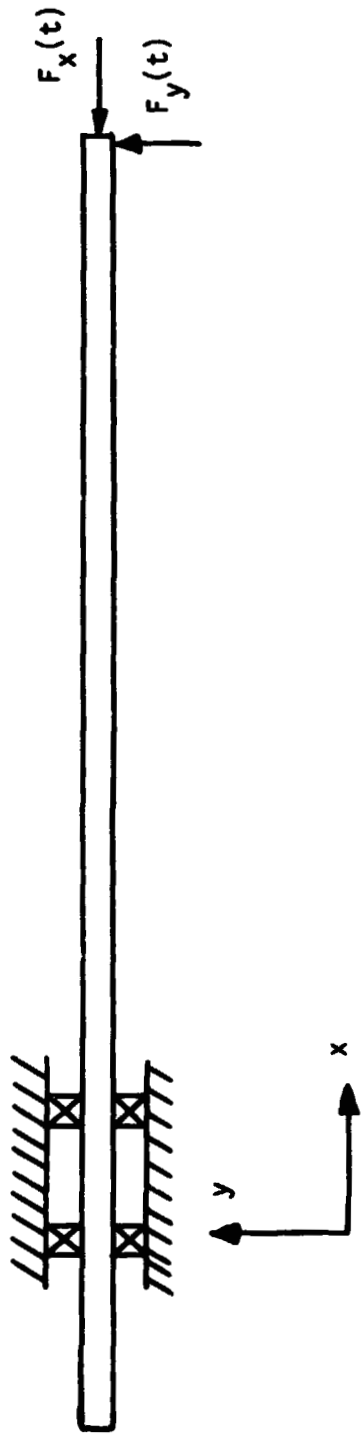


FIGURE 1. - SHAFT UNDER COMBINED TRANSVERSE AND RADIAL LOADING FREE TO SLIDE BETWEEN TWO BEARINGS

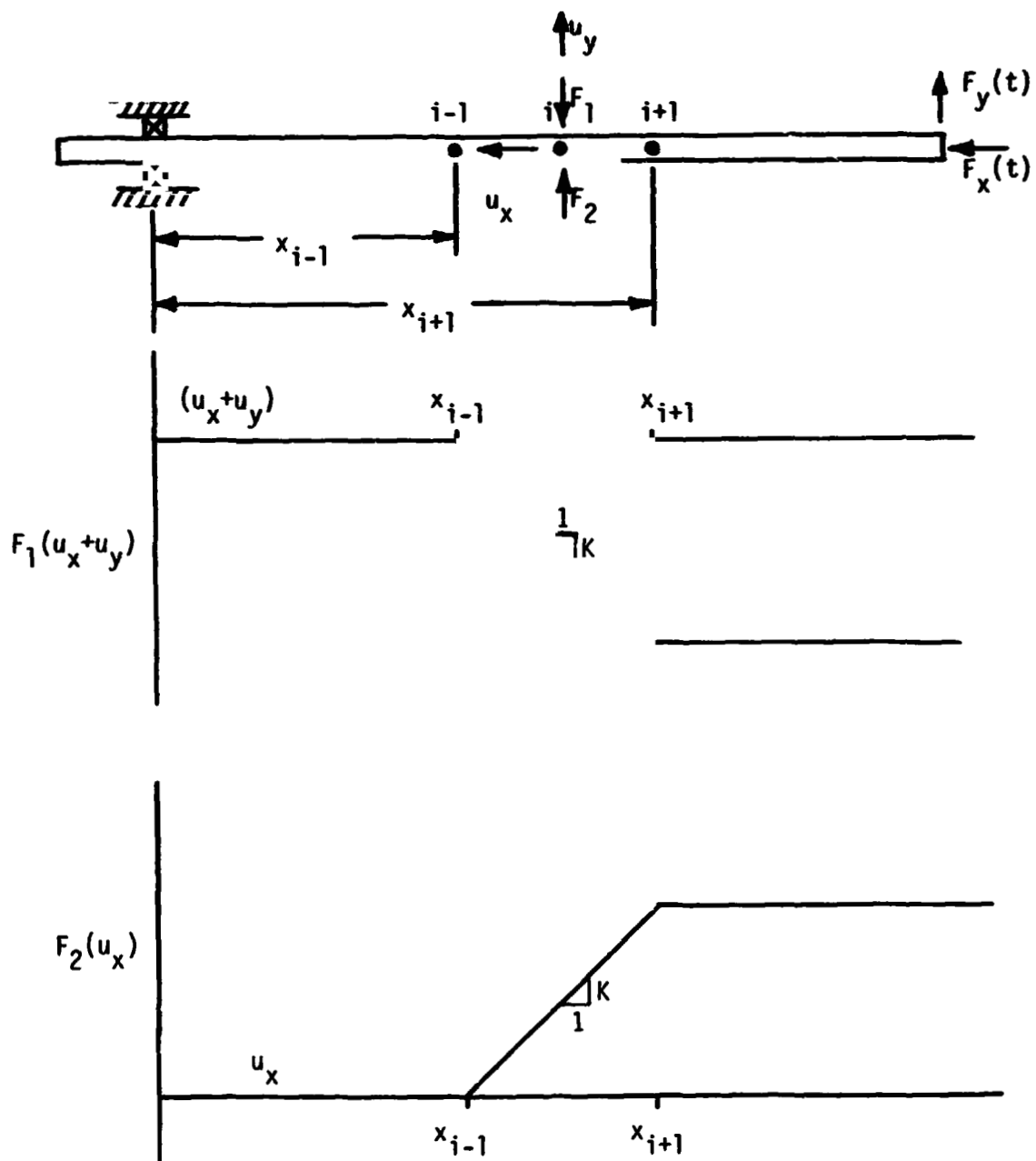
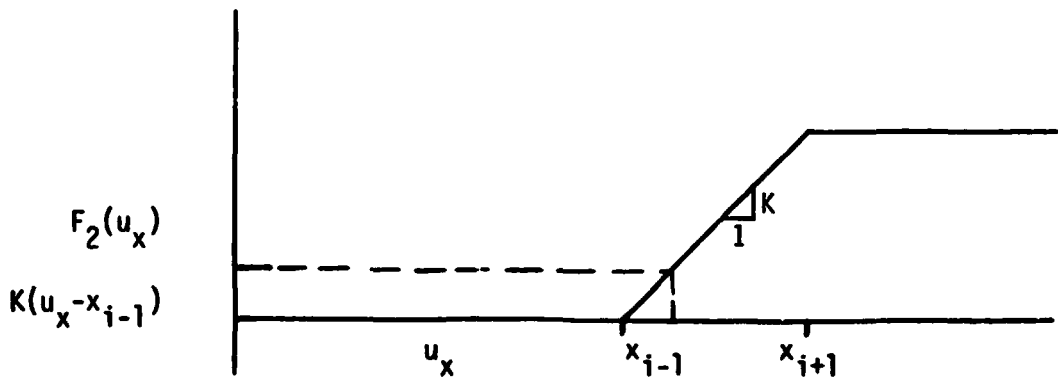
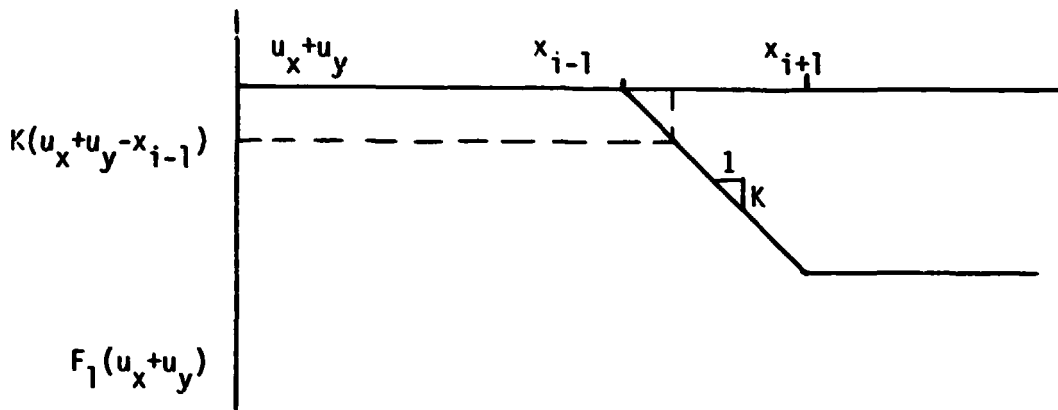
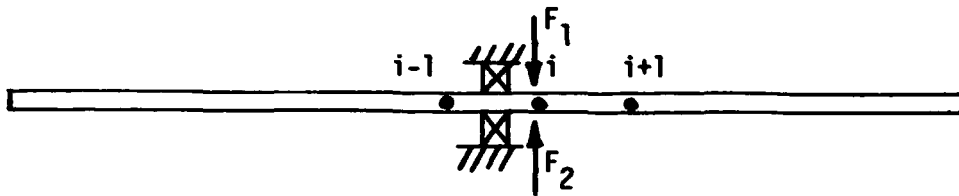
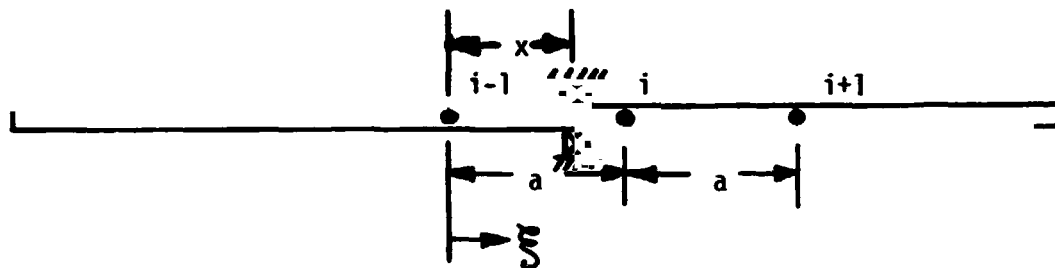


FIGURE 2. - NONLINEAR LOADING DIAGRAMS



$$\text{Net Load} = F_1 + F_2 = -Ks(u_x + u_y - x_{i-1}) + Ks(u_x - x_{i-1}) = -Ksu_y$$

FIGURE 3. - NONLINEAR LOADS WITH BEARING NEAR GRID POINT



$$K_{i-1} = K \frac{(a-x)}{a} \quad ; \quad K_i = K \frac{x}{a} \quad 0 < x < a$$

$$K_i = K \frac{(2a-x)}{a} \quad ; \quad K_{i+1} = K \frac{(x-a)}{a} \quad a < x < 2a$$

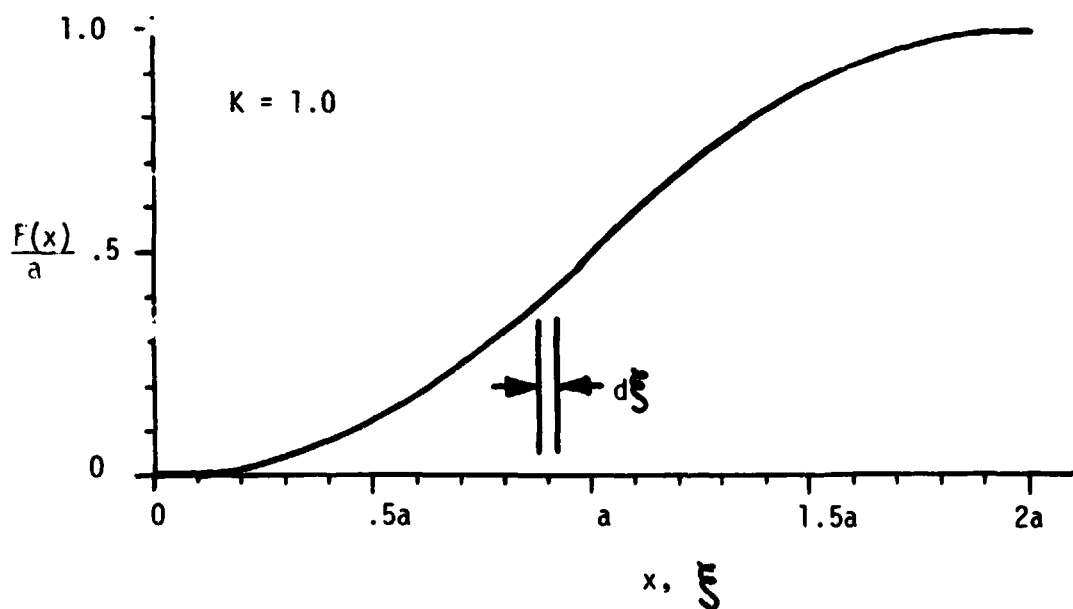


FIGURE 4. - PROPORTIONAL STIFFNESS SHARING SCHEME

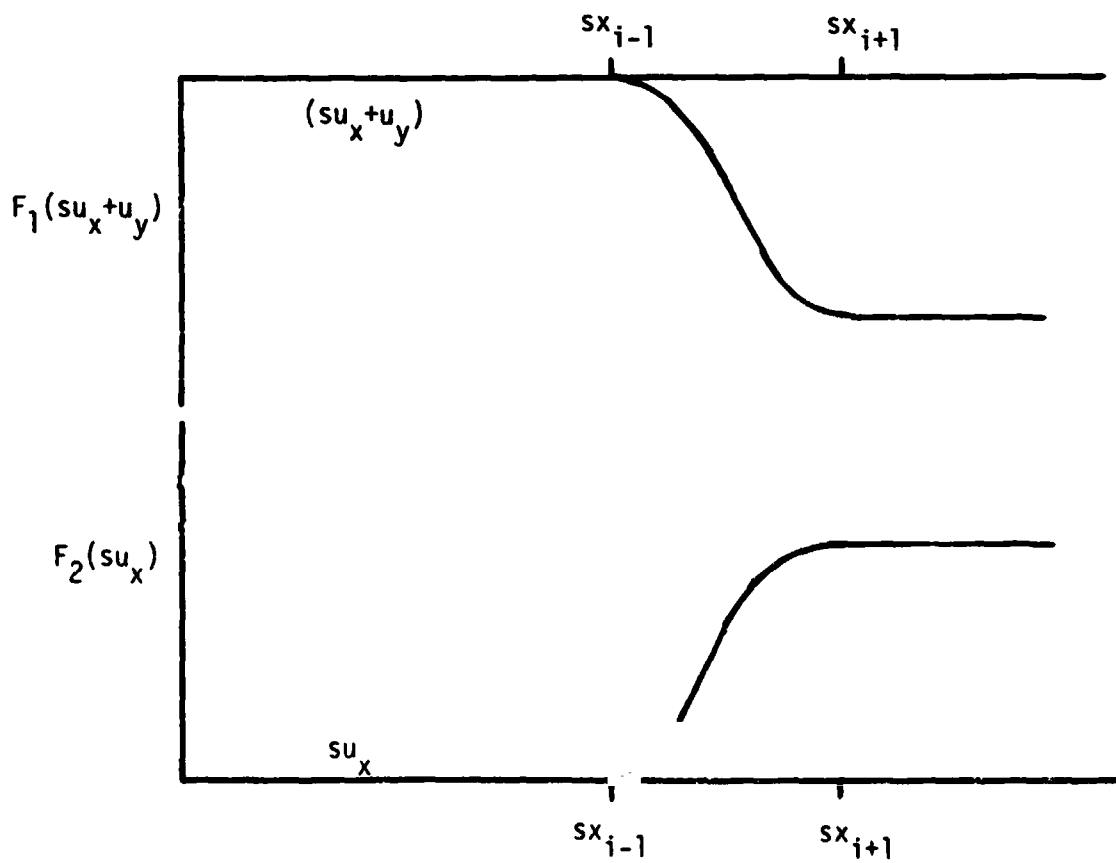
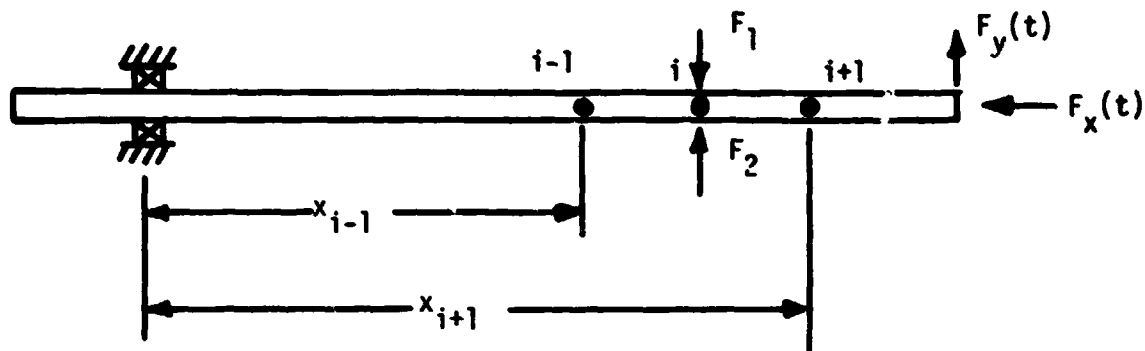


FIGURE 5. - ADDITION OF SCALE FACTOR s TO ELIMINATE ROUND OFF ERROR

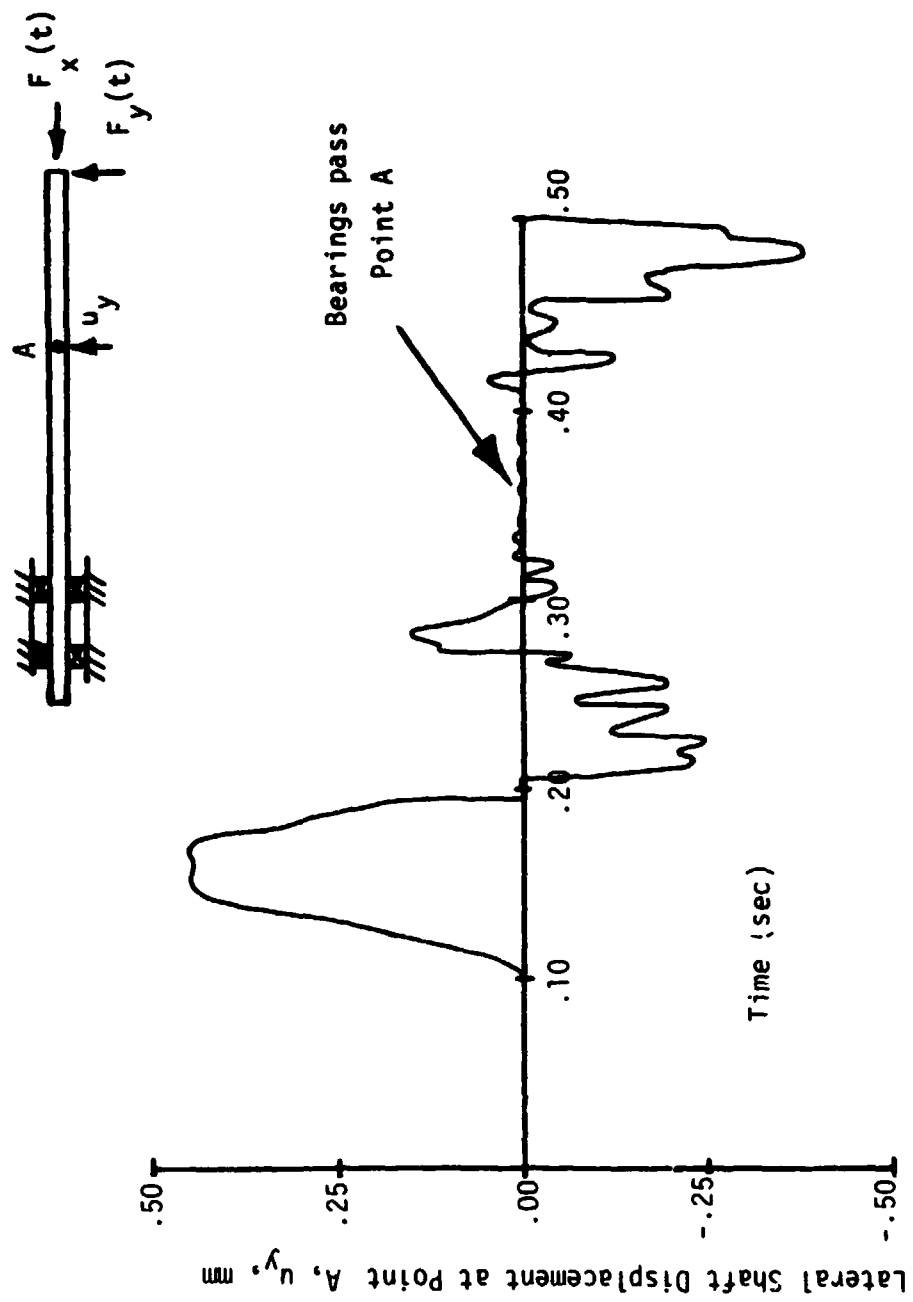


FIGURE 6. - TYPICAL RESULTS FOR LATERAL DISPLACEMENTS OF POINT ON SHAFT SLIDING BETWEEN TWO BEARINGS

N75 31507

APPLICATION OF NASTRAN IN NONLINEAR ANALYSIS
OF A CARTRIDGE CASE NECK SEPARATION MALFUNCTION

Jackson C.S. Yang
University of Maryland

and

Diana L. Frederick
U.S. Army, Frankford Arsenal

22

SUMMARY

The problem of case neck separation malfunction in the field of ammunition structural analysis is investigated. The axi-symmetric solid of revolution RING element was utilized in the manual piece-wise linear analysis to obtain the expansion of the wall of the cartridge case and barrel chamber by the pressure of propellant gases and the stresses in the structure. The analysis included the varying material properties along the wall of the case and the chamber. Additional instructions were provided to change the element material ID's without recomputing the entire stiffness matrix.

INTRODUCTION

A characteristic problem in the field of ammunition structural analysis is the interaction between the cartridge case and gun barrel chamber. Specifically of interest is a case neck separation (CNS) malfunction where rupture occurs at the neck-shoulder section, see Figure 1. CNS presents serious problems in double ended linkless feed systems, i.e., system in which the fired cases and released rounds are returned to the storage drum. Round control of cases with partially or completely separated necks is lost by the hand-off sprockets, resulting in a system jam. In systems where the fired cases are dumped overboard, CNS presents no problems unless the separated case neck remains in the gun barrel chamber, which can result in a jam when a subsequent round is fed into the same barrel.

When a round is fired, the powder pressure builds up and the sidewall expands elastically to its yield point and then completes its expansion plastically. Although the sidewall may or may not enter the plastic range before taking up the initial clearance between the case and the chamber, it will be completely plastic when the pressure reaches its maximum value. At this instant of maximum pressure, both the case outside diameter and chamber inside diameter will have expanded together to a common maximum value. Here the cartridge case sidewall will be acted upon on the inside by the internal pressure and on the outside by the chamber-cartridge case interface friction and pressure. The chamber wall will be acted upon by equal and opposite friction and pressure. Knowing the radial loads on the cartridge case at this instant of maximum pressure, the associated state of stress in the sidewall can be determined for various assumed values of axial (longitudinal) stress in the sidewall. This is done by applying the Von Mises or the Tresca law of yielding together with its associated flow rule.

In the problem of expansion of the wall of cartridge case and barrel chamber by the pressure of propellant gases and the stress analysis of the structure, it is desired that the axi-symmetric solid of revolution RING element be utilized. This element offers both simplicity and accuracy over other elements. Since the piece-wise linear analysis option of NASTRAN has not been developed for this element, a program was initiated to perform the piece-wise linear analysis manually (see Reference 1). A summary flow diagram is given in Figure 2.

INTERNALLY PRESSURIZED CARTRIDGE CASE

We now proceed to investigate the design of the cartridge case neck and barrel chamber interface section of a high pressure ballistic system. Figure 3 depicts the finite elements used in synthesizing the NASTRAN model of part of the cartridge case, barrel chamber and projectile. The case and chamber are assumed to be free at one end and clamped at the other end while the projectile was assumed to be free at both ends. Rigid Format 1 and trapezoidal RING elements were used. The overall model had 254 elements, yielding a total of 654 degrees of freedom. Bi-linear stress-strain curves are selected for the elastic-plastic materials which varied along the cartridge case. MPC was used at the interfaces of the chamber-case and case-projectile. Displacement and force conditions for skewed boundary are imposed on some part of the structure whose boundary surface is not oriented with respect to the global axis system. Internal pressure is applied in increments. The incremental displacements and stresses were cataloged and filed after each run. These were then added to the previous results to obtain the total displacements and stresses. After each run the stresses were tested with the Von Mises Condition. The elastic material properties of those elements that satisfied the yield criterion are changed into plastic material properties.

In order to form a manual piece-wise linear analysis and to change the element material ID's without recomputing the entire stiffness matrix, the following changes are needed in the NASTRAN DMAP instructions.

To use files rather than tapes for data storage, the following card must be inserted before the Executive Control Deck, see Reference 2.

```
NASTRAN SYSTEM_(45) __ = _ 1920, _ CONFIG = 6$
```

For Run 1 the following cards are inserted in the Executive Control Deck in order to change the rigid format.

```
ALTER 32
OUTPUT1 ,,,,//C,N,-1/C,N,2 $
OUTPUT1 KGGX,,,,//C,N,0/C,N,2 $
ALTER - 110
OUTPUT 1, __, ,,,,//C,N,-1/C,N,0/C,N,USERPLA __ $
OUTPUT 1 __ __ UGVV,,,,//C,N,0/C,N,0/C,N,USERPLA __ $
END ALTER
```

For Run 2

```
ALTER 31
PARAM //C,N,NOP/V,N,IM1=-1 $
INPUTT1 /,,,/C,N,-1/C,N,3 $
INPUTT1 /KGGXX,,,/C,N,0/C,N,3 $
CHKPNT KGGXX $
ELCHANG MPT,ECPT/ECPT1,ECPT2/V,N,NOCHAN $
SAVE NOCHAN $
EQUIV KGGXX,KGGX/NOCHAN $
COND YANG1,NOCHAN $
SMA1 CSTM,MPT,ECPT1,GPCT,DIT/KGGX1,,GPST1/V,N,NOGENL/V,N,NOK4GG/V,
Y,OPTION $
SMA1 CSTM,MPT,ECPT2,GPCT,DIT/KGGX2,,GPST2/V,N,NOGENL/V,N,NOK4GG/V,
Y,OPTION $
ADD5 KGGX1,KGGX2,KGGXX, /KGGXXX/C,Y,ALPHA=(1.,0.)/C,
Y,BETA=(-1.,0.)/C,Y,GAMMA=(1.,0.) $
CHKPNT KGGXXX $
EQUIV KGGXXX,KGGX/IM1 $
JUMP YANG1 $
MATPRN KGGXXX,,,// $
ALTER 32
LABEL YANG1 $
OUTPUT1 ,,,,//C,N,-1/C,N,2 $
OUTPUT1 KGGX,,,//C,N,0/C,N,2 $
ALTER 110
INPUTT1 /UGPREV,,,/C,N,-1/C,N,1/C,N,USERPLA _ $
ADD _ UGPREV, UGV/UGVV _ $
OUTPUT 1, _ ,,,,//C,N,-1/C,N,0/C,N,USERPLB _ $
OUTPUT 1 _ _ UGVV,,,//C,N,0/C,N,0/C,N,USERPLB _ _ $
ALTER 121
SDR2 _ CASE CC, SDTM, MPT, DIT, EOEXIN, SIL, GPTT, EDT, BGPDT, PGG, OB, UGVV,
EST,/
_ OPG2, OOG2, OUGV2, OES2, OEF2,/C,N,STATICS _ $
OFP _ OUGV2, OPG2, OOG2, DEF2, OES2, //V,N,CARDNO/V,Y,OPTION _ $
END ALTER
```

For Run 3, USERPLA is changed to USERPLB and USERPLB is changed to USERPLC.

Alters 31 and 32 are used in conjunction with CHANGEL cards for changing element material ID's without recomputing the entire stiffness matrix, along with output tape INP2 and input tape INP3.

Alters 110 are used to perform a manual piece-wise linear analysis, along with output tape INPT and input tape INP1. Alters 121 allow the incremental stresses, forces, and displacements to be printed out.

The following control cards are needed:

Run 1

```
Request, INPT, *PF.  
Request, INP2, *PF.  
Request, IDLF, *PF.  
Rewind, INPT, INP2, IDLF.  
NASTRAN(, IDLF)ATTACH.  
Catalog, INPT, INPT, ID=FREDERICK.  
Catalog, IDLF, IDLF, ID=FREDERICK.  
Catalog, INP2, INP2, ID=FREDERICK.
```

Run 2

```
Request, INPT, *PF.  
Request, INP2 *PF.  
Request, IDLF, *PF.  
Rewind, INPT, INP2, IDLF  
Attach, INP3, INP2, ID=FREDERICK.  
Attach, INP1, INPT, ID=FREDERICK.  
Rewind, INP3, INP1.  
NASTRAN(, IDLF)ATTACH.
```

Output data is saved on the IDLF file which is the punch file by using the options available in the Case Control Deck, see Reference 1.

```
Example: DISP(PRINT,PUNCH) = ALL  
         STRESS(PRINT,PUNCH) = ALL
```

In order to have a realistic model after each run the elements actually change position according to their displacement. Some Fortran routines were developed to incorporate these changes in the model.

Program WIDEF initially converts GRID data to 16 column fields in order to allow the displacement values to be utilized regardless of how small the numeric value is. (Run once.)

Program GEOMX takes the displacement values from the IDLF file and adds them to the GRID values from the file created by WIDEF. The new data input file is the new NASTRAN run. GEOMX allows the user to change the LOAD card, the material properties by the use of CHANGE card (explained below) and insert any other new data cards to the NASTRAN deck.

CHANGE Cards

```
CHANGE ELID OMID ELID OMID ELID OMID ELID OMID +A  
+A      ELID OMID ..... ENDT
```

ELID is an element ID number.

OMID is the old material ID for that element. The new material ID must be placed on the element connection card.

ENDT is required.

If no CHANGEL cards exist, the previously computed stiffness matrix (from INP3) will be used. All material cards referenced on property cards, connection cards, and CHANGEL cards must be included. If restarting after DMAP number 33, do not include any alters, INP2 or INP3 tapes. These changes work for all elements with material. ID's for elements with more than one material ID, just the first one indicated on the property card can be changed with this method.

In addition, two other Fortran programs take the output from IDLF. The first program sums up the individual normal stresses (R, θ ,Z) and shear stresses (ZX) and applies the Von Mises Law of Yielding together with its associated flow rule. The second Fortran routine sums up the displacements (R,Z). Thus at each step while performing a piece-wise linear analysis the data is organized results are easily studied.

ACKNOWLEDGEMENT

The authors would like to thank Mr. J. McKee and Mr. M.M. Hurwitz of the Naval Ship Research and Development Center for their helpful assistance and suggestions.

REFERENCES

1. "Application of Nonlinear Analysis to NASTRAN Using Ring Elements Including Aspect Ratio Effect," J.C.S. Yang and D. Frederick, Frankford Arsenal Technical Note TN-1178, August 1973.
2. The NASTRAN User's Manual, NASA SP-222, September 1970, Section 3.

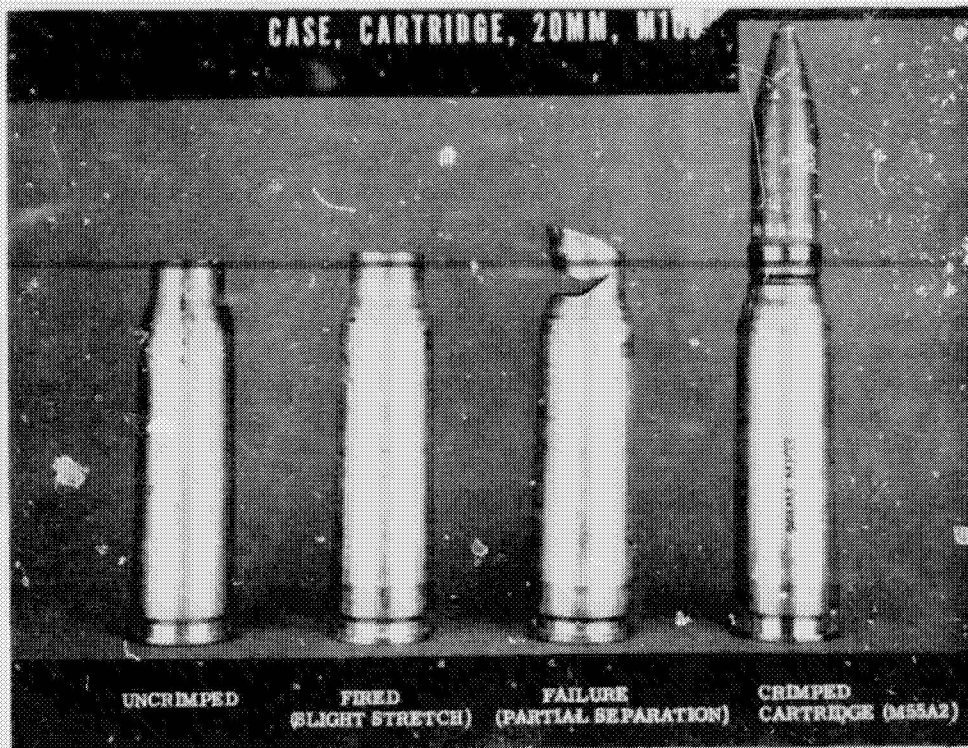


Figure 1.- Case neck separation.

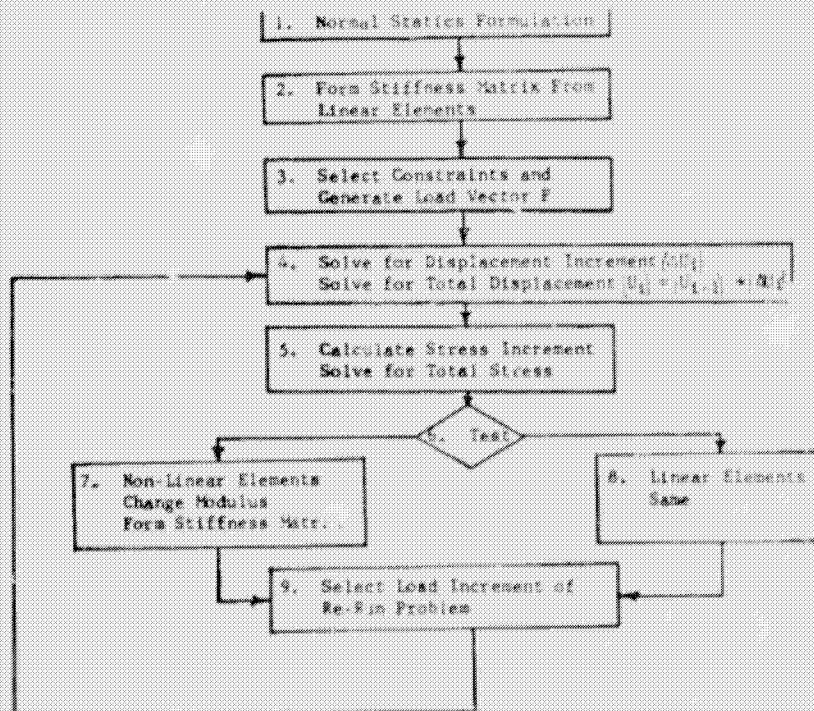


Figure 2.- Manual piece-wise linear flow diagram.

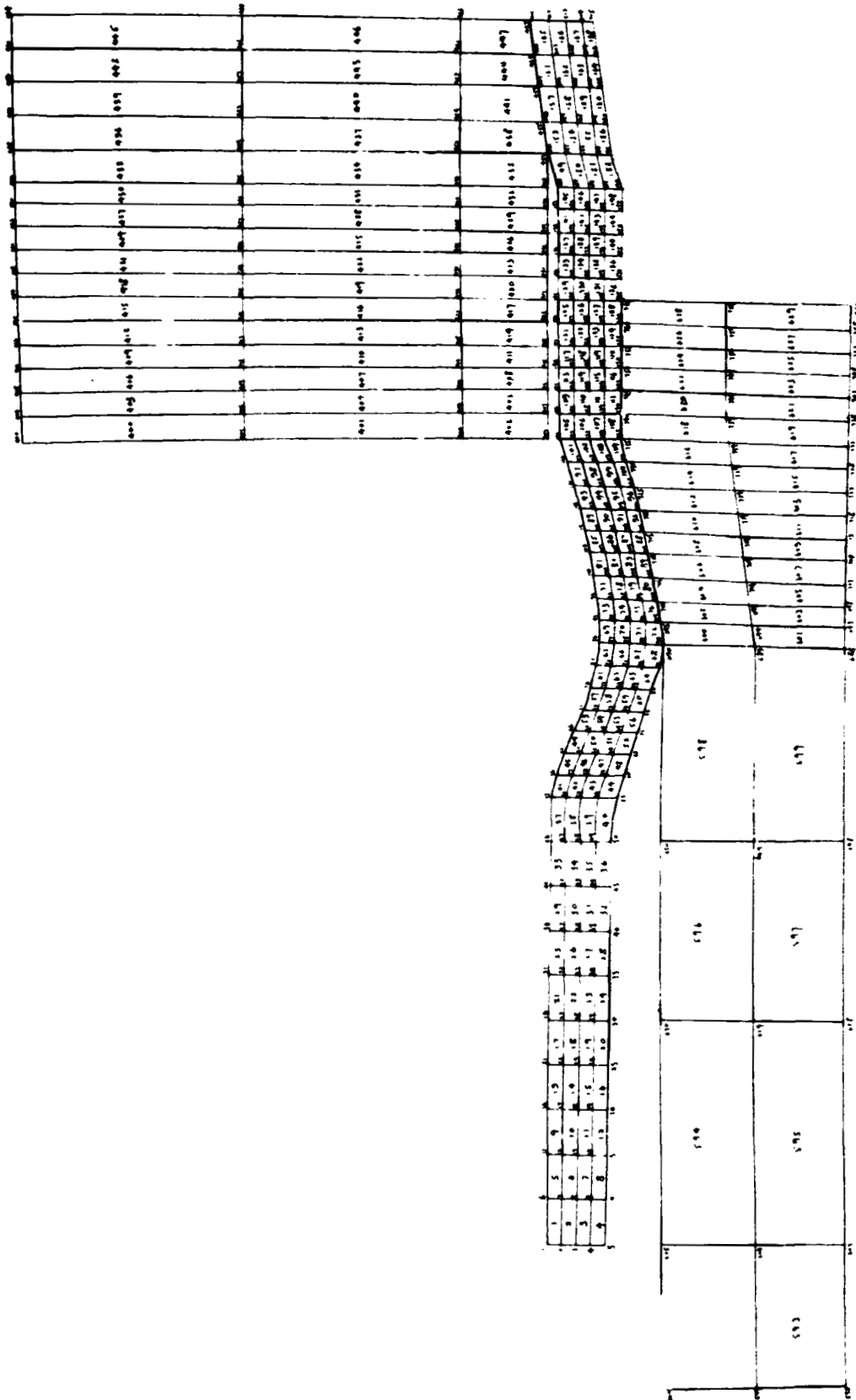


Figure 3.- NASTRAN model of internally pressurized case, chamber and projectile.

N75 31508

NONLINEAR SEISMIC ANALYSIS OF A REACTOR STRUCTURE
WITH IMPACT BETWEEN CORE COMPONENTS

Ronald G. Hill

Hanford Engineering Development Laboratory*

23

SUMMARY

The seismic analysis of the FFTF-PIOTA (Fast Flux Test Facility-Postirradiation Open Test Assembly), subjected to a horizontal DBE (Design Base Earthquake) is presented. The PIOTA is the first in a set of open test assemblies to be designed for the FFTF. Employing the direct method of transient analysis, the governing differential equations describing the motion of the system are set up directly and are implicitly integrated numerically in time. A simple lumped-mass beam model of the FFTF which includes small clearances between core components is used as a "driver" for a fine mesh model of the PIOTA. The nonlinear forces due to the impact of the core components and their effect on the PIOTA are computed.

INTRODUCTION

The reactor core of the FFTF** is designed to accommodate bowing of fuel assemblies which is caused by the core's neutronic and thermal environment. The individual fuel assemblies have a floating collar design at the above core load pad where adjacent assemblies contact to take into account the deformations of the core components. During certain periods of the reactor cycle small clearances may exist between core components; hence, it is important to determine the effect of design impact loads between these structural components to preclude unacceptable stress levels and failures.

The topic of impact is the subject of numerous studies. Special purpose computer program solutions have been developed for analysis of impact of reactor internal structures by Bohm and Nahavandi, reference 1, using explicit integration procedures. The analysis reported in this paper uses implicit integration procedures through the transfer function capabilities of the general purpose computer program NASTRAN to solve for the nonlinear loads due to impact between structural members.

*The Hanford Engineering Development Laboratory is a United States Energy Research and Development Administration Laboratory. HEDL is operated by the Westinghouse Hanford Company.

**See Nomenclature Table.

NOMENCLATURE*

FFTF-PIOTA	Fast Flux Test Facility-Postirradiation Open Test Assembly
DBE	Design Base Earthquake
NASTRAN	<u>NASA STRUCTURAL ANALYSIS</u>
OTA	Open Test Assembly
DOF	Degrees of Freedom
BANDIT	Computer Program -- to determine minimum bandwidth
PWR	Pressurized Water Reactor
IVHM	In-Vessel Fuel Handling Machine
HEDL	Hanford Engineering Development Laboratory
CYBER	HEDL Computer-Control Data Corporation Model 74-18
TRD	Transient Response Displacement
DMAP	Direct Matrix Abstraction Program
PNDL	A DMAP Module
MSC	McNeal Schwendler Corporation
INFONET	Computer Sciences Corporation Computer Network System
COSMIC	Agency for United States Government Release of Computer Programs
I/O	Input/Output Units
CPU	Central Processing Units
SDRC	Structural Dynamics Research Corporation
CYBERNET	Control Data Corporation Computer Network System

*In order of use.

SYMBOLS

Baa	damping matrix
Kaa	stiffness matrix
Maa	mass matrix
Ua	a set of coordinates expressed as a column matrix of two terms for each grid point; y, θ_z (see figure 3)
ω_3	pivotal frequency
f(t)	seismic forcing function
f(n)	nonlinear impact load
g	percent critical damping

MODELING PROCEDURES

Figures 1 and 2 portray the salient points of the FFTF reactor. The reactor is idealized with lumped-mass, spring, gap and beam elements for translation and rotational motion. The DBE, a translational input is applied directly to the reactor head. The core components, fuel assemblies, etc., are pinned at the core barrel and lateral support is provided at the pad locations by the gap elements. The core components, if permitted to rotate, may be considered as inverted pendulums. The core components (reflector, fuel assembly, OTA), figure 3, are expanded horizontally until a return is made to the core barrel, for an enclosed representation of the FFTF core.

Figures 3 and 4 show the grid point and finite element notation for the coarse FFTF reactor model and the fine mesh PIOTA model. A fine mesh was used to model the PIOTA, figure 4, because of the boundary conditions between the PIOTA's components, the close coupling of its natural frequencies, and the predicted critical stress area at the PIOTA's outlet ports. The coarse reactor model is numbered in the 1000 series of grid points and 2000 for the element numbers. The model parameters such as size, mass, stiffness, and damping values are described for the respective models in references 2 and 3. The coarse reactor model is like the FFTF systems model used for both SCRAM and nonlinear seismic analysis, reference 2, with the exception that certain reactor components are not included in the subject model; i.e., Instrument Tree, IVHM, etc. The SCRAM and nonlinear seismic analysis, reference 2, was performed using proprietary (Westinghouse Advanced Reactor Division) special purpose computer programs.

The set of equations used to determine the seismic response is

$$[Maa] \{\ddot{U}_a\} + [Baa] \{\dot{U}_a\} + [Kaa] \{U_a\} = \{f(t)\} + \{f(n)\}$$

The physical set of equations for the models shown in figures 3 and 4 has 927 DOF, of which 537 belong to the PIOTA. The DOF after reduction for coordinates y and θ_z , boundary conditions, constraints, etc., is 297. This problem size (297 DOF, time step increment of 0.0005 second and a 5 second earthquake) involves a sizeable computation investment, approximately 3×10^6 iterations. Hence, further reduction of the problem was desirable. Of the three reduction methods considered, substructuring, modal synthesis and Guyan, the Guyan method was found best for minimum loss of accuracy in conjunction with nonlinear dynamic analysis. Its basis is that fewer DOF are needed to describe the inertia of a structure than are needed to describe its elasticity with comparable accuracy. In using the Guyan method NASTRAN recovers directly, displacements, accelerations, etc., for the coordinates used in the reduction process. The Guyan reduction method was used to reduce the 297 DOF to an analysis set of 104 DOF. The Guyan reduction process increased the bandwidth from 3 to 45; however, the run time was reduced by 65% based on CPU, see table I. The preprocessor BANDIT was used to reduce the bandwidth for the PIOTA model, figure 4. BANDIT was not applied to the FFTF model, figure 3, because of the gap elements and the straightforwardness of the model.

NONLINEAR TRANSIENT ANALYSIS

In this transient solution, the coupled equations of motion are integrated directly without any uncoupling by modal methods, Rigid Format No. 9. The two basic methods used for direct numerical integration are explicit integration in time and implicit integration in time. Difference formulas that relate the accelerations, velocities and displacements are used in both the explicit and implicit integration methods. NASTRAN (reference 4) uses a form of the Newmark Beta Method, implicit integration in time, that yields an unconditionally stable solution for a wide range of transient dynamic problems. The stability limit is a function of the period of the highest vibration mode of the system. Though the implicit integration method is not as fast per time step as the explicit method, the unconditional stability permits the use of large time steps. A time step of 0.0005 second was selected for the runs described herein and no numerical stability problem was encountered. The introduction of nonlinearities in the implicit method of integration may cause numerical stability problems in addition to those mentioned above. These problems are due to the inconsistent definition of displacement and velocity between linear and nonlinear forces and may result in the presence of a parasitic mass on the coordinates to which nonlinear forces are applied. The remedy is to add sufficient mass to the coordinate directly or to reduce the time step of integration so that the parasitic mass effect is negligible in

comparison to the nodal mass. A time step of 0.005 second was used to obtain a linear solution for the model shown in figure 3. This is the same time interval as the input acceleration-time history. With the addition of gap elements to the model, figure 3, the time step was reduced to 0.0005 second through the above parasitic mass consideration.

In NASTRAN, the nonlinear effects (gap elements) are treated through the use of an additional applied load vector. The gap element and the respective applied load vector are user-created by means of transfer functions. Gap elements similar to the ones shown in figure 3 are described in reference 5 with transfer function and nonlinear load card images.

DAMPING AND THE GAP ELEMENT

Two forms of damping* are used in this seismic analysis, structural and impact. In both forms, assumptions concerning the effects of damping on the nodal coordinates are based on a viscous model in which the energy dissipated per cycle is proportional to frequency. A uniform structural damping of 2% of the critical for the DBE was input to the model (figure 2) in terms of stiffness, as follows:

$$[Baa] = \frac{2g}{\omega_3} [Kaa]$$

This method, reference 4, of inputting equivalent viscous damping is an approximation, since the viscous damping forces are larger at higher frequencies and smaller at lower frequencies. The structural damping, Baa, has small effect, or is of no effect, on the response of the model. This is due to the overruling effect and nature of impact damping (10% vs 2% of the critical).

The impact damping is related to the nonlinearities of the gap element. The impact damping and stiffness, c and k, figure 5, are based on a coefficient restitution method (rebound) and the Hertz theory of impact of two solids, i.e., an elastic statical consideration. The relationship between coefficient of restitution and critical damping is derived in reference 2 and is shown in this report as figure 6. An impact damping value of 10% of the critical was used in this analysis. This represents high viscous damping. Impact damping values for FFTF reflector and fuel assemblies have not been measured experimentally. However, there are data available from PWR fuel assemblies tests, reference 2, and from a FFTF IVHM test, reference 5, to corroborate the high impact damping value. Figure 6 shows a comparison of these impact damping values, 19% for PWR fuel assemblies and 15% for the vertical IVHM test. The

*Structural - hysteretic damping
Impact - Maxwell representation of viscous damping

IVHM 15% value was determined from the rate of decay of successive re-bounds. Therefore, the 10% of the critical damping is considered conservative for these analyses.

The vertical drop IVHM test, reference 5, affords a means to assess the validity of the NASTRAN gap element. In comparing the experimental results with those computed from the simple scalar lumped-mass NASTRAN model, there was close agreement. The free fall times and displacements for this test and model were readily calculated by hand methods.

The general form of the gap element used in this analysis is shown in figure 5(a). Gaps in positive and negative directions (for example, the boundary conditions of a rod moving within a tube), can be represented by this element. A gap element with closing capability only (i.e., that portion of the force deflection curve shown in the third quadrant, figure 5(b), and the analogous mechanical model shown in figure 5(c)), was used to represent the clearances between the core components, at twelve places (figure 3). The expanded representation of the core with the gap closure described above, yields a closed core configuration for impact analysis of individual core components. Figure 5(c) shows the mechanical model where the impact spring and gap are accompanied by energy dissipation, and viscous damping. Functionally, the viscous damper, c_1 should act only when the gap is closed, $x_1 > u_1$. At the time these seismic analyses were performed, a switchable, viscous damper had not been verified for use in NASTRAN. A pseudo Maxwell model, figure 5(c), was used in this analysis; the Maxwell model does not necessitate a switchable damper, since the damper c_1 is in series with the impact spring k_1 . The linear spring k_3 , which was small compared with k_1 , improved the stability of the numerical solution, i.e., a larger time step was used.

SEISMIC TIME HISTORY

The input to the FFTF seismic model, Grid Point 1001, figure 3, consisted of an acceleration time history with data points at 0.005 second intervals. This seismic transient is the singular output at the concrete ledge from a two-dimensional finite element soil interaction model of the containment building (reference 6). The dynamic coupling between the containment building and the reactor vessel is assumed to be negligible.

A DBE with 2% of the critical damping, and a duration of 20 seconds was specified (reference 6). Previous investigations (reference 2) revealed that only the accelerations from 1.5 seconds to 6.5 seconds were significant; this then is the seismic transient that was used for the PIOTA analysis (figure 7). The DBE earthquake was divided into ten increments, as shown in figure 7, for computer restart advantage and clarity of output. The printout time interval was ten times the integration time step, or 0.005 seconds. The analysis was started at 1.5 seconds; thus, there is a 1.5 second time shift in the output response, see figure 7.

SOFTWARE AND COMPUTER FACILITIES COMPARISON

This section compares the off-load* results with those obtained on the HEDL-CYBER for a 0.5 second DBE input to the FFTF-PIOTA model. The CYBER was not available to perform the 5 second DBE due to other commitments.

In performing the CYBER and off-load benchmark runs we found that the COSMIC version of NASTRAN, Level 15.5, computed incorrect nonlinear loads. The nonlinear load computations were evaluated by the IVHM model described in reference 5; the results for the IVHM model can readily be checked by hand methods. The IVHM evaluation revealed that the PNLD module in NASTRAN Level 15.5 was not functioning correctly. DMAP instruction number 139, NASTRAN Rigid Format No. 9 gives the relationship of the PNLD module to the computations of TRD. The source language for NASTRAN is essentially written in FORTRAN IV; the DMAP instructions are a compilation of this source language. The IVHM analysis was successfully performed in 1972 on the UNIVAC 1108 using Level 15.1, hence a CDC 6600 version of NASTRAN Level 15.1 was installed on the CYBER and used for the CYBER computations described in this report.

Benchmark runs were performed at the four computing facilities shown on table I. The CYBER run was used as a reference for evaluating the off-load results. The reference run column II, table I, is identical to the FFTF-PIOTA runs described herein with the exception of the OMIT 1 cards. The OMIT bulk data cards are used to achieve the Guyan reduction described previously in this report. It is difficult to compare results from dissimilar computing facilities because of timing algorithms, input-output variances, system dependent software, etc. These problems were alleviated in the FFTF-PIOTA evaluation by comparing the run time required for the TRD module, see table I; this module uses the majority of the central processing time needed for direct transient analyses.

Table I, columns III through VI, show that the MSC version of NASTRAN gives significant reductions in run time when compared to the HEDL or INFONET COSMIC version of NASTRAN. The benchmark run that the MSC performed in Los Angeles, column IV, had two alterations, the transfer functions used for the gap elements were replaced by multipoint constraint equations to utilize the more efficient symmetric matrix decomposition rather than unsymmetric decomposition, and certain data that was transferred to peripheral storage in Level 15.1 was held in main core in MSC-20, thus eliminating peripheral processing-calls. The above alterations account for the reduction in I/O time of 1237 to 26 seconds and CPU reduction of 864 to 569 seconds. The MSC-Los Angeles results shown in column IV were obtained subsequent to the analyses described in this report.

*Off-load -- Computer facilities other than available at HEDL-CYBER

The deck used by SDRC in their benchmark run was identical to the CYBER run, columns II and III, table I. The improvement in run time, I/O 3300 versus 1237 seconds and CPU 1134 versus 864 seconds, is due primarily to the version of NASTRAN utilized, COSMIC Level 15.1 versus MSC-20; the operating systems, CYBER and CYBERNET, are similar, both are basically CDC 6600 machines. The solution for the SDRC benchmark run was identical to the CYBER results, columns II and III. Therefore, as a result of these benchmark evaluations and the need for off-load capability, the SDRC facilities at Cincinnati, Ohio, NASTRAN MSC-20 and the CYBERNET operating system were used to perform the 5 second earthquake run described in this report, see column VI, table I.

RESULTS

NASTRAN, as a large, general-purpose, structural-analysis program, has features, through checkpoint and restart, to recover and compute element stresses, forces and moments for each of the elements shown in figures 3 and 4. Output for this analysis was restricted to bending moment and shears for the boundary-adjacent elements numbers 1, 24 and 52, and for element number 46, a reduced section on the output port of the holddown tube, figure 4. Tabulated peak values for each increment are shown in table II. Figures 8 through 11 show typical load versus time plots. The amplitude of these PIOTA loads are largely dependent on the nonlinear loads caused by impact between core components, see figure 9. The effect of the impact load on the wave form of the element loads can be seen by noting that core impacting at Grid Point 1022 does not occur until 0.18 seconds, figure 9; the corresponding loads in Element 52, figure 11, are very low until this time. The wave form of the PIOTA loads at the head, figure 10, is not directly influenced by the impacting of core components, the PIOTA acts as a mechanical filter.

CONCLUDING REMARKS

A seismic analysis of a reactor internal component with impact between core components has been performed. From this effort, it can be concluded that NASTRAN has good nonlinear transient analysis capabilities. At the present time, solutions are relatively expensive from a computational standpoint when compared with solutions from special purpose computer programs. However, with the efficiencies projected for Level 16 and the use of certain operating system and modeling procedures noted in this report, NASTRAN can effectively be used for nonlinear seismic analysis.

In using NASTRAN's nonlinear features, it is suggested that one begin with small sample problems with known solutions. The setup of nonlinear elements using NASTRAN's transfer function capabilities is a user-oriented function which presents opportunities for data errors; data checking by NASTRAN is minimal since the nonlinear features are mathematical abstractions.

The design of the PIOTA was found to be structurally adequate for the DBE.

ACKNOWLEDGEMENTS

The principal collaborators in these analyses were L. K. Severud, J. M. Anderson, R. A. Lujan, HEDL Engineering Department; W. A. McClelland, SDRC, and J. A. Joseph, MSC.

REFERENCES

1. Bohm, George J., and Nahavandi, Amir N.: Dynamic Analysis of Reactor Internal Structures with Impact Between Components, Nuclear Science and Engineering, Vol. 47, 1972.
2. Morrone, A.: FFTF Scram and Nonlinear Reactor System Seismic Analysis, FRA-1074, October 1973.
3. Anderson, J. M., and Lujan, R. A.: FFTF - Post Irradiation Open Test Assembly Design Support Document: Preliminary Stress Analysis, HEDL-SR2, September 21, 1973.
4. The NASTRAN Theoretical Manual, NASA SP-221, 1969.
5. Hill, R. G.: Transient Analysis of an IVHM Grapple Impact Test. NASTRAN: Users' Experiences, NASA TM X-2637, 1972, pp. 161-178.
6. Final Seismic Analysis Report for the FFTF: (Bechtel Report) BR-5853-C-2, January 18, 1974.

TABLE I
 FFTF-PIOTA FINITE ELEMENT MODEL--SEISMIC BENCHMARK-COMPARISON(2) --NASTRAN RUN TIME-MODULE TRD(1)

	BENCHMARK RUNS					V	V1(9)
	I	II	III	IV			
	CDC6600						
	IBM360-195						
	DENVER	HEDL	SDRC-OHIO	MSC-LOS ANGELES			
	INFONET	CYBER	CYBERNET	CYBERNET			
	LEVEL 15.5 (6)	LEVEL 15.1 (6)	MSC-20(7)	MSC-20			
DOF (3) - PHYSICAL SET Up	927	927	927	927	388(8)	925	
DOF - ANALYSIS SET Ua(1)	297	297	297	282	95	104	
BANDWIDTH - B(4)	3	3	3	8 rms(5)	95	45	
ACTIVE COLUMNS - C(4)	25	25	25	-	0	2	
MODAL REDUCTION	-	-	-	-	YES(8)	-	
GUYAN REDUCTION	-	-	-	-	-	YES	
TRD - IO, SEC	3263	3300	1237	26	996	997	
TRD-CPU, SEC	388	1134	864	569	458	392	
TRD - COST \$	294	312	453	136	240	205	

- NOTES:
- (1) TRD - TRANSIENT RESPONSE DISPLACEMENT U_a , $[M] (\ddot{u}_a) + [B] (\dot{u}_a) + [K] (u_a) = \{f(t)\}$
 - (2) FFTF - DESIGN BASE EARTHQUAKE 2.25 - 2.75 SECONDS, INTEGRATION TIME STEP 0.0005 SEC
 - (3) DOF - DEGREES OF FREEDOM OR NUMBER OF EQUATIONS
 - (4) MATRIX PROPERTIES 
 - (5) THE NASTRAN PREPROCESSOR WAVEFRONT WAS USED FOR MINIMUM BANDWIDTH, ON ALL OTHER RUNS THE NASTRAN PREPROCESSOR BANDIT WAS USED TO MINIMIZE THE BANDWIDTH
 - (6) NASA PUBLIC RELEASE THROUGH COSMIC
 - (7) PROPRIETARY SOFTWARE, McNEAL SCHWENDLER CORP (MSC)
 - (8) STRUCTURAL DYNAMICS RESEARCH CORP (SDRC) PROPRIETARY NASTRAN PREPROCESSOR NIP WAS USED TO REPRESENT THE 537 Up SET OF THE PIOTA THROUGH MODAL SYNTHESIS METHODS
 - (9) USED FOR 5 SECOND EARTHQUAKE ANALYSIS OF THE PIOTA

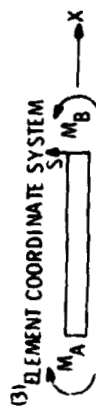
ORIGINAL PAGE IS
OF POOR QUALITY

TABLE II
SUMMARY-PIOTA
DESIGN BASE EARTHQUAKE LOADS (1)

INCREMENT	ELEMENT NO. 1 (4)			ELEMENT NO. 24			ELEMENT NO. 46			ELEMENT NO. 52						
	$N_A^{(2,3)}$	$M_B^{(2,3)}$	$S^{(2,3)}$	$t^{(2)}$	M_A	M_B	S	t	M_A	M_B	S	t	M_A	M_B	S	t
1	-5,114.0	-6,336.0	172.0	0.485	84.8	-1,507.0	47.0	0.475	3,655.0	3,532.0	30.7	0.490	211.0	-254.1	62.0	0.485
2	-9,216.0	-11,631.0	262.0	1.0	-1,191.0	-2,117.0	66.2	0.990	5,207.0	4,811.0	98.9	1.0	331.0	-409.8	98.8	1.00
3	-9,216.0	-11,631.0	262.0	1.0	-3,322.0	-5,906.0	184.6	1.385	13,900.0	13,800.0	24.9	1.345	4,023.0	3,096.0	123.5	1.315
4	-2,966.0	-3,817.0	92.4	1.78	-1,084.0	-1,839.0	57.4	1.785	-10,859.0	-10,181.0	-169.0	1.93	-574.0	998.0	-209.6	1.93
5	4,566.0	5,703.0	-123.4	2.025	-1,084.0	-1,928.0	60.2	2.16	-11,980.0	-11,212.0	-191.8	2.035	-901.5	229.9	-151.0	2.485
6	341.0	419.0	-84.6	3.00	991.0	1,762.0	-55.1	2.525	11,312.0	-10,785.0	-132.0	2.985	1,445.0	2,622.0	-157.0	2.535
7	4,666.0	6,027.0	-148.0	3.06	719.0	1,277.0	-40.0	3.060	-11,888.0	-11,076.0	-203.0	3.015	-982.0	468.0	-193.0	3.030
8	-4,927.0	-6,121.0	130.0	3.87	-682.0	-1,213.0	38.0	3.870	9,286.0	8,635.0	163.0	3.825	694.0	-345.0	138.0	3.935
9	3,469.0	4,566.0	-119.0	4.46	-1,030.0	-1,831.0	57.0	4.305	2,138.0	-2,464.0	418.0	4.315	-1,208.0	-1,199.0	-1.2	4.255
10	2,542.0	3,031.0	-53.0	4.87	-454.0	-808.0	25.0	4.670	-5,676.0	-5,313.0	-91.0	4.510	-389.0	408.0	-106.0	4.505
MAXIMUM LOADS	9,216.0	11,631.0	262.0	--	3,322.0	-5,906.0	184.0	--	13,900.0	13,800.0	-373.0	--	4,023.0	3,096.0	328.0	--

(1) FET - DESIGN BASE EARTHQUAKE

(2) UNITS: M_A, M_B in-lb; S , lb; t , sec. 1 in-lb = 0.11298 N-m; 1 lb = 4.448 N



(4) MAXIMUM VALUES FOR EACH INCREMENT, BASED ON M_A

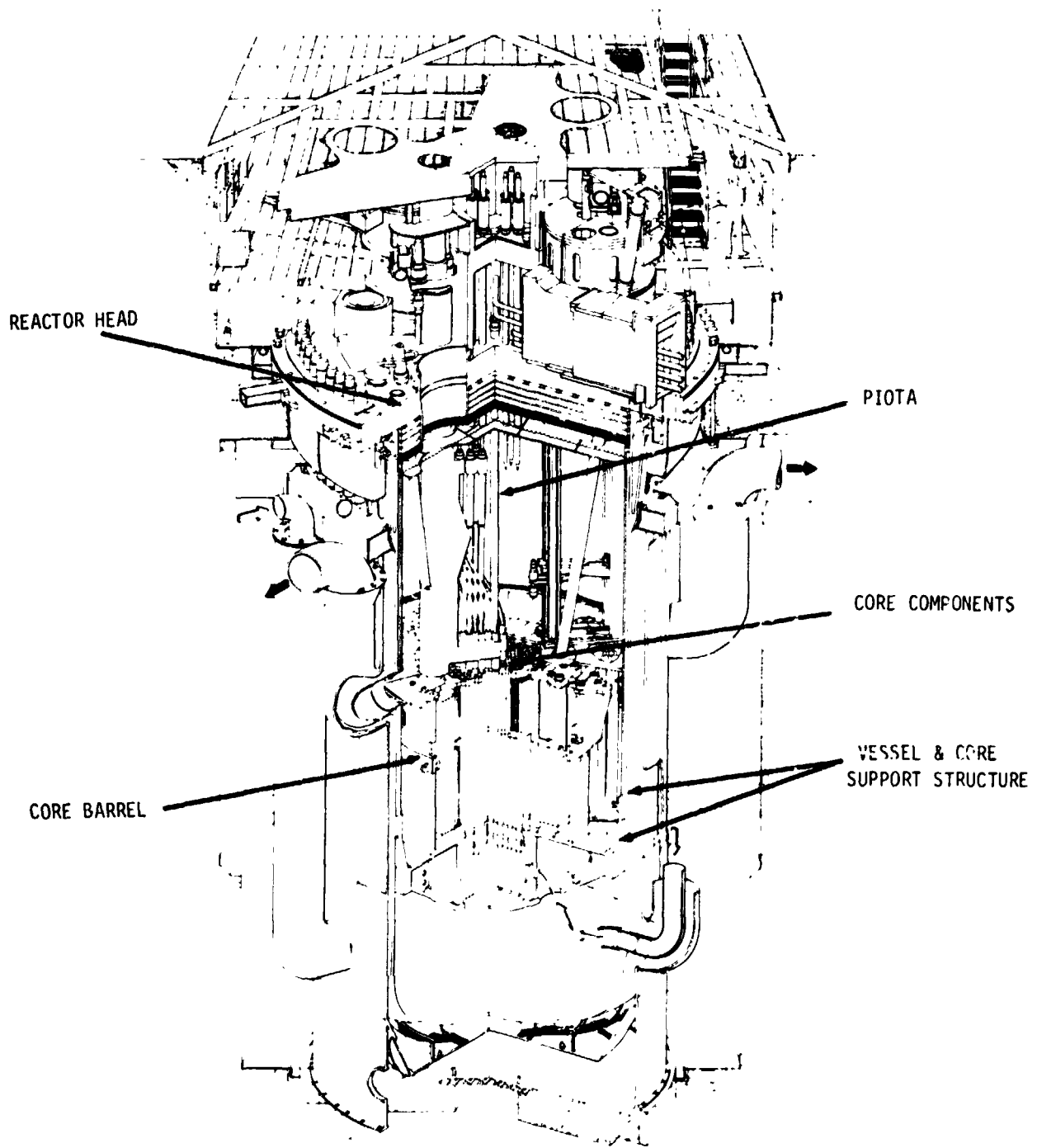


Figure 1.- FFTF reactor.

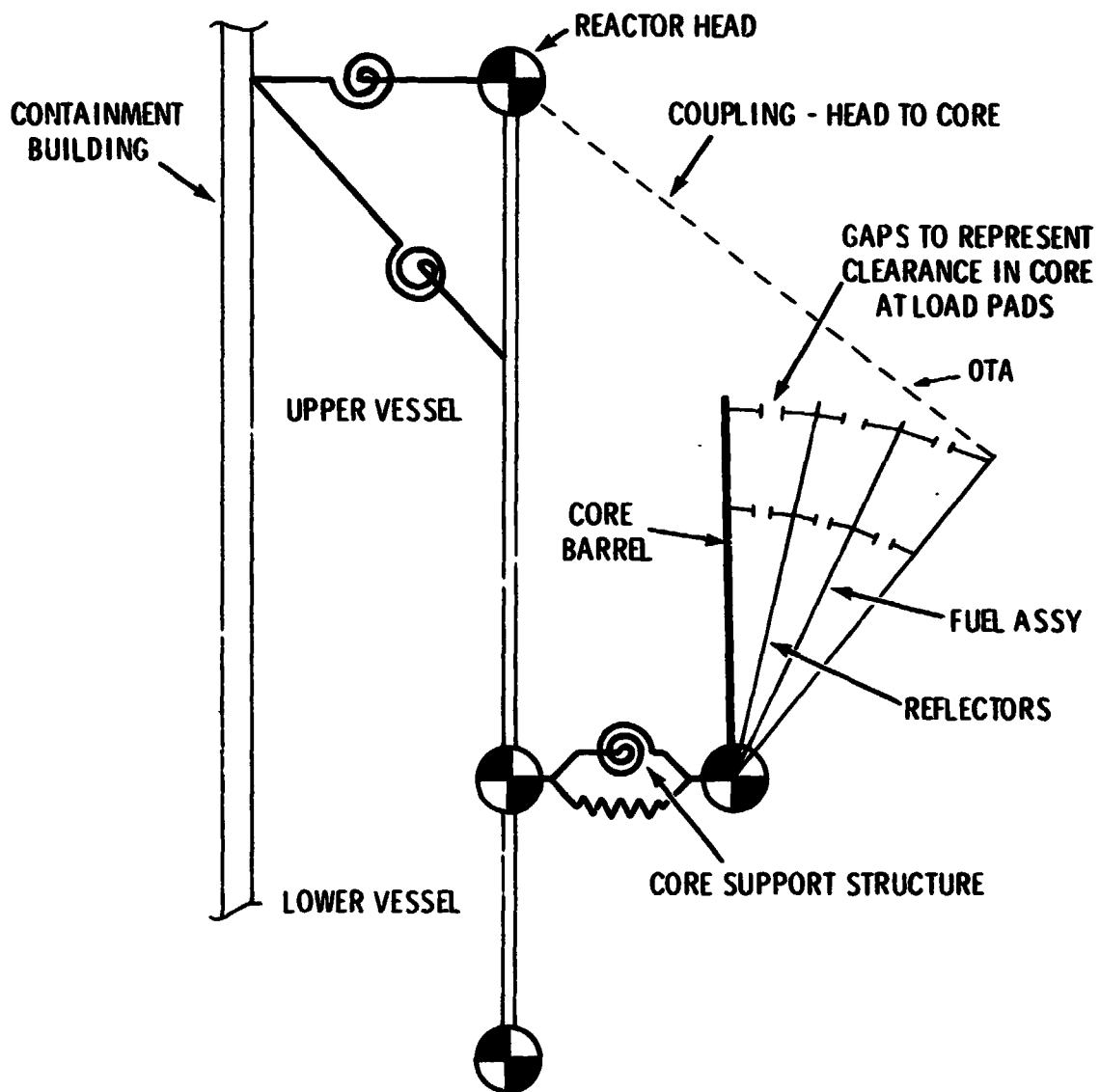


Figure 2.- Schematic of FFTF lumped-mass beam model.

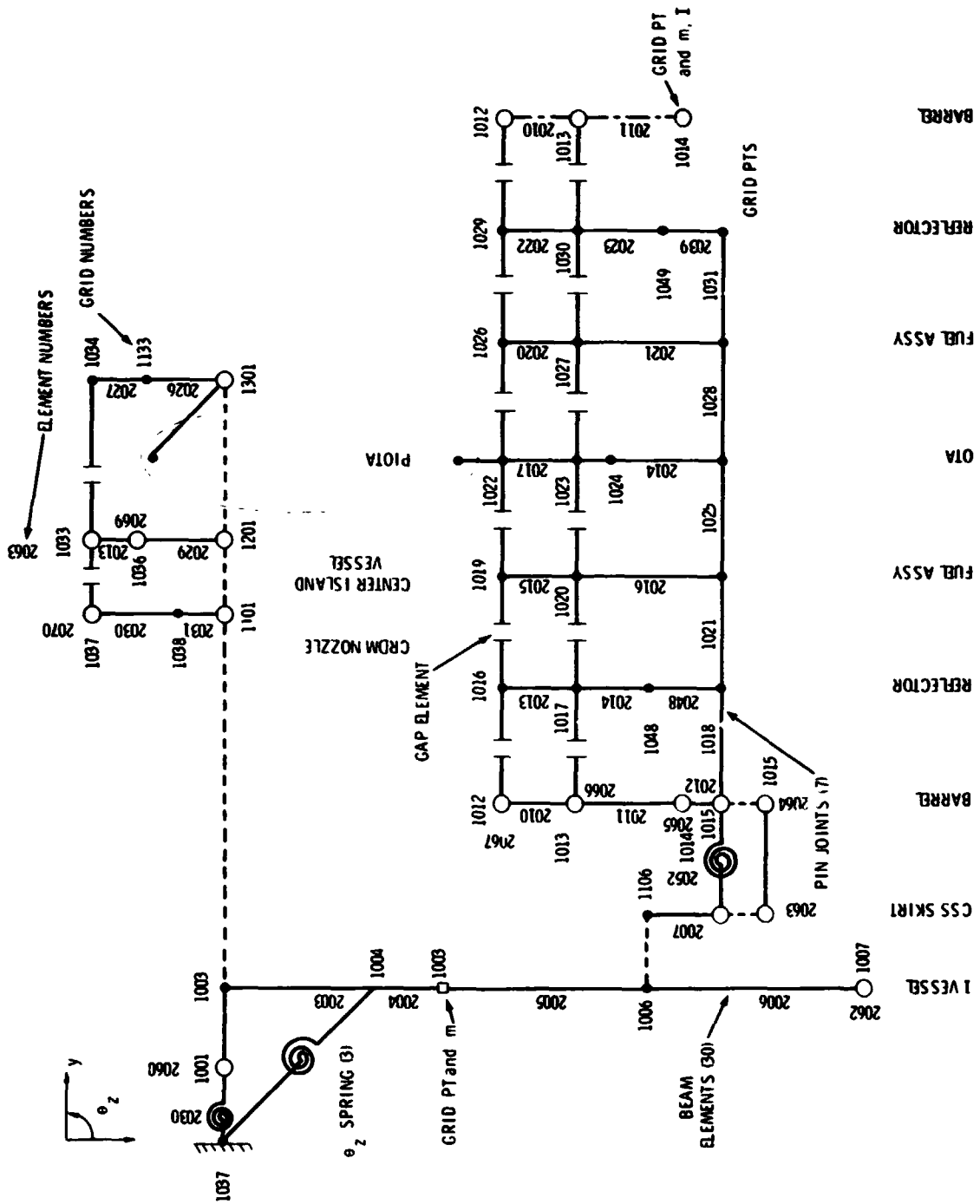
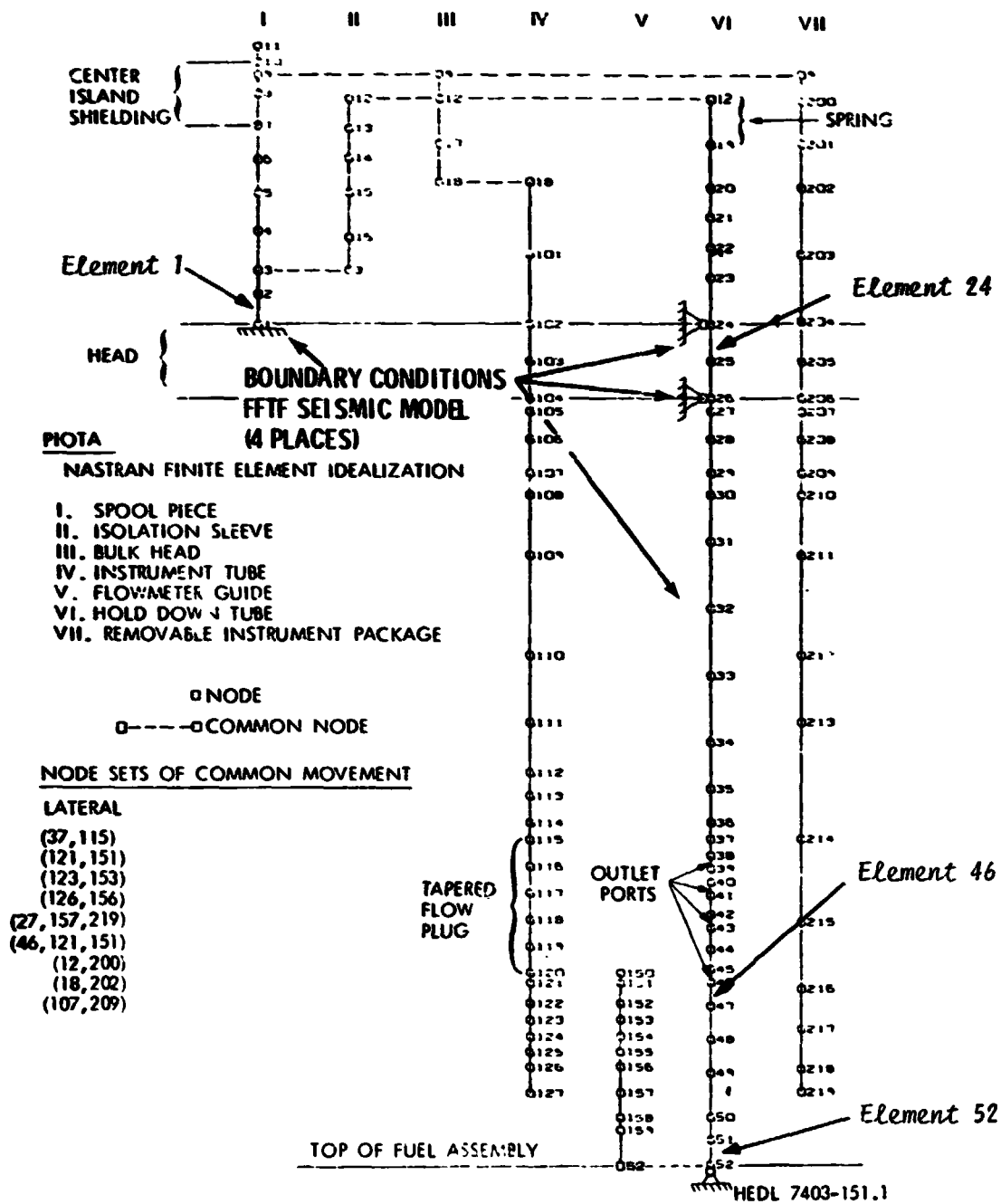


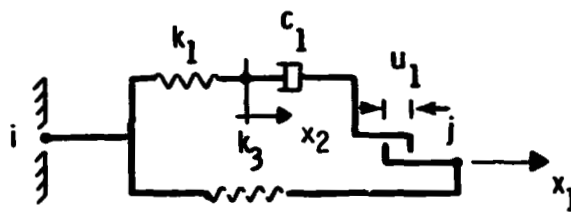
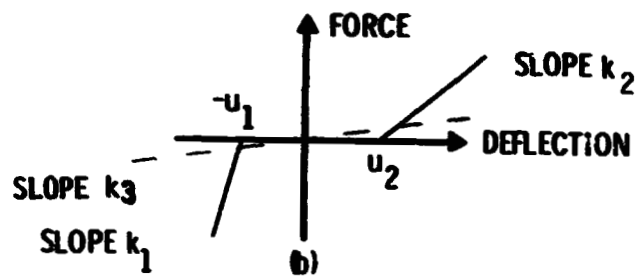
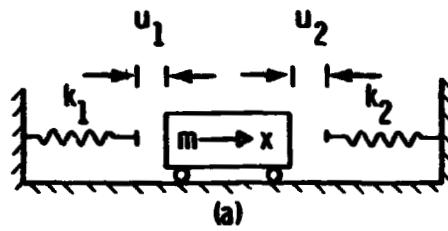
Figure 3.- FFTF seismic model.



POST IRRADIATION OPEN TEST ASSEMBLY
REAL MODEL

UNDEFORMED SHAPE

Figure 4.- PIOTA model.



$$x_1 > u_1 \text{ AND } k_3 \neq 0$$

$$f_1 = k_1 x_1 + c_1 (\dot{x}_1 - \dot{x}_2) = \text{FORCE @ } j$$

MAXWELL MODEL
(c)

Figure 5.- Gap element.

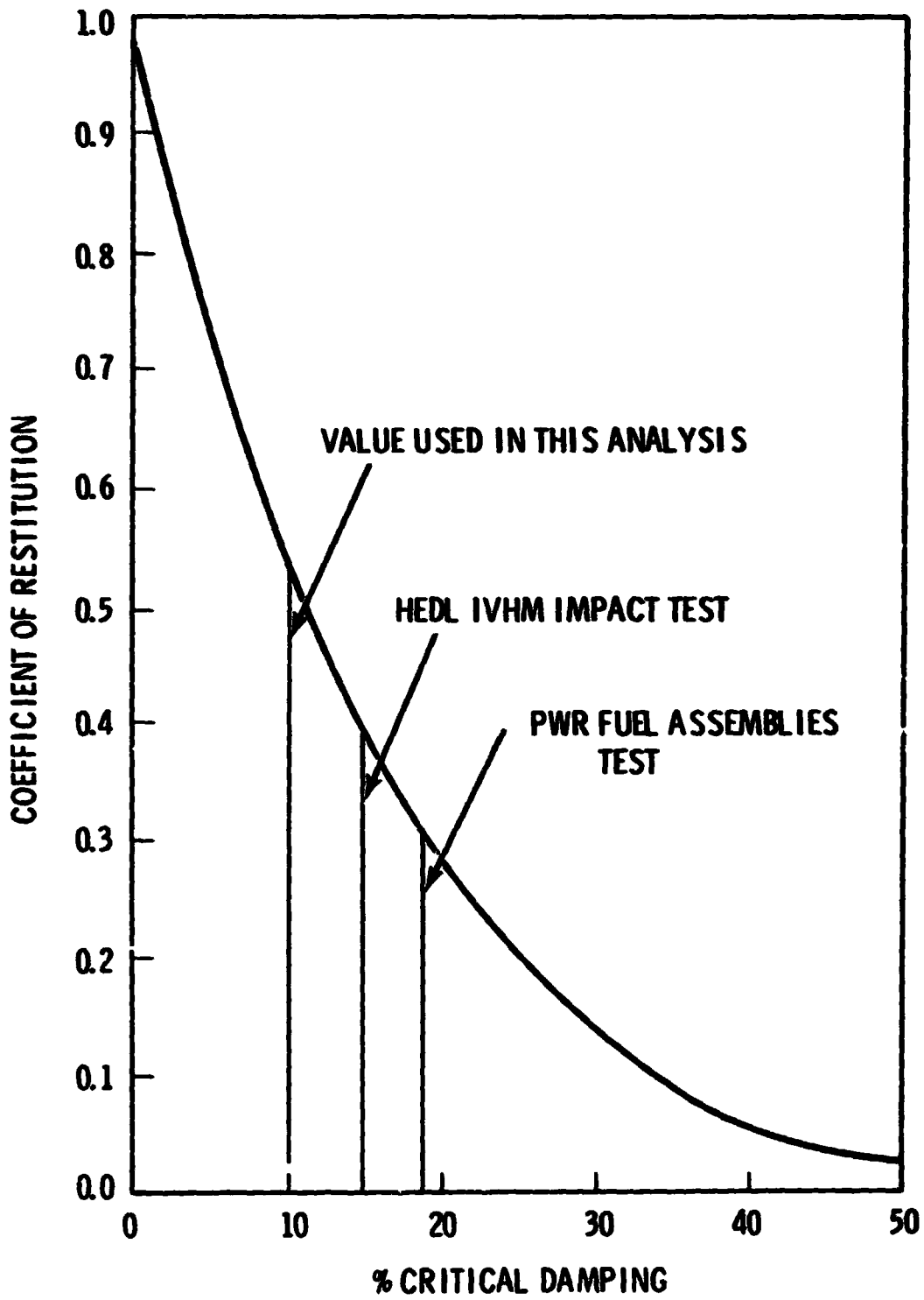


Figure 6.- Coefficient of restitution vs percent of critical damping at impact.

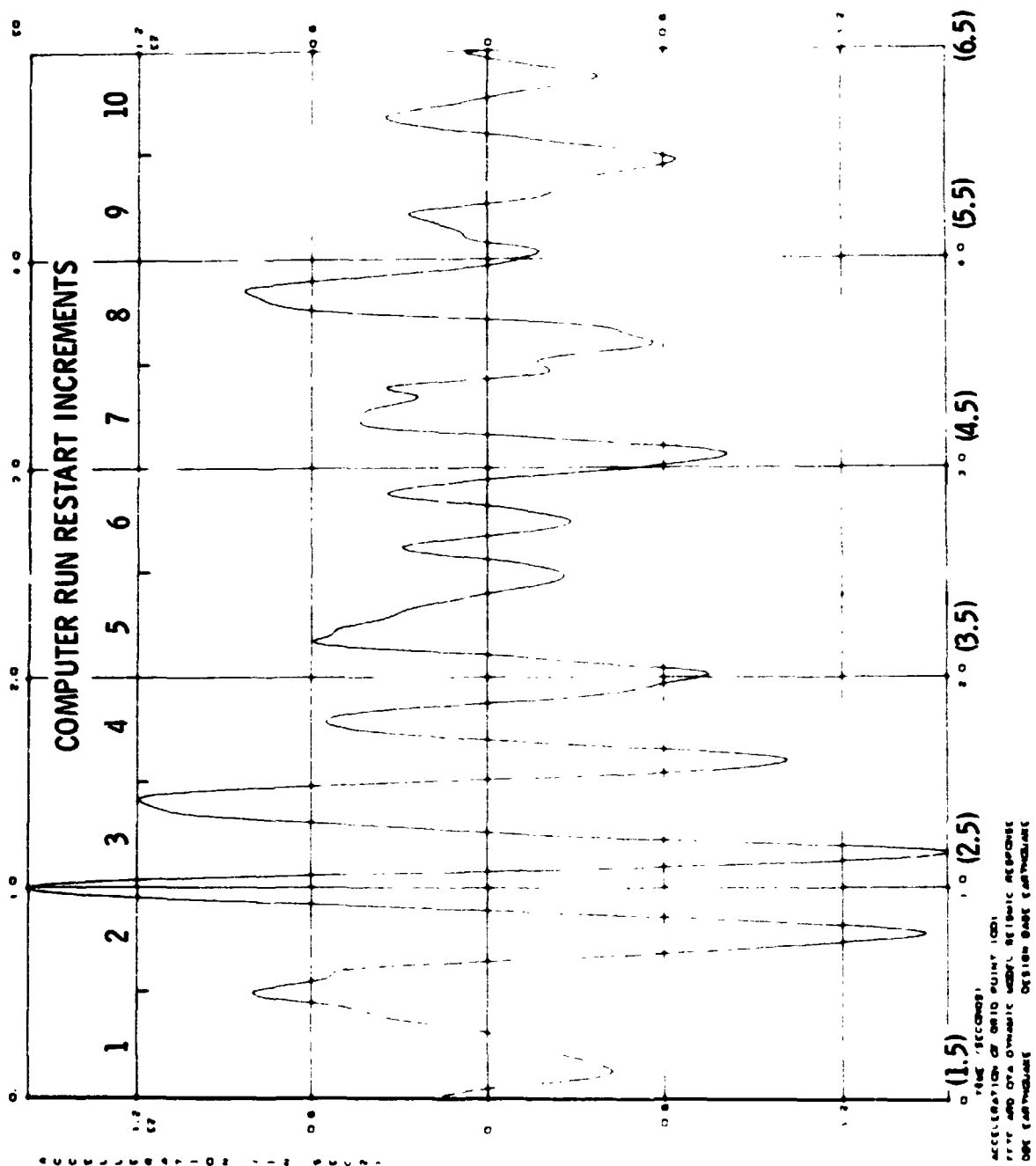
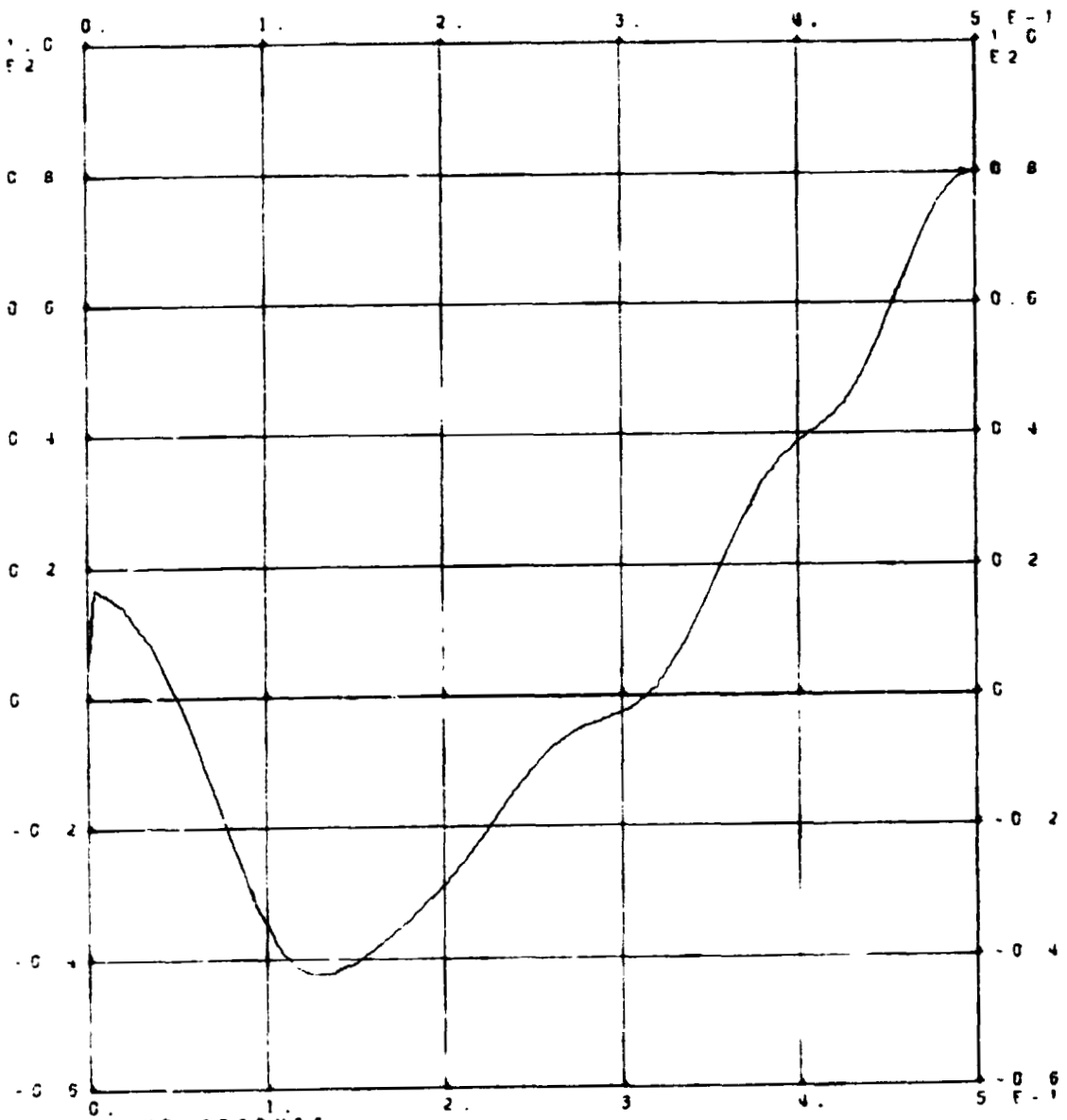


Figure 7.- Design base earthquake. $1 \text{ in/sec}^2 = 0.0254 \text{ m/sec}^2$.

DESIGN BASE EARTHQUAKE INPUT



DESIGN BASE EARTHQUAKE INPUT
 VESSEL AND REACTOR INTERNALS PLUS P10TA - SEISMIC MODEL
 DESIGN BASE EARTHQUAKE - DAMPERS IN SERIES WITH GAP ELEMENTS
 SUBCASE 1

Figure 8.- Increment 1 - acceleration input (see figure 7).
 1 in/sec² = 0.0254 m/sec².

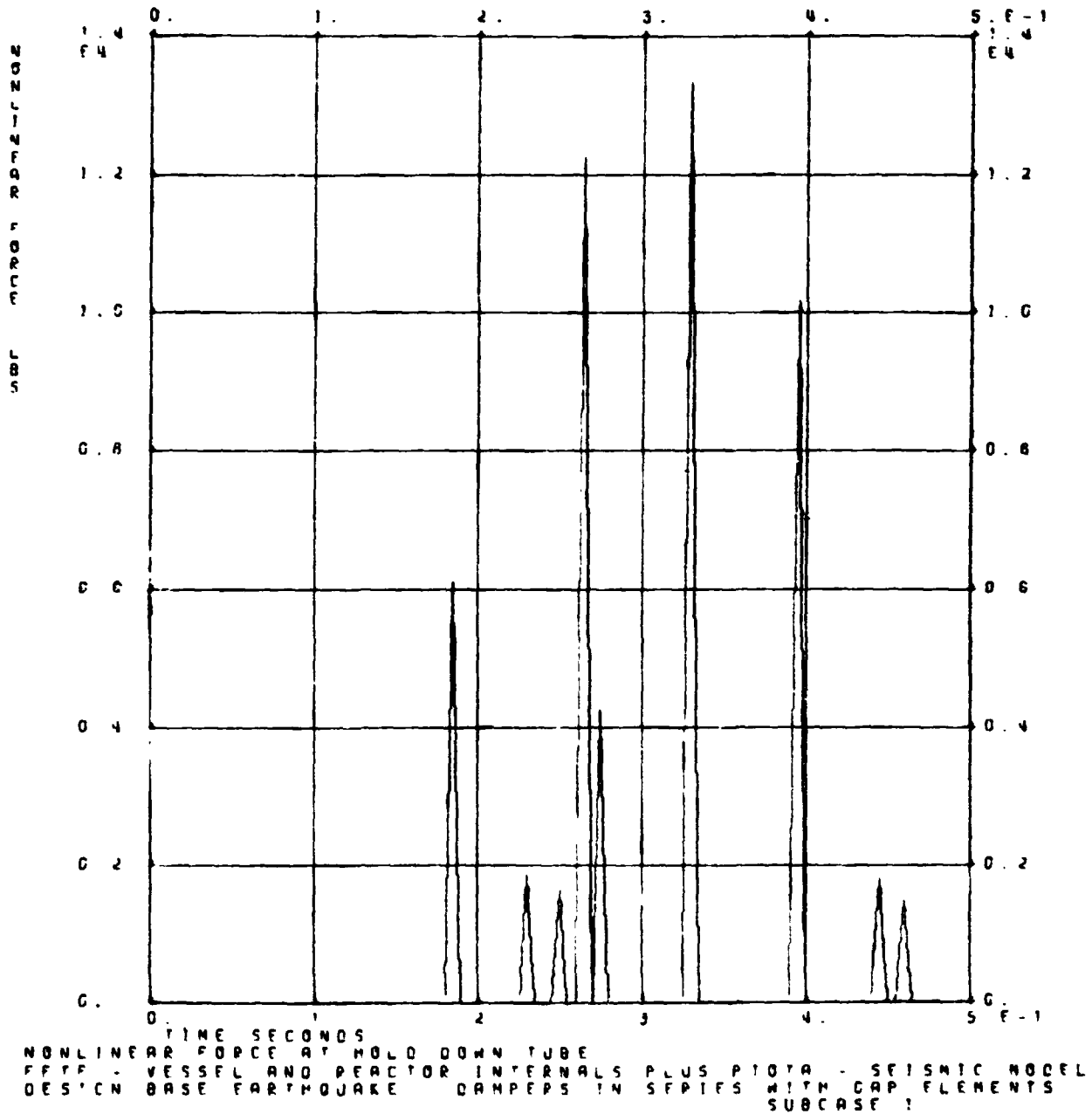


Figure 9.- Increment 1 - impact load grid pt 1022 (see figure 3).
 1 lb = 4.448 N.



Figure 10.- Increment 1 - moments, element 1 - PIOTA
 (see figure 4). 1 in-lb = 0.11298 N-m.

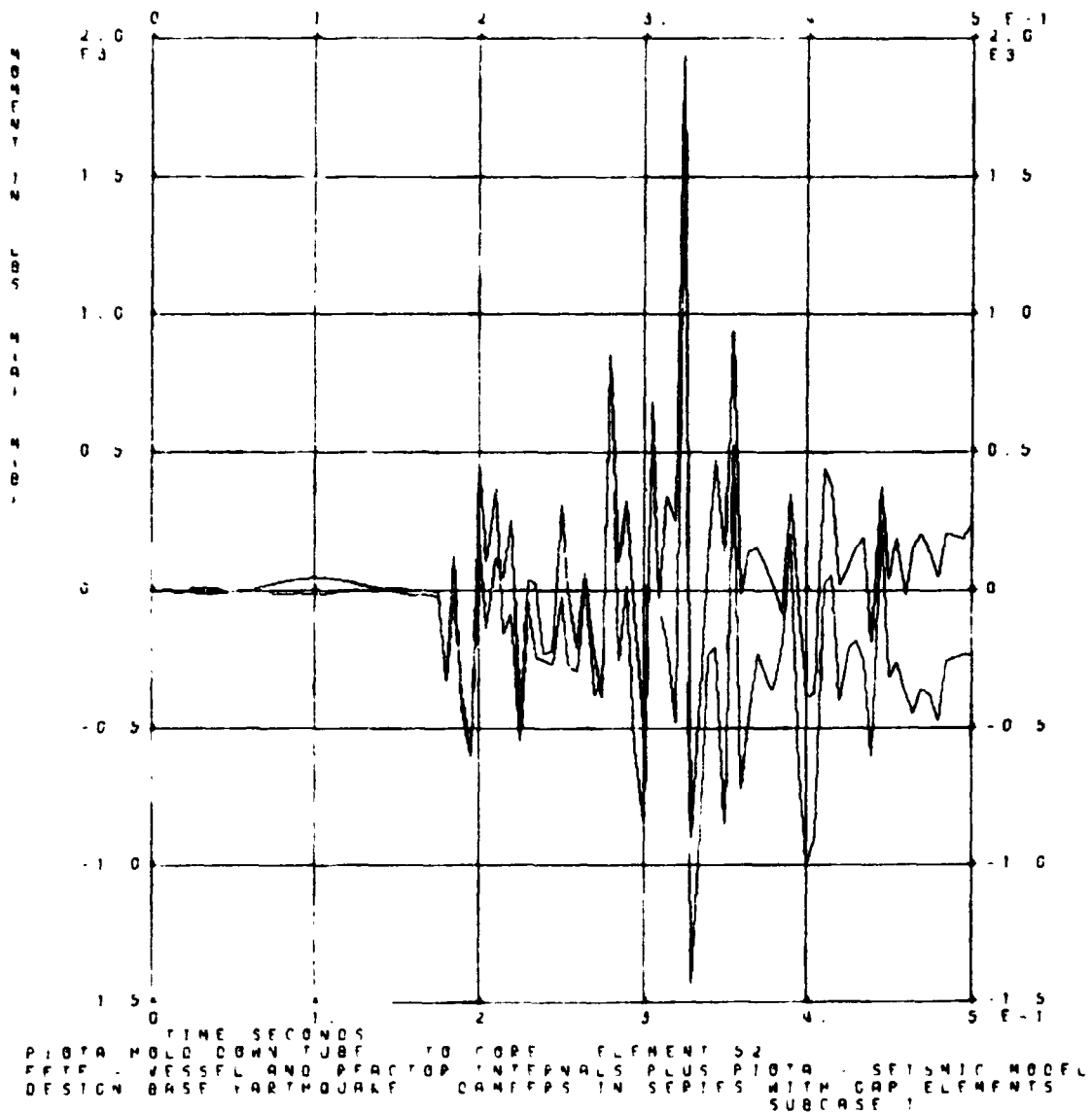


Figure 11.- Increment 1 - moments, element 52 - PIOTA
 (see figure 4). 1 in-lb = 0.11298 N-m.

N75 31509

THE DYNAMIC ANALYSIS OF SUBMERGED STRUCTURES

By Gordon C. Everstine, Erwin A. Schroeder,
and Melvyn S. Marcus

Computation and Mathematics Department
Naval Ship Research and Development Center
Bethesda, Maryland 20084

SUMMARY

Methods are described by which the dynamic interaction of structures with surrounding fluids can be computed by using finite element techniques. In all cases, the fluid is assumed to behave as an acoustic medium and is initially stationary. Such problems can be solved either by explicitly modeling the fluid (using pressure or displacement as the basic fluid unknown) or by using decoupling approximations which take account of the fluid effects without actually modeling the fluid.

INTRODUCTION

Recently there has been a growing interest in solving problems in which structures interact with fluids. Within the Navy, for example, application areas include underwater vibrations, ship silencing, shock response of ships, underside slamming, flow-induced vibrations, and the motions of liquids and gases in containers. The last two problem areas are also of interest to the aerospace community.

Concern here is with the dynamic structural response of submerged structures, including the determination of natural frequencies and the response of submerged structures to sinusoidal and general transient excitations. In the latter category, a very important application is the shock response of submarines to underwater explosions.

In all problems considered here, the structure is assumed to be initially at rest with respect to the fluid; i.e., there is no fluid flow initially. Also, the fluid is assumed to behave as an acoustic medium in which each material point undergoes only infinitesimal displacement from the static equilibrium position.

Such problems were apparently first formulated by using finite elements by Zienkiewicz and Newton (refs. 1 and 2). Choosing pressure as the basic fluid unknown, they applied a variational process to obtain the finite-element equations for the fluid. These were then coupled to the usual structural

equations in a consistent manner. The application of Zienkiewicz's approach with NASTRAN (refs. 3 and 4) is straightforward but requires program modifications. In fact, a similar approach was adopted in the development of the NASTRAN hydroelastic analyzer (refs. 4 and 5). This latter capability is restricted to the case of fluids contained in axisymmetric containers, although the motions of the coupled fluid-structure system need not be axisymmetric.

Another approach to the interaction problem uses fluid displacements (rather than pressures) as the fundamental unknowns (ref. 6). In brief, this approach converts standard NASTRAN elements into "mock" fluid elements by defining (in three dimensions) the 6 x 6 material matrix \underline{G} to be

$$\underline{G} = k \begin{bmatrix} 1 & 1 & 1 & 0 & 0 & 0 \\ 1 & 1 & 1 & 0 & 0 & 0 \\ 1 & 1 & 1 & 0 & 0 & 0 \\ 0 & 0 & 0 & 0 & 0 & 0 \\ 0 & 0 & 0 & 0 & 0 & 0 \\ 0 & 0 & 0 & 0 & 0 & 0 \end{bmatrix} \quad (1)$$

In equation (1), the bulk modulus k is given by

$$k = \rho c^2 \quad (2)$$

where ρ and c are the unperturbed mass density and sonic speed, respectively, of the fluid. To the NASTRAN user, Kalinowski's displacement approach (ref. 6) has the advantages of using a standard version of the program and of generating symmetric matrices (in contrast to Zienkiewicz's approach which generates nonsymmetric matrices). However, Kalinowski's method has the disadvantage of requiring three unknowns per fluid point rather than one (pressure). This penalty affects adversely both the order and the bandwidth of the assembled matrices.

The purpose of the remainder of this paper is to describe two additional methods for solving fluid-structure interaction problems. Both use only standard versions of NASTRAN.

A PRESSURE ANALOG METHOD

All approaches described in this paper treat the fluid as an acoustic medium: a compressible, inviscid fluid which is initially stationary and undergoes only small amplitude motion, and whose pressure satisfies the wave equation

$$\nabla^2 p = \ddot{p}/c^2 \quad (3)$$

where overdots denote partial differentiation with respect to the time t . The boundary condition at the fluid-structure interface can be obtained from momentum and continuity considerations:

$$\frac{\partial p}{\partial n} = -\rho \ddot{u}_n \quad (4)$$

where n is the unit outward normal from the solid at the fluid-solid interface, and ρ is the fluid mass density. A special case of equation (4) occurs at rigid walls where

$$\frac{\partial p}{\partial n} = 0 \quad (5)$$

At a free surface, in the absence of surface waves, the boundary condition is simply

$$p = 0 \quad (6)$$

The goals here are to solve fluid-structure interaction problems in which the fluid is described by equations (3) to (6) and to use only standard capabilities available in structural analysis codes such as NASTRAN.

In classical elasticity theory (ref. 7), the x component of the momentum equation is

$$\sigma_{xx,x} + \sigma_{xy,y} + \sigma_{xz,z} + \rho f_x = \rho \ddot{u} \quad (7)$$

where ρ is the mass density of the (solid) medium, u is the x component of displacement, f_x is the x component of body force, and the partial differentiation with respect to a coordinate is abbreviated with commas:

$$(\quad)_{,x} \equiv \frac{\partial}{\partial x} (\quad) \quad (8)$$

In programs such as NASTRAN, the stress and strain components are generally described with vector notation as follows:

$$\underline{\sigma} = \begin{Bmatrix} \sigma_{xx} \\ \sigma_{yy} \\ \sigma_{zz} \\ \sigma_{xy} \\ \sigma_{yz} \\ \sigma_{xz} \end{Bmatrix}, \quad \underline{\epsilon} = \begin{Bmatrix} \epsilon_{xx} \\ \epsilon_{yy} \\ \epsilon_{zz} \\ \gamma_{xy} \\ \gamma_{yz} \\ \gamma_{xz} \end{Bmatrix} = \begin{Bmatrix} u_{,x} \\ v_{,y} \\ w_{,z} \\ u_{,y} + v_{,x} \\ v_{,z} + w_{,y} \\ w_{,x} + u_{,z} \end{Bmatrix} \quad (9)$$

where u , v , and w are the three Cartesian displacement components. Thus, for linear materials, Hooke's law can be written in terms of a systematic 6×6 material matrix \underline{G} , where

$$\underline{\sigma} = \underline{G} \underline{\epsilon} \quad (10)$$

By substituting the strain definitions (9) into (10) and (10) into (7),

the wave equation (3) can be obtained if

$$u = p \quad (11)$$

$$v \equiv w \equiv 0 \quad (12)$$

$$\left. \begin{aligned} G_{14} = G_{16} = G_{46} = 0 \\ G_{11} = G_{44} = G_{66} = \rho c^2 \end{aligned} \right\} \quad (13)$$

$$f_x = 0 \quad (14)$$

In other words, the x component of displacement u can represent fluid pressure p if v and w are fixed everywhere in the fluid, if no body forces are applied, and if six of the material constants are as prescribed in equation (13). Although the other 15 constants can be arbitrarily chosen, it is convenient to choose them so that \underline{G} is invariant under a coordinate system rotation (i.e., \underline{G} is isotropic). A necessary and sufficient condition for \underline{G} to be isotropic is that it have the general form

$$\underline{G} = \begin{bmatrix} \lambda+2\mu & \lambda & \lambda & 0 & 0 & 0 \\ \lambda & \lambda+2\mu & \lambda & 0 & 0 & 0 \\ \lambda & \lambda & \lambda+2\mu & 0 & 0 & 0 \\ 0 & 0 & 0 & \mu & 0 & 0 \\ 0 & 0 & 0 & 0 & \mu & 0 \\ 0 & 0 & 0 & 0 & 0 & \mu \end{bmatrix} \quad (15)$$

where λ and μ are the Lamé constants (ref. 7). The only \underline{G} matrix satisfying both equations (15) and (13) is

$$\underline{G} = \rho c^2 \begin{bmatrix} 1 & -1 & -1 & 0 & 0 & 0 \\ -1 & 1 & -1 & 0 & 0 & 0 \\ -1 & -1 & 1 & 0 & 0 & 0 \\ 0 & 0 & 0 & 1 & 0 & 0 \\ 0 & 0 & 0 & 0 & 1 & 0 \\ 0 & 0 & 0 & 0 & 0 & 1 \end{bmatrix} \quad (16)$$

With \underline{G} isotropic, there is no need to be concerned about using finite elements whose material matrices are based on some local element coordinate system.

To summarize, the fluid is modeled with standard elastic finite elements (e.g., QDMEM in 2-D and general solids in 3-D) having material properties given by equation (16), where fluid pressure is represented by the x displacement u .

Boundary Conditions

Interface Condition

The boundary condition that the pressure p must satisfy at a fluid-solid interface is given by equation (4). To evaluate the left-hand side of equation (4), compute the directional derivative of p in the direction of the unit outward normal \underline{v} from the fluid at a surface point. Replacing p with its structural analog u yields

$$\frac{\partial u}{\partial v} = \underline{v} \cdot \underline{\nabla} u = u_{,x} v_x + u_{,y} v_y + u_{,z} v_z \quad (17)$$

By using the constitutive equations (10) and (16) with equation (17) yields

$$\frac{\partial u}{\partial v} = \frac{1}{\rho c^2} (\sigma_{xx} v_x + \sigma_{xy} v_y + \sigma_{xz} v_z) \quad (18)$$

where the parenthetical expression is equal to the x component of the stress vector $\underline{T}^{(v)}$ acting on a surface with unit outward normal \underline{v} (ref. 7). Hence,

$$\frac{\partial u}{\partial v} = \frac{T_x^{(v)}}{\rho c^2} \quad (19)$$

If the surface is discretized by a finite number of grid points, the surface traction $T_x^{(v)}$ can be replaced by its lumped equivalent

$$T_x^{(v)} = \frac{F_x}{A} \quad (20)$$

where F_x is the x component of the force applied to a particular point (on the surface with outward unit normal \underline{v}) to which the area A has been assigned. Hence, from equations (19) and (20), the final expression for the directional derivative is obtained as

$$\frac{\partial u}{\partial v} = \frac{F_x}{\rho c^2 A} \quad (21)$$

Since all symbols in equation (21) refer to the fluid, including u which represents the pressure p , merely combine equation (21) with the boundary condition of equation (4) at the interface to obtain the lumped interface condition

$$F_x^p = (\rho c)^2 A \ddot{u}_n \quad (22)$$

in which $\underline{n} = -\underline{v}$ and the superscript p has been placed on F_x to emphasize that the "force" is applied to the pressure variable. That is, if the outward normal component of structural acceleration at a point is \ddot{u}_n , the effect on the fluid pressure is that of a "force" given by equation (22) applied to the fluid

variable p . In equation (22), ρ and c refer to the fluid.

Equation (22) provides the influence of the structural motion on the pressure. The inverse relationship (that of fluid pressure on the structural motion) is obtained merely by applying a normal force to the structural point equal to pA .

The final set of matrix equations takes the form

$$\underline{M}\ddot{\underline{U}} + \underline{K}\underline{U} = \underline{F} \quad (23)$$

where, with the subscripts s and f denoting solid and fluid,

$$\underline{U} = \begin{Bmatrix} \underline{u} \\ \underline{p} \end{Bmatrix} \quad \underline{M} = \begin{bmatrix} \underline{M}_{ss} & \underline{0} \\ \underline{M}_{fs} & \underline{M}_{ff} \end{bmatrix} \quad \underline{K} = \begin{bmatrix} \underline{K}_{ss} & \underline{K}_{sf} \\ \underline{0} & \underline{K}_{ff} \end{bmatrix} \quad (24)$$

In equation (23), the vector of unknowns \underline{U} includes both the structural displacements and the fluid pressures. In equation (24), \underline{M}_{fs} is a matrix which is assembled by placing the term $-(\rho c)^2 A$ in the row corresponding to each interface p variable and the column corresponding to the associated structural normal displacement. Similarly, \underline{K}_{sf} is a matrix which is assembled by placing $+A$ in the row corresponding to each surface normal displacement and the column corresponding to the associated p . In NASTRAN, both \underline{M}_{fs} and \underline{K}_{fs} can be inserted by using direct matrix input (DMIG cards).

Infinite Fluids

The foregoing derivations apply directly to a wide variety of fluid-solid systems of finite extent. For structures in "infinite" fluids, interface disturbances travel far without reflection so that radiation damping may be significant. Although one should generally consider other approaches to solve such problems, approximations involving the current method can also be derived.

The approach here is to truncate the fluid model at a distance "sufficiently far" from the structure and apply the radiation condition (ref. 8) there:

$$\frac{\partial p}{\partial n} = -\frac{1}{c} \frac{\partial p}{\partial t} \quad (25)$$

This condition has also been referred to as the nonreflecting boundary condition (ref. 1) or the wave-absorbing boundary condition (refs. 6 and 9).

Equation (25) can be applied with NASTRAN by combining with equation (21), where again the pressure p is replaced by its structural analog u . Hence, the radiation condition becomes

$$\mathbf{F}_x^p = -\rho c A \dot{p} \quad (26)$$

In other words, a grounded scalar dashpot with damping constant $\rho c A$ should be connected to each p variable.

Numerical Example

These concepts can be illustrated by considering the two-dimensional problem of a steel ring vibrating in water (ref. 10). The ring has a radius of ten inches and a radial thickness of one inch. The inside is evacuated. The fluid region is a circular annulus with an outer radius of 32.6 inches. The outer surface is a "free" surface (where $p=0$). The problem was solved (ref. 10) by modeling with NASTRAN a 90° sector comprised of eight BAR elements representing the ring and an 8x6 mesh of QDMEM elements representing the fluid. Typical results for the in-fluid natural frequencies (in radians/second) are as follows:

Fourier Harmonic	NASTRAN frequency	Analytical frequency
0	4333.	4364.
2	231.6	226.1
4	1486.	1432.
6	3884.	3724.

The analytical results were derived by Schroeder and Marcus (ref. 11) based on a method developed by Junger (ref. 12). Calculations reported in Ref. 10 indicate that grid refinement does result in convergence to the analytical results.

DECOUPLING APPROXIMATIONS

For problems in which a structure interacts with a fluid of infinite extent, it may be expensive to model enough fluid to produce satisfactory results, even if the radiation condition (eqs. (25) and (26)) is applied at some arbitrary outer surface. Since the interest is in the structure rather than in the fluid, various schemes can also be used that approximate the fluid effects without actually modeling the fluid (refs. 13 and 14). These schemes, generally referred to as decoupling approximations, result in an analytical expression (in differential equation form) describing the relationship between the fluid pressure at the interface and the interface motion.

For certain dynamics problems in which the source of the disturbance is in the fluid rather than in the structure (e.g., underwater explosions), the decoupling approximation supplies only the radiation pressure. However, the

other contributors to the total dynamic pressure (the incident free field pressure and the scattered pressure) can be computed as if the structure were rigid and stationary and thus comprise the usual right-hand-side forcing function.

One decoupling approximation which has been used with NASTRAN was developed (but not yet published) by Dr. Hansen Huang of the Naval Research Laboratory. For axisymmetric cylinders modeled with conical shell elements, the interface pressure-motion equation is approximated by

$$\dot{p}_n + (cn/r)p_n = \rho c \ddot{w}_n \quad (27)$$

where p_n is the n^{th} Fourier harmonic of the radiation pressure

c is the speed of sound in fluid

ρ is the mass density of fluid

r is the radius of cylinder

w_n is the n^{th} Fourier harmonic of the outward normal component of shell displacement

Equation (27) is equivalent to the so-called doubly asymptotic approximation of Geers (ref. 13), which was formulated for more general three-dimensional situations.

To illustrate how approximations such as equation (27) are applied with NASTRAN, consider a cylindrical shell subjected to an underwater shock loading (ref. 15). In the absence of radiation pressure p , the usual transient matrix equation would apply

$$\underline{m} \ddot{\underline{u}} + \underline{k} \underline{u} = \underline{f}(t) \quad (28)$$

where the forcing function f consists of the sum of the incident and scattered pressures. The radiation pressure, which depends on the shell motion, supplies an additional load on the structure so that the equilibrium equations for the structure, from equation (28), become

$$\underline{m} \ddot{\underline{u}} + \underline{k} \underline{u} + \underline{h} \underline{p} = \underline{f}(t) \quad (29)$$

where \underline{p} is the vector of radiation pressures at each point, and \underline{h} is a matrix of area factors converting pressure to force.

Because of the mutual dependence of the shell motion and the radiation pressure on each other, equations (27) and (29) must be solved simultaneously. This solution is accomplished in NASTRAN by defining a new set of scalar degrees of freedom representing the radiation pressure at each surface point. The set of all such pressures is grouped into the vector \underline{p} . Thus, to NASTRAN, the vector of unknowns (displacements and pressures) is

$$\underline{U} = \begin{Bmatrix} \underline{u} \\ \underline{p} \end{Bmatrix} \quad (30)$$

After equation (27) has been written at each point and combined with equation (29), the resulting matrix equation which NASTRAN integrates is of the usual form

$$\underline{M}\ddot{\underline{U}} + \underline{B}\dot{\underline{U}} + \underline{K}\underline{U} = \underline{F}(t) \quad (31)$$

The contributions to \underline{M} , \underline{B} , and \underline{K} corresponding to the \underline{u} variables are computed directly by NASTRAN based on geometry and material properties. The contributions to \underline{M} , \underline{B} , and \underline{K} corresponding to the radiation pressure variables (\underline{p}) are the coefficients appearing in equation (27). Hence, they are computed externally to NASTRAN and input directly (using the TF bulk data card) into the program. Thus, the matrices \underline{M} , \underline{B} , \underline{K} , and \underline{F} in equation (31) take the unsymmetric form

$$\underline{M} = \begin{bmatrix} \underline{m} & 0 \\ \underline{d} & 0 \end{bmatrix} \quad \underline{B} = \begin{bmatrix} 0 & 0 \\ 0 & \underline{a} \end{bmatrix} \quad \underline{K} = \begin{bmatrix} \underline{k} & \underline{h} \\ 0 & \underline{b} \end{bmatrix} \quad \underline{F} = \begin{Bmatrix} \underline{f}(t) \\ 0 \end{Bmatrix} \quad (32)$$

NASTRAN integrates equations (32) by using the Newmark-Beta finite-difference algorithm, which is unconditionally stable if equation (32) is stable.

Unfortunately, specific numerical results are not yet available for general publication. However, early success with decoupling approximations has convinced the authors that such approaches have great promise as an alternative to the explicit finite element modeling of fluids of "infinite" extent.

GENERAL REMARKS

Two methods by which NASTRAN can be applied without modification to the solution of fluid-structure interaction problems have been described.

The first, the structural analog, is the "lumped" equivalent of the consistent formulation described by Zienkiewicz and Newton (refs. 1 and 2). However, the lumped approach has the advantage for the NASTRAN user that it can be applied without program modification. Otherwise, the two pressure formulations have similar characteristics, including nonsymmetric matrices. This is in sharp contrast to displacement approaches (ref. 6) which assemble symmetric matrices, but at the expense of having three times the number of fluid unknowns.

It should be emphasized that although the analog method was developed specifically for an acoustic fluid, the same technique could be applied to a wide variety of problems in mathematical physics, including heat conduction (ref. 16), the Helmholtz equation, electrical or magnetic potential problems, the torsion of prismatic bars, potential fluid flow, or seepage through porous media. In the present context of fluid-structure interaction problems, the calculation of added mass matrices can be accomplished directly, since it

involves solving Poisson's equation in the fluid region where the source terms occur only at the fluid-structure interface. Such equations can also be solved with standard three-dimensional steady-state heat conduction codes such as those contained in NASTRAN Level 15.5 (ref. 4), the Navy's thermostructural NASTRAN (refs, 17 and 18), or the CINDA thermal analysis program (ref. 19).

For infinite media, the explicit modeling of the fluid is often uneconomical compared with some of the competitive methods. For fluid-structure interaction problems, the use of decoupling approximations provides an attractive alternative. For other general field problems (e.g., potential flow), integral equation techniques are widely used (ref. 20).

REFERENCES

1. Zienkiewicz, O.C., and Newton, R.E.: "Coupled Vibrations of a Structure Submerged in a Compressible Fluid," Proc. Int. Symp. on Finite Element Techniques, Stuttgart, 1969.
2. Zienkiewicz, O.C.: The Finite Element Method in Engineering Science, McGraw-Hill Publishing Company Limited, London, 1971.
3. Butler, T.G., and Michel, D.: "NASTRAN: A Summary of the Functions and Capabilities of the NASA Structural Analysis Computer System," NASA SP-260, Washington, D.C., 1971.
4. MacNeal, R.H., editor: "The NASTRAN Theoretical Manual," NASA SP-221(01), Washington, D.C., 1972.
5. Mason, J.B.: "The NASTRAN Hydroelastic Analyzer," NASA X-321-71-174, Goddard Space Flight Center, March 1971.
6. Kalinowski, A.J.: "Fluid-Structure Interaction Problems using Finite Elements," Proceedings of the Fifth Navy-NASTRAN Colloquium, CMD-32-74, Naval Ship Research and Development Center, Bethesda, Maryland, September 1974, pp. 71-86; also, Defense Documentation Center (DDC) Report No. ADA 004604.
7. Sokolnikoff, I.S.: Mathematical Theory of Elasticity, second edition, McGraw-Hill Book Company, Inc., New York, 1956.
8. Dettman, J.W.: Mathematical Methods in Physics and Engineering, McGraw-Hill Book Company, Inc., New York, 1962.
9. Lysmer, J., and Kuhlemeyer, R.L.: "Finite Dynamic Model for Infinite Media," J. Engr. Mech. Div., ASCE, vol. 95, no. EM4, Proc. Paper 6719, August 1969, pp. 859-877.

10. Schroeder, E.A., and Marcus, M.S.: "Finite Element Solution of Fluid-Structure Interaction Problems," Naval Ship Research and Development Center Report 4707, October 1975.
11. Schroeder, E.A., and Marcus, M.S.: "Natural Frequencies of a Submerged Ring," CMD Report 27-74, Naval Ship Research and Development Center, Bethesda, Maryland, October 1974.
12. Junger, M.C.: "Vibrations of Elastic Shells in a Fluid Medium and the Associated Radiation of Sound," J. Appl. Mech., vol. 19, 1952, pp. 439-445.
13. Geers, T.L.: "Residual Potential and Approximate Methods for Three-Dimensional Fluid-Structure Interaction Problems," J. Acoust. Soc. Amer., vol. 49, no. 5 (part 2), 1971, pp. 1505-1510.
14. Clark, A.V., Jr.: "A Study of Fluid-Structure Interaction and Decoupling Approximations," Naval Research Laboratory Report 7590, Washington, D.C., December 1973.
15. Everstine, G.C.: "The Transient Interaction of Axisymmetric Structures with Fluids," Proceedings of the Fifth Navy-NASTRAN Colloquium, Naval Ship Research and Development Center, CMD Report 32-74, September 1974, pp. 87-92.
16. Mason, J.B.: "The Solution of Heat Transfer Problems by the Finite Element Method using NASTRAN," NASA X-321-70-97, Goddard Space Flight Center, Greenbelt, Maryland, February 1970.
17. Hurwitz, M.M.: "Additions to the NASTRAN User's Manual and Theoretical Manual for a Thermostructural Capability for NASTRAN Using Isoparametric Finite Elements," Naval Ship Research and Development Center Report 4134, May 1973.
18. Hurwitz, M.M.: "Programmer's Manual Additions and Demonstration Problems for a Thermostructural Capability for NASTRAN Using Isoparametric Finite Elements," Naval Ship Research and Development Center Report 4656, March 1975.
19. Gaski, J.D.: "Chrysler Improved Numerical Differencing Analyzer (CINDA)," Report No. TN-AP-66-15, Chrysler Corporation Space Division, New Orleans, Louisiana, April 1966.
20. Dawson, C.W., and Dean, J.S.: "The XYZ Potential Flow Program," Naval Ship Research and Development Center Report 3892, June 1972.

N75 31510

THE IMPACT OF "FOURTH GENERATION" COMPUTERS
ON NASTRAN

James L. Rogers, Jr.
NASA Langley Research Center

INTRODUCTION

The NASTRAN computer program (ref.1) is currently capable of executing on three different "third generation" computers, the CDC 6000 series, the IBM 360/370 series, and the UNIVAC 1100 series. In the past, NASTRAN has proved to be adaptable to the new hardware and software developments for these computers. The NASTRAN Systems Management Office (NSMO), as part of NASA's research effort to identify desirable formats for future large general-purpose programs, funded studies on the impact of the STAR-100 (ref. 2) and ILLIAC IV (ref. 3) computers on NASTRAN.

The STAR-100 and ILLIAC IV are referred to as "fourth generation" or "4G" computers in this paper. "Fourth generation" is in quotes because the differences between generations of computers is not easily definable.

Many new improvements have been made to NASTRAN as it has evolved through the years. With each new release, there have been improved capabilities, efficiency improvements, and error corrections. The purpose of this paper is to shed light on the desired characteristics of future large programs, like NASTRAN, if designed for execution on "4G" machines.

Concentration will be placed on the following two areas:

1. Conversion to these new machines
2. Maintenance on these machines

The advantages of operating NASTRAN on a "4G" computer is also discussed.

BACKGROUND

Figure 1 shows an example of the system changes NSMO has dealt with in the past and of some changes presently being contended with. Minor changes had to be made to Level 15 of NASTRAN when IBM released their 3330 disk packs. The changes by CDC to a SCOPE 3.4 Operating System and by IBM to Virtual Storage systems are causing considerable modifications for the operation of NASTRAN.

25

The STAR-100 and ILLIAC IV computers both have significant hardware and software features to support their respective pipeline and parallel processing capabilities. Pipeline and parallel processors can result in significant increases in computation speed when used on vector-type operations.

A diagram depicting the pipeline operations of the STAR-100 is shown in figure 2. When operating on two vectors, A and B, the pipeline works in the following manner. Elements A(1) and B(1) are received into the pipeline. They then proceed to the next unit in the pipeline, which is sign control. At this time elements A(2) and B(2) are received into the pipeline. A(1) and B(1) move to the align unit, A(2) and B(2) move to the sign control unit, and A(3) and B(3) are received by the pipeline. Each pair of elements then proceeds down the pipeline, with a new pair of elements entering the pipeline at each transfer, until the result is calculated and placed in the result stream.

The conceptual design of the ILLIAC IV with its 64 processing elements (PE) is shown in figure 3. The parallel processors operate differently on vectors than a pipeline processor. With parallel processors, PE₁ operates on A(1) and B(1), PE₂ operates on A(2) and B(2), ..., and PE₆₃⁰ operates on A(64) and B(64).¹ All of these operations take place simultaneously.

The STAR-100 and ILLIAC IV studies were conducted to gain insight into the potential impact of major system changes on large finite element programs like NASTRAN. In each of these studies there was one main objective: to investigate the feasibility of modifying Level 16 of NASTRAN in order to make it execute efficiently on the subject computer. This objective was to be accomplished in the following four steps:

1. Identify and describe the areas in NASTRAN which (a) easily lend themselves to or (b) could cause problems in conversion to the subject computer.
2. Determine the areas of NASTRAN where (a) modifications are needed to improve efficiency, and (b) significant benefits could be expected from using new strategies or algorithms for the subject computers.
3. Determine whether or not the above changes can be made in a way that the efficiency of NASTRAN can be improved with little or no increase in the number of computer dependent subroutines.
4. Estimate the time and cost involved in designing, coding, and implementing each of the modifications identified above.

Many different aspects of NASTRAN were studied. These items include:

1. Linkage Editor
2. Input/Output

3. Paging Problems
4. Machine-Dependent Code
5. Matrix Operations
6. Checkpoint/Restart
7. Compilers

The details of these aspects are discussed subsequently.

The STAR-100 and ILLIAC IV are completely dissimilar in the method of operating on vectors. Because of this and other dissimilarities, finite element programs like NASTRAN may require distinctly different versions to function efficiently on each machine.

CONVERSION

This section is concerned with the effort required to convert an existing version of NASTRAN to execute efficiently on a "4G" computer. Two basic questions are answered in this section. (1) What is the scope of the required changes in terms of time and manpower? (2) Which areas of NASTRAN must be converted to exploit "4G" technology?

Scope

The conversion effort to a new computer may be conveniently divided into a two-step process. The first step involves converting the currently existing NASTRAN to execute on the "4G" computer. The second step takes the converted code and improves it so that NASTRAN will execute efficiently on that computer. Table 1 summarizes the total effort required to complete both steps on the STAR-100 and ILLIAC IV.

An effort of 67 man months (ref. 2) over 9 months is estimated to convert NASTRAN to execute on the STAR-100. This effort results in only a scalar version of NASTRAN, which does not exercise the vector processing capability, and results in almost no improvement over the CDC 6600. To exploit the vector processing capability of the STAR-100 would require another 30-60 man months over a 10-18 month time period. Of the 67 man months in the initial conversion step, only 12 man months are to be used in actual NASTRAN code conversion.

An effort of 60 man months over 18 months (ref. 3) is estimated to convert NASTRAN to execute on the ILLIAC IV. This effort would not make full use of the parallel processing capability, but it is estimated that this will give the user 37% faster NASTRAN execution than the same run on an IBM 370/165. To make efficient use of the ILLIAC IV would require another 50-80 man months over an 18-24 month period. This effort would

allow NASTRAN to execute an estimated 90% faster than on the IBM 370/165. Of the 60 man months in the initial conversion step, 43 man months were estimated for actual NASTRAN code conversion.

Required Changes to NASTRAN

The changes that would be needed in the NASTRAN system include the following:

1. The Linkage Editor - The modifications to the Linkage Editor depend on the particulars of the computer involved. Conversion to the ILLIAC IV could require the Linkage Editor to be completely rewritten (a formidable task), since the present Linkage Editor on the ILLIAC IV has no overlay capability (ref. 3). Whereas, conversion to the STAR-100 could involve dropping the Linkage Editor in favor of executing NASTRAN as a single controllee file (ref. 2).
2. Input/Output - There are several important differences between NASTRAN and STAR I/O techniques (ref. 2). NASTRAN has hundreds of data blocks allocated for over 50 files, while the STAR Operating System (OS) provides less than 15 files. NASTRAN has open-ended files, while STAR OS requires allocation of the file space at the time the file is opened. The NASTRAN GINO provides random access methods employing indexed-sequential files, while STAR OS employs a simple sequential record manager. On the ILLIAC IV, the NASTRAN I/O package must be optimized to handle the bulk of data transfers between the processing element memories and the ILLIAC IV disk memory. In either the STAR-100 or the ILLIAC IV computer, because of the increased computational speed, the I/O must be highly optimized so as not to decrease overall efficiency.
3. Paging Problems - In STAR, a Virtual Storage computer, paging is a method for associating virtual memory with real memory. Several major factors influence the page size determination in a scalar virtual machine, namely code organization, compression, transport time, and the page replacement algorithm. Additional factors influencing the page size are created with the introduction of the vector capability. These factors include the cost of halting a vector instruction to replace a page, the cost of restarting a vector instruction, and the vector length. Before any conversion could take place, all of these factors would have to be examined and an optimal page size determined.
4. Machine-Dependent Code - All machine-dependent subroutines would, of course, require complete recoding in a "4G" assembly language.

5. Matrix Operations - The matrix operation modules of NASTRAN should be highly optimized for a "4G" computer, in order to exploit the special advantages of these computers. It was suggested in reference 2 that the NASTRAN matrix file structure could be optimized for the STAR-100 by dividing the matrix files into two separate files. One file would contain all the control information such as column, row position, and members of coefficients. This often enables one to operate directly on the coefficients without intermediate reorganization of the coefficients that for efficient pipeline processing. It was suggested in reference 3 that matrix operation modules could be optimized on the ILLIAC IV by developing detail specifications before beginning implementation. These preliminary design criteria would consider definition of array storage conventions within the ILLIAC IV processing element memories, and specialized storage schemes and disk mapping criteria for internal file communications and external files used in intermodular communication.
6. Checkpoint/Restart - Indiscriminate checkpointing of data files is most undesirable on "4G" computers. The transfer rates to and from a disk and central memory are slow compared to the execution power of a "4G" computer. Often, therefore, the cost effective approach would be to recalculate rather than checkpoint and restart.
7. Compilers - The STAR-100 FORTRAN compiler encompasses the NASTRAN FORTRAN subset with one exception: the use of the ampersand symbol (&) in a calling sequence to signify a non-standard return label. FORTRAN specifies that the symbol be a dollar sign (\$). The ILLIAC IV has a compiler option which will convert standard FORTRAN to IVTRAN, the ILLIAC IV FORTRAN-based language. This option examines DO loops of standard FORTRAN programs and converts them into more efficient DO FOR ALL loops for use on the ILLIAC IV.

Although all of these aspects of conversion are important, both studies (ref. 2,3) concluded that the majority of time in any conversion effort would be spent in optimizing the matrix operations.

Single-Programming and Multi-Programming

The ILLIAC IV is a single-programming computer, i.e. it is dedicated to execution of only one job at a time. Whereas, the STAR-100 is eventually anticipated to operate in a multi-programming mode, i.e. it will execute many jobs simultaneously at any one time. Reference 2 concludes that the STAR-100 CPU would remain idle most of the time if NASTRAN were executed on the STAR-100 in a single-programming environment. This, of course, would be very inefficient. Because of its configuration, the ILLIAC IV cannot handle a multi-programming environment. Thus one must definitely take the configuration of the conversion computer into consideration before conversion begins.

"Front-End" and Complete Conversion.

One of the major questions that arose during both the STAR-100 and the ILLIAC IV studies was, Is the preferred configuration to have NASTRAN execute in a host plus "4G" computer ("front-end") environment (e.g. let STAR do what STAR does best and leave the rest to the CDC 6000) or for NASTRAN to be completely converted to the "4G" computer? Both studies concluded that if conversion were contemplated, the preferable mode is for NASTRAN to be converted to do all of its executions on a "4G" computer. There are several reasons for recommending the complete conversion concept over the "front-end" concept.

1. The STAR-100 requires 180 msec to transfer one page of data from the CDC 6000 to the STAR-100.
2. Once the "front-end" concept was working, the remaining conversion effort, to get all of NASTRAN on a "4G" computer, while involving significant volumes of code, would not require the further system type extensions.
3. The cost of total conversion is estimated to be less than that of the "front-end" concept.

There are some differences when converting to a host plus "4G" computer and a total conversion effort.

The conversion of NASTRAN to a host plus "4G" computer involves only a subset of NASTRAN. Prime candidates for the conversions are the functional modules which have modest input requirements, heavy computer and/or internal I/O requirements, and modest output requirements. New code must be generated to pass data between the "4G" computer and its host. Further, new code would have to be developed so that when NASTRAN is running on the host computer it can either continue processing or go into RECALL until a needed file is received from the "4G" computer.

If the complete conversion takes place, the resulting NASTRAN code would be computer dependent. It would no longer be compatible with a "third generation" NASTRAN and probably not even compatible with another "4G" NASTRAN. This would complicate the maintenance of NASTRAN, a situation discussed in the next section.

MAINTENANCE

Once a large computer program has been developed or converted and released to users, the maintenance of that program becomes the primary concern. NASTRAN's maintenance effort centers around an archive version.

This version is continually being modified and contains all of the latest error corrections and new capabilities. The CDC, IBM, and the UNIVAC versions are generated from this archive version. Each of these versions also has its own unique features which must be maintained separately. These features include machine-dependent subroutines, special linkage editor control cards, and subroutines with multiple entry points or non-standard returns.

As figure 4 shows, the archive version is used to create a particular test version. Demonstration problems are then run on this version. If an error occurred in a machine-independent subroutine, then its correction in the archive version probably results in a correction in all versions. However, if the error occurred in a machine-dependent subroutine, then it may or may not occur in other versions and further testing is required. After the known errors are corrected, the next version is tested. The looping of this procedure is continued until all three versions of NASTRAN are ready for delivery to the public. The extensive machine-independent code and other well developed relationships among the three versions are fully utilized to minimize the testing effort required.

The "4G" computers involve radical departures from the "3G" machines and strong variations among themselves requiring different special programming language. Thus, for such machines, all code is essentially "machine-dependent". The cost of maintenance efforts for different machine versions cannot be minimized through extensive commonality of code, as it is for the three existing NASTRAN codes.

ADVANTAGE OF CONVERTING NASTRAN TO A "4G" COMPUTER

The primary advantage in converting NASTRAN to a "4G" computer is the gain in computational speed, especially for vector-type operations. Tables 2, 3, and 4 show some timing comparisons for the ILLIAC IV, STAR-100, and present "third generation" NASTRAN computers. From table 2 it can be seen that the STAR-100 and ILLIAC IV are on the order of 5 to 10 times faster than the fastest "third generation" computer when a large number of steps are involved in the calculation. Table 3 compares the potential efficiency of NASTRAN operations performed on the ILLIAC IV with the IBM 370/165 and the CDC 6600 computers. For this comparison, the process of matrix decomposition was selected as a representative operation involving large amounts of both computation and input/output processing. The decomposition of the 10,000 degree-of-freedom matrix would take 100 hours on the IBM 370/165 or 150 hours on the CDC 6600 when spill occurs. This same job, however, could be run in 4 hours on the ILLIAC IV. Table 4 shows a time comparison between the STAR-100 (anticipated) and CDC 6600 computers for decomposing a stiffness matrix. The algorithms used are Gauss elimination (in symmetric form) or Cholesky decomposition (with or without square roots) (ref. 2).

The effective bandwidth depends upon the numerical algorithm used in implementing the mathematical algorithm. For this table, the effective bandwidth has been set to $4\sqrt{N}$, where N is the number of equations. It is also assumed that both computers have full machine utilization of CPU time. It can be seen from the table that for 20,000 equations, the Cholesky method on the STAR-100 is 30 times faster than the Cholesky (FORTRAN) method on the CDC 6600 (13 minutes on the STAR-100, 6 hours 38 minutes on the CDC 6600). For the above tables, it is obvious that "4G" computers have a speed advantage when performing the large vector-type operations that are so common in finite element programs.

CONCLUDING REMARKS

As a part of NASA's research toward identification of desirable forms for future large finite element programs, studies were made of the required scope and technical changes which would be necessary to make NASTRAN operate efficiently on two "4G" computers, the ILLIAC IV and the STAR-100. Conversion efforts for either of these two computers could conveniently be divided into two steps. The first step would result in a working, not efficient, version of NASTRAN. The second step would optimize the results of the first step and yield an efficient version of NASTRAN on a "4G" computer. The first step alone was found not worth the effort, since the resulting version of NASTRAN would show only small improvements in execution speeds over similar "3G" versions. The time frame to complete both steps and release a "4G" version of NASTRAN to the public would take a minimum of three years.

Numerous areas of NASTRAN would need modification to take advantage of the increased computational speed of a "4G" computer. Areas requiring changes include the Linkage Editor, input/output, machine-dependent code, matrix operation subroutines, and the checkpoint/restart capability. Most of the effort, however, would be spent optimizing the matrix operation subroutines to exploit the capabilities of "4G" computers. A total conversion to a "4G" computer appears to be preferable to using a host "4G" computer environment. However, the converted "4G" NASTRAN would not be cost effective. Moreover, required changes would yield essentially all machine-dependent code and greatly amplify the burden of maintenance.

There are no current plans for NASA to convert NASTRAN to a "4G" computer. There are, however, other projects to develop structural analysis codes for "4G" computers. These are the ILSA (ILLIAC IV Structural Analysis) project sponsored by the Advanced Research Projects Agency and supervised by the Defense Nuclear Agency and a project designated as FESS (Finite Element System for STAR-100) at Langley Research Center.

REFERENCES

1. McCormick, C. W. ed.: "NASTRAN Users' Manual, "NASA SP-222(01), June, 1971.
2. Control Data Corporation: "Study of the Modification Needed for Efficient Operation of NASTRAN on the Control Data Corporation STAR-100 Computer." NASA CR-132644, 1975.
3. Universal Analytics, Inc.: "Feasibility Study for the Implementation of NASTRAN on the ILLIAC IV Parallel Processor." NASA CR-132702, 1975.

TABLE 1
 EFFORT REQUIRED FOR EFFICIENT CONVERSION OF NASTRAN TO EXECUTE ON
 STAR-100 AND ILLIAC IV COMPUTERS

COMPUTERS	STEP ONE CONVERSION		STEP TWO OPTIMIZATION		TOTAL CONVERSION	
	MAN MONTHS	MONTHS	MAN MONTHS	MONTHS	MAN MONTHS	MONTHS
STAR-100	67	9	30-60*	10-18	97-127	19-27
ILLIAC IV	60	18	50-80	18-24	110-140	36-50

*ONLY INCLUDES VECTOR PROCESSING CAPABILITY, NO OTHER CONVENIENCE OR PERFORMANCE FACTORS.

TABLE 2

COMPARATIVE SPEEDS* OF EXECUTION BETWEEN
"THIRD AND FOURTH GENERATION" COMPUTERS

[For the ILLIAC IV and STAR, the figures are preliminary and for illustrative purposes only. For the 360/195 and 7600, the numbers are sensitive to the way the smaller, faster memories are used.]

Operation	Steps per stage	IBM 360/75	IBM 360/195	CDC 7600	CDC STAR	ILLIAC IV
Addition	N = ∞	0.24	4.6	5.2	50	50
Multiplication	N = 1	0.24	0.55	1.6	0.57	0.78
	N = ∞	0.14	4.6	5.2	25	44
Division	N = 1	0.14	0.53	1.5	0.57	0.69
	N = ∞	0.096	1.7	2.0	12.5	17
	N = 1	0.096	0.43	0.93	0.56	0.27

*64-bit precision computation speeds (memory to memory) in millions of operations per second.

TABLE 3

DECOMPOSITION TIMING ESTIMATES FOR NASTRAN

[For the ILLIAC IV, the figures are preliminary and for illustrative purposes only]

	IBM 370/165	CDC 6600	ILLIAC IV (After Step 1)	ILLIAC IV (After Step 2)
<u>Decomposition (no spill)</u>				
Matrix order 10000 dof	0.6 hours	1.3 hours	0.7 hours	0.01 hours
Semibandwidth 300 dof				
Active columns 50 dof				
<u>Decomposition (with spill)</u>				
Matrix order 10000 dof	100 hours	150 hours	9 hours	4 hours
Semibandwidth 600 dof				
Active columns 50 dof				
Working storage 50000 words				

TABLE 4
TIMING ESTIMATES FOR THE DECOMPOSITION
OF A STIFFNESS MATRIX

Number of Equations	Time (seconds)			
	STAR (FORTRAN)		CDC 6600 (CHOLESKY)	
	GAUSS	CHOLESKY	FORTRAN	COMPASS
100	.08709	.07469	2.7502	1.5520
250	.35107	.32035	10.862	6.1366
500	1.3634	1.3345	31.601	18.251
750	2.6060	2.6346	59.856	35.351
1000	4.0498	4.2010	94.844	57.041
3000	24.392	28.236	743.38	546.28
5000	55.013	67.703	2035.2	1612.2
10000	170.49	230.09	6839.7	5639.7
20000	537.25	798.85	23914.	20524.

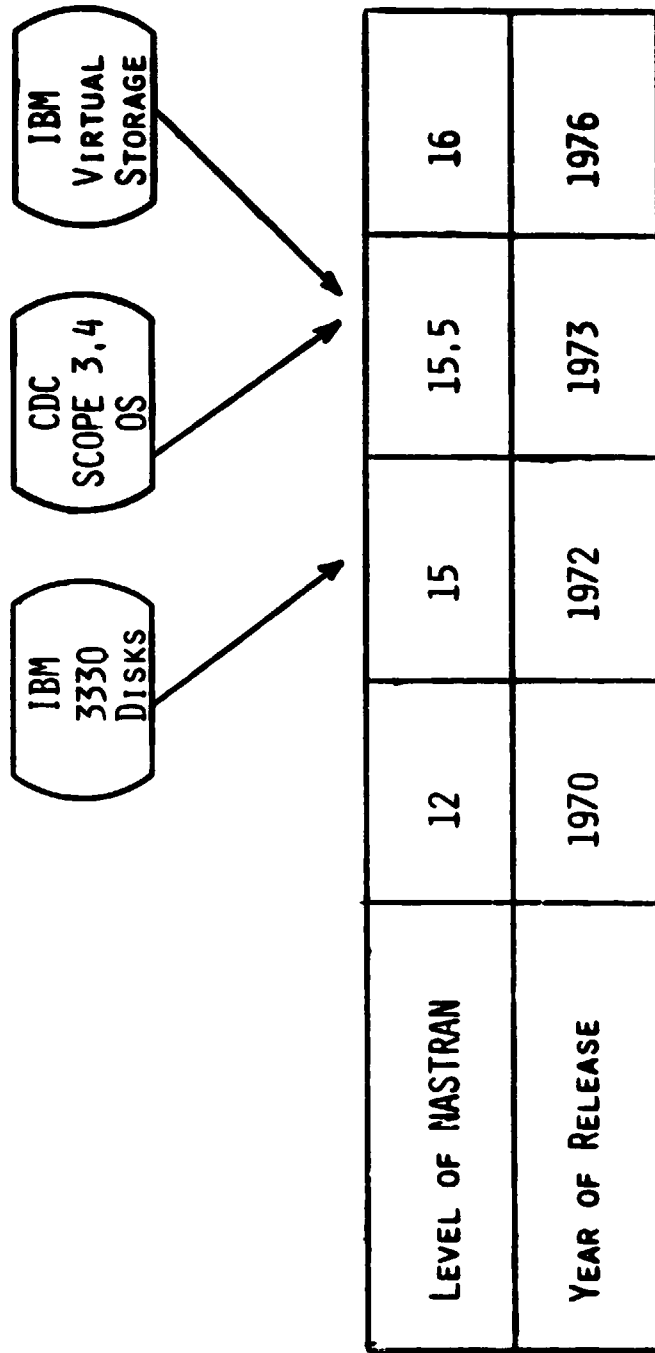
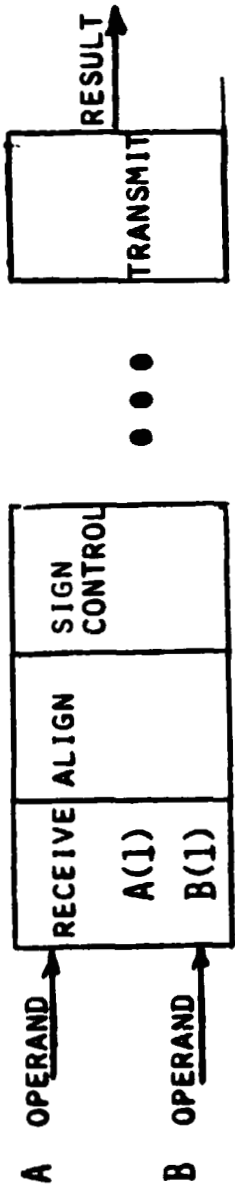
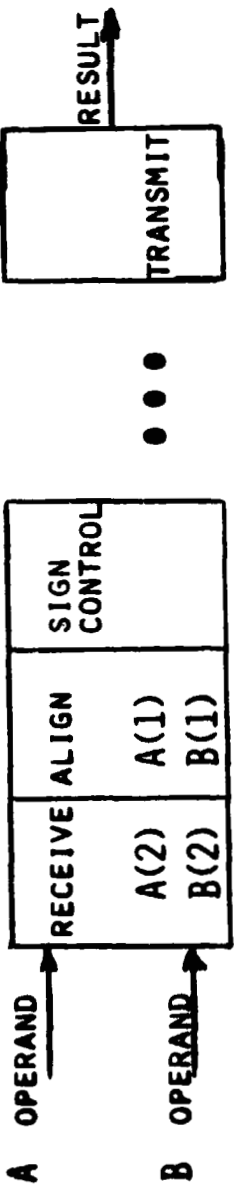


Figure 1 - Examples of Impacts of Hardware and Software Developments on NASTRAN Releases

STEP 1 - RECEIVE A(1), B(1)



STEP 2 - RECEIVE A(2), B(2), ALIGN A(1), B(1)



STEP 3 - RECEIVE A(3), B(3), ALIGN A(2), B(2), SIGN CONTROL A(1), B(1)

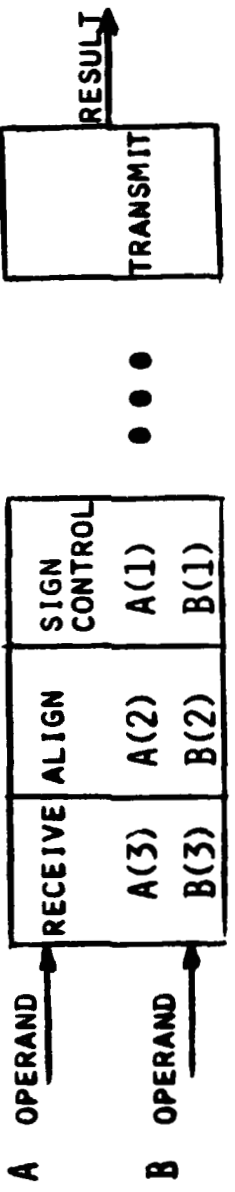


Figure 2 - Data Movement within the STAR-100 Pipeline

PROCESSING ELEMENTS

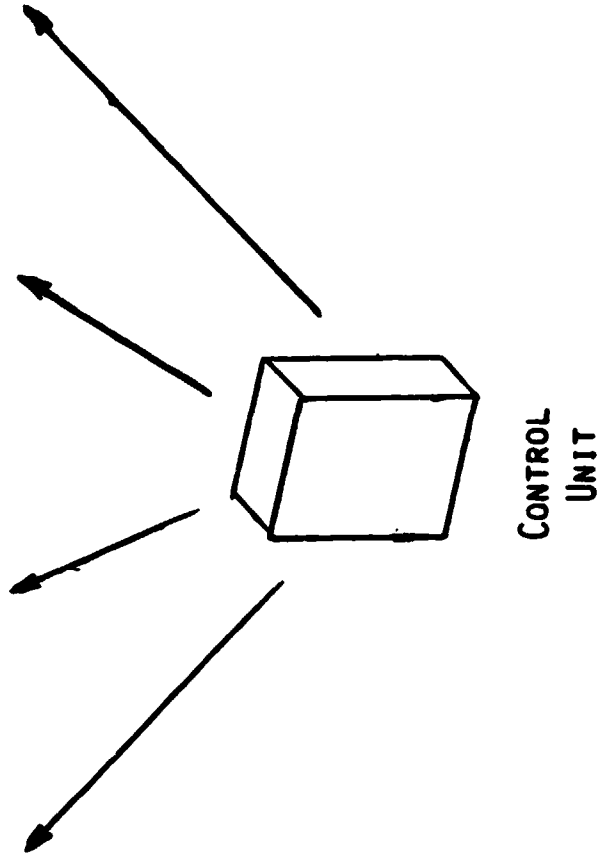
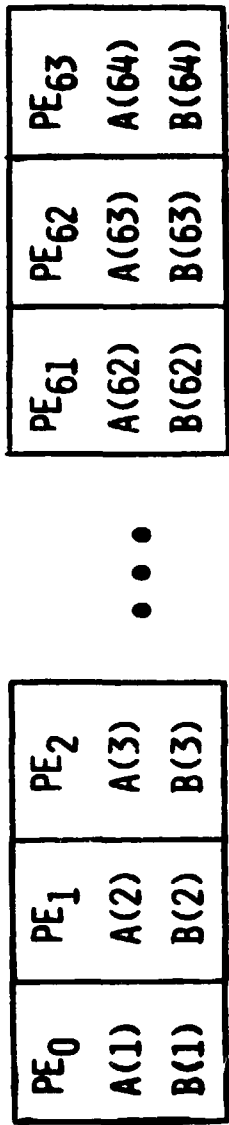


Figure 3 - Data Movement within the ILLIAC IV Processing Elements

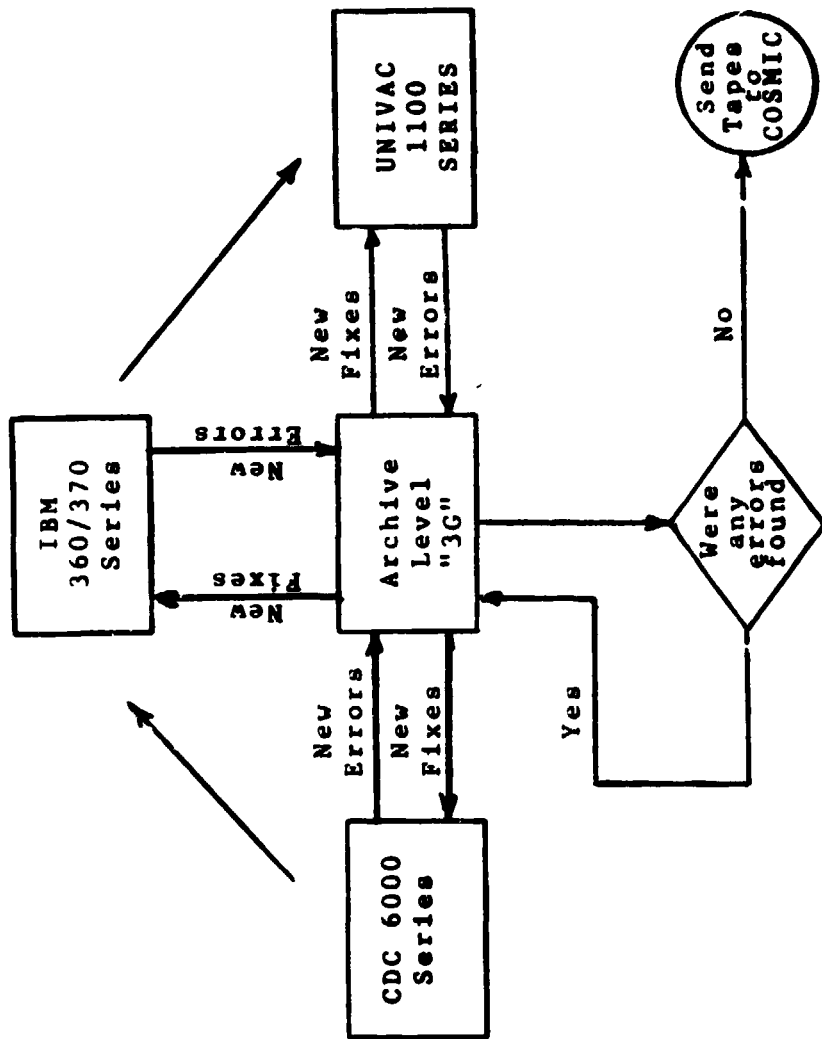


Figure 4 - Computers and the NASTRAN Maintenance Effort

N75 31511

NASTRAN PRE- AND POSTPROCESSORS
USING LOW-COST INTERACTIVE GRAPHICS

E. D. Herness and H. Z. Kriloff
Boeing Computer Services, Inc.

ABSTRACT

Low-cost graphics are now available to the engineer. The low-cost storage tube terminal, the time-sharing computers, and the communication through the ordinary telephone are the hardware advances that now make low-cost graphics a reality. Time-sharing system software and an easy to use graphics library are the software that make developing pre- and post-processors easy and inexpensive. A design for a NASTRAN preprocessor is given to illustrate a typical preprocessor. Several displays of NASTRAN models illustrate the preprocessor's capabilities. A design of a NASTRAN postprocessor is presented along with an example of displays generated by that NASTRAN processor.

INTRODUCTION

A large part of the cost for structural analysis is in the preparation of correct input data (Reference 1). Pre- and postprocessors are effective in reducing the cost of input data preparation and output analysis (Reference 2).

The data used to define a NASTRAN model and the results generated by a NASTRAN analysis are graphical. This is the reason the plotting capability has been so widely used. The major problem with the plotting package in NASTRAN is one of computer operations. The time it takes to get a NASTRAN job scheduled, run on the computer and plots returned is often several days. This is too long a time for an analyst to effectively check his input in this manner. As a result many expensive NASTRAN runs are made that solve the wrong model. This suggests a NASTRAN preprocessor using interactive graphics.

A NASTRAN preprocessor using low-cost interactive graphics can reduce the time and cost of making a NASTRAN analysis. Input errors can be located and corrected in minutes at very low cost. The NASTRAN input deck is more correct before the first NASTRAN run is made and the analyst has the confidence of seeing and verifying the input model.

28

A NASTRAN postprocessor using low-cost interactive graphics can replace pages of output with a few graphical displays. A displacement vector or mode shape can be displayed and visualized in minutes that may take several hours to understand from the listing. The speed with which one can see and interpret the results and the ability to interactively choose the data and view it are the major advantages of a low-cost interactive postprocessor over the NASTRAN plotting package.

The purpose of this paper is to discuss the advances in hardware and software that make low-cost interactive graphics easy to use. The design and capability of a NASTRAN preprocessor is discussed along with several displays of input models. The design and capabilities of a NASTRAN postprocessor that displays the NASTRAN results are also discussed.

LOW-COST GRAPHICS HARDWARE

The major reasons for the increased utilization of computer-based graphics have been the steady decrease in the cost of the hardware required and the improved performance of these systems. The decrease in cost is due to improved technology and the economics of increased utilization. These factors carry through to each of the components that make up the graphics system: the host computer, the communications lines and the graphic terminal (see Figure 1). New trends may change the present techniques for implementing graphics, but the direction of increased interaction with graphics images will continue.

The advent of time-sharing computing systems has decreased the cost of using a computer because now the user pays for only the resources that he uses, not those he has access to. This improved utilization allows the user to consider applications where little computation is performed and data are merely manipulated and reformatted by the computer. These applications instead of wasting resources allow more users to use a given computer system, decreasing the cost to each user. The user also has available the improved and specialized software development aids that are only economical when utilized by many users and he can share data storage costs among a number of application systems. The user is now not restricted to a specific package or hardware system but can now choose that system that best suits the needs of his application. This then decreases the costs to modify the software so that it will fit a given hardware configuration and system.

The user does not need to be geographically near the host computer. Due to advances in the field of telecommunications, standard telephone lines can be used to carry the signals from the host computer to a remote terminal. Since the computer signals are digital and the telephone lines transmit analog signals only, a device is used to modulate the analog carrier signal with the digital signal, and to demodulate (separate) the signals at the other end. This device is called a modem (modulation - demodulator) and has decreased in price while increasing in data transmission rate.

The largest cost decrease has occurred in the development of graphic terminals. Increased usage, simplified technology and improved design have made graphic terminals easier to use and less expensive. The three different types of terminals that will most affect graphics development in the next few years are the direct-view storage tube, the plasma panel and the intelligent terminal.

The direct-view storage tube (DVST) is a modified form of cathode ray tube (CRT) where an electron beam strikes the phosphor-coated face of the tube. This excites the phosphor which then emits light when it returns to the normal unexcited state. In the DVST a negatively charged grid is placed between the phosphor and a low energy unfocused electron beam. The negative charge prevents the electrons in the electron beam from reaching the phosphor and exciting it. However, a second, high energy focused electron beam is used to remove electrons from the grid, allowing the phosphor to be excited at that location. Therefore, the grid serves as a memory for the image being drawn. The use of the electrostatic grid memory allows the system to have both a low speed connection between the terminal and the computer and to provide storage for very complex graphical images. The DVST is widely marketed as a commercial terminal, thereby providing decreased cost due to mass production economics.

The plasma panel is a newer, less complex technology. The unit is totally digital, eliminating the need for circuitry such as digital-to-analog converters and can serve as both an input and a display device. While presently not in wide usage, these displays and other matrix displays similar to these should gradually replace the CRT displays in the next decade. The advantages of compactness, simplicity, and the optical mixing of photographic and computer-generated images will gradually overcome the advantages of the presently more widely used displays.

The third influence in the low-cost terminal market is the potential effect of the intelligent terminal. This is a display device combined with a micro- or miniprocessor. These processors are already in the under \$100 price range and can replace much of the specialized digital circuitry required by the present generation of terminals. Combined with the graphic display these processors provide a terminal that removes part of the processing load from the host computer, improves system response characteristics, and standardizes the user interfaces for many very different host computer systems. The advantages of personalized computing quickly outweighs any small additional cost (if any) required by adding the processor. The main deterrent to the widespread usage of such systems will be the high cost of developing software to support the terminal processing systems.

SOFTWARE FOR LOW-COST GRAPHIC TERMINALS

While the cost of the hardware used by graphic systems has steadily decreased, software prices have often increased the cost of using such systems. Since the software is as important as the hardware (sometimes more so since software can be used to modify the performance of the hardware while the hardware seldom changes the type of software required) the cost and usage of software is an important systems consideration.

The software required by a graphics system consists of a time-shared operating system, a higher level graphics language, and a graphics library. The time-shared operating system has two components that are very important for graphics systems. These components are the command interpreter and the text editor. The command interpreter provides the ability to select among a series of options, those programs, defaults and data files that will be used in a given task. The text editor is used to prepare programs and data for manipulation by the system.

A number of considerations must be addressed in the implementation of a higher level graphics language. These considerations are: the choice of an implementation language, the use of interpreters, the restrictions of device independent software and the use of general data structures.

The choice of a graphics language that would remove many of the difficulties of presently available languages is always a very tempting alternative. However, it takes from 7 to 15 years for a new programming language to be widely accepted no matter how many useful features are part of the language. Since graphics is only one part of the requirements for a programming language this long lead time prevents the utilization of a new language. However, there is a way to modify the syntax of a programming language without creating a new language. This is through the use of a precompiler that converts the modified syntax into some more widely used language. This gives the programmer the option to use the new syntax where it benefits the program development and the accepted language where the advantages of portability and greater utilization are more important.

Another choice in the implementation of a graphics system is whether the language should be provided as a compiler or as an interpreter. In a compiler the program code is translated into machine instructions as a complete entity. More than one language statement may be used to provide information about data structures, execution control or type of algorithm. Most of the execution decisions are made at this point allowing optimization of the final code. If an interpreter is used each statement is translated and immediately executed in the order determined by the program execution. This allows less optimization but greater flexibility in the execution of the program. As the graphic commands get higher level (i.e., each statement defines a more complex operation) the distinction between a compiler and an interpreter becomes less significant. The ideal mixture is a very high-level compiler allowing complex user-defined data structures and code optimization with statements that are mini-interpreters allowing greater freedom in the execution phase. Features such as data editing and execution control can thereby be utilized without recompiling the program.

The use of a compiler solves one other problem. Since there are a large number of graphic display devices, each with both desirable and undesirable features, the ability to use more than one device with the same program code (device independence) is an important feature of any graphics system. In an interpreter-based system the machine code for each display device would have to be part of the system and each time the program provided a display command it would have to check which device it was using. This would increase the size of the user program and decrease the execution speed. In a compiler this decision would be made only once and the system would load only those routines required by the devices being used. To change devices would require the recompiling or reloading of the user's program.

The data used to generate graphic images can exist in a number of different formats within the computer. These forms are dictated by the display hardware, the application program, or the operations that may be performed on the data. When these forms are simple (array type sequences) a wide variety of graphic software can be developed to edit or enhance the image to be displayed. As the data structures become more complex, less graphic software is available as a standard part of the system and it becomes the user's responsibility to provide the necessary routines. Therefore, the more complex data structures are used only where they add to the utility of the information representation.

Thus, a system implemented as a high-level precompiler with a simple data structure provides the best mixture of efficiency and flexibility in a graphics system. Where a large enough library of primitive operations are available to the system user, graphics can be simply and usefully added to application programs.

THE GRAPHICS DISPLAY LIBRARY

Each of the hardware, software or user-directed operations are implemented by one or more calls to library subprograms. These subprograms provide capabilities for accurate, fast and easy generation of the display portion of the application program. In order to provide for the device independence described above, the system should consist of two types of subprograms: those that communicate with the terminal (called the low-level routines) and those that manipulate the user's data (called high-level routines). A simple, flexible interface between the two levels allows the implementor to exchange low-level routines when he changes terminal systems. The low-level routines are provided by the terminal vendor (Reference 3) and simply draw lines, erase lines, and change the terminal state.

The higher level routines are the routines called by either the user or the precompiler in order to express the sequence of operations required to generate an image display or a user interaction. These allow the user to select and define defaults for a graphics terminal (initialization) to define the logical program control and the display format. The program control can be expressed through menus, function keys, input options and other types of processing of input from devices such as keyboards and crosshairs. The displays are generated by defining coordinate systems (rectangular or polar), scales (linear, logarithmic, etc.), labeling and

text generation. The scales are determined either automatically in order to fit the data or a section of the data (blowup) or explicitly by the user. Where data fall outside the screen scale, a scissoring routine is used to exclude all elements outside the region. Where the data are three-dimensional, routines are required to rotate the objects and to project the data into a two-dimensional system. Since all terminals do not have a device to generate a permanent copy of displays generated, a technique to preserve a representation of the object on the screen for later hardcopy plotting is also necessary. An example of a system that provides all these capabilities is the BCS (Boeing Computer Services) Interactive Graphics (BIG) System (Reference 4).

Once a system provides all the above facilities it can be used to generate programs that are easy to use, simple to implement and solve many different types of problems. Examples of the application of this system to NASTRAN are given in the following sections.

ADVANTAGES OF MULTIPLE PROCESSORS

In the implementation of a graphics display facility into an already existing computer program the designer has two options. He can insert the code into the program at the appropriate places or he can construct separate program modules that utilize the same data bases as the existing program. This latter choice often requires the reprogramming of certain operations that already exist in the functioning system. It also imposes additional overhead on the system because of increased disk input/output and data reformatting. However, in certain cases, the advantages of this second choice far outweigh the disadvantages.

A good reason for selecting the multiple processor form or design over the code insertion design is where the functioning program is already computationally bound. In that case the response time for the display part of the system will be increased due to the overhead calculations of the main program. Either complex logic must be incorporated into the program in order to improve system response or the display sections must be separated from the program logic sequence. Once this has been done the necessary additional programming for a pre- or postprocessor has been performed.

Another reason for using a separate processor is that as a program gets very large the slightest change tends to require a major effort. By building a separate processor the original program code is left undisturbed and the effort is minimized.

The last reason is that where the modules are small it is possible to create multiple versions of a subsystem for different classes of users. This can increase the utility of the program with very little additional effort since many sections of the programs will be identical.

Therefore the advantages for computer-bound NASTRAN tasks of improved response, minimal code disturbance and multiple versions led to the insertion of graphics displays using pre- and postprocessors.

NASTRAN PREPROCESSOR

An interactive graphics preprocessor for NASTRAN is a valuable addition to the NASTRAN capability. Errors in geometry and connectivity input can be identified and corrected in minutes from a terminal. These same errors may take days and several NASTRAN runs to find using a batch process with off-line plots. The relationship of the NASTRAN input display program to the rest of the system is shown in Figure 2. The time-share system command mode and editor are used to generate and update the NASTRAN deck and pass it to the NASTRAN Input Display program.

The program logic for the NASTRAN preprocessor is as follows: The program reads the NASTRAN deck. The grid cards are converted to the base XYZ system and stored in data arrays. The element connectivity cards are read and an element connectivity table is built. At the time the connectivity cards are read, a check is made to see that each grid reference on the connectivity card has been defined by a grid card. An error message is printed out that identifies the missing grid points. After the NASTRAN data has been read, the remainder of the program is executed interactively from the terminal. This provides the user with the opportunity to select those operations that contribute most to the data verification process. Since many types of errors might occur and only the user can detect most of them (that's why we use graphics) this type of operation is both cost-effective (less spoiled runs) and productive (the user does not have to observe useless data displays). The user then chooses the next step from the following menu:

DEFINE DISPLAY PARAMETERS
DEFINE DISPLAY SET
DISPLAY STRUCTURE

DEFINE DISPLAY PARAMETER allows the user to choose the view angle. By defining different view angles the structure may be rotated in any direction. Detail which is hidden because of a given orientation can be interactively changed to show clearly the structural idealization. Often several viewing angles are necessary in order to examine all of the geometry and connectivity of the model.

DEFINE DISPLAY SET allows the user to select any part of the model to be displayed. The linear elements, triangular elements and/or quadrilateral elements within one or more ranges of element ID's may be interactively selected as the display set. The linear elements, triangular elements and/or quadrilateral elements may be selected to be displayed individually or in combination. In addition specific element ID's or a range of ID's may be selected. The set selection option allows the model to be displayed section by section. Duplicate lines can be displayed in separate views.

DISPLAY STRUCTURE causes the program to create the previously defined display with user-chosen viewing angles. The user has the option to display gridpoint ID's and/or element ID's. Another important capability of this option is the BLOWUP feature. The corners of a new display window are defined as two points on the display. The window defined by these points are the new scale limits. The structure is displayed so that the window is expanded to the boundaries of the display screen. This is an important capability in viewing complex structural details

The NASTRAN preprocessor described above has been developed and extensively used. Figure 3 shows the NASTRAN demonstration problem 1-1 in a 3-dimensional view. The model includes several linear, triangular and quadrilateral elements. Figure 4 shows a spherical cap problem that is defined in the NASTRAN demo 1-2. The spherical cap model has been rotated counterclockwise so that the gridpoint ID's are more visible. Figure 5 shows a blown up portion of the same spherical cap. Notice the lines on the right and at the bottom are clipped at the display boundary.

The initial capability of the preprocessor includes the display of the gridpoints and element connectivity. Planned extensions include the display of single point constraints, multipoint constraints, forces and concentrated masses.

NASTRAN POSTPROCESSOR

A NASTRAN postprocessor that interactively displays deflections and mode shapes has been developed from the NASTRAN preprocessor capability. The source of the input data is now the checkpoint tape rather than the NASTRAN input deck. Usually it is advisable to extract from the checkpoint tape the data blocks BULKDATA, EQEXIN and UGY and save them on a separate file. The NASTRAN postprocessor then reads that file and builds the geometry array, the element connectivity and the displacement vectors. The highest level menu of the NASTRAN postprocessor is:

```
DEFINE DISPLAY PARAMETERS
DEFINE DISPLAY SET
DISPLAY UNDEFORMED STRUCTURE
DISPLAY DEFORMED STRUCTURE
DISPLAY UNDEFORMED AND DEFORMED STRUCTURE
```

The DEFINE DISPLAY PARAMETERS option allows the user to define the viewing angles, choose the subcase displacement vector and define the magnification factor on the displacement vector.

The DEFINE DISPLAY SET option is identical to the option in the NASTRAN preprocessor.

The three DISPLAY options display the undeformed structure, the deformed structure or both the undeformed and deformed structure. The user may choose to display the gridpoint ID's, the element ID's or both. On any display the user may choose to blow up a portion of the structure by selecting a viewing window defined by two points. That rectangle is then expanded to the full screen area.

The above program has been developed for the BCS MAINSTREAM-EKS System that runs on the CDC 6600 using the BCS Interactive Graphic System. Figure 6 shows the ninth vibration mode of the helicopter structure used in Reference 5.

CONCLUDING REMARKS

Advances in computer hardware, the low-cost graphics terminal and data communications make low-cost graphics feasible. Advances in graphics software allow the user to easily develop interactive pre- and post-processors for NASTRAN. The preprocessor provides a very effective way to interactively check the input data. The postprocessor provides immediate display of the results on low-cost interactive terminals.

REFERENCES

1. Tocher, J. L. and Felippa, C. A.: Computer Graphics Applied to Production Structural Analysis. Proceedings of the Symposium of the International Union of Theoretical and Applied Mechanics, Liege, Belgium, August 1970.
2. Herness, E. D. and Tocher, J. L.: Design of Pre- and Post-Processors. Proceedings of the International Symposium on Structural Mechanics Software, University of Maryland, June 1974.
3. Information Display Products: Tektronix Plot-10 Terminal Control System. Document No. 062-1474-00, Beaverton, Oregon (1972).
4. Quenneville, C. E.: BCS Interactive Graphic System. Boeing Computer Service Document No. 10201-044, June 1975.
5. Tocher, J. L. and Herness, E. D.: A Critical View of NASTRAN. Numerical and Computer Methods in Structural Mechanics, Academic Press, Inc., N.Y., 1973, pp. 151-173.

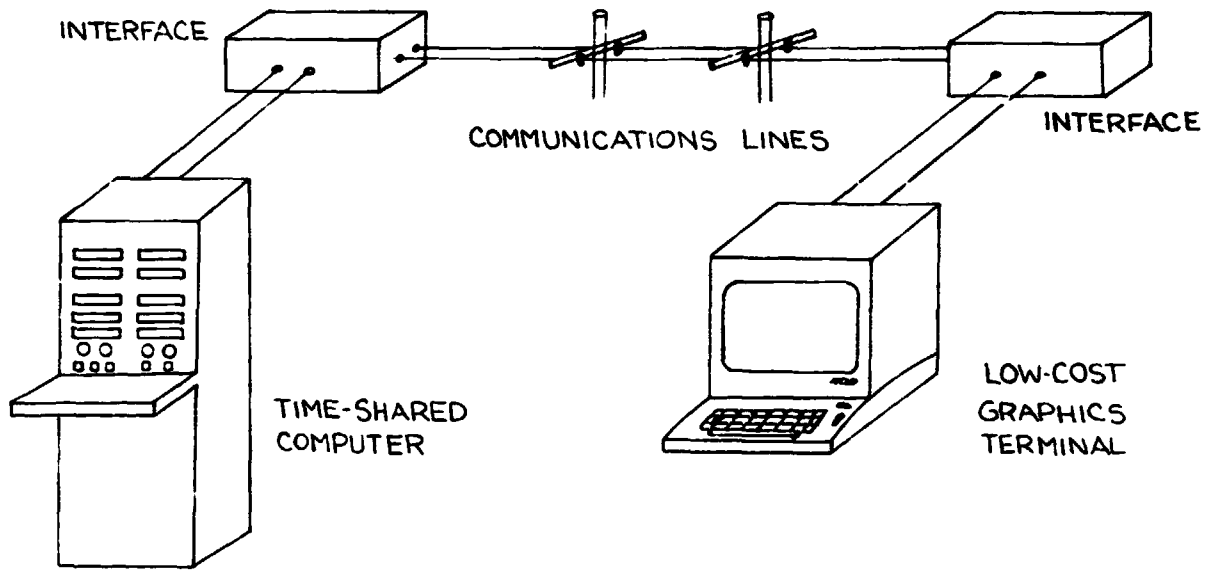


Figure 1.- Hardware Elements of a Low-Cost Graphics System.

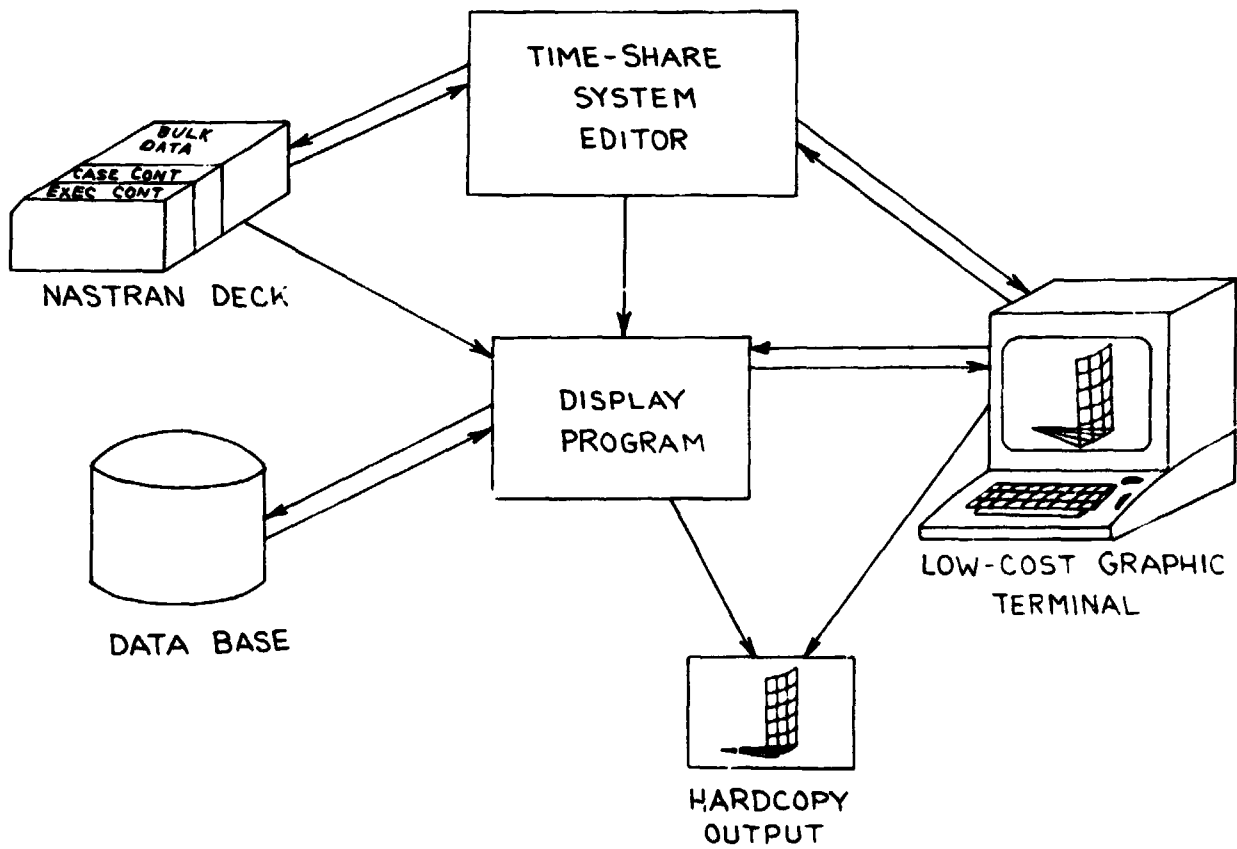


Figure 2.- Input Display Program Design.

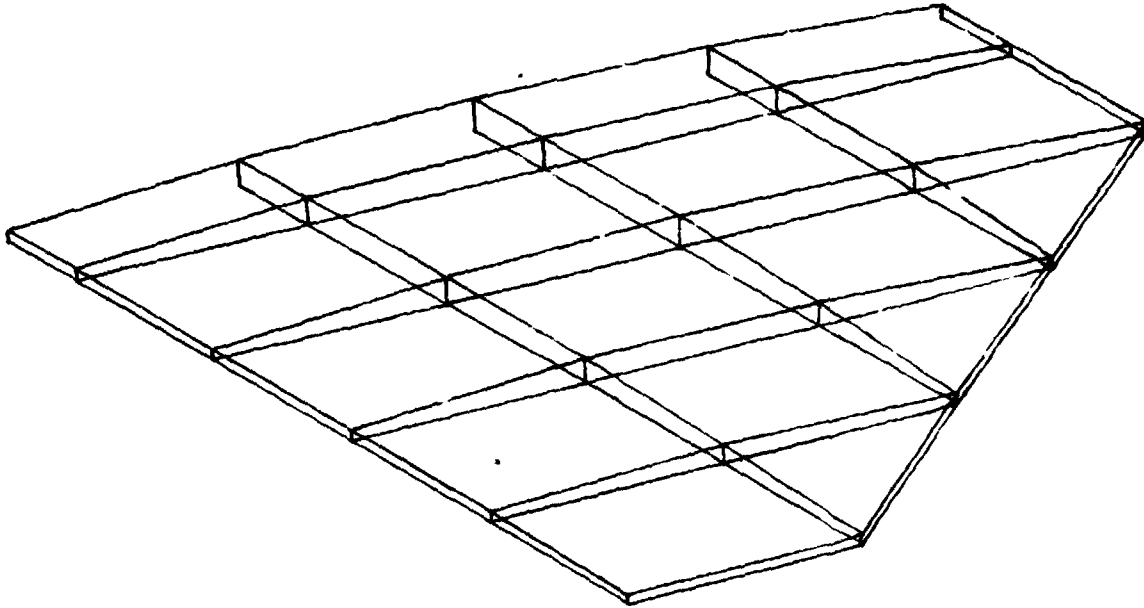


Figure 3.- Demo 1-1 Delta Wing.

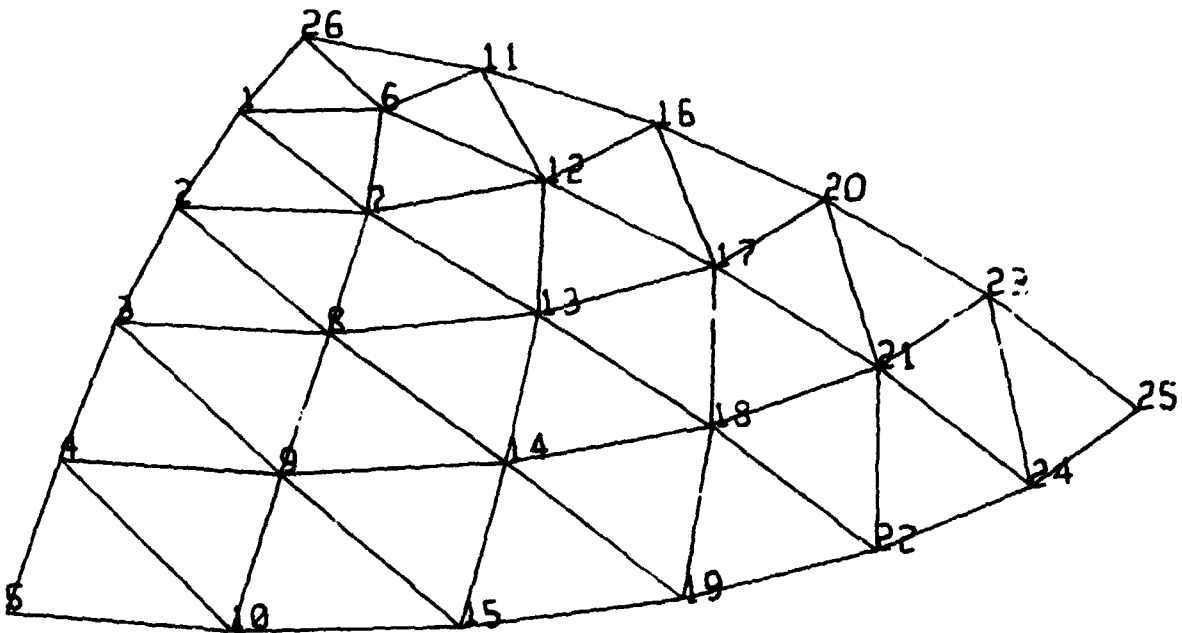


Figure 4.- Demo 1-2 with Grid ID's.

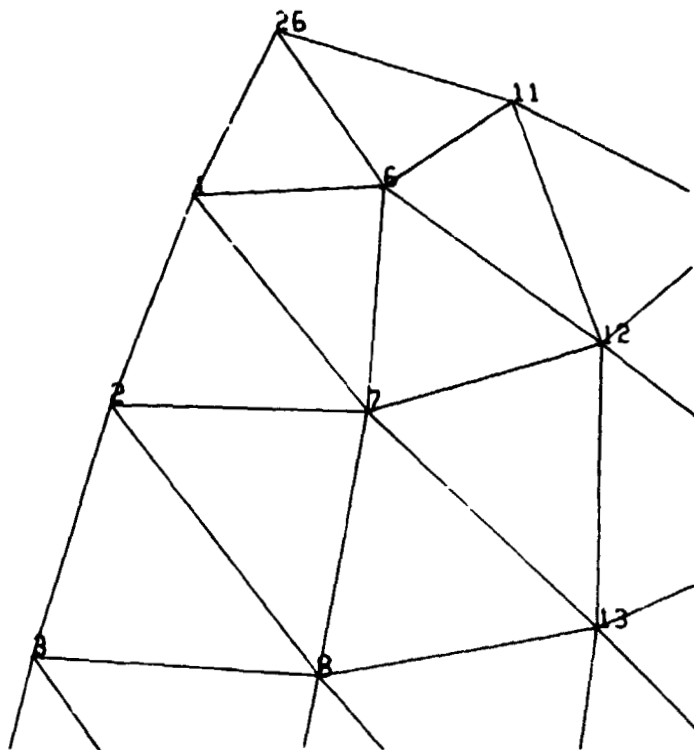


Figure 5.- Demo 1-2 Blowup.

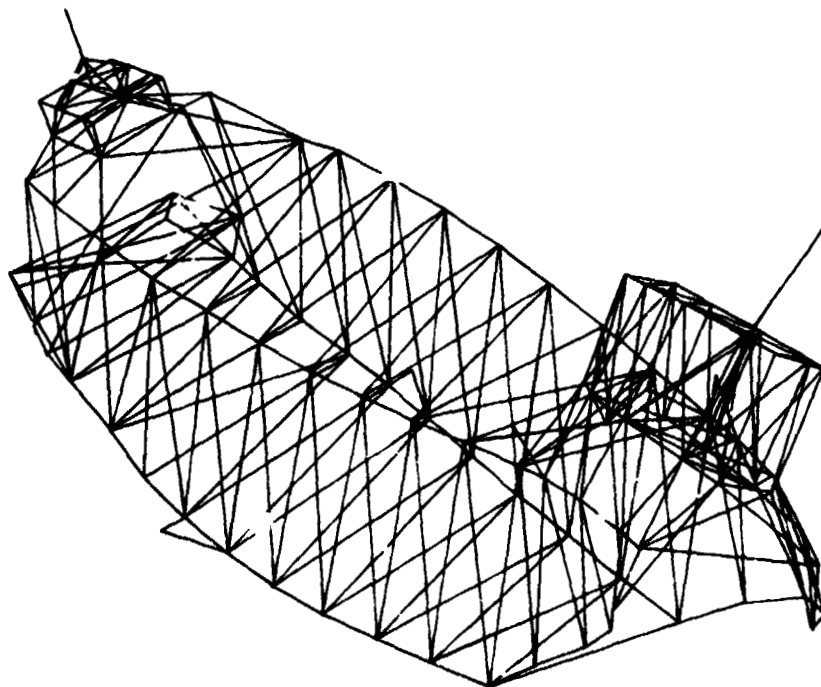


Figure 6.- Ninth Vibration Mode of a Helicopter Fuselage.

N75 31512

SCANNING NASTRAN OUTPUT DATA FOR
MAXIMUM AND MINIMUM VALUES

Donald C. Walker
Control Data Corporation
CYBERNET Service Division
Minneapolis, Minnesota

SUMMARY

A new computer program called NASCAN (NASTRAN scan) is offered as a service to NASTRAN users by Control Data Corporation CYBERNET Data Centers. NASCAN enables users to scan lengthy NASTRAN output files for maximum and minimum values in easy user-oriented categories. With this information quickly available through user terminals, a user can more confidently decide on what his next steps should be on the project. Areas of high stress or deflections in any of the NASTRAN rigid formats can be quickly detected and listed out for project documentations. The NASTRAN model can then be revised if necessary by updating an input file tape which is again processed through the NASTRAN program.

This relieves a user of the task of visually scanning lengthy output listings for this type of data. The text of the full output file listing can be used for more detailed documentation.

USING NASTRAN TO CREATE DATA FILES FOR SCANNING

Data to be saved for scanning by NASCAN are controlled by the user during his NASTRAN runs. The OUTPUT2 module of NASTRAN is utilized to request selected data blocks to be saved. Stresses, displacements, loads, velocities, accelerations, or eigenvectors can be chosen.

Figure 1 shows a tabulation of DMAP ALTER numbers and the corresponding NASTRAN data block name used in reference 1 that apply to each of the NASTRAN rigid formats. These names must be entered within the OUTPUT 2 DMAP ALTER statements by the user. The basic ALTER package within the NASTRAN executive control consists of the following cards:

```
ALTER yy  
OUTPUT2 a, b, c, d, e // C, N, -1/C, N/11/V, N, P3 = zzzz$  
SAVE P3$  
OUTPUT2, , , , //C, N, -9/C, N, 11/V, N, P3$  
ENDALTER
```

27

SYMBOLS

ALTER yy	rigid format sequence number where the OUTPUT2 or P instructions should be inserted into the rigid format
a, b, c, d, e	NASTRAN output data block names taken from table 1; one to five data blocks can be output with OUTPUT2 instructions
ll	signifies that NASTRAN should write its processing results onto file UT1; see page 5.3-20i of reference 2 for other options
zzzz	name assigned to the output tape for identification purposes; see reference 2 for more details

If the user does not wish the output listing for these data, the data block name can be removed from the CFP module instruction. This module formats tables and places them on the system output file; subsequently, these tables are printed.

If the user wants to scan large data blocks, separate tapes should be used to speed up the scanning process.

A sample statics solution (Rigid Format 1) NASTRAN Executive and Case Control creating two tapes for scanning with NASCAN is shown in figure 1. One tape will contain the stress output (data block OES1) on file UT1. The displacements (Data block OUGV1) will be saved on file UT2. Both are called for in the NASTRAN Case Control.

USING THE NASCAN PROGRAM

These data tapes can now be scanned by the NASCAN program which can scan several types of data blocks and multireel files in a single execution. NASCAN input is organized into easily defined major and minor scans. A major scan pertains to one type of NASTRAN output such as element stresses or grid point displacements. It includes a definition of subcase loadings, grid point sets, element sets, frequency ranges, eigenvalues, or time steps to be examined.

Within each major scan several minor scans may be specified to define stress components and element types.

Tables 2, 3, and 4 are taken from reference 3 and illustrate entries for major and minor scans, along with an explanation of the scan termination card.

To illustrate the use of NASCAN with dynamic analysis data, figure 2 is an example of program controls to scan a frequency response analysis run. Note the range of frequencies and the element components requested.

Sample NASCAN input for scanning a statics run with an explanation of the entries is shown in figure 3. The corresponding NASTRAN executive control which

created these data is shown in figure 4. Note that five data blocks were written on the same tape in this example. NASTRAN output results illustrating scannable output are shown in figure 5.

OUTPUT FROM NASCAN

All major scan parameters are clearly defined in a header block preceding the tabulation of results. The minor scan data are likewise identified with all output results. Maximum, minimum, and average values are given at each minor scan level.

The summary for each major scan (for example, stresses or displacements) gives the maximum and minimum values of all minor scans involved.

Sample output listings are shown in figures 6 and 7. It can be seen that these data have great value when they represent a summary of large files of information. Now the project engineer can quickly focus his attention on these regions of his model.

CONCLUDING REMARKS

A computer program called NASCAN (NASTRAN scan) has been described. NASCAN enables users to scan lengthy NASTRAN output files for maximum and minimum values in easy user-oriented categories.

REFERENCES

1. NASTRAN Programmer's Manual. NASA SP-223(01).
2. NASTRAN User's Manual. NASA SP-222(01).
3. NASCAN User Information Manual. Control Data Corporation Publication No. 76070200.

C-6

Table 1. Alter Numbers and Data Block Names for CDC/NASTRAN

Rigid Format Subset	1	2	3	4 1	4 2	5 1	5 2	6	7**	8**	9**	10**	11**	12**
Alters: Phy.	119	107	105	100	157	100	142	162	156	166	161	131	159	154
Alters: Sol.	-	-	-	-	-	-	-	-	145	143	143	121	130	127
NASCAN styp Parameter Entries														
D*SP	OUGV1	OUGV1		OUGV1	OUBGV1	OUGV1		OUGV1		OUPVC1	OUPV1		OUPVC1	OUPV1
>DISP*										OUDVC1	OUDV1		OUMVC1	OUMV1
EDISP			OPNIG				OPNIG		OPNIP				OPNIP	
SEDI*									OPNID				OPNID	
VELO										OUPVC1	OUPV1		OUPVC1	OUPV1
SVEL*										OUDVC1	OUDV1		OUMVC1	OUMV1
ACCE										OUPVC1	OUPV1		OUPVC1	OUPV1
SACC*										OUDVC1	OUDV1		OUMVC1	OUMV1
SPCF	OQG1	OQG1	OQG1	OQG1	OQBG1	OQG1	OQBG1	OQCI	OQPC1	OQPC1	OQP1	OQPC1	OQPC1	OQP1
OLQA	OPG1	OPG1		OPG1		OPG1		OPG1		OPPC1	OPP1		OPPC1	OPP1
MLLO*											OPNL1			OPNL1
STRE	OES1	OES1	OES1	OES1	OESB1	OES1	OESB1	OES1	OESC1	OESC1	OES1	OESC1	OESC1	OES1
ELFO	OEF1	OEF1	OEF1	OEF1	OEFB1	OEF1	OEFB1	OEF1	OEF1	OEF1	OEF1	OEF1	OEF1	OEF1

*Output from module VDR (solution set)
 **Do not use a subcase structure with: special alters

ORIGINAL PAGE IS
 OF POOR QUALITY

NOTE: COMP = 1 is also a valid entry for defining how a minor scan should be performed. See Table 3.

COMP(MAGN) = 1 = a grid data scanning sub-option that can be specified if the user wants NASCAN to determine vector sums of translations or rotations at a grid point. This only applies to real number data. Only the first component number (e. g. , 1 for translations or 4 for rotations) can be specified. A valid example of a translation vector sum is:

SET 100 = 1
DISP COMP(MAGN) = 100

A valid example pertaining to a rotation vector sum is:

SET 200 = 4
DISP COMP(MAGN) = 200

NOTE: Only data using the default CDC/NASTRAN SORT1 option can be input to NASCAN.

Table 2. Valid styp Entries for Major Scans

Valid Entry Columns 1-4	Function
STRE	Specifies that a stress scan should be performed. A BOTH entry is allowed when the user wants to select a sub-option for scanning fiber stresses on each side of selected plate elements. Table 4 lists valid elements and components. Table 3 lists valid parameters that are necessary when entering STRE with a minor scan.
ELFO	Specifies that an element force scan should be performed. Table 4 lists valid elements and components. Table 3 lists valid parameters that must accompany an ELFO entry when a minor scan is being defined.
DISP	Specifies a displacement scan (physical set); applies to grid data scans. *
SDIS	Requests a displacement scan (solution set); applies to grid data scans. *
EDIS	Specifies an eigenvector scan (physical set); applies to grid data scans. *
SEDI	Requests an eigenvector scan (solution set); applies to grid data scans. *
VELO	Specifies a velocity scan (physical set); applies to grid data scans. *
SVEL	Requests a velocity scan (solution set); applies to grid data scans. *
ACCE	Specifies an acceleration scan (physical set); applies to grid data scans. *
SACC	Requests an acceleration scan (solution set); applies to grid data scans. *

*Data blocks for the physical set are output from module SDR1, while blocks for the solution set are output from module VDR.

Table 2 . Valid styp Entries for Major Scans (Cont'd)

Valid Entry Columns 1-4	Function
SPCF	Specifies an SPC force scan; applies to grid data scans. *
OLOA	Requests a static or dynamic load scan; applies to grid data scans. *
NLLO	Specifies a non-linear load scan (solution set); applies to grid data scans. *

*Data blocks for the physical set are output from module SDR1, while blocks for the solution set are output from module VDR.

Table 3. Entries Accompanying STRE and ELFO (Minor Scans)

Entry	Function
COMP = <u>i</u>	This mandatory entry specifies the set number (<u>i</u> parameter) that identifies which components should be scanned. Table 4 lists the allowable integer values that represent entries that can be scanned for real and complex forces and stresses. NOTE: For complex numbers, the magnitude is always used. Only 10 entries can be specified for each request set.
ELEM = <u>bcd</u>	This mandatory entry specifies the appropriate element type. Valid entries for the <u>bcd</u> parameter are shown in the first column of Table 4. The minor scan option allows the user to determine the minimum and maximum value of all specified element types. Since this output is compared by component number in the final summary, the user should only specify similar element types (by grouping) as shown in Table 4 when he requests a major scan. NOTE: The <u>bcd</u> parameter refers to the same mnemonic that CDC/NASTRAN employs for element types. See Table 4 for a list of allowable element types. A valid example of COMP = <u>i</u> and ELEM = <u>bcd</u> is: ELFO ELEM = ROD COMP = 1.0
BOTH	This optional entry causes NASCAN to search the plate fiber stresses on each side of the element to locate a maximum absolute value. This value is then listed with an appropriate mathematical sign. Subsequently, the program finds a minimum absolute value for this side only (containing maximum) and lists it with its appropriate sign. If compressive stresses are higher than tension stress, they are listed as minimum. The BOTH option only applies to real element stresses. Table 4 lists allowable components. When selecting the BOTH option, users must enclose this entry within parentheses. This option can <u>not</u> be selected unless ELEM and COMP are also selected. A valid example of its use is: STRE ELEM = QDPLT COMP(BOTH) = 7.9

Table 4. NASCAN Element Types and Components for Minor Scans

Element Types	Stresses			Forces		
	Component Real	Code Complex	Component	Component Real	Code Complex	Component
BAR	2	2	Stress, A1	2	2	Bend-mom, A1
	3	3	Stress, A2	3	3	Bend-mom, A2
	4	4	Stress, A3	4	3	Bend-mom, B1
	5	5	Stress, A4	5	5	Bend-mom, B2
	6	6	Axial stress	6	6	Shear-1
	7	-	Max stress, A	7	7	Shear-2
	8	-	Min stress, A	8	8	Axial force
	9	-	Safety margin-ten	9	9	Torque
	10	12	Stress, B1			
	11	13	Stress, B2			
	12	14	Stress, B3			
	13	15	Stress, B4			
	14	-	Max stress, B			
	15	-	Min stress, B			
	16	-	Safety margin-com			
	TETRA	2	2	Normal-X	undefined	
HEXA1	3	3	Normal-Y			
HEXA2	4	4	Normal-Z			
WEDGE	5	5	Shear-YZ			
	6	6	Shear-XZ			
	7	7	Shear-XY			
	8		Octahedral			
	9		Pressure			
TRIM6†	3	-	Normal-X	undefined		
	4	-	Normal-Y			
	5	-	Shear-XY			
	6	-	Shear angle			
	7	-	Maj-prin			
	8	-	Min-prin			
	9	-	Max-shear			

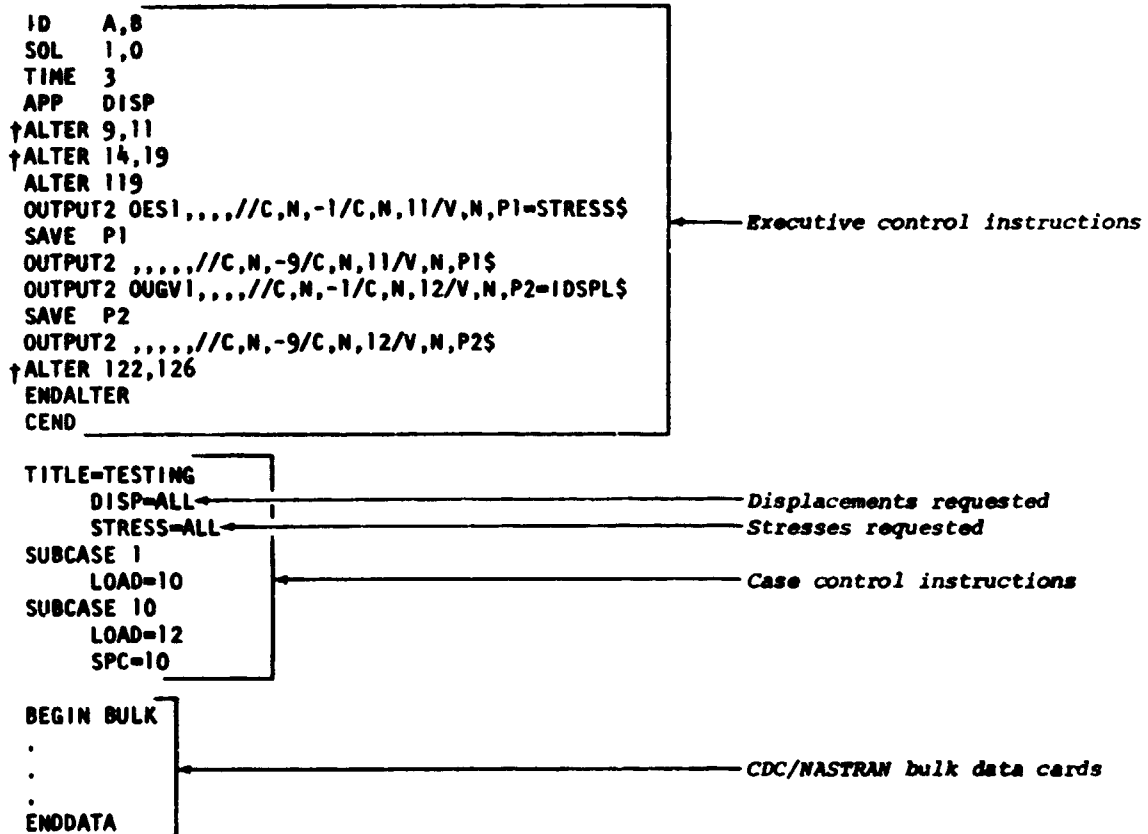
Major Scan Termination Card

A scan termination card (also called a FOR card) is required at the end of each major scan definition. Its purpose is to signal the end of the appropriate major scan data. This card should be filled out according to the following format:

$$\text{FOR } \begin{bmatrix} \text{ELEM} \\ \text{GRID} \end{bmatrix} = \underline{1}, \text{ SUBCASE} = \underline{1}, \text{ RANGE} = \underline{r_1}, \underline{r_2}$$

†All three corners and centers are scanned.

NASCAN



↑Required alters for Rigid Format 1 to bypass the plotting modules.

Figure 1.-- Generating SCAN data for the NASCAN Program with CDC/NASTRAN.

Figure 2 illustrates how to check NASCAN input data without mounting CDC/NASTRAN output tapes. This example also shows that the CDC/NASTRAN tapes should undergo a frequency response analysis (rigid format 8). In this second instance, the user must enter a COMPLEX = 1 option on his overall parameter card.

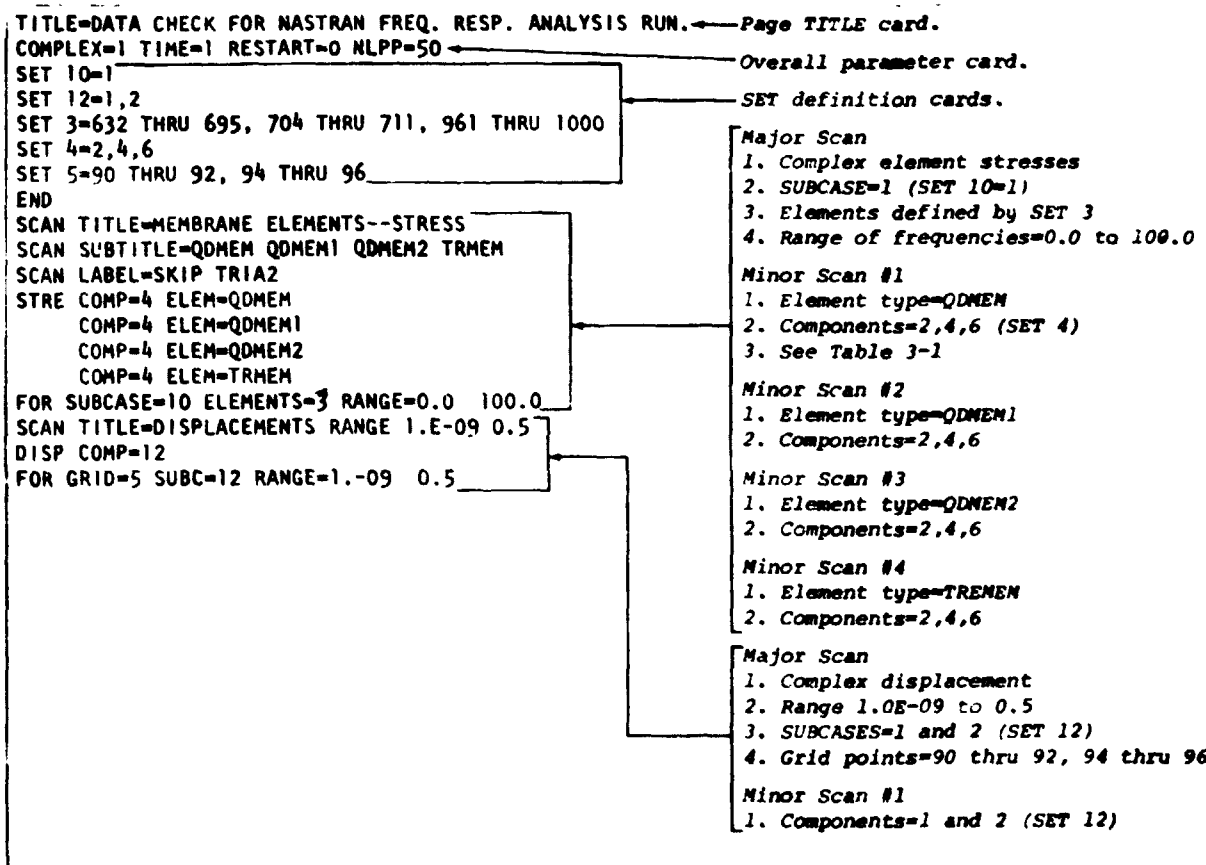


Figure 2.- Sample NASCAN Program controls: checking input.

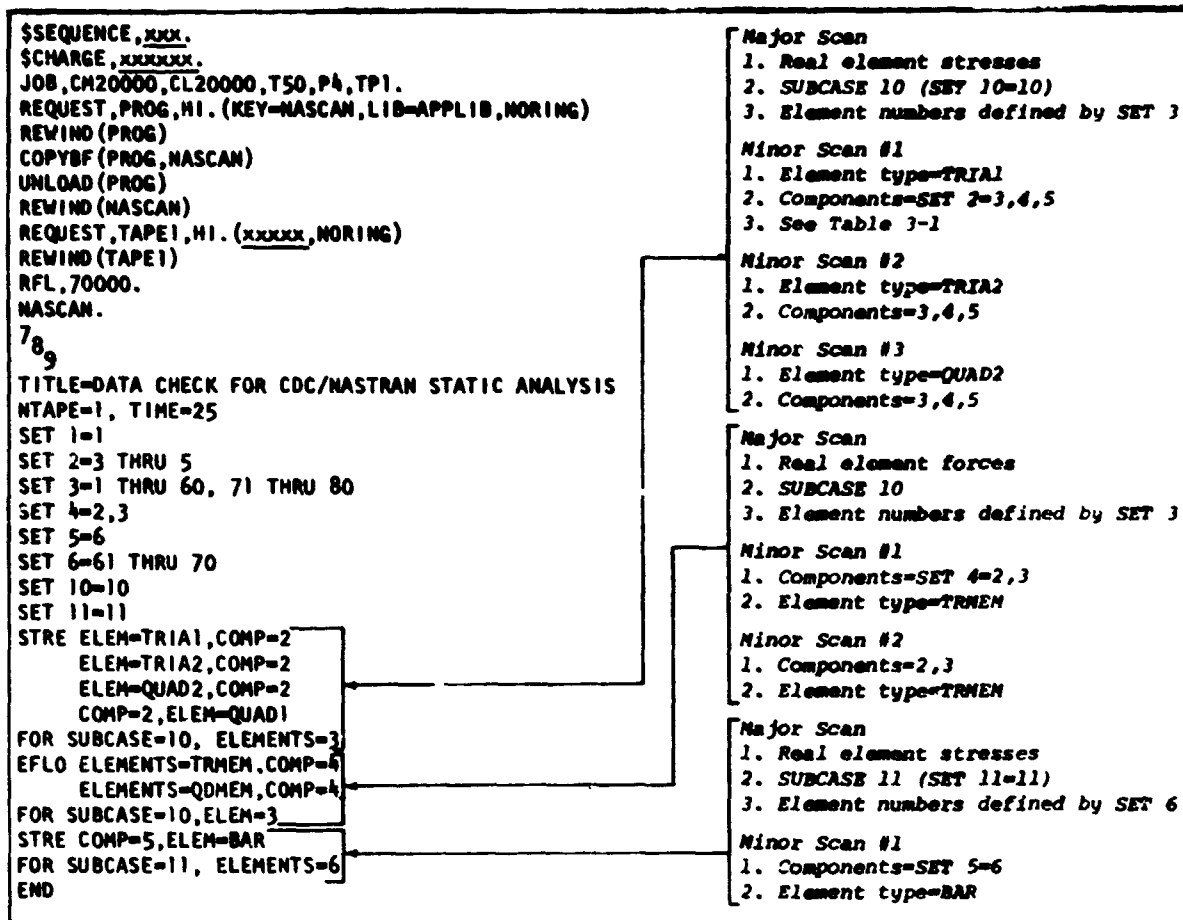


Figure 3.- Sample NASCAN entries: scanning a statics run.

```

SEPTEMBER 17, 1976  NASTRAN 7/26/76  PAGE 1
NASTRAN EXECUTIVE CONTROL DECK ECHO
10 STRESS ELEMENT OUTPUTS
APP DISP
TIME 3
SOL 1.0
ALTER 0-11
ALTER 10-10
ALTER 110
OUTPUT2 DES1,OUV1,REF1,OPB1,0001 // C.N.-1/C.N.11/V.N.P3=TEST2 0
SAVE P3 0
OUTPUT2: ...../C.N.-0/C.N.11/V.N.P3 0
ALTER 122-126
FINALTER
CEND

```

Figure 4.- NASTRAN input.

40	0	0.0	0.0	-0.03000E-01	-1.70000E-01	4.50000E-01	0.0
41	0	0.0	0.0	-1.17000E-01	1.12000E-02	1.00000E-01	0.0
42	0	-3.30000E-01	-3.30000E-01	0.0	0.0	0.0	0.0
43	0	0.0	0.0	0.0	0.0	0.0	0.0
44	0	0.0	0.0	0.0	0.0	0.0	0.0
45	0	-2.00000E+00	-2.00000E+00	0.0	-2.00000E-10	1.00000E-10	-2.00000E+00
46	0	-0.70000E+00	-0.70000E+00	0.0	0.0	0.0	0.0
47	0	-3.31000E+00	0.0	3.31000E+00	0.0	0.0	0.0
48	0	-0.70000E+00	2.30000E+00	0.0	0.0	0.0	0.0
49	0	-3.31000E+00	0.0	-3.31000E+00	0.0	0.0	0.0
50	0	0.0	0.0	0.0	0.0	0.0	0.0
51	0	0.0	0.0	0.0	0.0	0.0	0.0
52	0	0.0	0.0	0.0	0.0	0.0	0.0
53	0	0.0	0.0	0.0	0.0	0.0	0.0
54	0	0.0	0.0	0.0	0.0	0.0	0.0
55	0	0.0	0.0	0.0	0.0	0.0	0.0
56	0	0.0	0.0	0.0	0.0	0.0	0.0
57	0	0.0	0.0	0.0	0.0	0.0	0.0
58	0	0.0	0.0	0.0	0.0	0.0	0.0
59	0	0.0	0.0	0.0	0.0	0.0	0.0
60	0	0.0	0.0	0.0	0.0	0.0	0.0
61	0	0.0	0.0	0.0	0.0	0.0	0.0
62	0	0.0	0.0	0.0	0.0	0.0	0.0
63	0	0.0	0.0	0.0	0.0	0.0	0.0
64	0	0.0	0.0	0.0	0.0	0.0	0.0
65	0	0.0	0.0	0.0	0.0	0.0	0.0
66	0	0.0	0.0	0.0	0.0	0.0	0.0
67	0	0.0	0.0	0.0	0.0	0.0	0.0

TITLE CARD
SUBTITLE CARD
LOAN SET 1000
SEPTEMBER 17, 1974 NASTRAN 7/25/74 PAGE 52
SUBCASE 1

ELEMENT ID.	PIPING DISTANCE	STRESSES IN BENDING QUADRILATERALS			PRINCIPAL STRESSES (ZERO SHEAR)			SHA SHEAR
		STRESSES IN ELEMENT COORD SYSTEM NORMAL-X	NORMAL-Y	SHEAR-XY	ANGLE	MAJOR	MINOR	
44	-5.00000E-02	1.702374E-01	5.77710E-01	1.519010E-01	72.3665	0.000010E-01	7.994700E-02	7.010500E-01
	5.00000E-02	-1.702374E-01	-5.77710E-01	-1.519010E-01	-17.6355	-7.994700E-02	-0.000010E-01	7.010500E-01

TITLE CARD
SUBTITLE CARD
LOAN SET 1000
SEPTEMBER 17, 1974 NASTRAN 7/25/74 PAGE 53
SUBCASE 1

ELEMENT ID.	PIPING DISTANCE	STRESSES IN GENERAL QUADRILATERAL ELEMENTS			PRINCIPAL STRESSES (ZERO SHEAR)			SHA SHEAR
		STRESSES IN ELEMENT COORD SYSTEM NORMAL-X	NORMAL-Y	SHEAR-XY	ANGLE	MAJOR	MINOR	
47	-5.00000E-02	7.029596E-02	-2.207011E-03	0.931005E-03	0.0294	7.950250E-02	-3.410030E-03	0.100000E-02
	5.00000E-02	-7.029596E-02	2.207011E-03	-9.931005E-03	-03.0702	-7.950250E-02	3.410030E-03	-0.100000E-02
48	-5.00000E-02	-1.500166E-02	2.929553E-01	1.002037E-01	00.0130	3.300000E-01	-0.700000E-02	2.120213E-01
	5.00000E-02	1.500166E-02	-2.929553E-01	-1.002037E-01	-05.3070	-3.300000E-01	0.700000E-02	-2.120213E-01

TITLE CARD
SUBTITLE CARD
LOAN SET 2000
SEPTEMBER 17, 1974 NASTRAN 7/25/74 PAGE 74
SUBCASE 2

ELEMENT ID.	PIPING DISTANCE	STRESSES IN BENDING QUADRILATERALS			PRINCIPAL STRESSES (ZERO SHEAR)			SHA SHEAR
		STRESSES IN ELEMENT COORD SYSTEM NORMAL-X	NORMAL-Y	SHEAR-XY	ANGLE	MAJOR	MINOR	
44	-5.00000E-02	2.500740E-01	1.119504E+00	3.000021E-01	72.3665	1.212123E+00	1.500950E-01	5.201130E-01
	5.00000E-02	-2.500740E-01	-1.119504E+00	-3.000021E-01	-17.6355	-1.212123E+00	-1.500950E-01	5.201130E-01

TITLE CARD
SUBTITLE CARD
LOAN SET 2000
SEPTEMBER 17, 1974 NASTRAN 7/25/74 PAGE 75
SUBCASE 2

ELEMENT ID.	PIPING DISTANCE	STRESSES IN GENERAL QUADRILATERAL ELEMENTS			PRINCIPAL STRESSES (ZERO SHEAR)			SHA SHEAR
		STRESSES IN ELEMENT COORD SYSTEM NORMAL-X	NORMAL-Y	SHEAR-XY	ANGLE	MAJOR	MINOR	
47	-5.00000E-02	1.909911E-01	-0.010021E-03	1.900213E-02	0.0290	1.909911E-01	-0.000072E-03	0.201700E-02
	5.00000E-02	-1.909911E-01	0.010021E-03	-1.900213E-02	-03.0702	-1.909911E-01	0.000072E-03	-0.201700E-02
48	-5.00000E-02	-3.120333E-02	0.951100E-01	3.000070E-01	00.0130	0.000000E-01	-1.070000E-01	0.000000E-01
	5.00000E-02	3.120333E-02	-0.951100E-01	-3.000070E-01	-05.3070	1.070000E-01	0.000000E-01	0.000000E-01

Figure 5.- NASTRAN scannable output.


```

R = 0.      77=SID      Z=SUMC      2000=LOAD      MAX = 0.
R = A.      77=SID      Z=SUMC      2000=LOAD      MIN = 0.
O = 0.      COMPONENT 6      50 ENTRIES.      AVE = 0.
O = 0.      77=SID      Z=SUMC      2000=LOAD      MAX = 0.
O = 0.      77=SID      Z=SUMC      2000=LOAD      MIN = 0.

FOR ALL MINOR SCANS AND COMPONENTS. MAX = 4.000000E+00. MIN = -2.000000E+00

...PROGRAM NASTRAN CINC/NASTRAN TEST PROBLEM(RIGID FORMAT )
09/10/74 13.10.00. PAGE 14
*****
* MAJOR SCAN 15. REAL SPC-FORCES RANGE 0. TO 0.
* SUBCASE = 1 THRU 2
* GRID NO. = A1 THRU 100
* TEST FOR SPC FORCES
*****
* MINOR SCAN 1 - SUBOPTION 1
COMPONENT 1
R = 0.      03=SID      Z=SUMC      2000=LOAD      MAX = 3.200702E+01
R = A.      03=SID      Z=SUMC      2000=LOAD      MIN = -0.707400E+00
O = 0.      COMPONENT 2      50 ENTRIES.      AVE = 2.102500E+02
O = 0.      04=SID      Z=SUMC      2000=LOAD      MAX = 0.020000E+03
R = 0.      04=SID      Z=SUMC      2000=LOAD      MIN = -0.120370E+03
R = A.      COMPONENT 3      50 ENTRIES.      AVE = -3.167077E+01
R = 0.      04=SID      Z=SUMC      2000=LOAD      MAX = 1.713100E+05
R = 0.      04=SID      Z=SUMC      2000=LOAD      MIN = -1.107210E+05
R = 0.      COMPONENT 4      50 ENTRIES.      AVE = -7.300021E-10
R = A.      10=SID      Z=SUMC      2000=LOAD      MAX = 0.
R = 0.      01=SID      Z=SUMC      2000=LOAD      MIN = -0.002170E-10
R = 0.      COMPONENT 5      50 ENTRIES.      AVE = 0.920210E-10
R = A.      01=SID      Z=SUMC      2000=LOAD      MAX = 1.000325E-10
R = 0.      10=SID      Z=SUMC      2000=LOAD      MIN = 0.
R = 0.      COMPONENT 6      50 ENTRIES.      AVE = -0.270002E+02
R = A.      10=SID      Z=SUMC      2000=LOAD      MAX = 0.
R = 0.      A1=SID      Z=SUMC      2000=LOAD      MIN = -0.000000E+00

FOR ALL MINOR SCANS AND COMPONENTS. MAX = 1.213100E+05. MIN = -1.107210E+05

```

Figure 7.- Concluded.

N75 31513

UNDERSTANDING THE NASTRAN STRUCTURAL PLOTTER

Loren R. Kausinen

Universal Analytics, Inc.
Playa Del Rey, California

SUMMARY

Functions of the plotting hardware and the operations performed by the NASTRAN structural plotter are summarized to provide the user an insight into how the program works. The processing performed in response to each plot command is described and the interrelationships of the various parameters are explained. To assist in the effective and efficient utilization of the system, examples are provided which also illustrate several not yet documented capabilities of the Level 16 structural plotter.

INTRODUCTION

The NASTRAN structural plotting capability is used extensively for checking the structural geometry, plotting the deformations and preparing figures for reports. This paper is written, therefore, to provide some insight into the plotting procedures used by the upcoming NASTRAN Level 16. With this insight, the user can more confidently prepare his input to efficiently and effectively exploit this plotting capability.

The interface between NASTRAN and the basic plotting hardware is described. The key words input by the user to drive the NASTRAN plotter are explained in terms of the tasks performed according to each command. The algorithms which translate the structural data into plotting hardware commands are described in order to show how simple changes in the user's input can have significant effects on efficiency. Many illustrative examples are used. However, for brevity, the reader is assumed to have some familiarity with the basic input and access to the NASTRAN User's Manual (ref. 1).

In order to establish a common background of plotting terminology, the typical plotter hardware is described first, and the principles of computer graphics for structural plotting are summarized. Then, the NASTRAN plot files are identified, the algorithms are presented, and finally, examples of efficient input sequences are explained.

28

PLOTTING HARDWARE

All the plotting hardware supported by NASTRAN (see Table 1) requires the same basic output from NASTRAN. Therefore, rather than describing each plotter in

detail, only the fundamental characteristics are presented. The basic commands used by all plotters provide for the following:

1. Moving to a position
2. Drawing a line segment
3. "Typing" or drawing an alphanumeric or special character

The execution of these commands will differ, of course, depending on the type of plotter. If the plotter is a cathode ray tube type (CRT), these commands are translated into the movement of an electron beam across a luminescent screen (much like a television screen) from which a photograph is taken. That film can then be viewed through an enlarger or it can be printed on paper. In any case, the viewing area, or frame, is limited in size to the area provided by the CRT.

The other plotters use a pen and draw directly on paper or other media. These may be table plotters which are limited to an area the size of the table. Drum plotters, which use rolls of paper, are limited only to the width of the roll. Some maximum frame dimensions are always required to establish the working area. In place of pens, some plotters may use heat sensitive tips and special paper. In any case, the principles are the same.

To execute the plot commands, each plotter requires a method of positioning the pen or the electron beam. To accomplish this, each plotter works in an internal system of units usually called "rasters". This orthogonal, two-dimensional X and Y reference system has maximum raster values in the X and Y directions, limited mainly by the paper or film size. The number of rasters per inch is a constant value for the plotter selected.

Care must be taken in defining the sequence of positioning commands. For the CRT, this is not a great problem in that the electron beam can be moved virtually instantaneously. However, for pen plotters, the movement of the pen from one location to another requires considerable time with the pen either up or down. This is true even if the plotter provides a "zip" mode. An efficient sequence will also utilize a shorter magnetic tape, the normal output media for the plot commands.

The procedures for converting each of these commands for the plotter selected are supplied by functional utilities in NASTRAN. These routines convert the structural data into line segments and issue the commands to draw the lines desired, to "type" or draw the characters required for titles and other identifiers, and to start and stop the plotter.

BASIC FUNCTIONS

The tasks performed by the NASTRAN structural plot module are relatively simple. The plot routines must make two-dimensional drawings, provide labeling information and control the plotting sequence. The key words given here in

quotation marks are used and will be illustrated later as key words of the NASTRAN plot control language.

To create the two-dimensional image of a structural model, the program assumes a "plotting surface" exists in between the object to be plotted and the viewer. For orthographic plots, the viewing point is assumed to be an infinite distance from the plotting surface so as to prevent perspective line distortions. For perspective plots, a finite distance is used and line distortions are computed. For stereographic plots, two perspective plots are created from two different locations of the viewing point. The mathematical transformations used are presented in the Theoretical Manual (ref. 2) under Computer Graphics.

Once the plotter is selected and the frame size is established, a plotting "region" is established. This region, which allows for margins on each edge of the plot frame, will be varied to accommodate titling information, frame identification, and user-specified plot region sizes. Thus, the size may expand or contract at different phases of the plotting computations, but it never goes beyond the specified plotter's frame limits. All lines and characters must appear within the outer margins of the plot frame, otherwise they will be "clipped".

The picture on the plotting surface must not only be contained in the plotting region; it should be centered. To appropriately place the picture in the plotting region, a "scale" and "origin" approach is used. Note that for orthographic plots, moving the plotting surface towards or away from the object will not change the image size as it will for perspective plots. The program will select, or the user must specify, the scale and origin to be used. This scale is used as a conversion factor for transforming the model's projected structural coordinates into the two-dimensional raster coordinates within the frame's limits for the plotter. These raster coordinates are then shifted relative to the origin calculated for centering the final picture.

The viewable output is obtained by drawing lines to represent the element connectivities in either the model's deformed or undeformed "shape". Due to the difficulties encountered in viewing a complex three-dimensional deformed shape on paper, a line or "vector" can be requested to show only the components of deformation. These vectors are lines which may be attached to either the deformed or the undeformed shape of the model.

Since the relative dimensions of the grid point deformations are small compared with the structural coordinates of the model, NASTRAN exaggerates the magnitude of the deformations. This magnification factor must be specified by the user. He must give the length (in the structure's and not the plotter's raster coordinates) to which the maximum component of displacement is to be scaled.

To further assist the user in the task of checking out his NASTRAN input and/or output, the object to be plotted may be rotated for viewing from any angle. The picture to be plotted will show the view facing the plotting surface. This rotation is performed by specifying either "view" angles and/or "axes" to be interchanged. Symmetric plots may be requested. They necessitate

the interchange of axes to get a "left hand" coordinate system. Specifying view angles alone will not suffice.

Finally, a complex structure requires labels and special symbols to help identify the structural components for both the deformed and undeformed plots. Selected "symbols" may be used or identification numbers may be requested for grid points. For elements, "labels" can be requested to provide both the identification numbers and the element type information. Special care is taken in NASTRAN to position these labels to avoid misinterpretation and to enhance their legibility.

The processing to translate the structural data into two-dimensional plots using line segments, symbols and characters can be expensive. The resulting data files, described next, can be sizeable. To help avoid inefficient use of the basic functions, the subsequent chapters explain how the structural plotter commands are processed by the NASTRAN plot modules.

PLOTTING DATA FILES

The data files to be processed by the NASTRAN structural plot modules consist of control information and model data. The functions of the various input files will be shown. The names of the files, however, may differ depending on the rigid format.

The user defines his desired plot output via a separate section of the Case Control Deck. These physical cards are read and interpreted by a special preface routine. Unlike the other usual case control cards, the plot control commands are simply interpreted as BCD, real or integer data and stored in one file (PCDB) for future processing by the plot modules. All cards between the OUTPUT(PLOT) and the BEGIN BULK or the OUTPUT(XYPLOT) cards are assumed to be structural plot control cards.

The first phase of data analysis is performed by the PLTSET module which is executed only once in each run. Its function is to analyze the SET cards, output the GPSETS and ELSETS data files, issue error messages pertinent to the SET data on the PLTSETX file and rewrite the PCDB control data to the PLTPAR file with all SET definitions removed.

The two files GPSETS and ELSETS contain all the data required to specify the objects to be plotted. For every set of elements defined, one record of data is placed on each file whether it will later be used for plotting or not. Once these files have been established in the PLTSET module, no modification of these data is ever attempted.

For each set of elements, the ELSETS file lists the element type, its identification number and its connection points, which are entered as pointers into the GPSETS file. The corresponding GPSETS file contains the flags specifying all the grid points needed to draw those elements. It also specifies which points are to be identified by symbols or labels.

The actual plot tape is written by the PLOT module. The PLOT module analyzes the remaining plotter commands by sequentially interpreting the PLTPAR file. The processing of the data stored in each record of the ELSETS and GPSETS files is supported by the following standard input files as required:

- CASECC - provides plot headings
- BGPDT - provides undeformed grid coordinates
- EQEXIN - provides grid identification numbers
- SIL - controls use of PLTDSP1 and PLTDSP2 files
- PLTDSP1 - provides deformations for requests using STATIC
- PLTDSP2 - provides deformations for all other requests

The PLOT module is executed twice in most runs, first for undeformed and then for deformed plots depending on the value of a DMAP parameter. Input data on the PLTPAR file is interpreted sequentially. Plot requests applicable to the second pass are skipped on the first pass. Error messages and plot identification messages also occur in sequential order. Error messages pertinent to either the undeformed or deformed plots appear during the undeformed analysis. Messages pertinent to the deformed plots appear only on the second pass. All messages are output on the PLOTX file.

The deformation files, PLTDSP1 and PLTDSP2, are created for use by the PLOT module by the normal output processing modules of NASTRAN (e.g., SDR1). These data files contain only the three translational components in the basic coordinate system. Each set of data is identified as to type, subcase, and the appropriate frequency, eigenvalue or time.

The actual sequence of operations on these files is described next.

PROCESSING SEQUENCE

Lengthy calculations may be required of the plot modules, which suggests that care be given in the usage of certain input commands. These are described below to give the user insight into how the plotter will interpret each command. Since each card is acted upon in sequence, the usual structural plotter commands are presented below in the sequence that they should be input to the program. More detailed definitions for each key word can be obtained from reference 1. Table 2 illustrates the interaction of the plotting parameters for the discussion below. The next chapter presents many examples along with some interesting undocumented options.

The OUTPUT(PLOT) Card

This card indicates that the Case Control cards to follow are plot commands. All such cards up to an OUTPUT(XYPLT) or a BEGIN BULK are assumed to be structural plot commands.

The SET Card

This card initiates the creation of a scratch file containing all the plottable elements. These elements are those with geometric coordinates and at least two grid points. Only data on connections, element type and element number are on this file. This list is then scanned for each SET the user defines. Each SET card is then interpreted. Each element in the scratch file is scanned, and if its type and/or number is INCLUDED and not later EXCLUDED*, that element is accepted.

The SET card may also be used to restrict the output of grid point related labels, symbols and deformation vectors. The basic grid point data is obtained from the element set connectivities and therefore can not be expanded. Thus, INCLUDE GRID has no meaning unless it follows EXCLUDE GRID. Note here, that the key word GRID must always follow the INCLUDE, EXCLUDE or EXCEPT commands. In Level 16, some elements (e.g., AERO) automatically use EXCLUDE GRID.

The CSCALE Card

If used, this card must appear before each PLOTTER request to set the scaling parameter which allows the user to change the raster dimensions of the characters to be used in all subsequent operations. This scaling is useful if the plot output is to be post processed to enlarge a frame without also enlarging the characters or destroying their spacing. Thus, this parameter is input as the inverse of the factor the post processor will use to magnify the frame. Table 1 shows the character size for each plotter supported by NASTRAN.

The PLOTTER Card

To define the desired plotting hardware, the PLOTTER, PAPER SIZE and CAMERA or PEN parameters are specified. The first two set the parameters shown in Table 1 and initialize the plotter. PAPER SIZE controls the maximum plotting area for table or drum plotters. If a size larger than the maximum fixed dimension for that plotter is specified, the default is used. If the PLOTTER command is encountered later in the input stream, either by error or by design to change plotters, only those parameters following that card can be relied upon for use in subsequent computations. Therefore, all but the CSCALE parameter should be respecified.

The AXES, VIEW and MAXIMUM DEFORMATION Parameter

These three cards are used to orient and define the size of the object to be plotted. These parameters must be set before the FIND card is input. Once set,

* This feature now works in Level 16.

they are changed only by another AXES, VIEW, or MAXIMUM DEFORMATION card. However, if any one of these cards occur between a FIND and a PLOT card, the results may not be properly scaled and centered.

The MAXIMUM DEFORMATION parameter is used to scale up the deformations which are usually very small compared to the overall dimensions of the structural model. If the user does not specify a value, the program assumes a default of 5% of the maximum X or Y range in the structural coordinates of the current view. This is usually adequate. However, small deformations may not show up. Large deformations may cause undesirable distortions if this parameter is too large.

The SCALE and ORIGIN Card

Once the overall size of the object to be plotted is determined using the above parameters, it must be scaled and an origin selected to fit the picture in the frame. With these cards, the user can set the parameters himself, but the calculation process is error prone and the FIND option is recommended.

The FIND Card

This card is optional but it is recommended to let the program compute the SCALE, ORIGIN, and VANTAGE POINT parameters. The latter is only calculated if PERSPECTIVE or STEREO plots have been requested. If any word appears following the FIND, no defaults are used. Instead, it is assumed the unspecified parameters already have been set. Only the specified parameters will be calculated.

The data operations caused by the FIND card are extensive. After interpreting the input, the GPSETS record for the SET specified on the FIND card, or the first well-defined set in the plot input is read into core. The three geometric coordinates for the grid points in that set are read from the BGPDT file. These coordinates are transformed to correspond to the VIEW and AXES specified. From this transformed data, the minimum and maximum X and Y locations are obtained and added to the previously defined MAXIMUM DEFORMATION to determine the SCALE and ORIGIN required to place the object within the frame.

Another parameter, REGION, is a convenience parameter used to set up an origin and scale such that only part of the frame is available for plotting a given SET. Thus, more than one SET could be plotted on the same frame, but in different locations and with different options. Because only one SCALE exists, the sets to be plotted should be of similar dimensions. Different sets may be used but each will be plotted using the SCALE from the last FIND card processed before the PLOT command. Note, however, plotting may occur outside of this region since REGION is only a convenience parameter used by the FIND card. Its designed use is to facilitate the SYMMETRY option on the PLOT card. For user convenience when defining the REGION, the frame dimensions are scaled from 0.0 on the lower left to 1.0 on the upper right.

The PLOT Card

After the FIND card is processed, the program is ready to process the PLOT card. Following the word PLOT, additional identifying data are expected only if the request is to be for deformed plots. Otherwise, it defaults to undeformed plots. If a scale or an origin had not been set up, a default value is obtained and the first well-defined set is utilized. The words STATIC, MODAL, CMODAL, TRANSIENT or FREQUENCY may be used followed by DEFORMATION, VELOCITY or ACCELERATION. Note that the latter two are only valid for FREQUENCY or TRANSIENT requests. For deformed plots additional control parameters can be input. These parameters include RANGE or TIME and PHASE LAG or MAGNITUDE. RANGE or TIME (which are interchangeable key words) restrict the cases to be plotted. Units of frequency are used for RANGE when MODAL, CMODAL or FREQUENCY follow the word PLOT. For buckling analyses, the eigenvalue itself is used. For TRANSIENT, units of time are used. For STATICS, only the subcase number can be used to select the displacement set to be plotted. For CMODAL and FREQUENCY where complex variable deformations U are to be plotted, the user has a choice of PHASE LAG θ ($U = U_R \cos \theta + U_I \sin \theta$ with θ in degrees with a default of 0.0) or MAGNITUDE ($U = \sqrt{U_R^2 + U_I^2}$).

NASTRAN first processes all requests for undeformed plots. Then, once the desired solution is obtained, the plot requests are again scanned. On this pass, the undeformed plot requests are skipped and only the deformed plot requests are honored. On this second pass, each case on the appropriate deformation input file is checked against the subcase and range parameters specified. If not requested, that case is skipped until either one is found or no more cases exist.

Once a valid PLOT request is identified, the remaining parameters on the card are read. These parameters include SET, ORIGIN, SHAPE, SYMBOL, LABEL, VECTOR, DENSITY, PEN, SYMMETRY, ANTISYMMETRY, and MAXIMUM DEFORMATION. The first occurrence of SET is stored. Thereafter either an end-of-logical card or another SET request causes the stored parameters to be plotted. Before reading parameters for the next SET to be plotted, some parameters are reinitialized. These are LABEL, SHAPE, SYMBOL, SYMMETRY or ANTISYMMETRY, and VECTOR. These parameters must be respecified if they are to be used for plotting the next SET. SHAPE is used as a default.

For stereo plots, the control parameters are kept in core and the data files are reprocessed.

Plotting the SET

So far, the call to plot a set of elements has been described only in sketchy terms. This call needs to be explained in more detail. First, the remaining words of open core must exceed

NGP + 3 * NGPSET + N (undeformed plots)
NGP + 8 * NGPSET + M (deformed plots)

where NGP is the number of grid and scalar points in the model, NGPSET is the number of grids in the set being plotted, and where N is the number of words in 4 NASTRAN buffers plus the plotter buffer. To find the size of the plotter buffer, take the record size from Table 1 and divide by the number of characters per word for the machine being used. M is one NASTRAN buffer-size larger than N. What remains of open core is used, unless VECTOR NR is requested, to create a pen optimization sequence. This adds to the space required by at least NGPSET plus two times the number of edges on the elements in the set.

For the element set to be plotted, the displacements, velocities or accelerations for points in the set are read into core from the appropriate file and, if necessary, are converted from complex to real numbers as described above. At this time the maximum component is also found and stored. This is the maximum for all grid points, not just for those in the set.

For deformed plots, the deformations are processed according to the symmetry options and the values are rotated and scaled to the user requests. The scaling function is

$$u \left(\frac{M_c}{M_p} \right)$$

where M_c is from the MAXIMUM DEFORMATION card, M_p is the maximum specified on the PLOT card or alternatively the actual maximum component value, and u is each input component of the displacement, velocity or acceleration vector.

If the SHAPE (outline of each element) is to be drawn, phase one of the pen optimization is performed. The output is a list of pointers to a second array that lists all connections to the grid associated with the pointer. This process involves two sorts on the lines in the set. The core used for this operation may be monitored by turning on DIAG 25 in the Executive Control Deck. These sorts involve extensive calculations proportional to the square of the number of lines in the set.

These arrays are used for drawing the lines in both the undeformed and deformed SHAPE plots (phase 2). If the arrays could not be created in phase 1 due to core restrictions, optimization is not performed and all edges are drawn for each element directly from the ELSETS file.

The resultant plot for Demonstration Problem 1-2-1 shown in Figure 1 provides the following statistics for using the SHAPE option:

Number of rasters movement for	With Array	Without Array	Percentage increase
drawing lines.....	8,127	14,314	76%
repositioning pen.....	0	6,343	-
	8,127	20,657	154%

This data was calculated from a DIAG 30 dump using an SC 4020 plotter. Note DIAG 30 is special purpose and must not be set in the Executive Control Deck.

Drawing the VECTOR requests causes additional computation. Depending on the requests, as many as three lines may have to be calculated for plotting at each grid point, one for each component of deformation. These calculations, whether for components or the vector resultant, must include the appropriate axes transformation, rotation and projection onto the plotting surface.

Grid identification includes SYMBOLS and LABELS. The SYMBOLS are simply drawn (or typed) from standard tables available. The grid identification LABELS are obtained by searching the EQEXIN file to obtain the external grid point ID. Element identification numbers and element type identification LABELS are found by rereading the ELSETS file. These LABELS are centered and aligned relative to one of the element's edges. Such effort in locating and orienting each of these labels and symbols adds considerably to the computation time required for the PLOT module.

EXAMPLES AND ALTERNATIVES

Various input techniques are illustrated. Ways are shown for improving efficiency, simplifying the input, and exploiting the capabilities of the NASTRAN structural plotter.

Input Syntax

The formatting rules for the NASTRAN Case Control deck apply also to the plot command segment of that deck. Delimiters (e.g., "/", "=", "(", ")", and ",") may be used freely since they are ignored, that is, except for the comma if it is the last character on the card. Only the first four characters of the key word suffice unless the word would not be unique (e.g., PLOTTER and PLOT). Element names (QUAD1 and QUAD2, etc.) must be completely specified. Unlike normal Case Control, real numbers may be input as integers on the plot control card.

The four key commands (SET, PLOTTER, FIND and PLOT) must be the first word on the card. All the other key words may share the same card since they identify parameters which are stored. For example:

```
$ FIRST VIEW  
VIEW = 10.0, 20.5, 0.0  
AXES = Z, X, Y
```

could be specified as

```
VIEW 10, 20.5, AXES Z, X, Y $ FIRST VIEW.
```

This card also illustrates the use of "\$" for comments on a command card, and the acceptance of default values for the third VIEW angle. That default is 0.0 in this case because it is the "FIRST VIEW". Otherwise, the default would be the previously set value. If two angles had not been specified, the program would use the defaults for the second and third angle. Incidentally, using this combining

feature will not only reduce the size of the data files but will help preserve the sequence of the input deck if it is dropped.

Using the FIND Card

The FIND card is optional but recommended. The parameters SCALE and ØRIGIN could be calculated manually and input directly. An undocumented feature, used to manipulate the SCALE factor for special effects, illustrated by

FIND SCALE 0.9, ØRIGIN 100, SET 20

would reduce the calculated scaling factor to 90%. Note that SET 20 need not contain all the elements to be pictured later with the PLOT command. This set can be uniquely defined to establish a special scale factor and origin so that a limited area of a model may be selectively plotted. This concept depends on the fact that lines will be "clipped" if they fall outside the range of the plotter frame area. Hence, any elements outside the bounds of the SET used to define SCALE and ØRIGIN will be eliminated automatically.

The element SET created especially for use by the FIND card should be small. Recall that the coordinates for all grid points defined by a SET are read into open core. A 3 x 3 matrix transformation is performed to rotate them to the current view. Then, only the maximum and minimum values on the plotting surface are used to calculate SCALE and ØRIGIN. Also, the elements of the SET must be carefully selected to include the extremities of the object as it will appear when projected onto the plotting surface. For perspective projections, all three dimensions of the object must be considered.

For the plate model shown in Figure 2, the following commands could be used assuming the model includes only the first quadrant of the plate:

```
ØUTPUT(PLOT)
SET 2 = 1, 5, 31, 36
SET 1 = ALL
VIEW ...
AXES ...
FIND
PLOT SET 1
```

Note that the FIND card without any other key parameter will request all the defaults to be taken. SET 2 will be used since it is the first well-defined set. Had SET 1 been used, 36/16 more work would have been performed to find SCALE and ØRIGIN. On larger models, these savings would be substantial.

The REGION parameter on the FIND card can be used for plotting symmetric segments of the model illustrated in Figure 2. Assuming only the first quadrant of the square plate is specified in the model, all four quadrants could be plotted on the same frame with:

```

SET 1 = 1, 5, 31, 36
SET 2 = ALL
VIEW 60, 20, 0
FIND SCALE ØRIGIN 10 SET 1 REGION .43, .26, 1, 1
PLOT SET 1, SET 1, SYMMETRY X,
SET 1, SYMM Y, SET 1, SYMMETRY XY

```

Assuming the entire plate is to be centered in the plotting frame, the parameters were selected so that the first quadrant would be centered in the REGION specified. It should also be noted that the symmetry axes specified on the PLOT card are always assumed to refer to the basic coordinate system, not the axes of the plot frame. The SYMM plotter option can only work correctly if the plane(s) of structural symmetry align with the basic coordinate system axes.

An alternate method is available for plotting the entire plate shown in Figure 2 using the AXES card as follows:

```

ØUTPUT(PLOT)
SET 1 = 1, 5, 31, 36
SET 2 = ALL
VIEW 60, 20 $(QUAD 1 - AXES Z, X, Y)
PLOT SET 2
AXES Z, MX, Y
FIND $(QUAD 2)
PLOT SET 2
AXES Z, MX, MY
FIND $(QUAD 3)
PLOT SET 2
AXES Z, X, MY
FIND $(QUAD 4)
PLOT SET 2

```

This approach is more expensive due to the number of FIND requests. Also, not one, but four plots are required. If care is taken in defining the SET used to define SCALE, all the plots will be to the same scale and can later be integrated into one large figure. A more subtle method of forcing the same scale would be to add "ØRIGIN 1, SET 1" to all but the first FIND card. The first FIND would compute the scale factor. Because "SCALE" is not input on the subsequent FIND cards, that factor is used as the default.

PLOT Card - Deformation Selection

Eigenvalue analysis results usually include eigenvectors that need not be plotted. These may be the rigid body modes or, on restart, they might be the first 10 modes which were plotted previously. For these cases, since the frequency (or eigenvalue) already is known, the RANGE parameter on the PLOT card can be used. However, when the frequency is not known beforehand, a different approach must be used. Here is where the MODES Case Control card can be used to advantage. An example for plotting modes 5, 6, and 7 follows:

```

      :
      METHOD = 100 $ FIRST THRU FOURTH SUBCASE - MODES 1 THROUGH 4
SUBCASE 11
      MODES = 4 $ FIFTH THRU SEVENTH SUBCASE - MODES 5 THROUGH 7
SUBCASE 15
      MODES = 3
SUBCASE 18 $ REMAINING SUBCASE - ALL OTHER MODES
OUTPUT(PL0T)
      SET 1 = PL0TEL $ USED ONLY FOR * FIND * CARD
      SET 3 = ALL EXCEPT PL0TEL
      MAXI DEFORM, AXES Y, 3 X, VIEW 30, 45
      FIND SCALE 1.0, ORIGIN 1, SET 1, REGION 0.4, 0, 1, 1
      PL0T MODAL DEF 15 to 17, SET 1, SET 1 SYMMETRY X

```

These plots are controlled by the subcase numbers (e.g., 15 & 17) and not the mode number or RANGE of frequency. Note that Subcase 18 in Case Control had to be specified since MODES must not be used in the last subcase. The PL0TEL elements are introduced to define the model extremities for use by the FIND card. Notice that using the SYMMETRY option, mirror images are plotted for both the deformation and the model on the left and right sides of the plot frame. If instead, the ANTISYMMETRIC option were used, the direction of the deformation would be reversed for the mirror image only.

PL0T Card - Restricted Labeling

Being able to plot multiple sets per frame can be useful in providing different plot options for each SET. For example:

```

      SET 4 = PL0TEL $ FOR USE BY * FIND * CARD
      SET 3 = SHEAR, EXCLUDE GRIDS 100 THRU 276,
              EXCEPT GRID POINTS 123, 192
      SET 5 = BAR
              FIND SCALE, ORIGIN 5, SET 4
      PL0T FREQ VELOCITY 0, SET 3, SHAPE, LABEL (BOTH)
              SET 5, VECTOR NR, SYMBOL 7

```

illustrates a method for selectively labeling elements and grid points. Notice that all SHEAR elements, and not the BAR elements will be drawn and labeled. The BAR element set is used only to define the grid points to be associated with the VECTOR option. Only a portion of the grid points in SET 3 will be identified by number. Those in SET 5 will be identified by a symbol. Hence, some grids may be given both a symbol and a label.

The VECTOR NR option applies only to grid points in SET 5 preventing the plot of any underlay for these elements. However, the SHAPE of SET 3 will be drawn. Had grids been excluded from SET 5, both the vector and the symbol for those grids would not be plotted.

PLØT Card - MAXIMUM DEFØRMATION Parameter

With CRT film plots, a movie can be made from a transient solution. This requires the user to select a value for the maximum displacement applicable to all time steps. This value is specified with the MAXI DEFØ parameter on the PLØT card. If not used, the PLØT module would scale each time step vector differently, based on the maximum component for that one vector only. With the MAXI DEFØ parameter on the PLØT card, all time steps will be plotted to the same scale in order to preserve the relative difference from frame to frame.

The MAXI DEFØ parameter can also be used to modify the scale used in plotting the deformations of a subset of elements. This becomes important when a SET is located in the model where displacements are small relative to the overall maximum. Otherwise, the plotted deformations will be scaled to the maximum over all grid points in the model and not the maximum deformation of the grid contained in the SET.

PLØT Card - Element SET Selection

The issue here is efficiency. By choosing element SETs carefully, significant gains can be realized.

The SHAPE option on the PLØT card initiates two expensive sort operations which are always executed, unless open core is too limited. This sorting eliminates redundant lines encountered when more than one element connects the same pair of grid points. Once the unique lines have been identified, an optimum sequence for plotting these lines is established as described earlier and illustrated in Figure 1. However, if VECTØR NR is specified, any SHAPE or underlay requests and the associated line processing is bypassed.

Complicated models often include elements that add no unique lines. For instance, shear panels are frequently used with rod elements on all four edges. The most efficient choice would be to EXCLUDE the shear panel elements by its type or by the individual element number:

SET 5 = ALL EXCLUDE SHEAR 526, 15, 1025

Of course, for checking out a model, all elements should be plotted to verify overall consistency of the input. The alternative here is to divide the elements into subsets and request several SETs to be plotted on the same or on separate PLØT commands. Thus, the open core required to store data for any one set is reduced. Because the sorting time is proportional to the square of the number of lines in a SET, the CPU time also will be reduced.

CONCLUDING REMARKS

The examples throughout the paper have been designed to illustrate the flexibility and utility of the NASTRAN structural plotter. Each set of input commands was presented as a functional entity. The purpose was not to describe it in detail. The purpose was to inspire the reader to experiment.

REFERENCES

1. McCormick, C. W., Editor: The NASTRAN User's Manual. NASA SP-222, 1973.
2. MacNeal, Richard H., Editor: The NASTRAN Theoretical Manual. NASA SP-221, 1972.

TABLE 1. NASTRAN PLOTTER DATA

[1 inch = 0.0254 m]

Plotter Identification Data		Plotter Identification Data					Default Rasters X by Y	Rasters Per Inch	Character Rasters X by Y	Max. Line Length (Rasters)	Record Size (Characters)
Model	Type	Paper Size (Inch)	Line Size (Inch)								
EAI 3500	TABLE	30x30				16667x16667	666.7	66.7x133.3	83.33	2400	
EAI 3500	TABLE	45x45				17778x17778	444.4	44.4x88.8	55.56	2400	
BENSON LEHNER	TABLE	30x30				5000x5000	200.0	20x40	12	2400	
CALCOMP 565, 765	DRUM	12	.010			2400x2200	200.0	16x32	2	2400	
CALCOMP 565, 765	DRUM	12	.005			4800x4400	400.0	32x64	2	2400	
CALCOMP 563, 763	DRUM	30	.010			6000x5800	200.0	16x32	2	2400	
CALCOMP 563, 763	DRUM	30	.005			12000x11600	400.0	32x64	2	2400	
DATA DISPLAY 80	CRT					1023x1023	146.1	8x16	1023	1020	
STROMBERG CARLSON	CRT					1023x1023	136.4	8x16	63	720	
NASPLOT	CRT					1023x1023	146.1	8x16	1023	3000	
NASPLOT	TABLE/ DRUM					1000x1000	48.0	16x16	1000	3000	

TABLE 2. INTERACTION OF PLOTTING PARAMETERS

Other Parameters Affected	Default Options	Parameter Specified by User											
		ØRTHØGRAPHIC	PERSPECTIVE	STEREØ	PLØTTER	PAPER SIZE	ØRIGIN	SCALE	CSCALE	PRØJ PLANE	VANT PØINT	FIND	PLØT
ØRTHØGRAPHIC	YES	S						U				U U	
PEKSPECTIVE	NO		S					U	U	U	U	U	
STEREØ	NO			S				U	U	U	U	U	
PLØTTER	SC, 4020				A	U	U	U	U			U U	
PAPER SIZE	8-1/2x11				U	A						U U	
ØRIGIN	*	D	D	D	D		S					U U	
SCALE	*	D	D	D	D			S				U U	
CSCALE	1.0							U	S			U U	
PRØJ PLANE	1.0									S		U U	
VANT PØINT	*		D	D	D						S	R U	
FIND	*											A	
PLØT	REQUIRED												A
VIEW [†]	*	D	D	D								U U	
AXES [†]	X,Y,Z											U U	
MAXI DEPO [†]	0.0											U U	
CAMERA [†]	PAPER				D							U	
PEN [†]	1											U	
BLANK FRAME [†]	1											U	
ØCULAR SEPA [†]	2.756											U U	
SET	REQUIRED											U U	

Code

- * - Program generates all values required if not set by user.
- A - Action parameter. Activates computation when encountered.
- D - Default values restored. User must respecify if alternate values desired.
- R - Recalculated if requested.
- S - Stored for later use. Minor calculations may be initiated.
- U - Existing values utilized if required for projection, plotter.
- † - Stored for later use, does not cause change in other parameters.

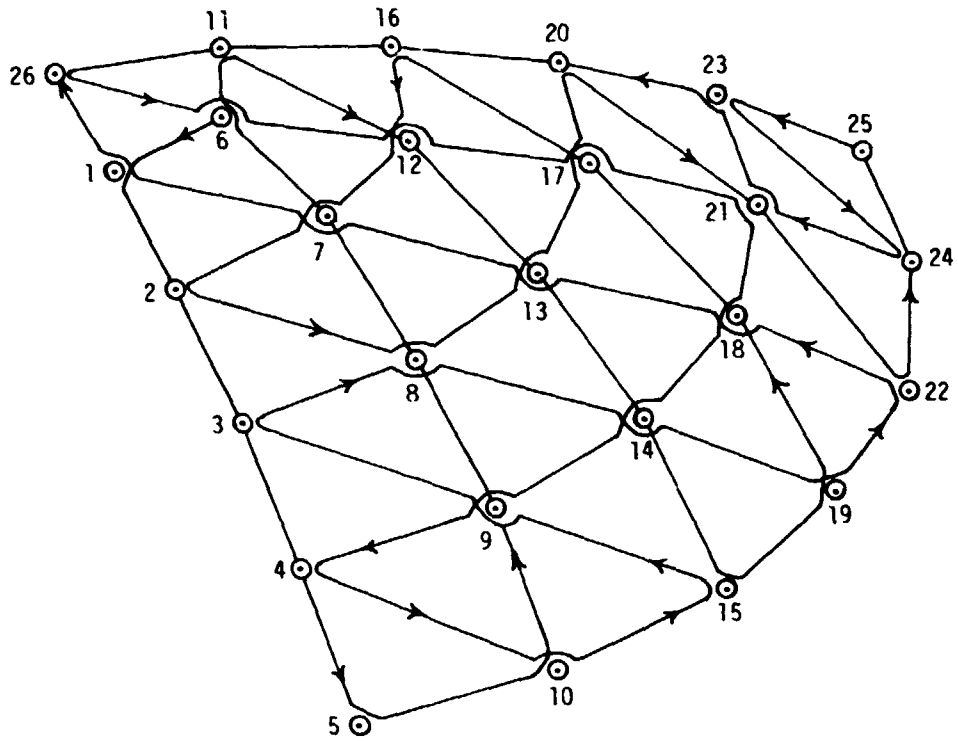


Figure 1.- Path of plotting pen for Demonstration Problem 1-2-1.

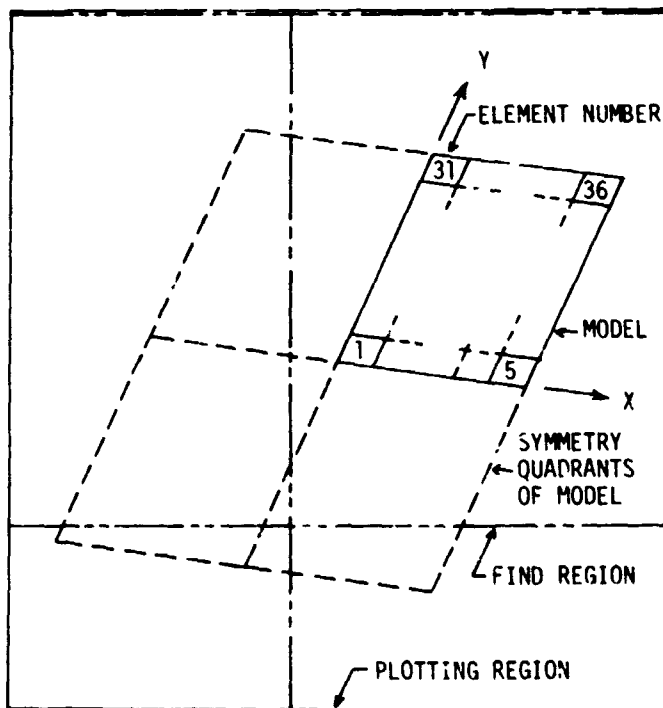


Figure 2.- Example illustrating SYMMETRY, REGION and SET, as used with the FIND and PLOT commands.

N75 31514

THE NASTRAN ERROR CORRECTION INFORMATION SYSTEM (ECIS)

David C. Rosser, Jr.

and

Janes L. Rogers, Jr.
NASA Langley Research Center

SUMMARY

A new data management procedure, called Error Correction Information System (ECIS), is described. The purpose of this system is to implement the rapid transmittal of error information between the NASTRAN Systems Management Office (NSMO) and the NASTRAN user community. This paper summarizes the features of ECIS and its operational status. The mode of operation for ECIS is compared to the previous error correction procedures. It is shown how the user community can have access to error information much more rapidly when using ECIS. Flow charts and time tables characterize the convenience and time-saving features of ECIS.

INTRODUCTION

In the past, NASTRAN users have been severely restricted in their access to NASTRAN error information. Access has been via telephone, correspondence, the NASTRAN Newsletter, and Software Problem Report (SPR) Log. Although many times temporary and permanent fixes were given to the originator of the SPR, these fixes were frequently not available to the entire NASTRAN user community until a new version of NASTRAN was released. In an effort to improve user access to NASTRAN error information, NSMO has initiated ECIS (ref. 1) on a commercial network, using an established data base management system (refs. 2 and 3).

THE ERROR CORRECTION INFORMATION SYSTEM

ECIS is a positive step by the NSMO to provide the NASTRAN user community with an expedient information storage and retrieval system for SPR's. This system will support the two-way transmittal of information and SPR fixes among the user community, NSMO, and the maintenance contractor on a daily basis.

Organization

The system consists of two distinct data bases. The first data base is the User Comment data base (Table 1). The User Comment Data Base has three purposes. The first and major purpose is for the two-way transmittal of information between NSMO and the user community. Through this data base the user can make general comments, describe difficulties, or submit an SPR. The second purpose is bookkeeping. Each time a user accesses this data base, the user's NAME, ORGANIZATION, DATE, and TIME OF DAY should be entered. From this information, NSMO can compile statistics on use of the system. The third purpose of this data base is for NSMO to respond to users. NSMO accesses the User Comment Data Base daily, records the user comments or problems, and then updates the data base with an acknowledgment, a solution to the problem, or an explanation of NSMC's plans with respect to the user's specific problem. Then the user can access the data base and learn that NSMO has received the data and what solutions or alternatives are available.

The second data base (Table 2), called ECIS, consists of information and updates pertinent to all active SPR's. When a new SPR is discovered, it is given a number and all known information about the SPR (shown in Table 2) is entered into the data base in the same manner as in the SPR Log. As the SPR is processed, a temporary fix, if available, and a permanent fix, when determined, are added to the SPR in the data base. This gives all users simultaneous access to all active SPRs with their current updates.

The system is accessible by users through CYBERNET, a national computer network maintained by Control Data Corporation. The resources needed to utilize ECIS are (1) a copy of NASA TM X-72651, (2) a desk-top, interactive computer terminal, and (3) a contract with Control Data Corporation for computer time on the CYBERNET System.

Querying ECIS

Software support for ECIS is a Data Base Management System called System 2000. System 2000 manages all definition, accessing, updating, quering, and retrieving of information to and from the data base. System 2000 organizes the data in a data base as an Element or a Repeating Group. The element consists of a name standing for data within the data tables. Each element has a name and a number which are synonymous as can be seen in Table 2. For example, if the user wants an output statement which prints SPR number and user name, he types "PRINT SPR NUMBER, USER NAME" or "PRINT C1, C2". SPR NUMBER is synonymous with C1 and USER NAME is synonymous with C2 in the ECIS data base.

The Repeating Group (RG) allows elements to take on multiple values. For each SPR entered into the data base, there will be only one SPR NUMBER but there might be several SUBROUTINE data items entered indicating which subroutines need modification. The name used for a Repeating Group is for definition only and

does not take on data values. For example, in Table 2 the only function of the Repeating Group described as PERMANENT FIXES is to define PERM FIX IBM, PERM FIX CDC, and PERM FIX UNIVAC as elements which may have multiple values.

ECIS retrieval commands range from the very simple to the very complex. The retrieval commands are in the form of PRINT (Something), or PRINT (Something) WHERE (Certain Conditions Exist). The quantity and form of the output is controlled entirely by the user through proper definition and ordering used in the retrieval commands.

There are two general forms of output statement: The first is of the form PRINT (Print Clause) and the second is of the form PRINT (Print Clause) WHERE (Condition Clause).

The print clause is the simplest form used in obtaining output from the data base. The print clause is only a list of data base items the user wants printed. The data can be printed in any order or number by listing in the print clause each item wanted and in the order wanted. The only restriction is that each item must be called by its proper name or element number as shown in the definition of the ECIS data base in Table 2. If data from Repeating Groups (RG) are included in the print clause, the name must be preceded with a (, BY ENTRY ,) operator.

Examples:

```
PRINT SPR NUMBER:  
PRINT SPR NUMBER, USER NAME, SUBROUTINE:  
PRINT C2, SPR NUMBER, C3, LEVEL FOUND:  
PRINT C1, BY ENTRY, SUBROUTINE:  
PRINT C1, C3, C4, C2:
```

The condition clause can take many forms, such as AND, OR EQUAL (EQ), NOT EQUAL (NE), GREATER THAN (GT), LESS THAN (LT), LESS THAN OR EQUAL TO (LE), GREATER THAN OR EQUAL TO (GE), EXISTS, AND FAILS. If data for repeating groups is included in a where clause, it must be preceded by an ENTRY HAS operator.

Examples:

```
PRINT SPR NUMBER WHERE SPR NUMBER EQ 395:  
PRINT C1 WHERE C7 EXISTS:  
PRINT C1 WHERE LEVEL FOUND GE 15.1:  
PRINT USER NAME WHERE SPR NUMBER LT 1000  
OR SPR NUMBER GT 200, AND USER NAME NE  
ROSSER, AND USER ORGANIZATION EXISTS:  
PRINT C1, BY ENTRY, C34 WHERE C6 FAILS AND  
ENTRY HAS MODULE EQ SDR2:
```

There are two special cases which may be needed by some users: the PRINT ENTRY and the PRINT ENTRY WHERE (Condition Clause). The PRINT ENTRY command will print out the entire data base. This command however will cause excessive printout. If all of this information is desired, it is suggested that the SPR

Log be purchased from COSMIC. The PRINT ENTRY WHERE command can be used to print one or many entire entries with one command. For instance, if one wanted the entire entries for all SPR's submitted by a particular user, he would type:

```
PRINT ENTRY WHERE USER NAME EQ WALL, JAMES
```

Several sample problems with user entries and system responses are given in Appendix A.

POTENTIAL OF ECIS

The old method of communicating and processing NASTRAN SPR's is diagramed in figure 1. The process began by the user mailing an inconsistency and its documentation (listing, dump, deck, etc.) to NSMO. NSMO then determined what caused the inconsistency. It may have been a user error, a previously reported error, or an SPR. NSMO then responded to the user by mail, possibly with a temporary fix. If enough documentation was sent to aid in correcting the error, the SPR was forwarded to the maintenance contractor. The maintenance contractor then recorded the error in the SPR Log, coded a fix, and implemented the fix into a new level of NASTRAN.

The disadvantage with this method was that there was no feasible way to rapidly distribute this error information to the entire user community. The old system for distribution of error information included the NASTRAN Newsletter (once every 6 months), the NASTRAN SPR Log (once every 8 months), or a new level of NASTRAN (once every 12-24 months). With over 1200 SPR's and 500 users on the mailing list, it was not feasible to mail a copy of the errors or fixes to each user as they became available. Thus the time span for receipt of error correction information was quite long. Minimum times are shown in figure 2. Note that long periods of time elapsed between the determination of a fix and its availability to the user community.

The new process for handling NASTRAN SPR's, with ECIS, is diagramed in figure 3. This method differs from the old method in that the user can immediately determine if the inconsistency is a reported SPR by examining ECIS. If it is a reported SPR and a temporary or permanent fix exists, the user can implement the fix into NASTRAN. If the SPR has not been reported, the user can report the error through ECIS and mail the appropriate documentation to NSMO. This way, the entire user community will have knowledge that the error exists. This method then proceeds the same as the old method except for one important difference. With the new method, any time a temporary or permanent fix is found, it is immediately put into ECIS and becomes available to the entire user community.

Once ECIS is accepted by the NASTRAN user community, the time spans from submission of error to receipt of fix are expected to greatly decrease, as shown in figure 4. With ECIS, all users could have knowledge of an SPR within one day, a temporary fix in one week, and a permanent fix in one month. These time spans are minimum time spans and are not meant to imply that all SPR's will be solved within this new time frame.

This procedure does, however, give all users immediate knowledge of the existence of a new problem, therefore eliminating the time and effort of many users responding to an SPR which is already being worked on or solved. If a fix is available, the user will save both time and computer cost normally spent in debugging NASTRAN or redesigning the problem. Thus, significant savings in computer time and manpower is expected when ECIS becomes an integral part of NASTRAN.

STATUS OF ECIS

ECIS was originally created by inputting all SPR's from the SPR Log into the data base. To reduce storage costs and extraneous material, all SPR's corrected before the release of Level 15 of NASTRAN were deleted from ECIS. Continuing efforts are being made to increase the readability and efficiency of ECIS. New SPR's, temporary fixes, and permanent fixes are frequently being added. The status of individual SPR's is updated as the SPR is fixed. When the code to implement a fix to an SPR is integrated into an archive version of NASTRAN, the number of that version is put into the LEVEL FIXED component of ECIS. Once that fix is verified as correct, the STATUS CODE component for that SPR is updated to FIN and the fix is placed in the PERM FIX components. At present, there have been 1202 SPR's reported to NSMO. The status of ECIS is:

- 587 SPR's
- 25 SPR's with permanent fixes
- 54 SPR's with temporary fixes
- 275 SPR's with a level fixed entry
- 164 SPR's with a status code of FIN
- 30 SPR's classified as previously reported errors

CONCLUDING REMARKS

By utilizing an organized procedure for storing, updating, and retrieving large volumes of data, an Error Correction Information System (ECIS) has been developed for NASTRAN. This system supports the two-way transmittal of NASTRAN information, errors, and error corrections between the user and the NASTRAN Systems Management Office; ECIS can be accessed by telephone through any desktop interactive computer terminal.

ECIS shows promise of greatly reducing the long times that heretofore have been needed to disseminate error correction information to the user community. Users of ECIS will have all SPR's, user information, and updates available on demand and fixes will be installed in the ECIS data base as they are devised.

APPENDIX A
SAMPLE PROBLEMS

1. **Problem:** Print all information for a particular SPR.
Entry: Print entry where C1 EQ 1190:
Response: SPR NUMBER = 1190
USER NAME = WINTER, RON
USER ORGANIZATION = TENNESSEE EASTMAN
COMPUTER = IBM 360
LEVEL FOUND = 15.10
DATE REPORTED = 04/02/1975
OPERATING SYSTEM = OCC
PRIORITY = 2.00
RIGID FORMAT = 1,0

MODULE = RBMG2

SUBROUTINE = SDCOMP

STATUS CODE = CKC

ERROR CODE = SOFTWARE ERROR

DESCRIBE ERROR = SPILL PROBLEM IN RBMG2 CAUSES SYSTEM
FAILURE

2. **Problem:** Find all SPR's associated with a particular user.
Entry: Print SPR number where user name EQ Walz, Joe:
Response: SPR NUMBER = 731
SPR NUMBER = 954
SPR NUMBER = 978
SPR NUMBER = 1006
SPR NUMBER = 1067
SPR NUMBER = 1068

3. **Problem:** Same as example 2 with C values substituted for element names.
Entry: Print C1 where C2 EQ Walz, Joe:

SAMPLE PROBLEMS (Cont'd.)

Response: SPR NUMBER = 731
SPR NUMBER = 954
SPR NUMBER = 978
SPR NUMBER = 1006
SPR NUMBER = 1067
SPR NUMBER = 1068

4. Problem: Find all SPR's reported in a particular time frame,

Entry: Print SPR Number where C7 GE 01/01/69 and C7 LT 01/01/70:

Response: SPR NUMBER = 13
SPR NUMBER = 69
SPR NUMBER = 115

5. Problem: Find all SPR's reported between two levels of NASTRAN.

Entry: Print C1 where C6 GT 15.5 and C6 LT 15.7:

Response: SPR NUMBER = 528
SPR NUMBER = 752
SPR NUMBER = 777
SPR NUMBER = 870
SPR NUMBER = 881
SPR NUMBER = 883
SPR NUMBER = 884
SPR NUMBER = 896
SPR NUMBER = 973
SPR NUMBER = 986
SPR NUMBER = 987
SPR NUMBER = 988
SPR NUMBER = 989
SPR NUMBER = 993
SPR NUMBER = 1007
SPR NUMBER = 1020
SPR NUMBER = 1049
SPR NUMBER = 1065

6. Problem: Print the SPR number and the description of any SPR that failed in a particular subroutine of a particular module.

Entry: Print C1, by entry, C34 where entry has C16 EQ TRHT and entry has C18 EQ TRHT1A:

SAMPLE PROBLEMS (Cont'd.)

Response: SPR NUMBER = 986
 DESCRIBE ERROR = SEVERAL ERRORS ARE PRESENT WITH RESPECT
 DESCRIBE ERROR = TO THE USE OF QVECT CARDS IN HEAT TRANSFER
 DESCRIBE ERROR = ANALYSIS.
 DESCRIBE ERROR = FOR IDENTICAL BULK DATA, QVECT LOADS ARE
 DESCRIBE ERROR = APPLIED DURING A NON-LINEAR STEAD STATE
 DESCRIBE ERROR = ANALYSIS, BUT NOT DURING A TRANSIENT RUN.
 SPR NUMBER = 1044
 DESCRIBE ERROR = THIS PROBLEM RAN SUCCESSFULLY, FOLLOWING
 DESCRIBE ERROR = WHICH TWO OF THE TEMP CARDS USED TO DEFINE
 DESCRIBE ERROR = SET 500 WERE REMOVED, LEAVING ONLY THE
 DESCRIBE ERROR = TEMPD CARD TO DEFINE THE SET.
 SPR NUMBER = 1083
 DESCRIBE ERROR = A TRANSIENT HEAT TRANSFER PROBLEM STOPPED
 DESCRIBE ERROR = IN MODULE TRHT WITH A USER ABEND OF 680.
 DESCRIBE ERROR = SUBR. TRH1A WAS TO CONTAIN 3 ERRORS IN
 DESCRIBE ERROR = THE CODE.

7. Problem: Print the SPR number, description, and temporary fix for a particular module that has a temporary fix.

Entry: Print C1, by entry, C34, by entry, C36 where entry has C16 EQ SMP1 and entry has C36 exists:

Response: SPR NUMBER = 1001
 DESCRIBE ERROR = AN OMIT CARD WAS ADDED TO A PREVIOUSLY
 DESCRIBE ERROR = OPERATIONAL TRANSIENT PROBLEM, AND THE
 DESCRIBE ERROR = ABOVE ERROR OCCURRED.
 DESCRIBE TEMP FIX = ALTER 65,65
 DESCRIBE TEMP FIX = SMP1 Huset, HKFF,,,/HGO, Hkaa, HKOO,
 DESCRIBE TEMP FIX = HLOO, HUOO,,,,,\$

8. Problem: Print the SPR number and permanent fix for a particular module that has a permanent fix.

Entry: Print C1, by entry, C39 where entry has C16 EQ XYTRAN and entry has C39 exists:

Response: SPR NUMBER = 1072
 PERM FIX CDC = TEST ALTER FOR LEVEL 15.5
 PERM FIX CDC = CARD *INDENT S1072L79
 PERM FIX CDC = CARD *INSERT RAND5.222
 PERM FIX CDC = CARD LLIST=LLIST-5*(II-ICDONE+1)
 PERM FIX CDC = CARD *DELETE RAND5.225
 PERM FIX CDC = CARD *COMPLETE RAND5

SAMPLE PROBLEMS (Cont'd.)

9. Problem: Find the number of SPR's now in ECIS

Entry: Tally/all/C1:

Response: *****
ELEMENT- SPR NUMBER

MINIMUM- 13

MAXIMUM- 9006

594 UNIQUE VALUES

594 OCCURRENCES

REFERENCES

1. Rosser, David C., Jr.: The Design and Use of an Error Correction Information System for NASTRAN. NASA TM X-72651, 1974.
2. The Information Network Division of Computer Science Corporation: System 2000 Reference Manual, E00209-01, 1973.
3. CYBERNET Service Control Data Corporation: System 2000 Level 2 User Information Manual, 86604500, 1974.

TABLE 1

DEFINITION OF USER COMMENT DATA BASE

- 1° USER NAME
- 2° USER ORGANIZATION
- 3° DATE
- 4° TIME OF DAY
- 5° USER COMMENTS (RG)
- 6° COMMENTS
- 7° NSMO COMMENTS (RG)
- 8° NSMO

TABLE 2

DEFINITION OF ECIS DATA BASE

THE DATA BASE IS COMPLETELY DEFINED BY THE FOLLOWING NUMBERED LIST OF COMPONENTS:

- 1° SPR NUMBER
- 2° USER NAME
- 3° USER ORGANIZATION
- 4° COMPUTER
- 5° LEVEL FOUND
- 6° LEVEL FIXED
- 7° DATE REPORTED
- 8° OPERATING SYSTEM
- 9° PRIORITY
- 10° RIGID FORMAT
- 11° R.F. SUBSET
- 12° ALTER
- 13° ERROR MESSAGE
- 14° PREVIOUS REPORTED BUG
- 15° MODULE NAME (RG)
- 16° MODULE
- 17° SUBROUTINE NAME (RG)
- 18° SUBROUTINE
- 19° DOCUMENTATION ERROR (RG)
- 20° DER NUMBER

TABLE 2 (CONT'D)

DEFINITION OF ECIS DATA BASE (CONT'D)

- 21° MANUAL
- 22° PAGE DATE
- 23° SECTION
- 24° PAGE NUMBER (RG)
- 25° PAGE
- 26° STATUS OF SPR (RG)
- 27° WHOM ASSIGNED
- 28° DATE ASSIGNED
- 29° STATUS CODE
- 30° ERROR CODE
- 31° EXPECTED COMPLETION DATE
- 32° STATUS COMMENTS
- 33° DESCRIPTION OF ERROR (RG)
- 34° DESCRIBE ERROR
- 35° TEMPORARY FIXES (RG)
- 36° DESCRIBE TEMP FIX
- 37° PERMANENT FIXES (RG)
- 38° PERM FIX IBM
- 39° PERM FIX CDC
- 40° PERM FIX UNIVAC

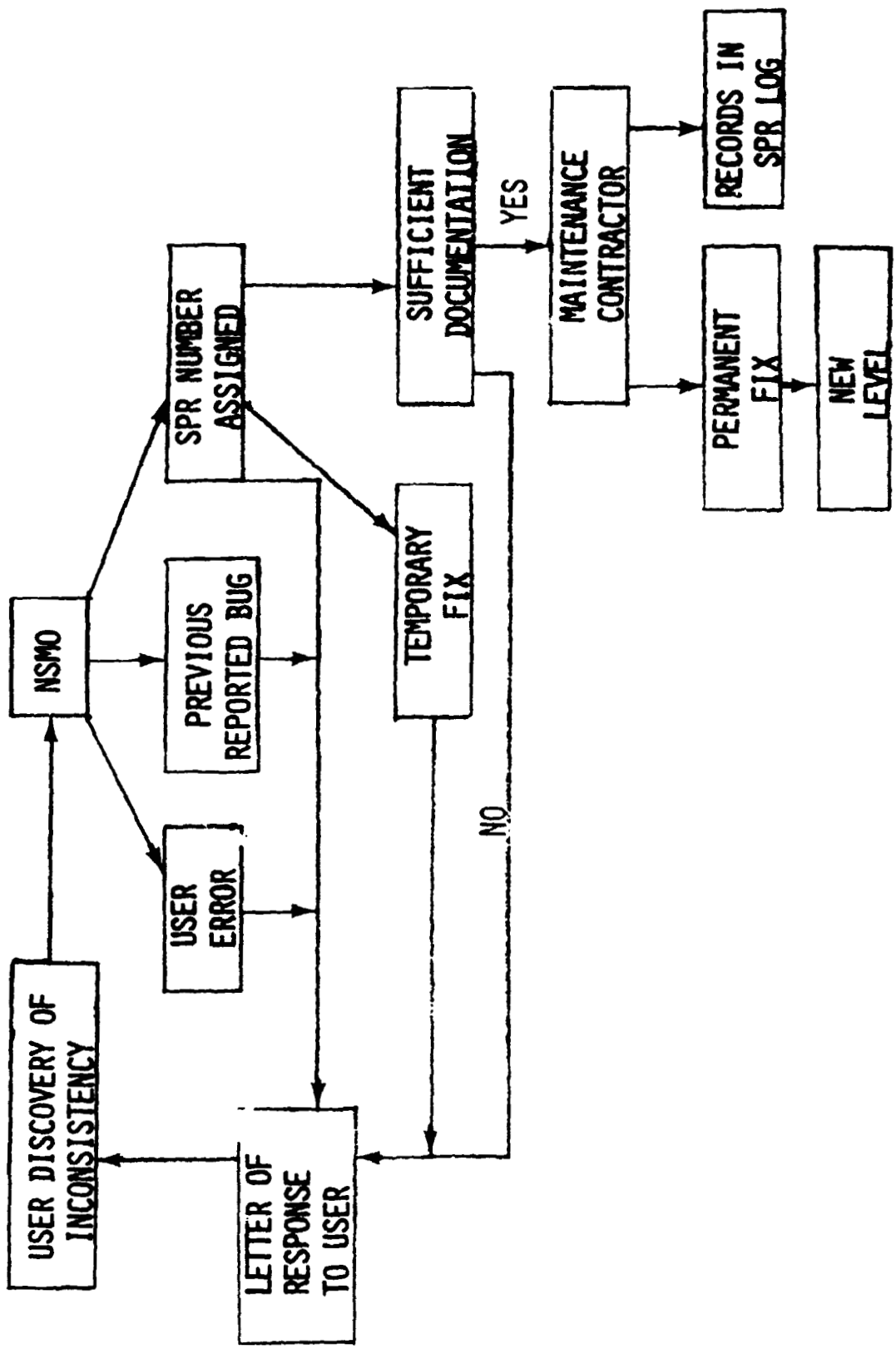


Figure 1 - Old Method for Handling NASTRAN SPR's

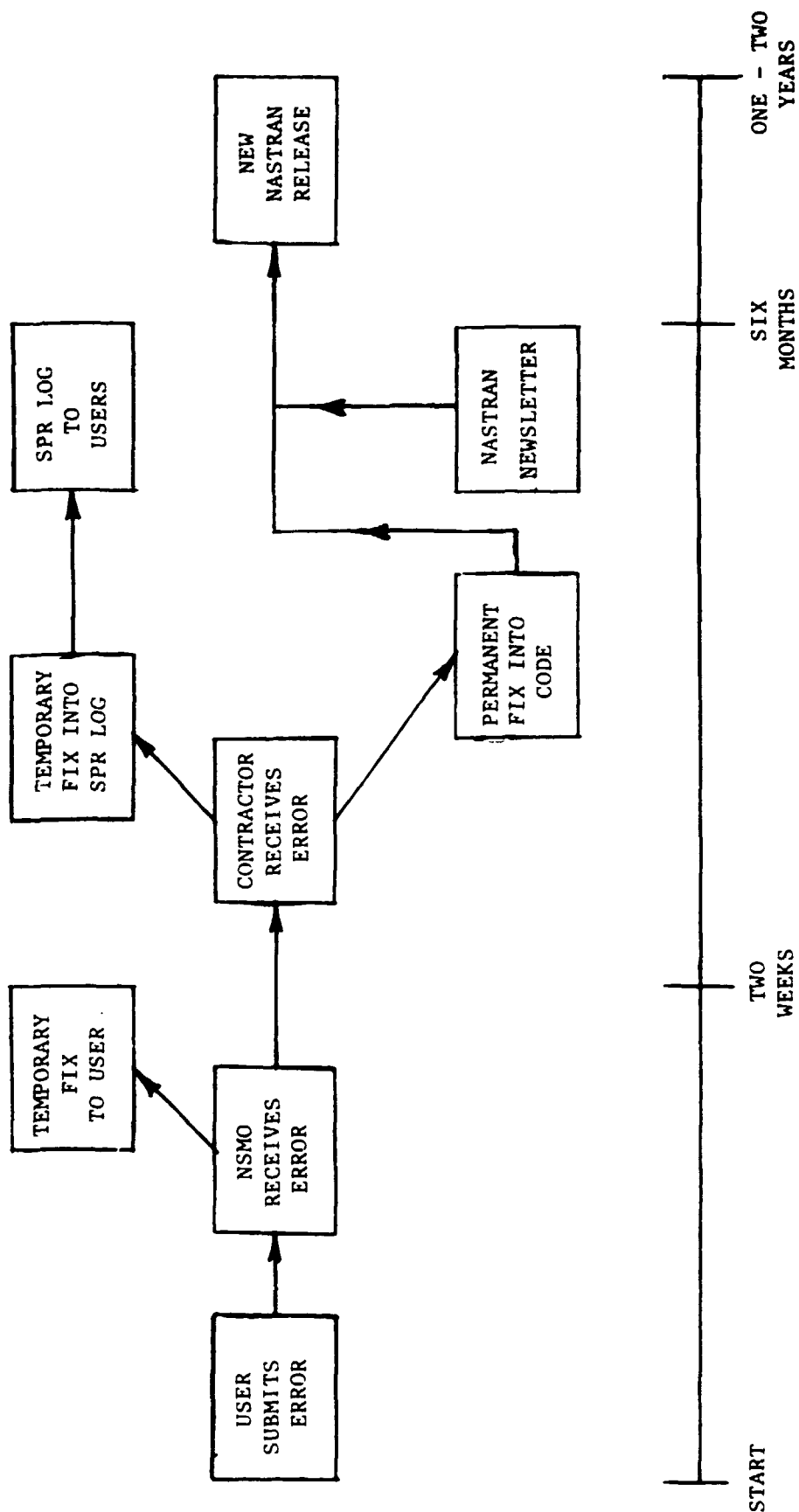


Figure 2 - Minimum Time Span for Old NASTRAN Method of Handling SPR's

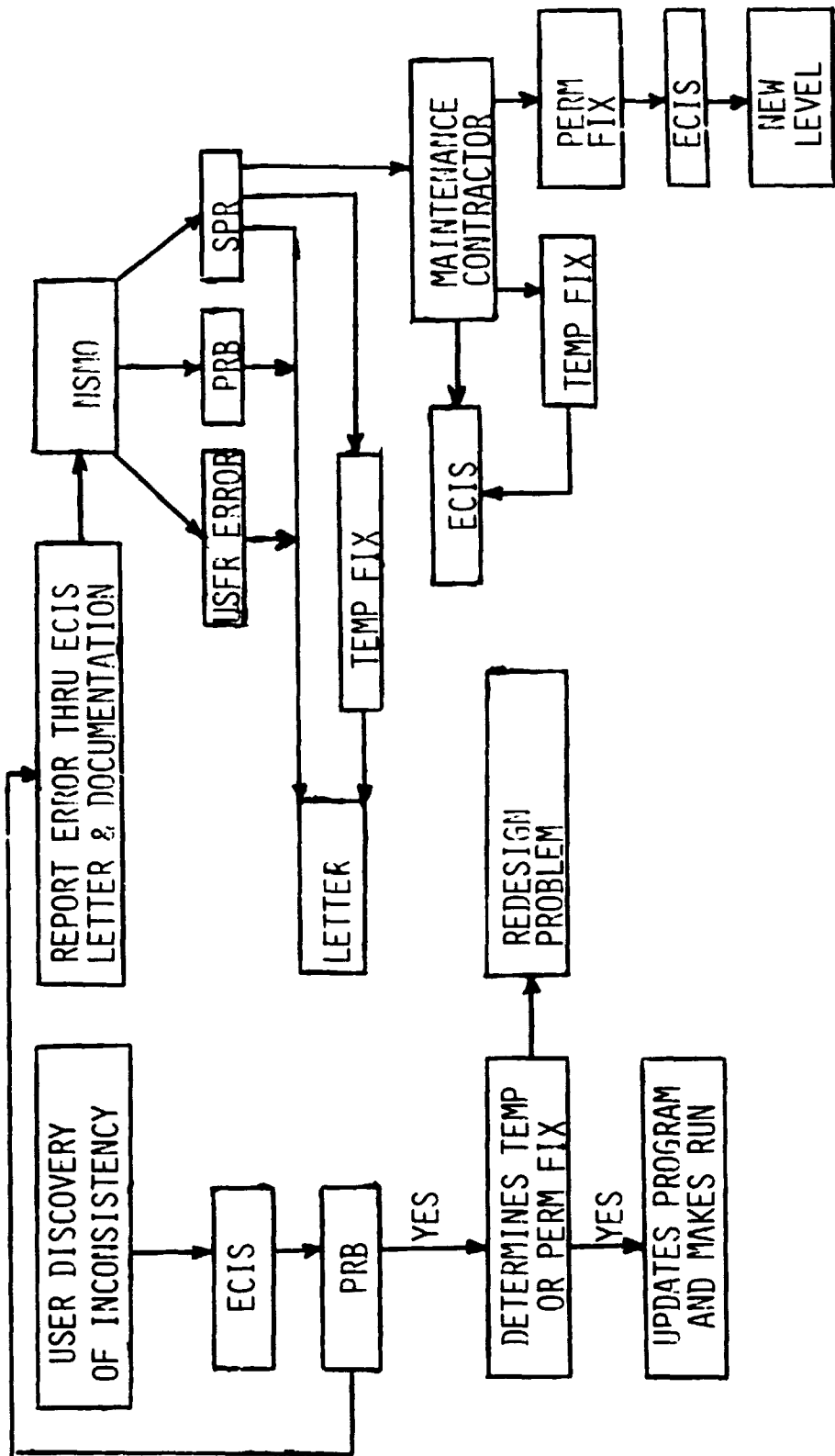


Figure 3 - New Method for Handling NASTRAN SPR's With ECIS

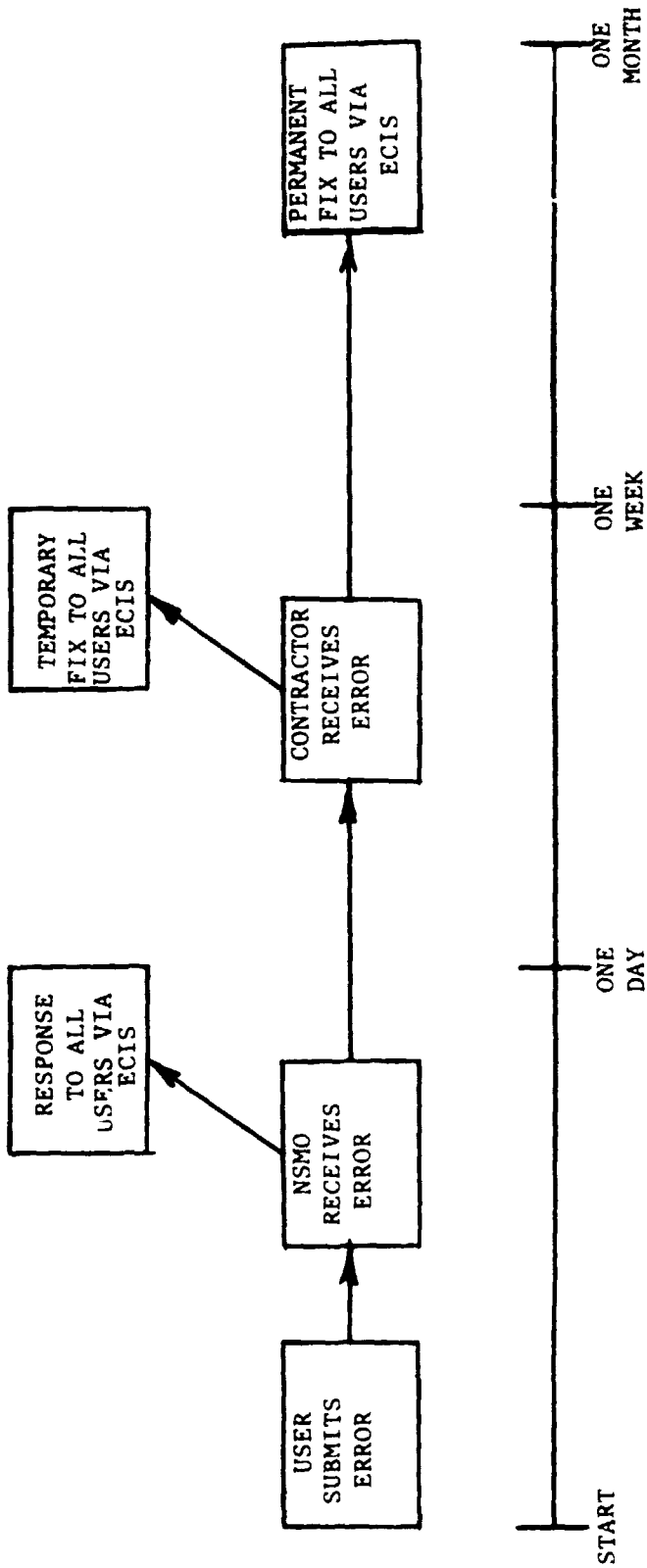


Figure 4 - Minimum Time Span for Handling NASTRAN SPR's with ECIS

N75 31515

RECENT IMPROVEMENTS TO BANDIT

Gordon C. Everstine

Naval Ship Research and Development Center
Bethesda, Maryland 20084

SUMMARY

The NASTRAN preprocessor BANDIT, which improves NASTRAN's computer efficiency by resequencing grid point labels for reduced matrix bandwidth, has been improved by the addition of (1) the Gibbs-Poole-Stockmeyer (GPS) algorithm, and (2) the user option to reduce matrix profile rather than matrix bandwidth. After describing these program additions, this paper shows that, compared to the Cuthill-McKee (CM) algorithm on which BANDIT was originally based, GPS is faster and achieves similar results. For completeness, BANDIT's current capabilities and options are summarized.

BACKGROUND

The NASTRAN structural analysis computer program (ref. 1, 2), as a finite element program, assembles matrices which are normally both symmetric and sparsely-populated. The locations of the nonzero terms in the matrices are determined solely by the choice of numbers (labels) assigned to the grid points. Like most finite element codes, NASTRAN's computer running time can be reduced if the labels can be chosen in such a way that the nonzero terms cluster tightly about the main diagonal. The NASTRAN user has complete control over that clustering by his choice of grid point labels and his optional use of SEQGP bulk data cards, which effect an internal grid point resequencing for calculation purposes.

Soon after NASTRAN became available some five years ago, it was apparent that the program user could benefit from an automatic capability to perform the resequencing and generate the SEQGP cards. Indeed, for large complex structures or those generated automatically, the job of determining a good grid point sequence manually was, at best, tedious and often very difficult.

To fill the need for an automatic capability, several NASTRAN preprocessor computer programs were developed: BANDIT (refs. 3, 4), WAVEFRONT (refs. 5-7), and BANDAID (ref. 8). (For a general survey of NASTRAN preprocessors and postprocessors, see reference 9.) Both BANDIT and BANDAID are intended to reduce matrix bandwidth, while WAVEFRONT is intended to

reduce matrix wavefront. (These terms are defined in the next section.) Of these preprocessors, BANDIT and WAVEFRONT appear to be the most popular. BANDIT was originally based on the Cuthill-McKee resequencing algorithm (ref. 10). WAVEFRONT and BANDAID are based on strategies developed by their authors, Levy (ref. 5) and Cook (ref. 8), respectively. These algorithms and others have been reviewed and compared by Cuthill (ref. 11).

Recently, a new bandwidth and profile reducing algorithm was developed by Gibbs, Poole, and Stockmeyer (GPS) (ref. 12) of The College of William and Mary. Since their testing of it showed it to be both effective and efficient (ref. 13), we have incorporated it in the BANDIT program to supplement the Cuthill-McKee (CM) strategy already there. (Actually, BANDIT uses the so-called reverse Cuthill-McKee algorithm since it was observed by George (ref. 14) and later proved by Liu and Sherman (ref. 15) that reversing the sequence generated by CM can never increase the profile and frequently reduces it. Such a reversal has no effect on the matrix bandwidth.) In general, GPS executes faster than CM and achieves comparable results. Unfortunately, for a given structure, it is not possible to predict a priori which strategy will yield the smaller matrix bandwidth or profile. However, since excessive resequencing time has never been considered to be a problem, BANDIT's current default mode of operation is to apply both CM and GPS to the structure in order to get the better of the two results.

DEFINITIONS

For the purposes of this discussion, some useful terms will be defined which generally follow the material given in Cuthill's survey (ref. 11).

Given a symmetric matrix A of order N , we define a "row bandwidth" b_i for row i to be the number of columns separating the first nonzero in the row from the diagonal. Alternatively, b_i is the difference between i and the column index of the first nonzero entry of row i of A . Then the matrix bandwidth B and profile P are defined as

$$B = \max_{i \leq N} b_i \quad (1)$$

$$P = \sum_{i=1}^N b_i \quad (2)$$

Let w_i denote the number of active columns in row i . A column j is active in row i if $j > i$ and there is a nonzero entry in that column in any row with index $k \leq i$. Thus, a given column is activated at the first nonzero encountered (reading from top to bottom) and remains active until the diagonal is reached. The matrix wavefront W is then defined as

$$W = \max_{i \leq N} w_i \quad (3)$$

Since the matrix A is symmetric,

$$P = \sum_{i=1}^N b_i = \sum_{i=1}^N w_i \quad (4)$$

Now, for row i , let \underline{b}_i denote the columnar distance between the diagonal and the last active column in row i . Then

$$B = \max_{i \leq N} b_i = \max_{i \leq N} \underline{b}_i \quad (5)$$

Since, by definition,

$$\underline{b}_i \geq w_i \quad (6)$$

for each i , it follows that

$$B = \max_{i \leq N} \underline{b}_i \geq \max_{i \leq N} w_i = W \quad (7)$$

and

$$S = \sum_{i=1}^N \underline{b}_i \geq \sum_{i=1}^N w_i = P \quad (8)$$

Hence, as a consequence of these definitions, the matrix wavefront W for a given matrix is less than the matrix bandwidth B , and the matrix profile P is equal to both the sum of the "row bandwidths" and the sum of the "row wavefronts."

These definitions are generally modified slightly by preprocessors such as BANDIT. Since NASTRAN requires all external resequencing via SEQGP cards to be performed at the grid point level rather than the degree of freedom (DOF) level, BANDIT treats each grid point as if it had only one DOF. In general, a NASTRAN grid point can have as many as six DOF's. Thus, to convert BANDIT's values of bandwidth and profile to meaningful approximate values for NASTRAN's structural matrices, one must multiply by the average number of DOF's per grid point.

A NEW RESEQUENCING STRATEGY

The principal recent improvement to BANDIT is the installation of the new bandwidth and profile reducing algorithm developed by Gibbs, Poole, and Stockmeyer (GPS) (refs. 12, 16) of The College of William and Mary. Rather than describe how GPS works, we shall instead demonstrate its performance on a set of test problems. The test problems used here constitute the current extent of a growing collection of diversified NASTRAN data decks to be

used for the testing of resequencing and equation solving algorithms. It is expected that a complete description of the set, including plots of each structure, will eventually be published.

The results of the resequencing tests are shown in Table 1. In that table, the following definitions apply:

N	=	number of grid points (nodes)
M	=	maximum nodal degree (i.e., the maximum number of nodes connected to any node)
B	=	matrix bandwidth (in terms of grid points rather than DOF)
P	=	matrix profile (in terms of grid points)
T	=	time, CDC 6400 CP seconds
Orig.	=	an original value (before resequencing) of B or P
CM	=	Cuthill-McKee strategy
GPS	=	Gibbs-Poole-Stockmeyer algorithm
Decomp.	=	matrix decomposition

For each of 20 structures, ranging in size up to 2680 grid points, the grid point labels were resequenced using both CM and GPS. Before and after results for both bandwidth (B) and profile (P) are shown. Since the test criterion was to reduce B rather than P, the P results are less significant. With CM, a user choice of profile reduction rather than bandwidth reduction will generally give different results for both P and B. All tests were run on a CDC 6400 computer with the SCOPE 3.4.2 operating system. Central processor (CP) times are given for both CM and GPS.

Since some of the structures are clearly very large, rough estimates of the NASTRAN real, symmetric, single-precision decomposition times on a CDC 6400 are given in the last column of Table 1. These values were computed using the following formula extracted from the NASTRAN subroutine RSPSDC:

$$T = T_B(n-2b/3)b^2/2 + T_P(n-b/2)b \quad (9)$$

For decomposition times in Table 1, it is assumed that (1) there are no active columns (in the NASTRAN sense), (2) no "spill" occurs, and (3) the structure has six DOF's per node. Hence $n=6N$ and $b=6B$, where the bandwidth B used is the minimum of that obtained by CM and GPS. The constants T_B and T_P are computer-dependent time constants equal, respectively, to 15 μ sec and 140 μ sec for the CDC 6400.

TABLE 1 - RESEQUENCING TEST RESULTS

Case	N	M	B (Orig.)	B (CM)	B (GPS)	P* (Orig.)	P* (CM)	P* (GPS)	T (CM)	T (GPS)	T (Decomp.)
1	59	5	25	8	8	405	256	283	1.25	0.283	7.78
2	66	5	44	3	3	574	157	127	1.46	0.378	1.91
3	72	4	12	7	6	172	284	267	0.903	0.270	6.05
4	87	12	63	17	19	2249	598	642	2.65	0.419	42.2
5	162	8	156	17	13	2644	1443	1500	4.80	0.903	52.2
6	193	29	62	42	42	7760	4671	4820	19.8	8.95	508.
7	209	16	184	33	42	9503	3742	4540	12.3	1.97	362.
8	307	40	63	40	44	7825	8645	9370	17.1	2.29	784.
9#	310	10	28	14	14	2696	2725	2726	29.9	3.57	117.
10#	346	18	318	43	46	8708	7180	7650	28.7	3.49	1021.
11	361	8	50	15	14	5084	4714	4699	21.8	2.76	137.
12	503	24	452	53	54	35914	15457	15571	80.4	6.44	2255.
13#	512	14	73	28	29	6018	4838	4669	25.3	10.2	697.
14	592	14	259	40	36	28805	14171	10725	83.7	6.86	1297.
15	758	10	200	26	25	23113	10644	7465	142.	8.62	845.
16	869	9	586	38	39	18987	14335	14587	183.	13.3	2136.
17#	918	12	839	46	49	108355	21479	20369	168.	16.1	3249.
18	992	17	513	52	35	262306	33992	33076	216.	47.8	2094.
19	1242	11	936	84	99	110188	50151	54496	221.	27.5	14065.
20	2680	18	2499	68	68	587863	102534	101451	602.	38.6	20643.

* The test criterion was to reduce bandwidth, not profile.

Denotes cases as presented in references 12 and 13.

Several conclusions can be drawn from the table:

1. CM and GPS generally obtain comparable bandwidth results, although occasionally one does significantly better than the other.

2. GPS is faster than CM.

Both CM and GPS are generally fast compared to estimated decomposition times. In the absence of resequencing, the decomposition times would usually be much larger.

Conclusions 1 and 3 indicate that the user would, in general, benefit from having both CM and GPS attempt to resequence his structure. Thus, the default mode of operation in BANDIT uses both and delivers to the user SEQGP cards for the better result.

REDUCTION OF MATRIX PROFILE

The second recent improvement to BANDIT is that the user now has the option of selecting matrix profile reduction rather than matrix bandwidth reduction. This option was installed primarily to facilitate testing with NASTRAN Level 15.9 to determine whether profile reduction has any advantages over band reduction. At this writing the question is still open. However, based on the close relationship between a matrix's bandwidth and its profile, it seems unlikely that major advantages will result. Indeed, in a larger sense, equation solvers which exploit matrix bandwidth, profile, or wavefront can all be classified under the general category of "envelope methods" (ref. 15), which ignore only those zeros in a matrix outside a particular region of the matrix. Distinct from the envelope methods are the general sparse methods, which ignore all the zeros in a matrix.

CURRENT BANDIT USAGE

This section summarizes briefly how a NASTRAN user runs BANDIT and what BANDIT's list of options are. It is assumed here that the prospective BANDIT user has already compiled the program and has it in executable form.

Versions of BANDIT exist for all computers on which NASTRAN runs: CDC 6000, IBM 360/370, UNIVAC 1100, and Honeywell 6000 (ref. 17).

Input to BANDIT generally consists of a standard NASTRAN data deck (ID through ENDDATA) plus one or more special \$ cards (which are comments to NASTRAN) for supplying various instructions to BANDIT. The minimum BANDIT data deck consists of \$ option cards, BEGIN BULK, element connection cards, and ENDDATA. BANDIT does not use GRID cards.

Output from BANDIT consists generally of printed output, punched output, and a file (FORTRAN logical unit 8) containing the complete input deck plus any SEQGP cards generated. This file, which is created automatically, is rewound before BANDIT execution terminates so that it is ready to be used as input to NASTRAN.

The current version of BANDIT, designated Version 5.1 and dated 04/28/75, contains in its element library all NASTRAN elements in Level 15.5 plus some additional elements appearing in several non-standard versions of NASTRAN. Multipoint constraint (MPC) cards are also recognized and accounted for if the user so elects.

Instructions from the user to BANDIT are passed via \$ cards having the general format

\$KEYWORD1 KEYWORD2

where the \$ must appear in card column 1, and the first letter of KEYWORD1 must appear in column 2. Otherwise, the format of such cards is free field: keywords, which can contain no embedded blanks, must be separated by one or more blanks, and at least two letters of each keyword are required for recognition by BANDIT. Since the \$ cards are interpreted by NASTRAN as comments, they can be left in the deck during a NASTRAN run.

The complete list of current \$ cards is summarized in Table 2. Such cards can appear in any order but must be placed somewhere ahead of BEGIN BULK. The cards defined under Part B are specialized cards created for particular users with special needs. For most \$ cards, a default is defined and denoted in Table 2 by underlining. The default applies whenever the \$ card is omitted from the deck.

For example, referring to Table 2, if resequencing is to be performed, the user inserts the card

\$SEQUENCE YES

into the deck anywhere before the BEGIN BULK card. In most cases, this is the only \$ card added to the deck.

Although many of the cards listed in Table 2 are probably self-explanatory, several require additional explanation. The \$GRID card is used to declare an upper bound (preferably least upper bound) on the number of grid points. The inclusion of this card is sometimes necessary (and never hurts) if BANDIT's default allocation of "open core" to various tables is inadequate. Generally, the default is such that the maximum nodal degree is limited to about 19. (The degree of a node is the number of other nodes connected to it.) Thus, for example, a \$GRID card is required whenever solid elements are present.

Sometimes, in order to induce active columns in NASTRAN, the user would like BANDIT to ignore connections to selected grid points. Such

TABLE 2 - SUMMARY OF BANDIT \$ CARDS

A. For General Use

\$SEQUENCE (NO, YES)	Is resequencing to be performed?
\$PUNCH (NONE, SEQGP, ALL)	What should be punched?
\$CRITERION (BAND, PROFILE)	What should be reduced?
\$METHOD (CM, GPS, BOTH)	By what method?
\$MPC (NO, YES)	Take MPC's into account?
\$PRINT (MIN, MAX)	What printed output?
\$GRID N	Upper bound on number of grids.
\$IGNORE G1,G2,...	Grid points to ignore.

B. For Particular Users

\$NASTRAN (NO, YES)	NASTRAN to follow BANDIT?
\$INSERT	Location of cards to insert.
\$INSERT N	Number and location of cards to insert.
\$LINES N	Number of lines per page.
\$PLUS +	User-defined plus sign.
\$CONNECTION (NO, YES)	Punch connection table?
\$START G1,G2,...	User-supplied CM starting nodes.
\$DEGREE N	Ignore nodes of degree exceeding N.

points are listed on the \$IGNORE card and are resequenced last.

The \$MPC card is used to tell BANDIT to modify the matrix connectivity according to the multipoint constraints (MPC's) in the deck. If this option is invoked, all MPC's present are included, regardless of any set ID's. The presence of MPC's creates a dilemma from the resequencing point-of-view, since resequencing is always performed at the grid point level, whereas MPC's are always applied at the DOF level. BANDIT treats MPC's by first generating additional connections between each independent point in the constraint relation and every other point to which the dependent point was previously connected. Second, each dependent point is eliminated from the connection table. Thus, if most or all of the DOF's for the dependent points appear in MPC relations (as, for example, with rigid links), MPC's should be taken into account. This guideline is based on experience with NASTRAN Level 15.5 and will probably have to be modified with Level 15.9 and subsequent versions, since a new equation solver has been developed for them (ref. 18).

The \$NASTRAN card was created for IBM users wanting to create a single BANDIT-NASTRAN cataloged procedure in which the user could execute either BANDIT or NASTRAN (or both) and be able to control the choice with \$ cards. The YES choice results in a FORTRAN STOP 5 at successful termination, thus supplying a testable condition code to the cataloged procedure.

CONCLUDING REMARKS

From the test results presented, it is clear that the addition of the new resequencing strategy by Gibbs, Poole, and Stockmeyer greatly enhances BANDIT's capabilities. The addition of the user option to reduce matrix profile rather than matrix bandwidth is a useful addition, but testing with NASTRAN Level 15.9 will be required to determine the extent of its usefulness. From the NASTRAN user's point of view, the relevant question is: For Levels 15.9 and 16, how should the grid point labels be sequenced? When these versions become available, this question will hopefully be answered by testing with band, profile, and wavefront reducers.

ACKNOWLEDGMENTS

The author is indebted to Professors N.E. Gibbs, W.G. Poole, Jr., and P.K. Stockmeyer of The College of William and Mary for supplying a copy of their source code, and to Mr. Curtis Glenn II of NSRDC for installing it into BANDIT and collecting and executing the test problems.

REFERENCES

1. MacNeal, R.H., ed.: The NASTRAN Theoretical Manual, NASA SP-221(01), Washington, D.C., 1962.
2. Butler, T.G., and Michel, D.: "NASTRAN: A Summary of the Functions and Capabilities of the NASA Structural Analysis Computer System," NASA SP-260, Washington, D.C., 1971.
3. Everstine, G.C.: "The BANDIT Computer Program for the Reduction of Matrix Bandwidth for NASTRAN," Naval Ship Research and Development Center Report 3827, March 1972.
4. Everstine, G.C.: "The BANDIT Computer Program for the Reduction of Matrix Bandwidth for NASTRAN," NASTRAN: Users' Experiences, NASA TM X-2637, 1972, pp. 407-414.
5. Levy, R.: "Resequencing of the Structural Stiffness Matrix to Improve Computational Efficiency," JPL Quarterly Review, vol. 1, no. 2, July 1971, pp. 61-70.
6. Levy, R.: "Savings in NASTRAN Decomposition Time by Sequencing to Reduce Active Columns," NASTRAN: Users' Experiences, NASA TM X-2378, 1971, pp. 627-631.
7. Levy, R.: "Structural Stiffness Matrix Wavefront Resequencing Program (WAVEFRONT)," JPL Technical Report 32-1526, vol. XIV, 1972, pp. 50-55.
8. Cook, W.L.: "Automated Input Preparation for NASTRAN," Goddard Space Flight Center Report X-321-69-237, April 1969.
9. Everstine, G.C., and McKee, J.M.: "A Survey of Pre- and Postprocessors for NASTRAN," in Structural Mechanics Computer Programs: Surveys, Assessments, and Availability, edited by W. Pilkey, K. Saczalski, and H. Schaeffer, The University Press of Virginia, Charlottesville, 1974, pp. 825-847; also, NSRDC Report 4391, June 1974.
10. Cuthill, E.H., and McKee, J.M.: "Reducing the Bandwidth of Sparse Symmetric Matrices," Proceedings of the 24th National Conference ACM 1969, pp. 157-172.
11. Cuthill, E.H.: "Several Strategies for Reducing the Bandwidth of Matrices," Sparse Matrices and Their Applications, edited by D.J. Rose and R.A. Willoughby, Plenum Press, New York, 1972, pp. 157-166.
12. Gibbs, N.E., Poole, W.G., Jr., and Stockmeyer, P.K.: "An Algorithm for Reducing the Bandwidth and Profile of a Sparse Matrix," Institute for Computer Applications in Science and Engineering (ICASE) Report, Hampton, Virginia, July 1974.

13. Gibbs, N.E., Poole, W.G., Jr., and Stockmeyer, P.K.: "A Comparison of Several Bandwidth and Profile Reduction Algorithms," Institute for Computer Applications in Science and Engineering (ICASE) Report, Hampton, Virginia, November 1974.
14. George, J.A.: "Computer Implementation of the Finite Element Method," Stanford University Computer Science Department Technical Report STAN-CS-71-208, Stanford, California, 1971.
15. Liu, W.H., and Sherman, A.H.: "Comparative Analysis of the Cuthill-McKee and the Reverse Cuthill-McKee Ordering Algorithms for Sparse Matrices," Department of Computer Science Research Report #28, Yale University, New Haven, Connecticut, 1974.
16. Crane, H.L., Jr., Gibbs, N.E., Poole, W.G., Jr., and Stockmeyer, P.K.: "Matrix Bandwidth and Profile Reduction," Institute for Computer Applications in Science and Engineering (ICASE) Report 75-9, Hampton, Virginia, April 1975.
17. Golden, M.E.: "Conversion of NASTRAN to the Honeywell H6000," Proceedings of the Fifth Navy-NASTRAN Colloquium, Naval Ship Research and Development Center, CMD-32-74, September 1974, p. 23; also, Defense Documentation Center (DDC) Report No. ADA004604.
18. McCormick, C.W.: "Review of NASTRAN Development Relative to Efficiency of Execution," NASTRAN: Users' Experiences, NASA TM X-2893, 1973, pp. 7-28.

N75 31516

31

NASTRAN THERMAL ANALYZER
STATUS, EXPERIENCE, AND NEW DEVELOPMENTS

H. P. Lee

NASA Goddard Space Flight Center

SUMMARY

The unique finite-element-based NASTRAN Thermal Analyzer originally developed at Goddard Space Flight Center is a general-purpose heat-transfer analysis capability that has been incorporated into the NASTRAN system in its standard version of Level 15.5. The current status, experiences from field applications, and new developments are reported herein.

INTRODUCTION

The unique finite-element-based NASTRAN Thermal Analyzer (NTA) is a general-purpose heat-transfer analysis capability that has been integrated into the NASTRAN system since its Level 15.5 version. It is a computer program fully capable of treating problems including conduction with convective boundary conditions and radiative exchanges in both steady-state and transient cases. NTA (refs. 1 to 3) was originated and developed at the Goddard Space Flight Center (GSFC) as one of the software products of a research program titled STOP (the Structural Thermal Optical Program). STOP was designed to advance capabilities in the interdisciplinary areas of heat transfer and structural analysis. Its main objectives were to provide greater solution accuracy for combined thermal and structural analyses and to eliminate any interpolations in intermodel transfer of temperature data. It was accomplished by adopting the unified finite-element approach for both the thermal and structural analyses; it thus eliminated the need to form separate analytical models with the concomitant requirement for intermodel data transfer. Such a unified approach is especially effective in applications involving space telescopes and antennas where small thermally induced deflections can cause significant degradations in performance. When NASTRAN is relied

upon for structural analysis, including thermal loadings, the reliability of the structural solution depends largely on the accuracy of the temperature data input. Therefore, the use of the $\bar{N}TA$ ensures a total structural-thermal model compatibility and avoids the tedious and time-consuming process of interpolation and extrapolation if temperature data were otherwise obtained by a heat-transfer computer program which is based on the lumped nodal method.

The development of the $\bar{N}TA$ was reported to the Second NASTRAN Users Colloquium (ref. 4) three years ago when this software was implemented and its IBM version was first installed at GSFC (ref. 5). Effort has since been spent in the verification of the delivered program, debugging and maintaining, application, and new developments. Since the $\bar{N}TA$ was integrated into the NASTRAN system in its Level 15.5 version which was made available for general use through the NASA software dissemination apparatus, COSMIC, in June 1973, frequent inquiries have reached us from various sectors. Other government agencies, private industries, and universities have requested details concerning the use of this program, modelling techniques, thermal analysis in tandem with structural analysis, accuracy and efficiency considerations, etc. This paper is a partial response to requests such as these and is designed to report the current status of the $\bar{N}TA$, our experience with this computer program, and new capabilities that have been developed.

STATUS

In NASTRAN Level 15.5, the $\bar{N}TA$ is a general-purpose heat-transfer computer program as opposed to the simple temperature analysis capability in Level 15.0 which was restricted to linear conduction problems only. This version of the $\bar{N}TA$ contains corrections for coding errors which were detected by GSFC in post-delivery verification runs. All findings, including possible error fixes, were reported to the NSMO through SPR's (Software Problem Reports), and corrections were made by the NASTRAN maintenance contract service. In addition, the GSFC NASTRAN Level 15.5 IBM-360 version has been updated continually via an in-house effort. Many error corrections and modifications to accommodate new capabilities for both R&D work and flight program support were promptly made to satisfy our immediate needs. These evolutionary changes were reflected in the program identification shown by the last digit following the version labeling 15.5. The latest operational version at GSFC is Level 15.5.3.

Although maintaining the NASTRAN system for general users is the responsibility of the NSMO, we at GSFC have assisted $\bar{N}TA$ users whenever they contacted us for advice. $\bar{N}TA$ users have included

NASA field installations, other Government agencies, private industry, and universities. Last March, the NSMO established a new service contract, with Universal Analytics, Inc. as the subcontractor to Computer Science Corp., for regular maintenance of the NTA. GSFC was requested officially by NSMO to be a consultant and to respond to all inquiries received in relation to the NTA.

APPLICATION EXPERIENCES

Since the delivery of the IBM-360 NTA to GSFC in June of 1972, the system checkout phase has been proceeding. Various types of test problems were designed to verify the program capabilities and to unearth programming defects. At the end of that year, the Colorado Experiment of the OSO-I (OSO-8) was selected as the first flight experiment to employ the developed analytical tools of the STOP program (ref. 6). Emphasis was placed on securing temperature data computed using the NTA. While many features made the NTA especially suitable for the solution of a problem of this size and complexity, certain important quantities such as thermal contact resistances and the physical properties of surface coatings were analytically indeterminate, and a laboratory test was therefore essential to verify the model. This was achieved by applying the boundary conditions of the thermal vacuum test to the basic NASTRAN thermal model to obtain predictions for the test results. If marked temperature differences were noted between the predictions and the measured temperatures, the basic thermal model would be adjusted to reflect the couplings which could be calculated from the test results. Modifications were continued until the predictions matched the measured temperatures, and the modified model would then be considered fully verified. This verified model could then be used with confidence to develop temperature predictions when thermal loads simulating the orbital environment were applied.

The economic advantage of using this computer program can be best expressed by examining the computer time expenditures required to complete a run. Again, the OSO-I Colorado telescope is used as an example. This model consisted of a total of 488 grid points. Each steady-state run required 10 min. of CPU time and 12 min. of I/O time, while a five-orbit transient solution with 120 time steps required 24 min. of CPU time and 28 min. of I/O time. It must be emphasized that structurally compatible temperature data cards were direct outputs included in these indicated computer time expenditures. The cost effectiveness is evident.

The NTA has since been used to support many scientific instrument packages for various programs at GSFC, such as IUE (International Ultraviolet Explorer Satellite), SMM (Solar Maximum

Mission), Thematic Mapper, EUV (Extreme Ultraviolet Experiment), and TDRSS (Tracking and Data Relay Satellite System) antenna.

Other users who have been in contact with us and are actively employing the NTA to solve various heat-transfer problems are working on tasks involving nuclear reactors, weaponry, computer hardware, etc.

NEW DEVELOPMENTS

New additions have been developed or are being implemented to enhance the capabilities or convenience of the NTA and may be summarized as follows:

A. The new capabilities already developed:

- (1) A highly stable explicit integration algorithm suitable for the finite-element transient application (ref. 7)
- (2) The temperature variance analysis (ref. 8)
- (3) The plotting of the boundary elements of the HBDY type (ref. 8)
- (4) A modification to the radiative matrix to accommodate the case of radiative exchanges with mixed diffuse-specular surface characteristics (ref. 9)
- (5) A modification that condenses the processing procedure for large radiation matrices by a factor of 40.

B. The new capabilities and convenience items currently being developed:

- (1) The condensation of a radiatively nonlinear finite-element thermal model
- (2) The entry of multiple boundary condition sets in one submission for execution (i.e., subcases)
- (3) The ability to input temperature-dependent emissivities and absorptivities
- (4) The one-dimensional thermo-fluid elements

Although these new capabilities have been developed for the GSFC version only, they can be made available to general users

if the NSMO will take up the responsibility of incorporating them into future levels of the standard version of NASTRAN. We at GSFC are willing to provide assistance in using these new capabilities as we have been doing for the present version of NTA and its associated VIEW program (refs. 10 and 11) (a view factor generation computer program totally compatible with the NTA).

A necessary item for general users of the NTA is a complete, self-contained document using physically meaningful heat transfer terminology that would be familiar to general thermal analysts who may not have prior experience in any NASTRAN modelling. We have undertaken the task of preparing a manual in the tutorial style that would consist of the underlying finite-element theory in its heat transfer application, the general structure of the NTA, the most commonly used NASTRAN data cards for thermal analysis, heavily commented illustrative examples to demonstrate various types of modelling techniques for different physical problems, etc. The material is an expanded written version of the lecture given at GSFC last May and will be made available to any interested groups or individuals upon receipt of a written request to this author.

REFERENCES

1. Lee, H. P.: Structural-Thermal-Optical-Program (STOP), Paper presented at NASA-GSFC 1970 Science and Technology Review, NASA-Goddard Space Flight Center, Jan. 13-14, 1971; also appears in: Significant Accomplishments in Technology: Goddard Space Flight Center, 1970, NASA SP-295, Washington, D.C., pp. 36-40.
2. Lee, H. P.: Application of Finite-Element Method in the Computation of Temperature with Emphasis on Radiative Exchanges, Progress in Astronautics and Aeronautics, Vol. 31--Thermal Control and Radiation, MIT Press, 1973, pp. 491-520.
3. Mason, J. B.: The Solution of Heat Transfer Problems by the Finite Element Method Using NASTRAN, NASA-GSFC, Test and Evaluation Div. Rept. X-321-70-97, Greenbelt, Md., 1970.
4. Lee, H. P., and Mason, J. B.: NASTRAN Thermal Analyzer: A General Purpose Finite-Element Heat Transfer Computer Program, The 2nd NASTRAN User's Colloquium, NASA TM X-2637, Sept. 1972, pp. 443-454.
5. McCormick, C. W.: The NASTRAN User's Manual, NASA SP-222, Sept. 1970, Washington, D.C.

6. Lee, H. P., and Jackson, C. E. Jr.: Using the NASTRAN Thermal Analyzer to Simulate a Flight Scientific Instrument Package, Proceedings of the 20th Annual Meeting of the Institute of Environmental Sciences, Apr. 1974, pp 152-158.
7. Baker, A. J., and Manhardt, P. D.: Finite Element Solution for Energy Conservation Using a Highly Stable Explicit Integration Algorithm, NASA CR-130149, Bell Aerospace Company, Oct. 1972.
8. Harder, R. L.: NASTRAN Variance Analysis and Plotting of HBDY Elements, NASA CR-139007, The MacNeal-Schwendler Corp., May 1974.
9. Lee, H. P., and Jackson, C. E. Jr.: Finite-Element Solution for a Combined Radiative-Conductive Analysis with Mixed Diffuse-Specular Surface Characteristics, AIAA Paper No. 75-682, AIAA 10th Thermophysics Conference, Denver, Colo., May 27-29, 1975.
10. Puccinelli, E. F., and Jackson, C. E. Jr.: VIEW: A Modification of the RAVFAC View Factor Program for Use with NASTRAN Level 15, The 2nd NASTRAN User's Colloquium, NASA TM X-2637, Sept. 1972, pp. 455-463.
11. Jackson, C. E. Jr: Programmer's Manual for VIEW--A Modification of the RAVFAC View Factor Program for Use with the NASTRAN Thermal Analyzer on IBM-360 Series Computers, X-322-73-120, Goddard Space Flight Center, March 1973.

N75 31517

APPLICATION EXPERIENCES OF NASTRAN THERMAL ANALYSIS

IN ENGINEERING

James Chi-Dian Go

Computer Sciences Corporation

32

ABSTRACT

This paper summarizes the experiences of the application of the thermal analysis phase of NASTRAN in engineering. Some illustrative samples are presented to demonstrate the applicability and limitation of NASTRAN thermal analysis capability in engineering. The results of the evaluation of the relative efficiency, applicability and accuracy among NASTRAN, other finite element programs and finite difference programs are also presented.

INTRODUCTION

Prior to the development of the finite element method, finite difference was one of the most practical analysis techniques for engineering thermal problems. Computer codes such as HEATING, TAP, etc. were developed and widely used. E. L. Wilson and others had shown that thermal problems could also be solved by finite element techniques. Subsequently, several finite element thermal analysis computer programs were developed; most of these were developed as part of a general purpose structural analysis code. For example, John Swanson implemented the finite element thermal analysis method into his proprietary program ANSYS in 1970 and it proved to be extremely popular among the structural engineers.

NASTRAN, being one of the most popular general purpose structural analysis programs, introduced many thermal analysts to finite element thermal analysis techniques. Subsequently, the application of finite element thermal analysis method was widely accepted by engineers and applied scientists. This paper summarizes some experiences of the application of NASTRAN in the analysis of engineering thermal problems.

COMPARISONS OF FINITE DIFFERENCE AND FINITE ELEMENT COMPUTER PROGRAMS

In assessing the relative merits of finite difference and finite element thermal analysis programs, we have to consider computational accuracy, efficiency of input preparation and output interpretation, computer requirements and some other factors. Some experiences are summarized in this section. It should be noted that the information was derived from a limited number of computer runs on currently readily obtainable programs.

In our evaluation of the accuracies of finite difference and finite element we selected several problems of various sizes and types covering ranges of our practical applications. In all cases the desired accuracies were easily obtained by adjusting the mesh or element sizes. Thus, the accuracy comparison by itself does not indicate preference among various finite difference and finite element computer programs.

Input preparation comparisons and output interpretation are more difficult to assess due to various degrees of familiarity with each of the computer codes. However, some distinctive advantages of finite element are evident:

- subsequent utilization of thermal analysis model for structural analysis
- thermal outputs conversion to structural analysis inputs
- program maintenance
- minimizing new users' learning time by running both thermal and structural analyses in one general purpose finite element analysis program

Computer requirements comparison is based on central memory, I/O and elapsed run time. For small problems, with two minutes or less run time and 140000 (octal) or less core, the relative efficiencies of the finite difference and finite element programs are not significant. However, some problems with run time of five minutes or over and requiring 142000 (octal) core for finite element programs required 300000 (octal) core and about the same run time for finite difference programs. It seems reasonable to project that this difference in core requirement will be widened as the problem sizes increase.

ADDITIONAL DESIRABLE FEATURES

In any computer program some additional features become desirable only after extensive actual applications. Based on our experiences, the following features would be extremely useful to the NASTRAN thermal analysis users:

- Internal Data Generation: During the course of our application of NASTRAN we developed several small programs to generate externally some NASTRAN input cards. After extensive application of NASTRAN and other finite element programs it has become apparent that internal data generation significantly increases users' efficiency.
- Simplification of Radiation Heat Transfer Inputs: The radiation heat transfer input cards RADMTX and RADLST should be simplified to reduce the input data preparation efforts.
- Contour Plot: A simple contour plotting for stress and temperature would be useful for the interpretation of the outputs.
- Addition of a Heat Transfer-Fluid Flow Element: This element is to be defined by two grids, each with only one degree of freedom. It should be capable of transferring heat and fluid between the two grids. The heat transfer should include the heat conduction within the fluid and the mass transport of the fluid.

CONCLUDING REMARKS

Based on our application experience, we have found that the finite element thermal analysis code significantly reduced analyst time and, in most cases, required less computer resources than finite difference codes. Current research and development of finite element programs by various groups is far more extensive than that of finite difference thermal analysis programs. This will lead to an even greater efficiency of finite element thermal analysis programs in the near future. This will provide another incentive for the adoption of the finite element method as a standard thermal analysis tool.

N75 31518

COMPARISON OF NASTRAN AND MITAS NONLINEAR THERMAL
ANALYSES OF A CONVECTIVELY COOLED STRUCTURE*

Earl A. Thornton
Old Dominion University

and

Allan R. Wieting
NASA Langley Research Center

33

ABSTRACT

Comparative steady-state nonlinear thermal analyses of a scramjet fuel injection strut are presented. The analyses were performed using the NASTRAN finite-element program and MITAS, a lumped-parameter thermal analyzer. The strut is subjected to aerodynamic heating on two sides and is internally cooled by hydrogen flowing from internal manifolds through heat exchangers bonded to the primary structure. Based on coolant temperatures determined by MITAS, NASTRAN predicted temperature distributions throughout the strut which were in close agreement with similar MITAS predictions.

INTRODUCTION

A research program is under way at the Langley Research Center to develop an airframe-integrated hydrogen-fueled scramjet (supersonic combustion ramjet) concept designed to operate over a flight Mach number range from 4 to 10. This concept (See fig. 1) utilizes the entire undersurface of the aircraft to process the engine air flow. The aircraft forebody serves as an extension of the engine inlet and the afterbody serves as an extension of the engine nozzle. Hydrogen fueled scramjets are of interest because no other airbreathing engine can match the efficiency of the scramjet above Mach 6 and hydrogen offers high energy content and cooling capacity along with minimal environmental impact. The high cooling capacity of the hydrogen can be used to cool the engine surfaces prior to combustion and thereby accommodate the extremely hostile environment which exists within scramjets.

*The NASTRAN analysis portion of this study was carried out by the first author at the Langley Research Center under support of NASA grant number NSG 1093 to the Old Dominion University Research Foundation.

A preliminary thermal/structural design and analysis study of the engine has been previously performed to determine design feasibility, coolant requirements, and structural mass estimates (ref. 1). Results of the study indicated that the fuel injection struts presented the most formidable cooling and structural problems. A more detailed study of the fuel injection struts is currently under way to further define cooling requirements and thermal/structural behavior. A thermal analyzer based on a finite element formulation is available in NASTRAN to provide thermal/structural analysis. However, there is little user experience with the NASTRAN thermal analyzer in the analysis of convectively cooled structures. Consequently, as part of the strut study, an evaluation of the NASTRAN thermal analyzer capabilities related to convectively cooled structures was undertaken. This evaluation is achieved through a comparison of results with an established finite-difference lumped-parameter thermal analyzer, MITAS (Martin Interactive Thermal Analysis System, ref. 2). The purpose of this paper is to present the results of this comparative evaluation.

SYMBOLS

- h Convective heat transfer coefficient, W/m^2-K (BTU/ft²-s-°R)
 h_0 Reference convective heat transfer coefficient, W/m^2-K (BTU/ft²-s-°R)
 k Thermal conductivity, $W/m-K$ (BTU/ft-s-°R)
 k_0 Reference thermal conductivity, $W/m-K$ (BTU/ft-s-°R)
 ℓ Strut thickness, 2.74 cm (1.08 in.)
 L Strut chord length, 30.7 cm (12.1 in.)
 \dot{q} Aerodynamic heating rate, W/m^2 (BTU/ft²-s)
 T Temperature, K (°R)
 x, y Distances along X- and Y-axes, respectively (origin at virtual apex)

FUEL INJECTION STRUTS

The three fuel injection struts (See fig. 1) resemble highly swept airfoils. The side struts are considered in the present study because their unsymmetrical configuration and loading lead to complex thermal/structural behavior. A chordwise cross section of a side strut is shown in figure 2. The side struts have a maximum thickness of 2.74 cm (1.08 in.), chord length of 30.7 cm (12.1 in.), a span of 45.7 cm (18 in.) and are swept back 48°. Each strut is subdivided internally into four chordwise compartments: the fore-and-aft compartments are coolant inlet and outlet

manifolds, respectively, and the central compartments are fuel manifolds for the strut trailing edge and wall fuel injectors. (Fuel injector details are not shown; see ref. 1). Heat shields are installed in all but the forward compartment, as shown, to eliminate direct convective heating from the hydrogen to the primary structure.

Coolant at 55 K (100°R) in the forward manifold is injected through a slot, impinges on the leading edge, and splits (unequally) to flow through an offset-fin plate-fin heat exchanger (See fig. 3) which is brazed to the primary structure. Flow proceeds along each wall to the trailing edge where it is collected in the aft manifold at approximately 890 K (1600°R).

The struts are subjected to severe temperature gradients because of non-uniform aerodynamic heating and variations in hydrogen temperatures in the manifolds. As shown in figure 4, the aerodynamic heating is different for each side wall and varies considerably along either wall because of flow stagnation at the leading edge, boundary-layer—shock interactions, and combustion. The thermal conductivities of the structure and the convective heat-transfer coefficient vary significantly with temperature as shown in figure 5, and thus a nonlinear steady-state thermal analysis is required to accurately predict strut temperatures. The strut is also subjected internally to high hydrogen pressures and must withstand a large unbalanced side loading resulting from possible unsymmetrical engine unstart.

NASTRAN ANALYSIS

A two-dimensional finite-element model of a typical chordwise cross section was formulated by using a total of 4657 elements. The discretization was made primarily to give an accurate temperature distribution throughout the strut, but an additional objective was to permit the same finite-element model to be used for both the thermal analysis and a subsequent plane strain structural analysis. It was desirable to use essentially the same models since the complex section and loadings required fine detail to predict temperature and stress distributions throughout the strut cross section.

The finite-element representation of conduction and convection heat transfer at a typical wall section is shown in figure 6. The NASTRAN CQDMEM element was used to represent the conduction heat transfer in the primary structure and the aerodynamic skin since this is the only NASTRAN quadrilateral element which has heat-transfer capability. Four membrane elements were used through the thickness of the primary structure because it was known from the preliminary study (ref. 1) that temperature gradients and wall bending stresses were significant. Since a nonuniform thermal gradient occurs across the coolant passage, conduction through the heat exchanger fins was represented by four rod elements in series. A total of 255 sets of four rod elements was used to represent the conduction through the heat exchanger fins for the strut cross section.

Line convection elements (shown in fig. 6 as dashed lines) were used to represent the convective heat transfer between the hydrogen in the manifolds and the primary structure and between the hydrogen and the wetted surfaces in the coolant passages. Convection elements were also used to represent the aerodynamic heating on the external skin.

A basic difficulty in the NASTRAN thermal analysis arose in modeling the convective heat transfer due to flow of the hydrogen coolant. NASTRAN has no direct means for modeling heat transfer due to fluid flow. Thus it was not possible by using NASTRAN to determine the coolant temperature distribution along the passage. Instead it was necessary to compute the coolant bulk temperatures by using the finite-difference thermal analyzer MITAS (ref. 2). These data were supplied to NASTRAN as a boundary condition using the convective line element.

Significant characteristics of the NASTRAN thermal finite-element model are shown in table I. The model is characterized by a large number of nodes and elements. The data cards for the model were generated by special purpose FORTRAN programs. The node and convection data were checked prior to execution by generating undeformed NASTRAN structural plots. Since NASTRAN does not have the capability to plot convection line elements, duplicate dummy plotting elements (PLOTTEL) were generated to represent convection elements. Most of the convection data were checked this way; however, it would be desirable to have a direct means of plotting the convection line elements.

TABLE I. CHARACTERISTICS OF NASTRAN FINITE-ELEMENT THERMAL MODEL

Item	Number
Nodes	
Known Temperatures	595
Unknown Temperatures	2812
Total	3407
Conductors	
Conduction	
Membrane elements	1517
Rod elements	1026
Convection	
Surface elements	2114
Total	4657

Before NASTRAN execution, the nodes were resequenced by using a FORTRAN program based upon the renumbering algorithm developed in reference 3. The NASTRAN conduction matrix of size 2812 had a semi-bandwidth of 278 for the original numbering scheme. The semi-bandwidth was reduced to 34 by renumbering of the nodes. The NASTRAN resequencing cards were generated by the renumbering program. The basic NASTRAN data deck which consisted of about 15000 cards was stored on a problem tape and executed by using the NASTRAN restart capability.

Two NASTRAN thermal analyses were performed. First, a linear analysis was made with constant values for the thermal conductivities and convection coefficients. Then, the resulting temperature distribution was used as the initial estimate for the iterative nonlinear NASTRAN thermal analysis.

MITAS ANALYSIS

The finite-difference thermal analyzer MITAS is used as the basis for the comparative evaluation. MITAS uses an equivalent lumped-parameter electrical-circuit analogue of the thermal system. In this technique the physical structure is divided into subvolumes which are assumed to be at a temperature corresponding to their center. The physical system is replaced by a network of conductors between the centers, or nodal points, of the subvolumes. The conductor may represent conduction, convection, or radiation heat flow paths. The electrical analogue of the thermal model for a typical section of the strut is given in figure 7.

Although a coarser model for MITAS may have been adequate, a one to one correspondence between the MITAS nodes and the NASTRAN grid points was established to eliminate discrepancies due to differences in discretization. Significant characteristics of the MITAS finite difference thermal model are given in table II. There were 3106 unknown temperatures in the MITAS analysis compared with 2812 unknown temperatures in the NASTRAN analysis. The additional MITAS unknowns are essentially the unknown coolant temperatures.

Data preparation for MITAS consisted of assigning node numbers, conductor numbers, and conductance values. With the MITAS internal generation capability, 98 percent, 82 percent, and 71 percent of the nodes, conductors, and conductances, respectively, were automatically generated. This represents an overall automated generation of 68 percent of the required input data. Spatial coordinates are not input to the MITAS model; consequently, plots of the finite-difference model could not be obtained for an input data check. The MITAS deck consisted of 3200 cards. MITAS, programmed as a preprocessor, reads the input data and incorporates it into a source program to obtain the required solution. This program was stored on a tape to yield a restart capability at any point within the solution sequence.

TABLE II. CHARACTERISTICS OF MITAS THERMAL MODEL

Item	Number
Nodes	
Known Temperatures	283
Unknown Temperatures	3106
<u>Total</u>	<u>3389</u>
Conductors	
Conduction	4443
Convection	
Surface	1862
Fluid	290
<u>Total</u>	<u>6595</u>

RESULTS AND DISCUSSIONS

Comparative NASTRAN and MITAS predicted temperature distributions within the strut cross section are presented in figures 8 to 11.

Of particular interest are the temperatures in the hydrogen coolant and the temperatures along the aerodynamic skin. Accurate prediction of the temperature distribution along the aerodynamic skin is required to predict the fatigue life of the heat exchanger. Plots of these temperature distributions are shown for the starboard side of the strut in figure 8. The temperature distribution in the hydrogen coolant was predicted by MITAS and used as input to NASTRAN.

The aerodynamic skin temperature distribution (fig. 8) basically reflects the aerodynamic heating distribution shown in figure 4. The skin temperature is high at the leading edge because of stagnation heating, drops sharply with a drop in the aerodynamic heating and maintains a nearly uniform value up to about $x/L = 0.5$, after which the temperature increases rapidly with rising aerodynamic heating first due to shock-boundary layer interaction and then combustion. The sharp rise of the skin temperature at $x/L = 0.59$ and at the trailing edge are local effects due to an absence of heat exchanger fins which result in a reduction of heat transfer to the hydrogen coolant. Heat exchanger fins were omitted in these regions because of possible fabrication problems.

The agreement between NASTRAN and MITAS predictions for this temperature distribution is very good. Some of the temperature values predicted by the two programs shown in figure 8 are tabulated in table III.

TABLE III. COMPARATIVE TEMPERATURE VALUES ALONG STARBOARD AERODYNAMIC SKIN

x/L	Temperature (K)		
	NASTRAN	MITAS	% Difference
0.05	955	951	0.4
0.1	137	139	1.4
0.2	142	143	0.6
0.3	148	148	0
0.4	154	154	0
0.5	165	165	0
0.6	307	318	3.5
0.7	463	465	0.4
0.8	639	650	1.7
0.9	759	770	1.5
1.0	881	887	0.7
1.05	1060	1120	5.7

The tabulated values indicate that agreement of temperatures predicted at the stagnation point is excellent and that the largest difference in the predicted temperatures, about 6 percent, occurs on the trailing edge. Similar results, which are not shown, were obtained for the port-side aerodynamic skin.

Of additional interest are the temperature gradients in the primary structure. In the previous study (ref. 1) these gradient were shown to introduce critical levels of thermal stresses. Temperature distributions in the starboard primary structure as predicted by NASTRAN and MITAS are shown in figure 9. Predictions for the structural temperatures along the hydrogen coolant passage and along the manifolds are shown. The temperatures in the primary structure reflect the hydrogen coolant temperature distribution and the heat transfer from the hydrogen in the

internal manifolds. On the coolant side of the primary structure, the structural temperatures basically follow the coolant temperature distribution shown in figure 8. On the manifold side the large increase in temperature of the structure at $x/L = 0.5$ is due to convective heating from the 890 K (1600°R) hydrogen in the adjacent manifold.

The agreement between the predicted temperatures is excellent. The programs calculate almost identical thermal gradients through the primary structure including the important reversal in sign of the gradient which occurs across the center bulkhead at about $x/L = 0.5$. The programs also show good agreement in calculating local effects such as the local peaks and valleys in the temperatures along the manifold side of the strut at the points of attachment to the thin interior bulkheads, e.g. at $x/L = 0.3$, and the rapid rise in temperature at $x/L = 0.5$.

Variations of the temperature through the thickness of the strut cross section are shown in figures 10 and 11 at the forward and aft main interior bulkheads. These plots show values of temperature at nodes on the aerodynamic skin, the heat exchanger fins, and on the primary structure. Figure 10 shows the temperature distribution through the center of the forward bulkhead. It can be seen that the temperature in the bulkhead at $y/l = 0.5$ approaches the temperature of the hydrogen in the adjacent manifold, about 55 K (100°R). NASTRAN and MITAS predictions show excellent agreement for all values of y . Figure 11 presents temperature distributions at the aft bulkhead for both the bulkhead and adjacent heat shield. The figure shows the effect of the heat shield on the temperatures in the bulkhead and walls of the primary structure. Although the bulkhead is heated close to the temperature of the hydrogen in the adjacent manifolds (890 K, 1600°R), the heat shield causes a substantial drop in the temperatures of the walls of the primary structure at $y/l = 0.15$ and $y/l = 0.75$. Values for the temperatures at $x/L = 0.686$ plotted in figure 11 are tabulated in table IV.

The most significant difference in predicted temperature occurs on the heat shield at the corners. The MITAS model predicts temperatures about 14 percent higher than the NASTRAN model at these points. This discrepancy appears to be attributable to differences in the NASTRAN and MITAS models of interior corners of the heat shield. Elsewhere, table IV shows that there is very good agreement between the two solutions.

A comparison of computer storage and run times for the NASTRAN and MITAS nonlinear thermal analyses is presented in table V. Both programs were executed on the Langley Research Center CDC 6600 computer. NASTRAN was executed in a larger field length and required less CPU time but more operating system calls than MITAS. By using the LRC cost algorithm, these two analyses cost about the same amount. It should be noted, however, that a prior additional NASTRAN linear analysis was used to provide an initial temperature estimate for the NASTRAN nonlinear thermal solution. It is also noteworthy that MITAS determined temperature values for 3106 unknowns in comparison with 2812 unknowns for NASTRAN. As a further point

of importance in the cost comparison, the MITAS solution includes the generation of a significant portion of its input data. As has been noted, the NASTRAN data were prepared by using special purpose programs at additional cost. Thus, when all factors are considered for the cost of a thermal analysis only, the MITAS solution was more cost effective.

TABLE IV. COMPARATIVE TEMPERATURE VALUES ON AFT HEAT SHIELD ON
REAR BULKHEAD

Temperature, K			
y/l	NASTRAN	MITAS	% Difference
0.023	261	261	0
.038	259	259	0
.063	266	264	0.7
.163	369	351	4.9
.205	696	792	13.8
.305	773	752	2.8
.405	778	770	1.0
.505	782	775	0.9
.605	776	770	0.8
.705	766	752	1.8
.784	695	792	14.0
.829	397	400	0.7
.929	314	318	1.3
.955	419	422	0.8
.969	443	444	0.2

TABLE V. COMPARISON OF NASTRAN AND MITAS NONLINEAR THERMAL
ANALYSIS COMPUTER RUNS
[Langley Research Center CDC 6600]

	<u>NASTRAN</u>	<u>MITAS</u>
Field length (octal words)	220 000	167 000
Computer time (CPU seconds)	967	1 780
Operating system calls	28 000	3 300
Comparative cost (per unit cost rate)	76.7	64.9

Of further interest are the relative merits of the two programs for use in a combined thermal/structural analysis. Incompatibilities between lumped-parameter programs such as MITAS and structural analysis programs such as NASTRAN have been cited (ref. 4) as one reason for development of NASTRAN thermal analysis capability. There did not exist any incompatibility between the MITAS thermal model and a NASTRAN structural model since a one-to-one correspondence between nodes was made in the development of the MITAS model. Thus, the incompatibility problem can be avoided by proper planning in development of the thermal and structural models. Of major importance, however, is that the verified NASTRAN thermal finite-element model can be used with only slight modification for a subsequent structural analysis. If a MITAS thermal analysis alone was performed, a completely new finite-element structural model would have to be generated and verified. This fact must be considered in a final evaluation of costs for a combined thermal/structural analysis.

For the thermal analysis of convectively cooled structures, a salient fact has already been noted. MITAS possesses the capability of modeling the convective heat transfer in the fluid flow. NASTRAN, level 15.5, is limited in representing heat transfer because of fluid flow as a convective boundary condition. This restriction offsets the advantages and limits the usefulness of the NASTRAN thermal analyzer for convectively cooled structures. The inability of the NASTRAN thermal analyzer to model convective heat transfer due to fluid flow is also characteristic of some other general purpose finite-element thermal analyzers.

CONCLUDING REMARKS

Comparative two-dimensional steady-state nonlinear thermal analyses of a scramjet fuel injection strut have been performed by using NASTRAN and

MITAS. Since NASTRAN does not possess the capability to represent heat transfer due to fluid flow, a MITAS solution was obtained first. The MITAS solution provided coolant temperatures which were used as boundary conditions for the subsequent NASTRAN analysis as well as temperatures throughout the structure which were used for comparison with the NASTRAN solution.

Comparison of predicted temperature distributions along the aerodynamic skin, heat exchangers, and primary structure of the strut showed good to excellent agreement. This close agreement verifies the capability of NASTRAN to solve a large nonlinear conduction heat-transfer problem with convective boundary conditions. The good agreement also demonstrates the MITAS capability for performing a complete thermal analysis of a convectively cooled structure. A final evaluation of the accuracy of the NASTRAN solution by comparison with MITAS must await the development within NASTRAN of a means of representing convective heat transfer due to fluid flow.

A comparison of costs for the analyses showed that MITAS was slightly less expensive with an additional advantage of automated input data generation capability. An advantage of the NASTRAN program was the ability to generate structural plots for data checking purposes. A part of this advantage was nullified by an inability to plot convective boundary elements.

Since general purpose finite-element thermal analyzers cannot presently represent convective heat transfer due to fluid flow there exists a basic need for development of this capability. In light of current interest in optimization of thermal/structural designs, a means of representing convective heat transfer due to fluid flow would offer potential for optimization studies of convectively cooled structures using finite-element analysis. Until such means are developed, thermal/structural analyses of convectively cooled structures must be performed by using other methods to determine either coolant temperatures or the complete thermal solution prior to a finite-element analysis.

REFERENCES

1. Wieting, A. R.; and Guy, R. W.: Preliminary Thermal-Structural Design and Analysis of an Airframe-Integrated Hydrogen-Cooled Scramjet. Aerospace Sciences Meeting, AIAA Paper No. 75-137, January 1975.
2. Staff of Martin-Marietta Corporation: Martin Interactive Thermal Analysis System, Version 1.0. MDS-SPLPD-71-FD238 (REV3), Mar. 1972.
3. Collins, R. J.: Bandwidth Reduction by Automatic Renumbering. *Internat. J. Numer. Meth. Eng.*, vol. 6, 1973, pp. 345-356.
4. Lee, Hwa-Ping; and Mason, James B.: NASTRAN Thermal Analyzer, A General Purpose Finite Element Heat Transfer Computer Program. NASTRAN Users' Experiences, NASA TM X-2637, 1972, pp. 443-454.

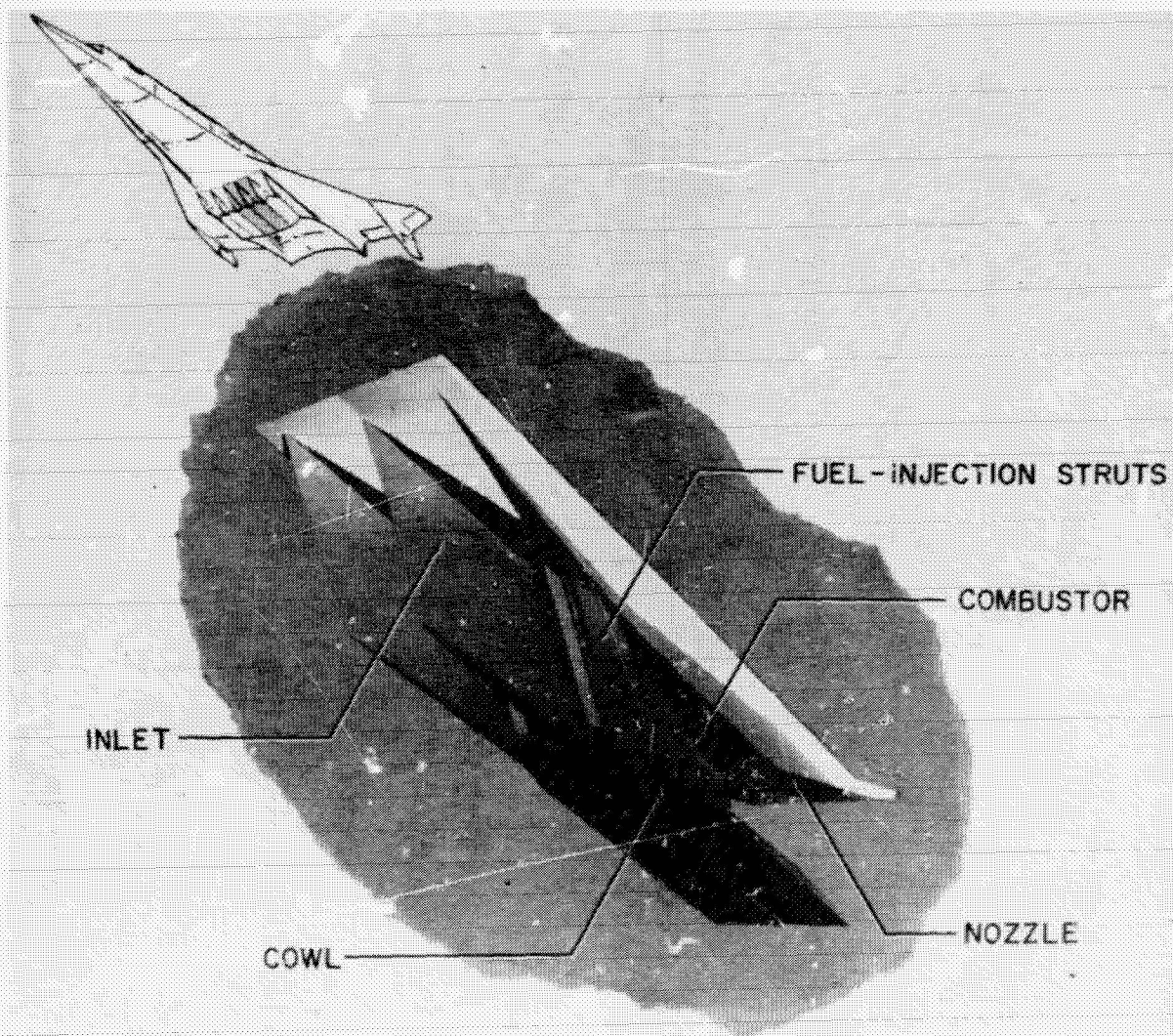


Figure 1. - Airframe-integrated scramjet concept.

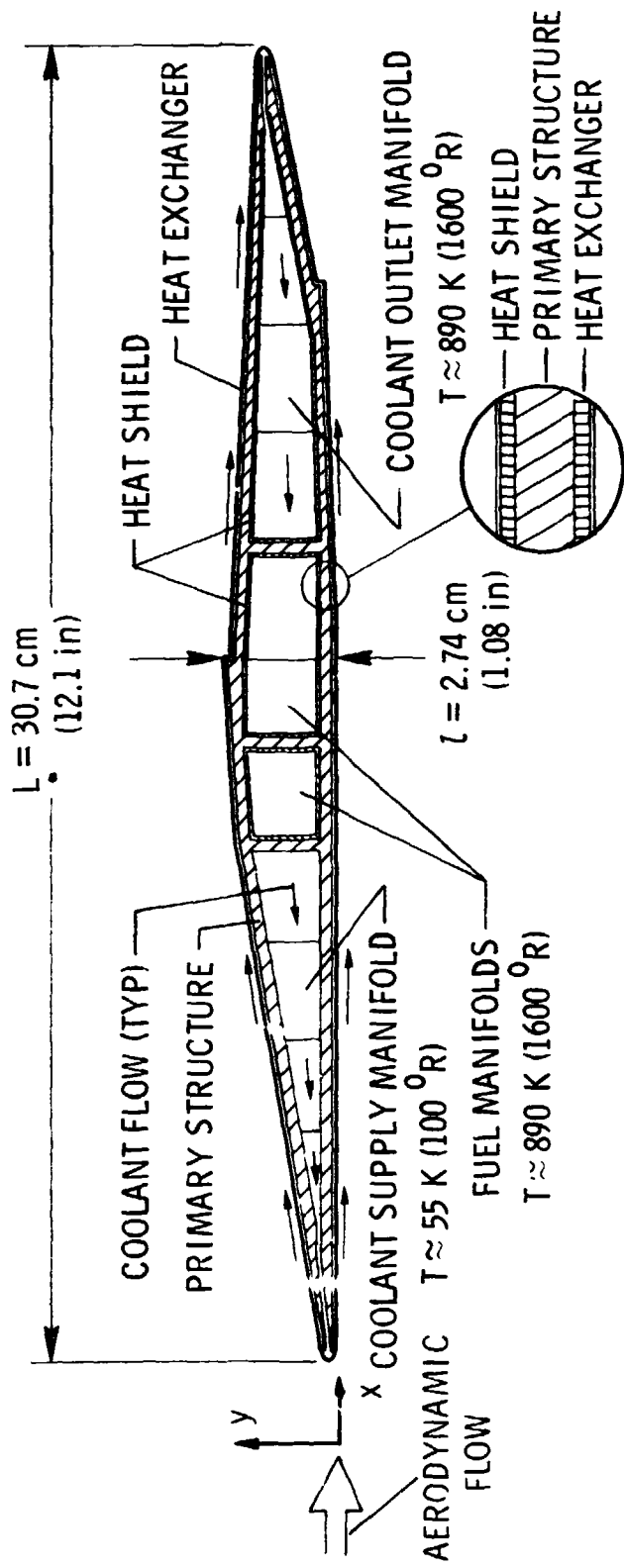


Figure 2. - Fuel-injection strut cross section (chordwise).

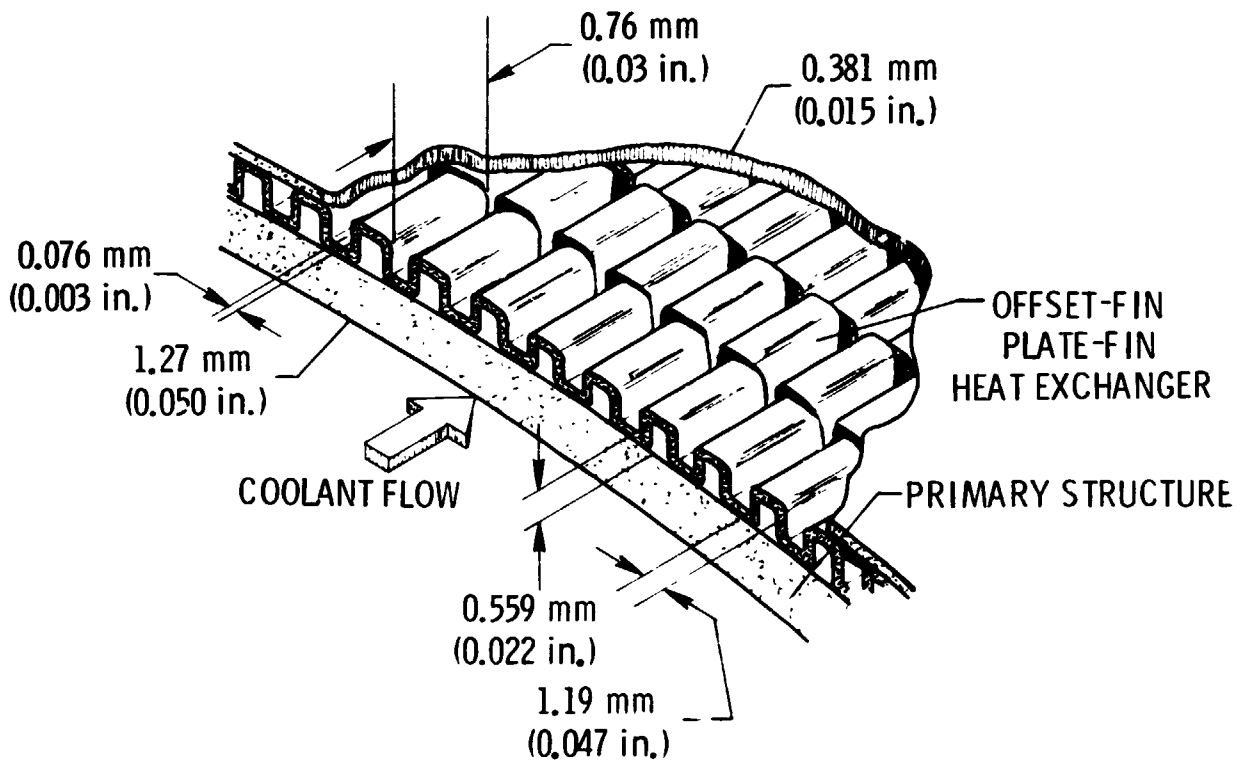


Figure 3. - Typical rectangular offset-fin plate-fin heat exchanger.

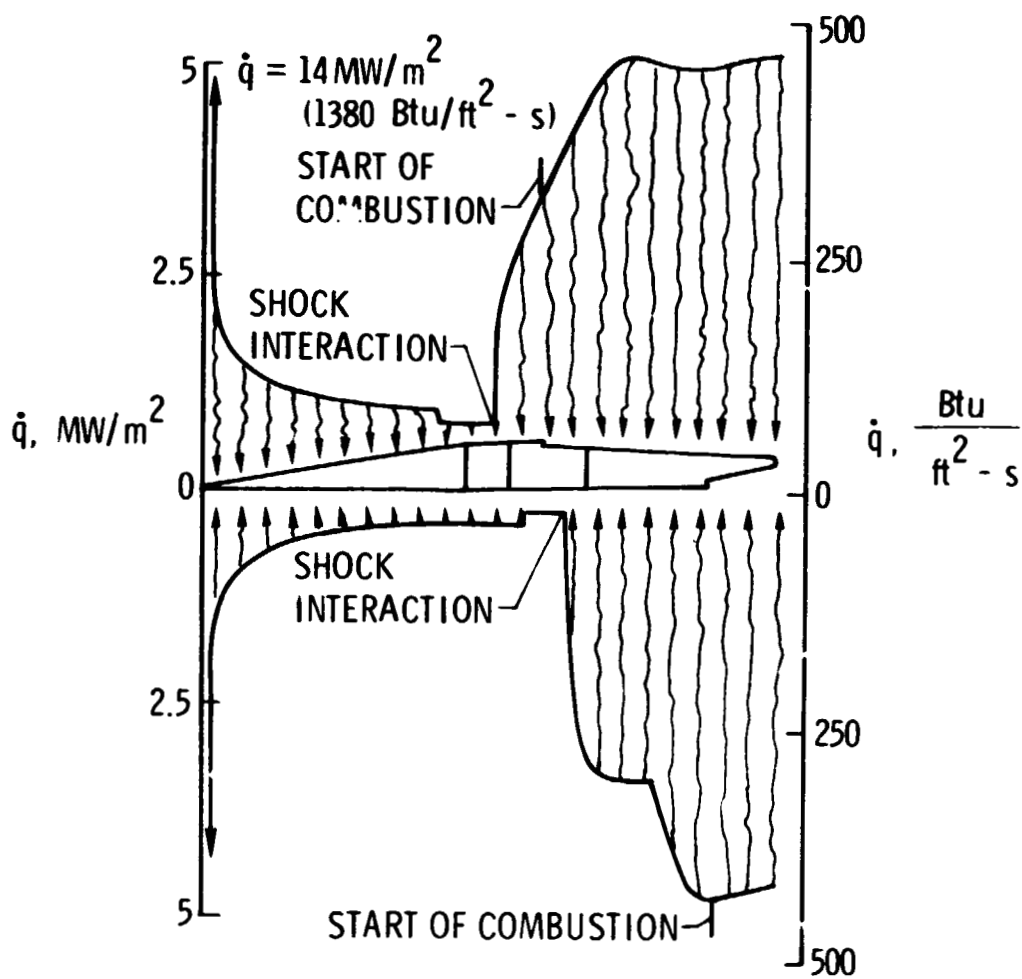


Figure 4. - Aerodynamic heating rate distributions.

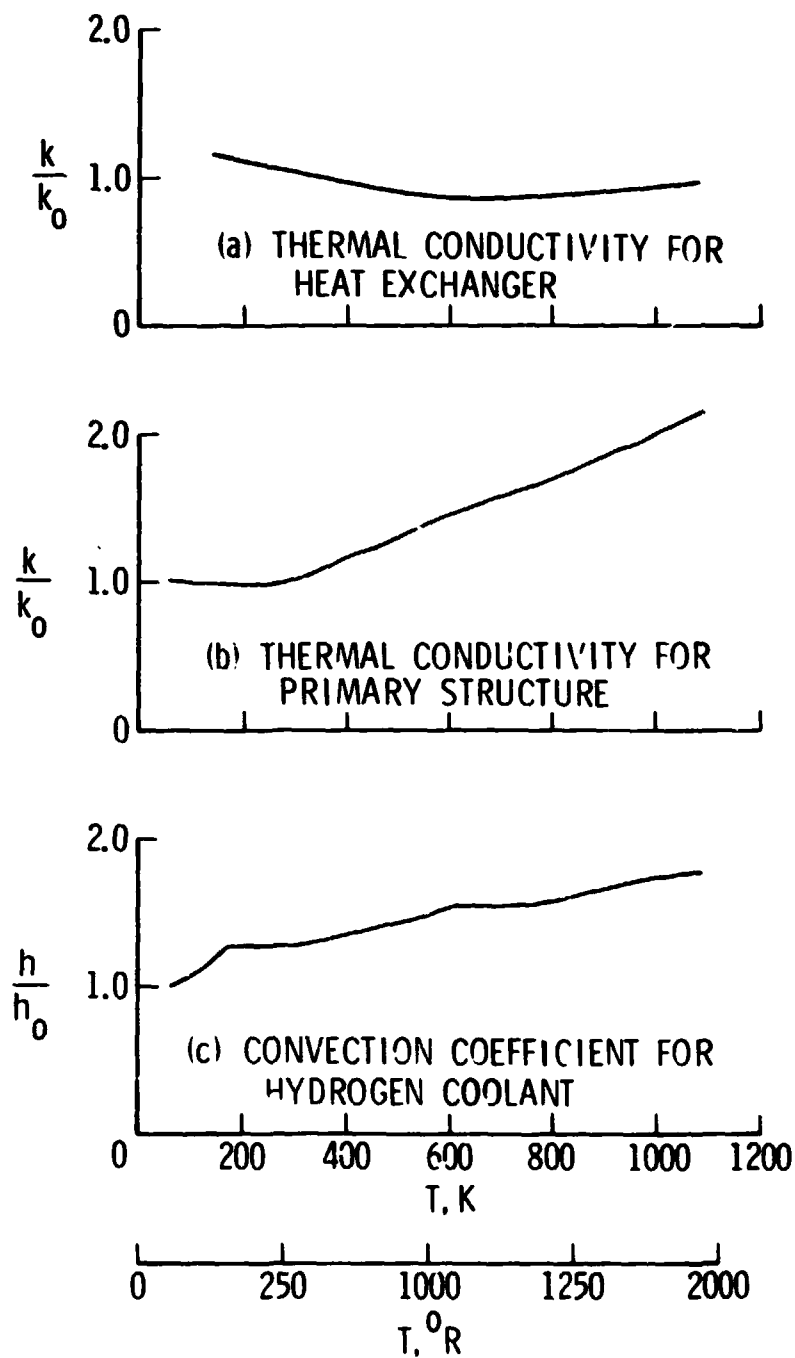


Figure 5. - Variation of heat-transfer coefficients with temperature.

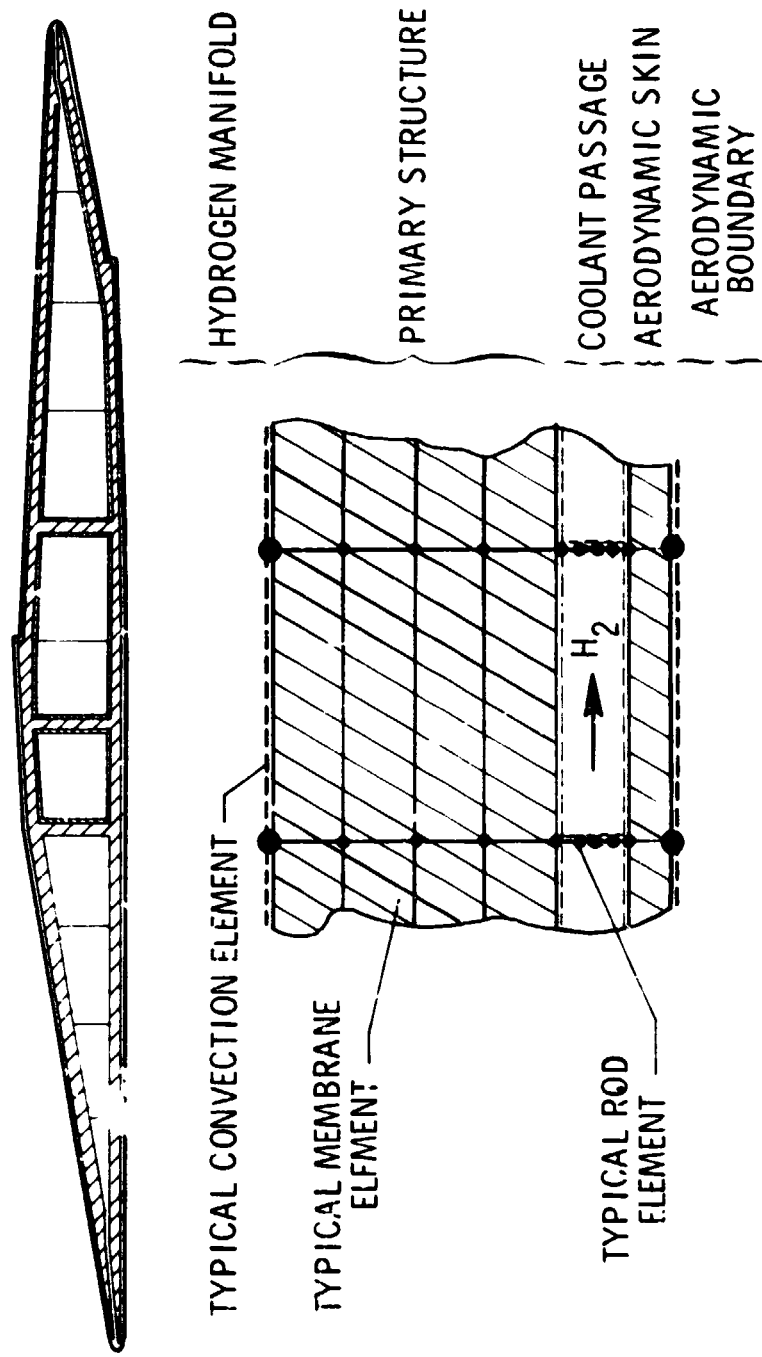


Figure 6. - NASTRAN finite-element model at a typical wall section.

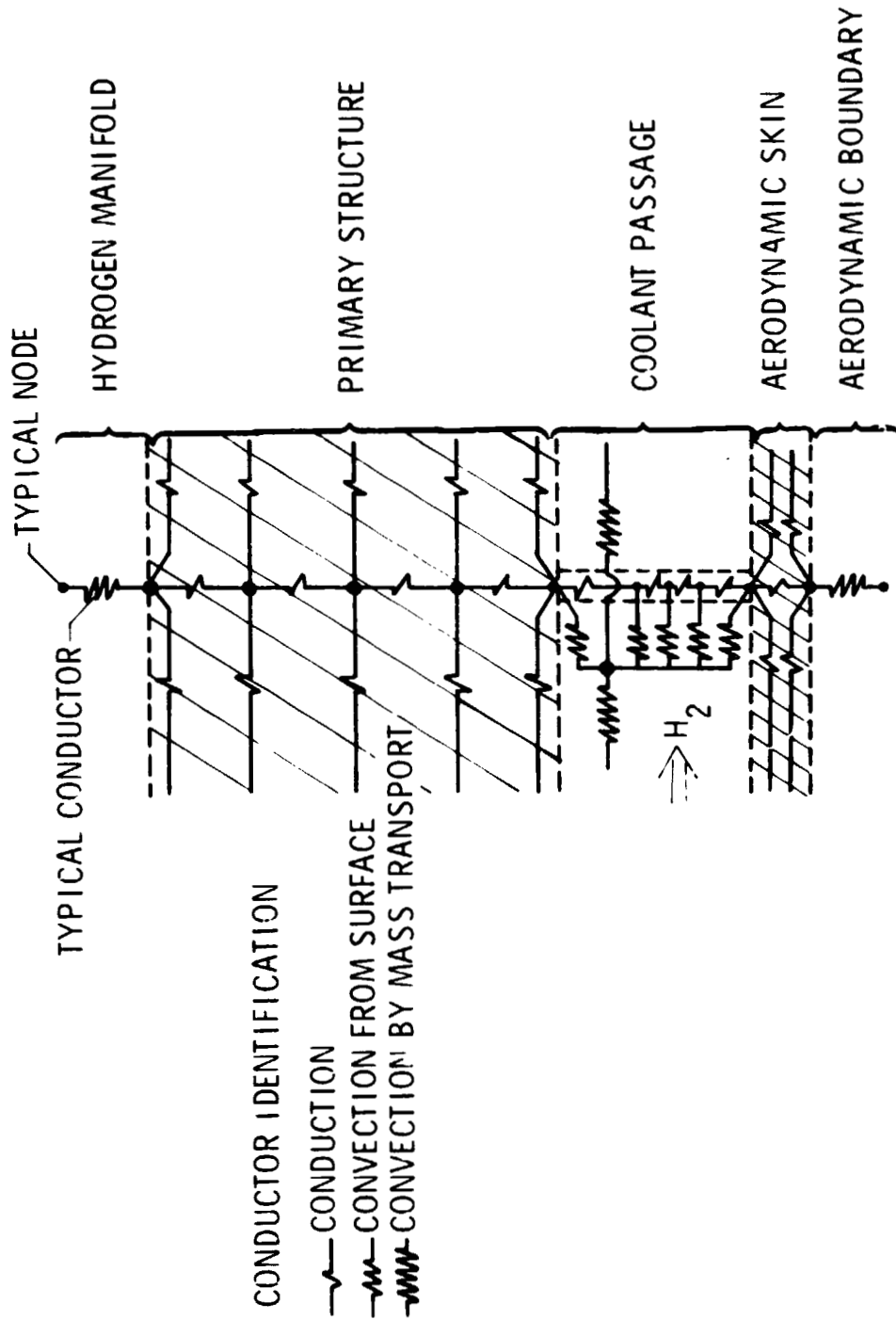


Figure 7. - Typical MIRA thermal model of strut wall section.

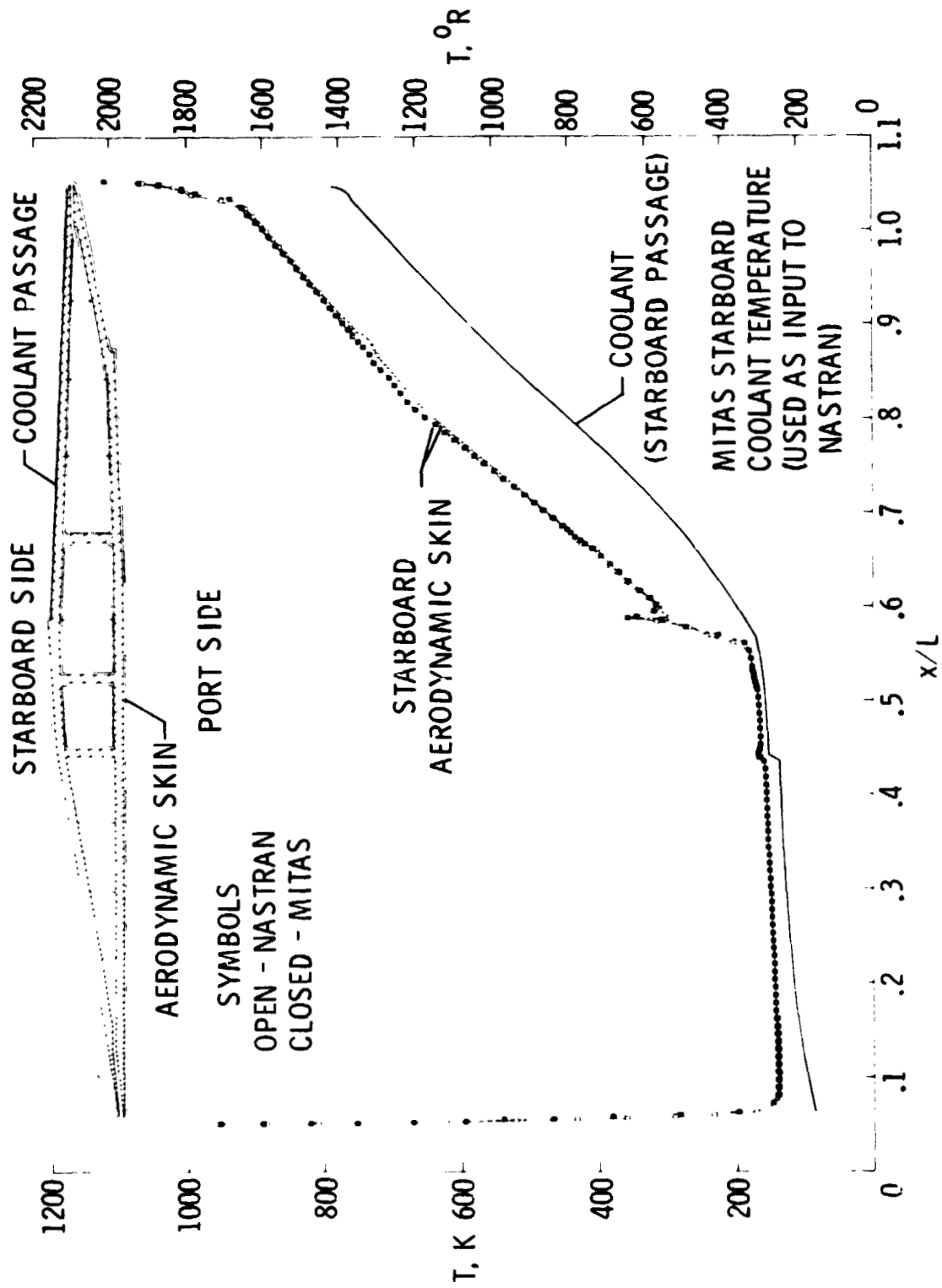


Figure 8. - Comparison of NASTRAN and MITAS predictions for temperature along starboard aerodynamic skin.

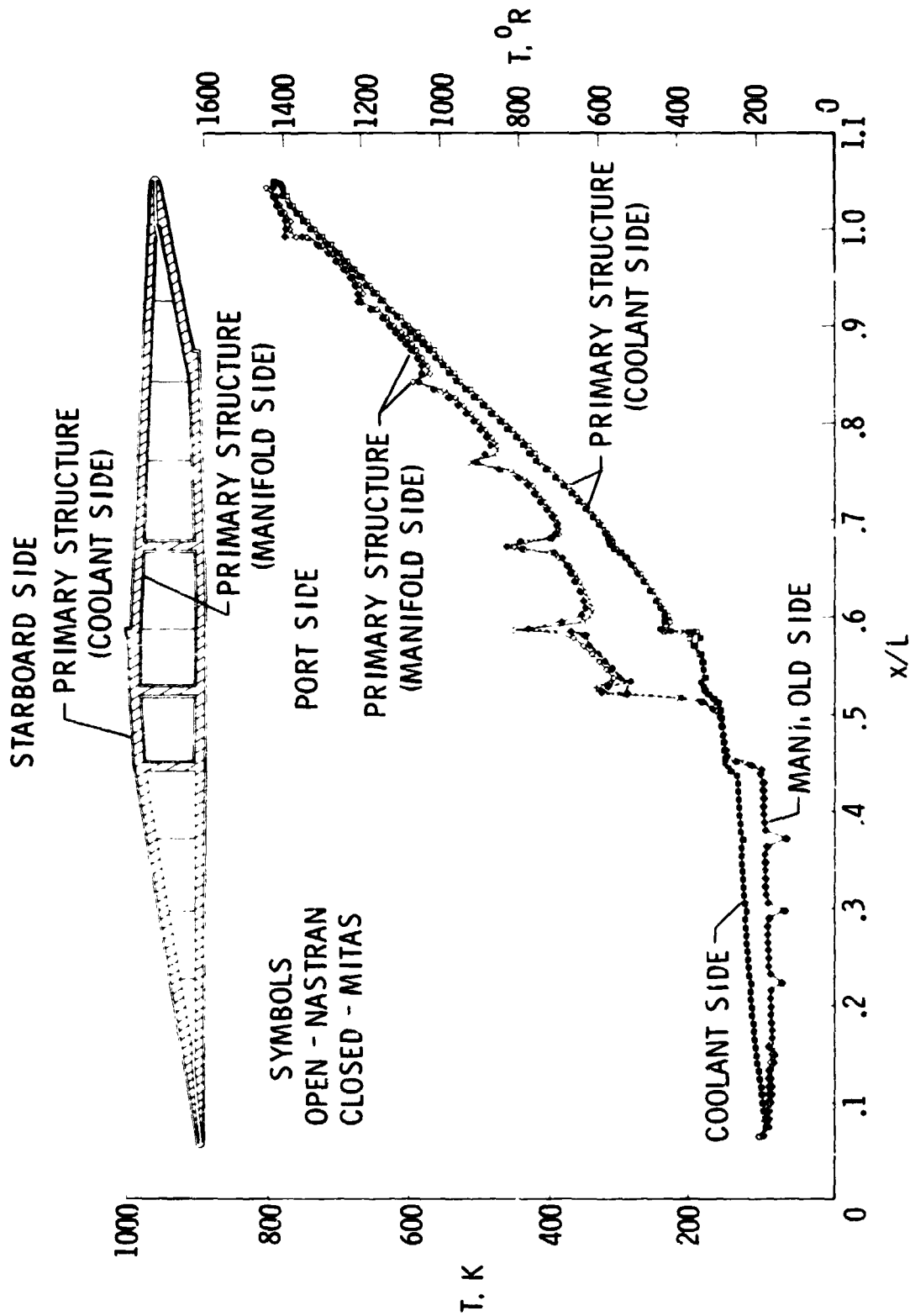


Figure 9. - Comparison of NASTRAN and MITAS predictions for temperature along starboard primary structure.

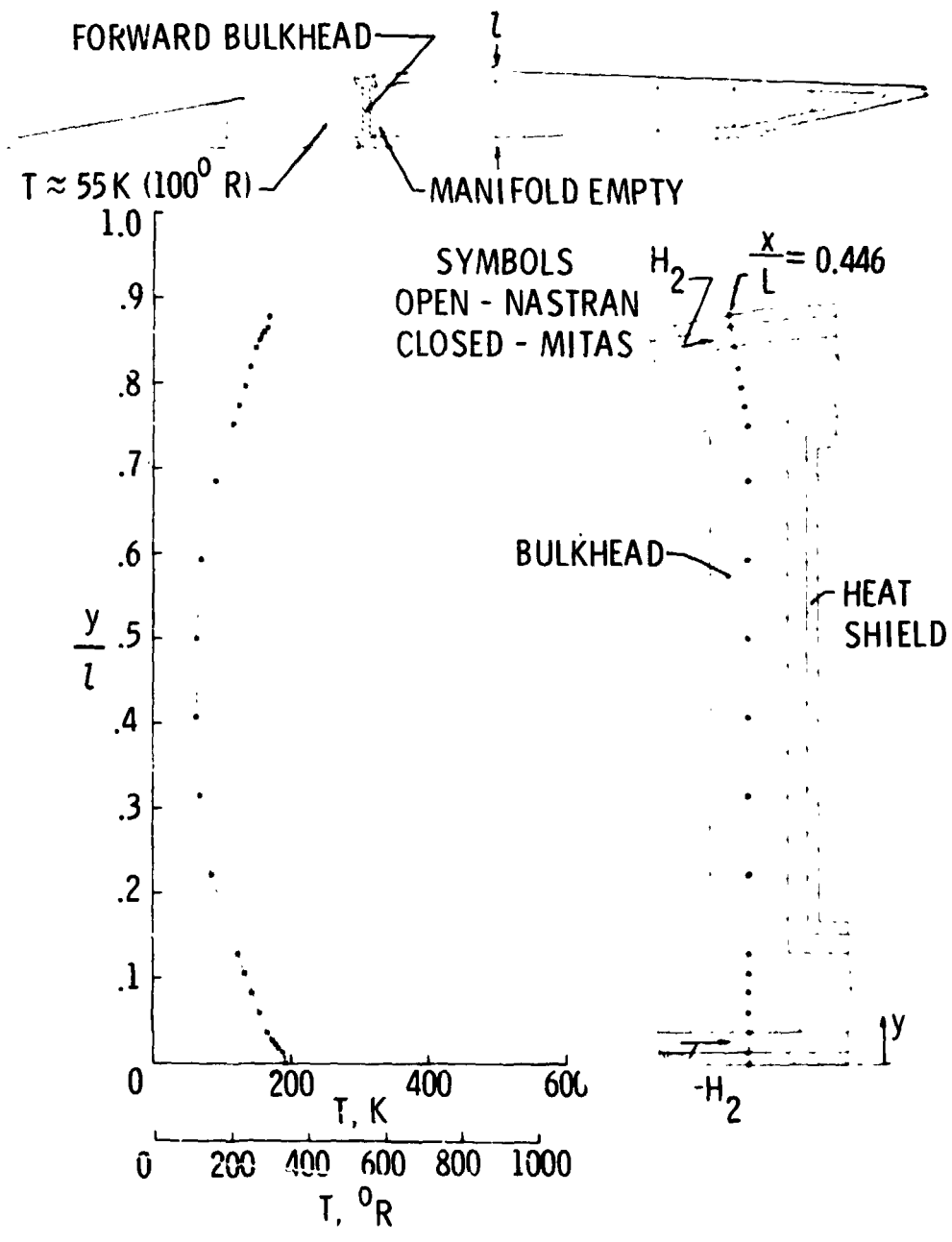


Figure 10. - Comparison of NASTRAN and MITAS predictions for the vertical temperature distribution at the forward bulkhead.

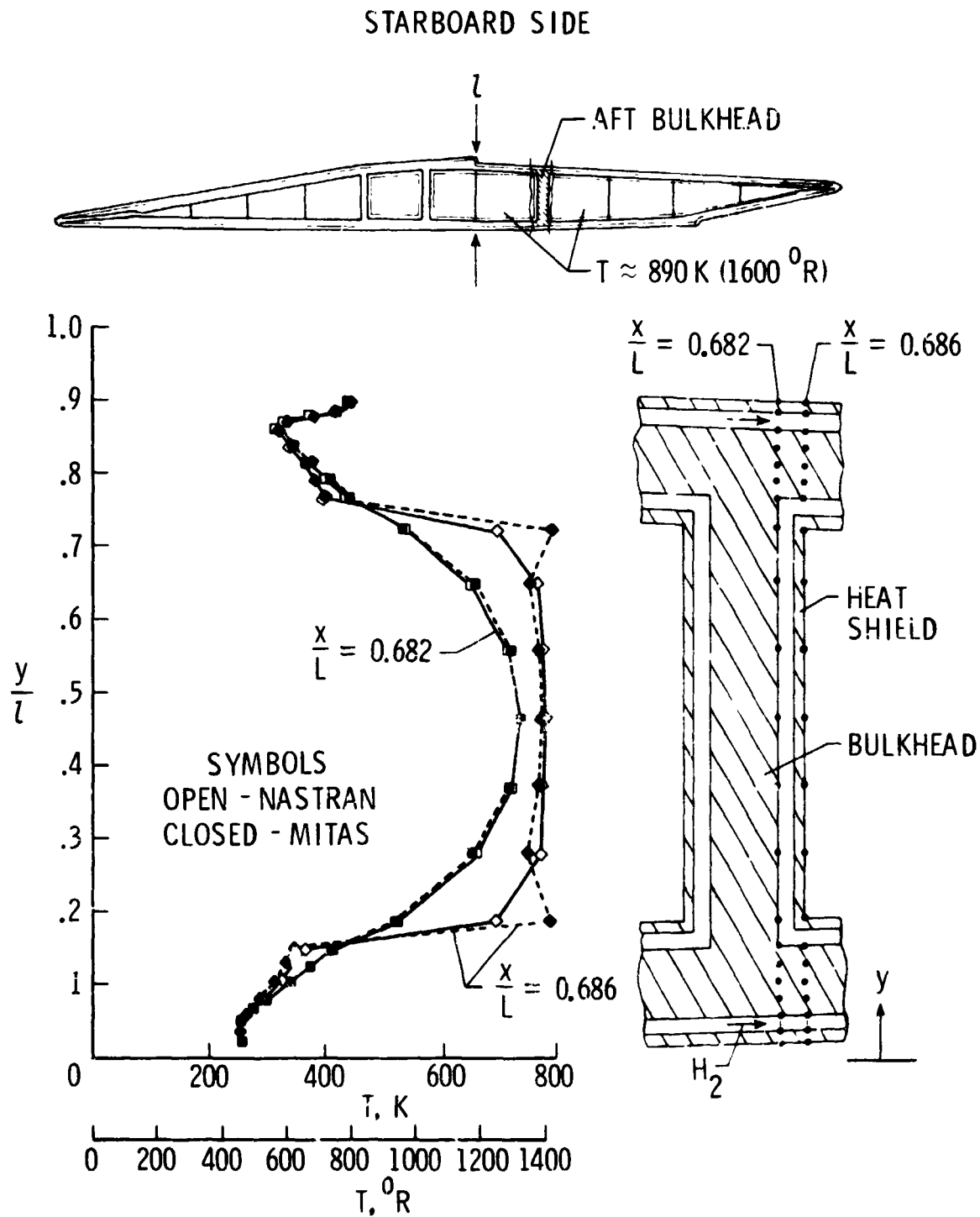


Figure 11. - Comparison of NASTRAN and MITAS predictions for the vertical temperature distributions at the aft bulkhead.

N75 31519

RIGID FORMAT ALTER PACKETS FOR THE ANALYSIS
OF ELECTROMAGNETIC FIELD PROBLEMS

E. Spreeuw Reactor Centrum Nederland

and

R.J.B. Reesman, Hazemeyer B.V.

SUMMARY

NASTRAN has been used to solve two types of electromagnetic field problems. The diffusion equation and the boundary conditions valid for problems of these kinds together with a replacing potential energy function have been given. The extent to which an analogy with finite element displacement and temperature approaches holds is indicated. The outputting of complex quantities is made possible after adjustment of standard rigid format 1 input data blocks to module SDR2. The applications made involve the study of the proximity effect in a system of three parallel conductors and the analysis of the magnetic field in the vicinity of the points of contact in circuit breakers.

34

INTRODUCTION

Obviously the knowledge of electromagnetic field distributions is of prime interest in Electric Power Engineering. Transient magnetic fields present in conducting materials cause the introduction of eddy currents in such materials. Energy losses leading to temperature increases result from these currents. The most familiar application of magnetic fields is in transformers where they determine the modification of current and voltage levels. They have also proven to determine the design of advanced types of power generators such as fusion reactors and MHD generators.

These and many other reasons explain why the analysis of electromagnetic problems is as important as it is. After finite difference techniques were used for these problems originally we now observe more and more interest in finite element methods. Among the applications of finite element techniques the works of Chari and Silvester (Ref. |1|), Chari (Ref. |2|), Silvester and Rafinejad (Ref. |3|) and Donea et al (Ref. |4|) have to be mentioned.

C-7

Rather than writing a stand-alone finite element code for the exclusive study of electromagnetic field problems it was felt worthwhile to investigate the applicability of the NASTRAN system.

When studying the equations and boundary conditions describing the problems involved it shows out there are many similarities with the ones NASTRAN is designed to deal with. The equation of balance valid here is identical to the equation of heat balance in solids except for the unknown quantity which is a vectorial instead of a scalar. When considering harmonic oscillations the transient term in the equation of balance may be transformed to a stationary one and a diffusion equation is obtained. In case the unknown field was a scalar quantity the solution to the magnetic field problem would be similar to the one valid for one-group neutron diffusion.

A NASTRAN solution to the neutron problem is reported in Ref. [5]. Electromagnetic field problems discussed in the present work mean a class of other nonstructural applications of NASTRAN and the approach applied here in fact means an extension of the research discussed in this reference.

FORMULATION OF THE ELECTROMAGNETIC FIELD EQUATIONS

Electromagnetic problems are described by Maxwell's equations. Without going into details these relations will be restated here for completeness.

Placing an electrically conducting body in a harmonically oscillating magnetic field \bar{B} will cause eddy currents to be introduced in it. The relation between \bar{B} and the electric field \bar{E} introduced is given by Faraday's law of induction:

$$\nabla \times \bar{E} = - \frac{\partial \bar{B}}{\partial t} \quad (1)$$

Current density \bar{J} is obtained from Ohm's law:

$$\bar{J} = \sigma \bar{E} \quad (2)$$

where σ denotes the conductivity.

These currents generate a magnetic field which interferes with the original one. When restricting ourselves to slowly changing systems ($f \leq 100$ Hz) we may use the relation:

$$\nabla \times \bar{B} = \mu \bar{J} \quad (3)$$

where μ stands for the permeability of the conductor.

We introduce the concepts of the magnetic vector potential \bar{A} which is related to \bar{B} by:

$$\bar{B} = \nabla \times \bar{A} \quad (4)$$

and the one of the electric potential ψ defined by:

$$\bar{E}_{el} = -\nabla\psi \quad (5)$$

\bar{E}_{el} indicates the electric field present when magnetic influences are omitted.
By definition

$$\nabla \cdot \bar{A} = 0 \quad (6)$$

Moreover

$$\bar{J} = -\sigma \frac{\partial \bar{A}}{\partial t} + \bar{J}_e \quad (7)$$

where \bar{J}_e represents the current caused by the electric potential.

Equations (1) ... (5) can be combined to obtain the diffusion equation

$$\nabla^2 \bar{A} = \mu\sigma \frac{\partial \bar{A}}{\partial t} - \mu \bar{J}_e \quad (8)$$

Since we are dealing with harmonic systems it is favourable to replace \bar{A} by $\bar{A}e^{j\omega t}$ and \bar{J}_e by $\bar{J}_e e^{j\omega t}$, with j standing for operator $\sqrt{-1}$. This will make Eq. (8) read:

$$\nabla^2 \bar{A} - j\omega\mu\sigma \bar{A} + \mu \bar{J}_e = 0 \quad (9)$$

which describes a stationary rather than a transient state.

However we have to pay a penalty since we are now dealing with complex quantity \bar{A} .

The boundary conditions valid in most cases are reflective ($\frac{\partial \bar{A}}{\partial n} = 0$) or consist of prescribed values of \bar{A} . For certain types of problems the location of the boundary may not be clearly established and is in fact situated at infinite distance from the area of interest. Moreover we have to meet the requirement that eddy currents should not give any contribution to the total current. This means the eddy current density integrated over the volume V vanishes, i.e.

$$\int_V \bar{A} dV = 0 \quad (10)$$

The solution of Eq. (9) is obtained by solving the equivalent variational problem, i.e. by imposing the requirement of the relevant energy functional P to be stationary.

$$P = \iiint_V \left(\frac{1}{2} \frac{\partial \bar{A}}{\partial x_i} \frac{\partial \bar{A}}{\partial x_i} - \frac{j\omega\mu\sigma}{2} \bar{A}^2 \right) dV + \iiint_V \mu \bar{J}_e \bar{A} dV = \text{Stationary} \quad (11)$$

When contrasting the first term of this functional with the thermal potential function it shows out to the neglect of a constant factor this term contains

the thermal potential function. Moreover when omitting a constant factor the capacitive energy function is implied in it.

This indicates electromagnetic field problems may be computed using finite element heat conduction computer programs at least modified in such a sense that the heat capacity matrix is added to the heat conduction matrix. Alternatively finite element structural mechanics codes with provisions to account for anisotropic material properties may be used. Specification of particular material properties and addition of the mass (or damping) matrix to the stiffness matrix is required in enabling the application of this alternative approach.

THREE PHASE BUS BAR SYSTEM

As a first example on how NASTRAN can be applied to deal with these problems we will discuss the interaction of electromagnetic fields in a system of three parallel conductors carrying alternating currents with mutual phase lags equal to $\frac{2\pi}{3}$.

For this type of problem the following assumptions are valid:

- 1) The magnetic vector potential and the source current densities in the bars have only components in the longitudinal direction of the system. They are invariant with this direction and vary sinusoidally with time, so the problem is essentially two-dimensional.
- 2) The fields are assumed quasi-stationary, so that displacement currents may be neglected.
- 3) Hysteresis, magnetic saturation and temperature effects of resistivity are negligible.

Because of the first of these assumptions \bar{A} and \bar{J} may be considered to be scalars. At infinite distance around the system this quantity vanishes and in order to apply this boundary condition properly it seems desirable to make use of something like the apparently contradictory concept of infinite finite elements recently introduced by P. Bettis, University of Wales. The lack of this type of elements can be overcome by restricting ourselves to a usual finite mesh (Fig. 11) and diminishing of the results with a certain quantity, resulting from Eq. (10).

The phase lagged volumetric quantity $\mu\bar{J}_e$ present in Eq. (9) is composed of three sets; one for each of the bars. Since the unknown is a scalar quantity and since in the displacement approach volumetric loading (GRAV bulk data cards) can neither be computed to obtain complex quantities nor be varied over subcases it is appropriate to use the NASTRAN heat conduction capability where we can use QVOL cards. Complex values of volumetric heat generation rate cannot be specified. This deficiency can be overcome by stepwise generation of the electromagnetic load in three different subcases and subsequent phase lagged superposition of the load vectors, making use of complex multiplication factors specified in the parameter section of DMAP module ADD.

The load vectors have to be computed separately instead of being appended.

This can be accomplished by specification of different single point constraints

for each of the individual subcases. Therefore an SPOINT has been introduced with three differing prescribed values. In order to determine the solution at the right level the subsidiary condition (Eq. 10) has to be applied. This means all elements of the solution vector $\{u_g\}$ have to be subtracted by its mean value:

$$u_m = \frac{1}{S} \int \{u_g\} dS \quad (12)$$

where S stands for the cross-sectional surface of the conductors. This multiplication factor is computed from:

$$\frac{1}{\rho S} \{u_g\}^T |M_{gg}| \{I_g\} \quad (13)$$

with $\{I_g\}$ denoting a vector of order g with all elements equal to 1.

Since SPR's 458 and 483 have not yet been corrected in Level 15.5 of NASTRAN module ADD is unable to add complex input matrices. Consequently, at present the subtraction mentioned has to be performed either by hand or in a stand-alone program. For the same reason the computation of the current density can not be done in NASTRAN.

Special care has to be taken that complex quantities are output from module SDR2. This requires reformatting of some of its input data blocks. In order to accomplish this a dummy table of eigenvectors CLAMA has been specified on DTI bulk data cards. A dummy EIGC card was used in order to have IFP create a DYNAMICS data block. Moreover modules CASE and DPD were introduced to provide CASEXX, EQDYN and SILD required to make SDR2 print complex eigenvectors. For the purpose of this application this means the printing of complex nodal vector potential values. The rigid format Alter resulting from these modifications is given in Appendix I.

The range of parameters used for the computation of \bar{A} reads as follows:

specific conductivity	$\sigma = 3.7_{10}^7 \text{ Ohm}^{-1} \text{ m}^{-1}$
permeability	$\mu = 4\pi_{10}^{-7} \text{ Henry m}^{-1}$
electrical current density	$J_e = 8.711 \text{ A m}^{-2}$
angular frequency	$\omega = 314.16 \text{ rad. sec}^{-1}$
RMS of total current through each conductor	$J = 1500 \text{ A}$
cross-sectional surface of one conductor	$S = 1722_{10}^{-6} \text{ m}^2$

The distribution of the current density \bar{J} derived from \bar{A} demonstrates the large impact on the uniform distribution due to the presence of the magnetic field. This phenomenon is called the proximity effect. For cross-sectional surface S and specific electric conductivity σ the heat production per unit length is computed from

$$Q = \iint_S \frac{1}{\sigma} |\bar{J}|^2 dS \quad (14)$$

Obviously, for any fixed net current through the system, the minimum value of Q ($=Q_{\min}$) is obtained when \bar{J} is uniformly distributed.

The economy of the conducting system is determined by the ratio of Q over Q_{\min} , which is called the resistance ratio. Q cannot be computed in the DMAP sequence since SPR's 458 and 483 prohibit the derivation of \bar{J} (Eq. 7). A stand-alone calculation of Q is simplified when making use of

$$ADJ2 = \{u_g\}^T |M_{gg}| \{u_g\}, \quad (15)$$

referred to in the ALTER packet.

To the neglect of J_e the heat production Q^* can be computed from

$$Q^* = \{u_g^*\}^T |M_{gg}| \{u_g\} \quad (16)$$

with $\{u_g^*\}^T$ standing for the transposed complex conjugate of $\{u_g\}$.

$$Q^* = \sqrt{\{Re(ADJ2)\}^2 + \{Im(ADJ2)\}^2} \quad (17)$$

For the present configuration the resistance ratio was found to be 2.4.

MAGNETIC FIELDS IN CIRCUIT BREAKERS

One of the aspects to be taken into account in the design of circuit breakers is the phenomenon of electrical discharge.

The occurrence of this phenomenon depends on the amplitude and phase angle of the magnetic field present in the neighbourhood of the contact. The magnetic field is studied in an arrangement of two parallel circular disks situated at the center of a Helmholtz configuration (Fig. |2|). This assembly of two identical coils with mutual distance equal to their diameter is known for the uniformity of the magnetic field that can be generated in it.

In contrast to the first application where we determined \bar{A} , this time the interest is in $\text{curl } \bar{A}$ (Eq. 4) which is obtained from linear combinations of its derivatives.

There is an analogy with the derivation of stresses from displacements and since the problem is essentially two-dimensional the choice for solid ring elements is obvious. However according to SPR 933 complex stresses cannot be derived for these types of elements. That is why the use of three-dimensional elements may be considered.

\bar{A} is no longer unidirectional and Eq. (9) in fact consists of two independent equations, one for each of the components of \bar{A} . Since no relation between these components exists the equations can be solved in two subcases using the dis-

placement approach. This requires that $E = G$ and $\nu = 0$ such that the stress-strain matrix transforms into the identity matrix multiplied by a constant. This stress-strain relation implies the material is anisotropic. It can be specified on MAT1 bulk data cards while for solid elements the material axes to which it refers are the axes of the basic coordinate system.

For the first subcase degrees of freedom 2 thru 6 of all grid points are constrained. This means the σ_x data of subcase 1 will denote $E \frac{\partial A_1}{\partial x}$, $\tau_{zx} = E \frac{\partial A_1}{\partial z}$ and $\tau_{xy} = E \frac{\partial A_1}{\partial y}$. When in the second subcase constraining all degrees of freedom but the third at all grid points stress data σ_z contain $E \frac{\partial A_3}{\partial z}$, $\tau_{yz} = E \frac{\partial A_3}{\partial y}$ and $\tau_{zx} = E \frac{\partial A_3}{\partial x}$. To the neglect of constant E the components of \bar{B} (Eq. 4) can now be obtained. The first component of $\text{rot } \bar{A}$ is found to be τ_{yz} given in the second subcase. The second component is represented by the τ_{zx} data obtained from a SUBCOM in which SUBCASE 1 data are subtracted from SUBCASE 2. The third component is the negative value of τ_{xy} output for the first subcase.

Unfortunately the SUBCOM results were erroneous which is presumably due to any of the SPR's mentioned before. As a consequence the subtraction of results has to be performed separately. Attempts to output complex stresses via OFP lead to PAKUNPK errors when more than one subcase is involved. Consequently τ_{yz} and τ_{xy} are obtained from a printout of table OES1.

The ALTER packet required for this class of applications is a simplification of the one given in Appendix I. The modifications made to it appear from the following:

- 1) The FILE instruction is removed.
- 2) Since the displacement approach is used the SMA2 instruction is the one standard in rigid format 1.
- 3) The part related to multiplication and addition of load vectors is deleted.
- 4) The instructions dealing with the computation of quantities required for heat production calculation are no longer appropriate.
- 5) The standard rigid format 1 call for SDR2 may be used but GES1 has to be printed out.

The resulting packet is given in Appendix II.

CONCLUDING REMARKS

Electromagnetic field calculations mean an area of relatively new finite element applications. Since the development of a production program based on finite element techniques has shown out to be an extensive task, those interested in these calculations are advised to verify to which extent they can reap the fruits of what has already been accomplished in structural analysis. The convenient way of programming offered in the DMAP language and the large number of available features such as checkpointing, direct matrix and table input, parameter operations and plotting facilities makes consideration of NASTRAN

application worthwhile. Since many of the problems dealt with in electromagnetic field analysis are axisymmetric it is felt desirable to increase the 1.0 priority status of SPR 933.

Moreover fixes of SPR's 458 and 483 will allow for proper execution of modules ADD, ADD5 and MPYAD when processing complex input matrices. Proper accounting for the boundary conditions and the capability of determination of quantities derived from the magnetic vector potential will be enabled by these corrections.

It is hoped the present work demonstrates the usefulness of NASTRAN in this area of engineering and will lead to the increasing number of non-structural applications it deserves.

APPENDIX I

```

$ *****
$ *
$ *   ALTER PACKET FOR THE COMPUTATION OF THE MAGNETIC   *
$ *   VECTOR POTENTIAL IN THREE-PHASE CONDUCTING SYSTEMS *
$ *
$ *****
$
ALTER 3
FILE          PG1=SAVE/PG2=SAVE $
ALTER 22,22
PARAM        //C,N,NOP/V,N,SKPMGG=1 $ GENERATE HEAT CAPACITY MATRIX
ALTER 35,35
SMAZ         CSTM,MPT,ECPT,GPCT,DIT/,MGG/V,Y,WTHASS=1.0/V,N,NOMGG/
              V,N,NOBGG/C,N,-1 $
ALTER 44,44
ADD          MGG,KGGX/KGG1/C,Y,OMEGA=(0.0,-314.1592654) $
CHKPNT       KGG1 $ NOW MODIFY TO ENABLE PROCESSING OF KGG1
EQUIV        KGG1,KGG/NOGENL $ EXCLUDES USE OF GENERAL ELEMENTS
ALTER 47,47
SMAZ         GEI,KGG1/KGG/V,N,LUSET/V,N,NOGENL/V,N,NOSIMP $
ALTER 89,89
PARAM        //C,N,NOP/V,N,COUNT=3 $ SET LOOP CONTROL COUNTER
DFCOMP       KLL/LLL,ULL/C,N,1/C,N,0/V,N,MINDIAG/V,N,DET/V,N,POWER/
              V,N,SING $          DECOMPOSITION BY RBMG2 REPLACED
SAVE         MINDIAG,DET,POWER,SING $
COND         HERPOR3,SING $ TERMINATE COMPUTATION IF KLL IS SINGULAR
ALTER 97,97
$           BEGIN OF ALTER TO MPYADD LOAD VECTORS OBTAINED
$           FROM SUBCASES 1, 2 AND 3
PARAM        //C,N,ADD/V,N,NSKIP/V,N,NSKIP $
PARAM        //C,N,SUB/V,N,COUNT/V,N,COUNT $
PARAM        //C,N,SUB/V,N,CASE3/V,N,COUNT $
PARAM        //C,N,SUB/V,N,CASE2/V,N,CASE3 $
COND         LOAD3,CASE3 $
COND         LOAD2,CASE2 $
ADD          PG,/PG1 $
CHKPNT       PG1 $
JUMP         END3 $
LABEL        LOAD2 $
ADD          PG,/PG2 $
CHKPNT       PG2 $
JUMP         END3 $

```

APPENDIX I - Concluded

```

LABEL          LOAD3 $
ADDS           PG,PG2,PG1,,/PSUM/C,Y,PHASE3=(-.5,-.8660254)/
              C,Y,PHASE2=(-.5, .8660254) $

CHKPNT        PSUM $
SETVAL        //V,N,REPEAT/C,N,-1 $
SAVE          REPEAT $
LABEL         END3 $
REPT         LBL7,2 $
$            END OF ALTER TO MPYADD LOAD VECTORS OBTAINED FROM
$            SUBCASES 1, 2 AND 3
EQUIV        PSUM,PL/NOSET $
ALTER 100,100
SSG2         USET,GM,YS,KFS,GO,DM,PSUM/QR,PO,PS,PL $
ALTER 103,111
$            SSG3 REPLACED BY FBS. LAST PARAMETER FOR CSP OUTPUT
FBS          LLL,ULL,PL/ULV/C,N,1/C,N,1/C,N,2/C,N,3 $
CHKPNT        ULV $
SDR1         USET,PG,ULV,,YS,GO,GM,PS,KFS,KSS,QR/UGV,PGG,QG/C,N,1/
C,N,STATICS $
CHKPNT        PGG,UGV $
$            BUILD VECTOR WITH ALL COMPONENTS EQUAL TO 1
VEC          USET/FSET/C,N,G/C,N,COMP/C,N,L $
VFC          USET/SSET/C,N,G/C,N,L/C,N,COMP $
CHKPNT        SSET,FSET $
ADD          SSET,FSET/UNIT $
MPYAD        MGG,UGV,/TST/C,N,0 $
CHKPNT        UNIT,TST $
MPYAD        UNIT,TST,/ADJ1/C,N,1 $ QUANTITIES ADJ1 AND ADJ2 ENABLE
MPYAD        UGV ,TST,/ADJ2/C,N,1 $ COMPUTATION OF HEAT PRODUCTION
CHKPNT        ADJ1,ADJ2 $
MATERM       ADJ1, ADJ2,,// $
ALTER 119,119
$            ADJUST SDR2 INPUT TO ALLOW FOR COMPLEX UGV OUTPUT
CASE         CASECC,/CASEXX/C,N,CEIGEN/V,N,REPEAT $
DPO          DYNAMICS,GPL,SIL,USET/GPLC,SILD,USED,,,,,,,,,EQDYN/V,N,
LUSET/V,N,LUSED/V,N,NOTFL/V,N,NODLT/V,N,NOFSOL/V,N,
NOFRL/V,N,NOFLT/V,N,NOTRL/V,N,NOEED/C,N,123/V,N,NOUE $
SDR2         CASEXX,CSTM,MPT,DIT,EQDYN,SILD,GPTT,EDT,BGPDT,CLAMA,QG,
UGV ,EST,/OPG1,00G1,0UGV1,0ES1,0EF1,PUGV1/C,N,CEIG $

ALTER 137
LABEL        HERROR3 $
POTPARM     //C,N,-3/C,N,HSTATICS $
ENDALTER

```

APPENDIX II

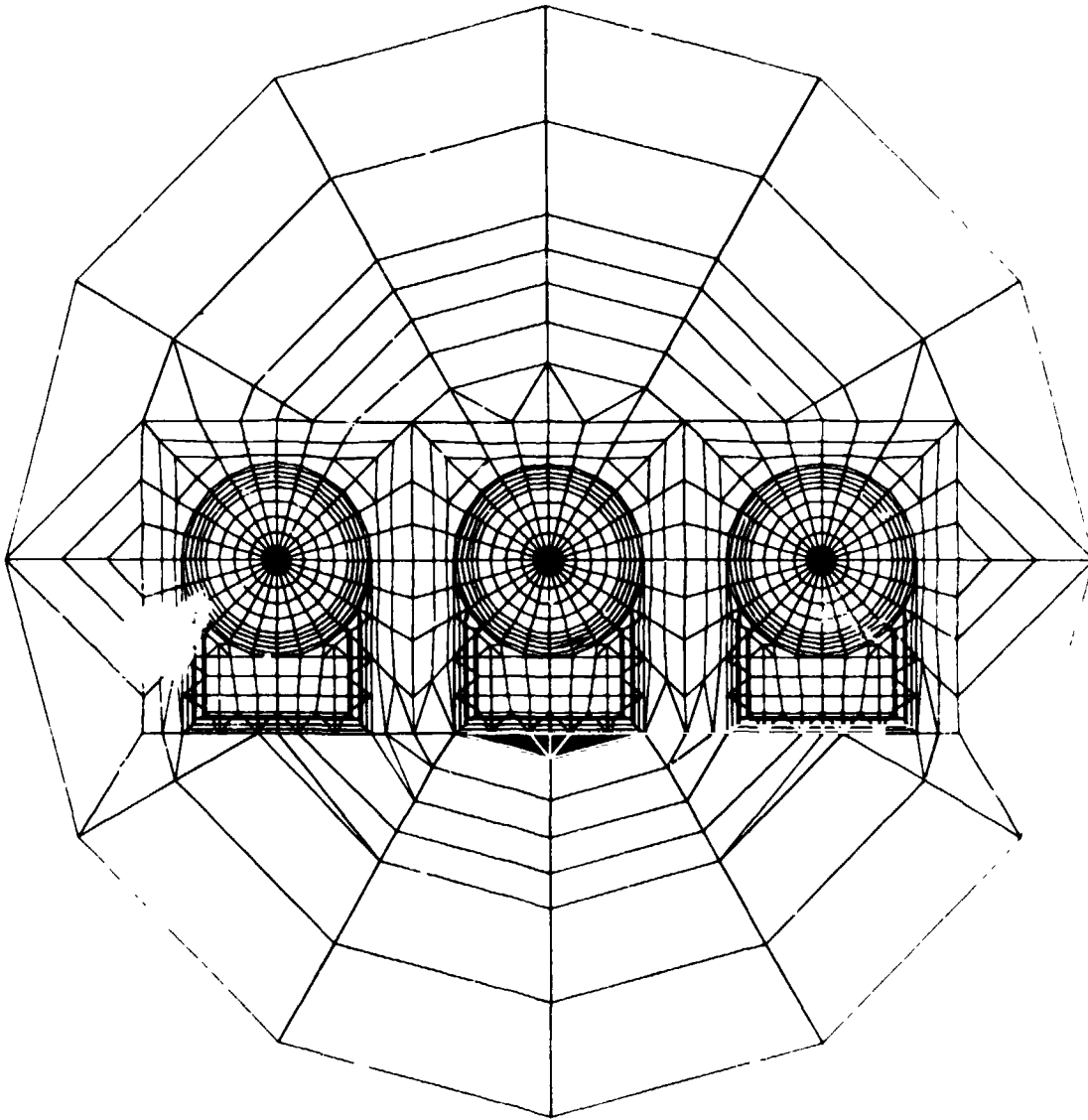
```

$ *****
$ *
$ *      ALTER PACKET FOR THE COMPUTATION OF MAGNETIC FIELDS *
$ *
$ *****
$
ALTER 22.22
PARAM // C.N.NOP/V.N.SKPMGG=1 & GENERATE MASS MATRIX
ALTER 44.44
ADD MGG,KGGX/KGGI/C.Y.OMEGA=(0.0,-314.1592654) &
CHKPNT KGGI & NOW RENAME TO ENABLE PROCESSING OF KGGI
FOHIV KGGI,KGG/NOGENL & USAGE OF GENERAL ELEMENTS IS EXCLUDED
ALTER 47.47
SMAR GEI,KGGI/KGG/V.N.(HSET/V.N.NOGENI /V.N.NOSIMP &
ALTER 89.89
DECOMP KLL/LLI.HLI /C.N.) /C.N.0/V.N.MINDIAG/V.N.DET/V.N.POWER/
V.N.SING & REPLACE PRMG2 DECOMPOSITION. KLL IS COMPLEX
MINDIAG.DET.POWER.SING
COND HEOROR3.SING & TERMINATE COMPUTATION IF KLI IS SINGULAR
ALTER 103.110
& CSO2 REPLACED BY FRS. LAST PARAMETER FOR CSR OUTPUT
FRS ILL.HLI.PI/HIV/C.N.1/C.N.1/C.N.2/C.N.3 &
CHKPNT ILLV &
SDR] HSET.PG.HLV..YS.GM.GM.PS.KFS.KSS.OP/HGV.PGG.QG/V.N.
NSKIP/C.N.STATICS &
ALTER 121.121
CHKPNT OES] & COMPLEX STRESSES ARE IN OES] BUT FORMAT
TARPT OES]....// & IS IMPROPER FOR CORRECT AEP PROCESSING
ALTER 137
[ARFI HEOROR3 &
POTPADM //C.N.-3/C.N.HSTATICS &
ENDALTER

```

REFERENCES

1. Chari, M.V.K. and P. Silvester: Analysis of Turboalternator Magnetic Fields by Finite Elements, IEEE Trans. Power Apparatus and Systems, Vol. 90, No. 2, pp. 454-464.
2. Chari, M.V.K.: Finite-element Solution of the Eddy-current Problem in Magnetic Structures, IEEE PES Summer Meeting & BHV/UHV Conference, Vancouver, B.C. Canada, July 15-20, 1973.
3. Silvester, P. and P. Rafinejad: Curvilinear Finite Elements for Two-dimensional Saturable Magnetic Fields, IEEE PES Winter Meeting, New York, N.Y. January 27 - February 1, 1974.
4. Donea, J., S. Giuliani and A. Philippe: Finite Elements in the Solution of Electromagnetic Induction Problems, Int. J. Num. Meth. Eng., Vol. 8., pp. 359-367 (1974).
5. Spreeuw, E.: Applications of NASTRAN to Nuclear Problems, NASTRAN: Users' Experiences, Second Colloquium, Hampton, Virginia, Sept. 11-12, 1972, NASA TM X-2637, pp. 429-441.



16/ 4/75

Fig. 1. Finite element model of bus bar geometry.

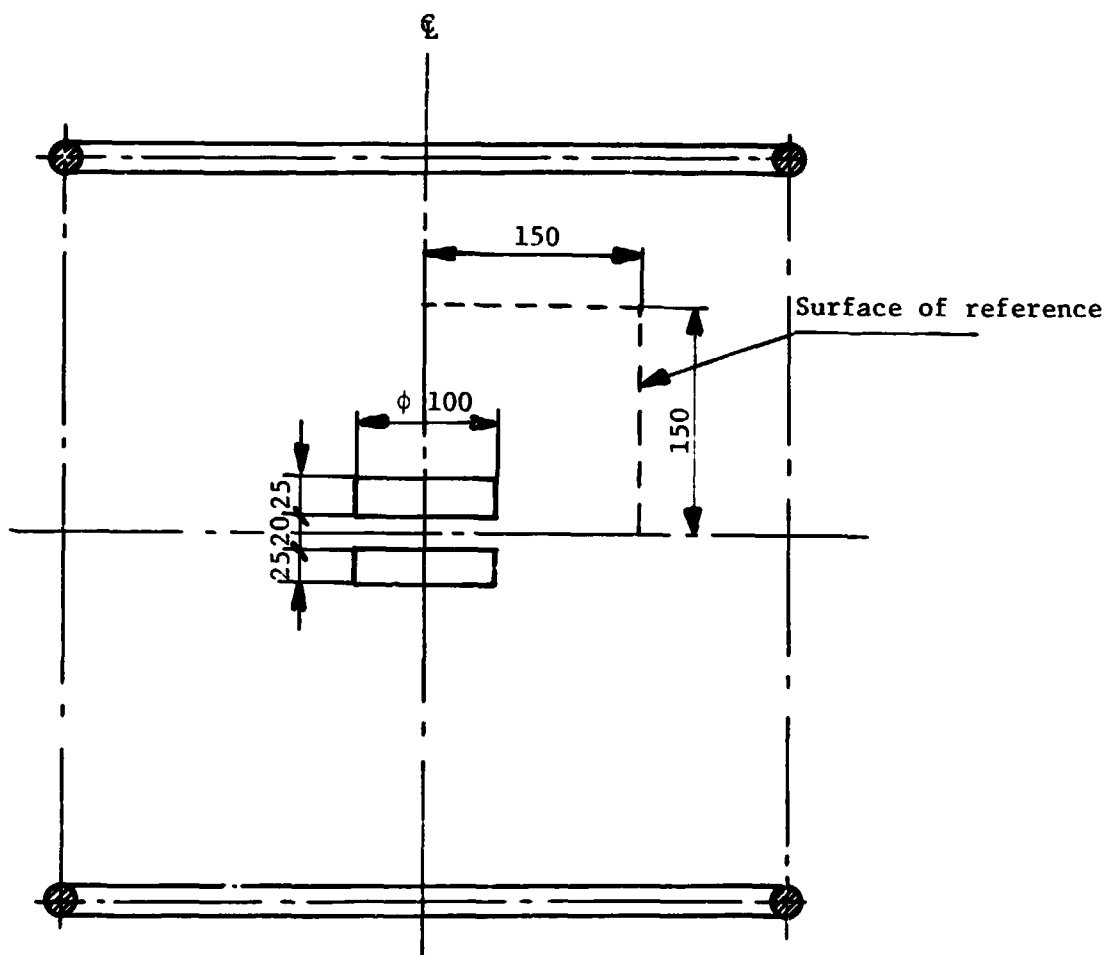


Fig. 2. Helmholtz configuration with two circular disks.

N75 31520

THE AUTOMATED MULTI-STAGE SUBSTRUCTURING
SYSTEM FOR NASTRAN

E. I. Field, D. N. Herting,
D. L. Herendeen and R. L. Hoesly

Universal Analytics, Inc.
Playa del Rey, California

SUMMARY

The new substructuring capability developed for eventual installation in Level 16 is now operational in a test version of NASTRAN. Its features are summarized. These include the user-oriented, Case Control type control language, the automated multi-stage matrix processing, the independent direct access data storage facilities and the static and normal modes solution capabilities. A complete problem analysis sequence is presented with card-by-card description of the user input.

INTRODUCTION

One of the most desired improvements in NASTRAN has been the capability for automated, multiple-stage substructuring analysis. The substructuring method reduces the difficulty of analyzing large and complex structures by dividing the analysis into small, more manageable tasks. Substructuring is a logical extension of the basic finite element method itself. That is, each component substructure is but a complex, finite part of the whole. This concept is easily extended to include the idea of combining substructures which are themselves combinations of component substructures. This process is called multi-stage substructuring.

The complex computational tasks of identifying the characteristics of each component, joining these components to form the final full model, and managing the associated data involve sophisticated computer program requirements beyond the existing scope of NASTRAN. Although the NASTRAN program currently provides the basic tools needed to perform simple substructuring analyses, the use of these capabilities requires significant experience and extensive intervention on the part of the user. Therefore, a new approach was proposed by Universal Analytics, Inc. This approach was presented by the NASTRAN Systems Management Office (NSMO) to a team of potential major aerospace users for their review and qualification to assure the viability and utility of the concepts proposed. Based on their review, the following final design criteria were established:

1. Analysis of large problems with a facility for unlimited multi-stage combinations of substructures.

2. Performance of both static and normal mode analyses (Rigid Formats 1, 2, and 3) at any stage of substructure combination with flexibility for extension at a later date to other Rigid Formats.
3. Execution on all three of the main frame computers on which NASTRAN is currently maintained (IBM, UNIVAC, CDC).
4. Elimination of all arbitrary restrictions on the sequencing of grid points and on the use of coordinate systems in defining the basic substructures.
5. Repeated application of the same basic substructure data for identical or symmetrical subcomponents of a model without redefinition of that model.
6. Communication of substructuring data between any two of the three main frame computers.
7. Simple user control by the novice while retaining existing NASTRAN flexibilities for the expert.

Each of these criteria was met with a minimum of machine-dependent programming using the following basic design features:

1. A bulk storage direct access file, independent of the standard NASTRAN file structure, was established for the Substructure Operating File (SOF) for storing all substructuring matrix and control data between each phase of processing.
2. A Master Data Index (MDI) file, also stored on the SOF, was designed to provide identification and control over all data sets on the SOF. A simply connected tree structure was selected to define all substructure component relationships and to provide unique trace-back facilities for retrieval of solution data at the basic substructure level.
3. A substructure Control Deck system of commands, using linguistic constructs, patterned after the current Case Control Deck, was developed for simple control over all steps of the analysis. To provide this feature, each command is automatically translated during execution into a set of DMAP instructions which are inserted as alters to the requested Rigid Format.
4. New Bulk Data Card options were provided so that all references to data contain only original basic substructure names and grid point identifiers.

The following sections provide an overview of how the system was implemented. The key user features are discussed and tables are included which list the substructuring commands and the Bulk Data options. A complete analysis sequence for a simple problem is illustrated in the appendix with a full card-by-card description of the input.

DESIGN SPECIFICATIONS

The specifications that were developed according to the criteria outlined above for implementing multi-stage substructuring into NASTRAN were based on a fully automated processing procedure. The alternative of enhancing the DMAP approach already available in NASTRAN was discarded to avoid: 1) the inherent requirement for user involvement in detail file maintenance, vector definition and matrix manipulations, 2) the overly constricting limitations on modeling of the substructures, and 3) the necessity of being an expert in NASTRAN to use this approach. Though the test system for the fully automated approach was implemented first in a Level 15.5 of NASTRAN, it was designed to minimize the effort of incorporation into Level 16.

The basic theory for the substructuring method is well known. The details of that theory to define each of the processing steps in NASTRAN need not be reviewed here. Substructure processing includes building the matrices for each of the basic substructures, defining the coordinate and matrix transformations needed for connecting two or more rotated, translated, or reflected component substructures, performing matrix reduction and solution, and computing the inverse transformations to recover solution results at any stage of the analysis. NASTRAN already provides a full set of modeling tools to generate the basic substructure matrices. It also provides most of the elementary matrix processing and output generating modules via the DMAP instruction set. The principal tasks were to develop the substructuring modules required to provide:

1. User control capabilities.
2. Data management features to maintain a Substructure Operating File (SOF) for storage and retrieval of substructuring data.
3. Program control for the execution of matrix operations requested by the user.

The user facilities provided by the new system are summarized below, followed by an overview of the SOF file maintenance utilities and of the methods used to control NASTRAN for automated substructuring.

USER CONTROL CAPABILITIES

A substructure analysis is performed in three phases. In Phase 1, the "basic substructures" are generated using the existing NASTRAN modeling data card input for elements, grid points, and constraints, etc. In Phase 2, various basic substructures may be "combined" and/or "reduced" in several steps to produce a "solution structure". Phase 2 also includes solution processing as well as the recovery of solution data for any previously defined level of substructure combination. In Phase 3, the basic Phase 1 processing is restarted using the check-pointed data or by resubmitting the original input data to obtain detailed displacement, force, and stress output for that basic substructure.

Each phase is run as a separate job step. Though the user may request all Phase 2 steps be performed in one execution, he will usually elect to subdivide the Phase 2 processing into several runs with each execution spanning one or more steps. This allows for examination and checkout of the intermediate results. This approach offers the following advantages:

1. Each component model of the overall structure (e.g., wing, fuselage, engine nacelles, landing gear, etc.) may be developed independently, even by separate contractors and on separate computer hardware systems.
2. Larger component substructures may themselves be assembled from yet smaller component substructures for multi-stage substructure analyses.
3. Each component substructure may be validated independently, plotted and analyzed prior to assembly and solution of the integrated whole model.
4. Changes due to errors, model modifications, and/or design alterations may be effected for any basic substructure and reintegrated into the overall structure at a minimum cost.
5. Via matrix reduction of the stiffness and mass matrices of neighboring substructures, their interaction effects on any given component can be economically included in the separate analysis of that particular component.

The user exercises control over the substructure operations via the "Substructure Control Deck" which contains a set of commands for directing the basic operations in each phase of the analysis. A summary of these commands and their associated subcommands is given in Table 1. The detailed data for defining transformations, connectivities, boundaries, constraints, etc., are input by the user via the new Bulk Data cards, summarized in Table 2. As can be seen the Substructure Control Deck options provided full control over each step in the analysis, selective output at each step, ample visibility into the contents of the SØF file, and simple management facilities to control the storage, purging, and retrieval of SØF data files. A detailed card-by-card description of the input for a simple problem is presented in the appendix to illustrate the convenience and simplicity of the s.

Each command uses terminology related to the operation performed. The primary operations of REDUCE, COMBINE, SOLVE, and RECOVER can be requested in any order desired by the user. The user is relieved of the tedious and error-prone tasks involved in keeping track of the matrices, partitioning vectors, internal numbering sequences, and details of the coordinate geometries, etc. Connections of component substructures may be found automatically or they may be specified manually. The component substructures which occur repeatedly may all be equivalenced to one component substructure and rotated, translated, or reflected into their respective positions in the final model. Undeformed plots may be requested at any step. If severe errors are detected, input checking on the remaining steps is performed and the time consuming matrix operations are skipped.

TABLE 1. SUMMARY OF SUBSTRUCTURE COMMANDS

A. Phase and Mode Control	
SUBSTRUCTURE #	- Defines execution phase (1, 2, or 3) (Required)
OPTIONS	- Defines matrix options (K, M, or P)
RUN	- Limits mode of execution (DRY, GØ, DRYGØ, STEP)
ENDSUBS #	- Terminates Substructure Control Deck (Required)
B. Substructure Operations	
COMBINE	- Combines sets of substructures
NAME	- Names the resulting substructure
TOLERANCE*	- Limits distance between automatically connected grids
CONNECT	- Defines sets for manually connected grids and releases
OUTPUT	- Specifies optional output results
COMPONENT	- Identifies component substructure for special processing
TRANSFORM	- Defines transformations for named component substructures
SYMTRANSFORM	- Specifies symmetry transformation
SEARCH	- Limits search for automatic connects
EQUIV	- Creates a new equivalent substructure
PREFIX*	- Prefix to rename equivalenced lower level substructures
REDUCE	- Reduces substructure matrices
NAME*	- Names the resulting substructure
BOUNDARY*	- Defines set of retained degrees of freedom
OUTPUT	- Specifies optional output requests
SOLVE	- Initiates substructure solution (statics or normal modes)
RECOVER	- Recovers Phase 2 solution data
SAVE	- Stores solution data on SØF
PRINT	- Stores solution and prints data requested
BRECOVER	- Basic substructure data recovery, Phase 3
SPLØT	- Initiates substructure undeformed plots
C. SØF Controls	
SØF #	- Assigns physical files for storage of the SØF (Required)
PASSWORD	- Protects and insures access to correct file
SØFØUT or SØFIN	- Copies SØF data to or from an external file
POSITION	- Specifies initial position of input file
NAMES	- Specifies substructure name used for input
ITEMS	- Specifies data items to be copied in
SØFPRINT	- Prints selected items from the SØF
DUMP	- Dumps entire SØF to a backup file
RESTØRE	- Restores entire SØF from a previous DUMP operation
CHECK	- Checks contents of external file created by SØFØUT
DELETE	- Edits out selected groups of items from the SØF
EDIT	- Edits out selected groups of items from the SØF
DESTROY	- Destroys <u>all</u> data for a named substructure and all the substructures of which it is a component

Mandatory Control Cards

* Required Subcommand

TABLE 2. SUBSTRUCTURE BULK DATA CARD SUMMARY

A. Bulk Data Used for Processing Substructure Command REDUCE	
BDYC	- Combination of substructure boundary sets of retained degrees of freedom
BDYS	- Boundary set definition
BDYS1	- Alternate boundary set definition
B. Bulk Data Used for Processing Substructure Command COMBINE	
CONCT	- Specifies grid points and degrees of freedom for manually specified connectivities - will be overridden by RELES data
CONCT1	- Alternate specification of connectivities
RELES	- Specifies grid point degrees of freedom to be disconnected - overrides CONCT and automatic connectivities
GTRAN	- Redefines the output coordinate system grid point displacement sets
TRANS	- Specifies coordinate systems for substructure and grid point transformations
C. Bulk Data Used for Processing Substructure Command SOLVE	
LOADC	- Defines loading conditions for static analysis
MPCS	- Specifies multipoint constraints
SPCS	- Specifies single point constraints
SPCS1	- Alternate specification of single point constraints
SPCSD	- Specifies enforced displacements for single point constraints

At each step in the analysis, the user identifies by name, e.g., HUB, WING, ROOT, etc., each substructure to be used in that step. All specific references to grid points for connection or boundary sets, releases, and loads, etc. are made with respect to the basic substructure name. The names of any component substructure can be used for the combine, reduce, equivalence, solve, and recover operations. Automatically the program retrieves all the relevant data for the named substructures from the SØF, performs the matrix operations requested, and stores the results on the SØF. Thus, the user is freed from the tedious task of bookkeeping. If the same component substructure is to be used more than once, e.g., identical components are to be used to create the full model, the "equivalence" operation must be used to assure unique names are assigned to each substructure and its contributing components.

Several features have been provided for input data checking. Principal among these is the DRY run option. This option allows the user to submit his run to have the program validate the consistency of his command structure and his data without actually performing the more time consuming matrix operations. Also available is a STEP option which first checks the data and then executes the matrix operations one step at a time. If errors are detected in the data, the matrix operations are skipped and the remainder of the processing sequence is executed as a DRY run only.

A second feature provided allows the user to process only selected matrix data. For example, if the user finds that after having assembled his solution structure he wishes to add new loading conditions, or he wishes to obtain normal modes but did not have the mass matrix, he may re-execute the sequence of matrix operations to process only the load or only the mass matrix.

A third feature is available for displaying all the relevant substructuring data generated by the program. The data items that can be printed automatically are listed in Table 3. Using the output options provided, the user can verify explicitly each and every connectivity. If desired, the user may also obtain lists of all the retained degrees of freedom of the resulting pseudostructure to verify the completeness and accuracy of his input. These are all identified by basic substructure grid point numbers.

The processing for any one analysis can be carried out across all three computer systems (CDC, IBM, and UNIVAC). That is, the SØF data file created on one computer may be written to magnetic tape and shipped to another center for processing on any of the three standard hardware systems. This facility allows for several contractors to participate in a cooperative analysis of complex structures using their own computer centers.

DATA MANAGEMENT

The key to data management for the new automated substructuring system is the Substructure Operating File, the SØF. This one file is structured to hold all the relevant information for each component substructure. All the data items required for any basic or component substructure are listed in Table 3. Also

TABLE 3. SØF DATA ITEMS REQUIRED FOR EACH COMPONENT SUBSTRUCTURE

<u>Item Name</u>	<u>Description</u>
EQSS	External grid point (using basic substructure IDs) and internal point equivalencing data including scalar indices and associated components for each internal point number
BGSS	Defines the geometric coordinates and local coordinate system ID for each internal point of a component substructure in terms of the basic coordinate system for that component
CSTM	Contains the coordinate transformation data for every local coordinate system referenced in the BGSS item
LØDS	Directory of set IDs for all loads on each contributing basic substructure defined in Phase 1
PLTS	Names of each contributing basic substructure and its basic coordinate system transformation data to be used in generating undeformed plots
SØLN	Contains either static solution vector identifiers by subcase or eigenvalue and eigenvector parameters
KMTX	Stiffness matrix
MMTX	Mass matrix
PVEC	Load vectors
PØVE	Load vectors on points omitted during matrix reduction
UPRT	Partitioning vector used in matrix reduction
HØRG	H or G transformation matrix
UVEC	Displacement vectors or eigenvectors
QVEC	Reaction force vectors

stored on the SØF are the Master Data Index (MDI) file which serves as the directory for each substructure, the Director Index Table (DIT) which contains the names of each component substructure in the MDI, and the NXT array which serves to chain together all the data blocks available on the SØF. To have access to any item of data on the SØF, only the item substructure names are required.

The SØF is a permanent file physically stored on a user disk pack, drum, or equivalent device. It is constructed as a direct access file to avoid long and costly searching. It is used to communicate the data between all different phases of a multi-level substructuring problem and is maintained independently from the usual NASTRAN files. This choice was made to avoid what would have been a severe overload of the existing NASTRAN facilities. For example, since each substructure requires at least 6 data blocks, a practical limit for the old NASTRAN facilities would have been reached with as few as 30 substructures. Table 1 lists the commands provided the user with which he can maintain and protect his data on the SØF.

A full set of utilities is provided to maintain the SØF as well as to store and retrieve specific data items as they are required by the processing modules. Though the SØF is considered to be a single logical file, it may be physically stored on one to ten devices. This feature provides the user with an open-ended file capability which may be extended dynamically as the analysis progresses and more space is required. It therefore serves as a combination data block pool and a checkpoint file between job steps.

By interrogating the MDI, the DIT and the NXT, the SØF utilities provided can be used to:

1. Create or destroy a substructure
2. Delete items associated with a substructure to recover from errors
3. Equivalence substructures
4. Randomly locate in the file selected items associated with any substructure
5. Read and write items on the SØF
6. Dump and restore data to tapes as backup, or permanent storage, or as overflow to reduce the number of physical files required at any one execution.

A significant additional capability has also been provided, unique in the history of NASTRAN. The SØF data created on one computer may be written to tape, shipped to another center, and read into a different computer. This inter-computer communication capability allows for construction of complex structural system models from substructures developed by different contractors, at widely separated locations and even on different computers.

PROGRAM CONTROL

The user exercises primary control over the execution of his analysis with the Substructure Control Deck commands listed in Table 1. One of the eleven new modules developed especially for substructuring, ASDMAP, processes the Substructure Control Deck. Its design allows for future adaptation of the substructuring concepts to processing with other Rigid Formats than the three provided with the current system, Rigid Formats 1, 2, and 3.

The central concept of ASDMAP was to translate each primary command and its related subcommands into appropriate DMAP ALTERS to the Rigid Format being executed. The ASDMAP module was designed to recognize the various matrix and dry run options, tabulate and check the substructure names, and diagnose the substructure control deck for user errors.

In the actual implementation, each of the substructure commands is interpreted with the aid of built-in block data tables. For each substructure operation, the basic DMAP statements, the allowable subcommands, the optional cards, and the entries to be changed in the DMAP sequence all are stored in the form of simple control tables. These tables are then used to direct the program execution. The ASDMAP module reads the cards associated with a command. It then generates the ALTER and DMAP card images, merges these with user-specified ALTER cards, and writes the merged set on the existing XALTER file, a logical file on the problem tape. The experienced user of NASTRAN retains the full flexibility of modifying and adapting the DMAP sequence produced to meet his own specialized requirements.

Inherent in the philosophy behind the design for the ten remaining substructure modules was the concept of an independent system using the NASTRAN subroutines for convenience while minimizing interaction with the remainder of NASTRAN. For this purpose, all of the substructure modules and the SØF file utilities were isolated to link 9 of NASTRAN. The number of input and output NASTRAN data blocks in the modules has been kept to a minimum, using the SØF files for the majority of data storage. In addition to the normal rules and restrictions on NASTRAN module design, the basic criteria for substructure modules were:

1. The NASTRAN matrix utility subroutines should be used for all matrix operations. This maintains compatibility with possible changes in future levels of the system.
2. Machine-dependent coding should be kept to a minimum. Only the initial file allocation for the SØF and the one SØF input/output routine are machine dependent.
3. The SØF file is basically a storage device and is not directly accessible by the NASTRAN utility routines. Matrix data from the SØF should be transferred to a scratch file before using the NASTRAN matrix utilities.
4. The format of each SØF data item should be kept independent of the level of combination; i.e., a basic substructure is assumed to be a combination substructure made up of only one component.

5. In addition to the NASTRAN parameters, certain control options may be stored on the internal Case Control data block. In particular, this method is used for passing the extensive control data required by the COMBINE and REDUCE operations in Phase 2.
6. If a non-trivial error in the data is detected, the DRY run parameter should be set and all possible effort should be made to complete the execution of that module. When the DRY run parameter is "ON", all further time consuming matrix operations should be skipped and every attempt should be made to check user input data and control parameters.

Extensive documentation has been added to the NASTRAN Programmer's Manual for every subroutine, data block, and file structure that was developed and/or modified for automated substructuring.

CONCLUDING REMARKS

The automated substructuring capability described above has been installed and tested on all three major hardware systems, CDC, UNIVAC and IBM. It will be implemented in NASTRAN Level 16.

The test system is being verified at a number of facilities across the country. Several fixes have been made since its delivery and certain enhancements have been suggested by its users. These enhancements are being considered in preparing the specifications for Level 16 installation.

With the support of these users who have been willing to experiment with the new system, who have delved into the code and offered specific coding suggestions, and who have reported their performance timing history, the automated multi-stage substructuring system will become a welcome and reliable addition to NASTRAN.

ACKNOWLEDGEMENTS

The authors wish to express their appreciation to Dr. D. J. Weidman of NSMO, for sponsoring this development project, and to Mr. H. P. Adam and Dr. E. C. Stanton of Douglas Aeronautics Company West, for monitoring its program under contract 6-73-182H with Universal Analytics, Inc.

APPENDIX

The following example illustrates an entire simple substructuring analysis. Figure A1 shows the basic substructures, TABLE and LEGS. Each has a loading specified; each has a different basic coordinate system; and each uses the same grid point identifiers. Figure A2 shows how these two components can be combined to make the final model using the reflective symmetry option.

The complete data decks to generate and analyze this structure are listed in Tables A1-A4. These include the data for generating the basic substructures in Phase 1, the assembly of the complete structure, solution, and data recovery in Phase 2, and the data recovery in Phase 3. A card-by-card explanation of their input demonstrates the simplicity of the new NASTRAN automated multi-stage substructuring system.

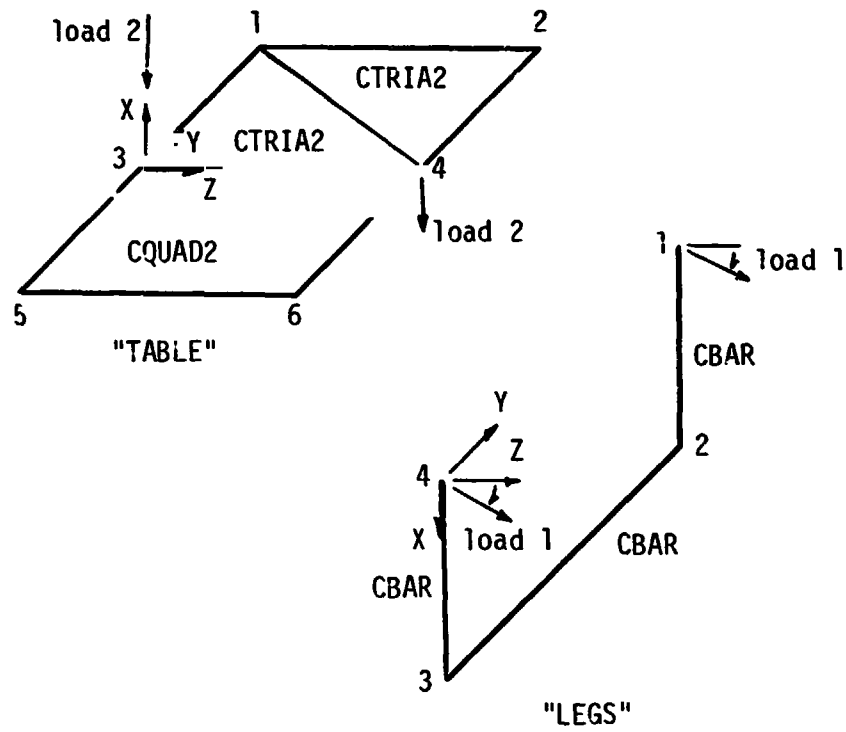


FIGURE A1. PHASE 1 - BASIC SUBSTRUCTURES (TABLE AND LEGS)

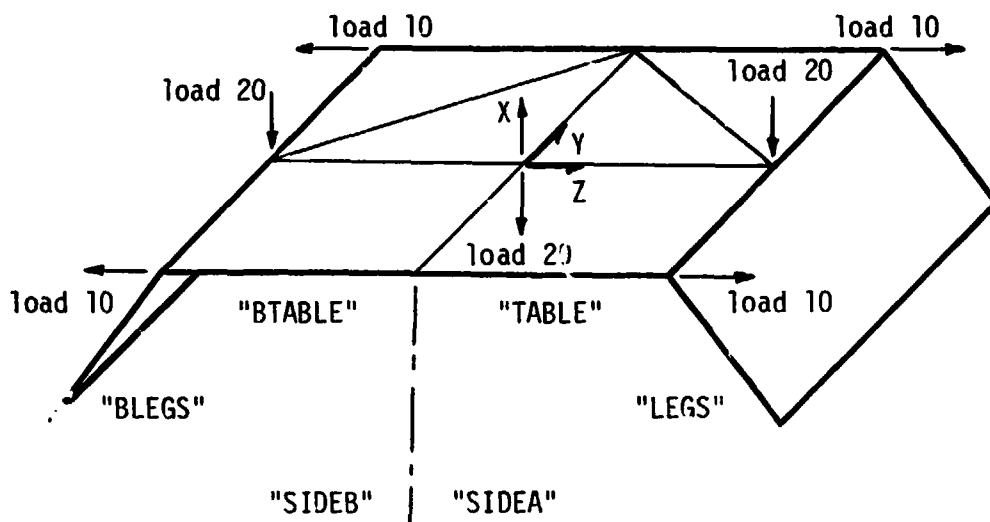


FIGURE A2. PHASE 2 - COMBINED SUBSTRUCTURE

TABLE A1. PHASE 1 DATA DECK FOR SUBSTRUCTURE TABLE

Card
No.

1 ID TABLE,BASIC
 2 APP DISP,SUBS
 3 SOL 2,0
 4 TIME 1
 5 CHKPNT YES
 6 CEND

 7 SUBSTRUCTURE PHASE1
 8 PASSWORD=PROJECTX
 9 SDF(1)=SDF1,250,NEW
 10 NAME=TABLE
 11 SAVEPLOT=1
 12 SDFPRINT TDC
 13 ENDSUBS

 14 TITLE=TABLE, PHASE ONE
 15 LOAD=2
 16 OUTPUT(PLOT)
 17 SET 1=ALL
 18 PLOT
 19 BEGIN BULK

	1	2	3	4	5	6	7	8	9	10
20	CQUAD2	3	2	5	6	4	3			
21	CTRIA2	1	1	1	2	4				
22	CTRIA2	2	1	3	4	1				
23	FORCE	2	3		10.0	-1.0				
24	FORCE	2	4		10.0	-1.0				
25	GRID	1		0.0	0.0	5.				
26	GRID	2		0.0	7.	5.				
27	GRID	3		0.0	0.0	0.0				
28	GRID	4		0.0	7.	0.0				
29	GRID	5		0.0	0.0	-5.				
30	GRID	6		0.0	7.	-5.				
31	GRID	7						123456		
32	MAT1	1	3.+7		.3	4.3				
33	PQUAD2	1	1	.1						
34	PTRIA2	1	1	.1						
35	ENDDATA									

TABLE A2. PHASE 1 DATA DECK FOR SUBSTRUCTURE LEGS

Card
No.

1 ID LEGS,BASIC
 2 APP DISP,SUBS
 3 SPL 2,0
 4 TIME 1
 5 CHKPNT YES
 6 CEND

 7 SUBSTRUCTURE PHASE1
 8 PASSWRD=PROJECTY
 9 SDF(1)=SDF4,7500
 10 NAME=LEGS
 11 SAVEPLOT=1
 12 SDFOUT INP3
 13 POSITION=REWIND
 14 NAME=LEGS
 15 EDIT(32) LEGS
 16 ENDSUBS

 17 TITLE=LEGS PHASE ONE
 18 LOAD=1
 19 OUTPUT(PLOT)
 20 SET 1=ALL
 21 PLOT
 22 BEGIN BULK

	1	2	3	4	5	6	7	8	9	10
23	CBAR	1	1	1	2	5			2	
24	CBAR	2	1	3	2	5			2	
25	CBAR	3	1	4	3	5			2	
26	FORCE	1	1		2.0	3.0	.0	4.0		
27	FORCE	1	4		2.0	3.0	.0	4.0		
28	GRID	1		0.0	10.	0.0				
29	GRID	2		5.	10.	0.0				
30	GRID	3		5.	0.0	0.0				
31	GRID	4		0.0	0.0	0.0				
32	GRID	5		100.	100.	0.0		123456		
33	MAT1	1	3.+7		.3	4.3				
34	PBAR	1	1	1.0	50.	100.	10.			
35	ENDDATA									

TABLE A3. PHASE 2 DATA DECK (COMBINE, REDUCE, SOLVE, AND RECOVER)

Card
No.

```

1 ID SUBSTR,PHASE2
2 APP DISP,SUBS
3 SOL 1,0
4 TIME 1
5 DIAG 23
6 CEND

7 SUBSTRUCTURE PHASE2
8 PASSWORD=PROJECTX
9 SDF(1)=SDF1,250
10 OPTIONS=K,M,P
11 SDFIN INP3,TAPE
12 POSITION=REWIND
13 NAME=LEGS
14 SDFPRINT TDC
15 COMBINE LEGS, TABLE
16 NAME=SIDEA
17 TOLER=0.001
18 OUTPUT=1,2,7,11,12,13,14,15,16,17
19 COMPONENT LEGS
20 TRANS=10
21 EQUIV SIDEA,SIDEB
22 PREFIX=B
23 COMBINE SIDEA,SIDEB
24 NAME=BIGTABLE
25 TOLER=0.001
26 OUTPUT=1,2,7,11,12,13,14,15,16,17
27 COMPONENT SIDEB
28 SYMT=Y
29 REDUCE BIGTABLE
30 NAME=SMALTABL
31 BOUNDARY=100
32 OUTPUT=1,2,3,4,5,6,7,8
33 SDFPRINT TDC
34 PLOT SMALTABL
35 SOLVE SMALTABL
36 RECOVER SMALTABL
37 PRINT BIGTABLE
38 SAVE BTABLF
39 SDFPRINT TDC
40 ENDSUBS

41 TITLE=PHASE TWO SUBSTRUCTURE
42 DISP=ALL
43 SPCF=ALL
44 LOAD=ALL
45 SPC=10
46 SUBCASE 1
47 LOAD=10
48 SUBCASE 2
49 LOAD=20
50 OUTPUT(PLOT)
51 SET 1=ALL
52 PLOT
53 BEGIN BULK

```

TABLE 12. (continued)

Card
No.

	1	3	4	5	6	7	8	9	10	
54	BDYC	100	LEGS	20	BLEGS	20				+A
55	+A		TABLE	10	BTABLE	10				
56	BDYS1	1C	4	1	3	4	5			
57	BDYS1	1C	123456	2	6					
58	BDYS1	20	123456	2	3					
59	LOADC	10	1.0	LEGS	1	1.0	BLEGS	1	1.0	
60	LOADC	20	1.0	TABLE	2	1.0	BTABLE	2	1.0	
61	SPCS1	10	BLEGS	123456	2	3				
62	SPCS1	10	BTABLE	4	1	3	4	5		
63	SPCS1	10	LEGS	123456	2	3				
64	SPCS1	10	TABLE	4	1	3	4	5		
65	TRANS	10	.0	7.0	-5.0	3.0	11.0	-5.0	+8	
66	+B	0.0	8.0	-5.0						
67	ENDDATA									

TABLE A4. PHASE 3 DATA DECK

Card
N.

1 ID TABLE,BASIC
2 APP DISP,SUBS
3 SOL 1,0
4 TIME 1
5 RESTART TABLE,BASIC (Restart deck)
6 CEND

7 SUBSTRUCTURE PHASE3
8 PASSWORD=PROJECTX
9 SDF(1)=SDF1,250
10 BRECOVER BTABLE
11 ENDSUBS

12 TITLE=PHASE THREE FOR REFLECTED TABLE
13 DISP=ALL
14 LOAD=ALL
15 SPCF=ALL
16 STRESS=ALL
17 SUBCASE 1
18 SUBCASE 2
19 LOAD=2
20 BEGIN BULK
21 ENDDATA

Phase 1 Data Deck for Substructure TABLE

- Card No.** Refer to Table A1 for input cards described below.
- 1-6 Standard NASTRAN Executive Control Deck except the 'SUBS' option is selected on the APP card.
 - 7 First card of Substructure Control Deck. Phase 1 is selected.
 - 8 Password protection on the SØF is 'PRØJECTX'.
 - 9 The SØF consists of one physical file with an index of one. (Indices must begin with one and increase sequentially.) The name of the file is 'SØF1' and it has a maximum size of 250,000 words. The file is to be initialized. (Internal pointers will be set to indicate that the SØF contains no data.)
 - 10 The basic substructure to be generated will be identified by the name TABLE.
 - 11 Plot set 1 will be saved on the SØF for performing plots of the combined structure in Phase 2.
 - 12 Print a table of contents for the SØF. This includes a list of all substructures and their data items.
 - 13 End of Substructure Control Deck
 - 15 Selects the load to be saved on the SØF for use in Phase 2. Note that multiple loads may be saved by using multiple subcases. In addition to external static loads, thermal loads and element deformation loads may be selected.
 - 16-17 Plot control cards are required if the SAVEPLOT subcommand is used in the Substructure Control Deck. These cards are used to define the plot sets for Phase 2 plotting. It is not necessary that a plot tape be set up in Phase 1.
 - 19-35 Standard NASTRAN Bulk Data Deck. These cards define the mathematical model of the basic substructure.

Phase 1 Data Deck for Substructure LEGS

- Card No.** Refer to Table A2 for input cards described below.
- 1-6 Standard NASTRAN Executive Control Deck except the 'SUBS' option is selected on the APP card.
 - 7 First card of the Substructure Control Deck. Phase 1 is selected.
 - 8 Password protection on the SØF is 'PPØJECTY'.
 - 9 The SØF consists of one physical file with an index of one. (Indices must begin with one and increase sequentially.) The name of the file is 'SØF4' and it has a maximum size of 7,500,000 words. The file has been used previously as an SØF.
 - 10 The basic substructure to be generated will be identified by the name LEGS.
 - 11 Plot set 1 will be saved on the SØF for performing plots of the combined structure in Phase 2.
 - 12-14 After substructure LEGS has been generated and saved on the SØF, it is copied out to user tape INP3.

Card
No.

- 15 All data items for substructure LEGS are removed from the SØF. (The substructure name remains in the SØF directory, however.)
- 16 End of Substructure Control Deck
- 18 Selects the load to be saved on the SØF for use in Phase 2. Note that multiple loads may be saved by using multiple subcases. In addition to external static loads, thermal loads and element deformation loads may be selected.
- 19-21 Plot control cards are required if the SAVEPLOT subcommand is used in the Substructure Control Deck. These cards are used to define the plot sets for Phase 2 plotting. It is not necessary that a plot tape be set up in Phase 1.
- 22-35 Standard NASTRAN Bulk Data Deck. These cards define the mathematical model of the basic substructure.

Phase 2 Data Deck

Card
No.

- Refer to Table A3 for input cards described below.
- 1-6 Standard NASTRAN Executive Control Deck except the 'SUBS' option is selected on the APP card. DIAG 23 requests an echo of the automatic DMAP alters generated.
- 7 First card of the Substructure Control Deck. Phase 2 is selected.
- 8,9 These cards specify the same SØF used in Phase 1 for substructure TABLE.
- 10 The card causes matrix operations to be performed on stiffness, mass, and load matrices. The default for Rigid Format 1 is stiffness and loads only. However, Rigid Format 2 was selected in the Phase 1 decks. This caused all three matrix types to be generated in Phase 1.
- 11-13 Basic substructure LEGS is copied to the SØF from user tape INP3.
- 14 Print the SØF table of contents.
- 15-20 Perform an automatic combination of substructures TABLE and LEGS. The resultant combined pseudostructure will be named SIDEA. The tolerance for connections is 0.001 units. Detailed output is requested. The basic coordinate system for substructure LEGS is transformed according to transformation set 10 in the Bulk Data.
- 21,22 Create a new secondary substructure SIDEB which is equivalent to SIDEA. This operation causes image substructures BLEGS and BTABLE to be generated.
- 23-28 Perform an automatic combination of substructures SIDEA and SIDEB. The resultant combined pseudostructure will be named BIGTABLE. The tolerance for connections is 0.001 units. Detailed output is requested. The basic coordinate system for pseudostructure SIDEB is symmetrically transformed about the XZ plane, identified by Y, the axis normal to the plane (sign change for all 'Y' degrees of freedom).
- 29-32 Perform a matrix reduction on the matrices of substructure BIGTABLE. The resultant reduced pseudostructure will be named SMALTABL. The retained degrees of freedom are selected in boundary set 100 in the Bulk Data. Detailed output is requested.
- 33 Print the SØF table of contents.
- 34 Plot pseudostructure SMALTABL. The plot control cards in the Case Control Deck are referenced.

- Card
No.
- 35 Perform a static solution of pseudostructure SMALTABL. The constraint sets and load sets selected in the Case Control Deck are used.
 - 36-38 Recover the displacements of substructures BIGTABLE and BTABLE from the solution of SMALTABL and save them on the SØF. Also, print the results for substructure BIGTABLE. The output requests in the Case Control Deck are referenced when the PRINT subcommand is invoked.
 - 39 Print the SØF table of contents.
 - 40 End of the Substructure Control Deck
 - 42-44 Case Control output requests. Referenced by the PRINT subcommand of the RECOVER command.
 - 45-49 Constraint and load set selections are referenced by the SØLVE command.
 - 50-52 Plot control cards are referenced by the PLØT command.
 - 54-58 These Bulk Data cards define the boundary set of retained degrees of freedom which was selected in the REDUCE operation (cards 29-32).
 - 59-64 These cards define the loads and constraints selected in the Case Control Deck for the substructure SØLVE operation.
 - 65,66 These cards define the transformation which is applied to the basic coordinate system of substructure LEGS in the first CØMBINE operation (cards 15-20).

Phase 3 Data Deck for Substructure BTABLE

- Card
No.
- Refer to Table A4 for input cards described below.
 - 1-6 Standard NASTRAN executive Control Deck except the 'SUBS' option is selected on the APP card. "Card" 5 is actually the Restart deck punched out in Phase 1 for substructure TABLE
 - 7 First card of the Substructure Control Deck. Phase 3 is selected.
 - 8,9 These cards specify the same SØF used in Phase 2.
 - 10 This card causes the data for the image basic substructure BTABLE to be copied from the SØF to GINØ data blocks. The data can then be used for data recovery operations, i.e., deformed structure plots, stresses, etc.
 - 11 End of Substructure Control Deck.
 - 13-16 Output requests for Phase 3 data recovery.
 - 17-19 The subcase definitions in Phase 3 must be identical to those used in the SØLVE operation in Phase 2. SPC and MPC constraints in Phase 3 must be the same as those used in Phase 1. Load sets selected in Phase 3 must correspond to those selected in Phase 2 for each subcase. However, load sets selected in Phase 2 which do not exist for this particular basic substructure can not be selected in Phase 3.

AUTOMATED MULTI-STAGE SUBSTRUCTURING ANALYSIS

COMPARED WITH SUPERELEMENT ANALYSIS

Lalit C. Shah

Rockwell International

ABSTRACT

Two large NASTRAN models for static analysis have been built by use of two different automated substructuring techniques currently available. The first model consists of about 30 000 degrees of freedom representing the Space Shuttle Crew Module. The second model consists of about 10 000 degrees of freedom representing the B-1 Nacelle. The automated multistage substructuring capability added to the level 15.5 was applied to the first model and some interesting lessons were learned from that experience. The superelement capability, available in MacNeal-Schwendler version of NASTRAN (CDC level 28), was applied to the second model. User convenience (automation) becomes increasingly important for large finite-element models. There are some significant differences between the two approaches in this area even though the basic matrix operations carried out are identical. In conclusion, some practical suggestions are presented that may be beneficial to other users.

(Paper was not available at time of publication.)

N75 31521

AN IMPROVED DMAP CAPABILITY

David L. Herendeen

Universal Analytics, Inc.
Playa Del Rey, California

SUMMARY

A set of improvements has been designed and implemented into a test version of the NASTRAN DMAP (Direct Matrix Abstraction Program) compiler. These modifications simplify the use of the DMAP control language while enhancing its power and versatility. The implemented changes are described and examples are presented to illustrate their use.

INTRODUCTION

Traditionally, the NASTRAN engineer-user has not felt comfortable with the DMAP capability. Its style is oriented to the programmer. It uses complicated semantic constructs that are overly formalized. Also, its implementation retains many undesirable and confusing restrictions.

Modifications have been made to the DMAP compiler to alleviate many of these disadvantages. Removal of certain restrictions has unlocked powers that have been imprisoned in the system since its inception. Full downward compatibility with currently operational DMAP has been retained.

These changes fall into three overlapping categories:

Improved Syntax

Removal of Restrictions

Extension of Capability

Improvements falling into the first two categories allow for the inadvertent introduction of errors into DMAP programs that previously would not be allowed. To protect the user, the extended capabilities include an error-handling facility, and a new class of POTENTIALLY FATAL ERRORS is defined. Thus, the system protects users from costly errors arising from incorrect DMAP while allowing the user freedoms he could not otherwise enjoy.

37

PRECEDING PAGE BLANK NOT FILMED

595

IMPROVED SYNTAX

Several cosmetic changes have been made by removing many of the semantic inconveniences. These syntax improvements include:

1. Abbreviation of the parameter section to eliminate the redundant use of the C, V, and N specifications. For instance, the parameter section of a DMAP instruction

```
/C,N,2/C,N,STATICS/V,N,NLOAD/V,N,PARAM=1.0
```

now may be written as

```
/2/*STATICS*/NLOAD/PARAM=1.0
```

2. Allowing the use of default parameters not only at the end of the parameter section, but also internal to it

```
/2/PARAM=1.0///4.5//NLOAD
```

3. Elimination of the need for trailing commas in both the input and output data block name lists when they are not required.

```
TABPT EST,,,// $
```

now may be written

```
TABPT EST// $
```

4. An automated checkpoint option controlled by a "predefined checkpoint" (PRECHK) declaration has been implemented. An analyst may generate all required checkpoint instructions by a single statement such as

```
PRECHK A,B,C,D,F,X $
```

Even more convenient forms have been implemented,

```
PRECHK ALL $
```

```
PRECHK ALL EXCEPT A,B,C $
```

This extension still allows the user to place the conventional CHPNT instruction throughout his program.

5. An automated SAVE specification to be included within the parameter section of the module instruction rather than a separate declaration.

```
MDX A,B/C/V,N,P1/V,N,P2 $
```

```
SAVE P2 $
```

now may be written

`MØDX A,B/C/P1/S,N,P2 $`

The effects of (4) and (5) above are much more than superficial. When combined and used appropriately, they reduce the length of DMAP routines (i.e., Rigid Format 1) by as much as 30%.

This more concise code is superior in structure and is made more readable by eliminating many statements that are not essential to the solution flow. Such structure allows for more rapid understanding of the solution algorithm. The automatic SAVE prevents the accidental misplacement of the SAVE instruction that formerly caused a dump. Such a misplacement is now handled correctly and does not cause an abnormal termination.

Though most of the above changes are cosmetic in nature, the improvements described next offer significantly improved capabilities.

REMOVAL OF RESTRICTIONS

There are many capabilities intrinsically available via the DMAP language that cannot be exploited because of the arbitrary restrictions imposed by the current DMAP compiler. The following changes have been made to remove these restrictions and greatly enhance the power of the language:

1. Data blocks may now appear as input before they appear as output.
2. Data blocks may now appear more than once as output.
3. The REPT instruction has been modified to allow a variable number of loops to be determined during execution. This usage is exemplified by

`REPT LØØPTØP,NLØØP $`

where `NLØØP` is a parameter output by some module prior to the REPT instruction.

4. The severely restrictive positional requirements of the EQUIV instruction have been eliminated.

The removal of the first two restrictions and the addition of the variable REPT instruction opens new vistas for the DMAP user. In addition, change (2) allows locally used data block names to be reused later; thus the efficiency of file allocation within the NASTRAN system is increased. The positional requirements of the EQUIV module that have accounted for many confused hours of debugging have been eliminated. The single requirement is that the primary data block of the EQUIV instruction must appear as output prior to the EQUIV.

The DMAP user now has the tools with which to design and execute sophisticated iterative algorithms. Such facilities have been long desired within the NASTRAN environment for solving complex nonlinear problems which involve either single or nested looping.

EXTENSION OF CAPABILITY

New capabilities have been added that on the surface appear to be very simple, yet they have profound effects on the flexibility of file operations, on user understanding, and on program control. These are

1. The implementation of two modules, COPY and SWITCH.
2. A new technique for user-specified compiler options, including a detailed cross reference of data block names, module names, and variable parameter names, and a complete and detailed OSCAR dump.
3. Specification and control of the extended error-handling facility.

The COPY and SWITCH modules are of great use in iterative DMAP routines. COPY performs a complete physical copy from the specified input data block to the output data block. SWITCH operates directly on the FIAT (File Allocation Table) to interchange data block names. It does not copy data.

The combination of these modules greatly simplifies and shortens DMAP looping. For example, in Figure 1, the DMAP code for raising a matrix [Q] to the rth power is shown in the original DMAP and again in the improved and extended DMAP. The simplification that results is immediately apparent.

Special compiler options may be elected, not through the DIAG, but by a new instruction XDMAP (Execute DMAP). Convenient options include: COPY/NOCOPY to allow a compilation only; LIST/NOLIST for DMAP compilation listing; DECK/NODECK to request the punching of the DMAP program; REF/NOREF to provide a cross reference; and OSCAR/NOOSCAR to print a detailed listing of all OSCAR records generated by the compiler. The OSCAR (Operation Sequence Control Array) is the "object" code that DMAP generates and is used to direct the actual computational flow. Also activated by the XDMAP instruction is the extended error-handling facility described below. These features are easy to use and helpful to both programmers debugging DMAP programs and engineers/analysts having to write their own routines or make local modifications to existing DMAP.

The extended error-handling facility justifies the removal of restrictions and improvement of capabilities in that it assures the user that gross logic errors in DMAP programs will not be costly. This feature helps the user diagnose and solve any problems caused by the new semantics. A new class of POTENTIALLY FATAL ERRORS warns the user to review his operations carefully. The user can select the error level (WARNING, POTENTIALLY FATAL, or FATAL) at which termination of the job will occur. Examples of XDMAP instructions are

XDMAP GØ,LIST,ERR=3 \$

XDMAP NØGØ,LIST,REF,ØSCAR,ERR=1 \$

Figure 2 shows a composite illustration of the detailed cross reference, while Figure 3 is an excerpt from an ØSCAR listing. Both of these figures are derived from the Level 15.5 Rigid Format 1.

CONCLUSION

Changes have been designed and implemented into the DMAP compiler that have improved the syntax and simplified DMAP usage for the engineer/analyst. Also, convenient mechanisms have been added to extend the file manipulation features. Finally, the removal of arbitrary compiler restrictions has unlocked implicitly existing capabilities which greatly enhance the flexibility of the language.

ACKNOWLEDGMENTS

The author wishes to express his appreciation to the NASTRAN Systems Management Office (NSMO) for sponsoring this effort. The work was performed by Universal Analytics, Inc., and monitored by McDonnell Douglas Astronautics Company - West. The author also wishes to thank Messrs. D. Herting and R. Hoesly for their valuable insight and diligent assistance in this effort.

OLD SYNTAX

```

1 BEGIN $
2 MATPRN Q,.,., // $
3 PARAM // C,N,NOP / V,N,TRUE=-1 $
4 PARAM // C,N,SUB / V,N,RR / V,Y,R=-1 / C,N,2 $
5 PARAM // C,N,NOP / V,N,FALSE=+1 $
6 COND ERROR1,RR $
7 ADD Q, / QQ $
8 LABEL DØIT $
9 EQUIV QQ,P / FALSE $
10 MPYAD Q,QQ, / P / C,N,0 $
11 EQUIV P,QQ / TRUE $
12 PARAM // C,N,SUB / V,N,RR / V,N,RR / C,N,1 $
13 COND STOP,RR $
14 REPT DØIT,1000000 $
15 JUMP ERROR2 $
16 LABEL STOP $
17 MATPRN P,.,., // $
18 EXIT $
19 LABEL ERROR1 $
20 PRTPARM // C,N,-1 / C,N,DMAP $
21 EXIT $
22 LABEL ERROR2 $
23 PRTPARM // C,N,-2 / C,N,DMAP $
24 EXIT $
25 END $

```

NEW SYNTAX

```

1 BEGIN $
2 MATPRN Q // $
3 PARAM // *SUB* / RR / V,Y,R=-1/2 $
4 COND ERROR1, RR $
5 COPY Q / P $
6 LABEL TØP $
7 SWITCH P,QQ // $
8 MPYAD Q,QQ / P / 0 $
9 REPT TØP,RR $
10 MATPRN P $
11 EXIT $
12 LABEL ERROR1 $
13 PRTPARM // -1 / *DMAP* $
14 END $

```

Figure 1.- Pairing a matrix Q to the power R.

LFVEL 2.0 DMAP COMPILEK - DMAP CROSS REFERENCE LISTING

DATA BLOCK	DMAP STATEMENT NUMBERS	PARAMETER	TYPE	DMAP STATEMENT NUMBERS	MODULE NAME	DMAP STATEMENT NUMBERS
RGFDT	0004*					
CASECC	0015	0025	I	0040	0095	0119 0123
CSTM	0004*	0006	I	0123		
DTT	0032	0035	I	0035	0040	0095 0119
DM	0057	0059	I	0093		0100
ECPT	0025*	0030	I	0032		
ECT	0027*	0004	I	0035		
ENT	0095	0119	I	0025		
ELSETS	0009*	0015	I	0019	0123	
EPT	0025					
EOEXIN	0004*					
EST	0025*	0010	I			
GEI	0025*	0010	I			
GEOM1	0004					
GFORM2	0004					
GFORM3	0020					
GFORM4	0053					
GM	0057					
GN	0057					
GPCT	0025*	0010	I			
GPT	0004*	0006	I			
GPL	0004*	0006	I			
GPSETS	0009*	0015	I			
GPST	0029	0030	I			
GPTY	0020*	0024	I			
KAA	0077	0078	I			
KFF	0071	0072	I			
KFS	0057	0059	I			
KGCX	0032*	0033	I			
KGG	0044	0045	I			
KLL	0083	0084	I			
KLR	0057	0059	I			
KNN	0058	0059	I			
KON	0057	0059	I			
KRR	0057	0059	I			
KSS	0057	0059	I			
LLL	0049*	0010	I			
LNO	0057	0059	I			
MCC	0021	0024	I			
MPT	0012	0035	I			
DEF1	0119*	0120	I			
DEF1	0119*	0120	I			
GPST	0029	0030	I			
GPNG	0040*	0041	I			
OPG1	0119*	0120	I			
OPG1	0119*	0120	I			

MODULE NAME	DMAP STATEMENT NUMBERS
COND	0014 0020 0031 0014 0039 0046 0055
EXIT	0099 0106 0112 0116 0122
GPSP	0061 0061 0061
GPNG	0040 0040 0040
GPI	0004 0004 0004
GP2	0007 0007 0007
GP3	0020 0020 0020
GP4	0053 0053 0053
JUMP	0051 0114 0127
MATGPO	0107 0108
MCF1	0046 0046 0046
MCF2	0048 0048 0048
OFF	0041 0041 0041
PARAM	0022 0022 0022 0050 0056 0115
PLOT	0115 0123 0123
PLTST	0009 0009 0009
PRMSG	0011 0011 0011 0125 0137
PRMAPH	0131 0131 0131 0135 0137
RAMP1	0046 0046 0046

Figure 2.- Composite illustration of the DMAP cross reference.

LEVEL 2.0 NASTRAN DMAP COMPILER - OSCAR LISTING

```

.....
OSCAR RECORD NUMBER 2  MODULE TYPE = 1
MODULE NAME - GP1  DMAP INSTRUCTION NO. 4

SUMMARY OF INPUT DATA BLOCKS( 3 )
GEOH1  0/ 2/0/  ?
GFGM2  0/ 17/0/  5
*****INPUT DATA BLOCK 3 IS NULL

SUMMARY OF OUTPUT DATA BLOCKS( 6 )
GPL  0/ 99/0/  55
EOEXIN  0/ 104/0/  47
GPOT  0/ 99/0/  22
CSTM  0/ 104/0/  13
RGPOT  0/ 104/0/  13
SIL  0/ 108/0/  13

SUMMARY OF PARAMETERS( 3 )
LUSET ( I ) 0
CONSTANT( I ) 123
NOGPOT ( I ) 0

OSCAR RECORD NUMBER 3  MODULE TYPE = 4
MODULE NAME - XSAVF  DMAP INSTRUCTION NO. 5

PARAMETERS TO BE SAVED( 1 )
LUSET 1

OSCAR RECORD NUMBER 4  MODULE TYPE = 4
MODULE NAME - XCHK  DMAP INSTRUCTION NO. 6

DATA BLOCKS TO BE CHECKPOINTED( 6 )
LQFXIN  GPOT  CSTM  BGPOT  SIL

OSCAR RECORD NUMBER 5  MODULE TYPE = 1
MODULE NAME - GP2  DMAP INSTRUCTION NO. 7

SUMMARY OF INPUT DATA BLOCKS( 2 )
GFGM2  0/ 17/0/  17
EOEXIN  0/ 104/0/  7

SUMMARY OF OUTPUT DATA BLOCKS( 1 )
ECT  0/ 22/0/  7

```

```

.....
OSCAR RECORD NUMBER 6  MODULE TYPE = 4
MODULE NAME - XCHK  DMAP INSTRUCTION NO. 8

DATA BLOCKS TO BE CHECKPOINTED( 1 )
FCY

OSCAR RECORD NUMBER 7  MODULE TYPE = 1
MODULE NAME - PLTSET  DMAP INSTRUCTION NO. 9

SUMMARY OF INPUT DATA BLOCKS( 3 )
PCOB  0/ 7/0/  7
EOEXIN  0/ 104/0/  13
FCY  0/ 22/0/  22

SUMMARY OF OUTPUT DATA BLOCKS( 4 )
PLTSETX  0/ 9/0/  9
PLTFAR  0/ 104/0/  13
GPSETS  0/ 108/0/  13
ELSETS  0/ 108/0/  13

SUMMARY OF PARAMETERS( 2 )
NSIL ( I ) 0
JUMPPLOT( I ) 0

OSCAR RECORD NUMBER 8  MODULE TYPE = 4
MODULE NAME - XSAVE  DMAP INSTRUCTION NO. 10

PARAMETERS TO BE SAVED( 2 )
NSTL 1
JUMPPLOT 2

OSCAR RECORD NUMBER 9  MODULE TYPE = 2
MODULE NAME - PRTHSG  DMAP INSTRUCTION NO. 11

SUMMARY OF INPUT DATA BLOCKS( 1 )
PLTSETX  0/ 9/0/  9

OSCAR RECORD NUMBER 10  MODULE TYPE = 2
MODULE NAME - SFTVAL  DMAP INSTRUCTION NO. 12

SUMMARY OF INPUT DATA BLOCKS( 1 )
*****INPUT DATA BLOCK 1 IS NULL

```

Figure 3.- Excerpt from an OSCAR listing.

DELTA WING FLUTTER BASED ON DOUBLET LATTICE

METHOD IN NASTRAN*

Howard Jew

N75 31522

Lockheed Electronics Company, Inc.,
Aerospace Systems Division
Houston, Texas

SUMMARY

The subsonic doublet-lattice method (DLM) aero-elastic analysis in NASTRAN was successfully applied to produce subsonic flutter boundary data in parameter space for a large delta wing configuration. Computed flow velocity and flutter frequency values as functions of air density ratio, flow Mach number, and reduced frequency are tabulated. The relevance and the meaning of the calculated results are discussed. Several input-deck problems encountered and overcome are cited with the hope that they may be helpful to NASTRAN Rigid Format 45 users.

PARAMETER SPACE

Flight velocity consideration and earth atmospheric properties suggest that subsonic aerodynamic wing flutter may take place in lifting flight through dense air (see Kuethe and Schetzer, reference 1). Based on atmospheric properties between 15-24 km (50 000 feet) altitude and the ground, the dimensionless air density parameter can be specified as follows:

$$.12 \leq \text{air density ratio} \leq .967$$

referred to sea level

In subsonic flight, a Mach number range can also be specified:

$$.25 \leq \text{Mach number} \leq .95$$

Another dimensionless parameter, the reduced frequency, may be assigned a usual flutter-producing range:

$$.10003 \leq \text{reduced frequency} \leq .200$$

These three-number intervals form a parameter-space volume within some part of which the delta wing could flutter.

*This work was performed under NASA Johnson Space Center contract NAS 9-12200.

THE NASTRAN AEROELASTIC METHOD

The organization of the aeroelastic analysis area in NASTRAN is described by figure 1, which shows the major program flow of a portion of Rigid Format 45.

A NASTRAN solution of the flutter equations goes through the 13-step sequence shown in figure 1. A short description of the thirteen (13) steps in terms of NASTRAN aeroelastic program modules follows.

- (1) Step 1 sets up tables, structural matrices, and geometry data after real eigenvalue analysis.
- (2) Module APD processes the aero data cards, and sets up aero tables. (SET1 referencing comes in here.)
- (3) Modules PLOT and PLTSET form undeformed aero/structure plots. (PLOT cards come in here.)
- (4) Module GI forms matrix G_{ka}^T for interpolation from structural to aerodynamic degrees of freedom. (CORE SIZE limit and matrix singularity may appear.)
- (5) Module AMG obtains aero matrix A_{jj} , area matrix S_{kj} , downwash matrices D_{jk}^1 and D_{jk}^2 .
- (6) Module AMP calculates the aero matrix list corresponding to the modal coordinates.
- (7) Module FA1 computes mass matrix M_{hh}^x , stiffness matrix K_{hh}^x , and looping table. (Doublet lattice computation enters at this point.)
- (8) Module CEAD extracts complex eigenvalues and normalizes eigenvectors. (Hessenberg solution enters here.)
- (9) Modules VDR and OFP prepare complex eigenvectors and place them on system output file for printing.
- (10) Module FA2 appends eigenvalues, eigenvectors, case control, and V-g plot data to appropriate tables.
- (11) Module XYTRAN prepares V-g plots under XYOUT requests, and module XYPLOT forms V-g plots for offline plot.
- (12) Module DDR1 converts eigenvectors from modal to physical coordinates. Module SDR1 recovers dependent components of eigenvectors and also single-point forces of constraint. Module SDR2 computes element forces and stresses for output.
- (13) Module PLOT obtains deformed plots of the structural and aero points.

DELTA WING MODEL DESCRIPTION

In this work the delta wing configuration is structurally modelled as in figure 2; aerodynamically, it is modelled as in figure 3. Figure 2, in fact, is a 3-dimensional figure, with only the top of the wing shown for sake of clarity. It should be noted that the modelled wing consists of a double delta, a flap, and an aileron. Furthermore, figure 3 shows respective trapezoidal boxes of the four panels used to represent delta 1 (boxes 101-108), delta 2 (109-144), flap (145-154), and aileron (155-166). The wing structure is represented by

18 quadrilateral panels
1182 rods
657 shear elements
90 triangular membranes
508 grid points
191 plot elements
4 splines

together with their respective physical properties and geometric coordinates.

RUN-DECK PROBLEMS

The several deck-associated problems found and eliminated are identified in figure 1, next to the modules where they were found.

- FLUTTER card specified surface splining when linear splining was needed; S was changed to L in field 7.
- EIGC card in conflict with FLUTTER card; number of eigensolutions didn't agree with number of eigenvectors; a weakness in the Hessenberg method was strengthened by setting the number of eigenvectors equal to the minimum of the number of desired eigenvectors (on FLUTTER) and the number of eigenvectors found (on EIGC).

SET1 referencing, insufficient core for splining, and XYPLOT peculiarity are really extra-deck problems found; they are beyond the scope of this paper, but their solutions were accomplished by Howard Jew and Edward Hess, at Lockheed Electronics Company, Inc.

FLUTTER COMPUTATION

The doublet-lattice method in NASTRAN is adequately described in Doggett and Harder (reference 2). Computation modularly goes through the 13-module package shown in figure 1. Flutter results for the delta wing were obtained at the Johnson Space Center and Lockheed, Houston, using the UNIVAC-1110 computer, and running on NASTRAN Level 15.6.4S.

First a checkpointed cold start was made, taking about 30 minutes SUP time. Subsequent runs, going through various points within the parameter space volume domain cited above, were made as restarts from this single checkpointed run, each restart finishing in about 29 minutes SUP time.

Although numbers entered the computer run deck in English units, the results were converted to the International System of Units for presentation in this paper.

FLUTTER RESULTS

Table 1 summarizes the available flutter boundary data of the delta wing for points in a parameter space subvolume having air density ratio, flow Mach number, and reduced frequency coordinates. The corresponding dependent quantities are the critical flow velocity in meters/sec and the critical flutter frequency in Hz. For example, in row 7 of table 1, at air density ratio = .967, Mach number = .70, and reduced frequency = .200, the delta wing, if flown, would flutter at frequency of 2.89 Hz for flow speed of 194 m/sec.

Figure 4 illustrates a typical damping coefficient as function of flow velocity for various reduced frequencies (k). For the $k = .200$ curve, the two values of flow velocity at which the damping coefficient vanishes, are critical flow velocities 219 and 283 meters per second as shown in table 1. At (.967, .45, .200) the delta wing would flutter at a frequency of 3.25 Hz for a flow speed of 219 m/sec. However, at (.967, .45, .200), within the flow speed range of 219 to 283 m/sec, any small disturbance on the delta wing would be aerodynamically amplified and destroy the wing if unchecked. At (.967, .45, .200), for flow speed < 219 m/sec and > 283 m/sec, any small disturbance on the wing would be aerodynamically damped. In other words, at (.967, .45, .200) the range of flow speed between 219 and 283 meters per second is unstable and small disturbances could build up through the mechanism of the fluttering wing continuously absorbing energy from the air stream (cf. Fung, reference 3).

Figure 5 illustrates flutter frequency as a function of flow velocity for various reduced frequencies. This is the companion figure to figure 4. Note that these frequency curves are all nearly linear functions of flow velocity. On the other hand, damping coefficient is a nonlinear function of flow velocity; see figure 4 curves. The flutter frequency as a function of flow velocity may be estimated from a very few points. However, reliable predictions of damping coefficient as a function of flow velocity cannot be made.

CONCLUDING REMARKS

- Delta wing flutter in the subsonic range could take place if the wing were flown, for a length of time, inside the flutter parameter space subvolume covered by table 1.
- Critical flutter frequency values summarized in table 1 are well within the expected range of 1-15 Hz for large wings.
- The flutter frequency results (see figure 5) appear not only reasonable but also consistent, indicating that a good flutter calculation has been achieved using the DLM in NASTRAN.

REFERENCES

1. Kuethe, A. M., and Schetzer, J. D.: Foundations of Aerodynamics, John Wiley & Sons, Inc., New York, Second Edition, 1963.
2. Doggett, Robert V., Jr., and Harder, Robert L.: Subsonic Flutter Analysis Addition to NASTRAN. NASTRAN: Users' Experiences. NASA TM X-2893, 1973, pp. 507-529.
3. Fung, Y. C.: The Theory of Aeroelasticity, GALCIT Aeronautical Series, John Wiley & Sons, Inc., London, 1955.

AIR DENSITY RATIO	FLOW MACH NUMBER	REDUCED FREQUENCY	CRITICAL FLOW VELOCITY (m/sec)	CRITICAL FLUTTER FREQUENCY (Hz)
.121	.85	.167	991	12.3
.484	.95	.167	208	2.57
.484	.95	.167	344	4.28
.484	.85	.125	184	1.71
.484	.70	.125	200	1.86
.484	.45	.125	169	1.58
.967	.70	.200	194	2.89
.967	.45	.200	219	3.25
.967	.45	.200	283	4.61
.967	.25	.200	200	3.00

Table 1. — Flutter boundary of delta wing.

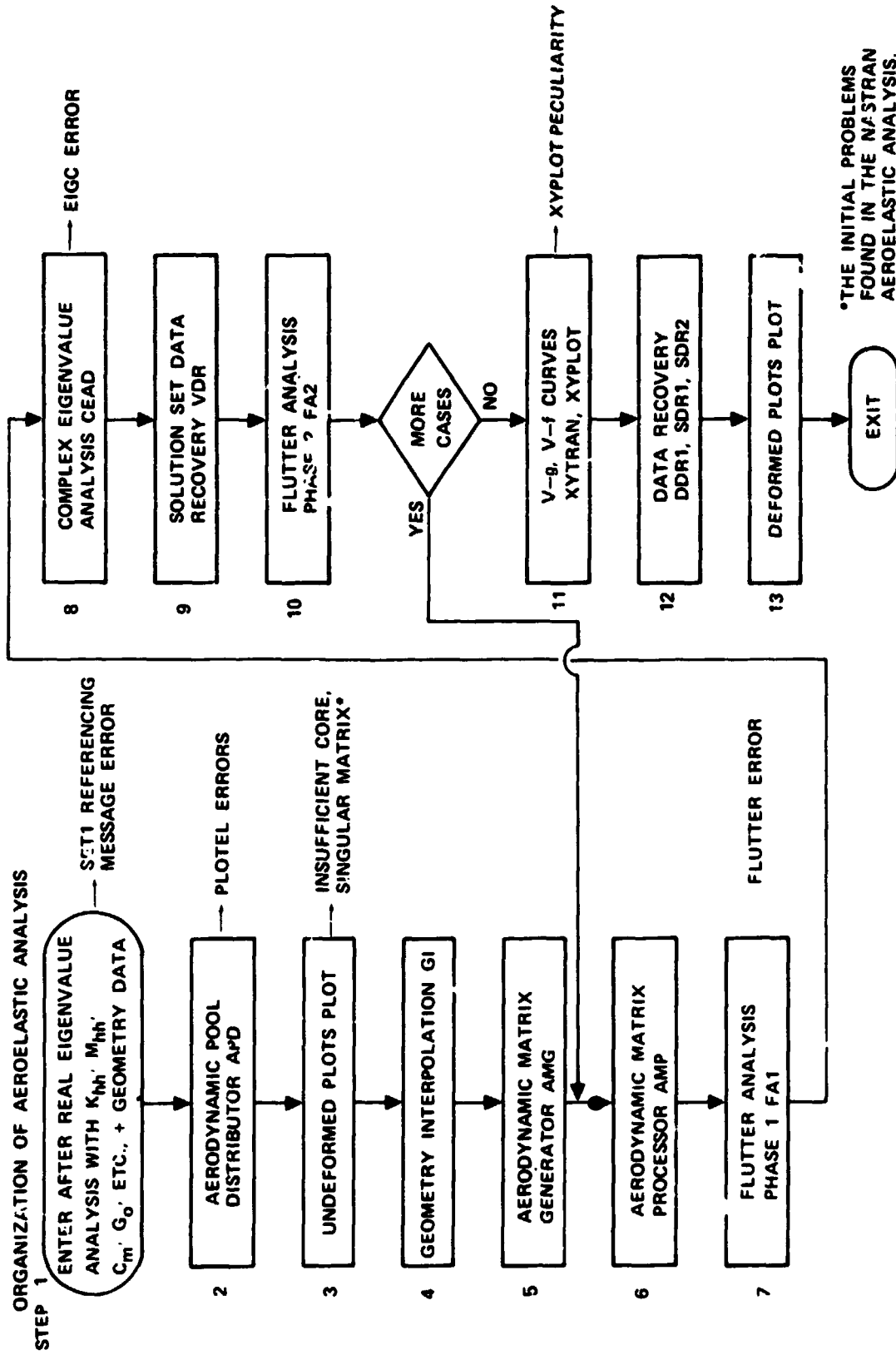


Figure 1. — Modal flutter analysis rigid format 45.

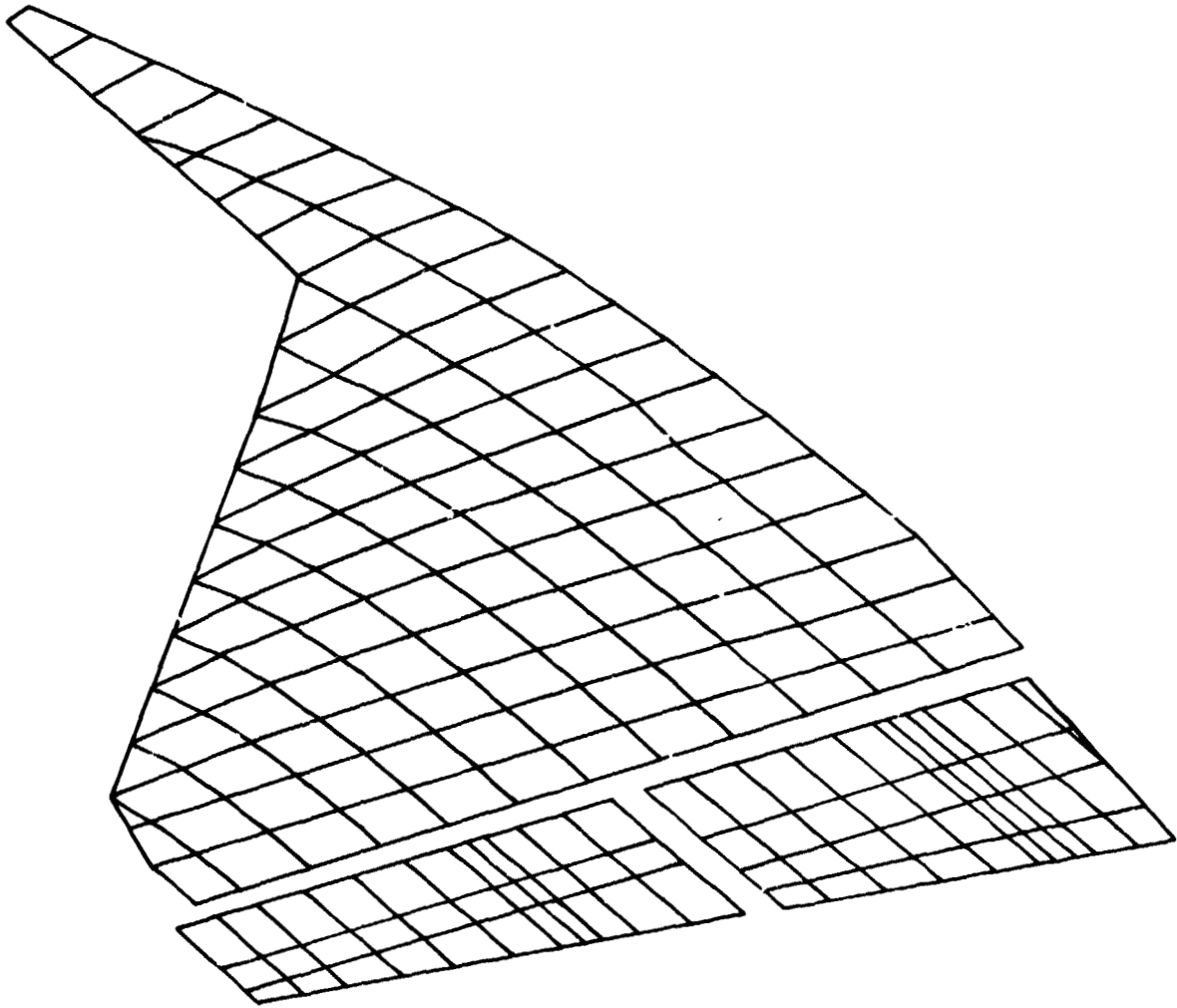


Figure 2. — Structural model of delta wing.

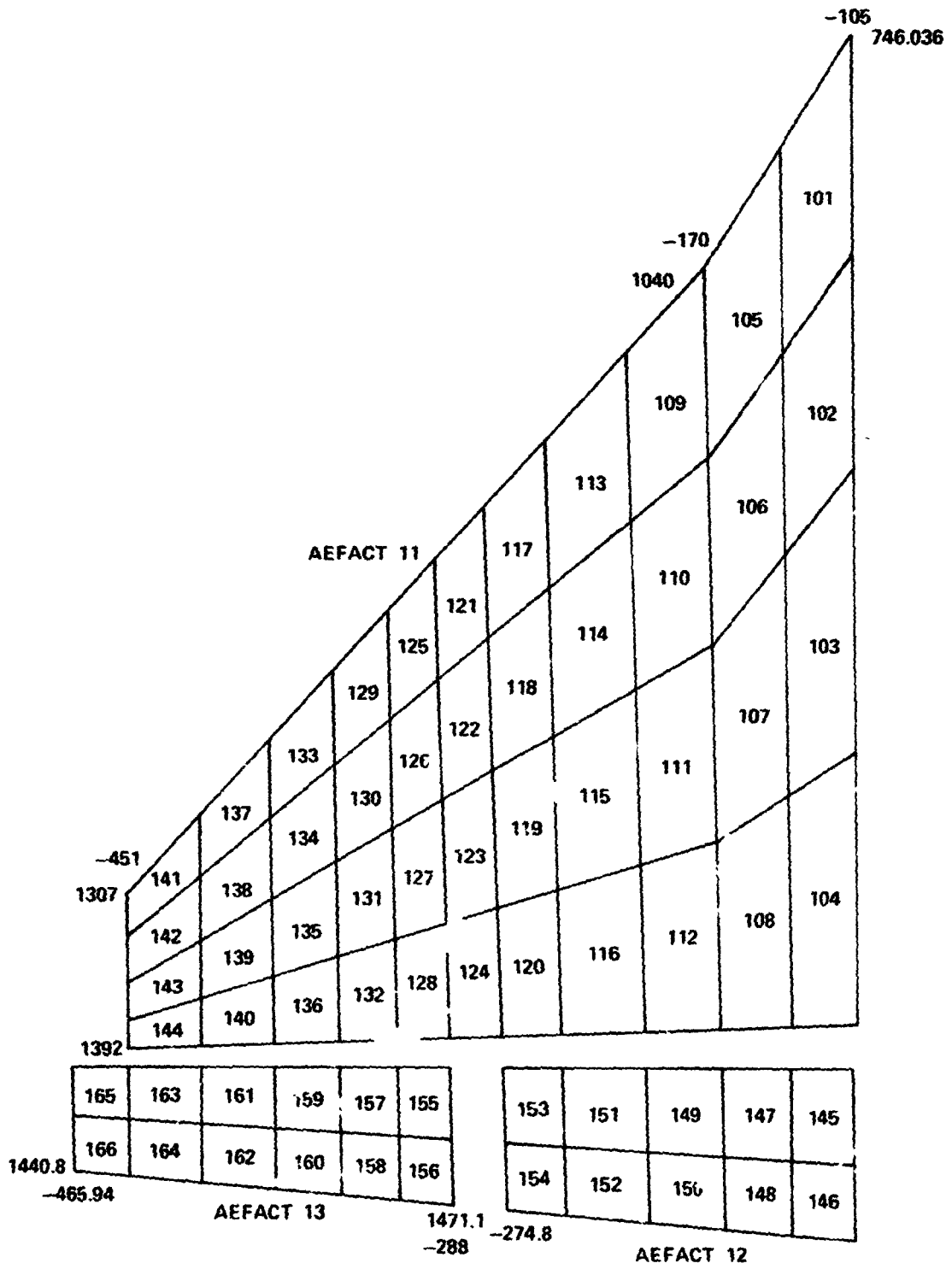


Figure 3. - 66 Aero-box model of delta wing.

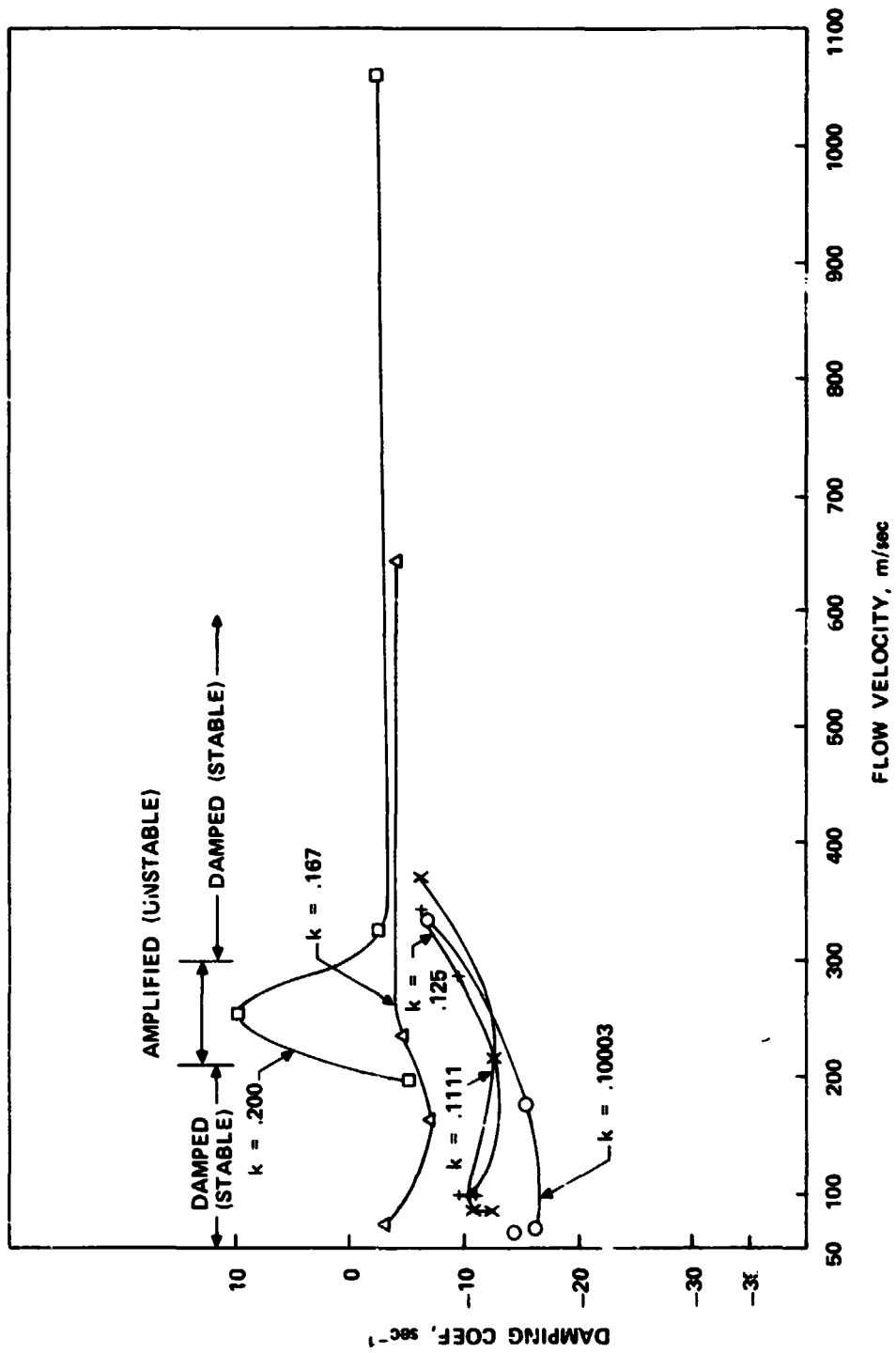


Figure 4. — Damping coefficient versus flow velocity at
 AIR DENSITY RATIO = .967
 FLOW MACH NUMBER = .45

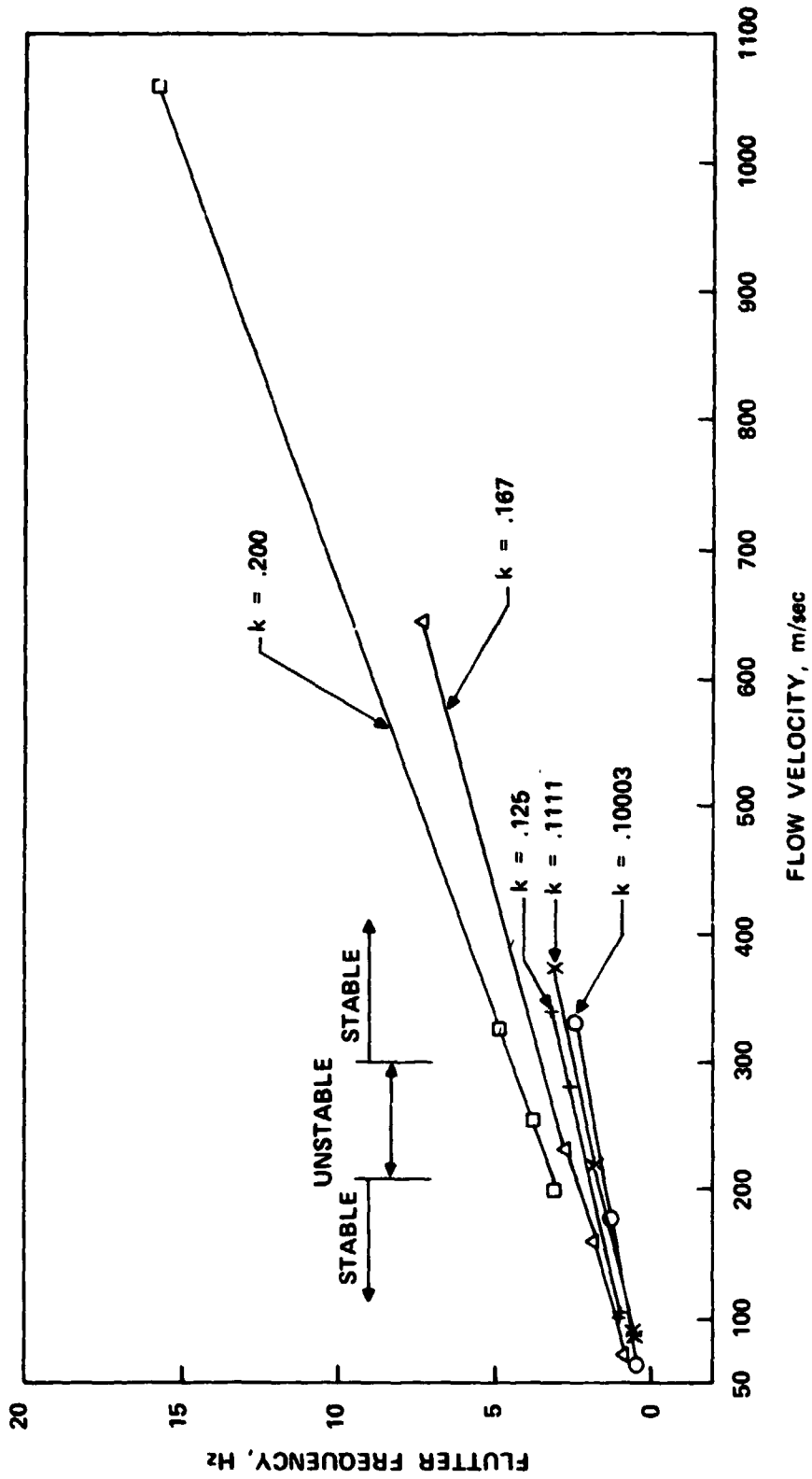


Figure 5. — Flutter frequency versus flow velocity at
 AIR DENSITY RATIO = .967
 FLOW MACH NUMBER = .45

N75 31523

NASTRAN MODELING AND ANALYSIS OF RIGID
AND FLEXIBLE WALLED ACOUSTIC CAVITIES

Joseph A. Wolf, Jr., and Donald J. Nefske

Research Laboratories
General Motors Corporation
Warren, Michigan

SUMMARY

The acoustic slot elements, CSLOTi, have been applied to analyze two-dimensional enclosures with fixed or moving boundaries. The capability has been utilized to compute (a) the acoustic natural modes and frequencies of a rigid walled enclosure and (b) the sound pressure at any point inside an enclosure when the surrounding walls are forced to vibrate. Applications to an automobile passenger compartment illustrate the technique.

The axisymmetric fluid elements, CFLUIDi, have been used in conjunction with a suitable choice of symmetry planes and a model of the surrounding structure to approximate a two-dimensional enclosure with flexible walls. The enclosure walls are modeled using finite elements or structural modes. Illustrative examples include a comparison of rectangular cavity modes with those calculated using the acoustic slot element and the free vibration modes of two enclosures coupled through a flexible rectangular panel.

INTRODUCTION

Modification of the NASA Structural Analysis (NASTRAN) program for connected slot acoustic analysis was first discussed by Herting et al. (Ref. 1) at the 1971 NASTRAN Users' Colloquium. This capability was later included in NASTRAN, along with an axisymmetric hydroelastic model, as documented in the NASTRAN Theoretical and User's Manuals (Refs. 2 and 3). The capability provided for therein includes rigid or moving wall two-dimensional slot models and rigid, moving, or elastic wall axisymmetric models.

The present paper describes some adaptations of this acoustic analysis capability which have not been described in the NASTRAN documentation, and it illustrates these adaptations through applications to some problems of practical interest. Examples include calculation of acoustic modes and frequencies for irregularly shaped cavities, calculation of frequency response for piston-like wall excitation of an acoustic cavity slot-model, use of axisymmetric hydroelastic elements to approximate a two-dimensional cavity with flexible walls, and modeling of cavities coupled through flexible panels. The implementation is within the present NASTRAN framework and involves no new element or rigid format alterations.

39

ACOUSTIC FINITE ELEMENT MODELING WITH THE CSLOT_i ELEMENT

The acoustic slot-element capability of NASTRAN was originally developed by Herting et al. (Ref. 1) and is described in Section 16.2 of the Theoretical Manual (Ref. 2) and Section 1.9 of the User's Manual (Ref. 3). While the slot elements -- CSLOT3 (a triangular element) and CSLOT4 (a quadrilateral element) -- were originally intended for analyzing slotted regions which extend radially outward from a central core (such as the lobes of a rocket motor cavity), it has been noted that "The slot elements can also be used . . . to solve both static and dynamic two-dimensional potential problems including, in addition to acoustic problems, fluid flow, heat conduction, gravity waves in shallow water, electrical wave transmission, etc." (Ref. 2, p. 16.2-2). However, the implementation of these elements to treat such two-dimensional problems has not been discussed in the NASTRAN documentation, and the purpose of this paper is to describe such an application to treat one of these problems -- namely, the acoustics of two-dimensional, irregularly shaped enclosures with rigid or moving walls. Specifically, the use of the slot elements is illustrated for computing (a) the acoustic natural modes and frequencies of a rigid walled enclosure (Normal Modes Analysis) and (b) the sound pressure at any point inside an enclosure when the surrounding walls are forced to vibrate (Direct Frequency Response). Examples include applications to the automobile passenger compartment.

NORMAL MODES ANALYSIS

Rigid Format number 3 -- Normal Modes Analysis -- can be used to extract the acoustic natural modes and frequencies of a slot-element model of the cavity. The bulk data cards which are required to implement this capability include:

<u>Card</u>	<u>Purpose</u>
AXSLOT	parameter definition
GRIDS	scalar point specification
CSLOT3, CSLOT4	element definition
EIGR	eigenvalue extraction technique

Plots of the finite element model may be obtained by using the standard NASTRAN plot request case control cards, with the exception of the card "SET n INCLUDE PLOTEL" (n = set number) which must be included.

To investigate the convergence of the slot element solution, computed eigenfrequencies for a one-dimensional tube with closed ends have been compared with the exact solution, and the results of this investigation are shown in Figure 1. The percentage error in the computed frequency can be deduced to be proportional to $(n/N)^2$ where n is the mode number and N is the number of elements used. These results can be applied to an irregularly shaped enclosure to estimate the number of elements required in a particular direction in order to attain a desired degree of accuracy of a particular mode.

For example, one can estimate that accuracy to within 10 percent can be obtained for the first four modes in a particular direction by using about ten elements in that direction.

Figure 2 illustrates the application of the slot elements to analyze an irregularly shaped enclosure, namely an automobile passenger compartment of the "hatchback" type. The computed resonant frequencies and the nodal lines for the lowest four modes are shown in Figure 3 for the compartment completely closed (for comparison, see similar computations reported in Refs. 4 & 5) and also for the compartment with the hatch open. (An open portion of the boundary can be modeled by applying single point constraints at the boundary GRIDS points.) The modes shown in the figure are analogous to the modes which occur in the tube except for the effects introduced by the irregular boundary shape. The open hatch configuration reduces the fundamental frequency, analogous to what occurs when one end of the closed-closed tube is opened, although in this case the fundamental frequency is not halved as it is for the tube. The figure shows some comparisons of the computed frequencies with experimentally obtained frequencies, and the agreement can be seen to be quite favorable.

DIRECT FREQUENCY RESPONSE

Rigid Format number 8 -- Direct Frequency and Random Response -- can be used to compute the sound pressure at the gridwork of points of the finite element model, for prescribed vibration input at the boundary. This capability, while not described in detail in the NASTRAN documentation, is alluded to on p. 1.9-2 of the User's Manual (Ref. 3) by the statement, "Dynamic load cards . . . may be introduced to account for special effects." Here the use of the RLOAD2 card with the slot-elements is described for the purpose of making direct frequency response computations of the acoustic sound pressure inside an enclosure.

The complete list of bulk data cards which are required includes:

<u>Card</u>	<u>Purpose</u>
AXSLOT	parameter definition
GRIDS	scalar point specification
CSLOT3, CSL0T4	element definition
RLOAD2	boundary condition specification
DAREA	vibration modeshape specification
DPHASE	vibration phase specification
FREQ1	vibration frequency specification
TABLED4	vibration type specification

To prescribe a vibration of the boundary, the RLOAD2 card is used to specify DAREA and DPHASE cards which are applied directly to the GRIDS points defining the boundary. The DAREA cards specify the modeshape of the vibration, and the DPHASE cards specify the phase of the vibration. The FREQ1 card determines the frequencies at which the computations are made, and the TABLED4 card specifies the type of modeshape (i.e., acceleration or displacement) being

input. Specifying only a constant on the TABLED4 card indicates an acceleration modeshape, and specifying only an f^2 dependence (f = frequency) indicates a displacement modeshape.

Figure 4 illustrates the scheme which has been used for discretizing the modeshape for preparing the DAREA cards. The scheme lumps the area in region I on the DAREA card for GRIDS point 1, the area in region II on the DAREA card for GRIDS point 2, etc., where the areas are defined by the bisectors of the distances between the points. For this scheme, width = 1 is assumed to be specified on the AXSIOT card.

Figure 5 shows a typical application of this capability to compute the sound pressure inside an automobile passenger compartment when the back windshield is vibrating in a prescribed modeshape with a prescribed acceleration. The figure illustrates the application which involves computing the pressure p_A at point A when a half-sine acceleration modeshape is prescribed. The response at A as a function of panel frequency ω can be obtained, and a plot of the solution is also shown in the figure. The frequencies f_1, f_2, f_3, \dots at which the response becomes infinite are the acoustic resonant frequencies of the compartment which can be computed as described above under "Normal Modes Analysis."

ACOUSTIC FINITE ELEMENT MODELING WITH THE CFLUIDi ELEMENT -- APPROXIMATION OF PLANE PROBLEM

In addition to possessing the rigid and moving boundary modeling capabilities of the slot element, the axisymmetric element may be connected to structural elements to provide flexible boundary models. By a judicious choice of overall geometry and of fluid symmetry planes, the CFLUIDi elements may be used to approximate a two-dimensional cavity and thus provide a flexible wall capability not otherwise available in NASTRAN. Referring to Figure 6, we see that if the radius R_0 is sufficiently large, and the angle $\Delta\phi$ is sufficiently small, the resulting thin slice can be made as close to a cavity of uniform depth as desired. The fractional difference in depth, $\Delta d/d$, is given by h/R_0 . Thus for a cavity depth variation of $\pm 1\%$ from nominal, one would select $R_0 = 50 h$. To complete the two-dimensional analogy, one assumes that the fluid motion normal to the cross section is negligible compared with the in-plane components. In the NASTRAN model, this is accomplished by selecting a NOSYM value of NO, and including only $N1 = 0$ (zeroth harmonic) in the harmonic numbers for solution on the AXIF card. To correctly model the interaction terms, a FLSYM card is included, with an even integer, $M = 360^\circ/\Delta\phi$, and $S1 = S2 = S$.

The influence of the out-of-plane curvature on the acoustic resonances is illustrated using a 2.0 by 1.1 m rectangular cavity previously discussed by Shuku and Ishihara (Ref. 4). The model chosen contained an 8 by 4 mesh of rectangular acoustic elements. Results are presented in Table I for three values of R_0 , along with results for the NASTRAN slot element and the exact analytical results. Even for a depth variation of $\pm 22\%$ ($R_0 = 2.31 h$), the

first four cavity frequencies are within one-half percent of the slot results and within five percent of the theoretical values, as predicted in Figure 1.

FLEXIBLE WALL MODELING

A sample axisymmetric hydroelastic model including structural boundaries is discussed in section 1.7.5 of Ref. 3. For the applications included herein, the model is nominally two-dimensional as far as the fluid is concerned. With this assumption the model may be applied as well to irregular cavities of uniform cross section, with any type of boundary structure. As before, the fluid motion is represented by its zeroth harmonic, and the coupling between boundary and fluid is obtained on the basis of including more than one structural grid (GRIDB) per fluid ring boundary (RINGFL). If an alternate solution is desired, requiring higher fluid harmonics (to include the effect of transverse cavity modes, for example), the limit $N < 100$ on the AXIF card must be modified somehow in the code, for with the thin slice concept used here, the first transverse (circumferential) symmetric harmonic would have a harmonic number exceeding this limit. For example, with $R_0 = 50h$ and $d = h$ (see Figure 6 for geometry), $\Delta\phi = 1.13^\circ$ and $M = N = 318$.

The boundary structure may be modeled by using the various NASTRAN plate, beam, etc. elements, or by means of structural modes, using MPC equations and modal mass and stiffness properties as described in section 14.1 of Ref. . When desired, forcing functions at the wall may be expressed in terms of time varying loads at one or more locations or in terms of a prescribed acceleration history at one or more locations. The latter is accomplished by the usual artifice of adding a large mass at each forced point and then applying a time varying force whose magnitude is determined from Newton's second law of motion to give the desired acceleration.

MULTIPLE CAVITY MODELING

There are many interesting technical problems which involve acoustic cavities coupled through flexible panels. Previous work in this area (Refs. 5 and 6, for example) has usually entailed the development of special finite element computer codes. The extension of the present modeling technique to encompass the analysis of this problem area within NASTRAN is conceptually straightforward, albeit somewhat tedious.

What is required is the definition of a second fluid-structure boundary for each coupling panel, along with the necessary constraint equation tying the two boundaries together. Two ways of accomplishing this are shown schematically in Figure 7. Simple rigid link type MPC equations are sufficient to tie the boundaries together. At the user's convenience, depending upon the previous modeling effort, the intervening plates may be defined to attach to one set of GRIDB points, or alternatively, the plate elements may be defined relative to a set of GRID points, to which both sets of GRIDB points are

connected via MPC equations. The resulting mass and stiffness terms are identical. Note that the coupled RINGFL and GRID elements defining the boundary are coincident in a given R-Z plane and are located on the panel mid-plane. If desired, the coupling panel may be modeled using its vibration modes, as discussed earlier.

To illustrate the technique, the free vibration modes of two equally sized enclosures coupled through an intervening flexible panel are calculated and compared with the results of Reference 6. The finite element model is shown in Figure 8. For the air in the cavities, the speed of sound $c = 344.4$ m/s and the density = 1.225 kg/m³. For the aluminum plate, the thickness = 3.2 mm, the density = 2865 kg/m³, the modulus of elasticity = 493 MPa and Poisson's ratio = 1/3. The plate model had four elements in the depth direction and was simply supported on all edges.

As a check, the uncoupled cavity and plate natural frequencies have been calculated and are presented in Table II, along with the results of two alternate solutions. The first five natural frequencies are within four percent of the theoretical values. The results for the coupled system are compared in Table III with the values published in Reference 6. The difference in frequencies is eight percent or less for the first seven modes. The first three mode shapes are shown in Figure 9 and illustrate the expected structural-acoustic interaction.

CONCLUDING REMARKS

As in other areas of use, the flexibility and redundancy inherent in the NASTRAN code permit the adaptation of the acoustic and hydroelastic modeling capability to several interesting applications not envisioned in the program documentation. The discussion and examples included herein are indicative of the practical structural-acoustic problems which may be analyzed using NASTRAN.

ACKNOWLEDGEMENT

The authors are indebted to Dr. D. L. Smith for providing the experimental data shown in Figure 3.

REFERENCES

1. Herting, D. N., et al.: Acoustic Analysis of Solid Rocket Motor Cavities by a Finite Element Method. Published in NASTRAN: USERS' EXPERIENCES, NASA TM X-2378, pp. 285-324, Sept. 1971.
2. MacNeal, R. H., editor: The NASTRAN Theoretical Manual. NASA SP-221(01), NASA, Washington, D.C., December 1972.
3. McCormick, C. W., editor: The NASTRAN User's Manual. NASA SP-222(01), NASA, Washington, D.C., May 1973.
4. Shuku, T., and Ishihara, K.: The Analysis of the Acoustic Field in Irregularly Shaped Rooms by the Finite Element Method. Journal of Sound and Vibration, Vol. 29, No. 1, pp. 67-76, 1973.
5. Craggs, A.: An Acoustic Finite Element Approach for Studying Boundary Flexibility and Sound Transmission Between Irregular Enclosures. Journal of Sound and Vibration, Vol. 30, No. 3, pp. 343-357, 1973.
6. Stead, G.: A Finite Element Approach to Sound Transmission Between Rooms. M.S. Thesis, University of Alberta, Edmonton, Alberta, Canada, September 6, 1973. Also presented with A. Craggs: Sound Transmission Between Enclosures: A Study Using Plate and Acoustic Finite Elements. Eighth International Congress on Acoustics, London, 1974.

TABLE I
 NATURAL FREQUENCIES IN HERTZ FOR A 2.0 BY 1.1 m RECTANGULAR CAVITY
 (Calculations Based on $c = 340$ m/s)

Cavity Mode	NASTRAN Axisymmetric Model			NASTRAN Slot Model	Theory
	$R_0 = 2.31$ h	$R_0 = 23.1$ h	$R_0 = 138.5$ h		
1,0	85.55	85.55	85.55	85.55	85.00
0,1	159.30	158.55	158.55	158.54	154.55
2,0	174.40	174.40	174.40	174.40	170.00
1,1	184.68	184.00	184.00	183.99	176.38

TABLE II
 NATURAL FREQUENCIES IN HERTZ FOR UNCOUPLED TWO CAVITY SYSTEM

Modal Description	NASTRAN Model	Model of Ref. 6	Theory
P(1,1) ⁺ : First Plate Mode	274	273	273
C(1,0) [*] : First Longitudinal Cavity Mode	293	289	289
C(0,1) [*] : First Transverse Cavity Mode	360	356	357
P(2,1) ⁺ : Second Plate Mode	366	373	371
C(1,1) [*] : First Mixed Cavity Mode	477	460	459

⁺Plate simply supported at all boundaries.

^{*}Pairs of modes with equal frequencies occur in the uncoupled system.

TABLE III

NATURAL FREQUENCIES IN HERTZ FOR COUPLED TWO CAVITY SYSTEM

Mode Number	Description*	NASTRAN Model	Model of Ref. 6
1	C(1,0) plus P(1,1) in phase	262	243
2	C(1,0), no plate mode	293	289
3	C(1,0) plus P(1,1) out of phase	307	312
4	C(1,1) plus P(2,1) in phase	348	336
5	C(0,1), no plate mode	360	356
6	C(1,1) plus P(2,1) out of phase	373	377
7	C(1,1), no plate mode	477	460

*The description "in phase" indicates that the pressure difference across the plate appears to produce the plate motion. "Out of phase" indicates that the plate motion appears to produce fluid over (under) pressure (see also Figure 9).

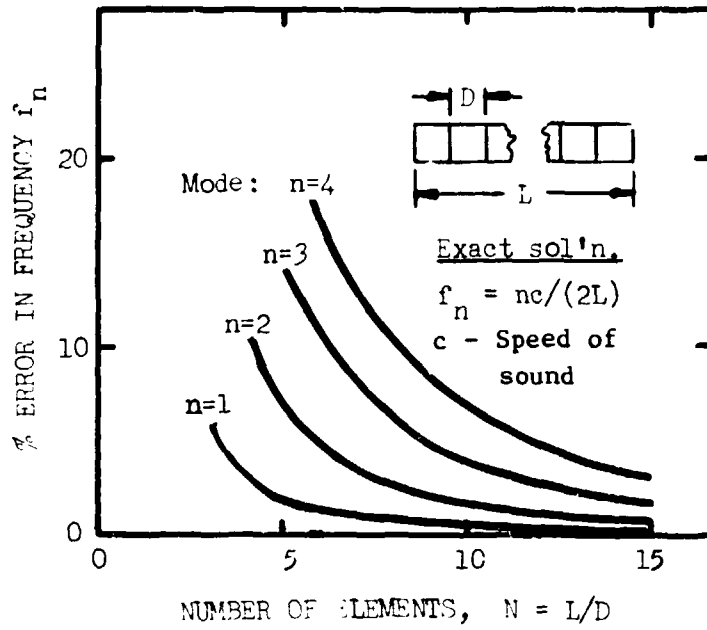


FIG. 1 RATE OF CONVERGENCE OF THE SLOT ELEMENTS

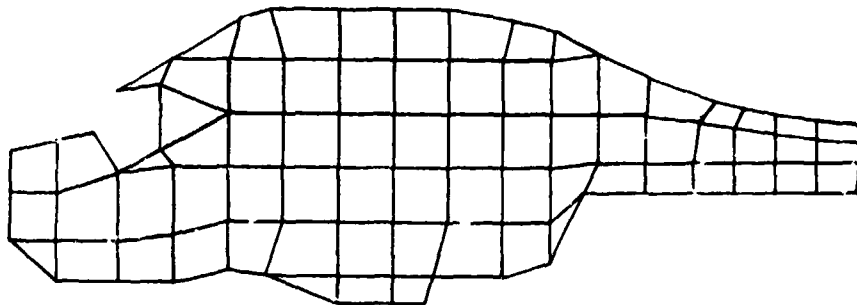


FIG. 2 FINITE ELEMENT MODEL OF AUTOMOBILE PASSENGER COMPARTMENT OF THE HATCHBACK TYPE

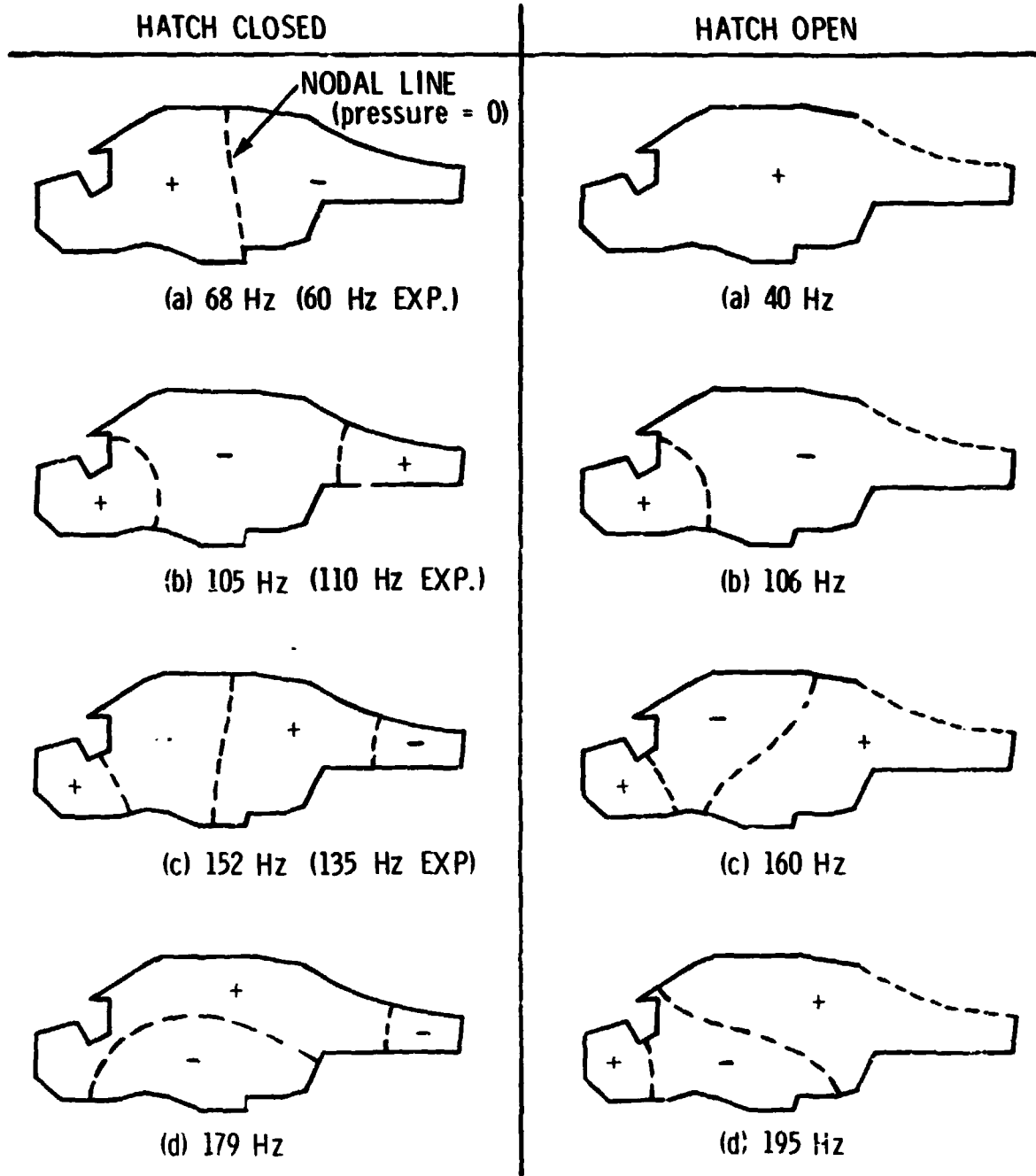


FIG. 3 ACOUSTIC RESONANT MODES AND FREQUENCIES OF PASSENGER COMPARTMENT ENCLOSURE (EXPERIMENTAL FREQUENCIES ARE SHOWN IN PARENTHESES. FOR COMPUTATIONS $c = 341$ METERS/SEC.)

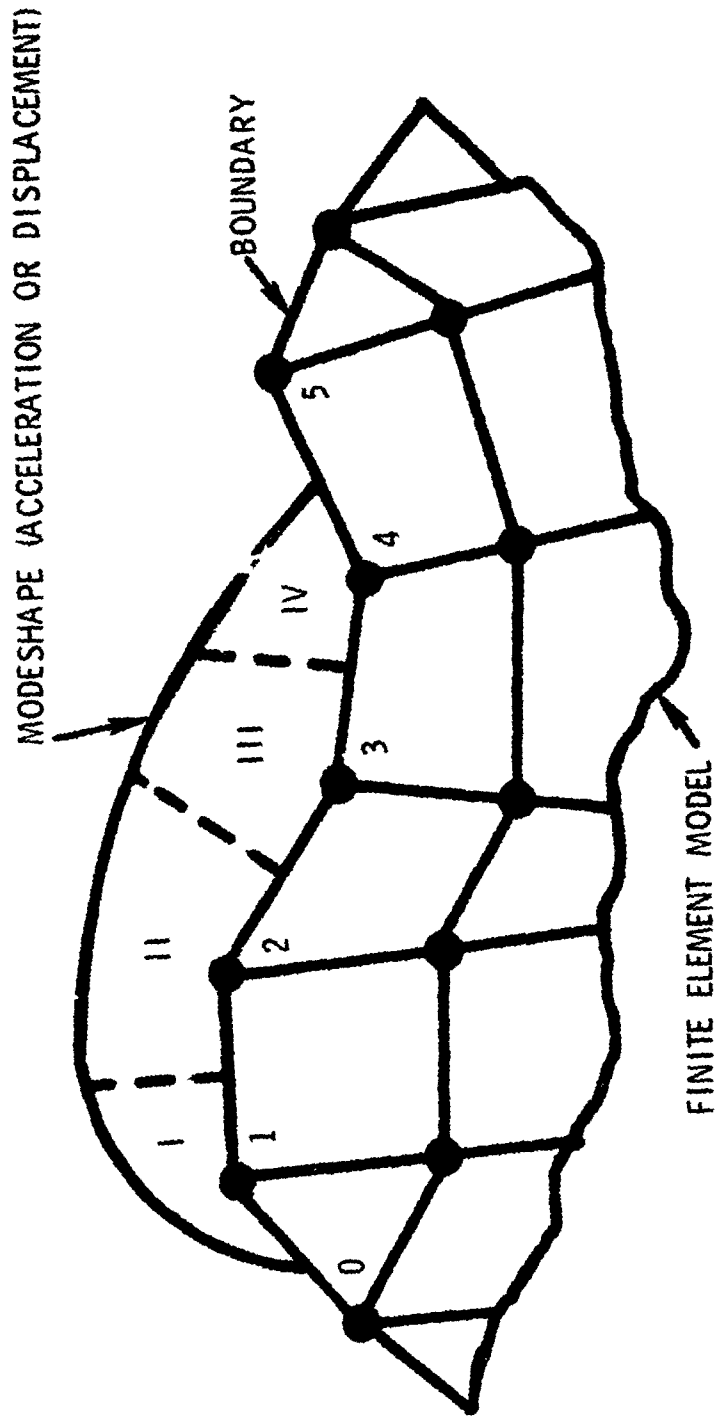


FIG. 4 SCHEME FOR DISCRETIZING PRESCRIBED BOUNDARY VIBRATION

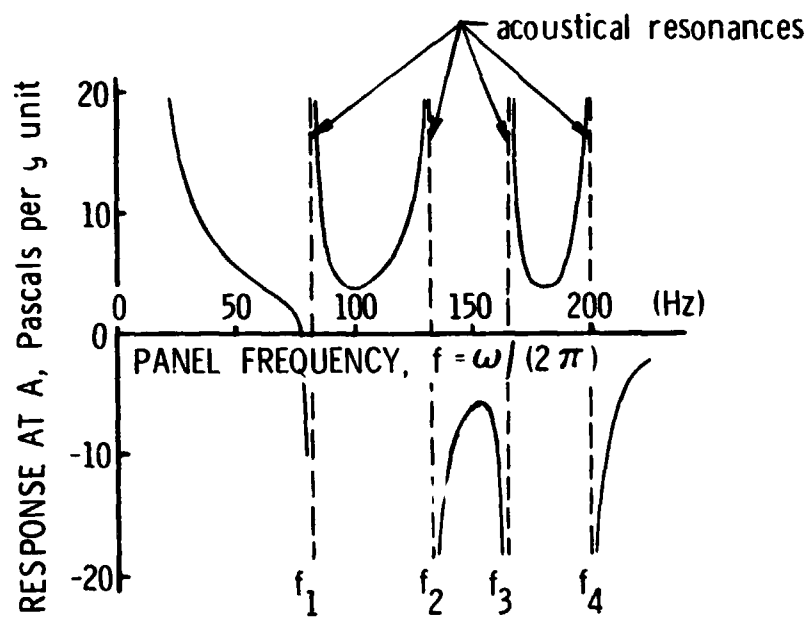
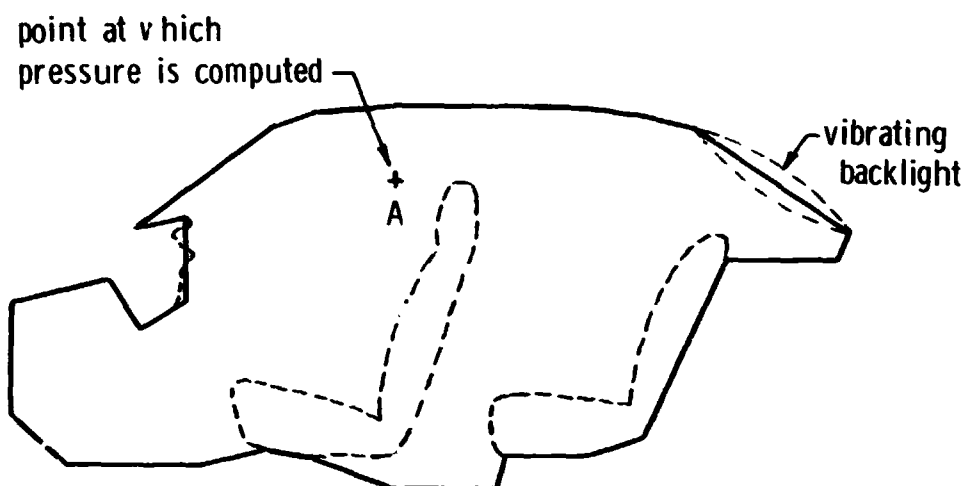


FIG. 5 FREQUENCY RESPONSE COMPUTATION OF THE SOUND PRESSURE AT THE FRONT PASSENGER EAR POSITION

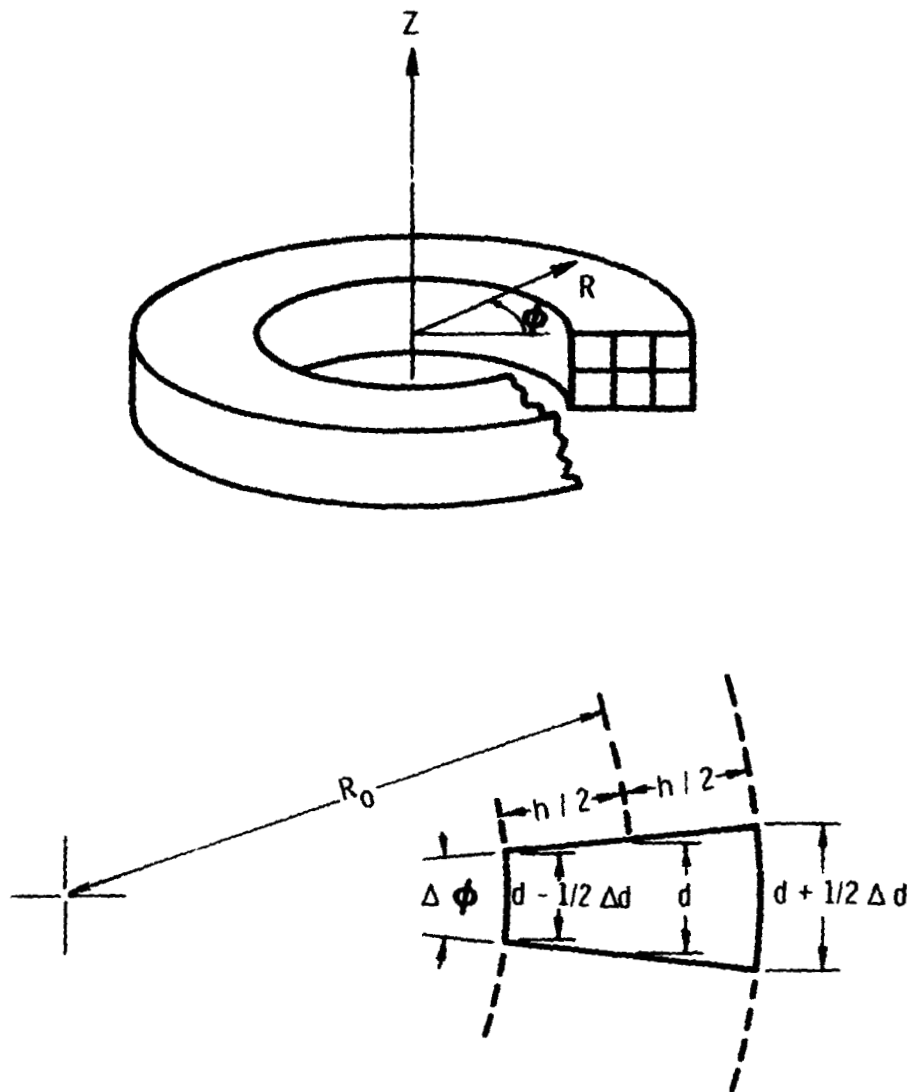
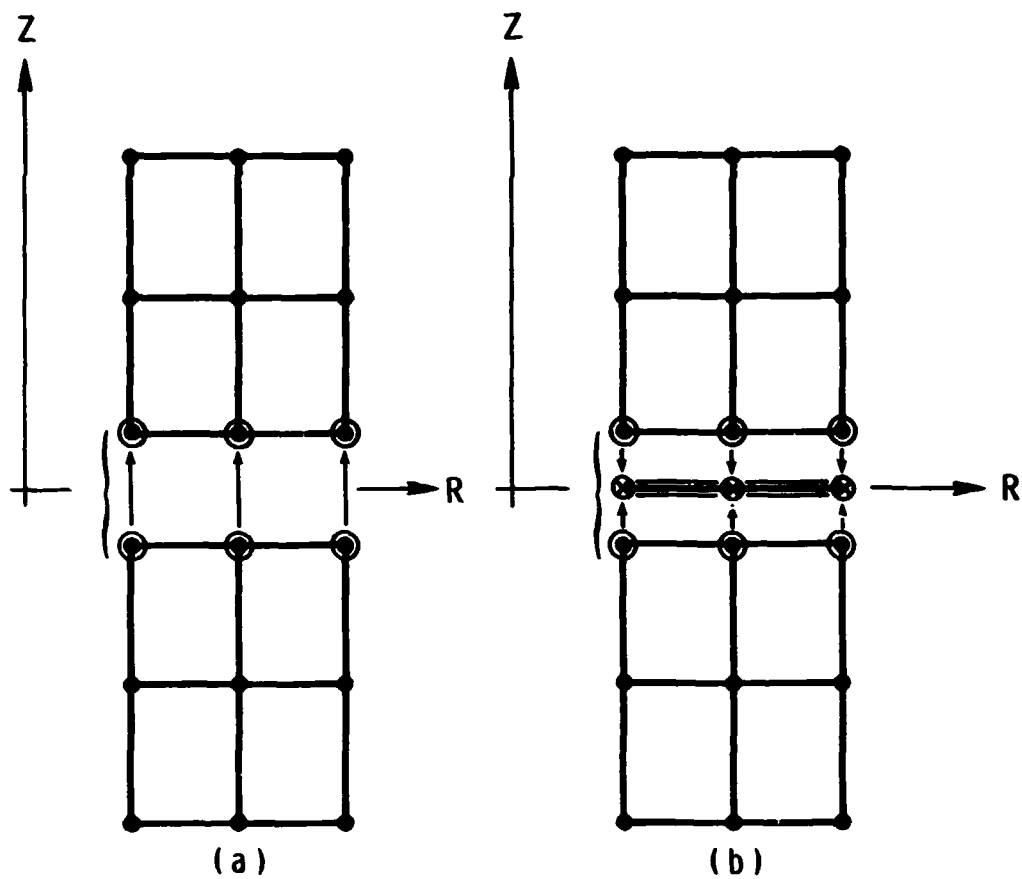


FIG. 6 USE OF AXISYMMETRIC ELEMENT TO APPROXIMATE A RECTANGULAR CAVITY



KEY:

- FLUID RING MESH POINT (RINGFL)
- ⊙ BOUNDARY GRID POINT (GRIDB)
- ⊗ STRUCTURAL GRID POINT (GRID)
- ══ FLEXIBLE BOUNDARY ELEMENT
- FLUID ELEMENT
- CONSTRAINT (MPC)
- { DENOTES COINCIDENT POINTS

FIG. 7 NASTRAN MODELING OF CAVITIES COUPLED THROUGH A FLEXIBLE BOUNDARY

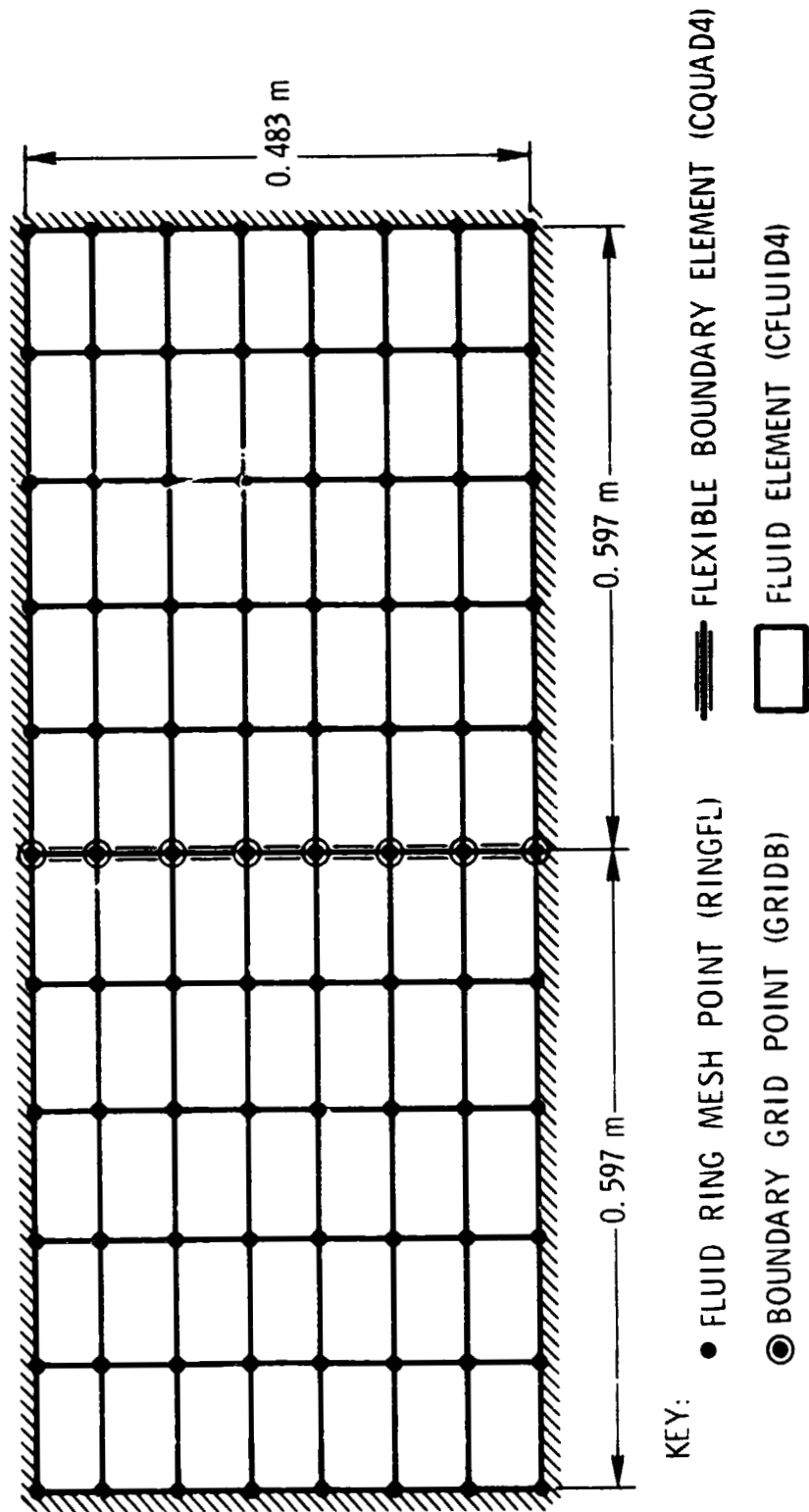
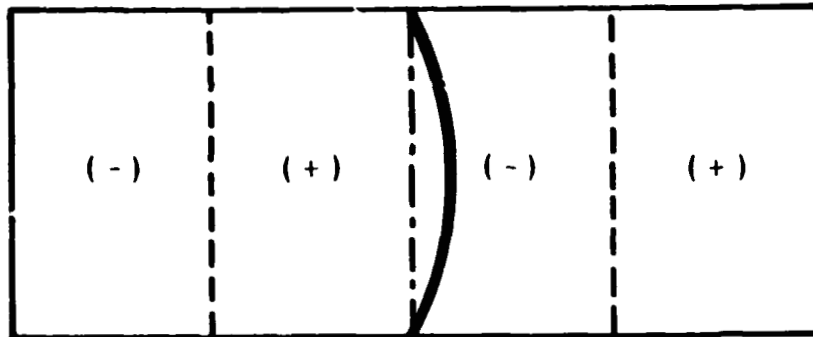
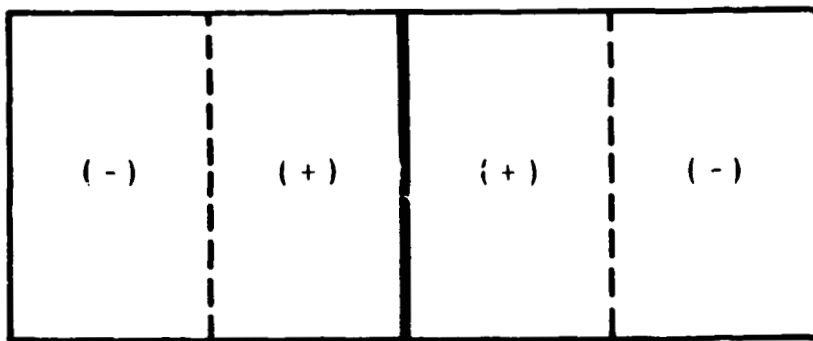


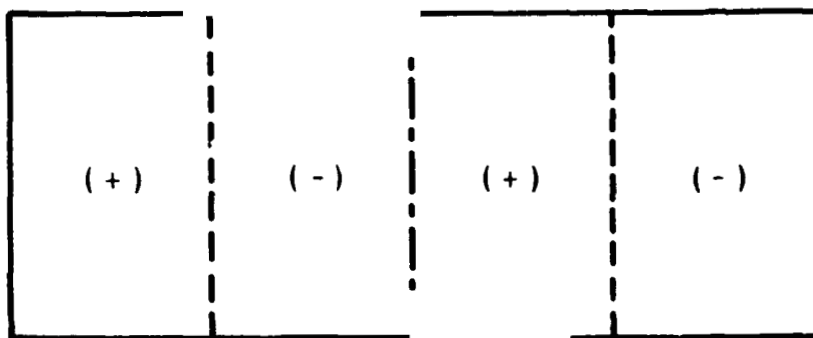
FIG. 8 NASTRAN MODEL OF TWO CAVITIES COUPLED THROUGH
A 0.483 BY 0.178 m ALUMINUM PANEL



(a) FIRST MODE - 262 Hz



(b) SECOND MODE - 293 Hz



(c) THIRD MODE - 307 Hz

——— ALUMINUM PANEL
 - - - - - NODAL LINE (ZERO CHANGE IN PRESSURE)
 (+), (-) RELATIVE SIGN OF OVER (UNDER) PRESSURE

FIG. 9 THREE MODES OF COUPLED TWO CAVITY SYSTEM